INVESTIGATION OF MITOCHONDRIAL TARGETS FOR CARDIOPROTECTION

Thesis submitted by

Rachel K. Dongworth

MBiol (First class with Honours)

For the degree of Doctor of Philosophy

University College London, UK.

Institute of Cardiovascular Science

The Hatter Cardiovascular Institute,
University College London,
67 Chenies Mews, London,
WC1E 6HX.

January 2014

DECLARATION

I, Rachel K. Dongworth confirm that the work presented in this thesis is my own. In cases where pilot data from other investigators within our laboratory is presented in the introductory sections of this thesis, the contribution of others towards this data has been duly noted. All technical assistance provided for the generation of experimental results presented here is noted alongside the presentation of methods and results in this thesis.

ABSTRACT

Background

Novel therapeutic strategies are required to protect the myocardium against ischaemia-reperfusion injury. Mitochondria are fundamental for the maintenance of cell function and survival in this setting. Although a number of mitochondrial therapeutic targets have been identified, their cardioprotective efficacy *in vivo* remains unknown.

Methods and Results

This thesis describes the establishment and validation of an important *in vivo* murine model of ischaemia-reperfusion injury for the first time within our laboratory. This model was used to investigate the cardioprotective potential of modulating three mitochondrial proteins. In addition, this thesis investigates the use of a novel cardiac MRI sequence to quantify myocardial area-at-risk, an essential pre-requisite for assessing the cardioprotective efficacy of therapeutic interventions.

Cyclophilin-D: Cyp-D has been implicated as a critical regulator of cell death by mitochondrial permeability transition pore opening upon ischaemia-reperfusion. Cyp-D genetic ablation evoked cardioprotection against myocardial ischaemia-reperfusion following extended reperfusion; thereby confirming the protective efficacy of this target.

Sirtuin-3: Post-translational protein deacetylation by Sirt-3 is an important regulator of mitochondrial biology and cell survival. Sirt-3 genetic ablation did not affect the susceptibility to myocardial infarction upon ischaemia-reperfusion under normal conditions. Fasting-induced Sirt-3 overexpression increased myocardial infarct size; thereby suggesting that Sirt-3 inhibition may be protective under certain conditions.

DJ-1: Preservation of mitochondrial function upon oxidative stress by the diverse actions of DJ-1 is critical for cell survival upon cerebral ischaemia-reperfusion. DJ-1 genetic ablation caused increased mitochondrial fragmentation but did not adversely affect cardiac function. DJ-1 knockout mice were more susceptible to myocardial infarction suggesting that this may represent an important target for cardioprotection.

Conclusions

This thesis confirms the role for CypD as an important target for cardioprotection, and provides experimental evidence implicating Sirt-3 and DJ-1 as novel mitochondrial targets for protecting the heart against ischaemia-reperfusion injury. We also provide initial data that arterial spin labelling cardiac MRI may be an important tool for the future assessment of novel cardioprotective interventions.

ACKNOWLEDGEMENTS

My sincerest thanks go to my supervisors, Dr Derek Hausenloy and Professor Yellon, who have provided me with the excellent opportunity to undertake my PhD under their exceptional guidance. I would specifically like to thank Dr Hausenloy for this continued direction and guidance over the past four years and for his expert vision which has allowed this work to come in to fruition. I would like to extend my sincere appreciation to Professor Yellon who has truly been a source of support and inspiration during this time. I feel most privileged to have undertaken my PhD in your laboratory with such a great team and will look back with immense fondness on my time here.

Thanks are also due to the excellent fellow researchers who have been a great source of support. My particular thanks go to Dr Andrew Hall who has kindly shared some of his exceptional knowledge and insight into all things scientific. I would also like to thank those who have provided preliminary data, namely, Dr Andrew Hall and Dr Sanjeev Kumar for their inspiring sirtuin-3 work and Ms U. Mukherjee for her efforts on the DJ-1 project. Thanks are extended to Dr Alex Dyson for his echocardiography expertise.

I would also like to thank Professor Mark Lythgoe and his team at the Centre for Advanced Biological Imaging for our MRI collaboration. Particular thanks to Dr Adrienne Campbell-Washburn for her extensive MRI expertise and sequence development which were integral for the realisation of this collaboration and to Mr Thomas Roberts for his expert assistance and many late weekends given over to scanning.

I wish to also extend my thanks to the Biological Services team, particularly Nick Davies who has been a superb source of advice and continued motivation, especially when I was attempting the seemingly insurmountable task of establishing the *in vivo* model.

Thanks are of course extended to the whole of the team at the Hatter Institute alongside which I have thoroughly enjoyed working; particularly to Hannah for the endless laughs. I am truly grateful to you all (of which you are simply too many to name on one page) for the light-hearted escapes which have provided a much needed check on my sanity!

Finally, my thanks to my parents and wider family who have provided me with untiring support and encouragement throughout. In particular, I thank Adrian for his absolute dedication and continued belief in me. I am truly grateful for this and can only hope that I will be able to return this, at least in part, over the coming years.

I was fortunate to be funded by the British Heart Foundation Four-Year PhD scheme and would also like to thank the BHF for this funding support during this time.

PUBLICATIONS

Below is a list of the primary research papers and first author poster abstracts resulting from the work presented in this thesis. Reference to the preliminary data previously presented in these publications is duly noted in this thesis.

Primary research publications

Dongworth R.K.*, Mukherjee U.A.*, Hall A.R., Astin R., Szabadkai G., Yellon D.M., Hausenloy D.J. Mitochondrial DJ-1 as a target for cardioprotection. Cell death and disease (in submission).

Dongworth R.K.*, Campbell-Washburn A.E.*, Roberts T.A., Yellon D.M., Lythgoe M.F., Hausenloy D.J. Cardiac magnetic resonance imaging for assessing area-at-risk *in vivo* in the murine heart (in preparation).

Oral presentations

Dongworth R.K., Campbell-Washburn A.E., Roberts T., Lythgoe M., Yellon D.M., Hausenloy D.J. Small animal magnetic resonance imaging for investigating ischaemia-reperfusion. Cardiovascular Imaging meeting, The Heart Hospital, London (UK). 2013.

Dongworth R.K., Campbell A.E., Roberts T., Lythgoe M., Yellon D.M., Hausenloy D.J. (Investigation of T2-Mapping cMR for area-at-risk assessment following ischaemia-reperfusion. BSCR UK-South Africa meeting, Cape Town (South Africa). 2012.

Poster abstracts

Dongworth R.K., Campbell-Washburn A.E., Roberts T., Lythgoe M., Yellon D.M., Hausenloy D.J. Murine Cardiac Magnetic Resonance T2-Mapping Imaging for Assessment of Area-at-Risk Following Myocardial Infarction. European Society of Cardiology, Varenna (Italy). *Translational Medicine,* S2 6; 6. 2013.

Dongworth R.K., Campbell A.E., Roberts T., Lythgoe M., Yellon D.M., Hausenloy D.J. T2-Mapping Cardiac MRI for assessing area-at-risk in a murine model of myocardial ischaemia-reperfusion injury. British Cardiovascular Society, London (UK). 2013.

Dongworth R.K., Campbell-Washburn A.E., Roberts T.A., Lythgoe M., Yellon D.M., Hausenloy D.J. Investigating the use of cardiac MRI for assessing *in vivo* area-at-risk in the mouse heart following ischaemia-reperfusion. UCL Innovations in Cardiovascular Science, London (UK). 2013.

Dongworth R.K., Yellon D.M., Hausenloy D.J. Long-term Cardioprotection of Cyclophilin-D in Acute Myocardial Infarction. *Cardiovascular Research,* 93(S1); P137. Frontiers of Cardiovascular Biology, London (UK). 2012.

Dongworth R.K., Yellon D.M., Hausenloy D.J. Investigation of the Role of Cyp-D in Cardioprotection following Ischaemia-Reperfusion. BSCR Autumn Meeting, London (UK). 2011.

CONTENTS

FIGURES

CHAPTER 1: GENERAL INTRODUCTION

CHAPTER 3: GENERAL RESEARCH METHODS

CHAPTER 4: ESTABLISHMENT OF AN IN VIVO MODEL OF MYOCARDIAL ISCHAEMIA-REPERFUSION INJURY

CHAPTER 5: INVESTIGATION OF CYCLOPHILIN-D INHIBITION AS A STRATEGY FOR CARDIOPROTECTION

CHAPTER 6: INVESTIGATION OF THE ROLE SIRTUIN-3 IN THE PATHOPHYSIOLOGY OF ISCHAEMIA-REPERFUSION INJURY

CHAPTER 7: INVESTIGATION OF THE ROLE OF DJ-1 IN THE PATHOPHYSIOLOGY OF ISCHAEMIA-REPERFUSION INJURY

CHAPTER 8: INVESTIGATION OF IN VIVO IMAGING OF THE MYOCARDIUM USING CARDIAC MRI

TABLES

ABBREVIATIONS

Standard units of measurement are used throughout this thesis according to accepted conventions. A comprehensive list of non-standard abbreviations is provided below.

AAR	Area-at-risk
ACE	Angiotensin-converting enzyme
Ab	Antibody
ADP	Adenosine diphosphate
ANT	Adenine nucleotide translocase
APS	Ammonium persulphate
ASK1	Apoptosis signal-regulating kinase I
ASL	Arterial spin labelling
ATP	Adenosine triphosphate
A.U.	Arbitrary units
BCA	Bicinchoninic acid
Bcl-2	B-cell lymphoma-2
Bp	Base pairs
BPM	Beats per minute (heart rate)
BSA	Bovine serum albumin
C106A	Cysteine 106 alanine (DJ-1 mutation)
CA	Carbonic anhydrase
Cine	Cinematic (imaging)
CK	Creatine kinase
COX-2	Cyclo-oxygenase 2
CsA	Cyclosporine-A
Cx	Circumflex (coronary artery)
Cyp	Cyclophilin
Daxx	Death-domain associated protein
dNTP	Dinucleotide triphosphate
DTPA	Diethylene-triamine penta-acetic acid
ECG	Electrocardiogram
ECL	Enhanced chemiluminescence
ECM	Extracellular matrix
ED	End-diastolic
EGE	Early gadolinium enhancement
ERK	Extracellular-regulated kinase
EM	Electron microscopy
eNOS	Endothelial nitric oxide synthase
ES (cell)	Embryonic stem (cell)
ES	End-systolic
ETC	Electron transport chain
FAIR	Flow alternating inversion recovery
FAD^+	Flavin adenine dinucleotide
FL	Floxed
FOXO	Forkhead box O
GC	Guanine-cytosine
Gd	Gadolinium
GPCR	G-protein coupled receptor
GSK-3β	Glycogen synthase kinase-3β
H_2O_2	Hydrogen peroxide
HAT	Histone acetyl transferase
HDAC	Histone deacetylase
HeLa	Human epithelioid cervix carcinoma
HET	Heterozygote (+/-)
HKII	Hexokinase II
HRP	Horseradish peroxidase
HSP	Heat shock protein
IDH2	Isocitrate dehydrogenase-2
IFM	Interfibrillar mitochondria
IL	Interleukin
IMM	Inner mitochondrial membrane
I.P.	Intraperitoneal
IPC	Ischaemic preconditioning
IPost	Ischaemic postconditioning
IS	Infarct size
I.V.	Intravenous

KAT	Lysine acetyl transferase
KDAC	Lysine deacetylase
KHB	Krebs-Henseleit buffer
KO	Knockout (-/-)
L116P	Lysine 166 proline (DJ-1 mutation)
LAD	Left anterior descending (artery)
LGE	Late gadolinium enhancement
LPS	Lipopolysaccharide
LV	Left ventricle
MALDI-TOF	Matrix-assisted laser desorption / localisation
MEF	Mouse embryonic fibroblast
Mer	Mutated oestrogen receptor
MHC	Myosin heavy chain
MMP	Matrix metalloproteinase
MnSOD	Manganese superoxide dismutase
mPTP	Mitochondrial permeability transition pore
mtCsA	Mitochondrial targeted CsA
mtRFP	Mitochondrial red fluorescent protein
mtYFP	Mitochondrial yellow fluorescent protein
MRI	Magnetic resonance imaging
NACWO	Named animal care welfare officer
NAD^+	Nicotinamide adenine dinucleotide
Neo	Neomycin resistance (gene)
NOS	Nitric oxide synthase
OMM	Outer mitochondrial membrane
PAF	Platelet activating factor
PBS	Phosphate buffered saline
PCR	Polymerase chain reaction
PE	Prostaglandins
PEP	Positive end pressure
Pi	Inorganic phosphate
PI3K	Phosphoinositide 3-kinase
PI	Propidium iodide
PKG	Protein kinase G
PPCI	Primary percutaneous coronary intervention
PPIase	Peptidyl-prolyl cis-trans isomerase
Ppif	Peptidyl-prolyl isomerase F
PTEN	Phosphatase and tensin homolog
RCA	Right coronary artery
RF	Radiofrequency
RIP	Receptor interacting protein
RIPost	Remote ischaemic postconditioning
RISK	Reperfusion injury salvage kinase
RNAi	Interference RNA
ROS	Reactive oxygen species
RV	Right ventricle
S.C.	Subcutaneous
SDS-PAGE	Sodium-dodecyl sulphate polyacrylamide gel electrophoresis
SfA	Sanglifehrin-A
sh-RNA	Short-hairpin RNA
Sirt	Sirtuin
Sir	Silent information regulator
SNO	S-nitrosylation
SOD	Superoxide dismutase
SPECT	Single photon emission computed tomography
STEMI	ST-segment elevation myocardial infarction
TAC	Transaortic constriction
TE	Echo time (MRI)
TEMED	Tetramethyl ethylenediamine
T_m	Melting temperature (DNA)
TMRM	Tetramethyl rhodaminemethyl
TNF	Tumour necrosis factor
TTC	Triphenyltetrazolium chloride
VDAC	Voltage-dependent anion channel
WT	Wildtype (+/+)
ZT	Zeitgeber time

CHAPTER 1: GENERAL INTRODUCTION

1.1. Cardiovascular disease and acute myocardial infarction

Coronary artery disease and its end consequence, acute myocardial infarction, is currently the leading cause of mortality worldwide. Indeed, almost 450,000 patients were admitted to hospital for acute myocardial infarction between 2004 and 2010 in England alone (Smolina et al., 2012). Furthermore, recent predictions suggest that the prevalence and consequent mortality of acute myocardial infarction will continue to increase during the coming decades, such that it will remain the leading cause of death worldwide in 2030 (Mathers and Loncar, 2006). These humbling statistics persist despite decades of basic and clinical research into the mechanisms of acute myocardial infarction and the development and implementation of reperfusion therapies for the treatment of myocardial infarction (Thygesen et al., 2007).

Acute myocardial infarction is the most significant clinical manifestation of coronary artery disease (Thygesen et al., 2007). During the progression of coronary artery disease, atherosclerosis of the major coronary arteries occurs due to accumulation of cholesterol-engorged macrophages which can cause plaques to develop within the arteries (reviewed by Lusis, 2000). Acute myocardial infarction is most commonly caused by rupture or erosion of an atherosclerotic plaque which results in the formation of a thrombus and subsequent distal occlusion of the artery. If the coronary artery occlusion is not rapidly removed, then sustained myocardial ischaemia will result in the death of cardiomyocytes within this area of ischaemia (Thygesen et al., 2007).

Clinical diagnosis of acute myocardial infarction is largely based on the presence of distinct electrocardiogram (ECG) features and elevated cardiac enzyme levels in blood, discussed in detail subsequently. Treatment of acute myocardial infarction comprises rapid restoration of coronary artery perfusion by removal of the occluding lesion. Current established reperfusion therapy for acute myocardial infarction comprises pharmacological thrombolysis or primary percutaneous coronary intervention (PPCI) to mechanically disrupt and remove the occluding lesion (Thygesen et al., 2007). Indeed, widespread and timely application of these reperfusion therapies has dramatically improved the early prognosis of acute myocardial infarction patients (Smolina et al., 2012). However, as short-term patient prognosis improves, the importance of studying long-term morbidity and mortality becomes increasingly important, particularly given the predicted increased prevalence of acute myocardial infarction and subsequent development of cardiac failure (Mathers and Loncar, 2006).

1.2. Myocardial ischaemia-reperfusion injury

The primary effect of coronary artery occlusion is myocardial infarction which is caused by the adverse effects of ischaemia and reperfusion. Myocardial ischaemia disrupts normal cellular physiology and initiates a sequence of events that ultimately result in death of ischaemic cardiomyocytes. In addition, reperfusion of the previously ischaemic myocardium also, paradoxically, causes a degree of damage, termed lethal myocardial reperfusion injury, which can result in further cardiomyocyte death (Manning and Hearse, 1984). Since it has long been appreciated that the extent of myocardial infarction strongly correlates with patient prognosis (Sobel et al., 1972), limiting ischaemia-reperfusion injury represents a significant target for the development of therapeutic strategies aimed at improving patient prognosis.

1.2.1. Overview of normal myocardial physiology

In order to understand the pathophysiology of ischaemia-reperfusion injury, it is necessary to appreciate the normal physiology of cardiomyocytes and their cumulative roles in normal cardiac function. Cardiomyocytes function as a highly ordered network of electrically and physically connected cells to allow efficient propagation of action potentials and contractile force. The helical macroscopic structure of the myocardium has been suggested to form the basis for efficient electrical and contractile functioning of the heart and is therefore important for overall cardiac function (Buckberg et al., 2001).

The heart is an exceptionally energy demanding organ and as such its constituent muscle cells, the cardiomyocytes, are densely packed with mitochondria (Katz, 2001). The main energy carrier in mammalian cells is adenosine triphosphate (ATP) which releases energy upon hydrolysis to produce adenosine diphosphate (ADP) and inorganic phosphate (Pi) (Alberts et al., 2002). Cardiomyocytes normally produce ATP by aerobic metabolism, predominantly by fatty acid oxidation and in part by aerobic glycolysis (Braunwald and Kloner, 1985). These processes produce acetyl-CoA which enters the citric acid cycle to produce ATP (Figure 1.1, stage 1 and 2). Electrons produced by the citric acid cycle are transferred along the electron transport chain (ETC) complexes in a process which establishes a proton electrochemical gradient across the inner mitochondrial membrane (Figure 1.1, stage 3). This causes proton flux across the mitochondrial inner membrane in to the matrix which drives ATP synthase to produce ATP by oxidative phosphorylation (Figure 1.1, stage 4). Oxidative phosphorylation dramatically increases overall ATP production by regenerating ATP from ADP and Pi. Importantly, reactive oxygen species (ROS) generated by the ETC are transferred to molecular oxygen to avoid oxidative damage (Katz, 2001; Alberts et al., 2002).

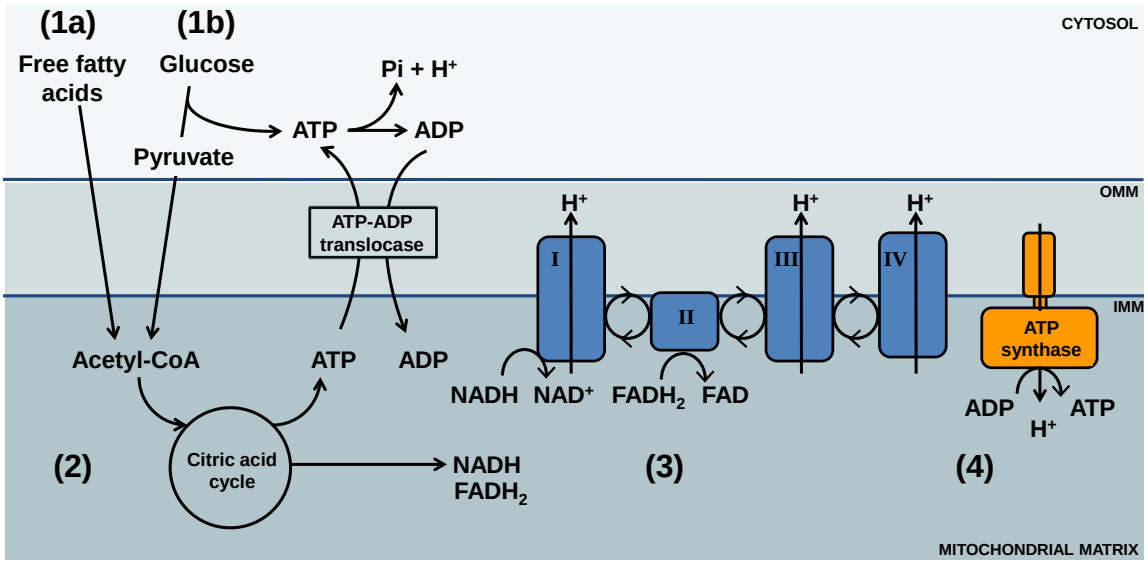

Figure 1.1: Energy production in normal cardiomyocytes
In the healthy normoxic heart, cardiomyocytes produce ATP by aerobic metabolism, predominantly by utilisation of free fatty acids: (1a) Free fatty acids are converted to acetyl-CoA. (1b) Aerobic glycolysis breaks down glucose to form ATP and pyruvate which is oxidised to form acetyl-CoA. (2) Acetyl-CoA enters the citric acid cycle which produces ATP and reduced NADH and $FADH_2$. (3) Electrons produced by the citric acid cycle are transferred to the ETC where transfer along the complexes (I, III and IV – dark blue) drives protons into the mitochondrial intermembrane space to create an electrochemical gradient across the IMM. (4) This causes proton influx across the IMM via the ATP synthase (orange) to generate ATP. Constructed from information provided by Katz (2001) and Alberts et al. (2002).

As with all cell types, energy is required for cellular homeostasis and in turn cellular signalling. Cardiomyocytes also utilise a significant amount of energy for contractility required for cardiac function (Davies, 1977). In healthy normoxic cardiomyocytes, ATP production is coupled to the demand for ATP by the availability of ADP and active regulation of ATP synthase (Das, 1998; Carmeliet, 1999). This regulation of ATP production ensures that in the normal heart, myocardial energy demands are constantly met thus ensuring that the contractile function of the heart is sustained (Katz, 2001).

Normal and sustained cardiac function therefore requires an uninterrupted supply of oxygen and nutrients to the myocardium by the coronary arteries. The myocardium is perfused by three main coronary arteries, the left anterior descending (LAD), right coronary artery (RCA) and circumflex (Cx), which each perfuse a distinct territory of the myocardium. Although there are subtle inter- and intra-species variations in coronary anatomy, these arteries consistently perfuse the myocardium in a subepicardial to subendocardial manner (Davies, 1977). A more detailed discussion of coronary anatomy is provided in chapter 4 with regards to animal models of ischaemia-reperfusion injury.

1.2.2. Pathophysiology of myocardial ischaemia

Coronary artery occlusion causes the region of myocardium normally perfused by the affected vessel to become ischaemic. The energy reserves of the ischaemic myocardium are rapidly depleted and the demand for oxygen exceeds the available supply. Given the substantial energy demands of the heart, ischaemia dramatically affects the cardiomyocytes and in turn, cardiac function (Reimer et al., 1977).

i Myocardial ischaemic milieu

The effects of myocardial ischaemia on the cardiomyocyte intracellular environment have been well-characterised and provide a basis from which to understand the pathophysiology of myocardial infarction (Reimer et al., 1977; Jennings and Reimer, 1981). The key intracellular events resulting from myocardial ischaemia are detailed below and their cumulative functional consequences are discussed subsequently.

Accumulation of ADP and inorganic phosphate: Severe hypoxia means that physiological aerobic metabolism cannot be sustained. This causes the affected myocardium to switch to anaerobic glycolysis within around 30 seconds of the onset of coronary artery occlusion (Davies, 1977; Jennings and Reimer, 1981) (Figure 1.2, stage 1). The inefficiency of ATP production by anaerobic glycolysis means that ischaemic cells are unable to generate sufficient ATP for normal cellular homeostasis and cardiac function and this in turn causes a series of cytosolic and mitochondrial changes including ADP and Pi accumulation (Katz, 2001; Alberts et al., 2002).

Intracellular acidosis: Acidification of the intracellular environment (to approximately pH 5.8 to 6.0) occurs due to lactate accumulation and hydrolysis of ATP. During anaerobic glycolysis the lack of oxygen means that pyruvate is reduced to lactate by lactate dehydrogenase in a process which also releases protons (Figure 1.2, stage 2). The accumulation of protons is further exacerbated by ATP hydrolysis which releases inorganic phosphate and protons (Figure 1.2, stage 3) (Davies, 1977; Katz, 2001). The cumulative effect of lactate and proton accumulation is progressive acidification of the cytosol and mitochondrial matrix. High lactate levels and intracellular acidosis also inhibit important glycolytic enzymes which further decreases the efficiency of ATP production and thus exacerbates ATP deprivation (Figure 1.2, stage 4) (Jennings and Reimer, 1981). In addition, protons accumulated within the cell can also interact with and affect numerous intracellular signalling pathways (Katz, 2001). Notably, voltage-gated ion channel inhibition and gap junction closure in the presence of high proton levels can cause slowed cardiac conduction and which can ultimately result in cardiac arrhythmias (Manning and Hearse, 1984; Carmeliet, 1999).

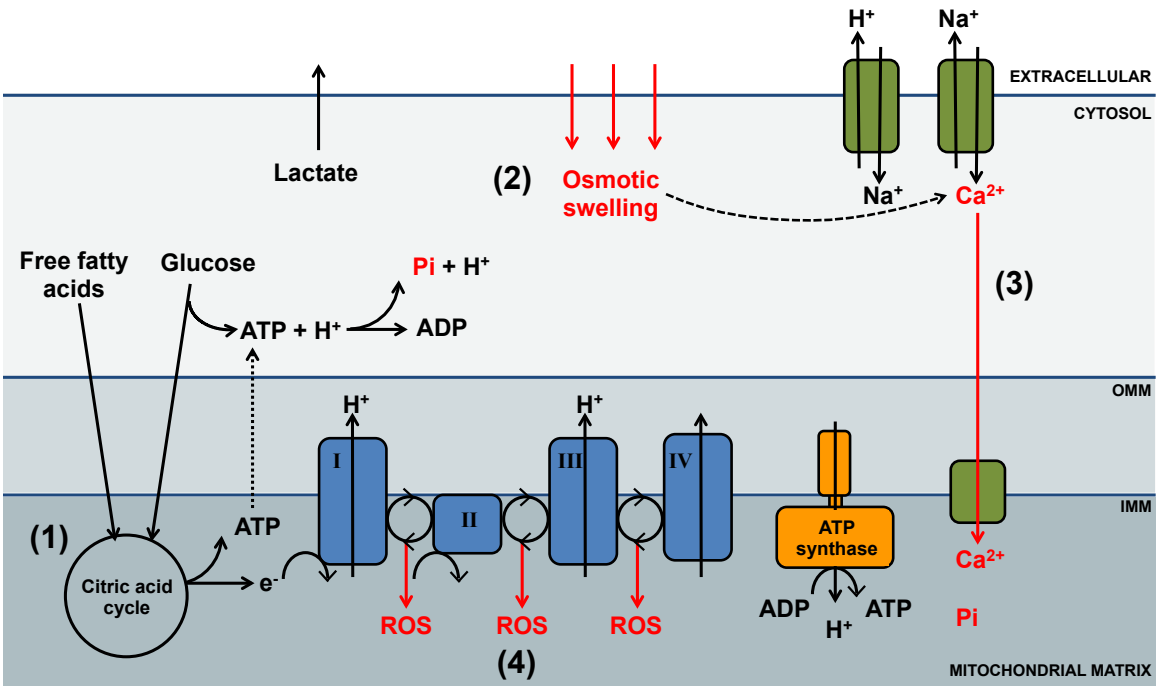

Figure 1.2: Energy production and homeostasis in ischaemic cardiomyocytes
Ischaemic cardiomyocytes respire via aerobic glycolysis. (1) Glucose is converted to pyruvate to generate small amounts of ATP. (2) In the absence of oxygen, pyruvate is converted into lactate in a process that releases protons. (3) ATP hydrolysis releases protons which exacerbates intracellular acidosis. (4) Lactate and proton accumulation decrease glycolytic efficiency. (5) High proton concentration causes Ca^{2+} influx and intracellular calcium overloading. (6) High intracellular Ca^{2+} leads to mitochondrial Ca^{2+} influx. Constructed from information provided by Noll et al. (1992), Katz (2001) and Alberts et al. (2002).

Calcium overloading: Increased intracellular proton concentration also results in calcium overloading of ischaemic cardiomyocytes. This is thought to be driven by ionic exchange mechanisms which attempt to maintain ionic homeostasis whereby the high intracellular proton concentration causes sodium ion influx (due to sodium and hydrogen ion exchange) and in turn increased intracellular calcium (due to sodium and calcium ion exchange) (Figure 1.2, stage 5) (Manning and Hearse, 1984; Kloner and Jennings, 2001). Intracellular calcium overloading accelerates interactions between contractile proteins which increases energy utilisation and thus exacerbates energy depletion of the ischaemic cardiomyocytes (Katz, 2001). Increased intracellular calcium also causes mitochondrial calcium overloading by rapid calcium influx by the calcium uniporter (Kristian and Siesjo, 1998) (Figure 1.2, stage 6).

Increased cellular osmotic load: A further effect of intracellular lactate and proton accumulation, alongside increased levels of inorganic phosphate, is an increased cellular osmotic load. Although this causes only modest cardiomyocyte swelling during ischaemia, the effect of increased osmotic load and resultant cellular swelling upon reperfusion is an important determinant of cardiomyocyte survival (Braunwald and Kloner, 1985; Katz, 2001), discussed below in relation to oedema (see section 1.2.3).

Accumulation of reactive oxygen species: Re-energisation of the ETC upon myocardial reperfusion generates a burst of reactive oxygen species (ROS). This is exacerbated by additional ROS production from ATP hydrolysis and metabolite breakdown and further by the loss of scavenging molecules, such as catalase and superoxide dismutase (SOD) due to compromised membrane integrity, described below (Braunwald and Kloner, 1985). ROS are highly reactive due to the presence of unpaired electrons in their outer shell. When ROS interact with cells they cause oxidative damage including denaturation of proteins and nucleic acids and lipid peroxidation of membranes, which can in turn disrupt membrane integrity (Forman et al., 1989). In perfused cardiomyocytes, unpaired electrons are transferred to molecular oxygen and combined with protons to form water. However, the lack of oxygen in ischaemic cardiomyocytes prevents sequestration of unpaired electrons causing accumulation ROS and ultimately oxidative damage (Katz, 2001).

ii Effects of myocardial ischaemia

The main pathophysiological effects of myocardial ischaemia are described below, where the severity of these effects depends largely on the duration of ischaemia.

Electrocardiogram changes: The electrocardiogram (ECG) depicts the sum of total electrical activity of the heart, where each segment of the integrated ECG trace is most heavily influenced by action potentials occurring in a distinct region of the heart. Myocardial ischaemia resulting from acute coronary occlusion causes significant changes to ventricular action potentials in the affected cardiomyocytes which can be visualised in the integrated ECG trace. Since the majority of acute myocardial infarctions occur in the left ventricle, it is predominantly the QRST, and specifically ST-segment of the integrated ECG trace that is affected (Katz, 2001; Herring and Paterson, 2006).

The primary cause of ECG ST-segment changes is thought to be differences in resting potential between perfused and ischaemic cardiomyocytes which abrogate the tight coupling of myocardial electrical activity (Katz, 2001). Slow electrical conduction and calcium overloading in the ischaemic myocardium perturb the plateau phase of ventricular action potentials, thereby giving rise to changes in the ST-segment of the integrated ECG trace. ATP depletion has also been shown to be an important factor in determining ST-segment changes upon myocardial ischaemia (Katz, 2001; Herring and Paterson, 2006; Sclarovsky, 2013). However, it should be noted that the exact causes of ST-segment changes upon myocardial ischaemia are not completely understood.

Nevertheless, ECG abnormalities provide a useful tool for diagnosis and classification of acute myocardial infarction; where ST-segment depression indicates subendocardial

ischaemia and ST-segment elevation indicates transmural left ventricular ischaemia. ECG ST-segment resolution confirms effective reperfusion (Thygesen et al., 2007).

Impaired cardiac function: Cardiac contractile function is rapidly reduced upon myocardial ischaemia, as evidenced by relative akinesis of the left ventricular free wall following LAD occlusion (Katz, 2001). Myocardial hypokinesis immediately upon the onset of ischaemia does not reflect impaired cardiomyocyte contractile function *per se* but an adaptive response to reduce ATP and oxygen use in an attempt to minimise the severity of ischaemia (Davies, 1977). Since myocardial hypokinesis reduces ejection fraction, its protective effect is limited to short ischaemic insults only (Katz, 2001).

If the period of ischaemia is prolonged then myocardial hypokinesis may persist even following reperfusion due to the extent of existing injury to the myocardium (Katz, 2001).

Cardiomyocyte cell death: If left unresolved, myocardial ischaemia will eventually result in death of ischaemic cells. Cardiomyocytes are the myocardial cell type most susceptible to ischaemic injury due to their extensive energy requirements (Frantz et al., 2009). The most effective strategy for reducing cardiomyocyte death, and thus infarct size, is rapid and effective restoration of coronary artery perfusion, discussed in detail below (see section 1.2.3). The recognition of infarct size progression with ischaemic duration was first formally postulated by Reimer et al. (1977) in the 'wavefront of necrosis' hypothesis which stated that cardiomyocyte death progresses from the subendocardial to subepicardial myocardium and is halted by myocardial reperfusion (Figure 1.3 B-C). Crucially, short durations of ischaemia (less than approximately 20 minutes in most species) cause only reversible injury to ischaemic cardiomyocytes (Figure 1.3 A) (Reimer et al., 1977; Jennings and Reimer, 1981).

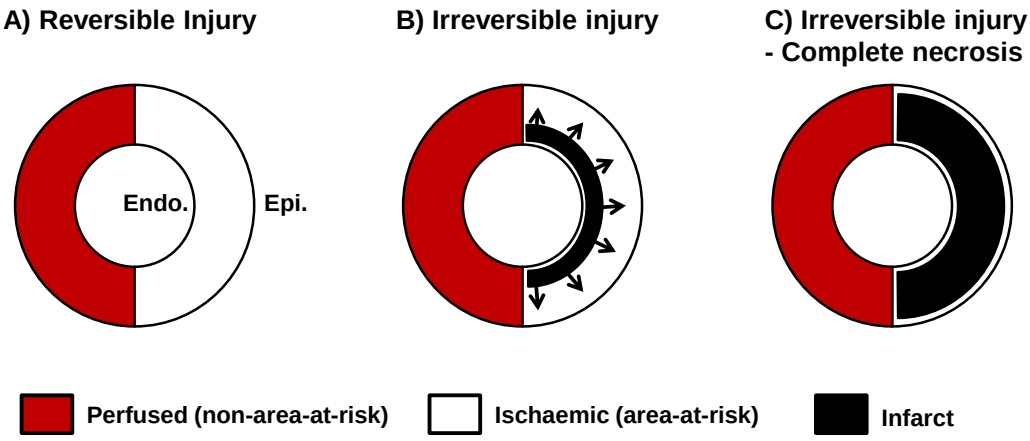

Figure 1.3: Ischaemic 'wavefront of necrosis' hypothesis
Representation of transverse myocardial section; within the ischaemic myocardium (white), necrosis (black) progresses from the subendocardium (endo.) to subepicardium (epi.). A) Short ischaemic durations cause only reversible injury. B) Intermediate ischaemic durations cause infarction in the subendocardial myocardium. C) Extended ischaemic durations cause transmural infarction. Adapted from Reimer et al. (1977) and Kloner and Jennings (2001).

The driving factor in the initiation of cardiomyocyte cell death following prolonged ischaemia is severe ATP depletion which results in deregulation of a number of critical cellular processes and pathways, described above (see section i). The distinct subendocardial to subepicardial nature of infarction is attributed to differences in perfusion and metabolic rates since the subendocardium is only perfused by the capillary bed and yet has a higher metabolic demand due to increased wall tension compared to the subepicardium (Davies, 1977; Reimer et al., 1993). There is a notable rim of non-infarcted subendocardial tissue which is likely spared due to oxygen diffusion from the left ventricle (LV) blood pool (Davies, 1977).

Ischaemic cell death is thought to occur predominantly by necrosis since apoptosis requires ATP; although it has been suggested that myocardial ischaemia may initiate apoptotic cell death pathways which are then executed in the presence of ATP upon reperfusion (Freude et al., 2000). Recent studies suggest that autophagy and necroptosis may also be important mediators of myocardial infarction (reviewed by Chiong et al., 2011); the contributions of these cell death pathways to myocardial infarction are discussed below (see section 1.2.3 ii).

1.2.3. Pathophysiology of myocardial reperfusion

Coronary artery reperfusion permits rapid return of oxygenated blood to the previously ischaemic tissue. Although early reperfusion is essential for cell survival and ultimately cardiac function (Reimer et al., 1977), reperfusion paradoxically also causes some injury, termed reperfusion injury. Reperfusion injury is discussed in detail subsequently (section ii) in the context of the intracellular events occurring upon reperfusion.

i Myocardial reperfusion milieu

The effects of myocardial reperfusion can be understood in the context of the intracellular changes caused by the preceding ischaemic insult, where rapid myocardial reperfusion temporarily worsens these intracellular imbalances. The ischaemic duration determines the extent of the principal intracellular changes (ATP depletion, increased osmotic load, acidification and ROS accumulation) and therefore the extent of subsequent reperfusion injury (Davies, 1977; Katz, 2001). In addition, myocardial reperfusion causes a transient increase in blood supply (reactive hyperaemia) proportional to the extent of the ischaemic insult, and this hyperaemia is a driving factor of immediate reperfusion injury (Katz, 2001). The intracellular changes occurring upon myocardial reperfusion following an intermediate ischaemic insult are described below and their cumulative effects discussed subsequently.

Rapid ATP production: The rapid restoration of myocardial oxygen supply by coronary artery reperfusion allows aerobic metabolism to re-start (Figure 1.4, stage 1). The resultant increase in ATP production efficiency redresses the balance of myocardial ATP supply and demand which, in turn, permits functioning of ATP-dependent cellular homeostatic mechanisms which, alongside washout of lactate, correct pH (Katz, 2001). However, rapid re-energisation and the resultant correction of intracellular acidosis may cause hypercontracture, discussed below (Piper and Garcia-Dorado, 1999).

Osmotic swelling – oedema: Ischaemia causes an increased cellular osmotic load which causes significant cardiomyocyte swelling upon myocardial reperfusion due to the rapid influx of fluids to the myocardium (Braunwald and Kloner, 1985) (Figure 1.4, stage 2). Homeostatic regulation of cellular swelling causes sodium ion efflux and calcium ion influx which exacerbates calcium overloading (Hoffman et al., 2004). Furthermore, excessive cell swelling can trigger cell death (Kloner, 1993), discussed below.

Calcium overloading: Intracellular calcium concentration is an important determinant of cardiomyocyte survival and function upon myocardial reperfusion. In moderately ischaemic cardiomyocytes, ATP-dependent ionic cellular homeostasis upon reperfusion attempts to restore intracellular calcium concentrations and thus preserve cardiomyocyte survival and contractile function (Braunwald and Kloner, 1985; Katz, 2001). However, upon reperfusion of severely ischaemic cardiomyocytes, membrane damage combined with homeostatic regulation due to cellular swelling can result in increased intracellular and mitochondrial calcium overloading (via the calcium uniporter) (Crompton and Costi, 1988; Vermeiren et al., 2000). (Figure 1.4, stage 3).

Intracellular calcium overloading in the presence of rapid re-energisation and pH correction can result in excessive cardiomyocyte contraction, termed hypercontracture, which if sustained can cause cell death. Hypercontracture also causes death of adjacent cardiomyocytes due to mechanical disruption and exposure to excessive extracellular calcium concentrations (Piper and Garcia-Dorado, 1999; Hoffman et al., 2004).

Further accumulation of ROS: ROS levels are further increased upon reperfusion due to increased ROS production in the presence of high tissue oxygen levels that occur upon myocardial hyperaemia (Manning and Hearse, 1984) (Figure 1.4, stage 4). ROS accumulation is exacerbated by further removal of ROS scavengers resulting from the combined effect of cellular leakage and myocardial perfusion (Braunwald and Kloner, 1985; Hoffman et al., 2004) and ROS production by infiltrating inflammatory cells (Braunwald and Kloner, 1985). ROS-induced oxidative damage can itself cause cell death (Braunwald and Kloner, 1985; Hoffman et al., 2004) in addition to the effects of high ROS levels on mitochondrial permeability transition described below (section iv).

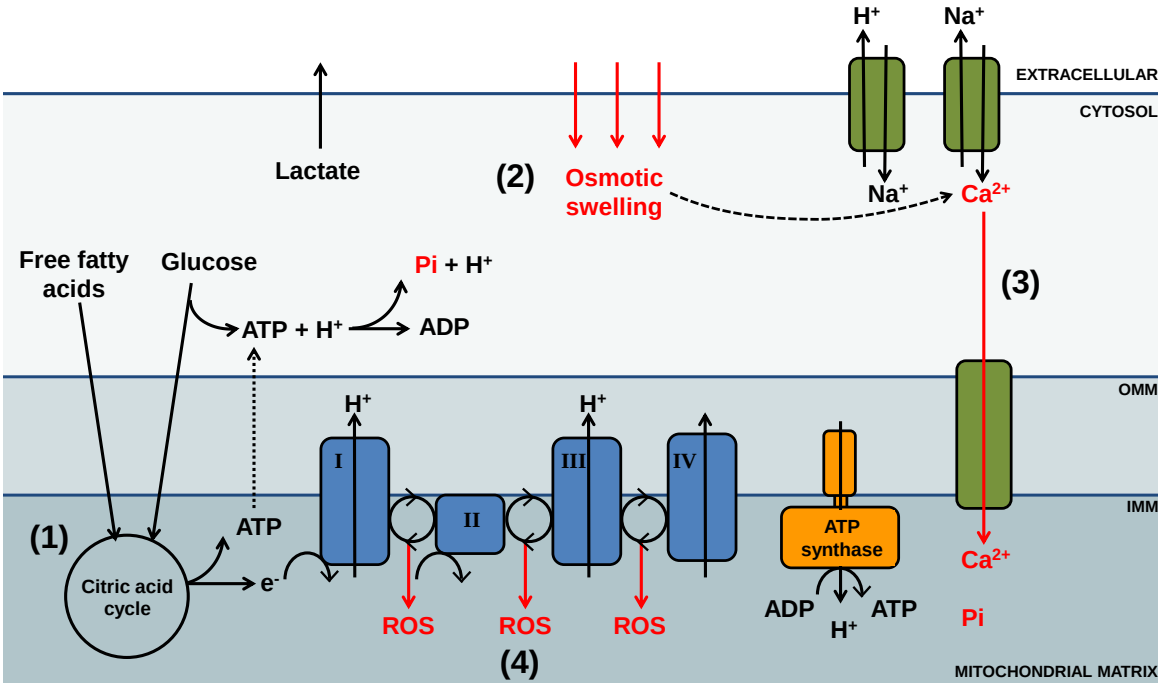

Figure 1.4: Energy production and homeostasis in reperfused cardiomyocytes
Myocardial reperfusion temporarily exacerbates the ionic imbalances caused by ischaemia. (1) Aerobic metabolism re-starts which increases ATP availability. (2) Cellular swelling occurs due to the increased osmotic load and presence of tissue fluid. (3) Calcium overloading is exacerbated by membrane damage and homeostatic attempts to correct osmotic swelling, which in turn cause mitochondrial calcium overloading. (4) Mitochondrial ROS accumulates due to ETC leakage resulting from oxidative damage. Constructed from information provided by Katz (2001), Alberts et al. (2002) and Hoffman et al. (2004).

The severity of these intracellular events upon reperfusion is largely dependent on the duration of the preceding ischaemic insult and thus the severity of the intracellular changes already initiated prior to reperfusion. The cumulative effects of the intracellular changes initiated by myocardial ischaemia and reperfusion are discussed below.

ii Effect of reperfusion – Lethal reperfusion injury

The wavefront of necrosis hypothesis postulated by Reimer et al. (1977) stated that myocardial reperfusion halts the progression of myocardial injury. However, despite the necessity of reperfusion for the preservation of viable cardiomyocytes, it is recognised that reperfusion itself results in some injury and cell death, termed reperfusion injury. The occurrence and molecular basis of reperfusion injury have been subject to extensive research and some controversy over the past decades (Kloner, 1993).

There are four recognised types of reperfusion injury: (1) lethal reperfusion injury, (2) reperfusion arrhythmias, (3) myocardial stunning and (4) no reflow (reviewed by Braunwald and Kloner, 1985; Kloner, 1993); summarised in Table 1.1.

TYPE OF INJURY	THEORETICAL BASIS AND OVERVIEW
Lethal reperfusion injury: (Braunwald and Kloner, 1985)	Death of cardiomyocytes that were only reversibly injured at the end of ischaemia but become irreversibly injured upon reperfusion. The occurrence of this form of reperfusion injury has been the most controversial – this discussed in detail in the main text.
Reperfusion arrhythmias: (Manning and Hearse, 1984)	Ventricular arrhythmias – experimentally generally only occur after brief periods of ischaemia and very rapidly upon reperfusion. The clinical occurrence of reperfusion arrhythmias is likely to be low and can be managed; if unresolved this can result in death.
Myocardial stunning: (Bolli et al., 1989)	Prolonged dysfunction of viable cardiomyocytes which represents a functional form of injury to the salvaged myocardium. This is expected to recover within 1 month of reperfusion and can be managed by administration of inotropes to stimulate contraction.
No-reflow: (Kloner et al., 1974) (Thygesen et al., 2007)	Perfusion defects within the area-at-risk due to vascular damage (particularly of the microvasculature) or cardiomyocyte swelling. This can result in sustained ischaemia of a region of the area-at-risk and results in poorer functional recovery. Effective reperfusion and thrombolysis are expected to reduce the severity.

Table 1.1: Predicted mechanisms of reperfusion injury
Summary of the four proposed types of reperfusion injury. References are provided for principal descriptions of these types of injury and their relevance in acute myocardial infarction.

The clinical occurrence and extent of reperfusion arrhythmias, myocardial stunning and the no-reflow phenomena have been largely elucidated and can be clinically treated; lethal reperfusion injury however, has been the subject of intense controversy over the past three decades (reviewed by Kloner, 1993; Garcia-Dorado et al., 2009). This is particularly pertinent given that lethal reperfusion injury is the only form of reperfusion injury where there is, as yet, no clinical treatment (Hausenloy and Yellon, 2013).

Lethal reperfusion injury causes death of some cells that were only reversibly injured by the preceding ischaemia (Figure 1.5) (Braunwald and Kloner, 1985; Kloner, 1993). Indeed, it has been suggested that in some circumstances lethal reperfusion injury could account for approximately 30-50% of myocardial infarct size. Precise delineation of ischaemic and reperfusion injury, and therefore direct evidence of lethal reperfusion injury, is complicated by the role of the preceding ischaemic insult in the occurrence and extent of reperfusion injury. It is now largely accepted that lethal reperfusion injury represents a true clinical phenomenon where studies have shown that pharmacological and mechanical interventions can reduce infarct size when administered at the onset of reperfusion (reviewed by Garcia-Dorado et al., 2009). Furthermore, a clinical study of cyclosporine-A administered at reperfusion significantly reduced infarct size (Piot et al., 2008), thereby confirming the clinical existence of lethal reperfusion injury and its potential as a therapeutic target for cardioprotection (discussed in section 1.4.1).

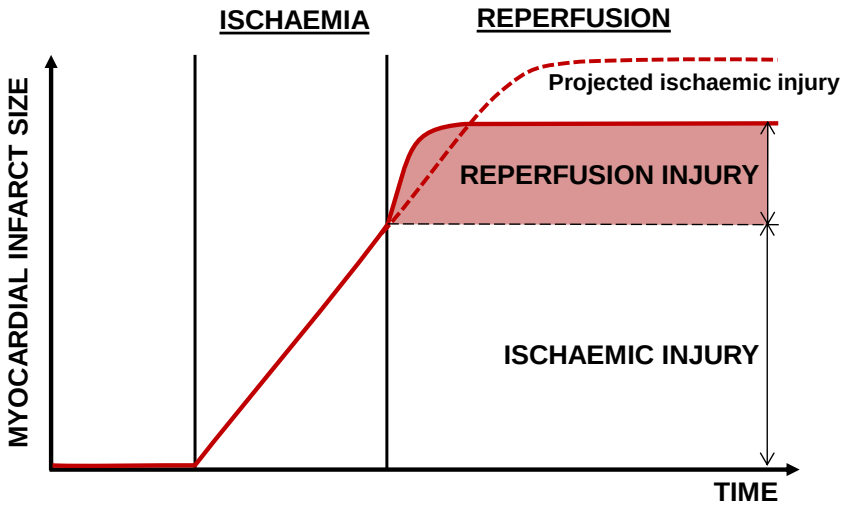

Figure 1.5: Lethal reperfusion injury
Infarct size (red line) increases with ischaemic duration and if left unresolved the total area of ischaemic myocardium will become infarcted (projected ischaemic injury– dashed red line). Reperfusion limits infarction but, paradoxically, causes some infarction itself, termed lethal reperfusion injury (shaded red area). Adapted from Garcia-Dorado et al. (2006).

Cardioprotection during the early phase of reperfusion is consistent with the occurrence of the numerous potentially injurious intracellular changes that occur upon myocardial reperfusion (reviewed by Garcia-Dorado et al., 2009), described previously (section i).

Given that early reperfusion is recognised as the most effective intervention for reducing infarct size (Kloner, 1993; Thygesen et al., 2007), it has been suggested that lethal reperfusion injury is likely to contribute to myocardial injury and therefore remains a significant and largely unmet clinical target for the treatment of acute myocardial infarction (Thygesen et al., 2007; Hausenloy and Yellon, 2013). This is crucial given the correlation between infarct size and patient prognosis (Sobel et al., 1972).

iii Lethal reperfusion injury – Mechanisms of cell death

Myocardial reperfusion causes cell death by necrosis, apoptosis, autophagy or necroptosis, although the precise contribution of these mechanisms to progression of myocardial infarction has not been fully elucidated (reviewed by Oerlemans et al., 2013).

Necrosis: Necrotic cell death is characterised by cellular swelling, membrane damage and ultimately cell rupture resulting in the loss of intracellular substrates which initiate a significant inflammatory response (Reimer et al., 1977). Myocardial ischaemia has been shown to cause necrosis (Jennings and Reimer, 1981), however, reperfusion has been suggested to initiate regulated necrosis by mitochondrial permeability transition (Figure 1.6 A) (reviewed by Baines, 2009a), discussed in detail subsequently (see section iv).

Apoptosis: Moderately injured cardiomyocytes may undergo apoptotic cell death which, due to the controlled nature of cell shrinkage and maintenance of membrane integrity, does not initiate an inflammatory response (MacLellan and Schneider, 1997; Piper and Garcia-Dorado, 1999). Apoptosis is triggered by intrinsic or extrinsic pathways:

Intrinsic apoptotic pathway: The precise mechanism of the intrinsic apoptotic pathway remains controversial. Tissue stress causes translocation and integration of pro-death B-cell lymphoma-2 (Bcl-2) proteins (Bax, Bak and Bid) into the outer mitochondrial membrane to cause its permeation (Figure 1.6 B). This allows release of pro-apoptotic proteins, such as cytochrome *c*, which bind to apoptotic protease activating factor-1 (APAF-1) to form the 'apoptosome' which subsequently activates 'effector' caspases, which are described in more detail below (Oerlemans et al., 2013).

Extrinsic apoptotic pathway: The extrinsic apoptotic pathway is the most well studied and involves receptor-mediated cell death. Tissue stress causes binding of extracellular death ligands (such as TNF-α) to cell surface membrane receptors to activate 'initiator' caspases including caspase-8 (Figure 1.6 C). Initiator caspases then activate 'effector' caspases which mediate cell death (Freude et al., 2000; Oerlemans et al., 2013).

Both intrinsic and extrinsic apoptotic pathways converge on activation of 'effector' caspases-3 and -9 which mediate destruction of cell structures and deregulation of protein activity (Hoffman et al., 2004). This causes membrane blebbing and surface exposure of phosphotidylserine residues which trigger phagocytosis by neighbouring cells. This complete and controlled removal of designated cells does not initiate an inflammatory response (MacLellan and Schneider, 1997; Hoffman et al., 2004). Due to its ATP-dependence, apoptosis occurs mainly following reperfusion, although there is evidence to suggest that ischaemia initiates apoptotic signalling cascades which are then executed in the presence of ATP at reperfusion (Freude et al., 2000).

Autophagy: Autophagy is a highly conserved process of lysosomal-mediated degradation of intracellular components initiated upon cellular stress events including hypoxia, nutrient starvation and ROS. Under physiological and mild stress conditions, autophagy is an adaptive response triggered by these cell stressors (Levine and Kroemer, 2008). Indeed, there is evidence that regulated autophagy in response to mild to moderate ischaemia may protect against the development of infarction by replenishing energy resources. However, prolonged ischaemia and subsequent reperfusion can trigger a dramatic and maladaptive upregulation of autophagy which is detrimental to cell survival. The precise molecular mechanisms of autophagy in response to acute myocardial infarction remain largely unknown (reviewed by Chiong et al., 2011) and thus are not discussed further in this thesis.

Necroptosis: More recent studies have suggested that a programmed form of necrosis, termed necroptosis, may also mediate cell death. Necroptosis is believed to be initiated by activation of classical death receptors such as TNF-α which in turn activate members of the receptor interacting protein (RIP) kinase family (reviewed by Long and Ryan, 2012). There is currently limited knowledge regarding the role of necroptosis in acute myocardial infarction and lethal reperfusion injury, however, this represents a potentially important cell death pathway for future research; this is not discussed further here.

A summary of the main cell death pathways implicated in lethal reperfusion injury to date is provided in Figure 1.6. The specific contribution of these death pathways is likely to depend on the prevailing pathophysiological conditions (reviewed by Oerlemans et al., 2013). It is evident that permeation of the inner and outer mitochondrial membranes represents a critical effector of cell death upon reperfusion (Figure 1.6 mechanisms A and B). The role of the mitochondrial permeability transition pore is discussed below.

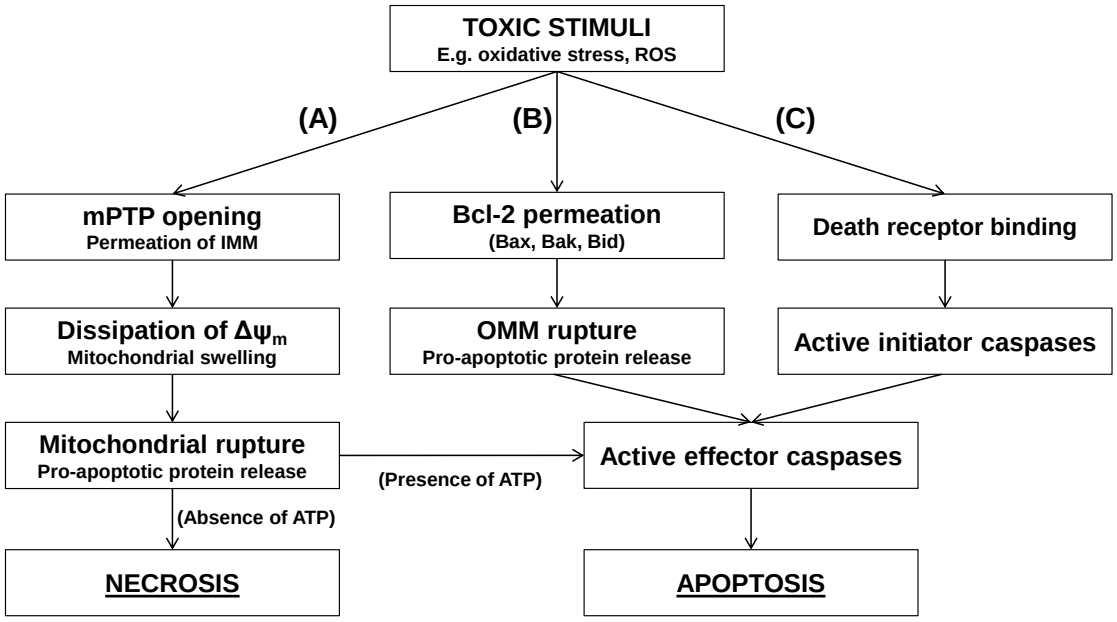

Figure 1.6: Pathways to cardiomyocyte death upon myocardial reperfusion
Reperfusion causes cell death primarily by necrosis or apoptosis. A) Necrosis can be regulated by mitochondrial permeability transition pore (mPTP) opening which causes mitochondrial swelling, rupture and cell death. In the presence of ATP, mPTP opening may cause apoptosis. B) Intrinsic apoptotic pathway: Mitochondrial permeability transition can be induced by Bcl-2 permeation of the OMM causing release of pro-apoptotic proteins and apoptosis. C) Extrinsic apoptotic pathway: Extracellular death ligand binding activates apoptosis. Constructed from information provided by Baines (2009a) and Oerlemans et al. (2013).

iv Lethal reperfusion injury – Mitochondrial permeability transition

The mitochondrial permeability transition pore (mPTP) is a key effector of necrotic and apoptotic cardiomyocyte death. The mPTP is a mitochondrial membrane pore that remains predominantly closed under physiological conditions. However, the intracellular, specifically mitochondrial, changes that occur upon reperfusion can trigger mPTP opening and thus permeation of the inner mitochondrial membrane which results in cell death. Although the molecular identity of the mPTP has been the subject of intensive research and controversy (discussed below), mPTP opening has been implicated in a number of pathological conditions (reviewed by Di Lisa and Bernardi, 2009).

The role of mPTP opening in mediating cell death upon myocardial reperfusion has been well characterised. The cellular conditions that activate and inhibit mPTP opening have been widely examined as potential therapeutic modulators. The principal activators of mPTP opening are: elevated calcium concentration, high levels of Pi and oxidative stress; conditions which prevail following myocardial ischaemia, although are strongly antagonised by low pH (Figure 1.7 A). Myocardial reperfusion exacerbates calcium and ROS accumulation whilst correcting the previous acidosis to remove antagonism of mPTP opening. Reperfusion therefore causes rapid and extensive mPTP opening within a few minutes (Figure 1.7 B) (Crompton et al., 1987; Baines, 2009a).

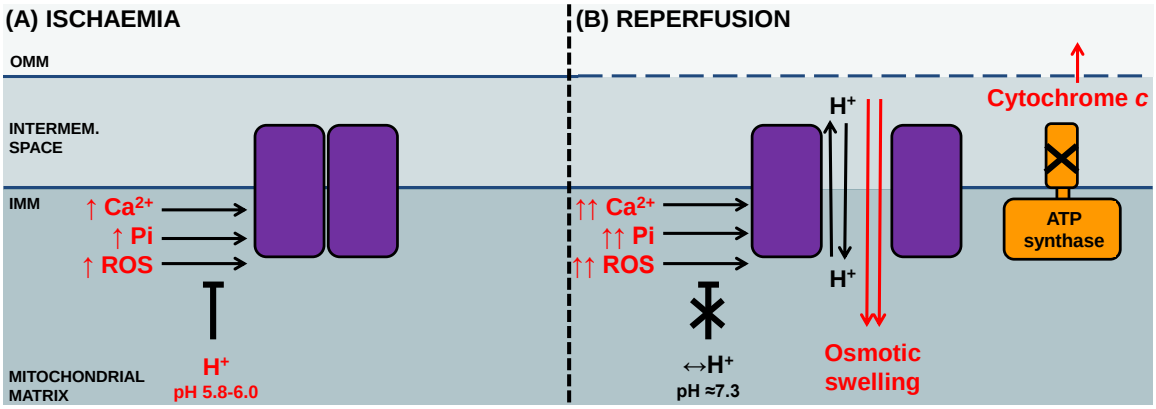

Figure 1.7: Cellular modulators of mitochondrial permeability transition pore opening
(A) Ischaemia: mitochondrial acidosis inhibits mPTP opening despite high calcium and inorganic phosphate levels. (B) Reperfusion: rapid pH correction and increased calcium, Pi and ROS levels trigger mPTP opening. Mitochondrial permeation allows equilibrium of protons across the intermembrane space which halts oxidative phosphorylation and allows mitochondrial swelling which in turn may result in OMM rupture and cytochrome *c* release. Constructed from information provided by Crompton et al. (1987) and Baines (2009a).

The initial effect of mPTP opening is permeation of the inner mitochondrial membrane which dissipates the electrochemical gradient resulting in cessation of ATP production by ATP synthase (Crompton et al., 1987; Baines, 2009a). Indeed, collapse of the electrochemical gradient may cause ATP hydrolysis by reverse ATP synthase activity. Mitochondrial permeability transition allows equilibration of solutes up to 1.5 kDa by passive diffusion through the pore, a process which results in mitochondrial swelling. Severe mitochondrial swelling can result in rupture of the outer mitochondrial membrane and release of pro-apoptotic proteins such as cytochrome *c* that could ultimately trigger apoptotic cell death (reviewed by Bernardi et al., 1999) (Figure 1.7). The final outcome of mPTP opening depends on the intensity of the trigger, severity of ATP depletion and the number of mitochondria affected (reviewed by Baines, 2009a). Although the mPTP is not a unique effector of lethal reperfusion injury, it does appear to be an important mediator of cell death in this setting and is investigated further in this thesis.

The proposed significant contribution of lethal reperfusion injury to myocardial infarction suggests that optimisation of reperfusion may reduce overall infarct size. This has been demonstrated, for example, by ischaemic postconditioning, whereby myocardial reperfusion is stuttered to reduce the severity of intracellular changes upon reperfusion and thus reduce the extent of cell death (discussed in detail in section 1.3).

Furthermore, the occurrence of lethal reperfusion injury presents the intriguing possibility that targeting both ischaemic and reperfusion injury may exert a combinatorial protective effect to further reduce infarct size and improve the prognosis of acute myocardial infarction patients (Hausenloy and Yellon, 2013). This thesis investigates mechanisms to reduce ischaemia-reperfusion injury in a mouse model of acute myocardial infarction.

1.2.4. Long-term effects of ischaemia-reperfusion injury

Elucidation of the cellular mechanisms of myocardial reperfusion injury demonstrates significant interplay of the cellular processes that occur upon ischaemia and reperfusion. It is therefore difficult to separate the long-term effects of these processes such that the effects of myocardial infarction are often described as a cumulative pathology, described here as ischaemia-reperfusion injury. The main phases of long-term progression of ischaemia-reperfusion injury are inflammation and ventricular remodelling (Pfeffer and Braunwald, 1990; Opie et al., 2006). The severity and outcome of these processes depends on the infarct size, area of affected myocardium, duration of ischaemia and conditions of reperfusion (reviewed by Frantz et al., 2009).

Inflammation: Myocardial reperfusion triggers rapid infiltration of neutrophils and macrophages which initiate the immediate inflammatory response that is essential for infarct healing and ventricular remodelling (Vermeiren et al., 2000; Frantz et al., 2009). Neutrophils contribute to the initial inflammatory response by release of pro-oxidant cytokines such as tumour necrosis factor alpha (TNF-α) and decrease of anti-oxidant cytokines which results in increased ROS production and in turn activation of cardiomyocyte apoptosis. Activation and infiltration of macrophages is critical for clearance of cellular debris by phagocytosis (Pfeffer and Braunwald, 1990). Successful clearance of cellular debris and associated pro-oxidant cytokine release dampens the immediate inflammatory response (Frantz et al., 2009).

Regulation of myocardial inflammation is important since, although crucial for infarct healing, extensive inflammation can cause adverse ventricular remodelling and subsequent impaired cardiac function (Gonzalez et al., 2011), described in detail below. In addition, activated neutrophils may cause direct injury due to microvascular obstruction resulting in microcirculatory ischaemia (no-reflow) and release of ROS which cause oxidative damage (discussed previously, section i) (Vermeiren et al., 2000).

Ventricular remodelling: Infarct expansion results in thinning and dilatation of the area of infarction (Weisman and Healy, 1987). This may be caused by cardiomyocyte 'slippage' resulting in fewer cardiomyocytes across the infarcted region due to increased ventricular wall stress and compromised structural integrity from extensive collagen degradation (Olivetti et al., 1990; Opie et al., 2006). Given the importance of the extracellular matrix (ECM) in infarct remodelling, the inflammatory response is a critical mediator of infarct remodelling due to the actions of neutrophils and macrophages on ECM degradation and expansion respectively. Neutrophils release matrix metalloproteinase (MMP) enzymes which breakdown extracellular collagen; extensive MMP activity can cause severe extracellular scaffold degradation (Vermeiren et al.,

2000; Gonzalez et al., 2011). Macrophages release pro-fibrotic cytokines such as TGF-β which stimulate fibroblasts to synthesise collagen that can cause myocardial fibrosis (Pfeffer and Braunwald, 1990; Vermeiren et al., 2000).

The long-term effects of extensive ventricular remodelling include cardiac rupture and myocardial hypertrophy which may ultimately lead to cardiac failure (Frantz et al., 2009).

Cardiac rupture: Rupture of the myocardium occurs most commonly in patients who have suffered LAD occlusion in which a large proportion of the LV wall is affected. Acute cardiac rupture occurs within the first few hours of reperfusion and is associated with adverse cardiac function and pressure overload. Sub-acute rupture results from myocardial thinning and adverse remodelling which render the LV wall incapable of sustaining high pressures and wall stress (Wehrens and Doevendans, 2004).

Myocardial hypertrophy: Extensive transmural myocardial infarction increases the workload of functional cardiomyocytes in the non-infarcted myocardium which can, in time, cause compensatory ventricular remodelling. Infarct expansion and uncontrolled LV remodelling cause increased ventricular volume and pressure load and these combined stresses lead to LV dilatation and compensatory hypertrophy. Sufficient hypertrophy can normalise ventricular wall stresses to maintain cardiac output (Opie et al., 2006); however, progressive LV dilatation with insufficient compensatory hypertrophy can cause cardiac failure (van den Borne et al., 2010).

There are currently no therapeutic interventions for treatment of lethal reperfusion injury (Hausenloy and Yellon, 2013). Patients with hypertrophy and high risk of cardiac rupture are managed by beta-blockers and angiotensin-converting enzyme (ACE) inhibitors (Wehrens and Doevendans, 2004; Thygesen et al., 2007). However, given the poor long-term prognosis following acute myocardial infarction (Smolina et al., 2012) and the predicted increase of acute myocardial infarction (Mathers and Loncar, 2006), the need for novel strategies to protect against ischaemia-reperfusion is ever more pertinent.

1.3. Cardioprotective interventions

Protecting the myocardium against the injurious effects of ischaemia-reperfusion injury is an essential focus for basic science and clinical research. Cardioprotection is defined as a significant reduction in myocardial injury; where myocardial infarct size has been the most widely assessed endpoint in this regard (Jennings, 2011) and forms the focus of the discussion of therapeutic efficacy of cardioprotective interventions here.

The notion that the myocardium can be protected from ischaemia-reperfusion injury is illustrated by the 'wavefront of necrosis' hypothesis which states the progressive development of infarction (Reimer et al., 1977). Indeed, early reperfusion is the most effective cardioprotective intervention for reducing infarct size (Yellon and Downey, 2003). The first demonstration of infarct size reduction by an external therapeutic intervention was ischaemic preconditioning (IPC) in 1986 (Murry et al.), described below. Despite the pre-clinical success of IPC, substantial research efforts are required to identify more clinically applicable cardioprotective strategies with similar potency.

1.3.1. Ischaemic conditioning

Ischaemic conditioning comprises mechanical administration of sublethal ischaemia either directly to the organ of interest or to a distant organ, in the case of remote ischaemic conditioning. Significant cardioprotection is elicited when ischaemic conditioning is applied either prior (pre-), during (per-) or after (post-) the main ischaemic insult. Extensive research has suggested that the molecular pathways elicited by these conditioning protocols are similar (reviewed by Hausenloy and Yellon, 2007); as such, pharmacological modulation of these pathways may provide a clinically applicable therapeutic intervention for cardioprotection. The discussion of ischaemic conditioning here will focus on IPC since this is the most widely studied and easily reproducible conditioning protocol to date.

i Classical ischaemic preconditioning

Ischaemic preconditioning consists of a short sublethal period of myocardial ischaemia (usually 3 to 5 minutes) followed by reperfusion (usually 5 minutes) immediately prior to the main ischaemic insult. Cardioprotection by IPC was first demonstrated by Murry et al. in the *in vivo* dog heart (Murry et al., 1986) and has since been shown to be efficacious in every species tested (Jennings, 2011). Indeed, IPC is recognised as the most potent cardioprotective intervention after early myocardial reperfusion (Yellon and Downey, 2003). The molecular pathways initiated by IPC are described below.

ii Molecular signalling of ischaemic conditioning

The signalling pathways elicited by ischaemic pre- and postconditioning have been largely elucidated and demonstrate striking convergence, although the precise details of the specific interactions between these components remains the subject of extensive research (reviewed by Hausenloy and Yellon, 2007). Understanding the molecular basis of ischaemic conditioning may allow cardioprotection by pharmacological modulation.

Direct effects: Ischaemic conditioning stimulates release of extracellular triggers, such as adenosine and bradykinin, which ultimately elicit cardioprotection. The primary action of these signalling autocoids is mediated via binding to G-protein coupled receptors (GPCRs) which initiate intracellular signal transduction. The multiple signalling autocoids and GPCR binding interactions provide functional redundancy to the conditioning stimulus. GPCR binding activates the intracellular reperfusion injury salvage kinase (RISK) signalling cascades: phosphoinositide 3-kinase (PI3K), Akt and Erk1/2. RISK pathway activation mediates intracellular signal transduction to the end-effector of ischaemic conditioning, believed to be the mPTP (Hausenloy et al., 2004b) (

Figure **1.8**).

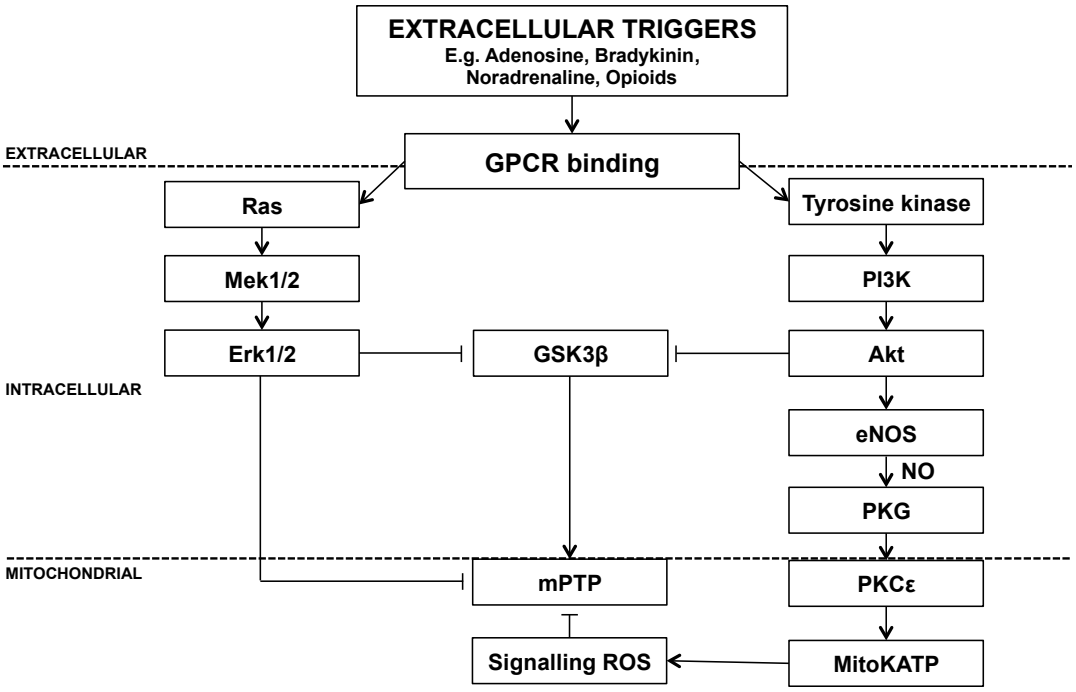

Figure 1.8: Ischaemic conditioning
Ischaemic conditioning produces autocoids which bind to GPCRs which activate intracellular signalling cascades. Activation of the RISK pathway relays the conditioning signal to mitochondrial targets which converge to prevent mPTP opening and thus reduce cell death. Constructed from information provided by Hausenloy and Yellon (2007).

The precise molecular pathways triggered by activation of the RISK pathway may vary between conditioning protocols and species, however, a number of common downstream effectors of ischaemic conditioning have been identified.

PI3K-Akt-eNOS-PKG: Phosphorylation of Akt activates endothelial nitric oxide synthase (eNOS) resulting in increased nitric oxide, which activates cytosolic protein kinase G (PKG). This nitric oxide may also directly inhibit mPTP opening (Hausenloy et al., 2009).

MitoKATP: PKG in turn phosphorylates mitochondrial PKC-epsilon (PKCε) which has been linked to opening of the mitochondrial membrane ATP sensitive potassium channel (mitoKATP) (Costa et al., 2005). MitoKATP channel opening upon reperfusion is controversial, it has however, been linked with production of signalling ROS and prevention of cell death by inhibition of mPTP opening (Hausenloy et al., 2007).

GSK3β: Akt and Erk1/2 activation cause inactivation of glycogen synthase kinase-3β (GSK3β) by phosphorylation. Juhaszova et al. (2004) implicated GSK3β as a point of convergence of cardioprotection on the mPTP. Recent evidence shows active GSK3β phosphorylates cyclophilin-D (Cyp-D) to enhance mPTP opening; thus inactivation of GSK3β reduces Cyp-D activity and mPTP opening (Rasola et al., 2010); section 1.4.1.

Indirect effects: Ischaemic conditioning may also indirectly inhibit mPTP opening by modulating mitochondrial conditions to favour mPTP closure:

Reduced calcium overloading: The precise mechanisms of reduced calcium overloading upon ischaemic conditioning have not been confirmed although there is evidence that it is linked to reduced acidosis which in turn reduces calcium influx through sodium-calcium exchange (see Figure 1.2) (Steenbergen et al., 1993). Ischaemic conditioning may also mediate increased calcium uptake by the sarcoplasmic reticulum to reduce intracellular and mitochondrial calcium overloading (Murphy and Steenbergen, 2011). Reduced mitochondrial calcium levels reduce mPTP opening.

Reduced detrimental ROS: Ischaemic conditioning reduces ROS production upon reperfusion, although the mechanism of this is not clear. Since oxidative stress is an important activator of mPTP opening, the effect of ischaemic conditioning on reducing ROS may in turn reduce mPTP opening (Murphy and Steenbergen, 2011). The roles of ROS in the setting of mPTP opening are complicated by the divergence of 'signalling' and 'detrimental' ROS, since it is well established that IPC-mediated ROS release is an essential signal transduction mechanism of the RISK pathway. These divergent effects of ROS may result from differences in the localisation, quantity, identity or timing of ROS release (Hausenloy and Yellon, 2007).

Transient mPTP opening: The precise mechanism of reduced calcium overloading and detrimental ROS levels have not been fully elucidated, however, there is evidence that these beneficial effects of IPC may be mediated by transient opening of the mPTP to a low-conductance state (Hausenloy et al., 2004a). Transient low-conductance mPTP opening is hypothesised to create a small diameter pore allowing passage of ions and solutes up to 300 Da. This low-conductance pore would therefore permit calcium and ROS efflux from the mitochondrial matrix whilst maintaining the electrochemical gradient for oxidative phosphorylation (Zoratti and Szabo, 1995; Ichas et al., 1997) (Figure 1.9).

It has been suggested that transient low-conductance mPTP opening may provide a mechanism for rapid regulation of mitochondrial matrix conditions which may in turn reduce activation of high-conductance mPTP opening and associated cell death (Hausenloy et al., 2004a) (Figure 1.9). It should also be noted that a similar effect may be mediated by transitory opening of the mPTP to a high-conductance state. The precise mechanism by which IPC triggers transient low-conductance or transient mPTP opening remains to be fully identified and has not yet been investigated as a mode of ischaemic postconditioning or pharmacological conditioning. The occurrence of transient low-conductance mPTP opening may be related to the physiological function of the mPTP, discussed subsequently (see 1.4.1).

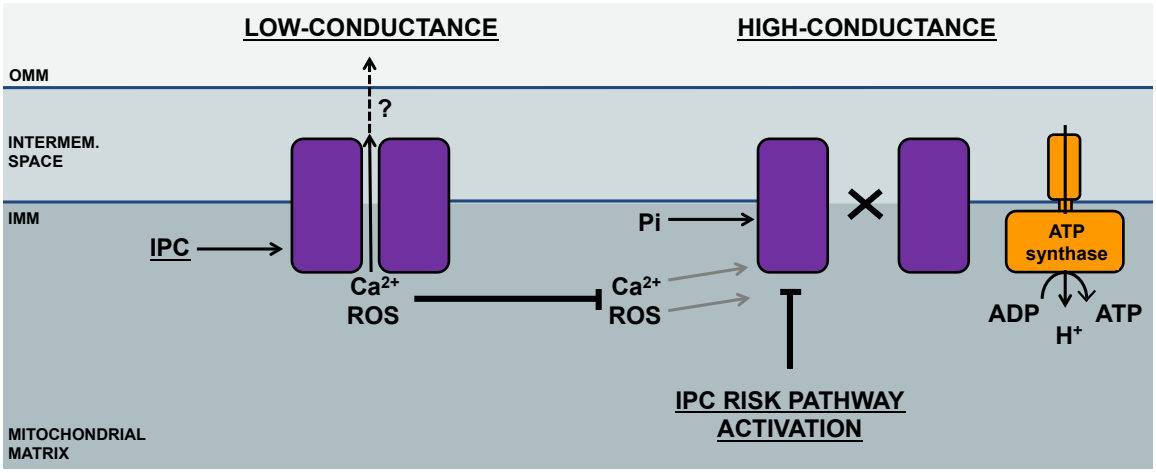

Figure 1.9: Model of transient mPTP opening in response to ischaemic preconditioning
IPC triggers transient low conductance mPTP opening which mediates Ca^{2+} and ROS release from the mitochondrial matrix which would otherwise trigger high conductance mPTP opening. Constructed from information provided by Zoratti and Szabo (1995) and Hausenloy et al. (2004a).

The cumulative effects of RISK pathway activation and decreased mitochondrial matrix calcium and ROS accumulation, reduce the probability of high conductance mPTP opening and cell death (Steenbergen et al., 1993; Baines, 2009a). Reduced calcium load upon ischaemic conditioning may protect against other mechanisms of cell death such as unregulated necrosis and hypercontracture (Garcia-Dorado and Piper, 2006).

iii Delayed ischaemic conditioning

The classical early IPC phenomenon described above elicits significant cardioprotection only if the delay between conditioning stimulus and ischaemic insult is less than approximately 2 hours. Subsequent studies have shown that a second phase of protection exists approximately 12 and 72 hours after the initial IPC stimulus, which has been termed the 'second window of protection' or 'delayed conditioning' (Marber et al., 1993; Baxter et al., 1997). The phenomenon of delayed conditioning suggests that it may be possible to target both the early and delayed components of protection to maximise cardioprotective potency, although this has not yet been confirmed.

The precise molecular mechanism for delayed IPC remains unclear; however, the temporal separation of the protective phases suggests that the conditioning stimulus evokes a memory response likely to involve *de novo* protein synthesis. The conditioning stimulus releases protective triggers, autocoids and cytokines, which in turn activate 'early' mediators to activate transcription factors causing synthesis of 'distal mediators' 12-24 hours later. The end-effectors of delayed conditioning include inhibition of mPTP opening (summarised in Figure 1.10) (reviewed by Hausenloy and Yellon, 2010).

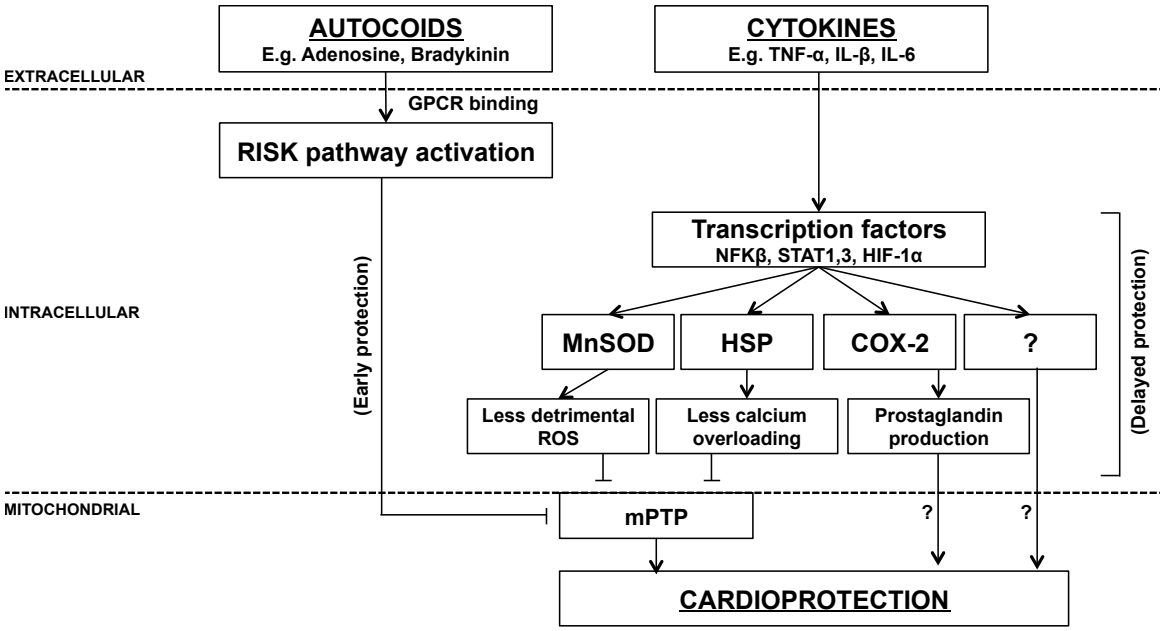

Figure 1.10: Delayed ischaemic conditioning
Ischaemic conditioning produces extracellular autocoids and cytokines which activate 'early mediators', such as the RISK pathway, which elicit early cardioprotection and induce transcription factor expression which triggers synthesis of 'distal mediators' 12-24 hours later. Distal mediators confer a delayed cardioprotective effect which is thought to converge on inhibition of mPTP opening. Constructed from information provided by Hausenloy and Yellon (2010).

Although the precise actions of these distal mediator proteins in cardioprotection have not been fully elucidated, the main roles identified to date are detailed below.

Manganese superoxide dismutase: MnSOD is an anti-oxidant enzyme elevated 24 hours after the initial conditioning stimulus, possibly in response to increased signalling ROS (Zhai et al., 1996). MnSOD expression is expected to decrease the levels of detrimental ROS and thus reduce mPTP opening (Hausenloy and Yellon, 2010).

Heat shock proteins: The role of heat shock proteins as mediators of cardioprotection is controversial, however, there is evidence that HSP70 may reduce calcium overloading and thus reduce mPTP opening (Marber et al., 1993; Hausenloy and Yellon, 2010).

Cyclo-oxygenase 2: Upon myocardial ischaemia, COX-2 produces prostaglandins (PE), PGE_2 and $PGF_{1\alpha}$, which have been shown to elicit significant cardioprotection by a yet unknown mechanism (Shinmura et al., 2000; Hausenloy and Yellon, 2010).

Although the clinical applicability of delayed IPC is limited in acute myocardial infarction, it presents the intriguing possibility that it may be possible to pharmacologically elicit delayed cardioprotection. Furthermore, it may be possible to achieve additive cardioprotection by targeting both early and late cardioprotective pathways, for example by inhibition of mPTP opening and prostaglandin expression; pharmacological conditioning for cardioprotection is discussed below.

1.3.2. Pharmacological conditioning

The molecular pathway of ischaemic conditioning provides a basis from which to investigate potential pharmacological interventions for clinical cardioprotection. In theory, delivery of a pharmacological agent that activates the RISK pathway or directly inhibits mPTP opening will elicit significant cardioprotection. Indeed, numerous pre-clinical studies have shown pharmacological activation of the RISK pathway is cardioprotective (Hausenloy and Yellon, 2007), and a proof-of-concept clinical study has shown that mPTP inhibition by cyclosporine-A (CsA) significantly reduced infarct size (Piot et al., 2008); cardioprotection by CsA is discussed below. Importantly, inhalation anaesthetic agents, including isoflurane, have been demonstrated to elicit significant cardioprotective effects at certain doses (reviewed by Stowe and Kevin, 2004).

Transgenic therapy also represents an intriguing possibility for cardioprotection and initial pre-clinical studies have shown adenoviral transfection of adult mouse hearts with inducible NOS was cardioprotective (Li et al., 2003; reviewed by Hausenloy and Yellon, 2013). This is less immediately clinically amenable and is outside the remit of this thesis.

1.4. Mitochondria as targets for cardioprotection

Mitochondria are fundamental organelles for the maintenance of cell function and survival. The importance of mitochondrial function is particularly pertinent in the heart given its substantial energy demand and the imperative nature of cardiac function for sustaining life. Indeed, mitochondria occupy around 30% of cardiomyocyte volume and supply more than 90% of the ATP required for contractile function (Javadov et al., 2009).

The central roles of mitochondria in cell survival extend beyond energy production to cell fate determination as end-effectors of cell death. This is demonstrated by the pathophysiology of ischaemia-reperfusion injury described above whereby mitochondrial dysfunction and permeability transition account for a significant extent of myocardial infarction (reviewed by Gustafsson and Gottlieb, 2008). Mitochondria therefore represent an important target for cardioprotection, whereby prevention of mitochondrial dysfunction and permeability transition is expected to reduce cell death and thus improve the prognosis of acute myocardial infarction patients.

This thesis will investigate the potential modulation of mitochondrial function and permeability transition to elicit cardioprotection against myocardial infarction.

1.4.1. Mitochondrial permeability transition and cyclophilin-D

Mitochondrial permeability transition is a key end-effector of cardiomyocyte death following ischaemia-reperfusion injury (as described above) and therefore represents an important potential target for conferring cardioprotection. Under physiological conditions the mPTP remains largely closed which is essential to maintain mitochondrial membrane integrity that is fundamental for the maintenance of the inner mitochondrial membrane electrochemical gradient ($\Delta\psi_m$) for ATP production by oxidative phosphorylation (Halestrap et al., 2007; Gustafsson and Gottlieb, 2008). However, prolonged high-conductance opening of the mPTP causes loss of inner mitochondrial membrane integrity which initiates a complex pathway of events that ultimately results in cell death by necrosis or apoptosis (see 1.2.3).

Given the importance of prolonged high-conductance mPTP opening in mediating cell death by necrosis and apoptosis upon myocardial reperfusion, it has been hypothesised that reducing mPTP opening will significantly reduce cell death and thus improve the prognosis of acute myocardial infarction patients (Hoffman et al., 2004; Yellon and Hausenloy, 2007). Extensive research efforts have investigated the potential of reducing mPTP opening by targeting the known mPTP regulatory protein, cyclophilin-D (Cyp-D).

i mPTP structure and regulation

Originally the mPTP was suggested to be formed by inner mitochondrial membrane adenine nucleotide translocase (ANT) (Tikhonova et al., 1994; Halestrap et al., 1997) and the outer mitochondrial membrane voltage-dependent anion channel (VDAC) (Szabo and Zoratti, 1993). However, numerous subsequent studies demonstrated that genetic ablation of both ANT and VDAC did not ablate mPTP opening (Kokoszka et al., 2004; Krauskopf et al., 2006) and therefore suggested that they acted only as mPTP regulatory proteins (Baines, 2009b). A very recent study by Bonora et al. (2013) implicated the c subunit of the ATP synthase enzyme (complex V, F_0F_1) in mPTP formation. Subsequently, Giorgio et al. (2013) extended this finding to provide the most direct evidence to date that the ATP synthase enzyme is a constituent component of the mPTP, whereby they proposed that dimers of whole ATP synthase form the mPTP in the inner mitochondrial membrane (Giorgio et al., 2013).

Given the only very recent suggestion of ATP synthase as a constituent of the mPTP, direct mPTP modulation has not yet been explored. However, interestingly a previous study by Giorgio et al. (2009) showed that Cyp-D interacts with the ATP synthase lateral stalk in a cyclosporine-A (CsA) dependent manner (Giorgio et al., 2009). Cyp-D regulation of mPTP opening is discussed below (see ii). Manipulation of mPTP opening to date has examined indirect modulation of mPTP opening by reducing cellular agonists of mPTP opening (namely high calcium levels, oxidative stress and high phosphate concentrations) and increasing antagonists of mPTP opening (enhanced acidosis). Numerous pre-clinical studies have shown that manipulation of the cellular environment upon reperfusion (for example by administration of ROS scavengers) can reduce mPTP opening and final infarct size (Crompton et al., 1987; Griffiths and Halestrap, 1995).

Direct manipulation of the known mPTP regulatory protein, Cyp-D represents an interesting and more elegant potential therapeutic approach for modulating mPTP opening; Cyp-D is the first cardioprotective target investigated in this thesis.

ii Cyclophilin-D as a mPTP regulatory target

Although the structural identify of the mPTP has been controversial, Cyp-D has long been appreciated as an important mPTP regulatory protein (Nicolli et al., 1996). Cyp-D confers calcium sensitivity to mPTP opening whereby it facilitates mPTP opening in conditions of elevated mitochondrial matrix calcium (Connern and Halestrap, 1994; Nicolli et al., 1996). Given the important regulatory role of Cyp-D, this protein represents an important potential target for pharmacological or genetic manipulation to indirectly affect mPTP opening and calcium sensitivity. It is predicted that inhibition of Cyp-D activity may therefore elicit a significant potential therapeutic benefit.

Cyclophilin protein family: Cyp-D is a member of the highly conserved and widely expressed cyclophilin (Cyp) protein family. The individual Cyp protein subtypes have varied molecular weights and intracellular locations but conserved peptidyl-prolyl cis-trans isomerase (PPIase) activity (Bergsma et al., 1991). This PPIase activity catalyses the otherwise slow cis-trans isomerisation of peptidyl-prolyl bonds. Rotation of proline peptide bonds causes conformational changes in the target protein which are crucial for facilitating protein folding and functional changes (Fischer et al., 1989; Barik, 2006).

The Cyp proteins also act as molecular chaperones, although this is less well understood and has been shown to be independent of their PPIase activity (Barik, 2006). The chaperone role of Cyp-D has not been implicated in mPTP opening and ischaemia-reperfusion injury and so is not discussed further here.

Cyclophilin-D: Cyp-D (originally termed hCyP3 and also known as Cyp-F in mice) is the only mitochondrial cyclophilin protein. Cyp-D is nuclear encoded by the *Ppif (peptidyl-prolyl isomerase F)* gene which contains 5.5 kb of genomic DNA and consists of six protein encoding exons separated by five intronic sequences. The *Ppif* gene is highly conserved within eukaryotic organisms (Bergsma et al., 1991; Basso et al., 2005).

The Cyp-D protein sequence is also highly conserved between eukaryotes and shares a large degree of homology to the other Cyp proteins (Bergsma et al., 1991). The full length Cyp-D protein (c. 22 kDa) consists of a highly conserved 109 amino acid Cyp domain which confers PPIase activity and a hydrophobic NH_2-terminus mitochondria-targeting sequence. This immature Cyp-D protein is produced in the cytosol and then specifically transported to mitochondria by the N-terminal mitochondria-targeting sequence which is predicted to be a mitochondria-transit peptide recognised by the outer mitochondrial membrane (Johnson et al., 1999). The Cyp-D protein is cleaved upon entry to the mitochondrial matrix to remove the targeting sequence and produce the mature functional protein (c. 18 kDa) (Bergsma et al., 1991; Johnson et al., 1999). The mature Cyp-D protein has a tertiary structure containing eight β-strands and two α-helices which are believed to be essential for PPIase activity (Kajitani et al., 2008).

Comparison of the human and rodent Cyp-D protein sequences has shown a very high degree of conservation in the functional PPIase Cyp domain but some divergence in the mitochondria-targeting sequence, although mitochondrial targeting does not seem to be affected (Woodfield et al., 1997). Given the large degree of conservation between the sequences and predicted structures of human and rodent Cyp-D proteins, it is expected that once the targeting sequence is cleaved, the function and regulation of Cyp-D is highly conserved between mouse and man (Woodfield et al., 1997; Barik, 2006).

Investigations of the role of Cyp-D and indeed the mPTP in both physiological and pathological settings require tools to selectively inhibit Cyp-D activity. The methods for inhibiting Cyp-D discussed here may also provide opportunities for clinical modulation of Cyp-D activity for future potential therapeutic approaches.

Pharmacological inhibition of Cyp-D: Pharmacological inhibition of protein function is the classical approach for investigating the role of a given protein; however, the usefulness of this approach is clearly determined by the selectivity and availability of inhibitors. The principal pharmacological inhibitors of Cyp-D are described below:

Cyclosporine-A: CsA is a widely used inhibitor of mPTP opening which led to the identification of Cyp-D as an important regulatory protein (Halestrap and Davidson, 1990) and has since been used to investigate the effects of mPTP opening in a number of pathophysiological models (Griffiths and Halestrap, 1993; Hausenloy et al., 2012).

CsA is a cyclic undecapeptide produced by the fungus *Trichoderma polysporum* and is clinically used for its immunosuppressant activities to prevent tissue rejection in transplant patients. Independently of its immunosuppressant activity, CsA inhibits Cyp-D activity by binding to the catalytic pocket of the PPIase domain, which is essential for Cyp-D regulation of mPTP opening. CsA reduces mPTP opening upon ischaemia-reperfusion (Crompton et al., 1988; Halestrap and Davidson, 1990) and reduces the extent of infarction in a number of *in vitro* and *in vivo* animal models (Nazareth et al., 1991; Griffiths and Halestrap, 1993; Hausenloy et al., 2002). Crucially, since CsA is cardioprotective when administered only at reperfusion (Hausenloy et al., 2002), CsA (and indeed mPTP inhibition) is a potentially clinically relevant therapeutic strategy.

To date, relatively few studies have investigated clinical use of CsA for cardioprotection. Initial *ex vivo* studies using isolated human atrial tissue have shown that CsA protects against ischaemia-reperfusion injury (Schneider et al., 2003; Shanmuganathan et al., 2005). Furthermore, a recent clinical proof-of-concept study demonstrated CsA administered 10 minutes prior to reperfusion in acute ST-segment elevation myocardial infarction (STEMI) patients significantly reduced infarct size (Piot et al., 2008). Importantly, since safety and regulatory approval for CsA in place for its clinical use as an immunosuppressant, larger clinical trials of CsA to protect as myocardial infarction could lead to its introduction as a widespread cardioprotective therapy.

However, the lack of specificity of CsA for Cyp-D represents an important caveat to the use of CsA as a research tool and potential therapeutic agent. As described above, CsA binds to the Cyp-D conserved PPIase domain and so also binds to and inhibits the PPIase activity of the other Cyp proteins (Kajitani et al., 2008), including cytoplasmic

Cyp-A. In addition, the bound complex of CsA–Cyp-A in turn binds to and inhibits calcineurin; a calcium / calmodulin dependent phosphatase which is involved in regulation of gene expression and other intracellular functions (Liu et al., 1991). This has required concurrent investigation of calcineurin inhibitors to confirm that CsA-mediated cardioprotection is not the result of calcineurin inhibition (Hausenloy et al., 2012).

The development of specific pharmacological inhibitors of Cyp-D may overcome this and has been the subject of much research in recent years. A number of purported Cyp-D selective inhibitors have been published and investigated in relation to their effects on Cyp-D inhibition of mPTP opening and protection against ischaemia-reperfusion injury; the main advances in pharmacological inhibition of Cyp-D are discussed below.

Sanglifehrin-A: Sanglifehrin-A (SfA) is an immunosuppressant distinct from CsA which tightly binds to and inhibits the Cyp proteins. SfA has been shown to inhibit Cyp-D activity and in turn reduce mPTP opening and improve cardiac function and increase cell survival upon ischaemia-reperfusion in animal models (Clarke et al., 2002; Hausenloy et al., 2003) and isolated human atrial tissue (Shanmuganathan et al., 2005). The main advantage of SfA over CsA is that the SfA-Cyp-A complex does not inhibit calcineurin, however, since SfA is not selective for Cyp-D, its effects may still be mediated by inhibition of other Cyp proteins (Clarke et al., 2002; Hausenloy et al., 2012).

Non-immunosuppressive CsA analogues: A number of small molecule CsA analogues have been developed which do not bind to calcineurin and so do not exert immunosuppressant activity (reviewed by Hausenloy et al., 2012). This group of inhibitors includes NIM-811 and Debio-025 which inhibit Cyp-D to reduce mPTP opening with increased potency compared to CsA (Hansson et al., 2004). Indeed, both NIM-811 and Debio-025 significantly reduce myocardial infarct size in *in vivo* models of ischaemia-reperfusion injury (Argaud et al., 2005; Gomez et al., 2007). However, these inhibitors may still bind to and inhibit other Cyp proteins to exert non-selective effects.

Mitochondria targeted CsA: Mitochondrial targeting of CsA has been investigated as an approach for sequestering CsA in the mitochondria to limit its binding to Cyp-D only. The mitochondrial CsA (mtCsA) molecule is formed by conjugation of CsA to a lipophilic cation (TPP^+) to give it a positive charge to drive its accumulation into the mitochondria due to the electrophoretic gradient imposed by the negative potential of the inner mitochondrial membrane. Although mtCsA can still bind to the other Cyp proteins, such as Cyp-A, sequestration of mtCsA in the mitochondrial matrix renders it selective for Cyp-D and thus also prevents its actions on calcineurin (Malouitre et al., 2010).

Initial *in vitro* studies showed that the CsA-TTP^+ (mtCsA) molecule is successfully accumulated in the mitochondrial matrix of cells and maintains its potency at inhibiting Cyp-D (Malouitre et al., 2010). Furthermore, *ex vivo* studies demonstrated increased potency of mtCsA compared to CsA at reducing cell death in *ex vivo* models of simulated ischaemia-reperfusion injury in rat hippocampal neurones (Malouitre et al., 2010) and cardiomyocyte preparations (Dube et al., 2012). Further studies are now required to assess the *in vivo* safety and cardioprotective efficacy of mtCsA.

Novel selective Cyp-D inhibitors may now be designed following the identification of a number of residues in proximity to the CsA binding site that are not conserved in the other Cyp proteins (Kajitani et al., 2008). In the meantime, since mtCsA and the non-immunosuppressant inhibitors are not widely available, CsA continues to be widely used to investigate Cyp-D and mPTP opening in ischaemia-reperfusion injury.

Genetic manipulation of Cyp-D: Genetic manipulation to modify Cyp-D expression provides an important tool for investigating the role of Cyp-D in mPTP regulation without the confounding effects of non-selective actions on the other Cyp proteins. There are a number of useful approaches for Cyp-D genetic manipulation, described below:

Genetic interference: Interference RNA (RNAi) is an interesting methodological approach whereby a recent study has demonstrated that RNAi knock-down of the Cyp-D gene product reduced ischaemia-reperfusion induced renal injury (Hu et al., 2010).

Overexpression: Limited studies have investigated Cyp-D overexpression (Lin and Lechleiter, 2002; Baines et al., 2005); however, this approach has been less widely employed and does not represent a therapeutic target for cardioprotection.

Genetic ablation: Whole body genetic ablation of Cyp-D in the mouse was achieved independently by several research groups in 2005 (Baines et al., 2005; Basso et al., 2005; Nakagawa et al., 2005). The precise details of Cyp-D genetic ablation varied between these studies but all demonstrated 100% absence of Cyp-D protein in all body tissues examined. A detailed description of the Cyp-D knockout mouse created by Baines et al. (2005) and used in thesis is provided in chapter 5.

The Cyp-D knockout mouse line has proved an invaluable tool for investigating the role of Cyp-D and mPTP opening in a number of pathological settings, including ischaemia-reperfusion. This is discussed in detail subsequently in relation to Cyp-D regulation of mPTP opening (see iv) and the physiological role of mPTP opening (see v).

iii Cyp-D and mPTP opening

The function of Cyp-D has predominantly been investigated in relation to its regulation of mPTP opening. Cyp-D was first implicated in mPTP opening by studies investigating the mechanism of mPTP inhibition by CsA, which demonstrated that Cyp-D is the singular mitochondrial receptor for CsA (Connern and Halestrap, 1994; Nicolli et al., 1996). CsA binds to the catalytic pocket of the Cyp protein PPIase domain thereby inhibiting its activity. Since CsA inhibits mPTP opening, it has long been hypothesised that Cyp-D facilitates mPTP opening by inducing a conformational change in a constituent protein of the pore that renders it open (Connern and Halestrap, 1994; Nicolli et al., 1996).

However, the precise mechanism by which Cyp-D activates mPTP opening is currently largely unknown due to the controversy surrounding the actual constituent proteins of the mPTP. The most recent model proposed by Bernardi's group states that the mPTP is formed from dimers of the F_0F_1-ATP synthase enzyme (Giorgio et al., 2013) (Figure 1.11 A) and suggests that Cyp-D is likely to mediate a conformational change in these dimers to facilitate pore opening (Bernardi, 2013; Giorgio et al., 2013) (Figure 1.11 B). The involvement of the ATP synthase enzyme in formation of the mPTP is also supported by an earlier study by Bonora et al. (2013) which implicated ATP synthase subunit c as a consistent protein of the mPTP. Indeed, a previous study by this group showed that Cyp-D interacts with the lateral stalk of the F_0F_1-ATP synthase to decrease its enzymatic activity. Furthermore, this study showed that CsA caused dissociation of the Cyp-D-ATP synthase interaction, in line with the CsA sensitivity of mPTP opening (Giorgio et al., 2009). This model of Cyp-D regulation of mPTP opening is reviewed by Bernardi (2013) and summarised in Figure 1.11.

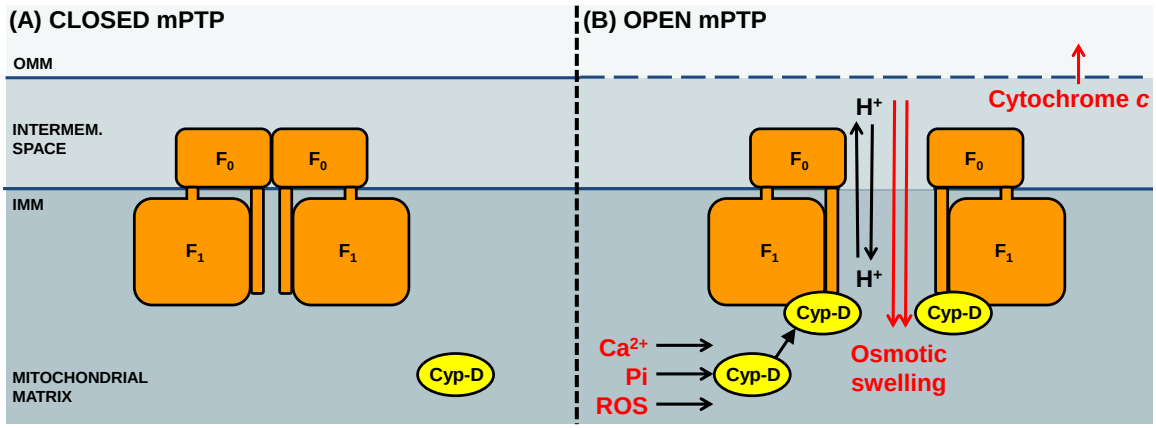

Figure 1.11: Revised model of mPTP and its regulation by Cyp-D
Proposed model of Cyp-D regulation of mPTP opening: the mPTP is formed of F_0F_1-ATP synthase dimers to which Cyp-D binds to induce a conformational change causing a high-conductance pore to form between the F_0 subunits. This still remains a putative model of the mPTP at this stage. Adapted from Bernardi (2013) and Giorgio et al. (2013).

The role of Cyp-D regulation in mPTP opening can be examined using pharmacological methods; however, Cyp-D genetic ablation has allowed more elegant dissection of the roles of Cyp-D. Complete genetic ablation of Cyp-D in mouse lines was completed independently by several research groups and reassuringly, demonstrated strikingly similar effects on mPTP opening (summarised in Table 1.2) (Basso et al., 2005; Baines et al., 2005; Nakagawa et al., 2005; Schinzel et al., 2005). Mitochondria devoid of Cyp-D were more resistant to loss of inner mitochondrial membrane potential, mitochondrial swelling and mPTP opening in response to common mPTP triggers including calcium and oxidative stress. However, it should be noted that these studies were mainly based on isolated liver mitochondria although Baines et al. (2005) confirmed these findings in cardiac mitochondria (Table 1.2). These studies also confirmed that Cyp-D is not a constituent of the mPTP since mPTP opening occurred in Cyp-D knockout mitochondria in response to increased severity of triggers (Basso et al., 2005; Baines et al., 2005; Nakagawa et al., 2005). Baines et al. (2005) demonstrated that the susceptibility to mPTP opening was restored in Cyp-D knockout mitochondria by reintroduction of wildtype, but not PPIase deficient Cyp-D protein, proving that Cyp-D PPIase activity is crucial in regulating the calcium sensitivity of mPTP opening (Baines et al., 2005).

Further to this, these studies demonstrated that Cyp-D knockout mouse embryonic fibroblast (MEF) cells were more resistant to cell death induced by ROS overload (upon treatment with hydrogen peroxide) (Nakagawa et al., 2005; Baines et al., 2005; Schinzel et al., 2005); although again it should be noted that these are not cardiac specific cells.

Importantly, Baines et al. (2005) and Nakagawa et al. (2005) showed that Cyp-D genetic ablation significantly reduced susceptibility to *in vivo* ischaemia-reperfusion injury. This provided the first conclusive evidence that Cyp-D ablation is a cardioprotective strategy. Subsequent studies have utilised the Cyp-D whole body knockout mouse line to further investigate the role of Cyp-D in regulating mPTP opening. Lim et al. (2011) showed that Cyp-D knockout mice had improved survival and cardiac function at 28 days of myocardial ischaemia, a model of pathological cardiac failure (Lim et al., 2011).

Further studies are required to investigate whether Cyp-D inhibition upon reperfusion is a feasible therapeutic strategy for conferring long-term cardioprotection. This is complicated by the unresolved physiological function of the mPTP and recent studies suggesting that chronic Cyp-D inhibition may be detrimental; discussed below (see v).

Table 1.2: Protective effects of Cyp-D genetic ablation
Initial studies examining the effect of whole body total ablation of Cyp-D (KO) on mPTP opening in response to environmental stressors. References provided. (Table overleaf)

STUDY	STRESSOR	EFFECT IN CYP-D KNOCKOUT
ISOLATED MITOCHONDRIA (Liver mitochondria unless otherwise stated)		
Baines et al. (2005) *Observed in heart, liver and brain mitochondria*	Calcium (250 µM) Calcium (25 µM) + atractyloside (200 µM)	• Resistance to mitochondrial swelling • Resistance to mPTP opening • Increased calcium uptake before undergoing mPTP opening • Less cytochrome *c* release These traits were all overcome by very high calcium loads
Basso et al. (2005)	Calcium (various concentrations to produce concentration response curves)	• Resistance to mPTP opening • CsA insensitivity
Nakagawa et al. (2005)	Calcium (50 µM) Atractyloside H_2O_2	• Resistance to loss of $\Delta\psi_m$ • Resistance to mPTP opening • Increased calcium uptake before undergoing mPTP opening • Less calcium induced cytochrome *c* release These traits were all overcome by very high calcium loads
Nakagawa et al. (2005)	Simulated ischaemia-reperfusion (30 min hypoxia)	• Resistance to loss of $\Delta\psi_m$ • Resistance to mitochondrial swelling • Preserved respiratory control compared to WT
Schinzel et al. (2005)	Calcium (100 µM)	• Resistance to mitochondrial swelling • Morphologically intact compared to WT (assessed by EM)
CULTURED MOUSE EMBRYONIC FIBROBLASTS		
Baines et al. (2005)	H_2O_2 (500 µM)	• Resistance to loss of $\Delta\psi_m$ and mPTP opening • Less cell death
Baines et al. (2005)	Calcium overload induced by thapsigargin (20 µM) or ionomycin (10 µM)	• Less cell death
Nakagawa et al. (2005)	H_2O_2 (500 µM)	• Less cell death
Schinzel et al. (2005)	H_2O_2 (various concentrations)	• Less cell death
IN VIVO		
Baines et al. (2005)	Cardiac ischaemia-reperfusion by LAD occlusion (60 min ischaemia, 24 hour reperfusion)	KO hearts showed 40% reduction in infarct size
Nakagawa et al. (2005)	Cardiac ischaemia-reperfusion by LAD occlusion (30 min ischaemia, 2 hour reperfusion)	KO hearts showed dramatic reduction in infarct size Very dramatic reduction in lactate dehydrogenase release
Schinzel et al. (2005)	Cerebral ischaemia-reperfusion (2 hour ischaemia, 24 hour reperfusion)	KO brains showed dramatic reduction in infarct volume and area

iv Regulation of Cyp-D activity

Cyp-D regulation of mPTP opening is crucial in determining cell survival; however, the mechanisms regulating Cyp-D activity remain largely unknown. Recent studies suggest post-translational modification of Cyp-D regulate its activity and in turn affect mPTP calcium sensitivity; the main putative post-translational modifications are described here:

Phosphorylation: The role of phosphorylation of Cyp-D remains controversial although there is evidence suggesting that GSK3β may translocate to the mitochondrial matrix to directly phosphorylate Cyp-D (Xi et al., 2009), however, this has not been shown *in vivo*. Rasola et al. (2010) recently showed GSK3β mediated Cyp-D phosphorylation resulted in increased mPTP opening and cell death; although this was in a cancer cell line where regulatory systems are known to be perturbed. Further studies are required to determine whether Cyp-D phosphorylation regulates mPTP opening.

S-nitrosylation: S-nitrosylation (SNO) is a reversible redox-dependent post-translational modification involving attachment of a nitric oxide moiety to a cysteine residue within the target protein. Previous studies have implicated SNO in modifying target protein activity and associated cardioprotection (Murphy et al., 2012). Cyp-D has been shown to be amenable to SNO at cysteine residue 203 (Kohr et al., 2011), where mutation of this residue conferred resistance to mitochondrial swelling and ROS-induced cell death (Nguyen et al., 2011). However, the causative relationship between Cyp-D SNO and mPTP opening remains unclear and it has been suggested that SNO may only indirectly affect mPTP opening by preventing its oxidation (Elrod and Molkentin, 2013).

Deacetylation: Several studies have suggested that deacetylation of lysine residues is an important regulatory mechanism. Two recent studies demonstrated that Cyp-D is deacetylated by sirtuin-3 (Hafner et al., 2010; Shulga et al., 2010). These studies suggest that Cyp-D acetylation increases mPTP opening and therefore, deacetylation by sirtuin-3 reduces Cyp-D activity and reduces mPTP opening. The precise mechanisms implicated by these two studies vary and are discussed in detail below (see 1.4.2).

The precise roles of these post-translational modifications in regulating Cyp-D activity remain unclear, however, it is likely that these mechanisms are important for 'fine-tuning' Cyp-D activity and thus mPTP opening and so may represent important cardioprotective targets. Indirect regulation of Cyp-D by modulation of post-translational regulation may provide a more subtle and therapeutically advantageous approach, given the complications of chronic Cyp-D inhibition. Modulation of sirtuin-3 as a potential cardioprotective target is discussed below (see 1.4.2) and investigated in chapter 6.

v Physiological role of Cyp-D and mPTP opening

The physiological role of Cyp-D and mPTP opening has remained largely unclear; however, Cyp-D genetic ablation has provided insights into the potential effects of long-term Cyp-D inhibition and the resulting calcium insensitivity of mPTP opening.

Baseline phenotype of Cyp-D knockout mice: The original publications describing generation of whole body Cyp-D genetic knockout mouse lines stated that there were no overt baseline phenotypic differences between wildtype and Cyp-D knockout (KO) animals (Nakagawa et al., 2005; Baines et al., 2005; Basso et al., 2005). Whole body genetic ablation of Cyp-D did not cause any adverse developmental defects and KO mice were born at the expected Mendelian ratio and did not show any difference in developmental survival (Baines et al., 2005). The baseline physiology and morphology of Cyp-D KO mitochondria appeared unaffected. In addition, cardiac function was not affected in young animals and there was no indication of cardiomyopathy (Nakagawa et al., 2005; Baines et al., 2005). These studies suggested that Cyp-D and mPTP calcium sensitivity are dispensable for development and exert only limited physiological function.

Adverse effects of Cyp-D inhibition: Recent studies, however, have suggested that Cyp-D KO mice may develop phenotypic differences with age or upon physiological stress. Elrod et al. (2010) showed that chronic Cyp-D inhibition may be detrimental, where Cyp-D KO animals exhibited an increased predisposition to hypertrophy and cardiac failure induced by physiological stresses such as swimming (Elrod et al., 2010). Chronic Cyp-D inhibition by CsA treatment has also been shown to exacerbate cardiac failure despite its significant effect in reducing hypertrophy (Oie et al., 2000); although it is not possible to preclude CsA effects independent of Cyp-D. However, a study by our laboratory showed that Cyp-D knockout mice were less susceptible to cardiac failure induced by the pathological stress of prolonged ischaemia (Lim et al., 2011).

Elrod et al. (2010) proposed that the adverse effects of chronic Cyp-D inhibition upon physiological stresses, such as excessive exercise, may relate to the physiological roles of mPTP opening, whereby transient low-conductance mPTP opening is critical for calcium release from the mitochondrial matrix (Elrod et al., 2010); discussed below.

Transient low-conductance mPTP opening: Transient low-conductance mPTP opening (see 1.3.1; Figure 1.9) may occur physiologically in response to slightly elevated mitochondrial matrix calcium, whereby mPTP 'flickering' may permit calcium homeostasis without affecting inner mitochondrial membrane potential (Figure 1.12 A). Chronic Cyp-D inhibition results in elevated mitochondrial matrix calcium which triggers a metabolic shift to glycolysis and a resultant propensity to cardiac failure (Figure 1.12 B) (reviewed by Elrod and Molkentin, 2013).

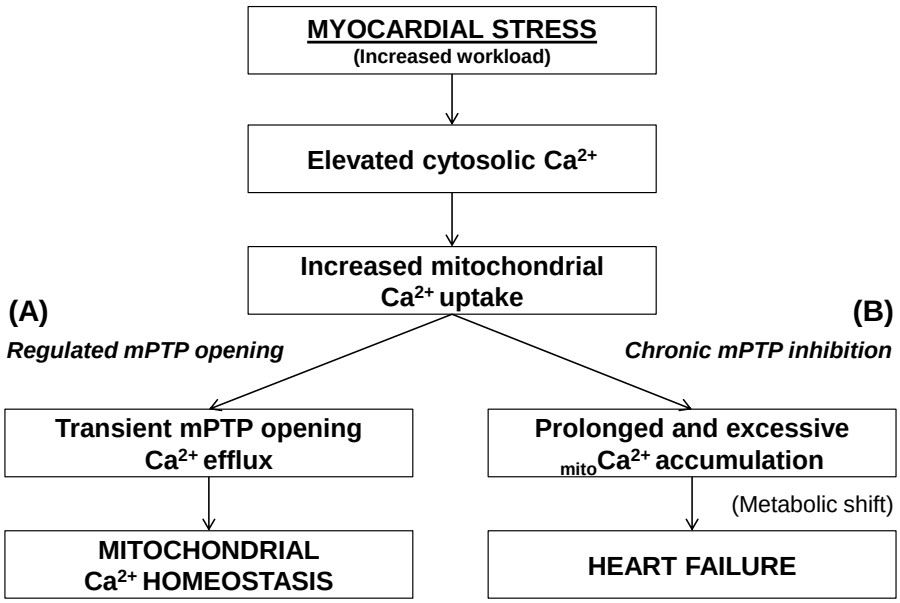

Figure 1.12: Physiological importance of transient low-conductance mPTP opening
Transient low-conductance mPTP opening is proposed to mediate physiological mitochondrial homeostasis (A). Inhibition of Cyp-D (B) or indeed any other mechanism inhibiting mPTP opening, causes mitochondrial calcium accumulation which results in a metabolic shift and ultimately cardiac failure. Adapted from Elrod and Molkentin (2013).

The metabolic shift associated with increased mitochondrial matrix calcium accumulation upon inhibition of mPTP opening is thought to be associated with the resulting increased activity of mitochondrial calcium-dependent dehydrogenases (Korge et al., 2011; Elrod and Molkentin, 2013). The precise molecular mechanisms of this process require further investigation; however, the potential role of Cyp-D in metabolic control further highlights the importance of careful modulation of Cyp-D activity as a potential therapeutic intervention.

The experimental evidence to date suggests that inhibition of Cyp-D may represent an important and efficacious method for reducing mPTP opening and thus preventing cell death upon myocardial reperfusion. However, the adverse effects of Cyp-D inhibition on prevention of physiological mPTP opening for mitochondrial matrix calcium homeostasis suggest that modulators of Cyp-D and mPTP activity should only be administered acutely. It remains to be seen whether acute Cyp-D inhibition confers long-term cardioprotection against ischaemia-reperfusion injury; this is investigated in chapter 5.

1.4.2. Regulation of mitochondrial proteins by sirtuin-3

Regulation of mitochondrial biology is crucial for cell function and survival in both physiological and pathological conditions. Control of mitochondrial biology can be exerted at a macro-level, for example by protein expression; however, more subtle and immediate regulation of mitochondrial proteins by post-translational modifications can also significantly affect mitochondrial physiology. Post-translational modifications of proteins regulate protein structure and function and therefore, post-translational modification represents an important biological regulatory mechanism (Balaban, 2010).

Mitochondrial proteins are subject to numerous post-translational modifications, including phosphorylation, S-nitrosylation and acetylation. Although phosphorylation has been the most widely studied, recent studies have shown that acetylation of proteins has a comparably widespread regulatory scope (Choudhary et al., 2009). Acetylation can occur on numerous amino acids but is most common on lysine residues. Indeed, acetyl-lysine residues have been identified in over 20% of mitochondrial proteins, including important respiratory proteins (Kim et al., 2006). These studies suggest that acetylation is a key regulatory mechanism of mitochondrial biology and as such may be an important target for modulating mitochondrial function to confer cardioprotection.

i Post-translational regulation by acetylation / deacetylation

Acetylation was identified as a post-translational modification affecting histone proteins; however, identification of acetylated non-histone proteins, including key mitochondrial proteins, suggested that acetylation may be a widespread and functionally important means of protein regulation. Given the prevalence of acetyl-lysine residues in important mitochondrial proteins, the balance of acetylation and deacetylation in regulating protein function has become an area of interest for mitochondrial research (Balaban, 2010).

Chemistry of acetylation and deacetylation: Lysine acetylation comprises the addition of an acetyl functional group ($O=C-CH_2$) to the ε-amino group of L-lysine (Figure 1.13 A) (Sauve, 2010). Lysine residues are often located in binding and catalytic sites of proteins where the positively charged amino side-chain (Figure 1.13 B) contributes to overall protein structure and function by bonding to negatively charged amino acids or non-protein atoms (Alberts et al., 2002). Addition of an acetyl group to lysine neutralises this positive charge (Figure 1.13 A) and can therefore influence its participation in protein binding and active sites which can thus affect overall protein structure and function (Choudhary et al., 2009). Deacetylation removes the acetyl functional group and restores the free amino group of the affected lysine residue therefore restoring its positive charge and functional capacity (depicted in Figure 1.13)

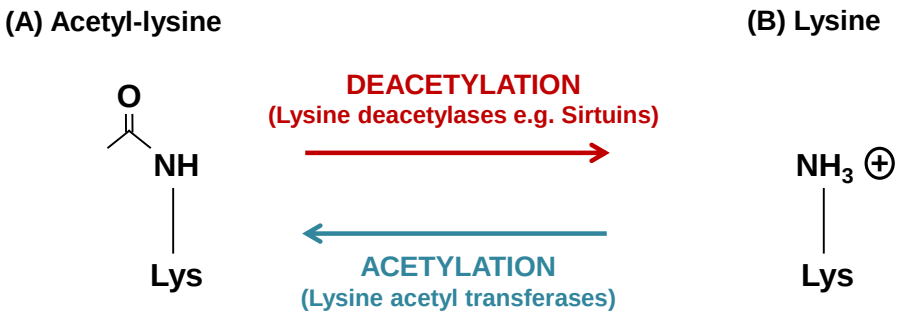

Figure 1.13: Schematic of lysine acetylation and deacetylation
Simplified chemical basis of lysine acetylation (A) and deacetylation (B) by acetyl transferases (blue) and deacetylases (red) respectively. Lysine contains a positively charged amino side-chain (+) which is neutralised by the addition of the acetyl group. Adapted from Sauve (2010).

Regulation of acetylation and deacetylation: Protein acetylation is a reversible post-translational modification involving a highly regulated balance between acetylation and deacetylation (Choudhary et al., 2009). These processes are catalysed by lysine acetyl transferase (KAT; previously known as histone acetyl transferase HAT) and lysine deacetylase (KDAC; previously known as histone deacetylase HDAC) enzymes respectively (Sauve, 2010; Fritz et al., 2012). Given the importance of lysine residue acetyl-status in protein structure and function, regulation of acetylation and deacetylation provides an interesting potential mechanism for modulating protein function.

Acetylation: The precise mechanisms catalysing acetylation in mitochondria have not been fully elucidated. It has been suggested that proteins with acetyl transferase activity are likely to reside in the mitochondrial matrix. In addition, auto-acetylation has been proposed. However, neither of these mitochondrial acetylation mechanisms has been confirmed to date and investigation of acetylation is on-going (Fritz et al., 2012).

Deacetylation: The regulation of deacetylation in mitochondria has been widely investigated and is much better understood. Deacetylation involves the removal of the acetyl group from lysine to restore its free amino group (Figure 1.13; red) (Sauve, 2010).

Deacetylation is catalysed by enzymes with deacetylase activity, termed lysine deacetylase (KDAC) proteins which are divided into four different classes (I - IV) based on sequence homology and function. KDAC proteins are generally zinc-dependent, except class III which are structurally and functionally divergent to the other KDAC enzymes (Dokmanovic et al., 2007). The sirtuin proteins are a major group of class III KDAC proteins which have been implicated in lysine deacetylation in a number of physiological and pathological settings (reviewed by Bao and Sack, 2010). Given the widespread roles of sirtuin proteins in lysine deacetylation, these proteins are an important regulatory mechanism of acetyl-post-translational modifications.

ii Sirtuin-3 as a post-translational regulatory protein

Activation of the catalytic activity of the sirtuin (Sirt) proteins results in rapid removal of acetyl groups from lysine residues. The Sirt proteins are known to deacetylate a diverse range of transcriptional regulators and intracellular proteins and have been widely investigated given the importance of acetyl-post-translational modifications in regulating protein activity (Bao and Sack, 2010). Sirtuin-3 (Sirt-3) has been implicated in regulating mitochondrial protein deacetylation (Shi et al., 2005) and is therefore an interesting target for cardioprotection by modulating mitochondrial function and thus survival.

Sirtuin protein family: Sirt-3 is a member of the highly conserved Sirt protein family of deacetylase enzymes. The yeast Sir2 (silent information regulator-2) protein was the first Sirt protein to be identified and there are now seven known mammalian Sirt proteins (Sirt 1-7). The mammalian Sirt proteins have varied subcellular locations but conserved nicotinamide adenine dinucleotide (NAD^+) dependent deacetylation activity. All the mammalian Sirt proteins contain a conserved NAD^+-binding and catalytic domain, termed the 'sirtuin core domain' (Frye, 2000) which confers their highly conserved NAD^+-dependence (Sauve, 2010), discussed below (see iii). The mammalian Sirt proteins have divergent N- and C-terminals where the N-terminus targeting sequence determines the protein subcellular location (Frye, 2000) and thus precise roles of the protein.

The Sirt proteins (including Sir2) also have putative roles in ribosylation (Onyango et al., 2002), where this has recently been reported specifically for Sirt-4 and Sirt-7 proteins. However, the ribosylation activity of the Sirt proteins is currently poorly understood and the source of some controversy; it is therefore not discussed in detail here.

The mammalian Sirt proteins are sub-divided into four classes defined by the degree of homology of the core 250 amino acid domain and their functional activity: class I (Sirt-1, -2 and -3), class II (Sirt-4), class III (Sirt-5) and class IV (Sirt-6 and -7) (Frye, 2000). The class I Sirt proteins exhibit the closest homology to yeast Sir2 and the most robust deacetylase activity. Although Sirt-1 has been the most widely studied member of the Sirt protein family, with regards to mitochondrial protein acetylation only Sirt-3, -4 and -5 proteins are located in the mitochondrial matrix (Shinmura, 2013). Of these mitochondrial Sirt proteins, Sirt-3 has been demonstrated to possess the most robust deacetylase activity. The role of Sirt-3 as the major Sirt deacetylase in mitochondria is demonstrated by extensive mitochondrial protein hyperacetylation in Sirt-3 genetic knockout mice (Lombard et al., 2007; Fritz et al., 2012). In comparison, genetic ablation of Sirt-4 or Sirt-5 caused very little difference to the acetylation status of mitochondrial proteins (Lombard et al., 2007). Sirt-3 is therefore the main focus for investigation of acetyl-post-translational regulation of mitochondrial proteins here.

Sirtuin-3: Sirt-3 is the main mitochondrial deacetylase protein identified to date. Sirt-3 is nuclear encoded to produce a 399 amino acids (c. 44 kDa) full length protein containing a 24 amino acid N-terminal mitochondria-targeting sequence and a conserved 'sirtuin core domain' described above. The immature full length Sirt-3 protein is transported to the mitochondrial matrix where this N-terminal sequence is removed to form the functionally active mature Sirt-3 protein (c. 28 kDa) (Frye, 2000; Schwer et al., 2002).

Sirt-3 is known to be enriched in mitochondria, which is evidenced by its high level of expression in mitochondria-dense tissues including heart, brain and liver (Lombard et al., 2007). Within the mitochondria, Sirt-3 is believed to be soluble in the mitochondrial matrix (Schwer et al., 2002; Lombard et al., 2007). An earlier study showing inner mitochondrial membrane bound Sirt-3 in cultured cells is likely to be an *in vitro* artefact. In addition to mitochondrial Sirt-3, a smaller nuclear pool of full length Sirt-3 has been identified in human brown adipose tissue samples (Scher et al., 2007), although this was not seen in mouse samples (Lombard et al., 2007). Although there is still some controversy, Sirt-3 is likely to only be active in the mitochondria since cleavage of the N-terminal sequence in the mitochondrial matrix is required for its function (Frye, 2000).

The human and rodent Sirt-3 protein sequences show a very high degree of conservation of the functional 'sirtuin core domain' (Frye, 2000). Initial studies suggested that the mouse Sirt-3 protein was shorter than the human isoform (Yang et al., 2000; Schwer et al., 2002); however, a subsequent study isolated a novel mouse Sirt-3 splice variant of increased length with a clearly identifiable mitochondria-targeting sequence (Cooper et al., 2009). Although there remains some controversy concerning the splice variants and isoforms of the mouse Sirt-3 protein, conservation of the functional sirtuin core domain suggests that the function and regulation of Sirt-3 in acetyl-post-translational modifications will be highly conserved between these species (Sack, 2011).

Investigations of the role of Sirt-3 in physiological and pathological situations have relied primarily on manipulation of Sirt-3 expression levels or activity since there is currently no known pharmacological activator or selective inhibitor of Sirt-3 (Sack, 2011). Cloning of the human and rodent Sirt-3 isoforms has allowed genetic overexpression, mutation and ablation studies *in vitro* in cultured cell lines (Frye, 1999; Frye, 2000; Michishita et al., 2005). Further to this, the role of Sirt-3 has been assessed *in vivo* using a Sirt-3 genetic knockout mouse model (Lombard et al., 2007) and by pathophysiological upregulation of Sirt-3 expression by fasting (Shi et al., 2005). Detailed descriptions of these approaches and the protocols used to manipulate Sirt-3 expression are provided in chapter 6.

iii Regulation of Sirt-3 mediated deacetylation

Deacetylation by Sirt-3 is highly regulated by intracellular and mitochondrial conditions. The key mechanisms regulating Sirt-3 are described below and discussed in detail subsequently in the relation to physiological and pathological conditions (see iv).

Regulation of Sirt-3 deacetylase activity: Sirt mediated deacetylation is dependent on activation of Sirt proteins by NAD^+ binding to the sirtuin core domain. Binding of NAD^+ to the Sirt protein induces its deacetylase activity thereby catalysing the removal of lysine acetyl groups on target proteins. NAD^+ also functions as a cofactor in the deacetylation reaction to produce nicotinamide, which under normal cellular conditions is regenerated to form NAD^+ (Revollo et al., 2004). Nicotinamide inhibits Sirt deacetylase activity by binding to a conserved regulatory pocket, termed the *c*-pocket (Bitterman et al., 2002). The balance of NAD^+ activation and nicotinamide inhibition of Sirt-3 deacetylase activity is the principal mediator of Sirt-3 protein activity (Sack, 2011), (Figure 1.14).

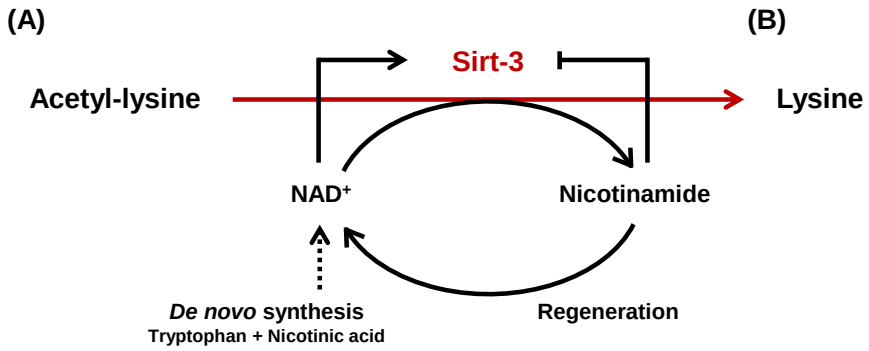

Figure 1.14: Regulation of Sirt-3 mediated deacetylation
Sirt-3 activity is dependent on binding to NAD^+ which is consumed by the deacetylation reaction. Sirt-3 deacetylase activity is regulated by the balance of NAD^+ which activates Sirt-3 and nicotinamide which inhibits Sirt-3. Constructed from information provided by Sack (2011).

<u>Regulation of NAD^+ levels:</u> Regeneration of NAD^+ from nicotinamide is the major source of NAD^+ in mammalian cells (Revollo et al., 2004) (Figure 1.14). However the precise regulation and availability of NAD^+ may vary between cell types and subcellular compartments (Bao and Sack, 2010). The processes regulating NAD^+ levels have been mostly studied in the cytosol in relation to Sirt-1 deacetylation, however, mitochondria-specific isoforms of the proteins regulating NAD^+ biosynthesis have been identified (Berger et al., 2005), suggesting that overall regulation of NAD^+ levels and thus Sirt deacetylase activity is conserved between the Sirt proteins.

The key role of NAD^+ in regulating Sirt (including Sirt-3) activity is likely to reflect the importance of Sirt proteins as metabolic sensors. Regulation of Sirt protein deacetylase activity by NAD^+ is conserved in all mammalian Sirt proteins. In normal cells where

energy production is not restricted, intracellular NADH levels increase at the expense of NAD^+ levels; therefore under normal conditions NAD^+ levels are low which prevents Sirt-3 mediated deacetylation. However, upon energy starvation, NAD^+ levels increase which activates Sirt-3 deacetylase activity (Rardin et al., 2013). Indeed, metabolic stress upon fasting also causes upregulation of the enzymes that convert nicotinamide to NAD^+ (Yang et al., 2007a), thereby increasing Sirt-3 activity upon fasting, discussed below.

Post-translational modification of Sirt-3: Post-translational regulation of Sirt-3 protein activity has not been widely investigated to date. It has been suggested that Sirt-3 may be carbonylated (carbon monoxide bound) upon certain stress conditions (Fritz et al., 2011), which inhibits Sirt-3 deacetylase activity (Fritz et al., 2012). It is unclear how widespread carbonylation controls Sirt-3 deacetylase activity in other cellular conditions.

Studies of cytosolic Sirt-1 protein regulation have shown that sumoylation is an important post-translational modification which activates Sirt-1 deacetylase activity (Yang et al., 2007b). Sumoylation of Sirt-3 has not yet been demonstrated. However, this may represent a potential Sirt-3 post-translational modification.

Regulation of Sirt-3 protein expression: In addition to regulation of Sirt-3 deacetylase activity described above, modulation of Sirt-3 protein expression is also likely to be an important mechanism of regulating Sirt-3 deacetylation and thus acetyl-post-translational modifications. The precise molecular regulatory mechanisms controlling Sirt-3 protein levels have not been well characterised, however, numerous studies have shown Sirt-1 protein expression is tightly regulated by transcription (e.g. Foxo-3a) and RNA stability (e.g. miRNA inhibition of Sirt-1 RNA). It is therefore expected that a similar scope of regulatory mechanisms will control Sirt-3 expression (Bao and Sack, 2010; Sack, 2011).

Although the precise molecular mechanisms controlling Sirt-3 protein expression levels are not well understood, it is widely appreciated that Sirt-3 protein levels are highly amenable to regulation by external cellular conditions. Most notably, calorie restriction and total fasting have been shown to trigger significant increases in Sirt-3 expression in *ex vivo* neonatal cardiomyocytes (Sundaresan et al., 2008) and *in vivo* in the liver (Lu et al., 2011). In addition, high ROS levels have been shown to induce increased Sirt-3 transcript and protein levels (Chen et al., 2011). Further to this, it has been shown that calorie restriction and concurrent increased Sirt-3 expression results in a significant decrease in mitochondrial protein acetylation in liver tissue samples (Hebert et al., 2013). Conversely, a high fat diet has been shown to downregulate Sirt-3 expression *in vivo* (Bao et al., 2010). The influence of calorie intake on Sirt-3 expression is likely to represent the role of Sirt-3 as an important sensor and regulator of metabolic stress (reviewed by Shinmura, 2013).

iv Physiological and pathophysiological roles of Sirt-3

Sirt-3 target proteins: Sirt-3 is known to deacetylate a number of mitochondrial proteins. Recent developments in large gene array and mass spectrometry technologies have allowed rapid identification of numerous lysine acetylation sites in *ex vivo* tissues (Kim et al., 2006). Furthermore, comparison of the 'acetylome' of Sirt-3 wildtype and knockout mice has identified lysine residues in at least 136 mitochondrial proteins that are specifically deacetylated by Sirt-3 (Fritz et al., 2012; Rardin et al., 2013).

Sirt-3 deacetylates a number of proteins involved in protein transcription, metabolism and cell survival (Sack, 2011; Nogueiras et al., 2012); as summarised in Table 1.3.

Transcription regulation: Sirt-3 has been shown to mediate deacetylation of Foxo3a, an important transcription factor; Foxo3a deacetylation increases its DNA binding activity and thus mediates transcription of a number of downstream genes, notably catalase and MnSOD (Jacobs et al., 2008; Kim et al., 2010). Sirt-3 induced Foxo3a mediated MnSOD expression was shown to protect against increased superoxide levels, where cells expressing mutant non-functional Sirt-3 exhibited increased superoxide levels (Jacobs et al., 2008). The role of Sirt-3 in regulating ROS levels is discussed further below.

Respiration: Sirt-3 is a crucial regulator of mitochondrial metabolism whereby Sirt-3 deacetylates and activates a number of key metabolic enzymes involved in oxidation of fatty acids and the electron transport chain (summarised in Table 1.3). Importantly, deacetylation of respiratory complexes I, II and V (Ahn et al., 2008; Finley et al., 2011; Wu et al., 2013) increases the enzymatic activity of the ETC to increase ATP production. The importance of the role of Sirt-3 in regulating metabolism is demonstrated in Sirt-3 knockout mice which have approximately 50% less cellular ATP (Ahn et al., 2008).

Cell survival: Sirt-3 mediated deacetylation is likely to influence cell survival by control of vital cellular processes including respiration (described above) and ROS scavenging. Sirt-3 increases the expression and enzymatic activity of MnSOD (Jacobs et al., 2008; Chen et al., 2011). Sirt-3 also deacetylates isocitrate dehydrogenase-2 (IDH2) to increase its activity, which as well as participating in the citric acid cycle, is an important antioxidant regulator (Yu et al., 2012). The cumulative actions of enhanced antioxidant activity upon Sirt-3 deacetylation, reduces overall ROS levels and thus oxidative damage (see section 1.2).

Table 1.3: Sirt-3 deacetylated proteins
Summary of proteins deacetylated by Sirt-3; this is in no way an exhaustive list of target proteins however, attempts to encompass the principal effects of Sirt-3 activity and explain Sirt-3 knockout (-/-) phenotypes. References provided. (Table overleaf)

STUDY	TARGET PROTEIN	EFFECT OF DEACETYLATION	RESULTANT PHENOTYPE IN SIRT3 -/-
TRANSCRIPTION / PROTEIN MODIFICATION			
Jacobs et al. (2008) Kim et al. (2010)	Foxo3a	Increased DNA binding activity: • Increased MnSOD transcription	(See effects of relevant target genes)
RESPIRATION (OXIDATIVE PHOSPORYLATION / TCA CYCLE)			
Hirschey et al. (2010)	Acetyl-CoA dehydrogenase	Increased enzymatic activity • Increases fatty acid oxidation	• Sirt-3 -/- exhibit blunted fatty acid oxidation
Hallows et al. (2006)	Acetyl-CoA synthase 2	Activates enzymatic activity	• Sirt-3 -/- exhibit blunted fatty acid oxidation
Lombard et al. (2007)	Glutamate dehydrogenase (GDH)	Increased enzymatic activity	• Sirt-3 -/- mice exhibit hyperacetylated GDH
Schlicker et al. (2008) Yu et al. (2012)	Isocitrate dehydrogenase-2 (IDH2)	Increased enzymatic activity By ≈44-fold (Yu et al., 2012)	• Sirt-3 -/- mice exhibit increased SO recovered by IDH2 deacetylation (Yu et al., 2012)
Ahn et al. (2008)	Complex I: NDUFA9	Increased enzymatic activity	• Sirt-3 -/- show approximate 20% reduction in complex I activity (Ahn et al., 2008) • Sirt-3 -/- exhibit compromised ETC complex activity and thus impaired ATP production (≈50% lower ATP levels) (Ahn et al., 2008) • Sirt suppression decreases ATP F_0F_1 activity
Cimen et al. (2010) Finley et al. (2011)	Complex II: Succinate dehydrogenase A / B	Increased enzymatic activity (Complex II activity unchanged in Sirt3 -/-)	
Finley et al. (2011) Wu et al. (2013)	Complex V: F1α OSCP	Increased enzymatic activity • Increased ATP synthesis	
CELL SURVIVAL			
Hafner et al. (2010) Shulga et al. (2010) Verma et al. (2013)	Cyclophilin-D	Inhibits Cyp-D PPIase activity • Reduces mPTP opening Dissociation of hexokinase II: • Stimulates OxPhos • Allows Bak/Bax apoptosis	• Sirt-3 -/- mice: Cyp-D hyperacetylation and increased Cyp-D activity • Sirt-3 depletion reduced Bax mediated cell death (Verma et al., 2013)
Chen et al. (2011) Tao et al. (2010) Jacobs et al. (2008) Ozden et al. (2011)	Maganese superoxide dismutase (MnSOD)	Activates enzymatic activity • Decreases mitochondrial ROS	• Sirt-3 -/- liver mitochondria exhibit increased superoxide levels (Chen et al., 2011) • Sirt-3 mutant cells have less SO (Jacobs et al., 2008)
Pellegrini et al. (2012)	Carbonic anhydrase (CA)	Increases enzymatic activity • Prevents intracellular acidification	• Sirt-3 silenced cells showed increased cellular acidification upon hypoxia
Sundaresan et al. (2008)	Ku70	Increased Bax binding – less apoptosis	• Sirt-3 overexpression reduced apoptosis
Li et al. (2010)	p53	Partially inhibits cell growth arrest	(Only examined in bladder cancer cell line)

Sirt-3 and mPTP opening: In addition to the effects of Sirt-3 on cell survival by regulation of respiration and ROS, Sirt-3 deacetylation may also affect cell survival by modulating mPTP opening. Recent studies have suggested that Sirt-3 deacetylation activity may control excessive mPTP opening due to its actions directly on Cyp-D and indirectly by its effects on reducing the intracellular conditions that favour mPTP opening. The potential regulatory actions identified to date are described below.

Cyclophilin-D: Sirt-3 has been shown to deacetylate Cyp-D to reduce its PPIase activity and thus reduce mPTP opening (Shulga et al., 2010; Hafner et al., 2010). Hafner et al. (2010) identified Cyp-D lysine 166 as the target for Sirt-3 deacetylation and showed that aged (16 month old) Sirt-3 knockout animals were more prone to calcium-induced mPTP opening. Although there was no difference in cardiac function, when subjected to hypertrophic stress by transaortic constriction (TAC), Sirt-3 knockout mice were more susceptible to hypertrophy and impaired cardiac function (Hafner et al., 2010). Shulga et al. (2010) showed a similar effect upon Sirt-3 inhibition and demonstrated that Cyp-D deacetylation causes hexokinase II (HKII) dissociation from the mitochondrial membrane to stimulate oxidative phosphorylation (Shulga et al., 2010).

F_0F_1 ATP synthase: Sirt-3 has been shown to directly interact with and deacetylate components of the F_0F_1 ATP synthase enzyme. Deacetylation of F_0F_1 ATP synthase significantly increases its enzymatic activity and thus increases ATP production (Finley et al., 2011; Wu et al., 2013). Given the recent studies by Bonora et al. (2013) and Giorgio et al. (2013) implicating the F_0F_1 ATP synthase as a constituent component of the mPTP, its regulation by Sirt-3 deacetylation poses the intriguing possibility that Sirt-3 may affect mPTP formation; this is likely to form a focus for future studies.

Reduced cellular triggers (ROS): Sirt-3 deacetylates several important ROS scavengers which increases their enzymatic activity to reduce overall ROS levels (as described above). This is particularly important since Sirt-3 deacetylation also increases ETC activity (Table 1.3) (Ahn et al., 2008; Finley et al., 2011; Wu et al., 2013), which would otherwise increase ROS levels and oxidative damage meaning that Sirt-3 may therefore indirectly reduce mPTP opening by reducing this important cellular trigger (see section 1.2). However, it should be noted that Sirt-3 also influences pH by deacetylation of carbonic anhydrase (CA) which has a major role in control of intracellular pH, whereby deacetylation of CA increases its enzymatic activity and therefore reduces intracellular acidosis upon hypoxia (Pellegrini et al., 2012). The effect of CA activity on mitochondrial pH is not known, however, it is possible that decreased intracellular acidosis during ischaemia may reduce the knock-on effect of increased mitochondrial acidosis and calcium overloading by the pathway described in Figure 1.4. Reduced mitochondrial

acidosis during ischaemia may also remove the inhibitory effect of low pH during ischaemia which is expected to inhibit mPTP opening during this period. Although the precise balance of these factors on indirectly promoting or inhibiting mPTP opening has not been investigated, reduced Cyp-D PPIase activity due to Sirt-3 mediated deacetylation reduces calcium-induced mPTP opening (Hafner et al., 2010).

Sirt-3 and apoptosis: Given the importance of mitochondria in mediating apoptosis, the role of Sirt-3 in regulating extrinsic apoptosis has been investigated.

Ku70: Sirt-3 has been shown to deacetylate Ku70 (Sundaresan et al., 2008) which in its deacetylated form binds to and sequesters Bax to prevent its translocation to the mitochondria where it induces apoptosis. Cytosolic Ku70 has previously been identified as an important target protein of Sirt-1; however, in cardiomyocytes Sirt-1 was shown to be ineffective at deacetylating Ku70, where Sirt-3 was instead implicated in this role (Sundaresan et al., 2008) (Figure 1.15). This remains controversial since it suggests a role for Sirt-3 outside the mitochondria and may represent an artefact of the *in vitro* cell expression model used and therefore requires further investigation in an *in vivo* setting.

p53: Sirt-3 also interacts with and deacetylates p53, a protein involved in regulating cell growth arrest and senescence by its actions in both the nucleus and mitochondria. Sirt-3 deacetylation of mitochondrial p53 partly abolishes its cell senescent activity to promote cell survival (Li et al., 2010) (Figure 1.15). However, this has only been investigated in a cancer cell line to date and it is therefore not clear whether Sirt-3-p53 regulation is important in normal cells and pathological settings such as ischaemia-reperfusion injury.

Hexokinase II: Sirt3 deacetylation of Cyp-D also results in dissociation of hexokinase II (HKII) from the outer mitochondria membrane. This was reported to be beneficial for cell survival since it stimulates oxidative phosphorylation (Shulga et al., 2010), described above. However, since binding of HKII to the outer mitochondrial membrane promotes membrane integrity, its dissociation upon Cyp-D deacetylation therefore allows Bak/Bax to disrupt the membrane to induce apoptosis. This has been demonstrated in human epithelioid cervix carcinoma (HeLa) cells where Sirt-3 deacetylation of Cyp-D and consequent HKII dissociation promoted apoptotic cell death (Verma et al., 2013). It has therefore been suggested that Sirt-3 deacetylation may actually promote cell death in certain settings. However, increased sequestration of Bax by deacetylated Ku70 may mitigate the susceptibility to Bax-mediated apoptosis upon HKII dissociation. Detailed investigations of the interplay between these death pathways are required in non-cancer cells to fully understand the effects of Sirt-3 activity on cell survival.

In summary, the precise effects of Sirt-3 deacetylase activity on cell survival are likely to depend on the cellular conditions and severity of stress which may dictate which cellular pathways prevail and determine cell fate. A summary of the potential effects of Sirt-3 on cell survival is provided in Figure 1.15 (where putative interactions are indicated in grey).

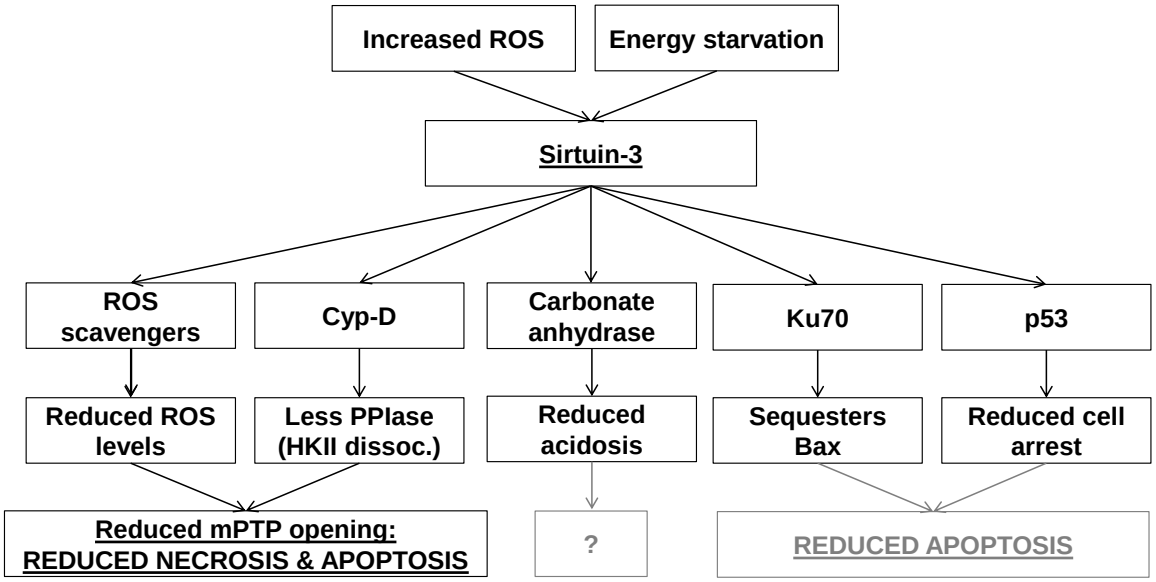

Figure 1.15: Putative effects of Sirt-3 mediated deacetylation upon cellular stress
Cell stress upregulates Sirt-3 deacetylation of a number of target proteins which affects their activity to influence important mediators of cell death including mPTP opening and putative effects on extrinsic apoptosis. Constructed from information provided by Sack et al. (2011).

Baseline phenotype of Sirt-3 knockout mice: Given the diverse targets of Sirt-3 deacetylation, it is intriguing that total Sirt-3 genetic ablation does not elicit any gross phenotypic abnormalities; Sirt-3 KO mice display no difference in oxygen consumption, physical activity or cell growth (Lombard et al., 2007) despite 50% less cellular ATP (Ahn et al., 2008). However, Sirt-3 KO mice show widespread protein hyperacetylation which is further enhanced upon cellular stress (Fritz et al., 2012; Rardin et al., 2013). The role of Sirt-3 appears to be more prominent under stress conditions, likely due its dependence on NAD^+ activation. Indeed, Sirt-3 KO mice develop overt phenotypic differences upon hypertrophic stress and aging (Hafner et al., 2010).

The experimental evidence to date suggests that Sirt-3 plays an important role in modifying mitochondrial metabolism and function in conditions of cellular stress. Myocardial ischaemia-reperfusion is known to elicit significant cardiomyocyte metabolic stress and cellular injury; however, the role of Sirt-3 deacetylase activity in this setting is largely unknown. It remains to be seen whether acutely increased Sirt-3 activity could provide a target to reduce myocardial infarction; this is investigated in chapter 6.

1.4.3. Mitochondrial oxidative stress and DJ-1

Oxidative stress is a critical mediator of cellular injury and has been implicated in a number of pathologies, including ischaemia-reperfusion injury (described in section 1.2). Under physiological conditions, mitochondrial respiration produces ROS which are usually scavenged by the many anti-oxidant and detoxification proteins. However, under pathological conditions, ROS rapidly accumulate and cause oxidative damage to mitochondria and wider cellular components, notably the lipid membranes (Anderson et al., 2012). Since oxidative damage is a key mediator of cardiomyocyte death following ischaemia-reperfusion, methods of reducing oxidative stress provide an important potential method to protect against ischaemia-reperfusion (Hoffman et al., 2004).

i Oxidative stress and mitochondrial function

Although ROS are known to be important cellular messengers, the effect of ROS accumulation caused by cellular insults such as ischaemia-reperfusion has been identified as a key factor in cell injury and death in these pathological conditions (Hoffman et al., 2004). The intracellular redox state is determined by the balance of oxidants (such as ROS) and antioxidants (such as enzymatic ROS scavengers) (Katz, 2001). Oxidants are produced in part as a by-product of mitochondrial oxidative phosphorylation which means that cells with a high metabolic demand, such as cardiomyocytes, are suggested to be at greater risk of redox imbalance upon stress (Jezek and Hlavata, 2005; Anderson et al., 2012).

Under physiological conditions, the cellular redox state is maintained by an array of homeostatic mechanisms, however, stress, such as myocardial ischaemia-reperfusion, disrupts the balance of ROS. The sequelae of events occurring upon myocardial ischaemia and reperfusion are outlined in section 1.2. The propagating nature of ROS accumulation following ischaemia-reperfusion is a key mediator of oxidative damage, whereby the initial increase in ROS further damages mitochondrial proteins which causes further ROS accumulation and oxidative damage (see 1.2.3) (Forman et al., 1989; Katz, 2001). Membrane lipid peroxidation is recognised as a major manifestation of oxidative damage resulting from ischaemia-reperfusion where ROS interact with the fatty acid side chains of membrane phospholipid proteins to produce lipid peroxidation products. Lipid peroxidation itself causes decreased membrane fluidity and increased membrane permeability which in turn contribute to mitochondrial dysfunction and cell death (Forman et al., 1989; reivewed by Anderson et al., 2012). In addition, the products of lipid peroxidation, for example reactive aldehydes, are also potent mediators of cellular oxidative damage. These lipid peroxidation products damage cellular proteins and nuclei acids including DNA and RNA (reviewed by Anderson et al., 2012).

Mitochondria possess an array of antioxidant proteins which are upregulated upon cellular oxidative stress. However, oxidative stress is also an important cell signalling method, where protein oxidation is a recognised post-translational modification (Shao et al., 2012). Since oxidative stress is highly regulated under physiological conditions and is a key mediator of mitochondrial dysfunction and cell death in many pathophysiological conditions, understanding the regulation of oxidative stress and its signalling effects may identify novel targets for protecting against ischaemia-reperfusion.

ii DJ-1 as a sensor of oxidative stress

Since mitochondria are regarded as the primary source of ROS under physiological and pathophysiology conditions, identification of mitochondrial proteins involved in regulating ROS directly by ROS scavenging or indirectly by sensing ROS to mediate wider responses, provides interesting scope for future potential targets for cardioprotection.

DJ-1 has recently been identified as an important stress response protein with purported roles in defending cells against ROS and mitochondrial damage. DJ-1 has been implicated in a diverse array of pathologies including multiple cancers, Parkinson's disease and cerebral ischaemia-reperfusion injury (reviewed by Cookson, 2010; Wilson, 2011). Although the precise functions of DJ-1 at baseline and under stress remain poorly defined, its apparent involvement as an oxidative stress response protein makes it a potential target for modulating cell stress and ultimately cell death.

DJ-1 protein family: DJ-1 is a member of the DJ-1/ PfpI superfamily of proteins for which DJ-1 homologs have been identified across all biological kingdoms. DJ-1 shares some homology to the bacterial cysteine protease enzyme PfpI, although the biological roles of DJ-1 are thought to extend beyond protease activity. DJ-1 has been investigated in Parkinson's disease where DJ-1 mutations have been implicated in rare heritable forms of this disease (reviewed by Wilson, 2011). The precise functions of DJ-1 remain elusive; an overview of its structure, regulation and proposed functions is provided here.

DJ-1 protein: DJ-1 is ubiquitously expressed in a number of human tissues, including the heart. DJ-1 is a small nuclear encoded protein of 189 amino acids (c. 20 kDa) which is encoded in humans by the *PARK7* gene (overview of protein provided by Wilson, 2011). The crystal structure of the DJ-1 protein was independently solved by five research groups which all showed that DJ-1 functions as a homodimer. These studies showed that the DJ-1 tertiary protein structure shares some homology to known cellular cysteine proteases and has an additional α-helix in the C-terminal region (Wilson et al., 2003; Honbou et al., 2003; Lee et al., 2003; Tao and Tong, 2003; Huai et al., 2003). This additional α-helix was suggested to block the catalytic site of the protein and was

therefore identified as a putative regulatory site (Honbou et al., 2003; Tao and Tong, 2003; Wilson et al., 2003). Importantly, a conserved cysteine residue (Cys106) in this region was shown to be critical for regulation of DJ-1 activity (Wilson et al., 2003); described in detail below. Dimerisation of DJ-1 was also shown to be critical for its activity where mutation of a conserved leucine residue (Leu166) located in the C-terminal α-helix impedes dimer formation (Huai et al., 2003; Tao and Tong, 2003; Olzmann et al., 2004) and results in poor DJ-1 protein folding and degradation.

Under normal cellular conditions DJ-1 protein is mainly located in the cytosol and to a lesser extent in the nucleus; however, cellular stress causes mitochondrial enrichment of DJ-1 by increased DJ-1 protein expression and translocation of cytosolic DJ-1 to the mitochondria (Canet-Aviles et al., 2004; Blackinton et al., 2005; Lev et al., 2008). Specifically, its conserved Cys106 residue is crucial for mitochondrial enrichment of DJ-1 upon oxidative stress (reviewed by Wilson, 2011); discussed further below.

Regulation of DJ-1 activity by cysteine oxidation: Cysteine oxidation of DJ-1 is a crucial regulatory mechanism serving to increase DJ-1 mitochondrial enrichment and activity upon oxidative stress. Although oxidation of proteins can be considered as a form of damage, it has also been proposed as an important post-translational modification in response to oxidative stress (reviewed by Wilson, 2011).

DJ-1 contains three potential targets for cysteine oxidative regulation (Cys-46, -53 and -106), of which Cys106 is the most highly conserved and has been strongly implicated in regulation of DJ-1 activity (Wilson, 2011). Potent oxidants cause oxidation of the cysteine thiol group to produce cysteine sulfinite (Cys-SO_2^-) or cysteine sulfonate (Cys-SO_3^-) (Figure 1.16). Cysteine oxidation of DJ-1 therefore produces a more acidic isoform of DJ-1 (Mitsumoto et al., 2001). Cysteine sulfonate is the highest oxidised form and is considered to be an irreversible modification (Shao et al., 2012).

Oxidation of DJ-1 Cys106 to cysteine sulfinate has been confirmed by biochemical and structural studies of DJ-1 under baseline and oxidative stress conditions. It should be noted that although mass spectrometry analysis demonstrated formation of DJ-1 cysteine sulfonate upon oxidative stress, this has yet to be confirmed by crystal structure analysis (reviewed by Wilson, 2011). It has been postulated that DJ-1 cysteine sulfonate formation may destabilise and inactivate DJ-1 and coincide with apoptosis (Zhou et al., 2006). It appears that the extent of DJ-1 oxidation may therefore determine the beneficial roles of DJ-1 in protecting against oxidative stress. This is supported by the cytoprotective effects of small molecule compounds that allow DJ-1 oxidation to cysteine sulfinate but not cysteine sulfonate (Miyazaki et al., 2008; Yanagida et al., 2009).

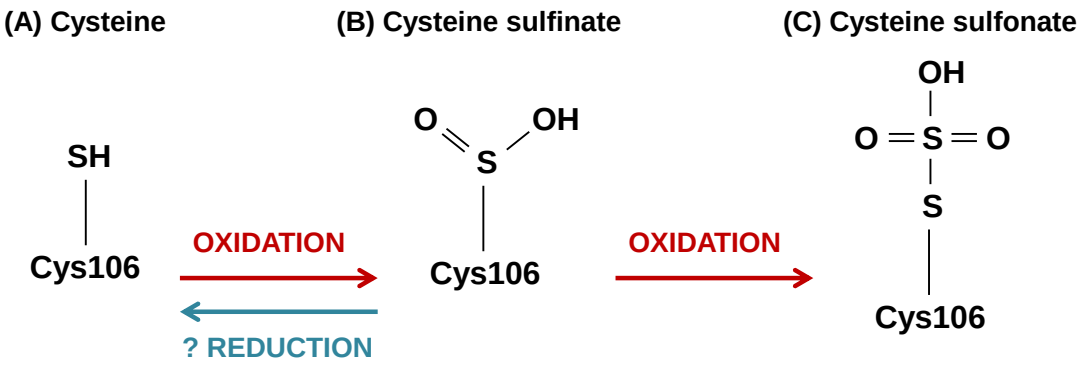

Figure 1.16: Modification of DJ-1 by cysteine oxidation
The cysteine thiol group can be oxidised to produce cysteine sulfinate or cysteine sulfonate. Constructed from information provided by Wilson (2011) and Shao et al. (2012).

Cysteine residues -46 and -53 have also been implicated in DJ-1 regulation by affecting Cys-106 oxidation capacity (Shendelman et al., 2004; Waak et al., 2009a); although these cysteine residues have been less well studied (reviewed by Wilson, 2011).

Although oxidation of cysteine residues to cysteine sulfinate (but not cysteine sulfonate) is theoretically chemically reversible (Shao et al., 2012), Duan et al. (2008) showed slow recovery of reduced DJ-1 protein levels following oxidative stress *in vitro*. In addition, since cyclohexamine (a protein synthesis inhibitor) inhibited the recovery of reduced DJ-1, it has been suggested that oxidation of DJ-1 is essentially irreversible and requires *de novo* protein synthesis (Duan et al., 2008). Further studies are now required to confirm the processes of DJ-1 protein regulation and turnover *in vivo* following oxidative stress.

The precise method of regulation of DJ-1 by cysteine oxidation has not been elucidated. Studies of other proteins have suggested that in some cases formation of cysteine sulfinate causes a conformation change in protein structure which modulates protein function (Shao et al., 2012). However, formation of cysteine sulfinate does not appear to cause conformational changes to DJ-1 (Canet-Aviles et al., 2004; Zhou et al., 2006).

Despite the unknown mechanism of regulation of DJ-1 by cysteine oxidation, several studies have confirmed the requirement for Cys106 oxidation for enhancing DJ-1 activity and translocation and conferring its protection against cell death (reviewed by Cookson, 2010; Wilson, 2011). Canet-Aviles et al. (2004) showed that mutation of Cys106 to alanine (C106A mutant) inhibited DJ-1 translocation to the mitochondria and abrogated its protective effect against cell death (Canet-Aviles et al., 2004). Further to this, Blackinton et al. (2009b) demonstrated that oxidation, specifically of Cys106, is crucial for mitochondrial localisation of DJ-1 in response to cellular stress (Blackinton et al., 2009b). These studies support the role of DJ-1 as an oxidative stress sensor and suggest that cysteine oxidation is an important post-translational modification of DJ-1.

iii Physiological and pathophysiological roles of DJ-1

The precise roles of DJ-1 under physiological and pathophysiological conditions remain the subject of intensive research. The requirement for DJ-1 cysteine oxidation (at Cys106) for its protective function suggests that DJ-1 has a role in responding to cellular oxidative stress. DJ-1 has been implicated in multiple cell survival pathways and the main putative roles for DJ-1 are described below:

ROS scavenger: Given the importance of cysteine oxidation of DJ-1 for mitochondrial translocation and increased activity, DJ-1 has been proposed to act directly as a ROS scavenger. Indeed, oxidation of DJ-1 necessarily consumes ROS (Wilson, 2011; Shao et al., 2012). However, the physiological relevance of direct ROS scavenging by DJ-1 is questioned by the relatively low capacity of DJ-1 to accept unpaired electrons and the partly irreversible nature of DJ-1 cysteine oxidation (Wilson, 2011). Further investigation of the direct ROS scavenging capabilities of DJ-1 is now required. The overall effect of DJ-1 function on reducing ROS levels upon oxidative stress has been confirmed by increased ROS levels *in vivo* in DJ-1 KO mice (Andres-Mateos et al., 2007).

Protease: Resolution of the crystal structure of DJ-1 showed some homology with members of the intracellular protease PfipI family (Honbou et al., 2003; Huai et al., 2003) which led to the suggestion that DJ-1 may function as a protease. Some studies have demonstrated that DJ-1 possess weak protease activity (Olzmann et al., 2004; Chen et al., 2010). However, it is now largely accepted that DJ-1 exerts minimal protease activity and this is unlikely to be a critical role of DJ-1. This is also supported by the absence of the conserved PfipI Cys-His-Glu catalytic site (Honbou et al., 2003; Huai et al., 2003; Wilson et al., 2003). It has been suggested that DJ-1 may indirectly induce protease activity upon cellular stress by regulating a protease enzyme (Wilson, 2011).

Protein chaperone: DJ-1 was first proposed to undertake putative protein chaperone roles based on the structural similarity of DJ-1 to the known chaperone HSP-31 (Lee et al., 2003). Shendelman et al. (2004) provided some experimental evidence that DJ-1 may function as a redox-sensitive chaperone in *in vitro* assays of protein chaperone activity. Interestingly, L166P mutated DJ-1 protein did not possess chaperone activity in this study which was interpreted as confirmation of the putative chaperone role of DJ-1 (Shendelman et al., 2004). However, a similar *in vitro* study by Olzmann et al. (2004) showed that DJ-1 did not mediate any significant chaperone activity (Olzmann et al., 2004). It is important to note that these *in vitro* chaperone activity assays may be subject to artefacts from the assay conditions and high levels of DJ-1 expression and thus may not reveal roles of DJ-1 under specific cellular conditions (reviewed by Wilson, 2011). The biological significance of DJ-1 chaperone activity therefore remains unclear.

Transcriptional regulator: DJ-1 has been suggested to regulate the transcription of a number of proteins and this has been proposed as the mechanism by which it is able to affect the diverse multitude of cellular pathways described in the various *in vitro* and *in vivo* models (van der Brug et al., 2008; reviewed by Wilson, 2011). Cookson's group proposed a model whereby DJ-1 binds to mRNA at nanomolar concentrations to slow translation and then dissociates from its mRNA targets upon oxidative stress to allow their efficient translation (van der Brug et al., 2008; Blackinton et al., 2009a). The direct role of DJ-1 as a transcriptional regulator however, requires further investigation of the precise mechanism by which DJ-1 is able to bind to mRNA since it lacks canonical RNA interaction motifs (van der Brug et al., 2008). The putative role of DJ-1 as a transcriptional regulator may explain the involvement of DJ-1 in modulating apoptotic cell death, although these actions may instead be mediated by indirect actions of DJ-1.

Apoptosis: DJ-1 has been shown to interact with and negatively regulate several critical mediators of cell death to promote cell survival upon cellular stress (Wilson, 2011).

PTEN/PI3K/Akt: DJ-1 directly interacts with phosphatase and tensin homolog (PTEN) to negatively regulate the P13K/Akt survival pathway (Kim et al., 2005a). PTEN is a pro-apoptotic phosphatase which antagonises the PI3K cell survival pathway resulting in reduced Akt phosphorylation and worsened cell survival upon cellular stress (reviewed by Mocanu and Yellon, 2007). DJ-1 inhibition of PTEN therefore causes increased PI3K and Akt phosphorylation and improved cell survival (Kim et al., 2005a). This DJ-1-PTEN interaction is also dependent on DJ-1 Cys106 oxidation (Kim et al., 2009). Although the biochemical nature of this DJ-1-PTEN interaction is unclear, the role of DJ-1 activity in enhancing PI3K/Akt pro-survival signalling has been implicated as an important protective response to oxidative stress (Kim et al., 2009; reviewed by Wilson, 2011).

p53: DJ-1 has also been shown to negatively regulate p53, an important tumour suppressor protein which is involved in transcriptional regulation of a number of proteins and can initiate apoptosis. Bretaud et al. (2007) showed that manipulation of DJ-1 expression levels in a zebrafish model showed concurrent changes to p53 levels and neuronal cell death (Bretaud et al., 2007). Further to this Fan et al. (2008b) showed that DJ-1 mediated inhibition of p53 activity causes decreased Bax expression and thus reduced caspase activation (Fan et al., 2008b). This group also suggested that DJ-1 sumoylation may be critical for its regulation of p53 activity (Fan et al., 2008a); although the precise roles of DJ-1 sumoylation have not been widely investigated. DJ-1 regulation of p53 activity and its subsequent effects on Bax-mediated cell death appears to be an important cytoprotective mechanism of DJ-1 activation in response to oxidative stress.

ASK1/p38/MAPK: DJ-1 activation has also been implicated in preventing Daxx/ASK1 mediated apoptosis by binding to death-domain associated protein (Daxx; a pro-apoptotic protein) to prevent its activation of apoptosis signal-regulating kinase 1 (ASK1) (Junn et al., 2005). Subsequent studies have shown direct interaction between DJ-1 and ASK1 (Waak et al., 2009a; Mo et al., 2010). These studies confirm further involvement of DJ-1 in reducing cell death and infer a cytoplasmic role for DJ-1. It is now widely accepted that DJ-1 activation reduces cell death from oxidative stress.

Genetic manipulation of DJ-1: As with many basic science studies, genetic manipulation provides an invaluable tool for investigating the roles of a specific protein both *in vitro* and *in vivo*. Many *in vitro* cell expression models have been used to assess the effect of overexpression of DJ-1 on important cell survival endpoints. Expression of mutant forms of DJ-1 has also provided insights into the importance of DJ-1 regulation by cysteine oxidation (reviewed by Wilson, 2011); this is discussed further in chapter 7.

Genetic knockout: The generation of DJ-1 genetic knockout mice has also led to a wealth of understanding of the roles of DJ-1 at baseline and following oxidative stress. The majority of studies of DJ-1 knockout mice have examined its effects on the brain. A summary of the main effects of genetic ablation of DJ-1 is provided above in Table 1.4.

Table 1.4: Effects of genetic ablation of DJ-1
Effects of whole body total ablation of DJ-1 (KO). This is in no way an exhaustive list of studies of genetic ablation of DJ-1 and attempts to encompass the principal effects of DJ-1 KO. A summary of *in vitro* studies is not provided here as an overview of these studies is provided in the main text in the description of the structure and regulation of DJ-1. References provided. (Table overleaf)

STUDY	BASELINE MEASURE / STRESSOR	EFFECT IN DJ-1 KNOCKOUT
CULTURED MOUSE EMBRYONIC FIBROBLASTS		
Giaime et al. (2012)	Baseline phenotype	• Reduced mitochondrial membrane potential • Increased mPTP opening • Increased ROS production • Reduced ATP levels • No effect on mitochondrial respiration or calcium
Krebiehl et al. (2010)	Baseline phenotype	• Reduced mitochondrial membrane potential • Increased ROS production • Impaired mitochondrial respiration • Accumulation of defective mitochondria • Reduced basal autophagy
Irrcher et al. (2010)	Baseline phenotype	• Increased mitochondrial fragmentation
PRIMARY EX VIVO PREPARATIONS		
Irrcher et al. (2010)	*Isolated mitochondria* - Baseline phenotype	• Increased ROS levels • Increased mitochondrial fragmentation
Waak et al. (2009b)	*Isolated astrocytes* - Lipopolysaccharide (LPS) stress	• Increased pro-inflammatory mediators; COX-2 and IL-6 • Increased nitric oxide (NO) by approximately 10-fold
Aleyasin et al. (2007)	*Granule neurones* - Glutamate excitotoxicity (ROS)	• Increased cell death
Andres-Mateos et al. (2007)	*Brain mitochondria* - Rotenone induced stress	• Increased hydrogen peroxide levels
Kim et al. (2005b)	*Embryonic cortical neurones* – H_2O_2 treatment (30 µM)	• Increased cell death
Martinat et al. (2004)	*Cultured embryonic stem cells* - H_2O_2 treatment (increasing concentrations)	• Increased cell death • No difference in ROS levels
IN VIVO		
Billia et al. (2013)	Myocardial infarction (Permanent LAD ligation)	• Increased myocardial infarct size
Billia et al. (2013)	Cardiac failure model of transaortic constriction (TAC)	• Increased susceptibility to hypertrophy and cardiac failure • Increased indicators of lipid peroxidation (4-HAE and MDA) • Decreased ATP levels
Lev et al. (2013)	Parkinson's disease model 6-hydroxydopamine (6-OHDA).	• Increased vulnerability to neuronal cell death • Lower expression of cell survival proteins; principally Nrf2
Aleyasin et al. (2007)	Cerebral focal ischaemia induced by endothelin-1	• Increased cerebral infarct size (approx. 4-fold increase)
Aleyasin et al. (2007)	Cardiac failure model of TAC	• Increased susceptibility to hypertrophy and cardiac failure • Increased oxidative damage to DNA

Pharmacological modulation of DJ-1: Pharmacological methods of increasing DJ-1 protein expression and activity have been investigated as potential therapeutic targets.

Small molecule regulators of DJ-1 oxidation: Miyazaki et al. (2008) undertook a screen of small molecule compounds which bind to the Cys106 region of DJ-1 to permit its oxidation to cysteine sulfinate but not cysteine sulfonate. Administration of these compounds was shown to reduce cell death in a drug-induced model of Parkinson's disease cell death suggesting that prevention of maximal oxidation of DJ-1 to prolong DJ-1 activation under oxidative stress may provide therapeutic benefit (Miyazaki et al., 2008). Further investigation of one of these, UCP0054278, showed a reduction in neuronal cell death in a cerebral ischaemia-reperfusion model (Yanagida et al., 2009).

Sodium phenylbutyrate: Several *in vitro* and *in vivo* studies have shown that treatment with sodium phenylbutyrate increases DJ-1 protein levels in neuronal cells and that this causes significant protection against oxidative-induced cell death (Zhou et al., 2011). However, sodium phenylbutyrate is not a selective pharmacological compound and is likely to exert other effects independent of DJ-1, indeed this compound is widely used as a histone deacetylase (HDAC) inhibitor (reviewed by Iannitti and Palmieri, 2011).

Although modulation of DJ-1 has been examined for potential therapeutic benefit in a number of pathologies, including cerebral ischaemia-reperfusion, its role in the heart remains largely unknown. The potential for modulation of DJ-1 as a therapeutic target to protect against myocardial ischaemia-reperfusion injury is investigated in chapter 7.

1.5. The future of cardioprotection

Cardioprotection has been an intense focus for basic science and clinical research for a number of decades, particularly following the first demonstration of significant protection against myocardial ischaemia-reperfusion injury by IPC in 1986 (Murry et al., 1986). However, despite numerous mechanical and pharmacological strategies showing promising reductions in infarct size pre-clinically in animal models, translation of these interventions to the clinical setting has proved incredibly poor (reviewed by Dirksen et al., 2007; Hausenloy et al., 2010). Although clinical translation is challenging in most fields of research, this appears to have been particularly severe for cardioprotection studies. Indeed, reperfusion therapy remains the only effective clinical intervention for reducing infarct size in acute myocardial infarction patients and there is currently no therapy for lethal reperfusion injury (Yellon and Hausenloy, 2007; Heusch, 2013).

Future studies of cardioprotection must attempt to address the shortcomings of previous experimental pursuits that may have contributed to their poor clinical translation.

1.5.1. Obstacles to clinical translation

The causes of poor clinical translation have been the subject of intense discussion within the field of cardiovascular research, leading to the publication of a number thought-provoking review articles on the subject by eminent researchers in the field (Kloner and Rezkalla, 2004; Hausenloy et al., 2010; Heusch, 2013). There appears to be good consensus of the principal obstacles to clinical translation concerning the design of animal models and notable differences compared to the clinical situation; indeed these same considerations are likely to apply to basic science studies in many research areas (Bolli et al., 2004). An overview of the main potential shortcomings of current research efforts into acute myocardial infarction is provided below and discussed subsequently in relation to the aims of this thesis.

i Experimental models

As with any pre-clinical research, experimental models emulating the pathology of interest are required to investigate, develop and refine potential interventions prior to their clinical application. A number of models of ischaemia-reperfusion injury have been developed and employed to investigate the mechanisms of ischaemia-reperfusion and efficacy of potential therapeutic interventions. This thesis will not examine *in vitro* models of ischaemia-reperfusion since these are employed mainly for the dissection of molecular pathways and interactions but will instead focus on the merits and limitations of current *in vivo* models and their relevance for clinical translation.

Good scientific practice requires the research model best represent the clinical situation and yet also controls possible experimental variables between subjects. Unfortunately this has often led to very simplified models of pathology. Pre-clinical studies are often only undertaken using young, male and otherwise healthy animals where the pathology of interest is initiated with a defined onset and severity. The potential effects of this for subsequent clinical translation are discussed below for acute myocardial infarction.

Gender: Epidemiological studies have highlighted the increased risk of cardiovascular disease in males suggesting that there is some inherent physiological difference in susceptibility to myocardial infarction. The majority of basic science research models utilise only male animals in efforts to reduce potential variables between study subjects, although clinical trials of potential cardioprotective therapies are necessarily conducted on mixed gender cohorts (reviewed by Bolli et al., 2004; Miura and Miki, 2008).

The potential effects of this bias of male subjects in the study of ischaemia-reperfusion injury are highlighted by studies comparing susceptibility to infarction between male and female animals where it has been demonstrated that females exhibit significantly lower occurrence of arrhythmias (Humphreys et al., 1999), improved functional recovery and reduced infarct sizes compared to their male counterparts (Song et al., 2003; Wang et al., 2005). Furthermore, young female mice have been shown to be more resistant to IPC and there is evidence to suggest that these sex differences may in part be due to increased Akt phosphorylation in females (Camper-Kirby et al., 2001; Turcato et al., 2006). Indeed, this increased Akt phosphorylation has been confirmed in human post-mortem myocardial samples (Camper-Kirby et al., 2001). It may be useful to use mixed sex groups with sufficient sample sizes to compare cardioprotection between sexes.

Co-morbidities and age: Acute myocardial infarction patients are often aged and present with comorbidities such as diabetes, hypercholesterolemia and hypertension and yet the majority of experimental studies utilise young otherwise healthy animals (reviewed by Bolli et al., 2004; Miura and Miki, 2008). This is particularly important since a number of co-morbidities cause altered pro-survival signalling, for example the PI3K-Akt signalling pathway is perturbed in the diabetic rat heart (Tsang et al., 2005).

A further effect of comorbidities is that acute myocardial infarction patients often have a background of long-term pharmacological treatment, for example with anti-diabetic or anti-hypertension agents. The potential effect of background of drug therapy was stressed by Ferdinandy et al. (2007) who highlighted the potential confounding effects of ‘poly-pharmacology’ and comorbidities on the response to ischaemia-reperfusion and cardioprotective therapies (Ferdinandy et al., 2007).

An exhaustive review of the effects of gender, comorbidities (including age) and concomitant drug therapies is beyond the scope of this thesis. However, the potential effects of these often neglected clinical variables may account in part for the poor clinical translation of cardioprotection research and should be considered when interpreting the results of basic science research models where these variables are not included.

ii Experimental endpoints

Further to concerns over the simplification of experimental models compared to the clinical setting, the focus and clinical relevance of endpoints for assessing efficacy are important potential factors affecting clinical translation of basic science research.

The majority of basic science cardioprotection studies use histological measurement of infarct size as the primary endpoint to assess cardioprotective efficacy. Infarct size is considered to be an important predictor of the long-term prognosis of acute myocardial infarction patients, as first formally demonstrated by Sobel et al. (1972) by correlation of serial serum creatine kinase (CK) levels with cardiac complications and long-term patient survival (Sobel et al., 1972). Given the prognostic value of infarct size, it is expected that histological assessment of infarct size in basic science studies should provide a good indicator of cardioprotective efficacy with some further considerations.

Time-points of infarct size assessment: Many basic science experiments measure infarct size at a single time-point and often following only a relatively short reperfusion duration. It is not clear whether infarct size at reperfusion durations as short as 2 hours correlates well with long-term infarct size and cardioprotection (Bolli et al., 2004). This is a potential factor affecting poor clinical correlation since clinical studies often use serial assessments of serum enzymes to assess infarct size (Thygesen et al., 2007).

Crucially, reductions in infarct size observed at short periods of reperfusion may not represent a true cardioprotective effect but may instead represent a temporary delay in infarct development and not an ultimate decrease in final infarct size (Kloner, 1993). This has been reported for platelet-activating factor (PAF) receptor antagonists which significantly reduced infarct size at 3 hours reperfusion but not at 6 hours reperfusion suggesting that PAF receptor antagonists delay but do not ultimately reduce infarct size in dog hearts (reviewed by Black and Rodger, 1996).

The duration of reperfusion at which infarct size is examined at may also reflect differences in infarct size limiting effects and long-term remodelling effects meaning that it is therefore pertinent that basic science studies of cardioprotection examine infarct size at reperfusion durations which are closely matched to meaningful clinical correlates.

Clinical correlates: Clinically, blood serum levels of cardiac enzymes are used as an important predictor of infarct size. However, small animal studies rely on histological measures of infarct size and rarely measure cardiac enzyme levels; this difference in endpoints of injury may affect the cardioprotective efficacy viewed between these studies and may therefore contribute to poor clinical translation (Miura and Miki, 2008).

It would be beneficial for pre-clinical and clinical studies to employ similar methods for determining primary endpoints, although this has been complicated by technical issues with repeated blood sampling of small animals and direct infarct size assessment in patients. Recent advances in pre-clinical and clinical imaging may ameliorate these differences in clinical correlates by enabling increasingly accurate *in vivo* measurements of infarct size (Thygesen et al., 2007); discussed in detail subsequently (see 1.5.2).

Myocardial salvage: Although imaging techniques permit *in vivo* assessment of myocardial infarct size and therefore longitudinal tracking of infarct size over prolonged reperfusion durations, these studies do not yet allow assessment of myocardial salvage. Myocardial salvage considers the area of ischaemic myocardium, termed the 'area-at-risk' (AAR) and therefore provides a more robust evaluation of the extent of protection (Reimer et al., 1977). However, current *in vivo* AAR measurements have not been fully validated and are often not undertaken in clinical assessments of infarct size. Since AAR is a strong determinant of final infarct size and is highly variable in patients, failure to consider AAR reduces the statistical power and thus ability to detect significant protection (reviewed by Miura and Miki, 2008).

Since clinical trials of potentially cardioprotective interventions often do not consider myocardial AAR when reporting infarct size as an endpoint, it is possible that the statistical power of these trials is insufficient to detect changes in absolute infarct size. This is beginning to be addressed in both pre-clinical and clinical studies by the use of novel *in vivo* imaging methods; this is discussed below and investigated in this thesis.

Although it is not feasible for each cardioprotection study to address all of the concerns of experimental design that may contribute to poor translation of pre-clinical research, it is advisable that the potential limitations of basic science studies are evaluated for the interpretation results. This thesis will investigate the use of longitudinal endpoints to assess cardioprotective efficacy of the mitochondrial targets described above (see 1.4).

1.5.2. Magnetic resonance imaging for evaluating cardioprotection

Magnetic resonance imaging (MRI) is a valuable, non-invasive imaging modality with significant potential for pre-clinical and clinical evaluation of cardiac function and infarct size in the setting of acute myocardial infarction (Thygesen et al., 2007).

i Basic overview of MRI

MRI provides an *in vivo* method to interrogate the characteristics of tissues within the body, including the heart, by exploiting its inherent physical properties and the effects of paramagnetic contrast agents on this. An in-depth discussion of the physical basis of MRI is beyond the scope of this thesis however, the specific MRI techniques employed in this thesis are described in detail in chapter 3. Briefly, a high strength magnetic field causes the natural proton spins of hydrogen atoms within the tissues to align in the direction of the magnetic field. Radiofrequency (RF) energy is then applied in short pulses which temporarily excite the proton spins away from the magnetic field direction. Between RF pulses, the protons release this energy and return to directional alignment with the magnetic field. The energy dissipated upon relaxation of the proton spins is recorded by array coils and is defined by two parameters: T_1 and T_2 which are characteristic of the tissue interrogated and the presence of any contrast agents (McRobbie et al., 2006; Edwards et al., 2009).

T_1 relaxation time: also termed spin-lattice relaxation time; this describes the rate constant of time taken for proton spins to realign with the main magnetic field and is greatest in water based tissues which appear dark on T_1-weighted MRI.

T_2-relaxation time: also termed spin-spin relaxation time; this describes the rate constant of time taken for proton spins to loose synchronicity with each other (i.e. become out of phase) and is greatest in water based tissues which appear bright on T_2-weighted MRI.

Since tissues vary in their inherent T_1- and T_2-relaxation characteristics, MRI allows interrogation of specific tissue characteristics and potential pathological changes. Contrast agents that specifically affect relaxation characteristics can provide further characterisation of tissues (McRobbie et al., 2006; Edwards et al., 2009).

Given its non-invasive and detailed tissue characterisation abilities, MRI represents an important tool for longitudinal studies of cardioprotective efficacy. A number of pre-clinical and clinical studies have examined the use of cardiac MRI to determine infarct size and cardiac function following acute myocardial infarction. The principal uses and advances in cardiac MRI are described below and investigated in chapter 8.

ii Infarct size assessment by MRI

Late-gadolinium enhancement (LGE) MRI allows *in vivo* assessment of infarct size. LGE imaging relies on administration of a paramagnetic gadolinium (Gd)-based contrast agents such as Gd-DTPA (diethylene-triamine penta-acetic acid). Gd-DTPA is a stable and highly paramagnetic contrast agent which reduces T_1-relaxation time at very low concentrations (Weinmann et al., 1984). Gd-DTPA is cell membrane impermeable and thus remains in the extracellular space; however, where membrane integrity is compromised, for example by infarction, Gd-DTPA enters damaged cells and therefore shows an increased distribution and thus hyperenhanced area on T_1-weighted MRI (McRobbie et al., 2006), (Figure 1.17).

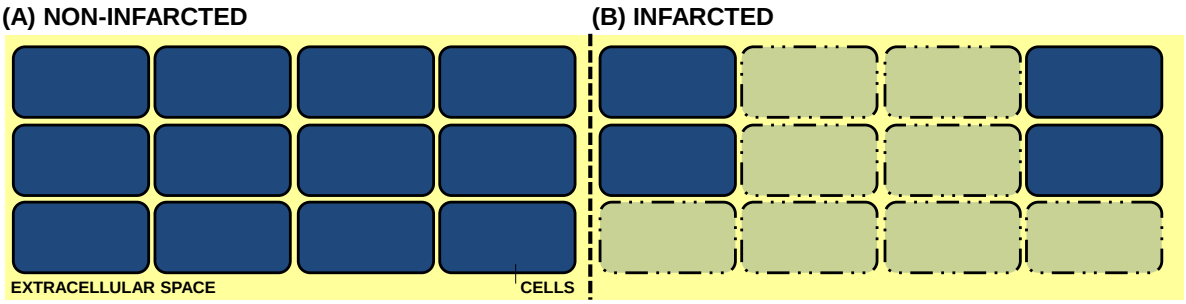

Figure 1.17: Late-gadolinium enhancement MRI of infarction
(A) Gadolinium-based contrast agents (indicated in yellow) are cell impermeable and thus remain in the extracellular space. (B) In areas of infarction, loss of cell membrane integrity permits a wider distribution of Gd and delayed T_1-relaxation. Modified from Ordovas and Higgins (2011).

LGE MRI was first used to assess myocardial infarction in 1984 to study dog hearts *ex vivo* following 24 hours coronary artery ligation (Wesbey et al., 1984). However, improved imaging techniques were required to facilitate the use of LGE imaging for infarct size quantification, namely increased magnetic field strengths and the development of inversion-recovery sequences (reviewed by Arai, 2011b). T_1-weighted inversion-recovery imaging increases the contrast of T_1-weighted images to produce heavily weighted T_1-images. This allows the signal from the normal myocardium to be effectively nulled to allow accurate delineation of the area of Gd-DTPA accumulation, which appears bright. Increased magnetic field strengths have also allowed relatively high resolution images of small animal hearts, including the mouse heart, using ECG-gated image acquisition (McRobbie et al., 2006).

LGE MRI is now commonly used to image myocardial infarction clinically and also a number of small animal models of ischaemia-reperfusion injury (reviewed by Geelen et al., 2012). LGE MRI has also been applied to assess chronic infarct remodelling since the extracellular space remains increased following fibrosis and infarct healing; this is discussed further in chapter 8 (reviewed by Ordovas and Higgins, 2011).

Validation of infarct size quantification: Numerous studies have validated the use of LGE MRI for infarct size quantification. Kim et al. (1999) first investigated the use of LGE MRI for infarct size quantification in dog hearts subjected to ischaemia with or without reperfusion by comparing LGE MRI quantification of infarct size to 'gold-standard' histological staining using triphenyltetrazolium chloride (TTC) (described in chapter 3). This study showed excellent correlations between infarct size quantification by LGE MRI and histology in both non-reperfused and reperfused hearts at 1 and 3 days and 8 weeks (Kim et al., 1999). Further studies have also validated the use of LGE MRI pre-clinically in numerous animal models of ischaemia-reperfusion injury, including the reperfused mouse heart. The seminal study by Yang et al. (2004) provided the first validation of LGE MRI determination of infarct size in mice following 60 minutes ischaemia and 24 hours reperfusion. Pre-clinical LGE MRI of small animals has since been established at a number of research centres.

Validation of LGE MRI for clinical assessment of myocardial infarct size has proved more challenging since it is not often possible to compare LGE and histological quantifications of infarct size. An initial study of LGE MRI for assessing patients prior to revascularisation surgery (non-acute patients) demonstrated that LGE was able to delineate areas of reversible myocardial dysfunction, however, this study did not quantify infarct size (Kim et al., 2000). A subsequent study by this group demonstrated that infarct size determined by LGE MRI is reproducible within patients and also correlated well with infarct size determined by single photon emission computed tomography (SPECT) (Mahrholdt et al., 2002). Further to this, Arai's group showed that infarct size quantification by LGE MRI in acute myocardial infarction patients correlated well with clinical indices of infarct size including serum cardiac enzyme level (troponin I), ejection fraction and regional wall thickening (Ingkanisorn et al., 2004). This was further confirmed in a large multi-centre study in 2008 which showed excellent agreement between LGE infarct size and creatine kinase (CK) serum levels (Kim et al., 2008). This latter study also constitutes an important landmark in the use of LGE since it confirmed that the technique is sufficiently robust to permit valid multi-centre trials.

These initial pre-clinical and clinical studies validated the use of LGE MRI to accurately determine the presence, spatial localisation and extent of infarction and formed the basis for the now widespread application of LGE MRI *in vivo* determination of infarct size (reviewed by Ordovas and Higgins, 2011). Given its non-invasive nature, LGE MRI provides an important tool for investigating infarct size in longitudinal studies of cardioprotective efficacy and will be examined further in this thesis.

iii Myocardial salvage – Quantification of area-at-risk

Infarct size is clearly an important factor in determining the prognosis of acute myocardial infarction patients and is therefore the most commonly assessed endpoint for clinical and pre-clinical studies of cardioprotective efficacy. However, interpretation of infarct size data requires an appreciation of the area of the myocardium that was 'at risk', termed the 'area-at-risk' (AAR). Assessment of infarct size alone does not consider the area of myocardium at risk of injury and therefore reduces the statistical power; this was discussed above in relation to poor clinical translation of cardioprotection studies and is therefore an important area for development of future studies.

In pre-clinical studies, AAR can be quantified by *ex vivo* histological staining following re-occlusion of the coronary ligation and perfusion of coloured dyes (such as Evans blue) or fluorescent microspheres (reviewed by Black and Rodger, 1996). However, this is not possible in clinical or longitudinal basic science studies and therefore presents the need for a method of quantifying AAR *in vivo*. A number of MRI-based protocols have been examined to this end; a basic overview and the theoretical basis of these methods is provided in Table 1.5 and further discussed below (reviewed by Arai, 2011a).

MRI METHOD	THEORETICAL BASIS AND OVERVIEW
T_2-weighted: (Aletras et al., 2006) (Friedrich et al., 2008)	Based on oedema. Relies on assumption that oedema is confined to AAR such that the area of oedema is equal to the AAR. Good agreement in AAR quantification with histology.
Pre-contrast T_1-weighted: (Ugander et al., 2012) (Ferreira et al., 2012)	Same basis as T_2-weighted MRI; Good agreement in AAR determined by pre-contrast T_1 and T_2 with histology – not as widely investigated. Likely to give similar problems as T_2-MRI (see text).
Early Gd enhancement: (EGE) (Matsumoto et al., 2011)	Gd enhancement images taken 2-3 minutes after Gd bolus. Good correlation of AAR determined by EGE and T_2-weighted MRI. May not be feasible in small animals due to longer scan times needed.
Late Gd enhancement: (O'Regan et al., 2009) (Ubachs et al., 2010) (Fuernau et al., 2011)	Estimate AAR based on transmural and circumferential extent of infarction. Shown to underestimate AAR. Unlikely to provide valid estimate in cardioprotected hearts. Poor correlation to AAR in patients (Fuernau et al., 2011) - Table 1.6
First pass perfusion: (Gonzalez et al., 2008)	Administration of Gd during ischaemia. Clinically impractical. Potentially beneficial since single administration allows AAR and infarct size quantification at different time-points. Gonzalez et al. (2008) have used first pass perfusion imaging to assess microvascular obstruction at reperfusion.
Manganese contrast: (Natanzon et al., 2005)	Manganese (paramagnetic cation) usually enters cells via voltage-gated calcium channels; uptake impaired during ischaemia. Administered during ischaemia and imaged 2 hours after reperfusion to accurately quantify AAR. Not ready for clinical tests.

Table 1.5: Potential MRI-based methods for *in vivo* quantification of AAR
Summary of MRI methods to quantify AAR *in vivo*. References provided for principal studies describing these methods and validation against histology. Reviewed by Arai (2011a).

Cardiac MRI therefore represents an important tool for potentially quantifying AAR *in vivo* in both pre-clinical and clinical studies of cardioprotection. Of the MRI methods detailed above, T_2-weighted based MRI has been most widely investigated, likely due to its methodological simplicity (reviewed by Arai, 2011a); AAR assessment by T_2-based MRI is discussed in detail below and examined in chapter 8.

Area-at-risk assessment by T_2-weighted MRI: Assessment of AAR by T_2-based MRI methods is based on the pathophysiology of ischaemia-reperfusion injury whereby the area of myocardium subjected to ischaemia and reperfusion develops oedema, as described previously (see 1.2.3). It has therefore been hypothesised that only the AAR (i.e. the area subjected to ischaemia) will develop significant oedema and thus the area of oedema may be used to approximate the AAR (Garcia-Dorado et al., 1993). Indeed, Abdel-Aty et al. (2009) showed that oedema develops within the AAR following only short durations of ischaemia that did not induce any infarction (Abdel-Aty et al., 2009). T_2-weighted MRI exploits the known linear correlation between tissue water content and T_2-relaxation time, whereby areas exhibiting oedema and thus increased water content appear bright on T_2-weighted MRI images (reviewed by Garcia-Dorado et al., 2012).

MRI T_2-relaxation times within the infarcted myocardium were first investigated by Higgins et al, in 1983 and were shown to correlate well with established measurements of myocardial water content (reviewed by Arai, 2011a). A number of pre-clinical and clinical studies have since investigated the use of T_2-based MRI to quantify myocardial AAR (reviewed by Ordovas and Higgins, 2011; Arai, 2011a). The first demonstration that *in vivo* cardiac T_2-weighted MRI could be used to accurately quantify myocardial AAR was published by Aletras et al. (2006) in dog hearts following 2 days reperfusion. Subsequent studies have extended these findings to numerous pre-clinical animal models of ischaemia-reperfusion injury and have demonstrated good correlations between the putative AAR determined by *in vivo* T_2-MRI and the true AAR determined by established histological methods (Bohl et al., 2010; Mewton et al., 2011; Beyers et al., 2012). Furthermore, recent clinical studies have suggested that T_2-weighted cardiac MRI may also permit *in vivo* AAR quantification in reperfused acute myocardial infarction patients (Berry et al., 2010; Fuernau et al., 2011).

A summary of the main studies validating the use T_2-MRI for *in vivo* quantification of AAR following ischaemia-reperfusion injury is provided in Table 1.6.

STUDY	METHODOLOGICAL DETAILS	SUMMARY OF FINDINGS
DOG		
Aletras et al. (2006)	90 minutes ischaemia and 2 days reperfusion, n=9; Cardiac T_2-weighted MRI; Compared to histological microsphere perfusion.	Good correlation between T_2-MRI and microsphere AAR (r=0.84). Oedema had completely resolved at 2 months reperfusion.
Ugander et al. (2012)	120 minutes ischaemia and 4 hours reperfusion, n=9; Cardiac T_2-weighted and T_1-weighted MRI Compared to histological microsphere perfusion.	Good correlation between T_2-MRI and histology AAR (r=0.96); Good correlation between T_1-MRI and histology AAR (r=0.94); Agreement in T_2- and T_1-MRI assessments of AAR (r=0.95).
PIG		
Mewton et al. (2011)	40 minutes ischaemia and 90 minutes reperfusion, n=15; Cardiac T_2-weighted MRI – both T_2(STIR) and T_2(ACUTE) - hybrid of SSFP and TSE. Compared to histological perfusion of Uniperse blue dye.	Good correlation between MRI and histology AAR for both T_2-MRI methods tested: T_2(STIR) (r=0.72); T_2(ACUTE) (r=0.65).
MOUSE		
Bohl et al. (2010) *Abstract only – few methodological details*	45 minutes ischaemia and 24 hours reperfusion Cardiac T_2-mapping MRI; Compared to histological perfusion of dye (details not given)	Correlation of MRI and histology AAR depended on analysis method (T_2-value 1, 2 or 3 S.D. ± mean): Best correlation using 1 S.D. ± mean with manual correction (r=0.99).
Beyers et al. (2012)	20 minutes ischaemia and 2 days reperfusion, n=10; Cardiac T_2-weighted MRI; Compared to histological perfusion of phthalo blue.	*AAR varied by differential placement of ligating suture to allow powerful correlation analysis.* Good correlation between T_2-MRI and histology (r=0.86).
HUMAN – ACUTE MYOCARDIAL INFARCTION PATIENTS (Reperfusion durations approximate only)		
Berry et al. (2010)	Acute myocardial infarction patients, n=50; Cardiac T_2-SSFP Compared to angiography jeopardy score (APPROACH).	Good correlation between MRI and angiography jeopardy score (r=0.78).
Fuernau et al. (2011)	Acute myocardial infarction patients, PPCI within 12 hours of onset of ischaemia, 2-4 days reperfusion, n=197; Cardiac MRI: T_2-weighted, LGE. Compared to angiography jeopardy score (APPROACH).	Good correlation between T_2-MRI and angiography jeopardy score (r=0.87). Poor correlation between LGE AAR and angiography (r=0.44) and between LGE AAR and T_2-MRI AAR (r=0.56).

Table 1.6: Area-at-risk quantification by *in vivo* T_2-based MRI
Summary of principal studies validating the use of *in vivo* T_2-based MRI for the quantification of myocardial AAR. Selected references provided for principal studies describing these methods and validation against histology.

Evaluation of area-at-risk quantification by T_2-based MRI: Given the promising nature of these initial studies validating the use of T_2-based cardiac MRI for quantifying myocardial AAR *in vivo*, there is considerable interest in the use of this technique for calculation of myocardial salvage (AAR minus infarct size) in studies of cardioprotection. As discussed previously, assessment of myocardial salvage is expected to improve clinical trials and longitudinal basic science studies by controlling for variation in AAR (see 1.5.1). Application of this method to the mouse heart is likely to prove more challenging given its smaller size and rapid heart rate. However, recent studies by Bohl et al. (2010) and Beyers et al. (2012) have shown that T_2-weighted based MRI can be used to quantify AAR in the reperfused mouse heart. T_2-mapping cardiac MRI protocols, such as that used by Bohl et al. (2010), are likely to provide improved resolution of myocardial oedema due to the averaging effect of combining the T_2-relaxation values from multiple images at different echo times; this approach is investigated in chapter 8.

However, despite these initial validation studies, there remain concerns over the robustness of T_2-based MRI quantification of AAR, particularly concerning the potential effects of cardioprotective interventions on the development of oedema (Wince and Kim, 2010; Mewton et al., 2011). To date this has not been sufficiently investigated and represents an important area of future research. Thuny et al. (2012) demonstrated that ischaemic post-conditioning (IPost) of acute myocardial infarction patients significantly reduced the area exhibiting oedema. This is supported by an early pre-clinical study of IPost in dog hearts where both IPC and IPost were shown to significantly reduce the extent of myocardial oedema (Zhao et al., 2003). Crimi et al. (2013) also recently showed a similar reduction in the area of myocardial oedema in patients treated with remote ischaemic postconditioning (RIPost) (Crimi et al., 2013). These studies therefore appear to invalidate the use of T_2-based MRI for quantification of AAR in subjects treated with these interventions. However, Lonborg et al. (2012a; 2012b) showed that infarct size reduction by exenatide did not affect myocardial oedema. These apparently conflicting results suggest a need for further validation of T_2-based MRI methods for *in vivo* AAR quantification and more robust MRI methods may be required.

Cardiac MRI represents a valuable tool for interrogating numerous myocardial parameters following ischaemia-reperfusion injury. There is a clear requirement for an *in vivo* method of determining AAR (combined with current methods for quantifying infarct size) for clinical and pre-clinical studies of cardioprotection. Although LGE MRI allows accurate and robust infarct size quantification, *in vivo* measurement of AAR remains a significant challenge. This thesis will investigate the use of small animal MRI to develop and validate a cardiac MRI method for determining AAR *in vivo* to facilitate subsequent longitudinal pre-clinical studies; described in chapter 8.

CHAPTER 2: RESEARCH OBJECTIVES

The overall aim of this thesis was to investigate the potential modulation of mitochondrial proteins to elicit long-term cardioprotection against myocardial ischaemia-reperfusion injury. The main objectives and research aims examined in this thesis are summarised below and described in detail in the following chapters.

Objective 1: The first objective of this thesis was to develop and characterise a mouse *in vivo* recovery model of ischaemia-reperfusion injury for subsequent investigations of long-term cardioprotective efficacy. The principal research aims to achieve this were:

(1) Establish a mouse *in vivo* recovery model of ischaemia-reperfusion injury;

(2) Validate this *in vivo* recovery model of ischaemia-reperfusion by application of known therapeutic interventions to demonstrate significant cardioprotection;

(3) Characterise this *in vivo* recovery model of ischaemia-reperfusion injury to determine the optimum protocol for subsequent applications of the model.

The completion of this objective is described in chapter 4.

Objective 2: The second objective was to investigate the role of Cyp-D inhibition (by genetic ablation) as a therapeutic target against the long-term effects of myocardial ischaemia-reperfusion injury. The principal research aims to achieve this were:

(1) Investigate the long-term cardioprotective efficacy of Cyp-D inhibition in the established model of global genetic ablation of Cyp-D;

(2) Investigate the role of Cyp-D in the heart by establishing and investigating a model of cardiac-specific genetic ablation of Cyp-D.

This objective was examined in chapter 5 of this thesis.

Objective 3: The third objective was to investigate modulation of Sirt-3 as a potential therapeutic target against the effects of *in vivo* myocardial ischaemia-reperfusion. The principal research aims to achieve this objective were:

(1) Investigate the effect of Sirt-3 genetic ablation on the development of myocardial infarction in response to *in vivo* myocardial ischaemia-reperfusion;

(2) Investigate the effect of fasting-induced Sirt-3 overexpression on development of myocardial infarction in response to *in vivo* myocardial ischaemia-reperfusion.

This objective was examined in chapter 6 of this thesis.

Objective 4: The fourth objective was to investigate the role of mitochondrial DJ-1 in the heart, specifically its potential role in the pathophysiology of ischaemia-reperfusion. The principal research aims to achieve this objective were:

(1) Investigate the role of DJ-1 in normal cardiac physiology and function;

(2) Investigate the role of DJ-1 in the pathophysiology of myocardial ischaemia-reperfusion injury.

This objective was examined in chapter 7 of this thesis.

Objective 5: The final objective of this thesis was to characterise and validate a method for determining area-at-risk *in vivo* in the mouse heart following ischaemia-reperfusion injury. The principal research aims to achieve this objective were:

(1) Develop and validate an *in vivo* cardiac MRI method/s for accurate assessment of myocardial area-at-risk in mice subjected to ischaemia reperfusion;

(2) Investigate the validity of these *in vivo* cardiac MRI assessments of AAR in the presence of cardioprotective strategies.

This objective was examined in chapter 8 of this thesis.

CHAPTER 3: GENERAL RESEARCH METHODS

This chapter describes the methodological approaches employed in this thesis with specific experimental details subsequently provided in the relevant results chapters.

3.1. Experimental use of animals

The use of animals in these studies was in accordance with the United Kingdom Animal (Scientific Procedures) Act of 1986 and local guidelines. All mice were subject to an initial examination prior to experimental use and any animals showing signs of poor health or barbarisation were excluded from use. Surgery was performed in accordance with best practice described by the Handbook of Laboratory Animal Management and Welfare (Wolfensohn and Lloyd, 2003) and extensive advice sought from the Named Animal Care Welfare Officer (NACWO) at the facility at University College London, UK.

Mice were housed in 12 hour light / dark cycles with standard chow provided *ad libitum*. All experiments used male mice aged 10-16 weeks old, unless otherwise stated. Daily care of animals was provided by technical staff at University College London, UK.

3.1.1. Standard mouse strains

All characterisation experiments presented here were undertaken using commercially available mouse strains of either B6/SV129 or C57BL/6 genetic backgrounds. B6/SV129 (B6SV129F1) mice were purchased from Harlan Laboratories, UK and C57BL/6 mice (inbred sub-strain C57BL/6NCrl) were purchased from Charles River Laboratories, UK. Mice were purchased aged 9-10 weeks and allowed a minimum of one week acclimatisation at the animal facility prior to experimental use. Most studies using commercially available mice presented here were undertaken on B6/SV129 mice since these were used previously within our laboratory and were considered the closest genetic background to the original Cyp-D genetic knockout mice utilised subsequently.

3.1.2. Transgenic mouse lines

A number of transgenic mouse lines were employed in this thesis; an overview of the methods concerning their use is provided here and specific details given subsequently.

Generation of transgenic mice: The transgenic animals used here were generated by external sources and imported into our facility. Transgenic animals were created using standard genetic modification methods involving generation of specifically mutated embryos and re-implantation to produce mutated progeny; this is summarised in Figure 3.1 and the specific details of each colony are provided in the subsequent chapters.

Briefly, transgenic animals were created by transfection of cultured embryonic stem (ES) cells with a targeting construct designed to disrupt or delete the target gene (Figure 3.1 A). Targeting vector constructs were specifically designed to contain homologous sequences to the target region of the endogenous ES cell genome and a neomycin-resistance gene (*neo*). Upon homologous recombination of the targeting vector and endogenous ES cell genome, the vector sequence becomes integrated into the ES cell genome causing mutation or total deletion of the target gene (Figure 3.1 B). Concurrent insertion of the *neo* gene confers neomycin resistance, which allows selection of mutant ES cells upon neomycin treatment which therefore kills only untargeted cells (Figure 3.1 C). Mutant ES cells were injected into blastocysts from donor mice and subsequently re-implanted into host mice to generate chimeric and wildtype progeny (Figure 3.1 D). Chimeric animals were crossed with wildtype mice to generate progeny including animals heterozygous for the mutation (Figure 3.1 E). Variations of this technique using sophisticated targeting vectors can be used for insertion or overexpression of the target gene, including cardiac-specific expression systems described below. This method of genetic modification produces stable germ line mutations to allow the subsequent generation of transgenic colonies (Mortensen, 1993; reviewed by Alberts et al., 2002).

All transgenic mice used here were backcrossed to differing degrees onto a C57BL/6 genetic background. Standard terminology is used throughout this thesis to describe the genotypes: wildtype (WT; +/+), heterozygote (HET; +/-) and knockout (KO; -/-).

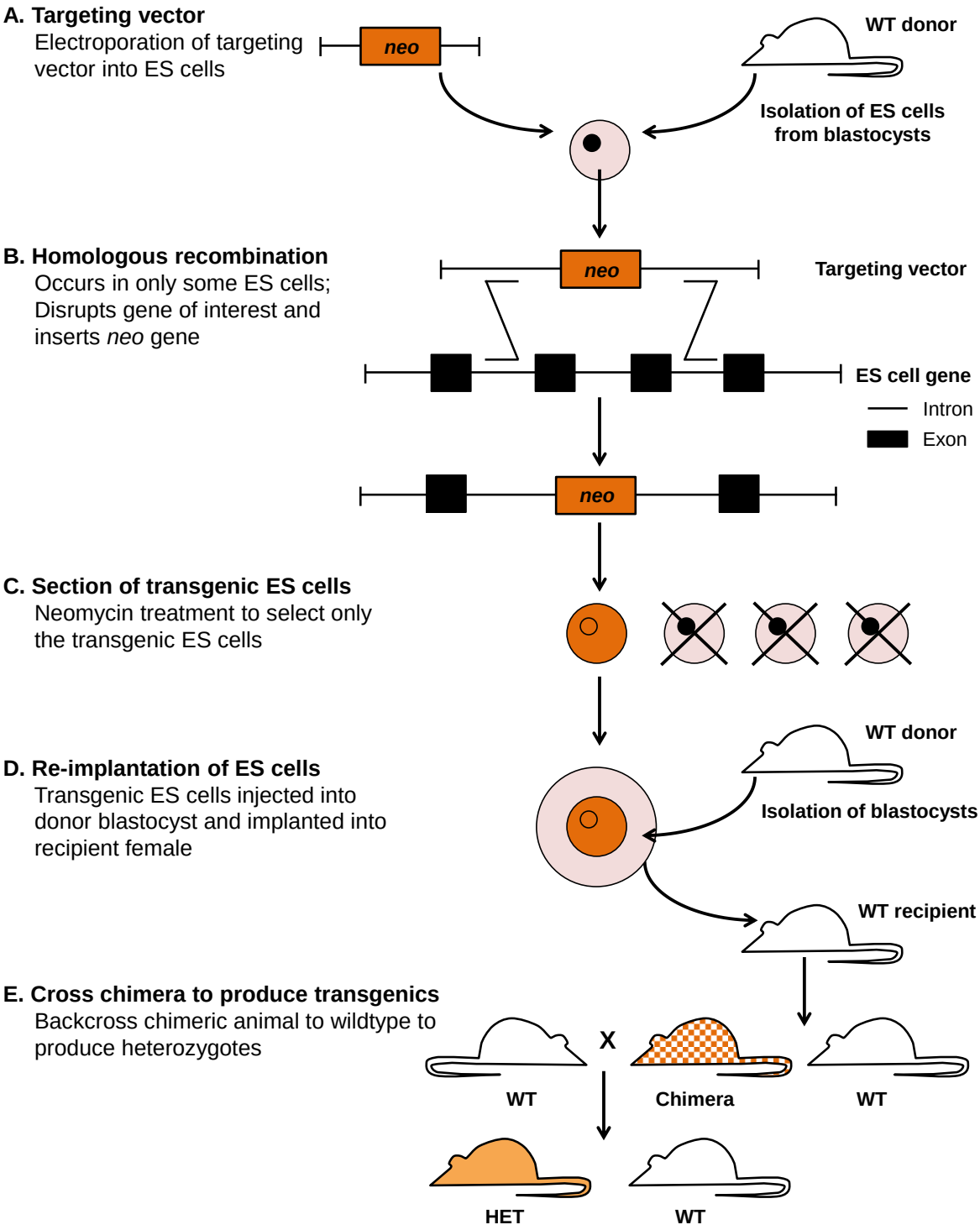

Figure 3.1: Standard method for generating transgenic mouse colonies
A) A targeting vector complementary to the target gene is inserted into ES cells. B) Homologous recombination occurs between the targeting vector and endogenous ES cell gene to disrupt the target gene and insert *neo*. C) Mutant ES cells can be selected by resistance to neomycin treatment. D) Mutant ES cells are microinjected into donor blastocysts to create progeny chimeric for the mutation. E) Chimeric animals are crossed with WT mice to produce heterozygous mice. Constructed from information provided by Mortensen (1993) and Alberts et al.(2002).

Generation of transgenic animals was completed by other research groups or commercial suppliers and animals from stage E imported into our laboratory.

i Global genetic ablation

The most widely used and simple transgenic system utilised in this thesis is global genetic ablation of the target gene. Global genetic knockout animals were originally created using the method described in Figure 3.1 above and imported into our laboratory. The precise details of these mice are provided in the results chapters.

***Colony maintenance*:** All breeding of animals undertaken as part of this thesis was in accordance with UK Home Office procedures and local guidelines. The health of all animals was closely monitored with particular attention given to breeding females.

Animals were bred as a ratio of two females per male and progeny weaned at 3-4 weeks old. All experiments using genetically modified animals were undertaken using true littermate control animals to minimise any effects of divergence of in-bred colonies over extended breeding periods. All transgenic colonies in these studies were maintained by heterozygote breeding crosses to give progeny of all combinations of genotypes according to expected Mendelian ratios (Figure 3.2). The genotype of each animal was determined prior to experimental use as described below in section iii.

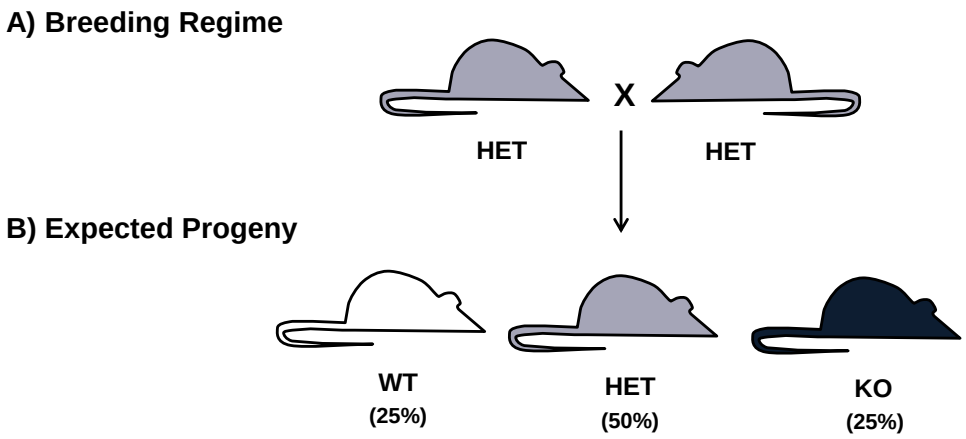

Figure 3.2: Standard maintenance of genetically modified mice colonies
A) Genetically modified mouse strains were maintained as heterozygote crosses (HET x HET). B) This produced progeny of all genotypes at expected Mendelian ratios (indicated in brackets).

ii Cardiomyocyte-specific genetic ablation

Temporal and spatial genetic ablation of a target gene was investigated using an inducible cardiomyocyte-specific knockout model. Inducible and tissue-specific genetic ablation of a gene of interest allows investigation of tissue- and time-specific roles of that gene; theoretically providing tissue and target selectivity advantages over many pharmacological inhibition studies (reviewed by Doetschman and Azhar, 2012).

Rationale of inducible cardiomyocyte-specific genetic ablation: Temporal and spatial regulation of genetic ablation is achieved by inducible site-specific genetic recombination. Generation of these animals was based on the transgenic method described above (Figure 3.1). An overview of the cardiac-specific model of genetic ablation used here is provided in Figure 3.3 and described below and in chapter 5.

Temporal regulation: Genetic recombination can be induced using Cre-recombinase technology which was first developed and successfully applied to mouse transgenic models in 1995 (Metzger et al., 1995). The Cre-recombinase protein (referred to as 'Cre') causes recombination of DNA recognition sites, *loxP* sites, placed flanking the target gene sequence (Figure 3.3 B). *LoxP* sites are specific 34 base pair (bp) sequences containing a core sequence (8 bp) surrounded by inverted repeated sequences (13 bp). The orientation of *loxP* sites determines whether Cre-recombination causes deletion or inversion of the flanked sequence (Figure 3.3) (Metzger et al., 1995).

Regulation of Cre-recombination is mediated by fusion of Cre to a mutated oestrogen receptor (Mer) which is insensitive to oestrogen but activated by tamoxifen (an oestrogen receptor antagonist) (Metzger et al., 1995). A double Mer-Cre fusion protein (MerCreMer) with significantly higher Cre-recombinase activity was used in this thesis (Sohal et al., 2001). MerCreMer is continually expressed and remains in the cytoplasm; however, upon tamoxifen exposure, MerCreMer enters the nucleus where it exerts its effect to cause *loxP* site recombination. This ensures that recombination occurs only upon tamoxifen treatment, thus providing temporal regulation (Metzger et al., 1995).

In addition to the use of *loxP* genetic manipulation for temporal regulation, a simplified protocol using insertion of *loxP* recombination sites surrounding the target gene (or specific exons) can be used to generate global genetic ablation models. This method involves crossing floxed animals with EIIa Cre-recombinase mice (developed by Lakso et al., 1996) which ubiquitously express Cre during early embryonic development, thereby allowing the genetic modification resulting from Cre-recombination to be transmitted to the progeny (Lakso et al., 1996). This method allows generation of mice with global genetic modifications for the development of a standard transgenic colony.

Spatial regulation: Tissue specificity of this genetic modification system is achieved by fusion of the MerCreMer complex to the cardiac-specific alpha-myosin heavy chain (α-MHC) promoter (Figure 3.3 A). This causes expression of Mer-Cre in cardiomyocytes, thereby meaning that Cre-driven *loxP* site recombination only occurs in cardiac tissue (Figure 3.3 C) (Sohal et al., 2001; Doetschman and Azhar, 2012). It is important to note that *loxP* target sites are inserted flanking the target gene in all tissues, where the tissue-specificity of recombination is driven by localised expression of MerCreMer, in

this case in cardiac tissue only. This α-MHC-MerCreMer – *loxP* system allows temporal and spatial regulation of a gene (Sohal et al., 2001; Doetschman and Azhar, 2012).

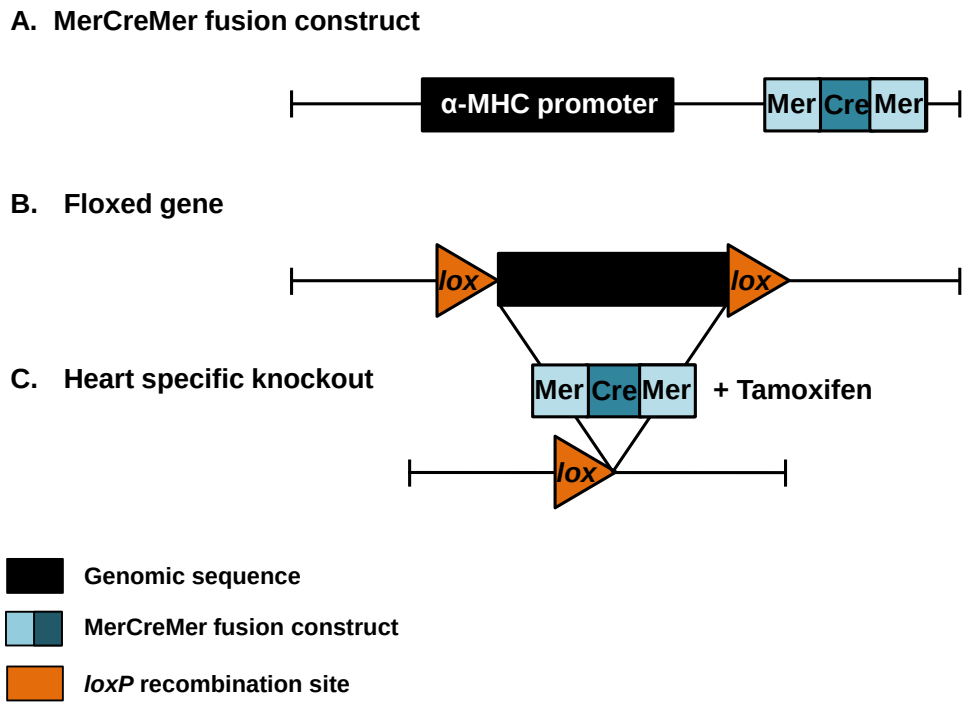

Figure 3.3: Inducible cardiac-specific genetic ablation
A) Cre-recombinase is expressed in a tamoxifen-sensitive manner due to fusion of MerCreMer to the α-MHC promoter. B) The target gene is flanked by *loxP* sites throughout the body. C) Treatment with tamoxifen drives MerCreMer expression in the heart which causes *loxP* site recombination to delete or disrupt the target gene in the heart. Constructed from information provided by Sohal et al. (2001) and Doetschman and Azhar (2012).

Colony maintenance: The precise details of the breeding schedule for the inducible cardiac-specific transgenic model used in this thesis are described in chapter 5.

Standard terminology is used to describe the genotypes of animals: the presence of the MerCreMer construct is described as wildtype (WT; +/+), heterozygote (HET; +/Cre) and mutant (Cre/Cre) and the presence of *loxP* sites is described as wildtype (WT; +/+), heterozygote (HET; +/FL) and mutant (FL/FL). The genotype of each animal was determined prior to use as described below (section iii) and in further detail in chapter 5.

Tamoxifen dosing: The MerCreMer – *loxP* system for genetic ablation described above requires induction of Cre-recombinase activity by tamoxifen (Figure 3.3). The final tamoxifen dosing regime used here was 18 mg/kg (thus 4.5 mg per 25 g mouse) administered as a single intraperitoneal bolus daily for 5 days. Tamoxifen (Sigma-Alrich, UK) was dissolved in vehicle comprising ethanol-100% and corn oil (1 part ethanol to 9 parts corn oil) agitated at 37ºC for a minimum of 4 hours until completely dissolved. Tamoxifen solutions were freshly prepared for each study and stored for a maximum of

6 days at 4ºC. This approximate tamoxifen dose and vehicle have been employed previously within our laboratory and in published literature (Sohal et al., 2001; 20 mg/kg). The precise details of this tamoxifen dosing regime are discussed in chapter 5.

Animals were dosed daily with tamoxifen between 09:00 and 10:00 and monitored closely for the duration of the protocol. Consistent timing of dosing was adhered to throughout the protocol to ensure that the effects of tamoxifen were matched between groups. Control animals were administered a matched volume of vehicle.

Experimental groups: Given the complexity of the genetic manipulation and treatment combinations employed by this genetic ablation model, it is necessary to include a number of control groups to assess the potential confounding effects of floxing (insertion of *loxP* sites) and tamoxifen toxicity. The experimental groups required are outlined in Table 3.1 (reviewed by Davis et al., 2012). Although many studies using this *loxP* – α-MHC MerCreMer system do not employ all of these control groups, it is important to appreciate the potential confounding effects in this model to select appropriate controls.

GROUP (Genotype and treatment)	**DESCRIPTION (Effect examined)**
$Gene^{FL/FL}$ MCM $^{WT/Cre}$ + Tamoxifen	Experimental group – genetic knockout
$Gene^{FL/FL}$ MCM $^{WT/Cre}$ + Vehicle	Experimental group – genetic wildtype
$Gene^{FL/FL}$ MCM $^{WT/WT}$ + Tamoxifen	Control group – controls for tamoxifen toxicity
$Gene^{WT/WT}$ MCM $^{WT/Cre}$ + Tamoxifen	Control group – controls for Cre toxicity
$Gene^{FL/FL}$ MCM $^{WT/WT}$ + Vehicle	Control group – controls for insertion of *loxP* sites

Table 3.1: MerCreMer – *loxP* experimental groups
Experimental groups required for studies of inducible genetic ablation to control for confounding effects of insertion of *loxP* sites and tamoxifen toxicity. Reviewed by Davis et al. (2012).

It is crucial to examine the potential effects of tamoxifen toxicity in this genetic system since tamoxifen has been shown to reduce cardiac function associated with some cardiac remodelling (although this usually resolved 7 – 14 days post-treatment) (Davis et al., 2012). Appropriate use of these control groups is discussed in chapter 5 (see 5.5.2).

Assessment of efficacy of cardiac-specific genetic ablation: The α-MHC-MerCreMer system is expected to result in approximately 70-90% knockdown of gene expression following 5-7 days tamoxifen treatment (Sohal et al., 2001; Davis et al., 2012). The effect of treatment on the levels of the target protein was assessed by Western blot analysis of heart samples isolated from mice following varied durations of tamoxifen dosing. The time-course of protein level reduction depends on the efficiency of genetic ablation and the turnover rate of the existing protein; this is discussed in chapter 5. A description of the Western blot technique used is provided below (see 3.4).

iii Genotyping genetically modified mice

Since all transgenic animals were bred as mixed genotypes (i.e. usually heterozygote crosses as described in Figure 3.2), it was necessary to determine the precise genotype of each animal. Genotyping was undertaken using standard polymerase chain reaction (PCR) of mouse DNA samples. The genotyping method is described below and specific details for each transgenic colony provided in the relevant chapters subsequently.

Mouse biopsies: Ear biopsies for genotyping were obtained from mice immediately following weaning (at approximately 3-4 weeks old). Ear biopsies were taken in a coded manner to allow subsequent identification of animals for genotyping. Ear biopsies were stored at 4ºC for a maximum of one week prior to processing for genotyping, after which ear biopsy lysates were stored at -20ºC until completion of the study.

Preparation of crude DNA lysates: DNA samples were obtained from ear biopsies by protein denaturation using Proteinase-K 1 mg/ml (Qiagen, UK) incubated in lysis buffer, Direct-PCR buffer (Ear, Bioquote, UK), at 55ºC in a heating block overnight. Samples were then mixed and incubated at 55ºC for a further one hour to ensure maximal lysis. Lysis was stopped by Proteinase-K denaturation by incubation at 85ºC for 45 minutes. Crude DNA lysates were cleared of hairs by centrifugation at 8000 RPM for 30 seconds, after which the pellet was discarded and the supernatant used for PCR as below.

Amplification of DNA – Polymerase chain reaction: DNA was amplified by PCR using a thermal cycler (Peltier Thermal Cycler, MJ Research, Canada) fitted with a heated lid. This genotyping technique relies on amplification of a specific region of DNA by assembly of DNA nucleotides (dNTPs) by *Taq* DNA polymerase. A commercially available DNA polymerase kit (Qiagen, UK) was used for all PCR genotyping reactions.

Primer design: Specific primers (short lengths of DNA) were designed for complementary binding to the template DNA to confer the specificity of DNA amplification which permits determination of the genotype of each animal. Primers were specifically designed with optimal DNA sequence, guanine-cytosine (GC) content and melting temperature, informed by established PCR protocols for each mouse strain. Primers were purchased from Eurofins (MG Operon, Germany) manufactured to standard PCR primer quality with MALDI-TOF (matrix-assisted laser desorption / localisation) mass spectrometry analysis and diluted to a stock concentration of 100 µM.

During the PCR, following separation of the double-stranded DNA template, the primers are able to specifically bind to the region of interest on the template DNA to allow amplification of this region only. The resulting DNA PCR products can be distinguished on the basis of their length depending upon the design of the primers. For example, for

genotyping Cyp-D global KO animals used here, primers were designed to bind to Exon-4, Exon-3 and Neo regions of the Cyp-D gene; since the knockout was created by deletion of Exons 1-3 and insertion of Neo, Cyp-D KO animals could be distinguished by generation of a shorter DNA product from Exon-4 (common) and Neo regions compared to the larger product produced by extension of Exon-3 and Exon-4 in wildtype samples.

PCR reactions: PCR reactions were based on a commercially available DNA polymerase kit (*Taq* PCR Core Kit, Qiagen, UK), where the precise constituents of these buffers is detailed in the manufacturer's guidelines (Qiagen, 2010). A PCR master mix was freshly made for each experiment, containing PCR buffer, dNTPs, DNA *Taq* polymerase, appropriate primers and autoclaved distilled water. The PCR buffer contained red and orange dyes (CoralLoad dye) to allow visualisation of the migration of the reaction upon electrophoresis. Crude DNA lysates were added to each reaction. All protocols were optimised to give a final reaction volume of 20 µl; precise details of PCR reactions are described for each transgenic colony in the subsequent chapters.

All PCR experiments included a negative control for DNA contamination comprising an aliquot of master mix (19 µl) and an equivalent volume of autoclaved distilled water (1 µl) in place of a DNA sample. The presence of DNA bands in this reaction indicated DNA contamination of some component of the master mix meaning that total PCR experiment was discarded and re-run using fresh reagents. In addition, all PCR experiments included positive controls for each band (a known heterozygote DNA sample) to confirm the presence and location of the DNA bands produced by the PCR.

Visualisation of DNA products – Gel electrophoresis: Since PCR amplification of DNA is expected to produce PCR products of distinct sizes (number of base pairs), the amplified DNA could be visualised by separation of PCR products using standard gel electrophoresis. Agarose gel electrophoresis allows separation of PCR DNA products on the basis of size whereby the agarose gel provides a matrix through which the DNA progresses upon application of an electrical charge due to the negative charge of DNA. This allows separation of DNA products where smaller DNA fragments travel easier through the gel (and thus further in a set time). The composition of the agarose gel determines DNA separation and so was optimised for the expected sizes of DNA bands.

PCR products obtained from the reactions described above were run on an agarose gel using a standard electrophoresis tank (Owl Easycast, BioRad, UK) set at 120 V for 45-60 minutes. Gel electrophoresis was conducted in a TAE running buffer (containing Tris 40 mM, acetic acid 20 mM and EDTA 1 mM). Electrophoresis of the PCR products was continued until the migration front of the PCR products had travelled approximately half the length of the gel. The approximate separation of DNA bands was determined by the

location of the red and orange dyes contained in the CoralLoad buffer: 2.0% agarose gel – red dye at 100 bp, orange dye at <10 bp; 1.5% agarose gel – red dye at 250 bp and orange dye at 20 bp. Agarose gels were made in TAE buffer with the addition of the fluorescent agent Syto60™ (0.001%: 1 µl in 100ml; Molecular Probes, USA). Syto60™ is a red fluorescent nucleic acid stain that is cell-permeant and binds to nucleic acid and therefore allows visualisation of distinct bands of DNA when the electrophoresed gel is scanned using a fluorescent imaging scanner (Odyssey, Licor, UK). DNA gels were scanned using a 700 nm laser at a resolution of 169 µm with focus offset of 2.0 mm for the standard thickness of gels used.

The molecular weights of the resulting PCR product bands were compared against a control molecular weight ladder (100 kbp Plus or MidRange, Qiagen, UK) and the genotype of each animal was determined by the presence or absence of each PCR product DNA band (representative example shown in Figure 3.4).

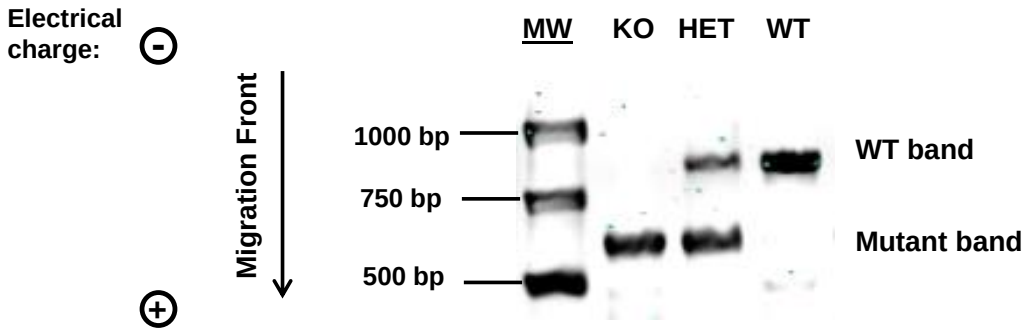

Figure 3.4: Representative visualisation of PCR products following gel electrophoresis
DNA lysates were amplified by PCR and separated by gel electrophoresis where DNA products migrate from the negative to positively charged ends of the gel. The Syto60™ containing gel was imaged using a fluorescent imaging scanner to visualise DNA bands: lane 1) molecular weight ladder, 2) KO band, 3) WT and KO bands corresponding to HET and 4) WT band.

3.2. Ischaemia-reperfusion *in vivo* recovery model

This thesis describes the development and characterisation of a mouse *in vivo* recovery model of ischaemia-reperfusion injury for the first time within our laboratory. An overview of the experimental rationale and surgical method is provided here and detailed descriptions of the precise surgical protocol and refinements provided in chapter 4.

This model of ischaemia-reperfusion injury comprised occlusion and reperfusion of the left anterior descending (LAD) coronary artery in the *in vivo* mouse heart followed by recovery of animals for subsequent investigation. This model was first described by Michael et al. (1995) and the method developed in this thesis was based on that presented by Fisher and Marber (2002) with modifications informed by van Laake et al. (2007). The use of animals was in accordance with the United Kingdom Animal (Scientific Procedures) Act of 1986 and local guidelines. General surgical advice was informed by the Handbook of Laboratory Animal Management and Welfare (Wolfensohn and Lloyd, 2003) and the NACWO at University College London, UK.

3.2.1. Surgical protocol

i Overview of surgical methodology

Experimental setup: All recovery surgeries were undertaken following strict aseptic operating practices in a sterile surgical theatre at University College London, UK. Animals were maintained on a thermostatically controlled heated operating table (Peco Services Ltd, UK) and body temperature was monitored (using a K-type thermocouple thermometer, Hanna Instruments, UK) and maintained at 37.0±0.5°C. Electrocardiograms (ECGs) were recorded throughout the procedure by a Powerlab setup coupled to Chart 7 software (AD Instruments, UK). All recovery surgeries were conducted with the aid of a high-powered surgical microscope set at custom magnifications (Zeiss Universal S2, Zeiss, Germany).

Surgical procedure: A simplified overview of the surgical procedure is summarised in Figure 3.5 and described below; chapter 4 provides a detailed methodological description of this protocol and the development and characterisation of this model.

For the main studies presented here, mice were anaesthetised by inhalation of isoflurane (Isoflo, Abbott Animal Health, USA) vaporised in oxygen (5% to 1.8% isoflurane in 1.5 L/minute oxygen) (Figure 3.5 A). Isoflurane is a halogenated ether which when vaporised provides rapid onset and stable maintenance of anaesthesia which has been reported for use in several experimental surgical models (Wiersema et al., 1997). Anaesthesia was initiated in an induction box supplied with isoflurane and

subsequently maintained by connection to a small animal ventilator connected to an isoflurane supply. Artificial respiration was provided by ventilation at a volume 200 µl and stroke rate 200 strokes/minute and supplied with oxygen (1.5 L/minute) (MiniVent Type 845, Hugo Sachs Electronik, Germany) (Figure 3.5 A). Surgical anaesthesia was confirmed by loss of the toe-pinch reflex and was continually monitored throughout.

Open-chest surgery was performed via a fourth intercostal space thoracotomy and retraction of the ribs using a small animal chest retractor (all surgical instruments are detailed in chapter 4) (Figure 3.5 B). The pericardium was gently opened to gain access to the heart. The LAD coronary artery was identified and under-run approximately 2 mm below the tip of the left atrium with an 8-0 polypropylene suture (8-0 prolene non-absorbable suture, W2775, Ethicon, USA). A custom-made snare system was assembled from polyethylene-50 tubing (PE50, Deutsch and Neumann, Germany) and a modified standard pipette tip (Figure 3.5 C); the precise components and assembly of this snare system are provided in chapter 4.

Myocardial ischaemia was induced by tightening the snare system to occlude the LAD, confirmed by: (1) ST-segment elevation, (2) myocardial pallor and (3) relative akinesis of the ischaemic area (AAR). Myocardial reperfusion was induced by release of the snare system for reperfusion of the LAD and was confirmed by resolution of the changes observed upon ischaemia, detailed above. Animals were excluded from the study where the onset of ischaemia or reperfusion was not accompanied by observations (1) and (2).

Following the onset of reperfusion, the snare system was disassembled and the LAD suture cut and left in place for subsequent analysis (Figure 3.5 D). All surgical openings were closed and the animal was recovered by cessation of the isoflurane supply (Figure 3.5 E). Ventilation was stopped only upon full return of independent breathing due to the known effect of isoflurane on reducing respiration rate (Abbott Animal Health, 2006).

Animals were monitored closely at regular intervals in the immediate post-operative period. Analgesia was provided by buprenorphine (0.1 mg/kg intramuscular, Vetergesic [Alstoe Animal Health, UK]) administered at the start and 6 and 24 hours post-surgery. Buprenorphine is a potent semi-synthetic opioid that exerts analgesic affects by its actions on opioid receptors (Reckitt Benckiser, 2011). Adequacy of pain relief was assessed by movement and general activity and advice sought from the NACWO if required. An additional buprenorphine dose was given 48 hours post-surgery if required.

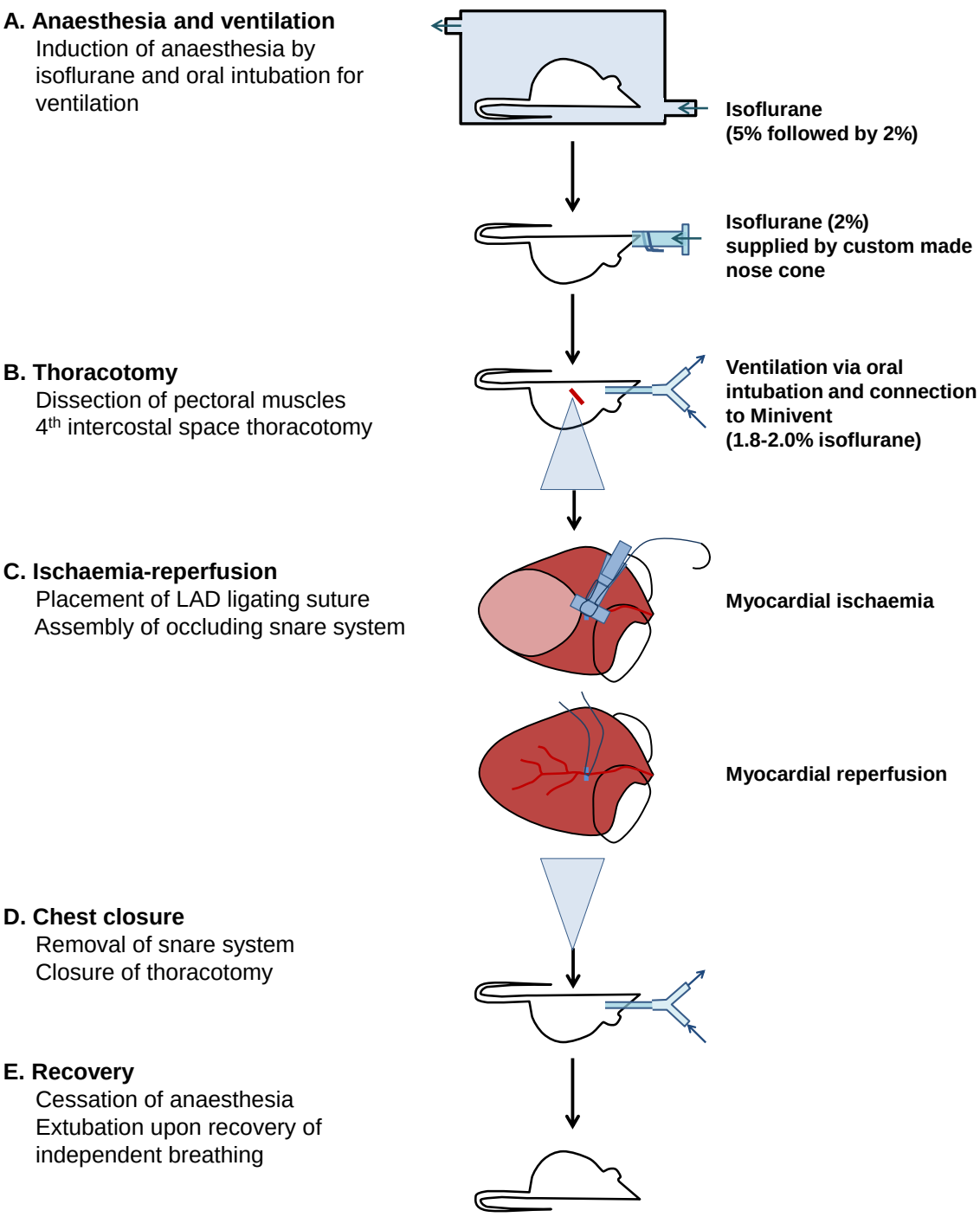

Figure 3.5: Overview of *in vivo* ischaemia-reperfusion injury recovery procedure
A) Mice were anaesthetised and ventilated by oral intubation and connection to a small animal ventilator. B) Access to the heart was gained by thoracotomy and opening of the pericardium. C) Myocardial ischaemia was induced by LAD ligation using a custom-made snare. Reperfusion was initiated by release of the LAD occlusion. D) The LAD snare system was removed leaving short lengths of ligating suture. The thoracotomy was closed. E) Animals were recovered by cessation of isoflurane supply and extubated. In depth surgical details are provided in chapter 4.

ii Ischaemia-reperfusion protocol

The standard protocol for *in vivo* recovery ischaemia-reperfusion was 30 minutes ischaemia and 72 hours reperfusion (Figure 3.6 B). Sham operated mice were subjected to the same surgical procedure including assembly of the snare system but without occlusion (Figure 3.6 A). Adjustment of the stabilisation duration in sham operated animals ensured that the anaesthetic duration of all *in vivo* recovery procedures was as closely matched as possible, unless specifically stated in the subsequent chapters.

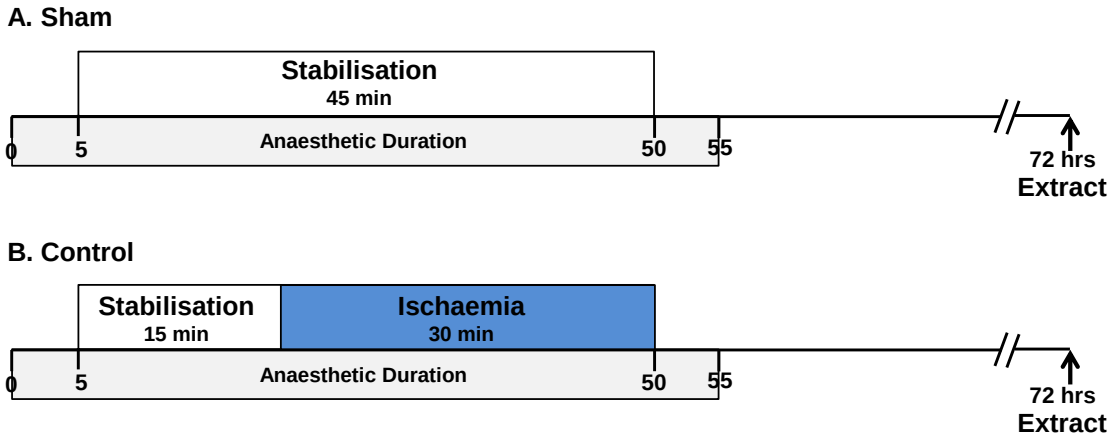

Figure 3.6: Standard ischaemia-reperfusion *in vivo* recovery protocol
A) Sham: 45 minutes stabilisation followed by disassembly of snare and recovery. B) Control: 15 minutes stabilisation followed by 30 minutes ischaemia and 72 hours reperfusion.

iii Surgical exclusion criteria

The pre-defined surgical exclusion criteria applied to this model were informed by the non-recovery *in vivo* model of ischaemia-reperfusion injury previously established at our laboratory. Animals were excluded from the experiment for the following reasons:

(1) Body temperature recorded was less than 35.5ºC or greater than 38.5ºC.
(2) LAD ligation caused severe mechanical damage or the myocardial AAR was clearly inappropriate (adequacy of AAR is described further below).
(3) Myocardial ischaemia or reperfusion was not confirmed by ST-segment elevation and myocardial colour changes (as described above).

The application of these exclusion criteria is described in detail in chapter 4 (see 4.3.2 iv). Further exclusion criteria concerning myocardial AAR were applied during the analysis stage of this model, as described below (see 3.2.4).

3.2.2. Treatments and interventions

i Ischaemic preconditioning

IPC is a well-recognised cardioprotective strategy whereby brief non-lethal periods of ischaemia immediately prior to the main ischaemic insult protects the heart against ischaemia-reperfusion injury (reviewed by Yellon and Downey, 2003). A standard IPC protocol of one cycle of 5 minutes ischaemia and 5 minutes reperfusion was applied prior to the main ischaemic insult. This IPC protocol significantly reduces infarct size in a similar non-recovery model of ischaemia-reperfusion within our laboratory (Lim et al., 2007). Control mice underwent 15 minutes stabilisation prior to the main ischaemic insult to ensure that the anaesthetic durations were equal between groups (Figure 3.7).

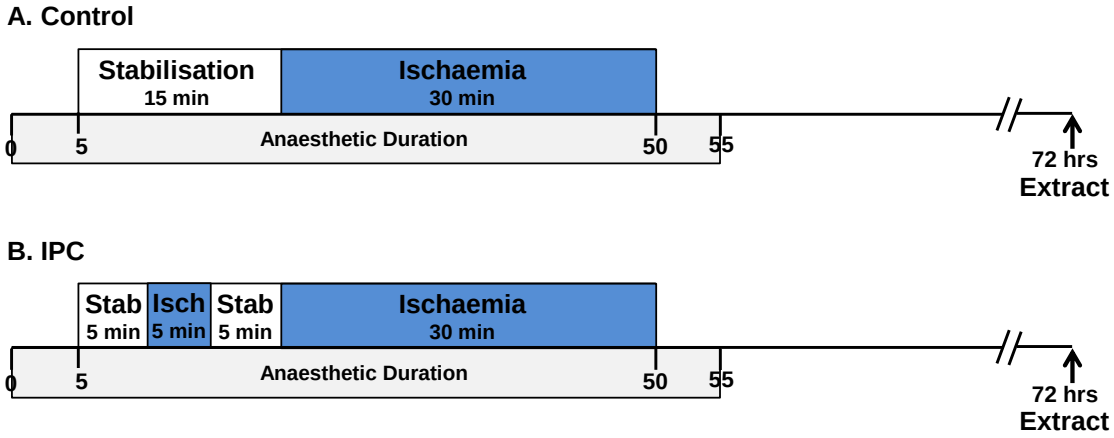

Figure 3.7: Standard ischaemic preconditioning protocol
A) Control: 15 minutes stabilisation, 30 minute ischaemia and 72 hours reperfusion. B) IPC: 5 minutes stabilisation, one cycle IPC of 5 minutes ischaemia and 5 minutes reperfusion, 30 minutes ischaemia and 72 hours reperfusion.

ii Pharmacological treatment

All pharmacological interventions were applied 5 minutes prior to the onset of reperfusion. Pharmacological agents were administered as a single intravenous (I.V.) bolus via either the left or right lateral tail vein using a 0.5 ml syringe (Beckton Dickinson, UK). Since core body temperature affects final myocardial infarct size (discussed in chapter 4), it was not possible to pre-warm animals to facilitate tail vein injections in accordance with standard practice for this procedure. Instead, a tissue swab soaked in warmed water was applied locally to the injection site to cause local dilation of the tail vein to aid placement of the injection needle.

Successful delivery of the intravenous bolus was confirmed by visualisation of washout of blood in the vein upon administration and subsequent return of blood following removal of the injection needle. Animals were excluded from the study if successful intravenous delivery of the pharmacological intervention could not be confirmed.

The optimal volume for administration was approximately 60 µl per 30 g animal (2 ml/kg; informed by previous studies within our laboratory) and all pharmacological interventions employed in this thesis were diluted such that this dosing volume was adhered to.

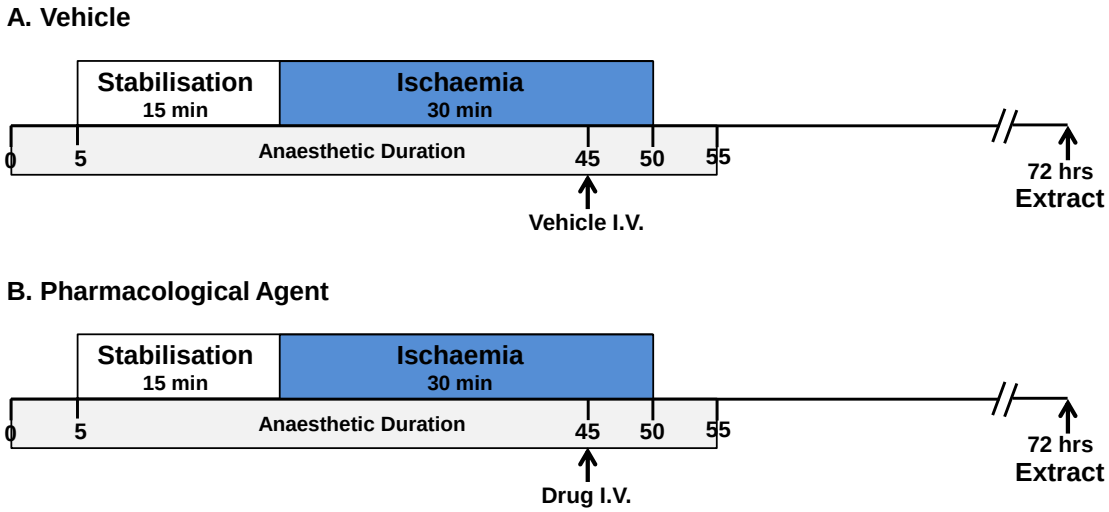

Figure 3.8: Standard pharmacological intervention protocol
Administration of pharmacological interventions was as a single I.V. bolus 5 minutes prior to the onset of reperfusion. A) Control: matched volume of vehicle. B) Drug treatment: 60 µl per 30 g mouse (2 ml/kg). Successful administration was confirmed by washout of blood in the tail vein.

iii Fasting

All animals were provided with standard chow and water *ad libitum*, unless specifically stated. A fasting protocol was employed in chapter 6 to investigate the effect of fasting on susceptibility to myocardial infarction. Fasting for a maximum of 16 hours is permitted without a specific Home Office protocol since it is not considered to be a procedure and therefore the fasting protocol employed here did not exceed 16 hours. Free access to water was ensured throughout this protocol and animals were carefully monitored.

3.2.3. Endpoint 1 – Survival

Survival of animals subjected to the *in vivo* recovery ischaemia-reperfusion procedure was recorded. Where animals died during the surgical procedure, the suspected cause of death was recorded and was most commonly the result of surgical error or in some cases cardiac failure during ischaemia. Deaths occurring post-surgery were investigated by post-mortem analysis to determine the suspected cause of death. Where there was no evidence of excessive surgical trauma or cardiac rupture, post-surgery deaths were thought to most often result from cardiac or respiratory failure. Cardiac rupture was evidenced by blood in the chest and visual rupture to the heart. However, death due to cardiac rupture was rare due to the relatively short ischaemic durations used. Surgical and recovery survival rates are reported in the subsequent chapters of this thesis.

Statistical analysis: Survival rates of animals subjected to this surgical protocol are presented as standard Kaplan-Meier survival plots constructed using GraphPad Prism® version 5.0 (GraphPad Software, USA). Statistical significance of survival was analysed by log-rank tests (Mantel-Cox) using GraphPad Prism® version 5.0 (GraphPad Software, USA). Log-rank tests were used since this analysis method places equal weight on deaths at all time-points, which is the most appropriate method for this analysis and is the more standard statistical analysis test applied to this type of data. Statistical significance was reported where $P<0.05$ using standard significance coding: *$P<0.05$, **$P<0.01$ and ***$P<0.001$. No statistical significance was reported where $P>0.05$ and was indicated as not significant (NS). Sample sizes and statistical significance are presented alongside all statistical tests.

3.2.4. Endpoint 2 – Histological staining for infarct size and area-at-risk

The primary endpoint of the *in vivo* ischaemia-reperfusion injury model was myocardial infarct size as a percentage of AAR (IS/AAR%). The AAR is defined as the region of myocardium subject to ischaemia. Infarct size and AAR were determined by histological staining of *ex vivo* heart preparations (summarised in Figure 3.9).

The area of myocardial infarction was determined by TTC staining whereby TTC serves as an enzymatic substrate for intracellular dehydrogenases in living cells causing it to change colour from an off-white precipitate to an intense red colour. Dead cells no longer contain these dehydrogenase enzymes meaning that TTC remains an off-white colour in areas of infarction. The colour of TTC stained tissues allows accurate distinction between the living and dead regions of myocardium (see Figure 3.9). This TTC-based staining method has been validated in numerous previous studies against classical microscopic histological indicators of cell death (reviewed by Kloner, 1993; Black and Rodger, 1996). The area of myocardium deemed ‘at-risk’ was delineated by perfusion of Evans blue dye following re-occlusion of the LAD suture which results in blue staining of the area of myocardium that was perfused during the ischaemic event; this staining method is summarised in Figure 3.9.

i Histological staining method

Hearts were extracted from mice anaesthetised with ketamine (100 mg/kg [Vetlar, Bioniche Animal Health, Canada]), xylazine (20 mg/kg [Rompun, Bayer, UK]) and atropine (0.6 mg/kg [Sigma-Aldrich, UK]). The chest was rapidly opened and the heart extracted by cutting the aorta immediately before the aortic loop. The aorta was cannulated onto a 21 gauge (G) standard metal perfusion cannula to allow retrograde perfusion of the heart (Figure 3.9 A).

The heart was perfused manually taking care not to exert excessive pressure that may damage the coronary system. The heart was first washed by perfusion of saline (1 ml) to remove blood from the coronary system (Figure 3.9 B). The area of infarction was then delineated by perfusion of TTC (7 ml of 1% TTC in phosphate-buffered saline [PBS], pre-warmed to 37°C) (Figure 3.9 C). The LAD suture from the surgical procedure was securely re-occluded and Evans blue dye (1.5 ml 0.5% Evans blue made in distilled water) then perfused under running water to delineate the AAR (Figure 3.9 D).

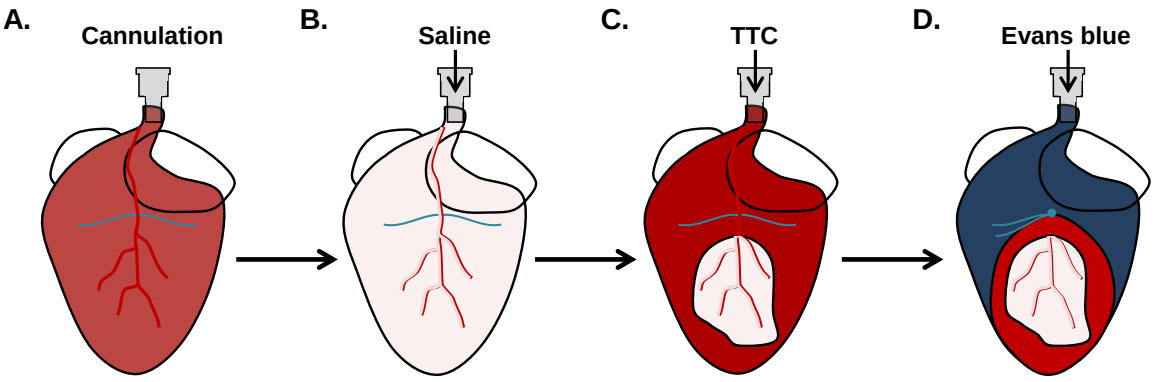

Figure 3.9: Histological staining method for myocardial infarction and area-at-risk
A) Hearts were extracted and the aorta cannulated for manual perfusion. B) Residual blood was removed by perfusion of saline. C) Staining for infarction was by TTC perfusion at 37ºC where living tissue stains bright red and dead tissue remains off-white in colour. D) The AAR was delineated by perfusion of Evans blue dye following re-occlusion of the LAD ligating suture whereby the non-AAR stains blue and the AAR remains unstained by Evans blue.

ii Processing of stained hearts

Hearts were immediately stored at -20°C for 1–2 days and then manually sliced using a sharp scalpel to give 5 transverse slices from the apex of the heart with the uppermost slice at the approximate level of LAD occlusion (Figure 3.10). Heart slices were washed in saline and fixed in 10% formalin for 90-120 minutes at room temperature. The right ventricle was dissected from each heart slice and the resulting left ventricle slices were imaged in a custom-made acrylic block spaced by 0.5 mm using an Epson scanner (Epson Perfection V100 Photo, Epson, UK) at 1200 dpi, 0%, 15% and 100% brightness.

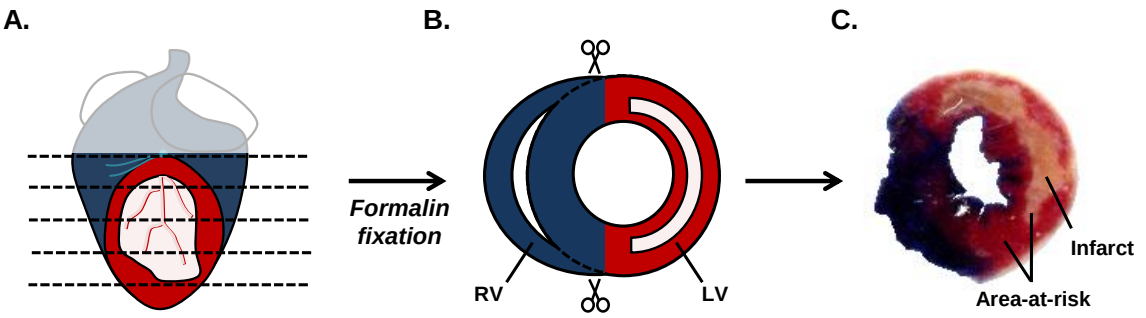

Figure 3.10: Processing method of preparing histologically stained hearts for imaging
A) Hearts were rapidly sliced using a sharp scalpel to take five transverse slices from the apex of the heart to the approximate level of the LAD suture. B) After briefly washing and formalin fixation for 90-120 minutes, the right ventricle (RV) was removed from each heart slice and discarded. C) Left ventricle (LV) slices were imaged using a scanner – example of mid-heart slice with area of infarction (off-white colour) and AAR (all of the area not stained blue) indicated.

iii Quantification of infarct size and area-at-risk

Infarct size and AAR were quantified by planimetry using ImageJ software (version 1.45s, National Institutes of Health, USA). Raw images (at 15% brightness) were assessed by manual thresholds to identify the total left ventricular area (LV area), area of Evans blue staining and area of infarction. Myocardial AAR as a percentage of left ventricle area (AAR/LV%) was calculated as: (LV area – Evans blue area) / (LV area). Infarct size as a percentage of AAR (IS/AAR%) was calculated as: (Infarct area) / (AAR/LV%). This method is summarised in in Figure 3.11 and the precise details and validation of this method is provided in chapter 4.

Figure 3.11: Planimetry method for quantification of infarct size and area-at-risk
A) Raw heart images were prepared by removal of the background image. B) AAR was quantified by manual threshold of the green channel image and the number of pixels of Evans blue staining recorded. C) Infarct area was quantified by manual threshold of the red channel image and the number of infarct pixels (off-white) recorded. Total LV area was quantified by manual threshold to record the number of pixels. AAR was calculated as (LV area – Evans blue area) / (LV area).

Hearts were excluded from the dataset if the myocardial AAR was outside the predefined inclusion range of 40–75% AAR/LV. No statistically significant differences were observed in AAR/LV% between groups within experiments presented. Mean AAR/LV% for each group are reported alongside the results for each experiment.

Statistical analysis: All percentage areas are reported as mean ± standard error of mean (SEM). Note that regression analysis values for slopes are given as the regression parameter ± standard deviation, as detailed below. Statistical analysis was completed using GraphPad Prism® version 5.0 (GraphPad Software, USA) or subsidiary GraphPad StatMate software version 2.0 (GraphPad Software, USA), as detailed below. Details of statistical tests and sample sizes are provided alongside all results.

Comparison of means: Sample means were compared using an appropriate statistical test determined by the number of groups and type of data being compared. Where two independent groups were compared, data were analysed using an unpaired t-test. Where more than two independent groups were compared, data were analysed by one-way ANOVA and Bonferroni test comparing relevant columns of data as indicated.

In cases where two dependent groups were compared, data were analysed using a paired t-test since measurements were made of the same parameter by two different methods. Paired t-tests were only appropriate for the comparison of histological and cardiac MRI endpoints where the use of paired t-tests is specifically reported in the text.

For all these statistical analyses, the statistical significance level was set at 5% (α=0.05) and statistical significance reported where the computed P-value was less than 0.05. Significance was reported using standard significance coding: *P<0.05, **P<0.01 and ***P<0.001. No statistical significance was reported where P>0.05 (indicated as 'NS').

Regression: Where appropriate, regression analysis of myocardial infarct size and AAR was undertaken using the Deming (Model II) regression method. Standard regression analysis was not appropriate in this case since it assumes that only the Y variable is subject to error, whereas in this case both measurement of AAR (X variable) and infarct size (Y variable) are subject to a similar degree of error. Deming regression analysis was therefore undertaken where the error of both the X and Y variables was assumed to be approximately equal. This regression analysis was used to define the relationship between infarct size and AAR and reported as: $y=mx+c$ where m is the slope and c is the intercept when $x=0$. Regression slope is reported as mean ± standard deviation (SD) and Y intercept reported for when $x=0$.

Regression values were reported as r^2 and the relationship determined for each group compared by evaluating the slopes. Where the slopes of the two groups were not

statistically significant, the elevation of the lines (intercepts) was compared. Statistical significance was set at 5% (α=0.05) and significance was reported when the computed P-value was less than 0.05 using standard significance coding.

Statistical power: Statistical power calculations were performed to determine the approximate sample sizes required for a prospective study or to retrospectively evaluate statistical power to ensure that sufficient sample sizes were investigated. For all tests, a statistical power of 80% was deemed the minimal acceptable level of power in accordance with published guidelines (Cohen, 1988; Townend, 2002). All power calculations were performed using GraphPad StatMate software version 2.0 (GraphPad Software, USA) according to the statistical power equations published by Cohen (1988).

Where no statistical significance was observed, the statistical power of the analysis was assessed using the observed sample sizes and standard deviations to determine the difference between groups that could be detected with 80% statistical power.

Sample size calculations for prospective studies were estimated based on 5% significance level (α=0.05) and 80% statistical power (β=0.2) and the required sample size estimated based on the predicted effect size. Specific details of power and sample size calculations for the assessment of statistical power are provided alongside results.

3.3. Ischaemia-reperfusion *in vivo* non-recovery model

A non-recovery *in vivo* model of ischaemia-reperfusion was also undertaken to permit assessment of myocardial infarct size following short durations of reperfusion. The surgical protocol was as described above (see 3.2.1) with minor modifications.

3.3.1. Non-recovery anaesthetics

It was not possible to undertake non-recovery surgery using isoflurane anaesthesia within our laboratory due to the constraints of ventilation systems and apparatus. A standard non-recovery injectable anaesthetic cocktail was therefore used for all non-recovery *in vivo* procedures undertaken. Mice were anaesthetised with an injectable anaesthetic cocktail containing ketamine (100 mg/kg [Vetlar, Bioniche Animal Health, Canada]), xylazine (20 mg/kg [Rompun, Bayer, UK]) and atropine (0.6 mg/kg [Sigma-Aldrich, UK]) administered as a single intraperitoneal bolus. Anaesthetic depth was monitored and maintained by additional anaesthetic doses. Ventilation stroke volume was 200 µl and stroke rate was 120 strokes/minute supplied with oxygen (1.5 L/minute).

3.3.2. Surgical procedure

The non-recovery *in vivo* procedure was undertaken using an identical surgical setup to that described for the recovery procedure but was performed within our laboratory (non-sterile environment) and used a standard surgical microscope (Gallenkamp, Weiss, UK).

Immediately following the initiation of myocardial reperfusion, the thoracotomy was loosely closed using a 5-0 braided suture (5-0 mersilk non-absorbable suture, W595, Ethicon, USA) and covered with a moistened tissue drape to prevent tissue desiccation. The standard protocol for non-recovery surgeries was 30 minutes ischaemia and 2 hours reperfusion (Figure 3.12). Animals were anaesthetised for the total duration (2 hours 50 minutes) and hearts then subjected to staining as above (see 3.2.3).

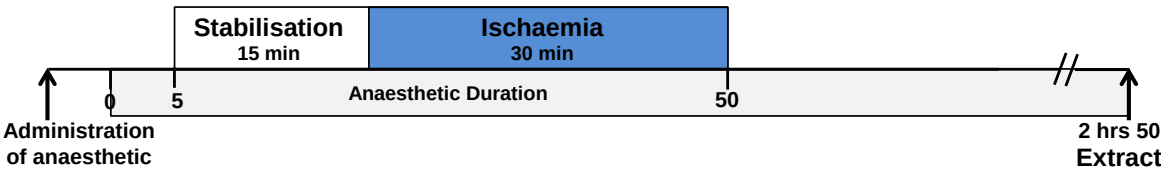

Figure 3.12: Ischaemia-reperfusion *in vivo* non-recovery protocol
Mice were anaesthetised using an injectable anaesthetic cocktail. The LAD ligating snare system was assembled and stabilised for 15 minutes followed by 30 minutes ischaemia and 2 hours reperfusion. Total anaesthetic duration was approximately 2 hours 50 minutes (pale grey box).

3.4. Analysis of myocardial protein levels

Myocardial protein levels were examined using standard Western blot techniques described below and detailed further in the relevant results chapters of this thesis.

3.4.1. Preparation of heart samples

i Extraction and processing of ventricular tissue

Hearts were extracted from anaesthetised mice and cannulated for manual perfusion exactly as described above (see 3.2.3: cannulation and saline perfusion only). Hearts were washed by perfusion of 1 ml chilled saline (4ºC) whilst submerged in ice-cold saline to remove residual blood from the ventricle lumen and coronary system. During processing, efforts were made to ensure that the ice-cold conditions were observed and the cannulation and perfusion process was completed as rapidly as possible to avoid changes occurring to the tissues. The atria were removed and discarded and the ventricles immediately transferred to a small container of liquid nitrogen and crushed using a cooled plastic tool to ensure rapid freezing of the tissue. Ventricle samples were stored in liquid nitrogen for 30 minutes and at -80ºC until processing.

Tissue samples were manually homogenised in standard homogenisation buffer for subsequent assays using a small glass pestle and mortar. This homogenisation buffer was based on a phosphate buffered saline (PBS) solution containing (in mmol/L): NaCl (137), KCl (2.7), $Na_2HPO_4.2H_20$ (10), KH_2PO_4 (2), pH 7.4 and supplemented with protease inhibitor and phosphatase inhibitor cocktails (diluted to 1X concentrations in PBS) and EDTA (pH 8.0) (Thermo Scientific, UK). The homogenisation buffer was freshly made for each experiment. Heart tissues were homogenised to a concentration of 0.1 g tissue in 0.1 ml buffer and stored at -80ºC prior to use in subsequent assays.

ii Isolation of mitochondria

Mitochondrial proteins were isolated from ventricular heart samples where required. Hearts were extracted from anaesthetised mice and cannulated for manual perfusion exactly as described previously. Hearts were washed by perfusion of 1 ml chilled saline (4ºC) whilst submerged in ice-cold saline to remove residual blood from the ventricle lumen and coronary system. The atria were removed and discarded and the left and right ventricular tissue immediately homogenised using a glass pestle and mortar in standard homogenisation buffer as previously described. Mitochondrial proteins were isolated using a commercial kit (Qproteome mitochondria isolation kit, Qiagen, UK) according to the manufacturer's instructions. Briefly, homogenised tissue was suspended in lysis buffer which selectively disrupts the cellular plasma membrane. The

resulting pellet (containing mitochondria, nuclei and other organelles) was re-suspended in disruption buffer to ensure complete disruption of the cells. The supernatant (which contained mitochondria) was re-centrifuged to pellet the mitochondria. Mitochondria were washed and re-suspended prior to Western blot analysis.

iii Quantification of protein concentration

The protein concentration of each tissue homogenate was assessed using a bicinchoninic acid (BCA) – copper(II) sulphate ($CuSO_4$) assay. This assay is based on the reduction of Cu^{2+} to Cu^{1+} by proteins in alkaline assay conditions where 2 molecules of BCA chelate one Cu^{1+} ion causing BCA to change from a green to purple colour where the purple intensity is proportional to the amount of protein (Figure 3.13).

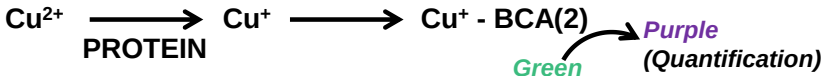

Figure 3.13: Molecular basis of BCA assay quantification of protein quantification
The chemical basis of this is described in the datasheet provided by Thermoscientific (2010).

Proteins were quantified by comparison to a normalised curve of BCA colour produced by known concentrations of bovine serum albumin (BSA) in homogenisation buffer. Heart samples and known BSA concentration control samples were added to the BCA and $CuSO_4$ solution and incubated for 30 minutes at 37 ºC with agitation. The resulting colour intensity was measured by a FLUOstar Omega microplate reader (BMG Labtech, USA) and the protein concentration of samples calculated by automatic software calculations using the standard concentration curve from the BSA samples.

Heart samples were subsequently diluted to a set concentration of the most dilute heart sample by addition of the calculated volume of homogenisation buffer required.

3.4.2. Western blotting protocol

i Gel electrophoresis

Western blotting was performed by standard sodium-dodecyl sulphate polyacrylamide gel electrophoresis (SDS-PAGE). This allows separation of proteins based on size and charge where SDS causes protein linearisation and negative charge.

Diluted heart samples (detailed above) were prepared for gel electrophoresis (100 µl aliquots) by addition of laemmli buffer (100 µl) and β-mercaptoethanol (10 µl). Laemmli buffer (containing mercaptoethanol and SDS) and additional mercaptoethanol cause denaturation of proteins within the samples so that they can subsequently be separated

by size upon gel electrophoresis. Laemmli buffer also contains glycerol to increase the density of the protein samples to facilitate their loading into the gel sample wells. These prepared heart samples were then incubated at 100ºC for 10 minutes prior to running.

SDS-PAGE gels were made using standard BioRad Mini Protean® Western blotting apparatus (BioRad, UK). Resolving gels were made containing 15% acrylamide, 0.1% SDS and Tris-HCl (pH 8.8) to a final concentration of 375 mM, tetramethyl ethylenediamine (TEMED, 7.5 µl) and the setting agent 10% ammonium persulphate (APS, 75 µl) added immediately prior to pouring the gels. Isopropanol water was gently poured onto the resolving gel whilst it set to ensure that a straight edge was formed. Following setting of the resolving gel and removal of isopropanol water, stacking gels were made containing 4.5% acrylamide, 0.1% SDS and Tris-HCl (pH 6.8) to a final concentration of 125 mM and TEMED (7.5 µl) and 10% APS (75 µl) added prior to pouring and 15 well combs inserted for loading.

The completed gels were placed in running cassettes (BioRad, UK) filled with running buffer comprising glycine (200 mM), SDS (1%) and Tris (25 mM). Gels were loaded with equal concentrations of proteins as calculated from the BCA protein assay (described above) such that 12.5 µl of heart homogenate was loaded per lane. A protein reference marker was loaded (7.5 µl Prevision plus, BioRad, UK) to allow determination of protein sizes. Gels were run at 180 volts for 1 hour or until separation of the protein ladder.

ii Western blot transfer to membrane

Following electrophoresis, proteins were transferred to nitrocellulose membranes by semi-wet transfer (Semi-Wet Transfer Cell, BioRad, UK) to allow interrogation of membranes by antibody binding (described below). Transfer of proteins was performed by mounting gels between wet blotting paper (Whatman, GE Healthcare, UK) next to a pre-prepared nitrocellulose membrane. This membrane was first prepared in 100% methanol for 2 minutes and washed in transfer buffer. Transfer buffer comprised glycine (200 mM) and Tris (25 mM) and 20% methanol. It was imperative that all air bubbles were removed from the assembly to avoid incomplete protein transfer. The transfer was run at 10 volts (<1 amp) for 45 minutes and confirmed by protein ladder transfer.

iii Antibody probing of gels

All washes of the membrane were conducted using PBS supplemented with Tween (0.1% Tween-20). Immediately prior to interrogating the membranes for proteins using selective antibodies, it was necessary to block non-specific antibody binding. Blocking was achieved by incubation in 5% milk (Marvel milk powder [Premier International Food Limited] made in PBS containing 0.1% Tween) for 45 minutes at room temperature.

Primary antibodies were diluted 1:1000 in 5% milk / PBS + Tween solution. Primary antibodies were incubated for 45-60 minutes at room temperature with agitation. The primary antibody epitopes were designed to recognise the protein of interest, as subsequently described in the relevant chapters. Excess unbound primary antibody was then removed by washing the membrane six times for 10 minutes each in PBS + Tween. Primary antibodies were detected by labelled secondary antibodies directed at a site-specific portion of each primary antibody. Secondary antibodies were diluted 1:5000 in 5% milk PBS + Tween solution. Secondary antibodies were incubated for 1 hour at room temperature with agitation. Secondary antibodies were conjugated to a horseradish-peroxidase (HRP) enzyme to allow subsequent detection by a standard chemiluminescence reaction (described below).

Details of the specific antibodies used for Western blot analysis of protein levels in these studies are provided in the applicable results chapters. The protein level of interest was normalised to the level of a relevant protein to control for differences in protein loading of the gels. For whole cell samples, α-tubulin was used as a loading control. Mitochondrial protein samples were compared against VDAC levels, however, since VDAC protein levels also appeared to be affected by the treatment tested, absolute protein levels of the mitochondrial protein of interest were assessed; described further in section 6.3.3.

iv Chemiluminescence detection of antibody binding

Protein bands were visualised using a standard HRP chemiluminescence reaction. Membranes were incubated in enhanced chemiluminescence (ECL) reaction (GE Healthcare, UK) for approximately 2 minutes. The HRP enzyme catalyses conversion of the ECL substrate into a luminescent product which can then be visualised using photographic development (Figure 3.14). Membranes were imaged using photographic film placed over the membrane and ECL for 10 seconds to 2 minutes Photographic films were scanned using an Epson scanner (Epson Perfection V100 Photo, Epson, UK).

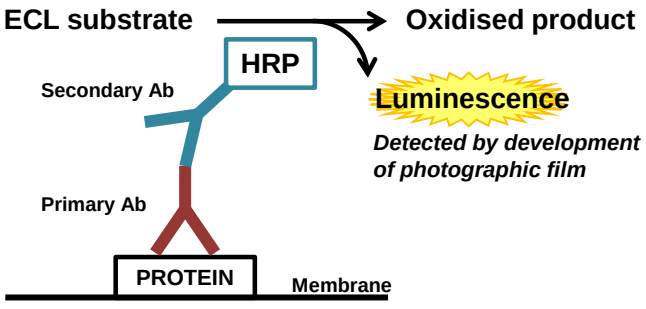

Figure 3.14: Molecular basis of enhanced chemiluminescence detection of antibody binding
Secondary antibodies were conjugated to HRP which catalyses conversion of the ECL substrate to evoke luminescence which can be detected by development of photographic film.
Modified from Cell Signalling (2012).

Quantification of protein levels: Since the intensity of chemiluminescence produced by the ECL reaction described above is proportional to antibody binding and therefore the amount of protein present on the membrane, the resulting bands produced on the photographic film are representative of the protein levels. This was quantified by densitometry of protein bands using ImageJ software (version 1.45s, National Institutes of Health, USA). Final protein levels were quantified and normalised against the loading control for each sample, where appropriate, and expressed as arbitrary units (A.U.).

All values are presented as mean A.U. ± standard error of mean (SEM). Data were analysed by one-way ANOVA followed by Bonferroni test comparing relevant columns of data using GraphPad Prism® version 5.0 (GraphPad Software, USA). The statistical significance level was set at 5% (α=0.05) and statistical significance was reported where the computed P-value was less than 0.05 using standard significance coding.

3.5. Assay of myocardial ATP levels

3.5.1. Langendorff preparation of heart samples

A Langendorff perfusion setup was used to prepare heart samples to assess ATP levels and permit investigation of the effects of myocardial ischaemia. A basic Langendorff constant pressure perfusion system was used to perfuse the hearts and initiate ischaemia. A detailed description of this model is beyond the scope of this thesis; a simplified overview is illustrated in Figure 3.15 and reviewed by Bell et al. (2011).

Mice were anaesthetised with ketamine (100 mg/kg [Vetlar, Bioniche Animal Health, Canada]), xylazine (20 mg/kg [Rompun, Bayer, UK]) and atropine (0.6 mg/kg [Sigma-Aldrich, UK]) administered as a single intraperitoneal dose. Upon surgical anaesthesia, hearts were extracted and rapidly cannulated onto a 21 G standard perfusion cannula as described above (see 3.2.3). The ideal time to perfusion was less than 3 minutes although this rarely took more than 2 minutes for the experiments presented here.

Langendorff perfusion chambers were filled with Krebs-Henseleit buffer (KHB) containing (in mmol/L): NaCl (118), glucose (11), $NaHCO_3$ (25), KCl (4.7); $CaCl_2$ (1.8), $MgSO_4.7H_2O$ (1.2) and pyruvate (0.5), equilibrated with 95% oxygen and 5% carbon dioxide to pH 7.4 and perfused at 80 mmHg. Physiological temperature of the heart was maintained by warming of the perfusion buffer and monitored by insertion of a fine tipped temperature probe into the LV wall (via Powerlab coupled to Chart 7 software, AD Instruments, UK). The temperature of the heart was maintained at 37.0±0.5ºC by subtle changes to the submersion of the heart in the warmed perfusate.

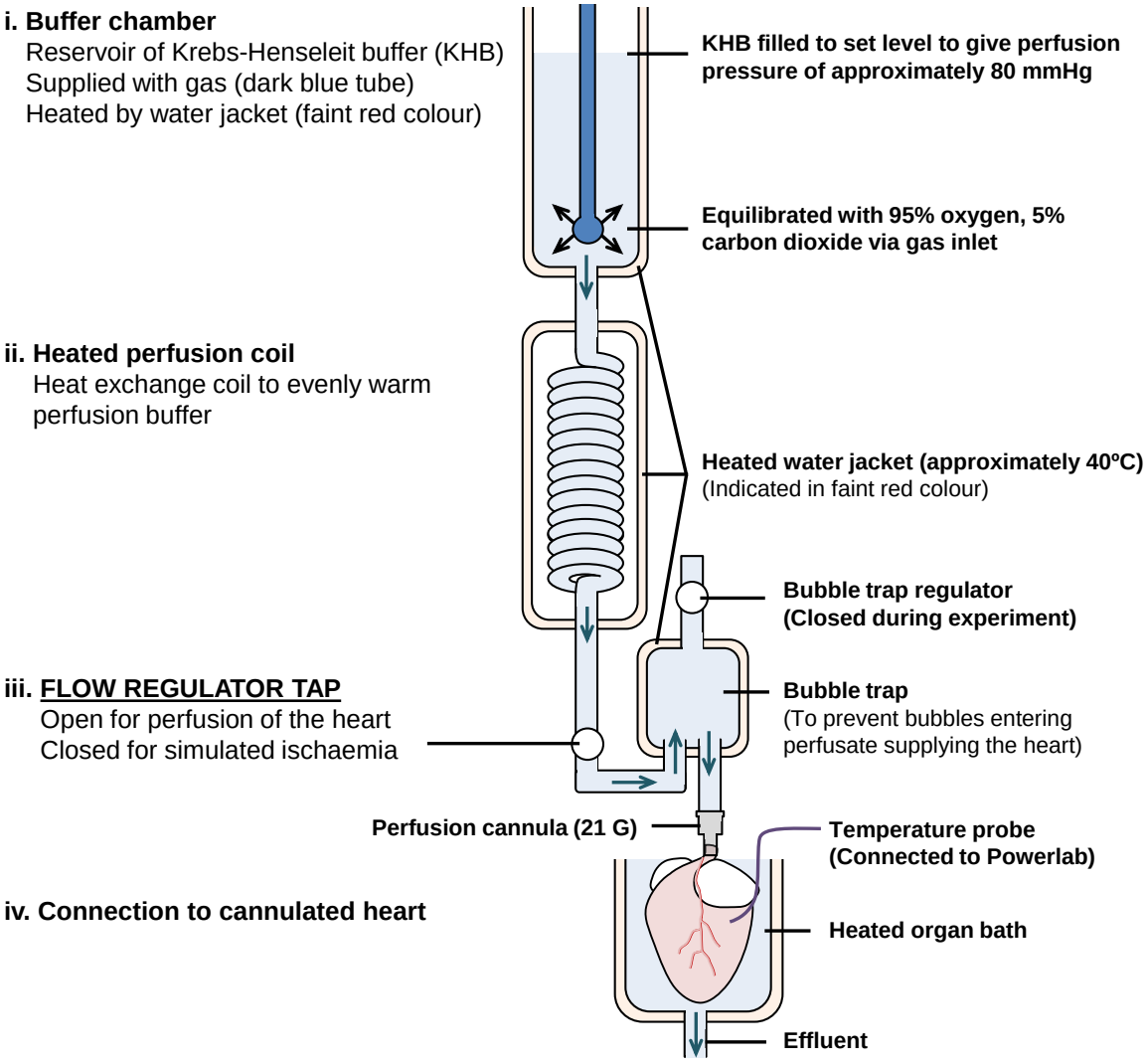

Figure 3.15: Overview of Langendorff perfusion system for preparation of heart samples
Simplified diagram of the constant perfusion pressure Langendorff system used to prepare control and ischaemic heart samples. Hearts were perfused with warmed Krebs-Henseleit buffer (KHB; indicated in pale blue). Buffer was gassed with 95% oxygen and 5% carbon dioxide (gassing rod shown in dark blue) and warmed by a system of heated jackets (indicated in faint red). A bubble trap system was used to ensure that no air bubbles could enter the perfusate. The heart was perfused in a retrograde manner via the aorta whilst submerged in a warmed organ bath. Buffer flow was regulated by opening and closing the flow regulator tap (iii) to allow perfusion (for stabilisation) and cessation of perfusion (for simulated ischaemia).

Immediately following cannulation of the heart, it was connected to the Langendorff apparatus and perfused at approximately 80 mmHg. Hearts were seen to contract rapidly upon perfusion and good function was confirmed prior to starting the experiment. Cardiac function was not formally assessed given the complications of inserting the pressure transducing balloon and often unreliable measurements using this system obtained with this setup in our laboratory. Perfusion of the heart was controlled by means of the flow regulator tap (see Figure 3.15) which remained in the open position for perfusion. Simulated ischaemia was induced by closure of the flow regulator tap and

thus cessation of perfusion and confirmed by the lack of effluent from the heart and the relatively rapid onset of dramatically reduced cardiac contractility.

Hearts were randomised to control and ischaemic groups, where control hearts were subjected to 30 minutes stabilisation and ischaemic hearts to 10 minutes stabilisation and 20 minutes global ischaemia (Figure 3.16). Upon completion of this protocol, hearts were removed from the Langendorff apparatus and the left ventricles dissected and immediately frozen by submersion into liquid nitrogen and then stored at -80ºC.

The period of stabilisation was started once the heart was securely attached to the Langendorff apparatus and good cardiac contractility had resumed. If the heart did not start contracting sufficiently it was discarded and the experiment started again to avoid any confounding effects on the final ATP assay conducted on this tissue. Two simultaneous perfusion experiments were conducted using this Langendorff system and the condition (control or ischaemia) randomised between hearts and perfusion rigs.

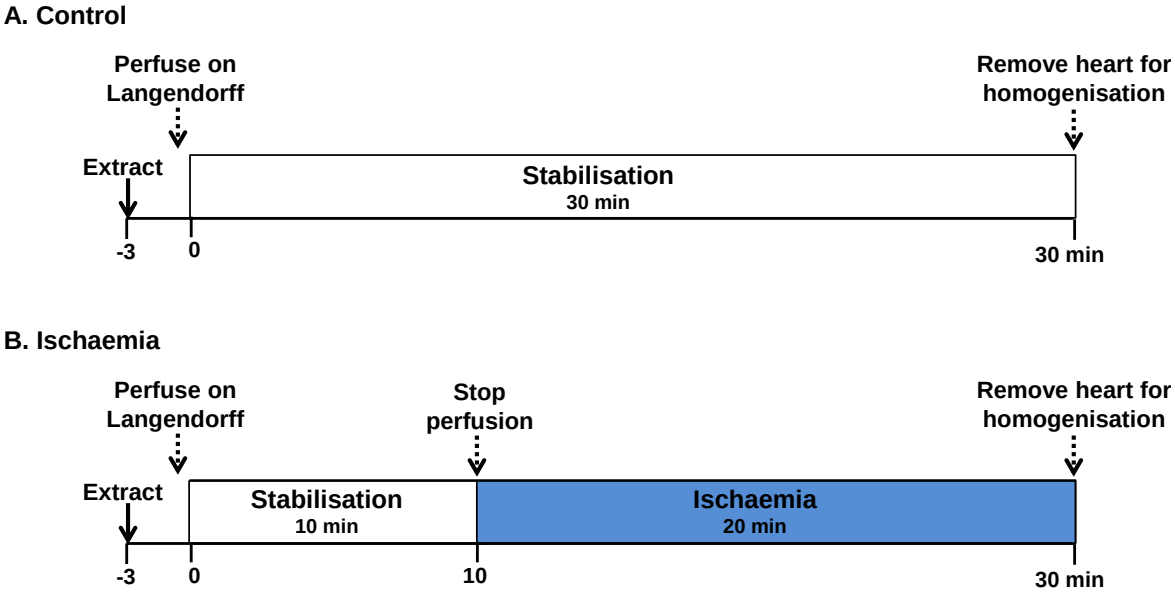

Figure 3.16: Langendorff perfusion protocol for the preparation of hearts for assay of ATP
Hearts were extracted from mice and cannulated to allow Langendorff perfusion. A) Control: 30 minutes stabilisation. B) Ischaemia: 10 minutes stabilisation and 20 minutes global ischaemia by cessation of perfusion. Left ventricles were then immediately frozen for subsequent processing.

Frozen heart samples were subsequently homogenised in ice-cold conditions in the standard homogenisation buffer described previously and the protein concentration of each sample assessed using a BCA assay, described above (see 3.4.1).

3.5.2. ATP luminescence assay

Myocardial ATP levels were measured using a commercial ATP assay kit (ATP Bioluminescent Assay Kit, Sigma-Aldrich, UK). This is a luciferase based assay whereby luciferin (the assay substrate) is converted to oxyluciferin by the luciferase enzyme in an ATP-dependent manner. When ATP is the limiting reagent, the intensity of the luminescence is proportional to the amount of ATP present (summarised in Figure 3.17).

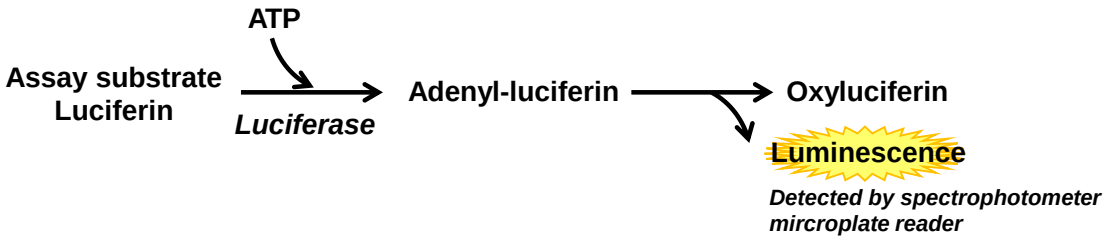

Figure 3.17: Molecular basis of luciferase assay quantification of tissue ATP levels
The chemical basis of this reaction is described in the datasheet by Sigma-Aldrich (2009).

This ATP assay was conducted in accordance with manufacturer's instructions (detailed by Sigma-Aldrich, 2009). This kit supplied an ATP assay mix (containing luciferase, luciferin, $MgSO_4$, dithiothreitol [DDT], BSA and tricine buffer salts) and ATP dilution buffer (containing $MgSO_4$, DDT, EDTA, BSA and tricine buffer salts).

Sample plate: Heart homogenates, prepared as described above, were diluted ten-fold in TAE buffer (buffer as above) and then incubated at 85ºC for 30 seconds. These heart samples were then transferred to a sample plate (standard clear 96-well microplate) to allow rapid transfer of samples when required, as detailed below.

Assay plate: The required volume of ATP assay mix was diluted 25-fold in the supplied ATP assay dilution buffer and vigorously mixed and rapidly transferred to the assay plate (white, clear bottom 96-well microplates; 100 µl diluted assay mix per well). The assay plate was swirled vigorously and incubated for 3 minutes to allow the signal from any endogenous ATP to be quenched to reduce any background luminescence signal.

Immediately following the 3 minute assay plate incubation period, the pre-prepared diluted heart samples were then rapidly added to the assay plate using a multi-channel pipette (100 µl heart sample per well) to ensure simultaneous addition of the heart samples to the assay plate for consistency of the luciferin reaction. The assay plate was then vigorously swirled and rapidly transferred to the microplate reader for assessment of luminescence every 5 seconds for 2 minutes using the FLUOstar Omega microplate reader (BMG Labtech, USA).

Statistical analysis of ATP levels: Luminescence values recorded during the first 20 seconds were used for all statistical analyses. These values were normalised to the average value recorded for wildtype control samples and expressed as a percentage of control ± standard error of mean (SEM). Data were analysed by one-way ANOVA, followed by Bonferroni test comparing relevant columns of data using GraphPad Prism® version 5.0 (GraphPad Software, USA). Statistical significance was reported where $P<0.05$ using standard significance coding.

3.6. Electron microscopy analysis of mitochondrial morphology

Examination of mitochondrial morphology in *ex vivo* tissues was undertaken using electron microscopy to evaluate mitochondrial length in *ex vivo* prepared heart samples.

3.6.1. Preparation of heart samples

Hearts samples were prepared from mice at baseline and following a sublethal ischaemic insult using the standard *in vivo* non-recovery ischaemia-reperfusion model exactly as described above (see 3.3.2). Mice were randomised to control or ischaemic treatment groups where the control group were subjected to 25 minutes stabilisation and the ischaemic group to 5 minutes stabilisation and 20 minutes ischaemia (Figure 3.18).

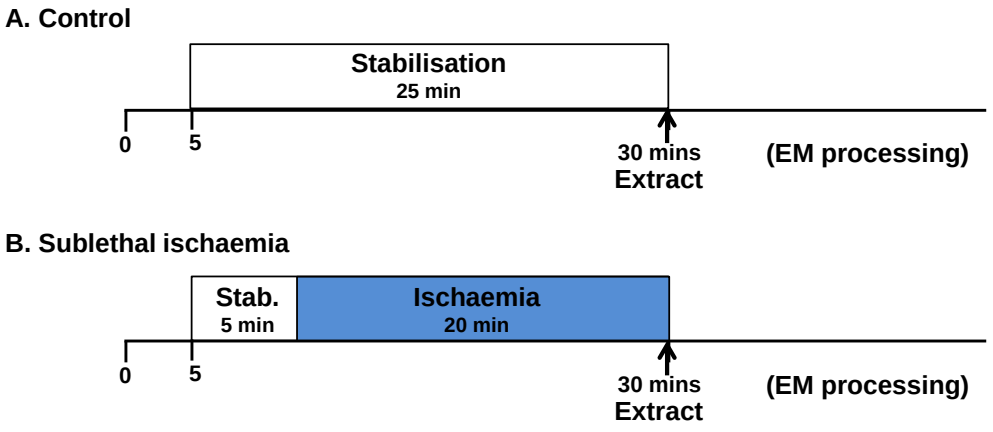

Figure 3.18: Non-recovery *in vivo* model protocol for assay of mitochondrial morphology
Mice were randomised to control or ischaemic groups. A) Control: 25 minutes *in vivo* stabilisation. B) Ischaemia: 5 minutes stabilisation and 20 minutes *in vivo* regional ischaemia by LAD ligation.

Hearts were then immediately extracted (with the LAD occluding snare still in place for the ischaemic group) and the aorta cannulated as described previously. Once cannulated the LAD occluding snare was released (in the ischaemic group) and residual blood removed by gentle perfusion of cold saline (1ml at 4ºC). Hearts were fixed for

electron microscopy (EM) imaging by perfusion of a standard EM fixative buffer consisting of standard PBS solution (described above) supplemented with paraformaldehyde 1%, glutaraldehyde 1%, $CaCl_2$ 0.5mM, glucose 0.031%, pH 7.3 and stored in this EM fixative buffer until further processing.

3.6.2. Electron microscopy

Subsequent processing and EM imaging described here was undertaken by Mr M. Turmaine (Electron Microscopy Services Facility, University College London, UK).

Hearts were prepared for EM imaging by removal of a 2 mm transverse slice of myocardium approximately 3 mm from the apex of the heart. Heart slices were fixed in an osmium buffer (consisting of: OsO_4 1% in standard PBS solution, pH 7.3) at 4ºC for 90 minutes and then washed in PBS buffer. Heart slices were En bloc stained with uranyl acetate (0.5% in distilled water) at 4ºC for 30 minutes to enhance the subsequent contrast of images. Heart samples were washed in distilled water and dehydrated in a graded ethanol-water series and then infiltrated with Agar-100 resin overnight (Agar Scientific, UK). Semi-thin sections of these slices were then cut at 1µm intervals and mounted on glass slides for staining with toluidine blue (1% in distilled water). Ultrathin sections were cut at 70-80nm using a microtome diamond knife (Reichert Ultra-cut, Reichert Microscope Services, USA). Sections were collected on mesh copper grids and stained with uranyl acetate and lead citrate. These processing steps were completed within one month of initial fixation of the heart samples.

Electron microscopy was performed on the stained ultra-thin sections and a random selection of 7 electron micrographs displaying longitudinally arranged cardiomyocytes taken for each heart (Jeol 1010 transition electron microscope, Jeol Ltd, UK).

Statistical analysis of mitochondrial morphology: Mitochondrial morphology was evaluated by assessment of the length of interfibrillar mitochondria (IFM) compared to sarcomere length where normal mitochondrial length was considered to be approximately 1 sarcomere length. Mitochondria were defined as less than 1 sarcomere length (fragmented morphology), equal to 1 sarcomere length (normal morphology) or greater than 1 sarcomere length (fused morphology). This method of evaluating mitochondrial morphology from *in vivo* prepared hearts has been previously validated by our laboratory (Ong et al., 2010). Analysis of EM images was performed by Dr S.B. Ong (previously of the Hatter Institute, UCL) who was blinded to the treatment groups.

The proportion of mitochondria defined as normal, fragmented or fused was calculated for each heart (total of 500-600 mitochondria per heart) and expressed as mean

percentage of mitochondria ± standard error of mean (SEM). All statistical analysis was completed using GraphPad Prism® version 5.0 (GraphPad Software, USA) to perform a one-way ANOVA and Bonferroni test comparing relevant columns of data. Statistical significance was reported where $P<0.05$ using standard significance coding.

3.7. Cardiac phenotyping by echocardiography

Echocardiography evaluation of mice in this thesis was undertaken in collaboration with Dr A. Dyson (Department of Medicine, University College London, UK).

Echocardiography examination of transgenic mice was undertaken to determine whether ablation of a particular gene of interest caused any overt cardiac phenotype.

3.7.1. Cardiac function at baseline

Assessment of cardiac function in transgenic mice was undertaken using ultrasound echocardiographic imaging to visualise *in vivo* functioning heart. Echocardiography was undertaken using a Vivid 7 dimension setup with 14 MHz probe (GE Healthcare, UK). Mice were anaesthetised with isoflurane vaporised in room air (3% isoflurane for induction and then maintained at 1.8-2.0% isoflurane). Animals were placed in the supine position for imaging and hair removed in the region of the heart to enable uninterrupted contact of the imaging probe. Upon steady anaesthesia using the minimal concentration of isoflurane required, echocardiographic measurements of cardiac dimensions and function were taken. Left ventricular end-diastolic (ED) and end-systolic (ES) dimensions were determined from a parasternal short-axis view at the papillary muscle level using time-motion (M) mode which allowed a quick succession of images to be taken to permit assessment of cardiac function (Rottman et al., 2007). The following echocardiographic measurements were taken:

(1) Anatomical measurements – Internal dimension of the left ventricle and the thickness of the left ventricle anterior and posterior walls (see Figure 3.19).

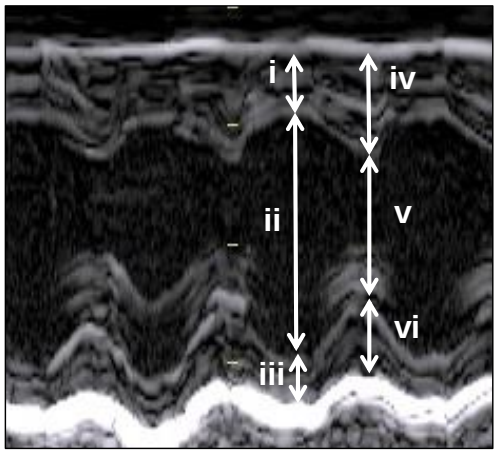

Diastole:
i) Anterior wall
ii) LV cavity
iii) Posterior wall

Systole:
iv) Anterior wall
v) LV cavity
vi) Posterior wall

Figure 3.19: Anatomical measurements of the heart by echocardiography
M-mode echocardiography of parasternal short axis view of the heart at the level of the papillary muscle. Anatomical measurements taken at diastole and systole.

(2) Aortic blood flow velocities – These were determined using pulsed-wave Doppler in the aortic arch immediately prior to the bifurcation of the right carotid artery. Blood flow direction was confirmed by colour Doppler. Peak aortic blood flow was measured as the average maximum velocity from 6 velocity-time traces.

(3) Heart rate – This was calculated by measuring the time between 6 consecutive cycles from the start of each Doppler trace.

(4) Stroke volume = velocity time integral * vessel cross sectional area
Where the vessel cross sectional area was calculated as: $(\pi \times [0.5 \times \text{diameter}]^2)$ where the diameter was assumed to be 1.34 mm based on a previous pilot study in age-matched wildtype mice (informed by Dr A. Dyson).

(5) Cardiac output = Heart rate * stroke volume

(6) Fractional shortening $= \frac{\text{(LV ED diameter - LV ES diameter)}}{\text{LV ED diameter}} * 100$

3.7.2. Cardiac function under pharmacological stress

The effect of a known cardiac stressor on the cardiac function of these mice was also examined. Isoproterenol is a non-selective β-adrenergic agonist that activates β_1-receptors on the heart to induce increased heart rate and force of contraction (Hoit et al., 1997). Normal functioning hearts are able to respond to this inotropic and chronotropic stimulation which should elicit a substantial increase in heart rate. Isoproterenol stress is commonly used to investigate potential differences in systolic or diastolic function that may not be evident at baseline (reviewed by Rottman et al., 2007). An isoproterenol stress protocol was optimised and used to assess cardiac function under stress.

Mice were administered isoproterenol (4 ng/g; intraperitoneal bolus) and echocardiographic measurements repeated after a 4 minute incubation period. This dosing protocol was optimised for use in this thesis and is described further in chapter 7.

3.7.3. Statistical analysis of echocardiography measurements

All values are presented as mean ± standard error of mean (SEM). Data were analysed by a one-way ANOVA and Bonferroni test comparing relevant columns of data using GraphPad Prism® version 5.0 (GraphPad Software, USA). Statistical significance was reported where the computed P-value was less than 0.05 and indicated using standard significance coding described above. No significance was reported where P>0.05.

3.8. Cardiac magnetic resonance imaging

Cardiac magnetic resonance imaging was undertaken in collaboration with Dr A. Campbell-Washburn and Mr T. Roberts, who were supervised by Prof M. Lythgoe (Centre for Advanced Biological Imaging, University College London, UK).

An overview of the relevant theory of magnetic resonance imaging (MRI) and its use for interrogating the physical properties of tissues *in vivo* is provided in chapter 1 (see 1.5.2). This thesis does not concern the development of the specific cardiac MRI sequences used here but assesses their application as potential tools for interrogating the reperfused mouse heart and for potentially assessing myocardial salvage.

The cardiac MRI sequences employed here were developed by our collaborators at the Centre for Advanced Biomedical Imaging (CABI) at University College London, UK. The development of the computational codes for the MRI sequences and data analysis used in this thesis have been reported by Dr A. Campbell-Washburn in the form of a PhD thesis. Readers are referred to Campbell-Washburn et al. (2012; 2013) for detailed descriptions of the arterial spin labelling MRI sequence and its development. Technical assistance for the later work presented here was provided by Mr T. Roberts at CABI.

The work presented in this thesis represents the first application of the MRI sequences developed at CABI to mice subjected to myocardial ischaemia-reperfusion injury.

3.8.1. Small animal magnetic resonance imaging setup

i Small animal cardiac MRI setup

MRI was undertaken using a 9.4 tesla horizontal bore scanner (Agilent Technologies, USA) fitted with 1000 mT/m gradient inserts (inner diameter of 60mm; Agilent Technologies, USA) running VNMRJ software (version 2.3A). Volume resonator quadrature RF coils (RAPID biomed, Ripmar, Germany) were used for RF transmission and signal reception. A detailed description of the MRI instrumentation at CABI is provided by Price et al (2011). MRI was undertaken according to the standard MRI protocol optimised at CABI and performed by Dr. A. Campbell-Washburn with final experiments assisted by Mr T. Roberts.

Mice were anaesthetised using isoflurane (approximately 1.5-2.0% isoflurane vaporised in 1.5 L/minute oxygen) and upon reaching a steady state of anaesthesia were transferred to the MRI small animal cradle (supplied with 1.0-2.0% isoflurane vaporised in 1.5 L/minute oxygen). Mice were securely fixed into the cradle and monitoring devices attached for real-time recording of respiration (neonatal apnoea sensor placed on the abdomen), ECG (two-lead setup, SA Instruments, USA) and body temperature (rectal thermometer attached to SA Instruments, USA). Body temperature was maintained at 36.5±0.5ºC using circulating warmed water (contained within tubing in close proximity to the animal) and a warm air fan placed at the entrance to the bore of the scanner. An intraperitoneal (I.P.) perfusion line containing gadolinium was attached to allow subsequent administration of gadolinium.

MRI acquisition was double-gated for both respiratory and cardiac gating to reduce motion artefacts. Respiration gating was applied by detection of chest movements using a pressure sensor (described above) to trigger image acquisition immediately following exhalation. Cardiac gating was achieved by detection of the integrated ECG trace to allow triggering of image acquisition immediately following detection of the ECG R-wave. This cardiac gating method ensured that images were obtained at the same phase of the cardiac cycle to allow compilation of final datasets of the whole heart and to allow subsequent quantification of cardiac parameters from these imaging protocols.

The main cardiac MRI protocol applied in this thesis comprised: (1) arterial spin labelling imaging (ASL) and (2) T_2-mapping and (3) late-gadolinium enhancement imaging; an overview of this protocol is shown in Figure 3.20 and described further below.

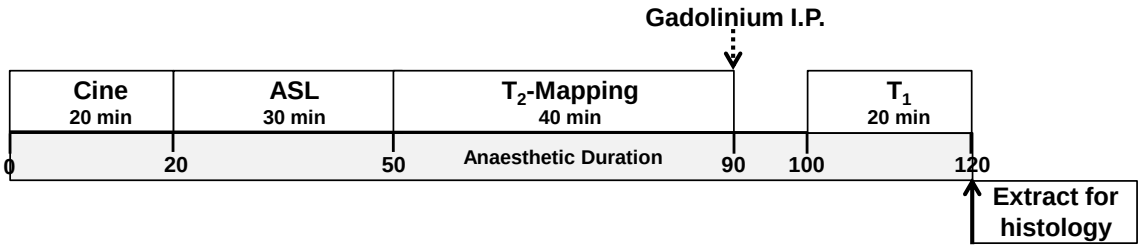

Figure 3.20: Cardiac MRI protocol
Animals underwent MRI comprising Cine imaging (volumes and function), T_2-mapping (putative AAR), arterial spin labelling (putative AAR) and late-gadolinium enhancement (infarct size). Immediately following cardiac MRI, mice were anaesthetised and hearts subjected to histological staining for validation of MRI measurements.

Cardiac MRI was performed by Dr A. Campbell-Washburn and Mr T. Roberts.

3.8.2. Cine imaging – Cardiac function

Cinematic (cine) images of the heart were first acquired to allow calculation of cardiac volumes and function of the reperfused mouse hearts examined in this thesis.

Theoretical basis: Cine imaging allows a series of single frame images of the heart to be captured throughout the cardiac cycle which can subsequently be used to create moving images of the heart to evaluate its contractile function. Cine imaging of the heart can be undertaken to give four-chamber (both ventricles and both atria), two-chamber (left ventricle and left atria) and short-axis (left ventricle and right ventricle) views of the heart. These images can be used to identify functional defects in contractile function and regional abnormalities in myocardial thickness. Cine imaging therefore allows an overall assessment of cardiac structure and function and is a widely used cardiac MRI protocol for animal and clinical studies of the heart (reviewed by McRobbie et al., 2006).

Method: The precise parameters of Cine imaging of the mouse heart used in this thesis are detailed by Price et al. (2011) and the salient points highlighted here. Initial scout images of the heart were first acquired in order to plan the two-chamber, four-chamber and short-axis views of the heart. For short-axis imaging of the heart, 10 myocardial slices of 1 mm thickness were imaged to approximately correspond to the whole left ventricle from apex to base. Cine imaging was performed using a double gated spoiled gradient echo sequence as detailed by Price et al. (2011). Two- and four-chamber cine images were used to assess cardiac contractile function and myocardial thickness only.

Quantification: Cardiac function was assessed from short-axis cine images. The myocardium was selected in these images by delineation of the epicardial and endocardial borders using semi-automated analysis by Segment software version 8 (Segment, http://segment.heiberg.se/). The blood pool volume (defined as the area

encompassed by the endocardial border) was then plotted against time to allow delineation of the phases of the cardiac cycle, specifically end-diastole (ED) and end-systole (ES). Manual correction of the segmentation of epicardial and endocardial borders was undertaken for the slices at ED and ES to ensure accurate calculations of cardiac function. Cardiac function was evaluated as detailed below:

(1) Anatomical measurements – Left ventricular wall mass (µg) was calculated as: Myocardial wall volume x 1.05 g/ml.

(2) Heart rate – This was calculated as the mean time between ECG traces.

(3) Stroke volume = (end-diastolic volume) – (end-systolic volume)

(4) Cardiac output = Heart rate * stroke volume

(5) $$\text{Ejection fraction} = \frac{\text{(LV end-diastolic volume - LV end-systolic volume)}}{\text{LV end-diastolic volume}} * 100$$

Statistical analysis: Quantification of these cardiac function measures was presented as mean ± standard error of mean (SEM). All statistical analysis was completed using GraphPad Prism® version 5.0 (GraphPad Software, USA). Where two groups were compared, data were analysed using an unpaired t-test. Where more than two groups were compared, data were analysed by one-way ANOVA and Bonferroni test comparing relevant groups. Statistical significance was reported where $P<0.05$.

3.8.3. Arterial spin labelling – Putative area-at-risk

This thesis investigates the use of arterial spin labelling (ASL) perfusion imaging as a potential method to quantify myocardial AAR *in vivo* in the reperfused mouse heart.

Theoretical basis: ASL MRI uses magnetically tagged water as an endogenous tracer to assess the movement of fluid within the myocardium. ASL uses radiofrequency (RF) pulses to affect the proton spins and in turn magnetically tag the blood water molecules (an excellent overview of this technique is provided by Petersen et al., 2006).

The ASL sequence applied in this thesis was a multi-slice flow alternating inversion recovery (FAIR) ASL (for precise details of this specific method see Campbell-Washburn et al., 2012). FAIR ASL uses two different inversion pulses to affect the proton spins within the tissue: (1) slice-selective inversion pulse (control condition – affects only proton spins in the imaging slice) and (2) global inversion pulse (tagged condition – affects proton spins throughout the body). ASL imaging is based on the T_1-relaxation (spin-lattice relaxation time) of protons spins. The global pulse inverts the proton spins of all blood within the myocardium such that the proton spins of the blood perfusing the

slice of interest are undergoing T_1-recovery with the T_1-relaxation parameters of blood. In comparison, the slice-selective inversion pulse inverts only the proton spins within that slice. The time delay between magnetic labelling (RF pulse inversion of proton spins) and acquisition (termed the inversion delay) allows new, unlabelled blood (with proton spins in equilibrium) to flow into the slice, thereby giving the appearance of accelerated T_1-recovery. Since the difference between control T_1-recovery (global inversion) and tagged T_1-recovery depends on the rate of myocardial perfusion, comparison of the T_1-values from control and tagged conditions can be used to provide an estimation of myocardial perfusion; further overview the theory of ASL MRI and its use for quantifying tissue perfusion is provided by Petersen et al. (2006).

Method: The ASL cardiac MRI method applied in this thesis was developed for application to the mouse heart by our collaborators at CABI (Campbell-Washburn et al., 2012; 2013). The studies presented in this thesis represent the first application of multi-slice ASL cardiac MRI to the reperfused mouse heart (discussed further in chapter 8).

Following completion of the cine imaging sequence, the multi-slice ASL cardiac sequence was initiated. T_1-relaxation was measured following slice-selective (control condition) and global (tagged condition) inversion RF pulses using a multi-slice segmented ECG-gated Look-Locker method. Scanning parameters were as follows: TE/TR(inv)/TR(RF) = 1.18 ms/13.5 s/3 ms, flip angle = 5°, FOV = 25.6 mm x 25.6 mm, matrix = 128 x 128, slice thickness = 1 mm, 6 slices total (3 slices/acquisition), number of points in recovery curve = 50 (as detailed by Campbell-Washburn et al., 2012; 2013). This ASL sequence was cardiac gated but not respiration gated which therefore resulted in some respiratory noise which is discussed in more detail subsequently. Multi-slice perfusion maps were calculated by comparison of T_1-recovery curves following slice-selective and global RF inversion pulses. This was performed on a pixel-by-pixel basis to generate ASL perfusion maps for each heart slice using scripts written in-house by Dr A. Campbell-Washburn (MATLAB Student Version R2008b, The MathWorks, USA).

The initial pilot study investigating the application of this ASL imaging method to reperfused mouse hearts in this thesis showed a large degree of variation in the perfusion values obtained for the most apical slice. This signal noise is thought to have resulted from respiratory motion since this ASL sequence was not respiratory gated. Since the perfusion values of the most apical slice did not seem reliable in the pilot studies, this slice was not acquired in the ASL imaging for the final datasets presented here. Since this method allowed acquisition of only 3 slices simultaneously, two acquisitions were required to image the whole left ventricle (6 short-axis slices).

Quantification: Perfusion was assessed from the ASL perfusion maps of 6 myocardial slices. Perfusion maps of myocardial slices produced by MATLAB compilation of raw T_1-values were displayed as heat-maps where normal perfusion appears in 'hot' colours (red – orange) and low perfusion appears in 'cold' colours (cyan - blue) (Figure 3.21).

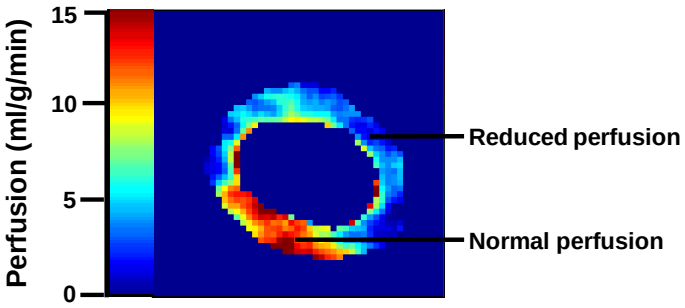

Figure 3.21: ASL perfusion map
Representative image of cardiac ASL perfusion map of mid-ventricle myocardial slice. Normal perfusion appears in 'hot' colours (red – orange) and low perfusion appears in 'cold' colours (cyan - blue). Segmentation of the myocardium means the background appears dark blue – this does not represent perfusion in these areas.

Normal perfusion values were defined for each heart by selection of a region of interest in the second from most basal slice, which is expected to be normal (corresponding to the non-AAR) in this mouse model of ischaemia-reperfusion. This area was used to define the mean normal perfusion. Reduced perfusion was defined as exhibiting a T_1-value less than 1 standard deviation below the mean normal T_1-value. This threshold analysis was performed by custom MATLAB scripts (as described above). The area of reduced perfusion was calculated as a percentage of the total number of myocardial pixels (area of perfusion deficit / myocardial area %). The area of reduced perfusion was investigated as a putative measure of myocardial AAR as described below (see 3.8.7).

3.8.4. T_2-mapping – Putative area-at-risk

Since previous studies have suggested that T_2-weighted based cardiac MRI can be used to determine the AAR *in vivo*, this thesis also investigated the use T_2-mapping MRI as a method to quantify myocardial AAR *in vivo* in the reperfused mouse heart.

Theoretical basis: T_2-weighted based MRI imaging is based on the T_2-relaxation (spin-spin relaxation time) of protons spins. T_2-relaxation is caused by interactions between proton spins whereby slower relaxation causes a faster T_2-relaxation time and reduction in the MRI signal. Since free water (fluid) contains small molecules that are far apart and rapidly moving, there are fewer spin-spin interactions resulting in slower T_2-relaxation (longer T_2-relaxation times). This slower T_2-relaxation results in less loss of T_2-signal at a given time thereby appearing bright on T_2-weighted images of the myocardium. T_2-weighted MRI exploits the known linear correlation between tissue water content and T_2-relaxation time to characterise pathological increases in tissue water content (McRobbie et al., 2006). Tissue oedema with increased fluid accumulation will therefore cause

slower T_2-relaxation resulting in increased T_2-relaxation times and brighter signals on T_2-weighted images. T_2-weighted based MRI sequences measure T_2-relaxation at a range of echo times (termed TE: defined as the time between RF pulse and signal measurement). At increased echo times there is more time for the protons to undergo T_2-relaxation resulting in reduced MRI signal, described by an exponential relationship. The T_2-relaxation times at multiple echo times can be used to construct exponential decay curves to determine the T_2 time constant (as described by McRobbie et al., 2006).

Method: The T_2-mapping cardiac MRI method applied here was developed for application to the mouse heart by Dr A. Campbell-Washburn at CABI. This method was loosely based on that briefly described in a presentation abstract by Bohl et al.(2010).

The MRI setup was as described above where 7 short-axis slices of the myocardium were interrogated. Following completion of ASL imaging, the multi-slice T_2-mapping cardiac protocol was initiated. T_2-relaxation was measured using a cardiac-gated spin echo sequence, with sequence parameters as follows: TE = (3.5, 7, 10, 12, 15, 17, 20, 25, 30) ms, repetition time (TR) = RR-interval, matrix = 128 x 128, field-of-view (FOV) = 25.6 mm x 25.6 mm, 7 slices, slice thickness = 1mm. A delay following the R-wave was introduced to this sequence to ensure that the MRI signal was measured at the same cardiac phase. Exponential decay curves of T_2-relaxation time were used fit to the myocardial signal intensity on a pixel-wise basis for each slice using scripts written by Dr A. Campbell-Washburn (MATLAB Student Version R2008b, The MathWorks, USA).

Quantification: Myocardial T_2-signal was assessed from the T_2-maps of the 7 myocardial slices. T_2-maps of each myocardial slice produced by MATLAB analysis were displayed as heat-maps in which normal T_2-signal appears in 'colder' colours (green-yellow) and elevated T_2-signal appears in 'hot' colours (red) (Figure 3.22).

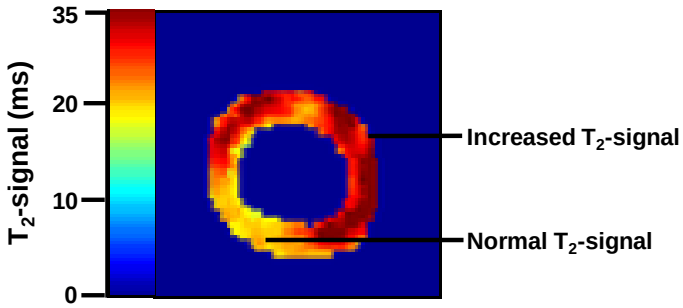

Figure 3.22: MRI T_2-map
Representative image of cardiac T_2-map of mid-ventricle slice. Normal T_2-signal appears in 'cold' colours (green – yellow) and increased T_2-signal appears in 'hot' colours (red). Segmentation of the myocardium means the background appears dark blue – this does not represent T_2-signal in these areas.

Normal T_2-signal values were defined for each heart by selection of a region of interest in the septum of the second from most basal slice, which is expected to be normal (non-AAR) in this mouse model. This area was used to define the mean normal T_2-value. Elevated T_2-values were defined as greater than 1 standard deviation above the mean

normal T_2-value. This threshold analysis was performed by custom MATLAB scripts (as described above). The area of elevated T_2-signal was calculated as a percentage of the total number of myocardial pixels (area of elevated T_2-signal / myocardial area %).

3.8.5. Late-gadolinium enhancement – Infarct size

Late-gadolinium enhancement (LGE) cardiac MRI has been widely used to quantify myocardial infarct size in experimental animal and clinical studies. This thesis applied a multi-slice LGE cardiac MRI protocol optimised and validated for use in rodents by our collaborators at CABI and described by Price et al. (2011).

Theoretical basis: The use of exogenous contrast agents can be used to affect T_1- or T_2-relaxation times and therefore provide enhanced signal within a region of interest. Gadolinium-based contrast agents have been widely used to highlight regions of myocardial infarction in cardiac MRI and have become a reference standard for this purpose. Gadolinium (Gd) acts as a paramagnetic agent due to its seven unpaired electrons which shorten T_1-relaxation time. Gd distributes throughout the vasculature and extracellular space but cannot transverse cell membranes due to its size and charge. However, in regions of infarction, disruption of cell membranes and the resulting increased extracellular space allows an increased Gd distribution which results in shorter T_1-relaxation times in this region of tissue. Late-gadolinium enhancement (LGE) imaging exploits this effect of Gd-enhanced T_1-relaxation by imaging the myocardium 10 minutes after Gd administration to allow sufficient Gd accumulation within the infarcted area. LGE allows clear visualisation of areas of infarction and has been widely validated to provide accurate infarct size quantification (overview provided by McRobbie et al., 2006); see 1.5.2 for a further overview of this method.

Method: The precise LGE imaging method used here is described by Price et al. (2011). Gadolinium diethylene-triamine penta-acetic acid (Gd-DTPA) was administered via an intraperitoneal infusion line as a single bolus of 0.6 mmol/kg Gd-DTPA (Magnevist, Germany). Following a delay of 10 minutes to allow for enhancement by Gd within the area of infarction, a further set of T_1-weighted images was acquired. A Look-Locker-style gradient echo acquisition was used to determine the null point of healthy myocardium in one mid-ventricle slice (one acquisition per cardiac cycle, TR(RF) = RR-interval, TE = 1.1 ms, FOV = 25.6 mm x 25.6 mm, slice thickness = 1 mm, flip angle = 10°, recovery delay= 1 s, acquisition time ~ 3 minutes). LGE images were acquired using the single inversion time point chosen with Look-Locker acquisition (typically 3 RR-intervals) (7 short axis slices acquired sequentially during systole per cardiac cycle, TE = 1.1 ms, TR(slice) = 3.1 ms, FOV = 25.6 mm x 25.6 mm, matrix = 128 x 128).

Quantification: Areas of infarction appear with an enhanced (brighter) signal on T_1-weighted images of the myocardium (Figure 3.23). Infarct area was determined using an automated delineation method constrained by the myocardial borders using Segment software (version 8, http://segment.heiberg.se/). Infarct size was calculated as the number of pixels with hyperenhanced T_1-signal as a percentage of the total number of pixels in the left ventricle. Analysis of this quantification is described below (see 3.8.7).

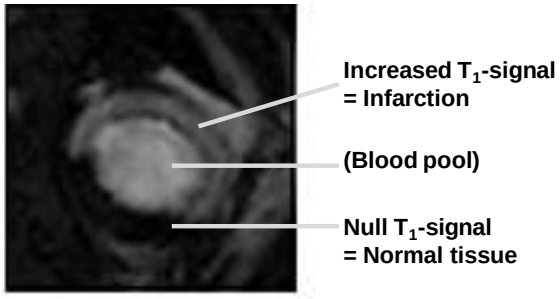

Figure 3.23: Cardiac MRI LGE image
Representative image of LGE imaging of mid-ventricle myocardial slice. T_1-images of the myocardium obtained at the null point of healthy tissue (appears dark). Accumulation of gadolinium within the area of infarction 10 minutes post-Gd-DTPA administration results in shorter T_1-relaxation within this area (seen as the region of bright signal intensity).

3.8.6. Histological staining for validation of cardiac MRI

In order to validate cardiac MRI measurements of infarct size and AAR, hearts were also subjected to classical *ex vivo* histological staining using TTC and Evans blue staining as described previously (see 3.2.4). Seven transverse slices of approximately 1 mm thickness were taken from apex towards base and imaged exactly as described above.

3.8.7. Statistical analysis of cardiac MRI and histological measurements

Percentage areas are reported as mean ± standard error of mean (SEM). All statistical analysis was completed using GraphPad Prism® version 5.0 (GraphPad Software, USA). Details of statistical analyses and sample sizes are provided alongside results presented in the subsequent chapters of this thesis. Validation of cardiac MRI quantification of myocardial infarct size and AAR was assessed by paired t-test comparison of MRI and histology endpoints for each group. For all statistical tests, statistical significance was reported where $P<0.05$ using standard significance coding.

To assess the overall agreement in cardiac MRI and histological methods, Bland-Altman plots were constructed for each experimental group. Although Bland-Altman plots do not provide a formal structure for statistical testing, they provide a useful method of visualising the differences between these two methods. The endpoint for each method was plotted for each heart as the difference between histological and MRI quantification (Δ = cardiac MRI – histology endpoint) against the average quantified by these methods.

CHAPTER 4: ESTABLISHMENT OF AN IN VIVO MODEL OF MYOCARDIAL ISCHAEMIA-REPERFUSION INJURY

4.1. Introduction

Ischaemia-reperfusion injury is the main clinical consequence of acute myocardial infarction. During acute myocardial infarction blockage of a coronary artery causes ischaemia within the area normally perfused by this vessel. Rapid reperfusion of the ischaemic myocardium is required to preserve the viability of 'at-risk' cardiomyocytes and is achieved clinically by primary percutaneous coronary intervention (PPCI) or pharmacological thrombolysis (Thygesen et al., 2007). However, myocardial reperfusion itself paradoxically causes a degree of myocardial injury (including cardiac arrhythmias, stunning and no-reflow) and cell death (lethal reperfusion injury). Although the former types of myocardial injury can be clinically managed, there remains no clinical therapy to protect against lethal reperfusion injury (reviewed by Hausenloy and Yellon, 2013).

Lethal reperfusion injury is thought to account for a significant proportion of the final myocardial infarct size in acute myocardial infarction patients. Since myocardial infarct size is a critical determinant of acute myocardial infarction patient prognosis (Sobel et al., 1972), lethal reperfusion injury represents a significant and largely unmet clinical target for cardioprotection (reviewed by Garcia-Dorado et al., 2009; Hausenloy and Yellon, 2013). It is therefore pertinent to investigate methods to protect the myocardium against both ischaemic and reperfusion injury. To this end, the first aim of this thesis was to establish an appropriate model of ischaemia-reperfusion injury which could be applied to investigate potential therapeutic targets for long-term cardioprotection.

There are numerous experimental research models of ischaemia-reperfusion including simulated ischaemia-reperfusion (hypoxia-reoxygenation) of preparations of *in vitro* cultured cells and *ex vivo* primary isolated cells. However, since this thesis aimed to investigate the long-term efficacy of cardioprotective interventions, an *in vivo* ischaemia-reperfusion model with long-term recovery of experimental subjects was essential.

The first results chapter of the thesis describes the establishment and validation of a mouse *in vivo* recovery model of ischaemia-reperfusion and the effects of important experimental variables central to the design of subsequent studies in this thesis.

4.2. Research objective and aims

The first aim of this thesis was to develop and characterise a mouse *in vivo* recovery model of ischaemia-reperfusion injury for subsequent investigations of long-term cardioprotective efficacy. The principal research aims to achieve this objective were:

(1) Establish a mouse *in vivo* recovery model of ischaemia-reperfusion injury;

(2) Validate this *in vivo* recovery model of ischaemia-reperfusion by application of known therapeutic interventions to demonstrate significant cardioprotection;

(3) Characterise this *in vivo* recovery model of ischaemia-reperfusion injury to determine the optimum protocol for subsequent applications of the model.

4.3. Aim 1: Establish *in vivo* recovery model of ischaemia-reperfusion

4.3.1. Background

Experimental models of *in vivo* ischaemia-reperfusion injury have been widely employed in this research field and have most commonly utilised large animal species including dog and pig (reviewed by Black and Rodger, 1996). However, although it is technically more challenging to establish *in vivo* models in mice due to their small size and rapid heart rate, recent advances in genetics and the resulting scope of genetically modified models make the mouse an important tool for investigating long-term cardioprotection.

Experimental research models of *in vivo* ischaemia-reperfusion injury most commonly comprise artificial occlusion of a main coronary artery to cause ischaemia followed by release of the occlusion to initiate reperfusion. This can be achieved using intra-coronary devices (for example coronary balloon inflation) in larger animals. However, in small animals this is usually undertaken by ligation and release of a fine suture placed around the coronary artery (reviewed by Verdouw et al., 1998; Klocke et al., 2007).

Clinically, occlusion of one of the main coronary arteries perfusing the left ventricle (LAD or circumflex arteries) results in the most significant patient morbidity and mortality due to the large area of myocardium affected and the essential role of the left ventricle in normal cardiac contractile function (Thygesen et al., 2007). Most animal models of ischaemia-reperfusion therefore comprise occlusion of one of these main left ventricle arteries, commonly the LAD (Verdouw et al., 1998). The LAD perfuses the majority of the left ventricle meaning that occlusion of the main LAD branch causes a large

regionally distinct area of ischaemia, termed the AAR (reviewed by Verdouw et al., 1998; Klocke et al., 2007). There are subtle differences in the LAD branch patterns of mice compared to other species; specifically, the mouse LAD does not perfuse the left ventricle septal wall (Kumar et al., 2005); this is, however, unlikely to influence the validity of the mouse model for cardioprotection studies. The mouse coronary anatomy exhibits a similarly low number of collateral vessels (those vessels serving the same vascular bed) as the healthy human heart. However, it should be noted that the occurrence of acute myocardial infarction in patients is preceded by the chronic pathological processes of cardiovascular disease which is likely to result in the develop and opening of collateral vessels (reviewed by Verdouw et al., 1998). These are important considerations for the development and interpretation of the model here.

The mouse *in vivo* recovery model of ischaemia-reperfusion was first described by Michael et al. in 1995 (Michael et al., 1995) and further refined by Fisher and Marber (2002). However, the mouse *in vivo* recovery model of ischaemia-reperfusion remains recognised as a challenging model to establish and further publications have aimed to provide detailed methodological protocols to expedite the setup of this model. Notably van Laake et al. (2007) published extensive troubleshooting advice which alongside the protocols from Michael et al. (1995) and Fisher and Marber (2002), provided a foundation for the establishment of the model in this chapter.

The main objective of this chapter was to establish and characterise a mouse *in vivo* model of ischaemia-reperfusion for the first time within our laboratory. The principal attributes of this model are: (1) use of mice to exploit genetic models, (2) defined periods of ischaemia and reperfusion and (3) recovery to permit long-term investigation.

Aim 1: The first aim of this chapter was to establish a mouse *in vivo* recovery model of ischaemia-reperfusion injury. The crucial milestones for development of the model were:

(1) Sufficient surgical survival – this is required by the UK Home Office to be greater than 75% immediate surgical survival of animals subjected to this protocol.

(2) Minimal and quantified effects of potentially confounding factors – this primarily concerns investigation of the potential conditioning effects of anaesthetic regime used and is described in more detail subsequently in this chapter.

4.3.2. Detailed methods

The mouse *in vivo* recovery model of ischaemia-reperfusion injury comprised occlusion and reperfusion of the LAD coronary artery followed by recovery of the animals for long-term investigation. The surgical procedure was based on that described by Fisher and Marber (2002) with modifications informed by van Laake et al. (2007). In addition to the brief description of the surgical model provided in chapter 3, this section provides a detailed description of the precise surgical protocol developed during the course of this study with the aim of providing a comprehensive resource for future operators.

i Ischaemia-reperfusion injury in vivo recovery model

Surgical setup: All recovery surgical procedures were conducted in a controlled sterile surgical theatre at University College London, UK. An overview of the surgical setup is illustrated in Figure 4.1 and the key components described below.

Aseptic operating practices were adhered to throughout the procedure as defined by the Handbook of Laboratory Animal Management and Welfare (Wolfensohn and Lloyd, 2003). Animals were prepared for surgery by hair removal and chlorhexidine cleansing of the chest and neck regions. Chlorhexidine washes were also undertaken prior to skin opening and immediately upon skin closure to reduce the possibility of infection.

Specialised small animal surgical instruments were used for all surgical procedures (instruments shown in Figure 4.1; purchased from World Precison Instruments, UK unless otherwise stated). All instruments were autoclaved prior to each operating session and a hot bead steriliser was used to sterilise instruments between surgeries.

Surgeries were conducted on a thermostatically controlled heated operating table (Peco Services Ltd, UK) covered with a sterile material drape. ECG recordings were taken throughout surgery by means of a three-lead ECG with electrodes attached subcutaneously on both forelimbs (positive and negative leads) and the right hind limb (reference lead) (Powerlab coupled to Chart 7 software, AD Instruments, UK). Temperature was monitored via a rectal thermometer (K-type thermocouple thermometer, Hanna Instruments, UK) and maintained at 37.0±0.5°C by manual adjustment of the heated operating table. All surgery was conducted with the aid of a surgical microscope (Zeiss Universal S2, Zeiss, Germany).

A

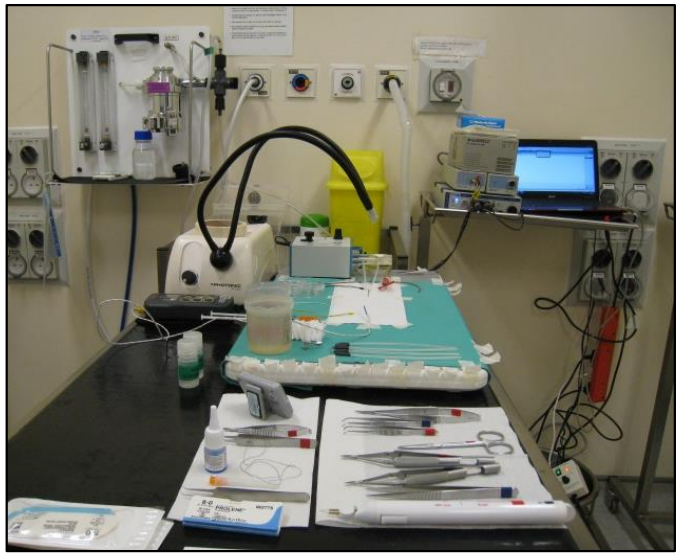

B

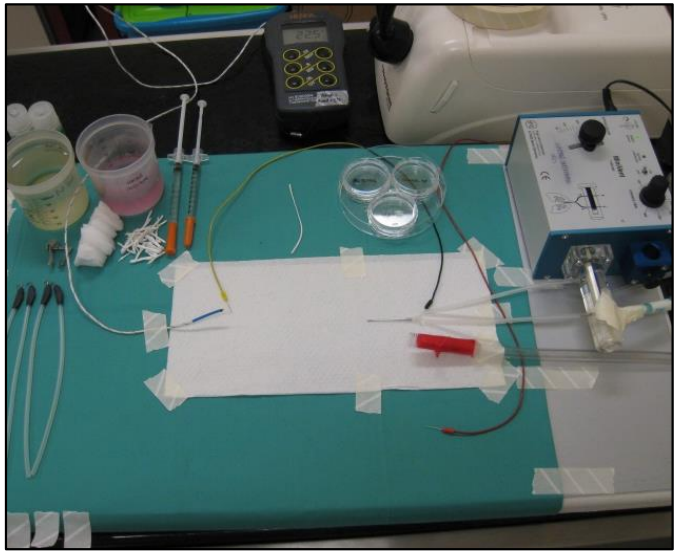

C

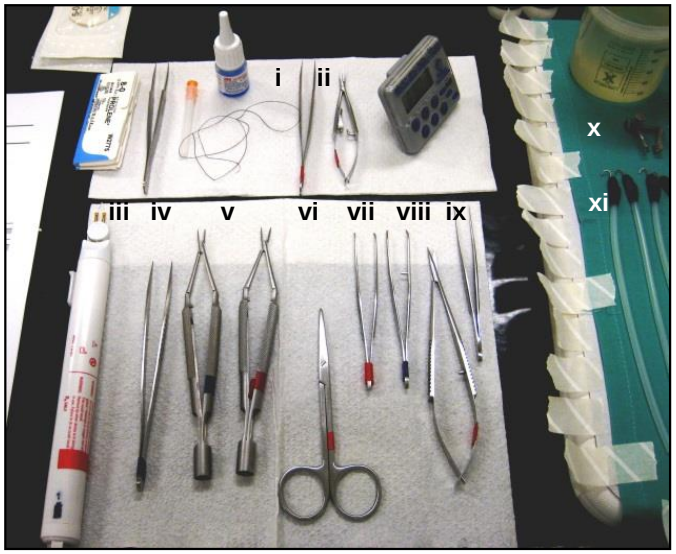

Figure 4.1: Surgical setup for *in vivo* model

A) Surgical setup: isoflurane vaporiser connected to oxygen supply, heated operating table prepared with sterile surgical drape, small animal ventilator and ECG setup. B) Operating table: ventilator, nose cone (red), temperature probe and ECG leads. C) Instruments: From World Precision Instruments, UK, unless stated otherwise in the text.

i) Fine forceps
ii) Small needle holder
iii) High temperature cautery
iv) Rat-toothed rib holder
v) Large needle holder
vi) Blunt round ended scissors
vii) Serrated tweezers
viii) Sharp microdissection scissors
ix) Smooth tweezers
x) Goldstein chest retractor
xi) Blunt stay hooks

Surgical procedure: Surgical depth of anaesthesia was assessed before starting the surgical procedure and regularly thereafter, where sufficient anaesthetic depth was confirmed by the loss of pedal reflex to toe-pinch stimulus. The anaesthetic regimes used are detailed subsequently. For isoflurane anaesthesia, breathing rate was also observed as an indication of anaesthesia; where slow shallow or deep gasping breaths were suggestive of too deep anaesthetic depth, as described by Wiersema et al. (1997).

The precise *in vivo* ischaemia-reperfusion surgical procedure is detailed below:

(1) Intubation – Mice were placed in the supine position and the neck extended using a suture hooked around the incisors and secured using adhesive tapes. Direct observation of the trachea was used to aid intubation by creating a small skin incision to the neck directly above the visible midline of the salivary glands. The trachea was exposed by gently teasing apart the skin, submaxillary glands and paratracheal muscles in turn. The ventilation cannula was passed through the mouth into the trachea (see Figure 4.4 i).

Successful intubation was confirmed once the intubation cannula could be directly visualised inside the trachea and further confirmed by observing regular chest movements upon ventilation. Unsuccessful intubation, corresponding to the placement of the ventilation cannula in the oesophagus, was judged by absence of the cannula inside the trachea and regular movements to the lower abdomen upon ventilation. In the event of unsuccessful intubation, the ventilation cannula was removed and further attempts at intubation made. Intubation was ideally completed within two attempts. The ventilation cannula was only connected to the ventilator once successful intubation was confirmed (see section ii). The final ventilation technique developed here is illustrated in Figure 4.6.

(2) Thoracotomy – For access to the LAD the mouse was repositioned by crossing the left leg over the body. A skin incision was made laterally across the chest at the approximate position of the fourth intercostal space. The major and minor pectoral muscles were blunt dissected and reflected outwards using blunt hook stays (Figure 4.1 xi); caution was taken to preserve integrity of the pectoral muscles for effective chest closure. The fourth intercostal space was identified by evaluation of the lung position - the fourth space being the one prior to the curvature of the base of the lung and confirmed by the presence of a large branching vessel along the surface of the rib. Opening of the intercostal space was performed by dissection to create a small entry hole using sharp pointed scissors (Figure 4.1 xiii) followed by insertion of a small animal chest retractor (Figure 4.1 x). Opening of the chest retractor was aided

by diathermic dissection using a high temperature cautery (Figure 4.1 iii; Bovie, USA). See Figure 4.4, stages ii-iv.

In occasional circumstances where the lung was positioned in close proximity to the chest wall opening, a small saline soaked swab was placed between the heart and lung in order to protect the lung. Extreme care was taken not to damage the lung. This swab was then removed at the end of the procedure prior to chest closure.

(3) Ischaemia / Reperfusion – Access to the LAD was facilitated by opening of the pericardium using blunt tweezers (Figure 4.1 vii, see Figure 4.4 v). The LAD was identified by its brighter red colour and often by its pulsating appearance; in cases where the LAD could not be visualised, the suture position was approximated from experience. The pericardium was used to slightly rotate the heart to facilitate access to the LAD. The LAD was under-run with an 8-0 polypropylene suture (8-0 prolene non-absorbable suture, W2775, Ethicon, USA) approximately 2 mm below the tip of the left atrium. A snare system consisting of several precisely cut lengths of polyethylene tubing (PE50, Deutsch and Neumann, Germany) and modified pipette tip was assembled onto the suture to allow LAD occlusion and release (Figure 4.2).

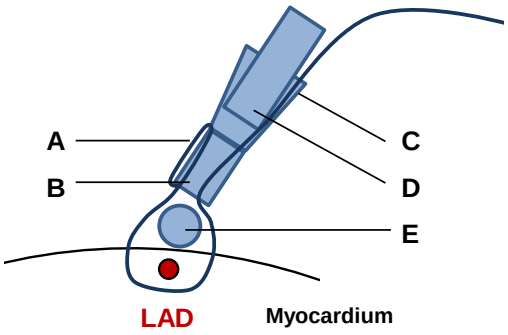

Figure 4.2: LAD snare system for ischaemia and reperfusion
Custom-made snare system for induction of ischaemia and reperfusion consisting of (a) 8-0 polypropylene suture, (b) suture tubing PE-50, (c) conical tubing pipette tip, (d) brake tubing PE-50 and (e) protective tubing PE-50. Ischaemia was induced by occlusion of the snare system and reperfusion initiated by release of the snare system.

(See Figure 4.4 for *in vivo* snare assembly)

Successful ischaemia upon occlusion of the snare system was confirmed primarily by appreciable myocardial pallor distal to the suture and ECG ST-segment change. Since the AAR was expected to be transmural across the free wall of the left ventricle, ischaemia was expected to induce elevation of the ST-segment (Figure 4.3 A). In cases where depression of the ST-segment was observed (indicative of subendocardial left ventricular ischaemia) the procedure was continued since AAR inclusion criteria were applied subsequently upon analysis (see section vi). In addition, successful ischaemia of a sufficiently large myocardial AAR was expected to cause noticeable akinesis of the left ventricle. Reperfusion upon release of the snare was confirmed by return of myocardial colour and resolution of the ECG ST-segment change (Figure 4.3 B). Precise exclusion criteria are detailed in section iv.

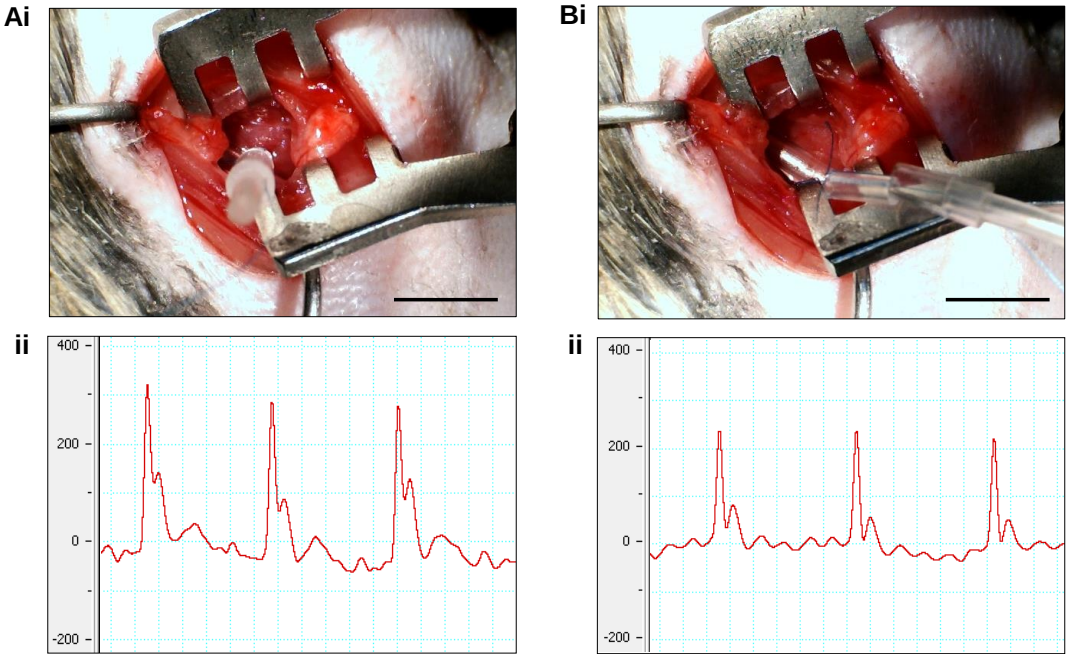

Figure 4.3: Confirmation of successful ischaemia and reperfusion
(A) Snare system *in vivo* (1 cm scale bar). (B) Example ECG for (i) stabilisation – loose assembly of snare and normal ECG trace, (i) ischaemia – occlusion of snare and ST-segment elevation and (ii) reperfusion – release of snare and resolution of ST-segment.

In sham operated mice the snare system was assembled but not occluded and all surgical timings observed to ensure equal anaesthetic duration between groups.

(4) Chest closure – Immediately following reperfusion, the snare system was disassembled and the suture cut leaving sufficient lengths for re-occlusion upon extraction of the heart. All parts of the snare except the LAD suture were removed and the ends of the LAD suture placed securely inside the chest cavity.

The intercostal space was closed using two 5-0 braided silk sutures (5-0 mersilk non-absorbable suture, W595, Ethicon, USA), where the lateral suture was tightened first to approximate the ribs and protect the lung. Ventilation positive end pressure (PEP) was then applied by submersion of the ventilator outlet tube in 2 cm of water to completely re-inflate the lungs, which was expected to improve respiratory function upon recovery. The medial suture was tightened upon simultaneous application of gentle chest compression to expel excess air to prevent pneumothorax. Effective closure of the intercostal space was facilitated by tissue glue (Vetbond, 3M, UK) applied to the suture sites and muscle opening. The major and minor pectoral muscles were unfolded to cover the underlying intercostal space opening and the skin closed with interrupted 5-0 braided silk sutures. Careful dissection of these muscles in stage 2 of this protocol preserves muscle integrity which in turn facilitates good closure of the intercostal space (see Figure 4.4 ix).

(5) Recovery – Cessation of anaesthesia is detailed for each anaesthetic regime below. When the animal had recovered independent breathing, extubation was facilitated by gentle removal of the ventilation cannula. Supplemental oxygen was provided via a nose cone for approximately 5 minutes after which animals were expected to have fully regained mobility. Animals were housed individually post-surgery and monitored hourly for the first six hours and twice daily thereafter.

Analgesia was provided by buprenorphine (0.1 mg/kg intramuscular, Vetergesic [Alstoe Animal Health, UK]) administered at the start of the procedure and 6 and 24 hours into recovery, as described previously in chapter 3.

A detailed pictorial summary of each stage of the mouse *in vivo* ischaemia-reperfusion surgical protocol is provided below in Figure 4.4.

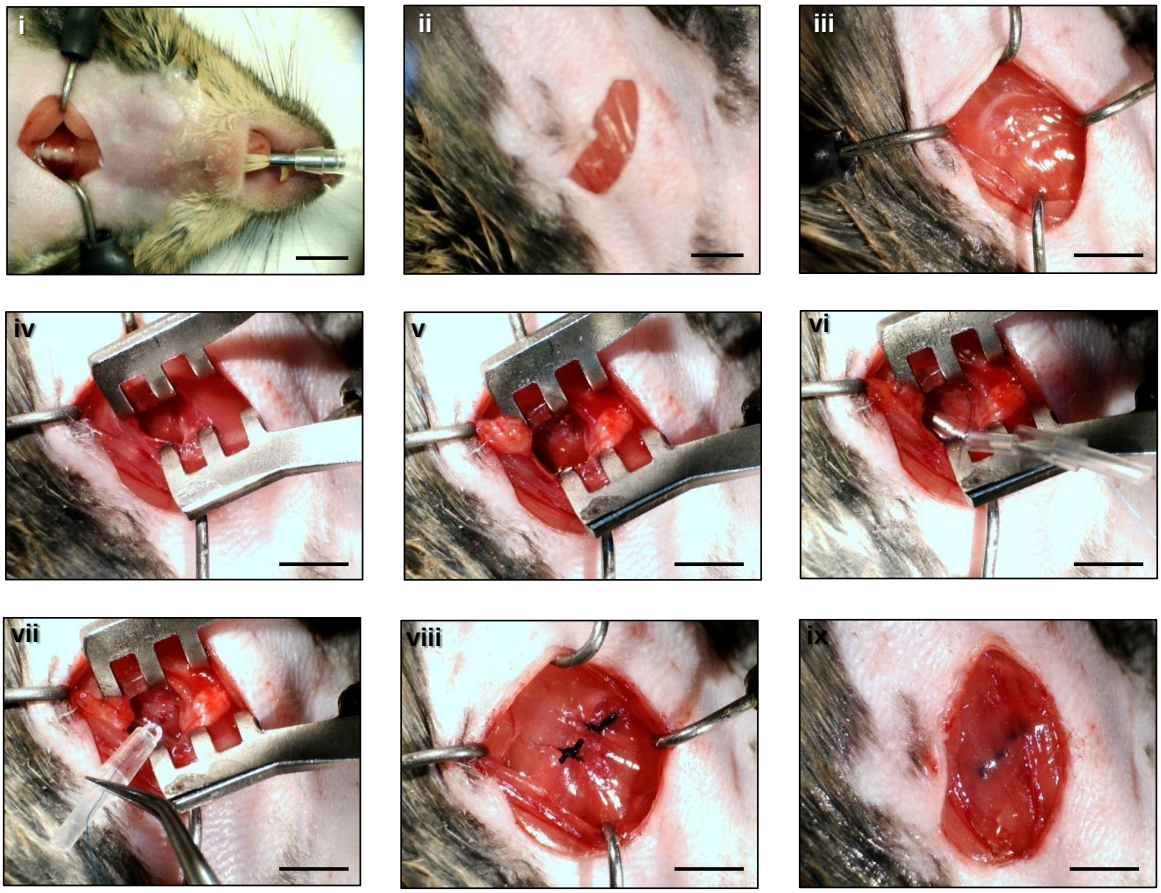

Figure 4.4: Summary of *in vivo* ischaemia-reperfusion injury recovery model
Main procedural stages (1 cm scale bar): i) Ventilation via oral intubation and connection to ventilator. ii) Preparation and opening of skin to reveal pectoral muscles. iii) Retraction of pectoral muscles using blunt hook stays. iv) Thoracotomy with the aid of a small chest retractor. v) Opening of pericardium to access the heart. vi) Placement of 8-0 suture around LAD and assembly of snare. vii) Occlusion of snare to induce ischaemia, followed by release and removal of snare. viii) Intercostal space closure using 5-0 sutures and tissue glue. ix) Release of pectoral muscles to complete chest closure.

The standard recovery *in vivo* ischaemia-reperfusion injury protocol was 30 minutes ischaemia and 72 hours reperfusion (Figure 4.5). A 15 minute stabilisation period was allowed prior to the onset of ischaemia to allow for extended durations of ischaemia or IPC in modified protocols without extending the total surgical duration. The total anaesthetic duration for this model was approximately 55±5 minutes and the anaesthetic duration was kept as consistent as possible between animals to reduce any potential interference of anaesthetic conditioning (discussed in section 4.6.1 i).

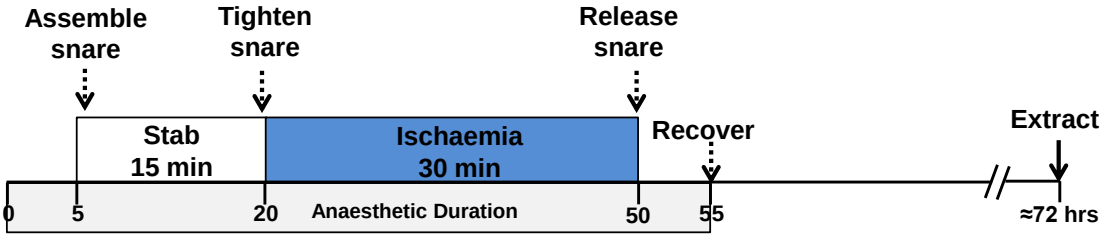

Figure 4.5: Standard *in vivo* recovery ischaemia-reperfusion protocol
Stabilisation was for 15 minutes followed by occlusion of the snare for 30 minutes ischaemia (blue box) and release of the snare to initiate reperfusion. Animals were recovered immediately upon reperfusion. Total anaesthetic duration was 55±5 minutes (indicated by pale grey box). Reperfusion was for 72 hours and hearts extracted for histological staining.

Recovery anaesthetics: Injectable and inhalation anaesthetic regimes were examined; the protocols are detailed below and their suitability discussed in section 4.6.1.

Injectable anaesthetics – This anaesthetic regime was based on that published by Cruz et al. (1998) and had previously been successfully employed within our laboratory for a short *in vivo* recovery procedure in mice. Mice were anaesthetised with an injectable cocktail containing ketamine (75 mg/kg [Vetlar, Bioniche Animal Health, Canada]) and medetomidine (1 mg/kg [Domitor, Orion Pharma, UK]) administered as a single intraperitoneal bolus. Commonly, two additional doses of 0.1 ml anaesthetic cocktail were required at 20-30 and 40-50 minutes to maintain surgical depth of anaesthesia. Ventilation stroke volume was 200 µl and stroke rate was 160 strokes/minute where the ventilator inlet was supplied with oxygen at 1.5 L/minute. This anaesthetic cocktail reduced heart rate to 200-250 BPM and had a profound effect on reducing body temperature, in line with published reports (Cruz et al., 1998), meaning that temperature control was critical for this anaesthetic regime.

Recovery of consciousness was induced by atipamezole (5 mg/kg [Antisedan, Pfizer, USA]) administered as a single intraperitoneal bolus matching the total volume of anaesthetic administered. Extubation was expected within approximately 15 minutes and recovery of movement within 3 hours, although animals remained drowsy and relatively inactive for several hours after this.

Inhalation anaesthetics – Mice were anaesthetised with isoflurane (Isoflo, Abbott Animal Health, USA) vaporised in oxygen. Induction of anaesthesia was in a gas chamber supplied with 1.5 L/minute oxygen and 5% isoflurane, reduced to 2% after 1 minute. Intermediate maintenance of anaesthesia was via a nose cone (custom made from the barrel of 2 ml syringe) supplied with 1.5 L/minute oxygen and 2% isoflurane. Long-term anaesthesia was via the ventilator supplied with 1.5 L/minute oxygen and 1.8-2% isoflurane, stroke volume of 200 µl and stroke rate of 200 strokes/minute. Isoflurane was regulated to the minimum concentration for the maintenance of surgical anaesthesia and ventilation parameters were optimised for each mouse strain to ensure there were no deep gasping breaths and surgical anaesthesia was easily maintained. Gasping breaths resulted from either lighter anaesthesia (despite absence of a toe-pinch reflex) or deep anaesthesia and in both cases correlated with poor recovery. Heart rate under this anaesthetic regime was 500–600 BPM and was unaffected by anaesthetic depth. This anaesthetic regime did not affect body temperature.

Recovery of consciousness was achieved by termination of the isoflurane supply, after which animals regained consciousness within 3-5 minutes. Recovery of movement was expected within 10 minutes and mice were expected to be active and alert within 1 hour.

ii Surgical complications

The *in vivo* recovery model of ischaemia-reperfusion is recognised to be complicated to establish in the mouse due to difficulties in part resulting from: (1) its small size, (2) its rapid heart rate and (3) the prolonged anaesthetic duration required (Fisher and Marber, 2002). During the course of establishing this model, several problems were encountered which required further refinement of the surgical protocol; the principal refinements are described below and extensive troubleshooting guidance is provided in Table 4.1. Following these refinements it was possible to produce a reliable and robust model of ischaemia-reperfusion *in vivo* with recovery using isoflurane anaesthesia. The suitability of the anaesthetic regimes is described in the results section below (see 4.3.3).

Ventilation technique: Initial surgeries showed that a number of mice subjected only to intubation and recovery exhibited poor recovery or death, thus indicating a potential problem with the anaesthetic regime or ventilation technique. Post-mortem examination of these mice revealed inflation of the bowels which sometimes resulted in distension of the diaphragm. The most likely cause of this was poor intubation technique where the intubation cannula was momentarily inserted into the oesophagus (the route of least resistance during intubation). The ventilation procedure was modified to only connect the cannula to the ventilator following confirmation of successful intubation to prevent bowel inflation; this seemed to resolve this complication and improved surgical survival.

This modified ventilation technique using inhalation anaesthesia is illustrated in Figure 4.6 below. It is imperative to note that the ventilation procedure had to be completed very rapidly during the periods in which the animal was not receiving isoflurane (highlighted in red in Figure 3.5). This ventilation technique required redirection of the gas supply and change of connection hoses, as indicated below, to ensure that the duration during which the animal received no isoflurane was minimised. Surgical survival of animals subjected to this procedure was improved following this procedural modification. This ventilation technique was used for all subsequent surgeries.

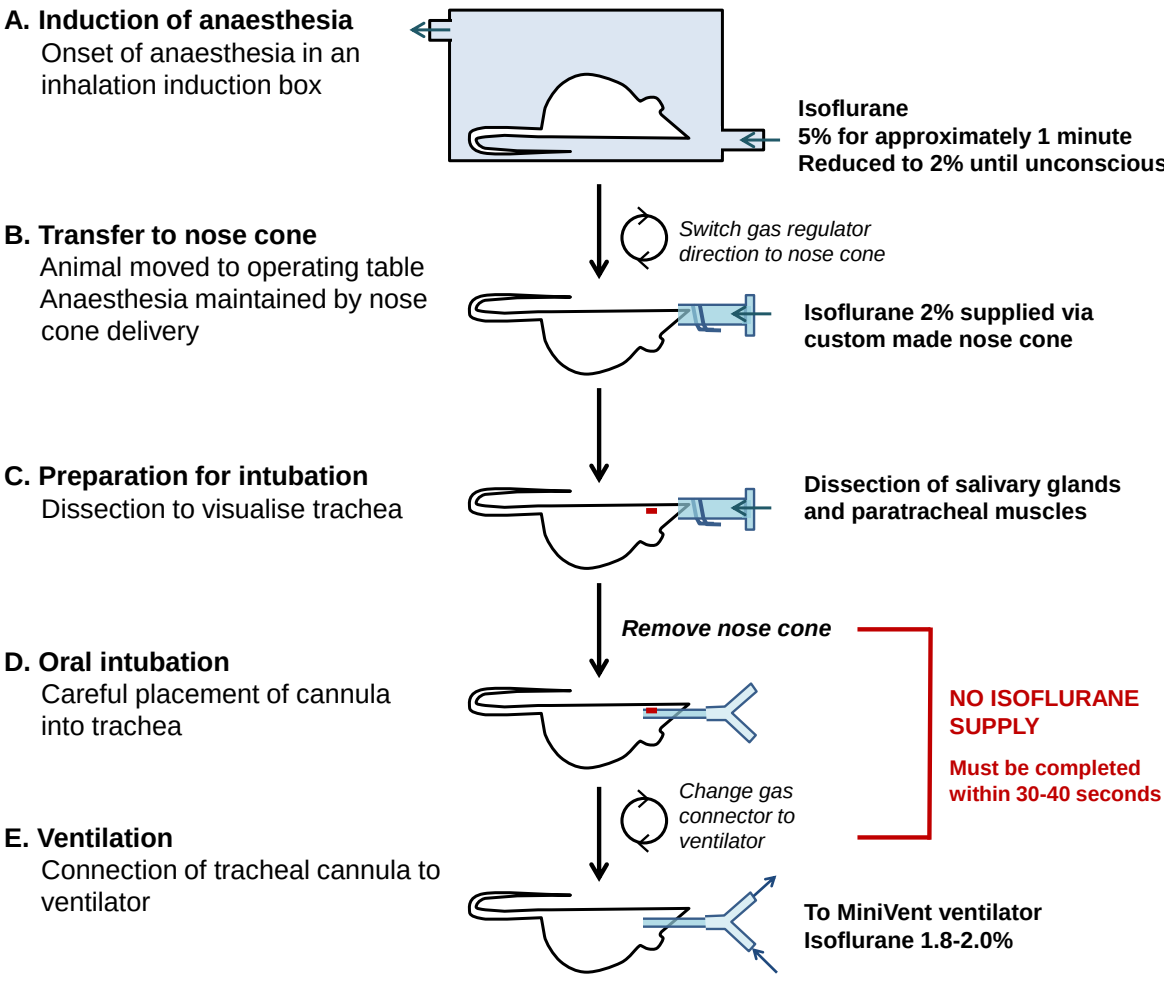

Figure 4.6: Modified ventilation procedure using isoflurane anaesthesia
Optimised ventilation technique developed for use with isoflurane anaesthesia. A) Anaesthesia was induced in a standard induction box after which animals were transferred to the operating table (B) where anaesthesia was maintained by connection to a custom made nose cone (modified 2 ml syringe barrel with metal clip to stabilise its location). C) Dissection of the neck region to visualise the trachea. D) The nose cone was removed to allow oral intubation. E) Mice were ventilated only upon confirmation of successful placement of the tracheal cannula.

COMPLICATION	POSSIBLE CAUSE	SOLUTION AND PROGNOSIS
(1) INDUCTION OF ANAESTHESIA AND INTUBATION		
Gasping on ventilation *(Note - C57BL/6 mice gasp slightly under isoflurane anaesthesia which is normal)*	Incorrect placement of ventilation cannula in oesophagus.	Re-intubate. Poor recovery prognosis due to inflation of bowels.
	Anaesthesia too deep or not deep enough. Check toe-pinch reflex and observe gasps: i) Too deep – very deep gasps, check toe-pinch reflex ii) Too light – frequent shallow gasps	i) Reduce isoflurane ii) Increase isoflurane Good prognosis provided rapidly corrected. Avoid problem by careful regulation of isoflurane dosing. Poor prognosis if unresolved.
	Blockage of ventilation tubing. Confirm by lack of bubbles from ventilator exhaust when submerged in water.	i) Tubing blocked – rapidly replace tubing. Good prognosis. ii) Intubation cannula blocked – prior to thoracotomy, remove and clean cannula and re-intubate (good prognosis). Cannot be resolved after thoracotomy - terminate experiment if any signs of respiratory distress.
(2) THORACOTOMY		
Difficulty identifying correct intercostal space	Lung is likely to be fully inflated over the heart meaning the edge of the lung cannot be used as a guide.	i) Manoeuvre angle of left leg over body to rotate heart and lungs. ii) Count ribs to identify fourth space. Easily resolved.
Left ventricle and atrium are not visible upon opening of the chest	Incorrect intercostal space. i) If only left atrium is visible then thoracotomy was at third intercostal space. ii) If only apex of left ventricle is visible then thoracotomy was at fifth intercostal space.	Open correct intercostal space in addition and continue with procedure. At the end of the procedure close thoracotomy by approximating 3 ribs. Prognosis is medium to poor depending on success of closure, pneumothorax may occur.
Upon opening the chest, the lung is covering the heart	Occurs even under optimal ventilation parameters.	i) Manoeuvre angle of left leg over body to rotate heart and lungs within chest. Good prognosis. ii) Move lung away using a sterile swab. Medium to good prognosis.
(3) ISCHAEMIA – REPERFUSION		
LAD is not readily visible.	Observing incorrect region of the left ventricle.	Use atrial appendage to identify correct region of left ventricle. Rotate the heart gently using the pericardium. Easily resolved.
	Anatomy of LAD – vessel runs deeper into the myocardium.	i) Increase microscope light intensity. ii) Approximate location by reference to atrial appendage. Good prognosis with experience.
Bleeding on placement of suture	Suture needle passed through a vessel.	Terminate experiment if bleeding is severe or if there is any visible damage to the myocardium
	Suture needle came into contact with the lung – evidenced by the lung becoming a deep red colour.	Terminate experiment if bleeding is severe or if there is any visible damage to the lung affecting ventilation.

COMPLICATION	POSSIBLE CAUSE	SOLUTION AND PROGNOSIS
No ST-segment elevation or myocardial colour change on ischaemia	Occlusion of snare system was not sufficient to induce complete ischaemia.	Immediately increase occlusion pressure. Note – this must be done simultaneously on induction of ischaemia to avoid potential inadvertent preconditioning, otherwise terminate the experiment.
	Incorrect placement of occluding suture.	Terminate experiment. Take detailed description of incorrect location to facilitate learning process.
Bleeding on occlusion of suture	Mechanical damage to myocardium (with or without severing the LAD). Caused by poor suture placement: i) Suture too wide ii) Suture too shallow	Terminate experiment if bleeding is severe or if there is any visible damage to the myocardium. If experiment is continued then take particular care to confirm reperfusion was successful.
ST-segment resolution or return to red myocardial colour during ischaemic period	Occluding snare system loosened during the procedure. Caused by: i) Incorrect tension of snare ii) Accidental movement of snare	Terminate experiment.
ST-segment elevation or myocardial colour change do not resolve upon reperfusion	Slight delay in total reperfusion due to normal processes.	Carefully observe LAD to determine whether it has fully reperfused. If changes have not occurred within 1 minute then terminate experiment.
	Mechanical damage to LAD or surrounding myocardium meaning LAD reperfusion will not occur.	Terminate experiment.
(4) CHEST CLOSURE		
Difficult or incomplete closure of intercostal space	Thoracotomy was too wide creating a large opening.	Place intermediate 5-0 suture to approximate ribs and then continue to close with 2 further sutures. Prognosis is medium to poor depending on success of closure, pneumothorax may occur.
Gasping immediately following chest closure	i) Increased depth of breathing upon chest closure is normal. ii) If very deep gasping occurs this may indicate unsuccessful re-inflation of the lungs.	i) Slight increased depth of breathing is normal, no action need be taken. ii) Upon deep gasping, further compress chest to remove residual air and apply tissue glue simultaneously.
(5) RECOVERY		
Independent breathing does not resume within 10 minutes	Slight overdose of isoflurane meaning recovery will be prolonged.	Stop oxygen supply to ventilator and wait a further 5 minutes if ECG confirms heart is still beating.
	Other problem with surgery meaning recovery may not be successful.	If independent breathing has not resumed following above step then remove ventilation cannula and observe. If breathing does not occur confirm death by cervical dislocation.

Table 4.1: Surgical refinements and troubleshooting for *in vivo* recovery model
Refinements to the *in vivo* recovery surgical protocol; identification of the common problems and their possible causes and solutions. Note that this table relates specifically to the isoflurane inhalation anaesthetic regime, although many problems were common to all anaesthetic regimes.

iii Ischaemia-reperfusion injury in vivo non-recovery model

A non-recovery *in vivo* model of ischaemia-reperfusion was developed for studies requiring assessment of infarct size after only short reperfusion durations. This model was previously established within our laboratory; however, the protocol was modified to ensure consistency of the *in vivo* procedures used in this thesis. The *in vivo* non-recovery protocol was exactly as above (section i) with the modifications detailed here.

Non-recovery anaesthetics: Mice were anaesthetised with an injectable anaesthetic cocktail containing ketamine (100 mg/kg [Vetlar, Bioniche Animal Health, Canada]), xylazine (20 mg/kg [Rompun, Bayer, UK]) and atropine (0.6 mg/kg [Sigma, UK]) administered as a single intraperitoneal bolus. Surgical depth of anaesthesia was continually monitored and maintained by additional doses of as required.

This anaesthetic regime reduced heart rate from 500-600 BPM to 300-400 BPM at surgical depth of anaesthesia. Ventilation stroke volume was 200 µl and stroke rate was 120 strokes/minute where the inlet was supplied with oxygen at 1.5 L/minute.

Surgical procedure: Non-recovery surgeries were undertaken in the laboratory instead of in a sterile operating theatre. The non-recovery surgical setup was identical to that described above (see section i) but used a standard dissection microscope (Gallenkamp, Weiss, UK). Following successful onset of reperfusion, the intercostal muscle opening was loosely closed using one 5-0 braided suture and covered with a moistened tissue drape to prevent tissue desiccation. Surgical anaesthesia was maintained throughout the reperfusion duration. At the end of reperfusion, hearts were extracted for histological staining (see section vi).

The standard protocol for the non-recovery ischaemia-reperfusion injury model was 30 minutes ischaemia and 2 hours reperfusion (Figure 3.12). The total anaesthetic duration was approximately 2 hours 50 minutes; however, this was more variable than the isoflurane recovery procedure due to the less predictable onset of anaesthesia.

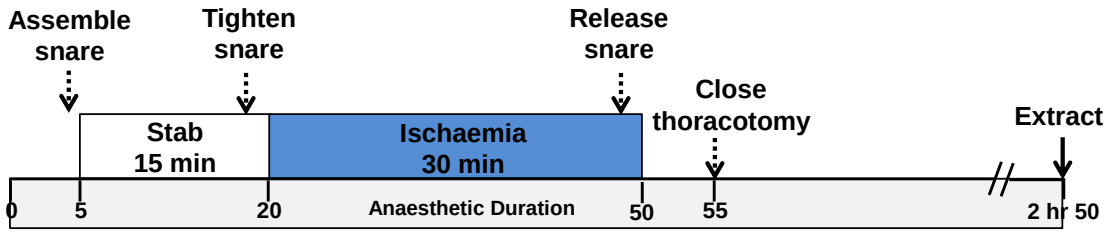

Figure 4.7: Standard *in vivo* non-recovery ischaemia-reperfusion protocol
Stabilisation was for 15 minutes followed by occlusion of the snare for 30 minutes ischaemia and release of the snare to initiate reperfusion. Reperfusion was for 2 hours. Animals were anaesthetised for the whole procedure (anaesthetic duration indicated by pale grey box).

iv Surgical exclusion criteria

Consistency of the surgical model was ensured by application of surgical exclusion criteria concerning: (1) body temperature, (2) LAD ligation and (3) ischaemia-reperfusion, described below. Following initial establishment of the model, exclusion of animals from a study on the basis of these criteria was rare.

(1) Body temperature – Body temperature was maintained at 37.0±0.5ºC throughout the surgical procedure. All efforts were made to ensure that body temperature was maintained within this ideal range. If temperature deviated by more than 1ºC (i.e. less than 35.5ºC or greater than 38.5ºC) the animal was excluded. Strict temperature control was imperative given the known cardioprotective effect of extremes of body temperature (van den Doel et al., 1998).

(2) LAD ligation – Ideal placement of the ligating LAD suture was approximately 2 mm below the tip of the left atrium. If the location of the ligating suture was visually too high or low then the suture was removed prior to snare assembly and replaced for a maximum of two attempts. If any visible damage to the myocardium or severe bleeding occurred from placement of the suture then the animal was excluded from the study to avoid any confounding mechanical injury to the myocardium. Further LAD ligation exclusion criteria were applied at the point of analysis of AAR as described below (see section vi).

(3) Ischaemia / Reperfusion – Successful ischaemia and reperfusion were confirmed by: (1) ECG ST-segment change, (2) myocardial colour change (3) contractile movement of the AAR. Animals were excluded where the onset of ischaemia or reperfusion was not accompanied by at least observations (1) and (2).

Animals were rarely excluded from the study due to unsuccessful ischaemia. Unsuccessful reperfusion was the most common cause of exclusion from a study and this was more frequent following extended ischaemic durations (for example 45 minutes ischaemia) or IPC due to mechanical damage to the myocardium.

v Endpoint 1 – Surgical survival

Surgical survival was evaluated by close monitoring of all animals post-surgery. Deaths were recorded to the nearest hour in the immediate post-operative period and the cause of death defined as: (1) surgical death from operative error, (2) surgical death from unexplained cause, (3) post-operative death from respiratory failure, (4) post-operative death from cardiac rupture or (5) post-operative death from unexplained cause.

Statistical analysis: Kaplan-Meier survival plots were plotted using GraphPad Prism® version 5.0 (GraphPad Software, USA). Statistical significance was analysed by log-rank

tests (Mantel-Cox) since this is the more standard and powerful relevant statistical test. Statistical significance was reported where $P<0.05$ using standard significance coding.

vi Endpoint 2 – Histological staining for infarct size and area-at-risk

Infarct size and AAR were assessed by classical histological staining in animals which survived to the pre-defined reperfusion duration. Staining for infarct size and AAR was by *ex vivo* perfusion of TTC and Evans blue dye.

For *ex vivo* histological staining, mice were anaesthetised with ketamine (100 mg/kg [Vetlar, Bioniche Animal Health, Canada]), xylazine (20 mg/kg [Rompun, Bayer, UK]) and atropine (0.6 mg/kg [Sigma, UK]) administered as a single intraperitoneal dose. Upon surgical anaesthesia, the chest was rapidly opened and the heart extracted by cutting the aorta immediately before the aortic loop. The aorta was cannulated onto a 21 G perfusion cannula to allow retrograde perfusion of the heart. Extreme caution was taken to maintain the location and integrity of the LAD ligating suture. The ideal time to perfusion was less than 4 minutes and with experience very rarely exceeded 3 minutes.

Residual blood in the coronary system was removed by manual perfusion of saline (1 ml). TTC solution (7 ml of 1% in PBS) was pre-warmed to 37°C and perfused within 3 minutes of heart extraction. For delineation of the AAR, the LAD ligating suture was re-occluded and Evans blue (1.5 ml of 0.5% Evans blue in distilled water) perfused whilst the heart was submerged in running water to prevent surface staining. All perfusion was completed manually with extreme care not to damage the coronary circulation.

Hearts were stored at -20°C for 1–2 days to facilitate slicing. Frozen hearts were manually sliced using a sharp scalpel to take 5 transverse slices from the apex with the uppermost slice at the approximate level of LAD occlusion. Heart slices were washed in distilled water and fixed in 10% formalin for 90-120 minutes at room temperature. The right ventricle was removed by careful dissection and the left ventricular slices placed in a custom-made acrylic block spaced by 0.5 mm and images taken using an Epson paper scanner (Epson Perfection V100 Photo, Epson, UK). Images were taken at consistent settings: 1200 dpi resolution, 0%, 15% and 100% brightness where 15% brightness images were used for analysis.

Images were analysed by planimetry using ImageJ software (version 1.45s, National Institutes of Health, USA). Raw heart images were prepared for analysis by manual removal of the background image to leave only the heart slices. These red-green-blue (RGB) images were then automatically split into separate colour channels for analysis. A threshold of pixel intensity was applied to each slice where the threshold level was determined manually by matching the highlighted areas to the representative regions of

the raw image. The area of Evans blue staining was quantified using the red channel image and the area of infarction quantified using the green channel image. Myocardial AAR was calculated as a percentage of LV area: (LV area – Evans blue area) / (LV area). Infarct size was calculated as a percentage of AAR: (Infarct area) / (AAR/LV%).

Quantification of infarct size and AAR using this threshold method was validated by assessing inter- and intra-observer variability. A batch of control operated hearts were analysed by two blinded observers and the IS/AAR% and AAR/LV% compared. The final quantifications for this batch of hearts was not significantly different between observers (assessed using paired t-test). In addition, IS/AAR% and AAR/LV% quantification by one observer was assessed between analyses of three blinded replicates of this batch of hearts and showed excellent consistency. All subsequent datasets were analysed by one blinded observer where all groups were blinded until completion of analysis for the total dataset.

The extent of AAR was determined by the location of the occluding suture in relation to the coronary anatomy. Hearts were excluded from the dataset if the AAR was outside the predefined inclusion range of 40–75% AAR/LV. This exclusion criterion was important since the assumed linear relationship between AAR and infarct size was expected to only apply to the central ranges of AAR (Fisher and Marber, 2002). For each dataset, the AAR (AAR/LV%) was compared between all groups to ensure that there were no differences in the extent of the myocardium subjected to ischaemia.

Statistical analysis: All values are presented as mean ± SEM. All statistical analysis was completed using GraphPad Prism® version 5.0 (GraphPad Software, USA). Where two groups were compared, data were analysed using an unpaired t-test. Where more than two groups were compared, data were analysed by one-way ANOVA and Bonferroni test comparing relevant groups. For all statistical tests, statistical significance was reported where $P<0.05$ using standard coding.

4.3.3. Results

This thesis describes the first successful establishment of this complex mouse *in vivo* recovery model within our laboratory. Initial surgeries encountered a diverse and somewhat extensive array of surgical complications, largely resulting from surgical inexperience. All initial surgeries were conducted using the recovery anaesthetic injectable regime described above (ketamine and medetomidine). A number of non-recovery surgeries were first undertaken in order to develop and refine the detailed surgical skills required for mouse cardiac surgery. The surgical procedure was refined incrementally and final myocardial infarct size and AAR determined for a batch of non-recovery procedures; the results of these preliminary studies are not presented here.

Further to this, incremental changes to the *in vivo* recovery protocol were refined where animals were recovered following each of the key surgical stages identified in the detailed description of the method provided above (induction of anaesthesia and intubation, thoracotomy, sham LAD ligation and ischaemia-reperfusion). These studies were conducted in mice from breeding stock within our laboratory and were of mixed genetic backgrounds (usually albino:SV129) and genotypes. Attempts were made to recover animals at each of these stages in order to establish and refine the procedure and identify recurrent complications. Several problems were identified primarily concerning correct identification and ligation of the LAD and recovery of animals subjected to long anaesthetic durations. These problems were largely overcome with extensive surgical practice and modification of the anaesthetic regime detailed below.

Histological staining of *ex vivo* prepared hearts from these surgeries was undertaken to refine the extraction, cannulation and staining protocols necessary for good quality staining and thus quantification of infarct size and AAR in subsequent studies. Infarct size was not formally quantified in these animals due to the mixed genetic backgrounds and genotypes; however, assessment of AAR in these early surgeries showed substantial variation in LAD suture location and thus AAR between animals.

These initial experiments led to extensive refinements of the surgical protocol (presented in Table 4.1 above) to eventually result in a relatively robust and reproducible model of *in vivo* ischaemia-reperfusion injury with reasonable recovery of animals. Following this, subsequent studies aimed to determine the most appropriate anaesthetic regime for use in consequent studies and investigate the potential anaesthetic conditioning effects of isoflurane; the key results of these studies are presented here.

i Anaesthetic regime

Surgical survival: An initial study aimed to establish surgical survival and infarct size in commercially available C57BL/6 and B6/SV129 mice using the injectable anaesthetic regime. However, this was hindered by very poor surgical survival in the pilot studies conducted on C57BL/6 mice using the injectable anaesthetic protocol of ketamine and medetomidine (Figure 4.8: surgical survival of sham operated animals to 72 hours was 25%; survival of 2/8 animals). Since these animals were only subjected to the sham procedure, this poor survival rate suggested a problem with a direct element of the surgical protocol itself. Attempts were made to further investigate this in B6/SV129 mice; however, this injectable anaesthetic regime (ketamine and medetomidine) did not provide sufficient depth of anaesthesia in a number of surgeries meaning that surgery could not be undertaken in these mice. Due to these complications, this ketamine and medetomidine injectable anaesthetic cocktail was not used for any further surgeries.

An alternative isoflurane inhalation anaesthetic regime was investigated for surgeries in both C57BL/6 and B6/SV129 mice. Surgical survival rates of sham operated animals for both mouse strains were greatly improved using this anaesthetic regime (Figure 4.8: C57BL/6 sham operated animal survival 100% to 72 hours post-surgery, B6/SV129 data not shown). This anaesthetic regime, however, did not reduce heart rate (500-600 BPM) meaning that identification and ligation of the LAD was appreciably more difficult in these animals compared to the recovery injectable anaesthetic regime used previously (ketamine and medetomidine, heart rate 200-250 BPM). Animals excluded from this study due to poor or incorrect placement of the LAD suture are not reported below.

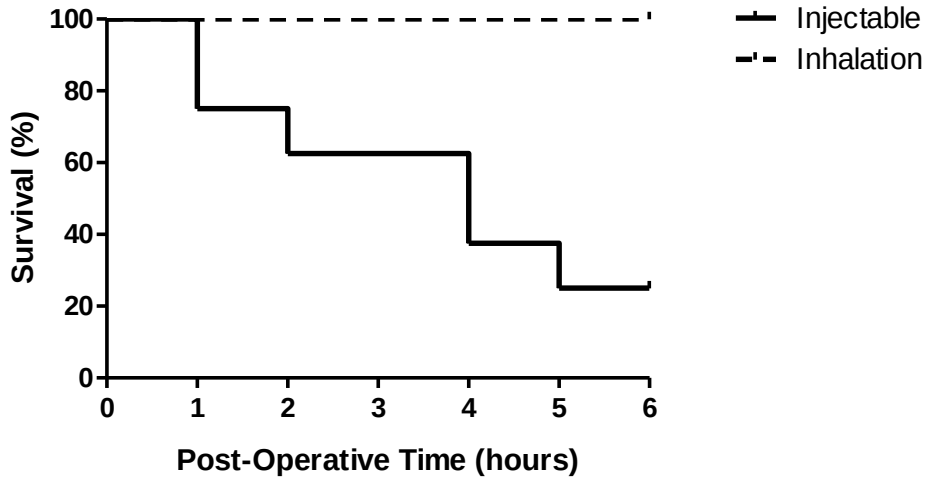

Figure 4.8: Surgical survival for injectable and inhalation anaesthetic regimes
Immediate post-operative survival of C57BL/6 mice subjected to sham operation using injectable (ketamine and medetomidine; solid line) or inhalation (dashed line) anaesthesia. Survival to 6 hours recovery was 25% for injectable anaesthesia (2/8 mice) and 100% for inhalation anaesthesia (6/6 mice). Statistical significance assessed by log-rank test, **P<0.01, (n≥6/group).

All subsequent validation and characterisation of the *in vivo* recovery model of ischaemia-reperfusion injury presented in this chapter was conducted in B6/SV129 mice since these were considered to be the closest genetic background to the cyclophilin-D genetically modified mice that were subsequently used (see chapter 5).

Potential anaesthetic conditioning: Given the reported cardioprotective effects of inhalation anaesthetics, including isoflurane (reviewed by Kato and Foex, 2002; Stowe and Kevin, 2004), subsequent experiments aimed to investigate the potential effects of the isoflurane dose used here. To this end, infarct size in B6/SV129 mice subjected to ischaemia-reperfusion injury under inhalation and injectable anaesthetic protocols was assessed. However, due to the complications of obtaining sufficient anaesthetic depth and surgical survival using the recovery injectable anaesthetic cocktail (ketamine and medetomidine), the non-recovery model of ischaemia-reperfusion injury had to be used. Surgical survival of sham operated B6/SV129 mice using this non-recovery model with injectable anaesthesia (ketamine, xylazine and atropine) was 100% (n=6).

It is important to note that this injectable anaesthetic regime (ketamine, xylazine and atropine) significantly reduced heart rate in these animals to approximately 300-400 BPM depending upon the anaesthetic depth. The potential effects of this with regards to infarct size are discussed subsequently (see section 4.6), however, the immediate result of this was an increased success rate of suitable AAR resulting from improved ligation of the LAD facilitated by the decreased heart rate. The surgical survival statistics presented below do not include animals excluded from the study based on inappropriate AAR.

Comparison of myocardial infarct size (IS/AAR%) in B6/SV129 mice subjected to 30 minutes ischaemia and 2 hours reperfusion between the injectable (ketamine, xylazine and atropine) and recovery inhalation anaesthetic regimes showed a striking agreement (Figure 4.9: IS/AAR% injectable anaesthesia 38.8±3.2 versus isoflurane 38.4±3.4; n≥6/group, $^{NS}P>0.05$). There was no significant difference in AAR between these groups (AAR/LV% injectable anaesthesia 61.8±3.3 versus isoflurane 63.1±5.0; n≥6/group, $^{NS}P>0.05$). Surgical survival of animals undergoing these regimes was not significantly different (surgical survival: injectable 85.7%, n=7 versus inhalation 88.9%, n=9).

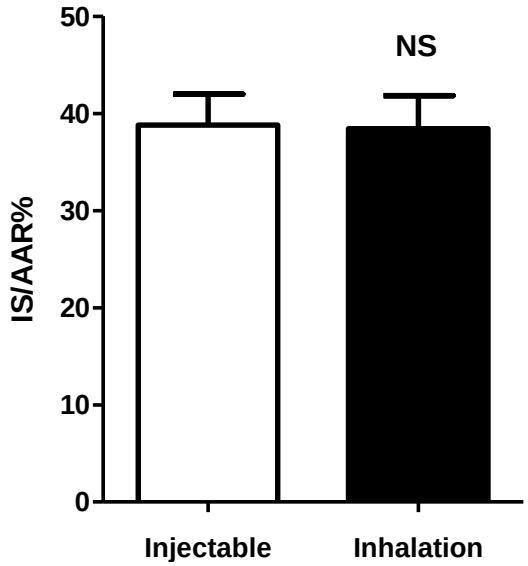

Figure 4.9: Infarct size using injectable and inhalation aesthetic regimes
Infarct size following 30 minutes ischaemia and 2 hours reperfusion in B6/SV129 mice using injectable (non-recovery: ketamine, xylazine and atropine) and isoflurane inhalation (recovery: isoflurane) anaesthetic regimes. IS/AAR% was not significantly different between anaesthetic regimes: IS/AAR% injectable anaesthesia 38.8±3.2 (n=6) versus inhalation 38.4±3.4 (n=7). Statistical significance assessed by unpaired t-test, $^{NS}P>0.05$.

This study was subsequently repeated following complete refinement and establishment of the surgical protocol to ensure the validity of this finding; this study also showed no difference in myocardial infarct size using these two anaesthetic regimes (data not shown). Given the lack of any profound cardioprotective effect of this anaesthetic regime, this protocol was used for all recovery surgeries of the *in vivo* ischaemia-reperfusion injury model presented here. Further investigation of a potential anaesthetic conditioning effect using this protocol is provided subsequently (see section 4.6)

Additional refinement of the surgical protocol was required to improve the success of LAD ligation using this isoflurane anaesthetic regime; these refinements are described in Table 4.1 and following extensive practice of this model, the surgical success rates in terms of survival and appropriate AAR were both substantially improved. Early studies aimed at characterising and establishing this *in vivo* recovery ischaemia-reperfusion model are not presented here due to the large variability of infarct sizes within experimental groups thereby questioning the validity of such data. During the first year of this project, extensive refinement of the model and staining techniques was completed to perfect the final model that was applied for the studies presented here.

All subsequent data presented in this thesis was conducted following this extensive refinement and establishment of the model and is therefore deemed robust and reliable.

4.4. Aim 2: Validation of the ischaemia-reperfusion injury model

4.4.1. Background

The overall aim of this thesis was to investigate the long-term cardioprotective efficacy of potential therapeutic interventions at reducing myocardial infarct size upon ischaemia-reperfusion. With any experimental model it is pertinent to validate the principal endpoint in order to verify that the model is robust and reproducible and capable of detecting differences between experimental groups. It was therefore important to ascertain whether the infarct size elicited by the mouse *in vivo* recovery of myocardial ischaemia-reperfusion injury developed in the first part of this chapter was sufficiently robust to allow a significant reduction in infarct size to be detected.

Validation of infarct size reduction requires the application of cardioprotective interventions which are known to elicit a significant cardioprotective effect, as tested by numerous previous research groups. As described in chapter 1 of this thesis, several mechanical and pharmacological interventions have been examined and shown to be cardioprotective in pre-clinical research models. IPC is considered to be the most powerful cardioprotective intervention after early reperfusion (Yellon and Downey, 2003) and thus represents an ideal positive control for cardioprotective efficacy here. IPC has been extensively tested and proven to significantly reduce cell death in *ex vivo* and *in vivo* models of ischaemia-reperfusion injury. Importantly, IPC has shown to be effective in every mammalian species tested to date and consistently reduces myocardial infarct size in the region of 50% (reviewed by Yellon and Downey, 2003; Jennings, 2011).

In addition to cardioprotection by the mechanical intervention IPC, it was important to demonstrate significant cardioprotective efficacy of a pharmacological intervention, for which the extent of infarct size reduction is expected to be more variable and slightly lower. This was critical to evaluate the robustness of the *in vivo* recovery model of ischaemia-reperfusion developed here with regards to the statistical power and thus sample sizes required to detect statistical significance. The smaller effect size elicited by pharmacological interventions such as cyclosporine-A (CsA) was predicted to be similar to those produced by genetic ablation of mitochondrial proteins investigated subsequently in this thesis (chapters 5 and 6). Cyclosporine-A is a pharmacological inhibitor of calcineurin and the cyclophilin proteins and has been shown to reduce infarct size in a number of *in vitro* and *in vivo* animal models (Nazareth et al., 1991; Griffiths and Halestrap, 1993; Hausenloy et al., 2002); see section 1.4.1.

This section describes validation of the *in vivo* recovery model of ischaemia-reperfusion injury recovery using two positive controls for cardioprotection: IPC and CsA.

Aim 2: The second aim of this chapter was to validate the *in vivo* recovery model of ischaemia-reperfusion injury by assessing the cardioprotective efficacy of two well-described cardioprotective interventions. The central hypotheses to validate and test the robustness of this model were:

(1) A standard IPC protocol would elicit a significant reduction in myocardial infarct size upon ischaemia-reperfusion.

(2) Administration of a known therapeutic dose of CsA immediately prior to reperfusion would elicit a significant reduction in infarct size upon ischaemia-reperfusion.

4.4.2. Detailed methods

Myocardial infarct size and AAR were assessed in mice subjected to the *in vivo* recovery model of ischaemia-reperfusion injury developed in part 1 of this chapter. The *in vivo* procedure was exactly as described above using isoflurane anaesthesia. The dose and duration of anaesthesia for each animal was kept as constant as possible where the specific surgical protocols for each group are detailed below. Following 72 hours reperfusion, mice were anaesthetised and hearts extracted for *ex vivo* histological staining using TTC and Evans blue exactly as described above. The surgical and myocardial AAR exclusion criteria were as described previously.

i Ischaemic preconditioning

B6/SV129 mice were randomised to receive ischaemia-reperfusion injury, with or without IPC. Control mice were subjected to 15 minutes stabilisation, 30 minutes ischaemia and 72 hours reperfusion (Figure 4.10 A). IPC mice were subjected to one cycle of 5 minutes ischaemia and 5 minutes reperfusion immediately prior to the main ischaemic insult (Figure 4.10 B). This IPC protocol has been shown to significantly reduce infarct size in a mouse *in vivo* non-recovery model of myocardial ischaemia-reperfusion within our laboratory (Lim et al., 2007).

Particular care was taken to ensure effective reperfusion in these groups since the IPC regime was more prone to causing mechanical damage to the surrounding myocardium which could impede successful reperfusion upon release of the snare system following the main ischaemic insult. Where clear recovery of myocardial colour and ECG ST-segment was not observed upon reperfusion, animals were excluded from the study.

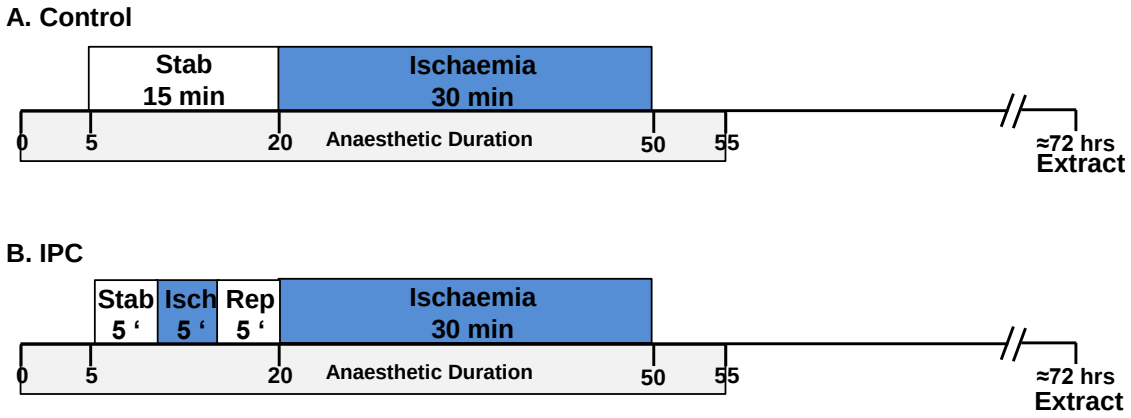

Figure 4.10: Ischaemic preconditioning protocol
A) Control: 15 minutes stabilisation, 30 minute ischaemia and 72 hours reperfusion. B) IPC: 5 minutes stabilisation, one cycle IPC consisting of 5 minutes ischaemia and 5 minutes reperfusion prior to the main ischaemic insult of 30 minutes and 72 hours reperfusion. Following 72 hours reperfusion, hearts were extracted for histological staining for infarct size.

ii Cyclosporine-A

B6/SV129 mice were randomised to vehicle control or CsA treatment groups. CsA or vehicle was administered during ischaemia, 5 minutes prior to the onset of reperfusion (Figure 4.11). This CsA dose has been shown to significantly reduce infarct size in the non-recovery ischaemia-reperfusion model within our laboratory (Lim et al., 2007).

CsA was dissolved in a solution of cremophor and ethanol-94% (0.65 g cremophor per 1 ml 94% ethanol where 94% ethanol was prepared in sterile saline). This vehicle solution was prepared under sterile conditions and stored at 4ºC for a maximum of 1 month with vigorous shaking prior to use. CsA solutions were made fresh on each operating day to ensure that there was no loss of drug activity between experiments. The CsA dosing stock solution was made directly in cremophor/ethanol-94% at a concentration of 5 mg/ml. The CsA dosing stock was administered at a volume of 2 ml/kg, and therefore 60 µl per 30 g mouse, to give a final dosing concentration of 10 mg/kg. Vehicle treated animals received a matched volume of cremophor/ethanol-94% instead of CsA.

CsA or vehicle was administered as a single intravenous bolus via either the left or right lateral tail veins immediately following regional warming of the tail vein using local application of a warmed tissue swab. Successful dosing was confirmed by washout of blood in the vein and return of blood following removal of the needle. Animals were excluded from the study where dosing could not be confirmed.

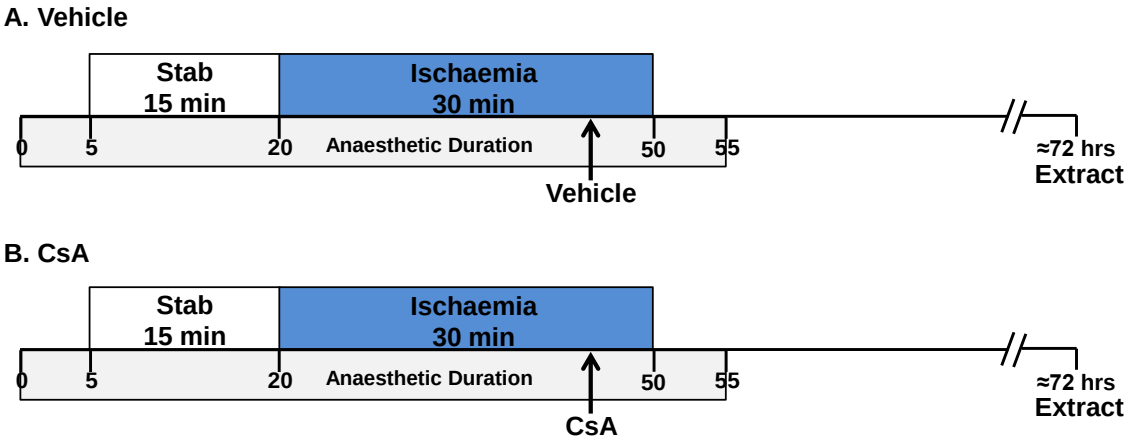

Figure 4.11: Cyclosporine-A protocol
A) Vehicle mice received a matched volume of cremophor/ethanol-94%. B) CsA mice received CsA 10 mg/kg in cremophor/ethanol-94%. All compounds were administered as a single I.V. bolus 5 minutes prior to reperfusion. All mice were subjected to 15 minutes stabilisation, 30 minutes ischaemia and 72 hours reperfusion. Hearts were extracted for staining for infarct size.

4.4.3. Results

To ascertain the scope for cardioprotection, the infarct size of animals subjected to the sham procedure (open chest surgery with no myocardial ischaemia) and control procedure (30 minutes ischaemia) was examined. The infarct size in sham operated B6/SV129 mice, in which the LAD snare system was assembled but not occluded and all surgical timings adhered to, was 6.2±0.2 IS/AAR%, n=4 (Figure 4.12 Ai). This was deemed an acceptable extent of injury for sham operated animals and was in the region of that obtained for the non-recovery ischaemia-reperfusion model within our laboratory.

The control infarct size resulting from 30 minutes ischaemia and 72 hours reperfusion was 32.0±3.7 IS/AAR%, n=7 (Figure 4.12 Aii). This was lower than expected based on the non-recovery *in vivo* model where 30 minutes ischaemia and 2 hours reperfusion resulted in 38.8±3.2 IS/AAR% (Figure 4.9). The absolute difference between sham and control infarct sizes (i.e. the effect size) in this model was 25.7 IS/AAR%, which was lower than expected from the non-recovery model; this is discussed in section 4.6.2.

i Ischaemic preconditioning

A standard IPC protocol of 5 minutes ischaemia and 5 minutes reperfusion known to be cardioprotective was applied to the *in vivo* recovery model developed here. IPC significantly reduced the infarct size in B6/SV129 mice subjected to 30 minutes ischaemia and 72 hours reperfusion (Figure 4.12: IS/AAR% control 32.0±3.7 versus IPC 16.2±0.7; n≥6/group, **P<0.01). There was no difference in AAR (AAR/LV% control 57.0±1.8 versus IPC 55.9±5.5; n≥6/group, ^{NS}P>0.05) or survival between control or IPC groups (survival to 72 hours reperfusion: control 87.5% versus IPC 75%, ^{NS}P>0.05).

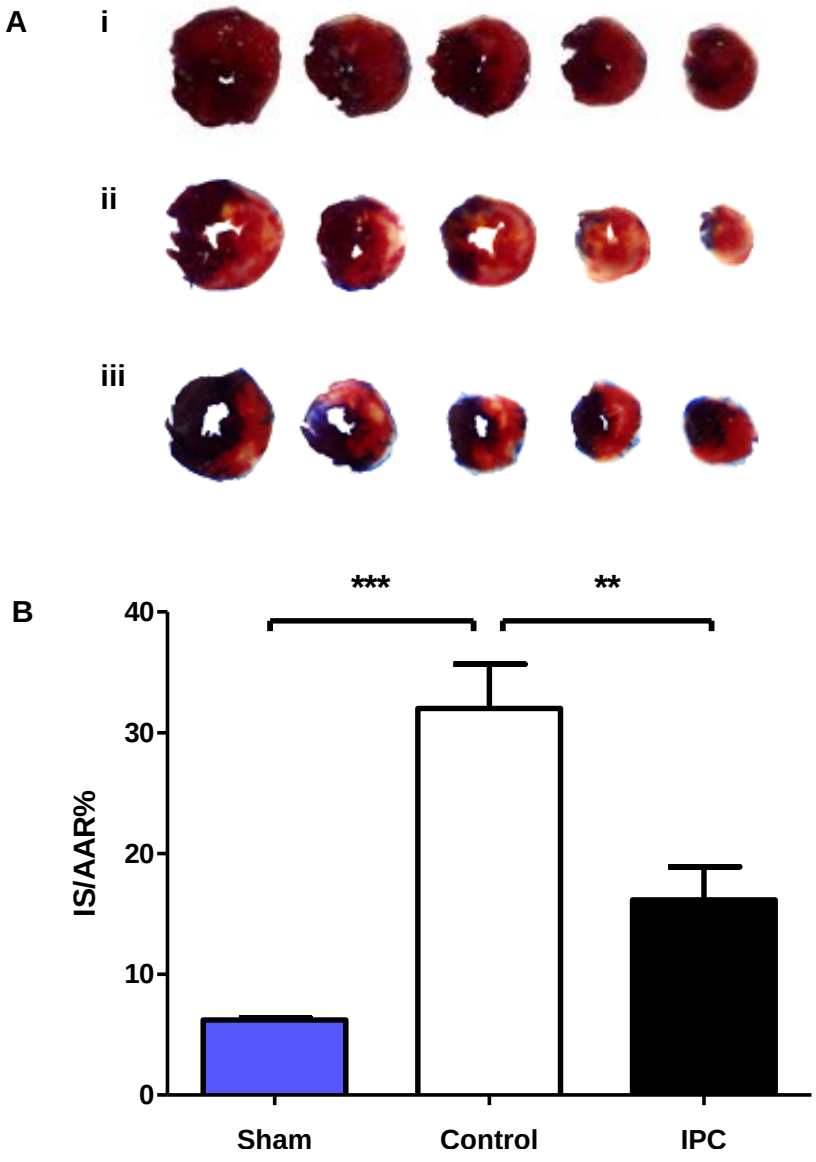

Figure 4.12: Infarct size reduction following ischaemic preconditioning *in vivo*
A) Representative infarct size in B6/SV129 mice subjected to i) sham, ii) control 30 minutes ischaemia and 72 hours reperfusion or iii) IPC (5 minutes ischaemia and 5 minutes reperfusion) prior to 30 minutes ischaemia and 72 hours reperfusion. B) Infarct size in sham operated mice was 6.2±0.2% (n=4). Infarct size was significantly reduced by IPC: IS/AAR% control 32.0±3.7 (n=7) versus IPC 16.2±0.7 (n=6). Statistical significance assessed by one-way ANOVA comparing sham versus control and control versus IPC, n≥4/group, **P<0.01 and ***P<0.001.

ii Cyclosporine-A

Treatment with a known cardioprotective dose of CsA treatment 5 minutes prior to the onset of reperfusion in this model also significantly reduced infarct size resulting from the standard protocol of 30 minutes ischaemia and 72 hours reperfusion (Figure 4.13: IS/AAR% vehicle control 43.1±1.5 versus CsA 29.9±3.1; n=4/group, *P<0.05). There was no difference in AAR (AAR/LV% vehicle 67.7±8.8 versus CsA 69.7±2.0; n=4/group, ^{NS}P>0.05) or survival between vehicle and CsA treated mice (survival to 72 hours reperfusion: vehicle 100% versus CsA 100%, ^{NS}P>0.05, excluding those animals excluded due to unconfirmed dosing).

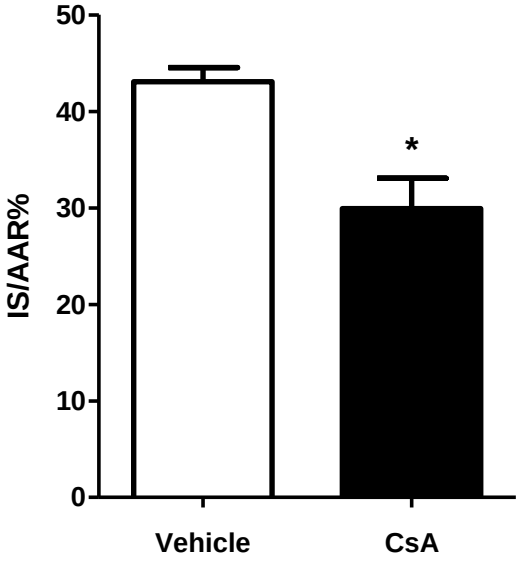

Figure 4.13: Infarct size reduction following CsA administration *in vivo*
Infarct size resulting from 30 minutes ischaemia and 72 hours reperfusion in B6/SV129 mice administered either vehicle or CsA bolus I.V. 5 minutes prior to reperfusion. IS/AAR% was significantly reduced by CsA: IS/AAR% vehicle control 43.1±1.5 (n=4) versus CsA 29.9±3.1 (n=4). Statistical significance assessed by unpaired t-test, *P<0.05.

The infarct size in B6/SV129 mice treated with vehicle only (cremophor/ethanol-94%) was slightly larger than for control only animals (IS/AAR%: Figure 4.13 vehicle 43.1±1.5 n=4, versus Figure 4.12 control 32.0±3.7 n=7). It was not appropriate to perform statistical analysis of these groups since they were completed as separate experiments and so were not randomised. Although no firm conclusions regarding the effect of the vehicle on infarct size could be made, this is an important consideration.

These initial experiments demonstrate that two known cardioprotective interventions, IPC and CsA, elicit significant cardioprotection against ischaemia-reperfusion injury in the *in vivo* recovery model developed in this thesis using a standard protocol of 30 minutes ischaemia and 72 hours reperfusion, thereby validating this model for further studies of cardioprotection undertaken subsequently in this thesis.

4.5. Aim 3: Characterisation of ischaemia-reperfusion injury model

4.5.1. Background

With any research model it is essential to control all possible confounding experimental variables in order to reduce the variability within groups and to enhance the statistical power and reduce the sample sizes required. Further characterisation of the *in vivo* ischaemia-reperfusion recovery model developed here was examined to determine the optimal experimental design of subsequent studies to be undertaken.

Optimisation of the ischaemic duration was particularly important in the present study given the smaller infarct size of control operated animals subjected to 30 minutes ischaemia and 72 hours reperfusion demonstrated in part 2 of this chapter (see 4.4.3). This 30 minute ischaemic protocol was used since this was the standard protocol used within our laboratory for the mouse *in vivo* non-recovery ischaemia-reperfusion injury model to generate control infarct sizes in the region of 40% (IS/AAR). Despite the demonstration of significant infarct size reduction using known cardioprotective interventions, it was pertinent at this stage to investigate the optimal ischaemic duration for subsequent studies in this thesis. Given the wavefront of necrosis hypothesis postulated by Reimer et al. (1977), it is expected that increased ischaemic duration will increase the extent of myocardial infarction. The optimal ischaemic duration is a trade-off between a sufficiently large infarct size to obtain large effect sizes in experimental treatment group balanced with the potential complications associated with a greater extent of injury including surgical survival and other forms of injury including cardiac arrhythmias and rupture (reviewed by Sane et al., 2009). The effect of ischaemic duration on infarct size in this model was investigated and is reported in this section.

Reperfusion duration may also influence the quantification of infarct size, whereby the processes of infarct expansion and subsequent myocardial thinning may affect the quantification of myocardial AAR and thereby unduly affect infarct size calculation (IS/AAR%). Myocardial thinning is known to occur during infarct remodelling and although this is expected to be more profound in non-reperfused infarcts (Michael et al., 1999; Vandervelde et al., 2006), it is possible that subtle changes to myocardial thickness may affect the calculation of IS/AAR% in this study. Furthermore, there is some debate as to the validity of infarct size quantification based on TTC staining at various durations of reperfusion due to the enzymatic nature of the staining reaction and impaired metabolic function of irreversibly injured cardiomyocytes at early durations of reperfusion (Black and Rodger, 1996; Redel et al., 2008). These potential confounding factors are discussed in detail in section 4.6.

A number of experimental variables have been reported to affect myocardial infarct size following ischaemia-reperfusion injury including temperature, time of day and gender (reviewed by Black and Rodger, 1996). It is therefore imperative to control as many of these potentially confounding variables as possible and this has led to a bias in the use of male subjects only in many studies of cardioprotection, as discussed in chapter 1.

Operative time of day has also been suggested to affect myocardial infarct size, where an elegant study by Durgan et al. (2010) demonstrated a 3.5 fold increase in infarct size across the extremes of the operating day (12 hour spacing of surgeries). The potential effects of these experimental variables are particularly important given the identification of significant differences in cardioprotective signalling pathway activation, for example the level of phosphorylated Akt (Durgan et al., 2010). The final part of this chapter investigates the effect of operative time of day and gender, on the infarct size obtained in the mouse *in vivo* recovery model of ischaemia-reperfusion injury developed here.

The final section of this chapter describes characterisation of the optimal ischaemia and reperfusion durations and the effect of potentially important experimental variables to inform the methodological details and acceptable variables for subsequent studies.

Aim 3: The final aim of this chapter was to characterise the potential effects of experimental variables on infarct size resulting from the *in vivo* recovery model of ischaemia-reperfusion. The hypotheses relating to these experiments were:

(1) Ischaemic duration: Increased ischaemic duration would increase infarct size.

(2) Reperfusion duration: Infarct size would increase slightly over the initial period of myocardial reperfusion.

(3) Operative time of day: Mice subjected to ischaemia-reperfusion in the afternoon may exhibit slightly larger infarct sizes than those in the morning.

(4) Gender: Infarct size resulting from ischaemia-reperfusion in females would be slightly lower than in male mice.

It was not expected that operative time of day or gender would elicit statistically significant differences in infarct size in this model; however, it was imperative to investigate and quantify the effect of these variables on infarct size in order to inform the experimental design of subsequent studies to be undertaken in this thesis.

4.5.2. Detailed methods

The *in vivo* procedure was exactly as described above using the isoflurane anaesthetic regime. Following the defined period of reperfusion, mice were anaesthetised and hearts extracted for *ex vivo* staining using TTC and Evans blue exactly as described above. The surgical and myocardial AAR exclusion criteria were as described previously and there were no differences in AAR between groups. The survival of animal subjects was recorded, including the number of animals excluded on a procedural basis (e.g. due to unsuccessful reperfusion) in order to evaluate the optimal protocol for subsequent studies. The precise calculation of survival statistics is detailed here.

Statistical power calculations were performed to retrospectively evaluate the statistical power of tests undertaken to facilitate the interpretation of these results. When it was clear that statistical power was not reached using the sample sizes presented here, a prospective calculation based on the expected effect size and standard deviation of these studies was used to determine the sample size required to reach sufficient statistical power. For all tests, the minimal level of statistical power was judged to be 80%, in accordance with published guidelines (Cohen, 1988; Townend, 2002). All power calculations were performed using GraphPad StatMate version 2.0 (GraphPad Software, USA) according to the statistical power equations published by Cohen (1988).

i Ischaemic duration

B6/SV129 mice were randomised to receive 30 or 40 minutes ischaemia followed by 72 hours reperfusion (Figure 4.14). The stabilisation period for each group was modified to ensure that the total anaesthetic duration was equal between experimental groups.

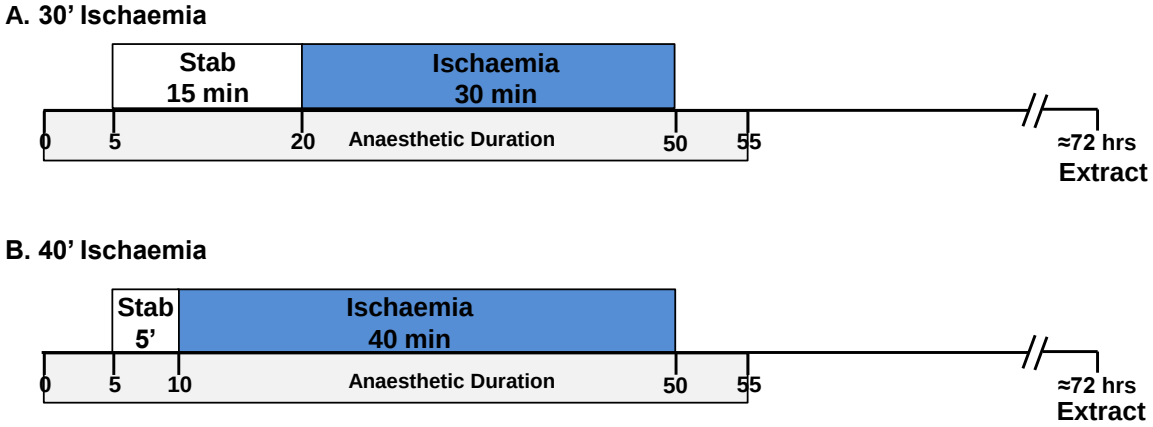

Figure 4.14: Ischaemic duration protocol
B6/SV129 mice were randomised to either A) 30 minutes or B) 40 minutes ischaemia. Stabilisation duration was modified to ensure total anaesthetic duration was approximately equal between experimental groups. Following 72 hours reperfusion hearts were extracted for staining.

ii Reperfusion duration

B6/SV129 mice were subjected to 30 minutes ischaemia and hearts extracted following defined reperfusion durations of 2, 6, 24 or 72 hours (Figure 4.15). Separate groups of animals were required for each of the reperfusion durations examined due to the terminal nature of the histological endpoint for infarct size and AAR assessment. All groups, including those subject to short reperfusion durations only, underwent the recovery procedure with isoflurane anaesthesia to ensure consistency protocols.

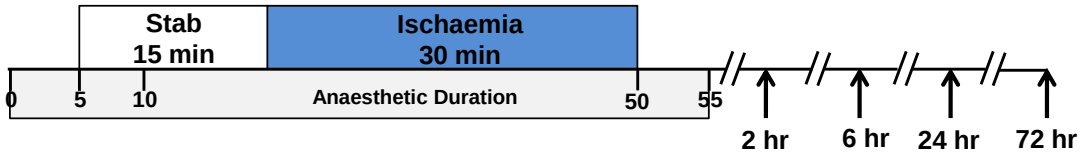

Figure 4.15: Reperfusion duration protocol
B6/SV129 mice were randomised to receive 30 minutes ischaemia followed by reperfusion for i) 2 hours, ii) 6 hours, iii) 24 hours or iv) 72 hours. Following the defined duration of reperfusion, hearts were extracted for histological staining (indicated by arrows).

iii Operative time of day

All surgeries presented in thesis were conducted during full day operating sessions from 08:00-18:00. A retrospective analysis of infarct size from morning and afternoon surgeries was conducted for B6/SV129 mice subjected to the standard protocol (30 minutes ischaemia and 72 hours reperfusion) and standard IPC protocol (5 minutes ischaemia, 5 minutes reperfusion and standard ischaemia and reperfusion insult) described above (Figure 4.10). For this retrospective analysis, previously operated animals were assigned to morning or afternoon operative sessions depending on the time of the onset of ischaemia; where morning sessions were defined as onset of ischaemia 08:00-11:00 and afternoon sessions were defined as onset of ischaemia 14:00-17:00. Animals were excluded from this sub-analysis where the start of ischaemia was outside of these morning and afternoon operating session definitions.

iv Gender

All previous studies described in this thesis were conducted on male mice only. To investigate the potential difference in infarct size with gender, commercially available male and female B6/SV129 mice were subjected to the standard *in vivo* recovery protocol of 30 minutes ischaemia and 72 hours reperfusion described previously.

4.5.3. Results

i Ischaemic duration

The standard ischaemic protocol employed in this thesis was 30 minutes ischaemia, however, increasing this to 40 minutes ischaemia only slightly increased infarct size, where this difference was not significant (Figure 4.16: IS/AAR% 30 minutes ischaemia 32.0±3.7 versus 40 minutes ischaemia 40.1±5.0; n=7/group). However, the small effect size and relatively large variability meant that an unfeasibly large sample size would be required to reach statistical power; thus limiting the conclusions of this experiment. There was no significant difference in AAR between groups (AAR/LV% 30 minutes ischaemia 57.0±1.8 versus 40 minutes ischaemia 61.1±2.1; n=7/group, $^{NS}P>0.05$).

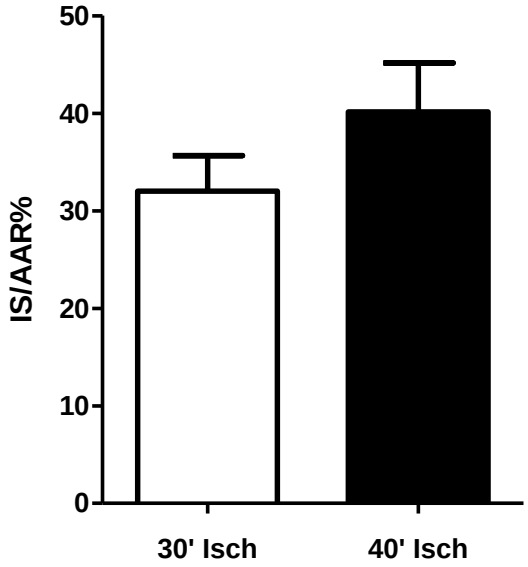

Figure 4.16: Infarct size following increased ischaemic insult
Infarct size resulting upon 30 or 40 minutes ischaemia and 72 hours reperfusion in B6/SV129 mice. There was a slight but non-significant increase in infarct size upon 40 minutes ischaemia: IS/AAR% 30 minutes ischaemia 32.0±3.7 (n=7) versus 40 minutes ischaemia 40.1±5.0 (n=7). Statistical significance assessed by unpaired t-test, however, this is statistically underpowered.

The surgical and post-operative survival of animals subjected to the 30 and 40 minute ischaemic protocols was also recorded, including exclusion of animals from the study based on procedural reasons such as unsuccessful reperfusion. Recovery of animals to 72 hours reperfusion (the pre-defined endpoint) was slightly lower in the 40 minute ischaemic groups compared to the standard 30 minute ischaemic protocol (Figure 4.17: % survival to 72 hours reperfusion: 30 minutes ischaemia 87.5% n=8, versus 40 minutes ischaemia 63.6% n=11). The majority of animals lost in the 40 minute ischaemic group were excluded due to unsuccessful reperfusion (time 0, Figure 4.17).

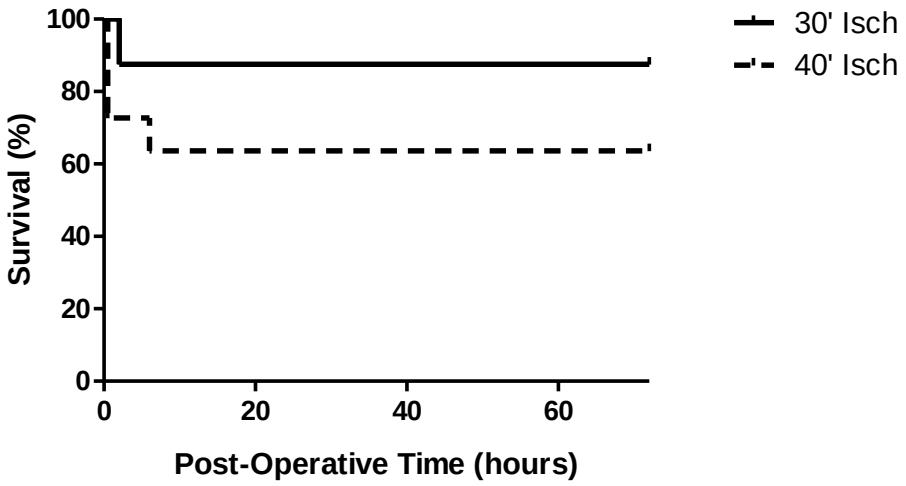

Figure 4.17: Survival following increased ischaemic insult
Survival of B6/SV129 mice subjected to 30 or 40 minutes ischaemia and 72 hours reperfusion. Survival was slightly lower in 40 minute ischaemic group: survival % 30 minutes ischaemia 87.5% (7/8) versus 40 minutes ischaemia 63.6% (7/11). However this was not statistically significant; significance assessed by log-rank test (Mantel-Cox), $^{NS}P>0.05$.

Further to this, a standard IPC protocol was investigated in animals subjected to 40 minutes ischaemia and 72 hours reperfusion and was shown to significantly reduce infarct size by approximately 44% (40 minutes ischaemia with standard IPC protocol; IS/AAR% control 40.1±5.0 versus IPC 22.5±2.1, n=7/group **P<0.01). However, inclusion of the IPC protocol in this 40 minute ischaemic protocol meant that the total anaesthetic duration (and thus isoflurane dose) was increased by 10 minutes compared to the other surgeries in this chapter since the standard protocol devised in part 1 was not designed to accommodate this extended protocol.

Although the difference in survival rates between the two ischaemic protocols (30 minutes and 40 minutes ischaemia) was not statistically significant, the increased exclusion of animals subjected to the 40 minute ischaemic protocol meant that the 30 minute ischaemic protocol represented a more feasible protocol. All surgeries for this thesis were conducted using 30 minutes ischaemia unless otherwise stated.

ii Reperfusion duration

The effect of reperfusion duration on infarct size development was examined to investigate the potential reason for slightly reduced infarct size in the *in vivo* recovery model (standard protocol: 72 hours reperfusion) compared to the well-established *in vivo* non-recovery model (standard protocol: 2 hours reperfusion) within our laboratory.

B6/SV129 mice were subjected to 30 minutes ischaemia and hearts extracted at defined reperfusion periods. Increased reperfusion duration over the time-points investigated did not significantly affect infarct size, although there was a non-significant trend of decreased infarct size at extended reperfusion durations (24 and 72 hours) compared to earlier time-points (Figure 4.18). There was no significant difference in AAR between groups, however, AAR in the 2 hour reperfusion group was slightly smaller compared to later time-points (AAR/LV% 2 hours 63.1±5.0 versus 6 hours 57.1±3.9, 24 hours 57.5±4.4 and 72 hours 57.0±1.8; n≥7/group, $^{NS}P>0.05$).

Although this experimental model is not sufficiently sensitive to detect such small effect sizes, this study provides an important interpretation of the slightly lower infarct sizes obtained following the standard *in vivo* recovery protocol at 72 hours reperfusion as compared to the previous studies reported within our laboratory at 2 hours reperfusion.

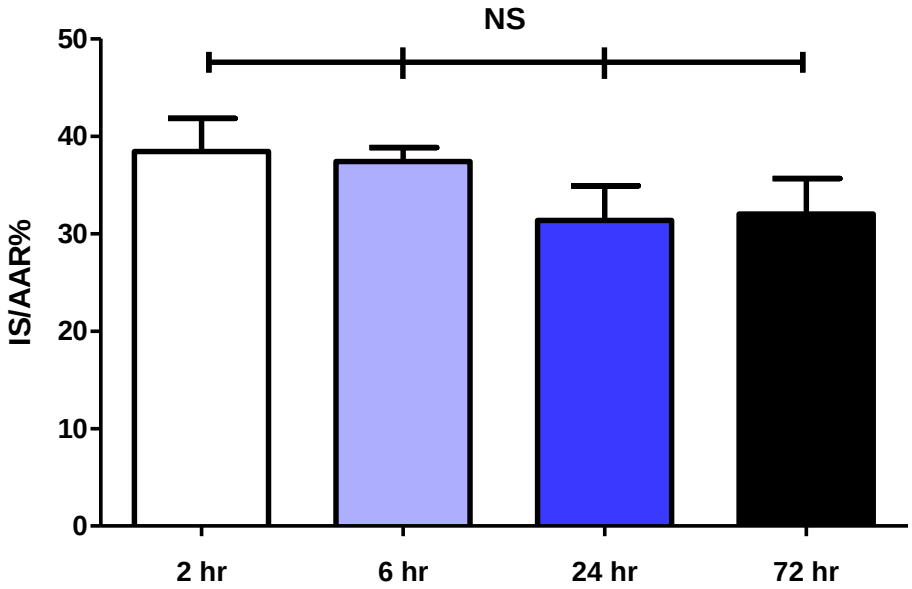

Figure 4.18: Infarct size following varied reperfusion duration
Infarct size resulting from 30 minutes ischaemia and varied durations of reperfusion in B6/SV129 mice. Infarct size was slightly decreased at longer durations of reperfusion: IS/AAR% 2 hours 38.4±3.4 (n=7), 6 hours 37.4±1.4 (n=8), 24 hours 31.4±3.5 (n=8) versus 72 hours 32.0±3.7 (n=7). However this was not statistically significant; statistical significance assessed by one-way ANOVA comparing all groups, $^{NS}P>0.05$.

iii Operative time of day

The effect of operative time of day on myocardial infarct size in this model was investigated in B6/SV129 mice subjected to standard control and IPC protocols. Infarct size data was retrospectively grouped into morning or afternoon sessions defined by the time of onset of ischaemia. There was no significant difference between morning and afternoon surgeries for control (Figure 4.19 A: n≥6/group, $^{NS}P>0.05$) or IPC operated animals (Figure 4.15 B: n≥3/group, $^{NS}P>0.05$); although it should be noted that the sample size for the IPC comparison is low. There was no significant difference in AAR or survival between these (AAR/LV% control AM 56.0±1.9 versus PM 56.9±4.0; n≥6, $^{NS}P>0.05$; AAR/LV% IPC AM 54.5±4.8 versus PM 63.7±8.3; n=4/group, $^{NS}P>0.05$).

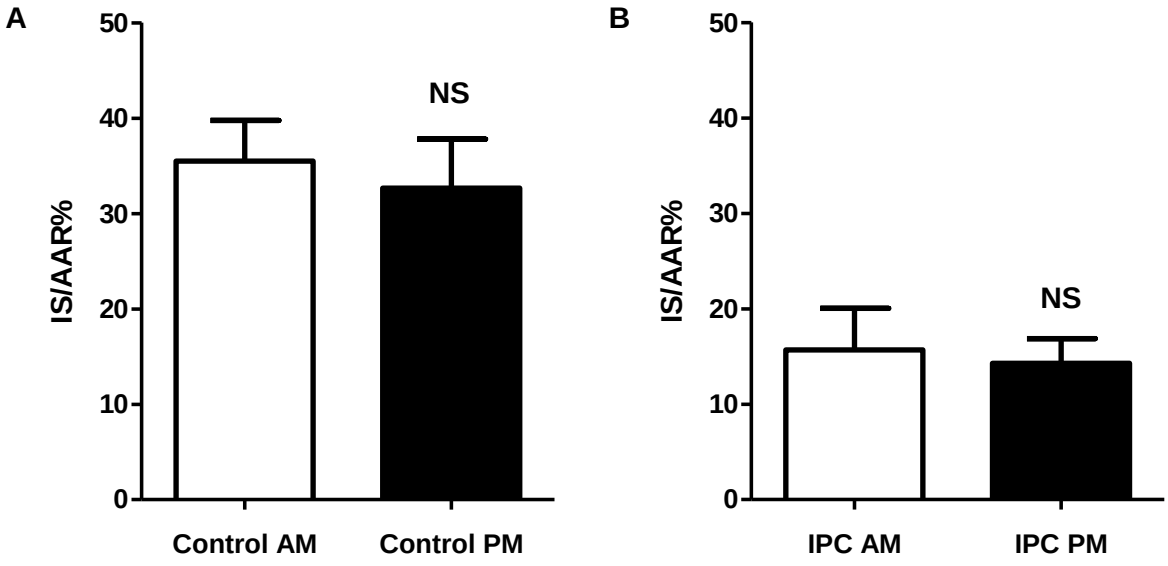

Figure 4.19: Infarct size resulting from morning and afternoon surgeries
B6/SV129 mice were subjected to ischaemia and reperfusion during morning (white bars, 08:00 – 11:00) and afternoon (black bars, 14:00-17:00) operative sessions. A) Control mice subjected to 30 minutes ischaemia and 72 hours reperfusion. There was no statistically significant difference in infarct size between morning or afternoon sessions (IS/AAR%: morning 35.5±4.3 (n=8) versus afternoon 32.7±5.2 (n=6), $^{NS}P>0.05$). B) IPC mice subjected to IPC 5 minutes ischaemia and 5 minutes ischaemia prior to main ischaemic insult of 30 minutes and 72 hours reperfusion (IS/AAR%: 15.7±4.4 (n=4) versus afternoon 14.3±2.6 (n=3), $^{NS}P>0.05$). Statistical significance assessed by unpaired t-test comparing AM (white bar) versus PM (black bar), $^{NS}P>0.05$.

An additional sub-analysis of control infarct size data was conducted to compare infarct size at the extremes of time of day (onset of ischaemia defined as 08:00-09:00 or 16:00-17:00). In line with the analysis presented above, there was no statistically significant difference in infarct size between these groups. This sub-analysis could not be undertaken for the IPC group due to its small sample size.

All subsequent experiments presented were conducted in full day operating sessions and mice were randomly assigned to morning or afternoon surgeries and an equal mix of operating sessions ensured between groups.

iv Gender

All previous experiments presented in this thesis were conducted on male mice only. The effect of gender on infarct size in the present study was investigated in male and female B6/SV129 mice subjected to the standard control ischaemia and reperfusion protocol (30 minutes ischaemia and 72 hours reperfusion). This demonstrated that there was no significant difference in myocardial infarct size between male and female mice (Figure 4.20: IS/AAR% males 34.8±3.8 versus females 36.2±5.1; n=7/group, $^{NS}P>0.05$). There was no significant difference in AAR between these groups (AAR/LV% male 58.7±2.2 versus female 61.5±5.8; n=7/group, $^{NS}P>0.05$).

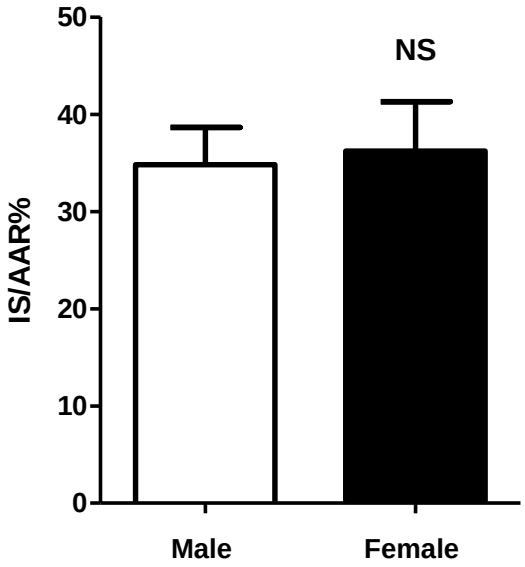

Figure 4.20: Infarct size in male and female mice
Infarct size in male and female B6/SV129 mice subjected to 30 minutes ischaemia and 72 hours reperfusion. There was no statistically significant difference in infarct size between males and females: IS/AAR% males 34.8±3.8 (n=7) versus females 36.2±5.1 (n=7). Statistical significance assessed by unpaired t-test, $^{NS}P>0.05$.

All subsequent surgeries in this thesis were undertaken in male mice only, other than where this is specifically indicated in the methods of the relevant section.

This chapter has described the standard protocol for the mouse *in vivo* ischaemia-reperfusion injury model subsequently applied in this thesis for the investigation of cardioprotective efficacy of a number of potentially therapeutic interventions.

4.6. Discussion

The main objective of this chapter was to develop and characterise a mouse *in vivo* model of ischaemia-reperfusion injury for subsequent investigations of cardioprotective efficacy. Although this model has been established by other research groups, this was the first establishment of this important research model within our laboratory.

This chapter describes the extensive development and characterisation of the *in vivo* recovery ischaemia-reperfusion model undertaken in this thesis and intends to provide a comprehensive surgical protocol to facilitate transfer of this protocol to future operators.

4.6.1. Aim 1: Establish *in vivo* recovery model of ischaemia-reperfusion

The mouse *in vivo* recovery model of ischaemia-reperfusion injury developed here was loosely based on previously published surgical protocols (Michael et al., 1995; Fisher and Marber, 2002; van Laake et al., 2007). This model comprises open-chest surgery for occlusion of the LAD coronary artery to induce regional myocardial ischaemia followed by release for myocardial reperfusion and recovery. The key attributes of this model are described in detail in the introduction of this chapter (see 4.3.1) and include: (1) use of mice to exploit genetic models, (2) defined periods of ischaemia and reperfusion and (3) recovery to permit long-term investigation.

This *in vivo* recovery model is recognised as being complex to establish in mice due to their small size and rapid heart rate (Fisher and Marber, 2002; van Laake et al., 2007). The first part of this chapter describes the difficulties encountered in efforts to establish this model within our laboratory. Despite the difficulties encountered with initial establishment of this model, it was imperative to persevere with this recovery model in order to permit the subsequent investigation of long-term cardioprotective efficacy. Extensive development and refinement of surgical skills and the protocol itself led to the establishment of a robust and reproducible model of *in vivo* ischaemia-reperfusion injury, described in part 1 of this chapter. The early results from this model are not presented in this thesis due to the large degree of variability in myocardial infarct size within experimental groups. All data presented in this thesis were conducted following the refinement of this model to ensure validity of the data and interpretations presented.

Surgical survival and anaesthetic regime: Initial surgeries were conducted using a recovery anaesthetic protocol (consisting of ketamine and medetomidine and reversal by atipamezole) which was previously published and used within our laboratory for *in vivo* recovery procedures of short anaesthetic durations (Cruz et al., 1998; Lim et al., 2011). However, modification of this anaesthetic regime to the substantially longer

anaesthetic duration required for the ischaemia-reperfusion model presented here resulted in very poor surgical survival of animals (Figure 4.8: surgical survival to 6 hours post-surgery 25%) which was clearly unacceptable for an experimental model.

Further to this, the insufficient depth of anaesthesia of B6/SV129 mice observed in initial trials of this anaesthetic regime meant that it was not appropriate to continue with this anaesthetic protocol. The additional effects of this anaesthetic regime on heart rate and body temperature are discussed below. Given the strict UK Home Office guidelines and local rules governing *in vivo* recovery procedures it was not feasible to investigate other injectable regimes without rapid reversal agents, such as sodium pentobarbital and ketamine xylazine regimes (Nossuli et al., 2000; Fisher and Marber, 2002; Pons et al., 2003) since this would have substantially reduced the throughput of this model.

Initial investigations of the isoflurane inhalation anaesthetic regime demonstrated substantially improved surgical survival (Figure 4.8: surgical survival to 6 hours post-surgery 100%) and permitted the assessment of myocardial infarct size as a percentage of AAR in a number of animals subjected to this protocol (Figure 4.9). Isoflurane anaesthesia also conferred several further procedural advantages including: (1) rapid onset and reversal of anaesthesia, (2) ease of delivery and modulation of dosing and (3) no effect on physiological heart rate or body temperature. The lack of interference on heart rate and body temperature confer clear advantages over the injectable regimes described in this thesis given the known effects of lowered cardiac function (Appleton et al., 2004) and temperature (Schwartz et al., 1997; van den Doel et al., 1998) on infarct size. Indeed, Kober et al. (2004; 2005) reported that isoflurane exerts significantly less effect on haemodynamics and cardiac function than ketamine and xylazine anaesthesia.

Anaesthetic conditioning: The use of isoflurane anaesthesia in this model presents the possibility of anaesthetic conditioning effects which have been reported to reduce final myocardial infarct size in some previous studies (reviewed by Kato and Foex, 2002). Investigation of this in animals subjected to this protocol using non-recovery injectable (ketamine, xylazine and atropine) and isoflurane inhalation anaesthetic regimes showed a striking agreement in myocardial infarct size between them (Figure 4.9), thereby suggesting that the isoflurane protocol here does not exert an appreciable cardioprotective effect. However, interpretation of this effect is limited by the short reperfusion duration (2 hours only) imposed on this study due to the complications of the recovery protocol described above, whereby it is possible that this isoflurane dose may exert delayed conditioning effects that would not be detected in this study. Tsutsumi et al. (2006) showed that isoflurane mediated cardioprotection elicited an acute memory phase up to two weeks following *in vivo* ischaemia-reperfusion in mice. However, the

isoflurane dose examined in this published study was sustained for 30 minutes prior to the onset of ischaemia (Tsutsumi et al., 2006), which differs substantially from the protocol used in this thesis. Indeed, the main studies reporting significant cardioprotective effects of isoflurane in this model of ischaemia-reperfusion use similarly high and prolonged isoflurane doses (reviewed by Kersten, 2011).

Interestingly, a comprehensive study of the cardioprotective effects of isoflurane dosing by Redel et al. (2009) showed that 30 minutes and not 15 minutes administration of isoflurane prior to ischaemia-reperfusion in mice was required to significantly reduce myocardial infarct size. However, it should be noted that 18 minutes post-conditioning by isoflurane dosing also significantly reduce myocardial infarct size (Redel et al., 2009), confirming the potential postconditioning effect of isoflurane in mice. This study demonstrates that, as expected for any cardioprotective intervention, the threshold required for cardioprotection is dose and time dependent, where it appears that the isoflurane protocol used in this thesis does not reach the threshold required for cardioprotection. This further demonstrates the importance of strict control of isoflurane concentration and duration of dosing in the model presented here.

Furthermore, since it has been suggested that anaesthetic and ischaemic conditioning are mediated by the same cardioprotective pathways (see chapter 1) (Kober et al., 2004; Stowe and Kevin, 2004; Tsutsumi et al., 2006), the demonstration of a significant reduction in myocardial infarct size by IPC (Figure 4.12), in the region of that expected from previous IPC studies (reviewed by Yellon and Downey, 2003), also suggests that this isoflurane protocol does not elicit significant cardioprotection.

It should be noted however, that it is possible that isoflurane may be mediating more subtle effects including (1) lowering the threshold for other conditioning protocols with shared pathways, such as IPC (Kober et al., 2004; Stowe and Kevin, 2004; Tsutsumi et al., 2006) or (2) exhibiting delayed conditioning effects that could be observed at prolonged reperfusion durations (Tsutsumi et al., 2006). Further investigation of potential anaesthetic conditioning by examining the isoflurane dosage required to significantly reduce infarct size is outside the remit of this thesis. However, this may have provided further confirmation that the dose used in the present study was not approaching the threshold dose required for cardioprotection.

An additional possible mechanism of inadvertent cardioprotection in the *in vivo* ischaemia-reperfusion model developed here is the administration of the analgesic buprenorphine; a semi-synthetic opioid which exerts its analgesic effects by acting on opioid receptors (specifically mu and kappa receptor subtypes) (McCormack and Chapleo, 1998). Opioid compounds have been reported to exert significant

cardioprotective effects in *in vivo* models of ischaemia-reperfusion (reviewed by Peart et al., 2005). However, for the same reasons as discussed above relating to similarity of infarct sizes obtained using the non-recovery (injectable anaesthesia without buprenorphine administration) and the recovery (isoflurane anaesthesia) protocols and the demonstration of significant cardioprotection by IPC, it is not expected that buprenorphine administration here exerts any significant cardioprotective effect here. Consistency of buprenorphine dosing was ensured to minimise the interference of any possible effects in the studies presented in this thesis.

In summary, consideration of possible complications due to inadvertent isoflurane or opioid conditioning should not be discounted in the model presented here; however, attempts were made to limit any potential conditioning effects by using the minimal dosing concentration required for effect and close matching of dosing between animals. This isoflurane anaesthetic protocol permitted establishment of a robust and reproducible *in vivo* recovery model of ischaemia-reperfusion in mice. The subsequent sections of this chapter described the validation and characterisation of this model.

4.6.2. Aim 2: Validation of ischaemia-reperfusion injury model

Since this thesis intended to apply the *in vivo* ischaemia-reperfusion model developed here to investigate the long-term cardioprotective efficacy of therapeutic interventions, it was necessary to validate the use of this model for detecting reductions in myocardial infarct size. This was completed by application of two well-described cardioprotective strategies, IPC (Figure 4.12) and CsA (Figure 4.13). Both of these interventions significantly reduced myocardial infarct size at 72 hours reperfusion and thus confirmed that the infarct size evoked by this model is amenable to modification. This was particularly important in the present study given that the infarct size in control operated animals at 72 hours reperfusion was smaller than that expected from previous studies with 2 hours reperfusion, meaning that the absolute infarct size difference between the sham and control infarct sizes was only 26% IS/AAR.

Cardioprotection by ischaemic preconditioning: IPC is a powerful cardioprotective intervention whereby brief sublethal episodes of ischaemia immediately prior to the main ischaemic insult protect against ischaemia-reperfusion injury (Murry et al., 1986). Although this specific intervention is of limited clinical relevance since it must be administered prior to the main ischaemic event, it provides a useful experimental tool since it elicits a robust cardioprotective effect that has been confirmed in every mammalian species tested to date (reviewed by Jennings, 2011). A standard IPC protocol of one cycle of 5 minutes ischaemia and 5 minutes reperfusion prior to the main

ischaemic insult elicited significant cardioprotection against both 30 minute (Figure 4.12) and 40 minute (data not shown) ischaemic insults. Importantly, this experiment demonstrated that the variation of infarct size within these groups and the cardioprotective effect size were sufficient to demonstrate statistical significance to **P<0.01 with six animals per group (Figure 4.12). Furthermore, the extent of infarct size reduction by IPC (49% reduction) is in agreement with that expected from previous studies of IPC in numerous models (reviewed by Yellon and Downey, 2003); as discussed above in relation to potential inadvertent conditioning effects.

Cardioprotection by cyclosporine-A: Administration of CsA 5 minutes prior to the onset of myocardial reperfusion also mediated significant cardioprotection in this model (Figure 4.13). Although the extent of infarct size reduction was lower than that conferred by IPC (IS/AAAR% reduced by approximately 31% for CsA compared to 49% for IPC), statistical significance was obtained with small sample sizes (Figure 4.13: n=4/group).

It should be noted that the control infarct size in vehicle treated animals in this CsA study was slightly larger than control animals previously (Figure 4.13: 43.1% in vehicle treated controls compared to Figure 4.12: 32.0% in controls). This suggests that the vehicle used in this study (cremophor/ethanol-94%) evoked increased myocardial injury. The potentially injurious effect of this vehicle has not been investigated further in this thesis and it remains unclear which component of the vehicle exerted this effect. Ethanol has previously been reported to be cardioprotective in this model (reviewed by Krenz et al., 2002), although only as a preconditioning mimetic which is distinct to the timing of administration in this study. A previous study by Tatou et al. (1996) in an *ex vivo* working heart model of myocardial infarction showed that cremophor significantly impaired cardiac function (Tatou et al., 1996); however, this has not been confirmed *in vivo*.

Since all animals in this study received matched doses of vehicle (either with or without CsA) this does not affect the interpretation of the cardioprotective effect of CsA. However, the increased control infarct size may increase the absolute effect size of infarct size reduction in this study, thereby increasing the statistical power at this small sample size. The precise influence of this increased control infarct size on effect size cannot be evaluated from this data because infarct size was not assessed in sham operated mice receiving this vehicle. Although administration of this vehicle could not be avoided due to the solubility properties of CsA, this study highlights the importance of well-designed studies with appropriate control groups, where the inclusion of vehicle treated controls in this experiment permits the conclusion that CsA treatment is cardioprotective in this model. This was also an important consideration for the experimental design of a further CsA study in chapter 8.

In summary, this initial validation study confirmed that the infarct size evoked by this model is amenable to reduction by known cardioprotective interventions. The scope for increased infarct size has not been examined here since this was not the focus of the subsequent applications of this model; this is however, discussed further in chapter 6.

4.6.3. Aim 3: Characterisation of ischaemia-reperfusion injury model

Further characterisation of the *in vivo* ischaemia-reperfusion model developed in this thesis was examined to determine the optimal ischaemic and reperfusion durations and the effect of other experimental variables on the infarct size evoked by this model.

Ischaemic duration: The optimal myocardial infarct size of control operated animals should be such that it permits scope for increase or decrease upon application of experimental treatments. The optimal ischaemic duration, in terms of the resultant infarct size, was examined in this section since it is known that ischaemic duration correlates with infarct size, as explained by the wavefront of necrosis hypothesis by Reimer et al. (1977) described in chapter 1 (see 1.2.3). This investigation of infarct size was particularly pertinent in the present model given the slightly smaller infarct size obtained in this recovery model (Figure 4.12; 30 minutes ischaemia, 72 hours reperfusion) than that expected in animals subjected to the *in vivo* non-recovery model within our laboratory (Figure 4.9; 30 minutes ischaemia, 2 hours reperfusion).

An additional 10 minutes myocardial ischaemia resulted in a slight but non-significant increase in myocardial infarct size (Figure 4.16, comparing 30 versus 40 minute ischaemic insults). Although there was no statistical difference, there was a trend towards decreased survival in the group subjected to the increased ischaemic duration (Figure 4.17: 40 minutes ischaemia 63.6% survival compared to 30 minutes ischaemia 87.5% survival), where the majority of those animals that did not survive to the pre-defined endpoint were actually excluded due to incomplete reperfusion upon release of the occluding snare. This is important for evaluating the most appropriate ischaemic duration for subsequent studies, where a standard model of 30 minutes ischaemia was used in all subsequent experiments unless otherwise stated.

Although the increased ischaemic duration examined in this study did not significantly increase myocardial infarct size, it is likely that this reflects an insufficient increase in the ischaemic duration tested, such that this produced only a small effect size for which this study is likely to be underpowered to detect. It is unlikely that the lack of a significantly increased infarct size following 40 minutes ischaemia reflects secondary selection of smaller infarct size by death of animals with larger infarcts, since the majority of ‘non-survivors’ were excluded and did not die spontaneously (Figure 4.17), described above.

The wider potential effects of secondary selection for smaller infarct sizes by death of animals with larger infarct sizes are discussed in detail below. Further studies could have assessed the effect of further incremental increases in ischaemic duration, however, given the increased exclusion of animals in the 40 minute ischaemic group due to poor myocardial reperfusion; this would be unlikely to lead to the development of an improved model and was not therefore investigated further.

It is important to note that neither of the ischaemic durations tested in this chapter resulted in any noticeable myocardial haemorrhage within the AAR (which would have been visualised by the rust-red appearance of blood upon scanning of the hearts). This is in line with the expected progression of infarction predicted by Reimer et al. (1977) where myocardial haemorrhage is predominantly expected in fully transmural infarcts. A further interesting observation of the myocardial infarctions evoked by this *in vivo* model is the unusual subepicardial dominance of infarction (see Figure 4.12 A), which is not as predicted by the wavefront of necrosis hypothesis demonstrated by Reimer et al. (1977) in dog hearts (see 1.2.3). This may result from species differences between coronary anatomy and myocardial thickness, specifically in terms of the proportion of subendocardial tissue that is amenable to residual delivery of oxygen by diffusion from the lumen of the left ventricle. The unexpected morphology of infarction in the mouse heart does not impact on the overall applications of this model; however, it is important to highlight a potential confounding factor that may affect the visualisation and measurement of infarction in subsequent applications of this model.

A further consideration for the interpretation of infarct sizes in this thesis is that infarct size was only assessed in animals which survived to the pre-defined reperfusion endpoint, in order to ensure consistency of the model. However, this may have introduced some selection of animals with smaller infarcts which are expected to have an increased survival rate. It was not feasible to quantify infarct size in those animals which died spontaneously, due to the questionable validity of delayed TTC staining for infarction in dead animals where further cell death will occur and enzymatic washout may not be complete; this has not been directly addressed in the literature. Although a previous study by Pons et al. (2003) did report post-mortem measurements of infarct size and showed a trend towards larger infarct sizes in animals that died spontaneously, caution should be exercised in the interpretation of this study especially since the time delay between death and TTC staining is not detailed. In the present thesis, exclusion of animals that died spontaneously during the reperfusion period may result in some secondary selection of lower myocardial infarct sizes. This is likely to be more acute in experiments resulting in larger infarct sizes and is therefore discussed in more detail in relation to the results presented in chapter 6.

Reperfusion duration: The overall aim of this thesis was to investigate the long-term efficacy of potentially cardioprotective interventions and it was therefore pertinent to investigate the effect of extended reperfusion duration on myocardial infarct size assessed in this model. It was hypothesised that infarct size would increase over the immediate reperfusion duration as the full extent of infarction due to ischaemic and lethal reperfusion injury and the initial remodelling effects of myocardial thinning and infarct expansion occur. This was based on studies of larger species and it is important to note that the metabolic rate and velocity of remodelling in the mouse heart are known to be faster (Patten et al., 1998; Fisher and Marber, 2002; Dewald et al., 2004).

This study showed that although there was no statistically significant difference in infarct size between the reperfusion durations tested, there was a trend towards decreased infarct size at the extended reperfusion durations (24 and 72 hours) compared to earlier reperfusion durations (2 and 6 hours) (see Figure 4.18). Closer examination of published studies revealed that Tsutsumi et al. (2006) observed a similar non-significant decrease in myocardial infarct size at 2 hours and 14 days reperfusion (Tsutsumi et al., 2006).

The study presented here was not adequately powered to detect a significant difference between each of these reperfusion durations since this model is not sufficiently sensitive to undertake such studies. The terminal nature of this histological staining method used for infarct size and AAR quantification further decreases the statistical power of this study, whereby an *in vivo* method of examining the progression of infarct size within the same cohort of animals would likely provide a valuable insight into the processes of infarct development. The use of cardiac MRI for *in vivo* myocardial infarct size and AAR is the focus of chapter 8 and may provide a valuable tool for future studies.

It is also important to note that although TTC is considered to be a 'gold-standard' method for identifying and quantifying infarct size, it is recognised that there are potential factors that can affect its validity including: (1) time for enzymatic washout (Redel et al., 2008), (2) impaired metabolic activity of living cells (Tsutsumi et al., 2006) and (3) lack of distinction between cell types. The time required for enzymatic washout and recovery of metabolic activity of cells following ischaemia and reperfusion should not affect the infarct sizes reported in this study since the shortest reperfusion duration examined was 2 hours. It is possible that the slight reduction observed in infarct size at 72 hours compared to 2 hours reflects an artefact from positive TTC staining of infiltrating inflammatory cells at this later reperfusion endpoint. Further investigation of the effect of reperfusion could be undertaken using immunohistochemical approaches; however, the lack of a validated method for determining AAR using this method would hinder interpretation of this data and has not therefore been undertaken here.

An additional consideration for interpreting the data presented in this study is the potential effect of remodelling whereby extensive myocardial thinning at extended reperfusion durations would be expected to reduce the measured AAR. This is unlikely to represent a significant bias in the present study since no appreciable myocardial thinning was observed at any endpoint and furthermore, there was no difference in AAR between these groups. This is further supported by Vandervelde et al. (2006) who concluded that myocardial thinning of the mouse heart following a similar ischaemic insult is very limited (Vandervelde et al., 2006). Potential changes in the measured AAR at extended reperfusion durations remain an important consideration, particularly since remodelling may be further affected by interventions. This is discussed further in chapter 8 which aims to develop an *in vivo* method for determining AAR to overcome the problems associated with extended reperfusion.

The effect of reperfusion duration on infarct size was not investigated further in this thesis given the recognised limitations of this study design. However, the experiment presented here was important to further evaluate and support the infarct size reported at 72 hours reperfusion in this model since it suggests that this is not an unduly small infarct size but is actually in good agreement with the extent of infarction obtained at 2 hours reperfusion (non-recovery model) by previous operators within our laboratory and previously in this thesis (Figure 4.9).

Operative time of day: A further important consideration for the experimental design of subsequent studies in this thesis is the potential effect of diurnal changes that have previously been shown to affect myocardial infarct size in a similar *in vivo* mouse model. Durgan et al. (2010) demonstrated a 3.5 fold increase in infarct size (following 45 minutes ischaemia and 24 hours reperfusion) in mice subjected to this ischaemic insult at zeitgeber time (ZT) zero (equivalent to 06:00) compared to ZT12 (equivalent to 18:00). Further to this, levels of phosphorylated Akt and GSK-3β were shown to decrease during the period, in accordance with the inverse correlation with infarct size (Durgan et al., 2010), as expected given the cardioprotective actions of these kinases.

All surgeries in this thesis were conducted during full day operating sessions during which the time of onset of ischaemia was between approximately 08:00 and 18:00. A retrospective analysis of myocardial infarct size in morning and afternoon operated animals in the present study demonstrated that there was no significant difference in infarct size for either control or IPC groups (Figure 4.19 i and ii). An additional more detailed sub-analysis was conducted for control operated animals to compare only early and late surgeries (08:00-09:00 versus 16:00-17:00) and this also showed no significant difference in infarct size. Although it is possible that diurnal variations may be exerting

more subtle effects that cannot be seen in this retrospective investigation of infarct size, to reduce the potential of any such effects, an equal mix of morning and afternoon surgeries was ensured between groups for all studies reported in this thesis. Although this variation in operating time may slightly increase the variability of final infarct size data, it was not feasible to restrict the operating day to only morning or afternoons due to the long surgical protocol and throughput required.

Investigation of diurnal variations in infarct size resulting from this *in vivo* recovery model of ischaemia-reperfusion injury was not a primary objective of this thesis; however, it is reassuring to demonstrate that the variation in operating time of day in the model developed here does not significantly affect infarct size. The absence of any obvious diurnal effects on myocardial infarct size may result from the less extreme operating times investigated (8:00 versus 17:00) or compared to those examined by Durgan et al. (2010) (6:00 versus 18:00). It should also be noted that the model of infarction investigated here comprised 30 minutes ischaemia and 72 hours reperfusion compared to 45 minutes ischaemia and 24 hours reperfusion investigated by Durgan et al (2010). The precise reasons for the absence of obvious diurnal effects on infarct size resulting from the model presented in this chapter was not investigated further since it was not the focus of the overall research objectives of this thesis. This finding supported the use of full day operating sessions for all other studies presented in this thesis.

Gender: Previous basic science and clinical studies have shown that females are inherently more cardioprotected than males, in part due to oestrogen levels (reviewed by Murphy and Steenbergen, 2007). The majority of basic science cardioprotection studies have historically only investigated male subjects due to the potential increased variation between females due to oestrogen-cycling (Black and Rodger, 1996). It has, however, been suggested that this gender bias of pre-clinical studies may affect the success of clinical translation; this is discussed in detail in chapter 1 (see 1.5.1). Gender did not appear to significantly affect infarct size observed in the model presented here (Figure 4.20). The absence of a significant difference in infarct size between male and female mice in this study may result from the relatively young age of these animals (10-12 weeks old), although these animals are expected to be sexually mature. It is likely that any subtle effect of gender on myocardial infarction in the experiments presented here would be minimal based on this study, however, the majority of studies in this thesis continued to use male subjects only since this is more conventional for publication purposes. The gender of animals used in subsequent studies is specifically detailed.

In summary, part three of this chapter has investigated the effects of a number of potentially important experimental variables to define the optimal experimental protocol for the subsequent applications of this *in vivo* recovery model of ischaemia-reperfusion.

4.6.4. Potential limitations of the ischaemia-reperfusion injury model

An important consideration for the suitability of the model of ischaemia-reperfusion presented here is the invasive nature of the surgical protocol concerning: (1) open-chest preparation of the animal and (2) direct mechanical occlusion and reperfusion of the LAD. It is likely that these surgical interventions will evoke a confounding inflammatory response concurrent with that resulting from myocardial ischaemia-reperfusion itself.

Nossuli et al. (2000) have reported a closed-chest model of ischaemia-reperfusion injury by externalisation of the LAD ligating suture for subsequent ischaemia-reperfusion one week post-surgery (Nossuli et al., 2000). Further studies have attempted to enhance the closed-chest surgical protocol and Gao et al. (2010) recently reported a closed-chest model of ischaemia-reperfusion without the need for artificial ventilation which resulted in lower inflammatory responses and improved surgical recovery. More recently, Liao et al. (2013) published a modified closed-chest method to allow application of ischaemic conditioning protocols. However, there remain potential limitations with these closed-chest models including the lack of direct visualisation of the AAR in the delayed model presented by Nossoli et al. (2000) and the relatively poor surgical survival reported by Liao et al. (2013). Given the complications associated with establishing the recovery model of ischaemia-reperfusion presented in this thesis, subsequent modifications to this protocol to enable closed-chest induction of ischaemia were not investigated here.

Although the open-chest model of ischaemia-reperfusion developed here is likely to evoke a significant background inflammatory response, which limits the investigation of precise inflammatory pathways, the effect of this on the measurement of infarct size and cardiac function is likely to be limited. The effect of background responses to injury evoked by open-chest surgery is discussed further in chapter 6, where it was shown that sham operated animals exhibited a significant increase in myocardial expression of Sirt-3, an important mitochondrial stress protein (see 6.3.3).

Another potential confounding variable in the open-chest model of ischaemia-reperfusion injury presented in this thesis is myocardial temperature. Although it is known that core body temperature profoundly affects myocardial infarct size (van den Doel et al., 1998), Schwartz et al. (1997) showed that myocardial temperature may vary despite the use of a thermostatically controlled operating table. Although myocardial

temperature was not examined in this thesis, use of sterile drapes covering the chest opening may have helped to reduce any variations in myocardial temperature.

Direct external manipulation of the LAD using a suture occlusion to induce ischaemia is notably different from the spontaneous occlusion of a vessel by atherosclerotic plaque rupture in the clinical setting (reviewed by Black and Rodger, 1996). It is not clear whether the difference in means of occlusion between these settings would dramatically affect results from this model; however, it is difficult to overcome this given the technical restraints concerned with using an intra-coronary device in the mouse.

It is also important to note that this model of ischaemia-reperfusion injury has been developed in otherwise young, healthy animals which is distinct from the clinical setting of acute myocardial infarction whereby patients usually present with several comorbities (as discussed in 1.5.1. i). In particular, the pathophysiological responses induced by the defined onset of ischaemia in an otherwise healthy vessel (as in the model presented here) may differ from the pathological setting of chronic cardiovascular disease. Although it is complicated to develop a research model including this pathological background, this potential limitation of the current model should be appreciated.

4.6.5. Summary

This chapter describes the development and characterisation of a reproducible and robust model of ischaemia-reperfusion to permit future investigation of long-term cardioprotective efficacy. The key findings of this chapter are summarised below:

(1) The surgical protocol for the mouse *in vivo* recovery model of ischaemia-reperfusion has been developed with extensive procedural refinements to facilitate a high surgical survival rate of animals subjected to this model. A detailed surgical protocol and an extensive troubleshooting guide are provided in this chapter and aim to facilitate subsequent establishment of this model by future operators.

    Isoflurane anaesthesia was required to achieve sufficient surgical anaesthesia and survival for this model and steps have been taken to ensure any potential cardioprotective effects of this regime are reduced by using minimal and consistent isoflurane doses between animals. An initial investigation of the potential cardioprotective effects of isoflurane demonstrated that there was no significant difference in myocardial infarct size between animals subjected to the inhalation isoflurane and injectable anaesthetic regimes in this protocol, thereby suggesting that any cardioprotective effect of isoflurane in this protocol is minimal.

(2) The mouse *in vivo* recovery ischaemia-reperfusion model developed here has been validated for the evaluation of cardioprotective efficacy in terms of myocardial infarct size reduction by the application of two well-described cardioprotective interventions. Both ischaemic preconditioning and cyclosporine-A significantly reduced myocardial infarct size as expected and thereby demonstrated that the infarct sizes produced by this model are amenable to reduction in the presence of a cardioprotective intervention. These experiments also confirm that the infarct sizes evoked by this model and the quantification methods used are robust and reproducible.

(3) The potential effects of several potentially important variables were investigated in this *in vivo* recovery model of ischaemia-reperfusion thus informing the optimal design of future studies in this thesis. An optimal protocol of 30 minutes ischaemia and 72 hours reperfusion was shown to elicit an appropriate extent of myocardial infarction and was used for all subsequent studies presented in this thesis unless otherwise stated. The timing of surgeries during standard operating days had no significant effect on infarct size confirming that it is appropriate to utilise full operating days to maximise the throughput of this model. Gender did not affect infarct size and thus justifies use of mixed gender groups for subsequent studies if required.

CHAPTER 5: INVESTIGATION OF CYCLOPHILIN-D INHIBITION AS A STRATEGY FOR CARDIOPROTECTION

5.1. Introduction

Mitochondrial dysfunction and mitochondrial permeability transition pore opening account for a significant proportion of cell death upon myocardial ischaemia-reperfusion. The mitochondrial proteins involved in these processes represent critical targets for interventions to regulate these processes and potentially reduce infarct size and thus ultimately improve patient prognosis (reviewed by Gustafsson and Gottlieb, 2008).

Mitochondrial permeability transition upon mPTP opening is a key effector of cell death upon myocardial ischaemia-reperfusion due to its effects on dissipating the inner mitochondrial membrane electrochemical gradient and resultant loss of ATP production and subsequent necrotic or apoptotic cell death; outlined in chapter 1 (see 1.2.3, Figure 1.6) (reviewed by Baines, 2009a; Oerlemans et al., 2013). Although the molecular composition of the mPTP has been subject to intensive research and conflicting models, Cyp-D is accepted as an important regulatory component which confers calcium sensitivity to mPTP opening (Connern and Halestrap, 1994; Nicolli et al., 1996).

Cyp-D inhibition has been identified as an important potential target for reducing mPTP opening and thus cell death upon ischaemia-reperfusion. Genetic ablation or pharmacological inhibition of Cyp-D renders the mPTP less sensitive to calcium, thereby requiring significantly higher calcium concentrations to trigger mPTP opening. Previous studies have shown that Cyp-D inhibition reduces cell death following ischaemia-reperfusion, including in *in vivo* models of myocardial ischaemia-reperfusion injury (Nakagawa et al., 2005; Baines et al., 2005; Gomez et al., 2007); outlined in chapter 1 (see 1.4.1). Indeed, Gomez et al. (2007) showed that a single intravenous dose of the Cyp-D inhibitor, Debio-025, preserved cardiac function and improved survival to 30 days in mice subjected to *in vivo* myocardial ischaemia-reperfusion (Gomez et al., 2007); thereby suggesting that Cyp-D represents a target for long-term cardioprotection. However, since Debio-025 also inhibits other cyclophilin proteins, the long-term efficacy of Cyp-D inhibition for cardioprotection against ischaemia-reperfusion remains unclear.

The long-term efficacy of Cyp-D inhibition in this setting remains pertinent given the suggestion by some studies that long-term Cyp-D inhibition can be detrimental. Importantly, Oie et al. (2000) suggested that chronic Cyp-D inhibition by CsA may exacerbate cardiac failure and Elrod et al. (2010) showed that Cyp-D knockout mice

have a higher predisposition to cardiac hypertrophy and cardiac failure upon physiological stress. Although the divergent effects of Cyp-D inhibition in the settings of cardiac failure and ischaemia-reperfusion injury may result from the divergent pathophysiological processes in these settings, it is crucial to assess the long-term efficacy of Cyp-D as a therapeutic target against myocardial ischaemia-reperfusion. This is particularly relevant given the complexity of the long-term pathophysiology of myocardial ischaemia-reperfusion, including lethal reperfusion injury, inflammation and ventricular remodelling, as described in chapter 1 (see 1.2.4). Indeed, the lack of long-term trials of cardioprotective efficacy has been identified as a potentially important obstacle to the poor translation of therapeutic interventions from basic science research to the clinical setting (Hausenloy et al., 2010), as discussed previously.

This chapter aimed to investigate the long-term efficacy of Cyp-D inhibition (by genetic ablation of Cyp-D) in conferring cardioprotection against ischaemia-reperfusion injury.

5.2. Research objective and aims

The main objective of this chapter was to investigate the potential role of Cyp-D inhibition (by genetic ablation) as a therapeutic target against the long-term effects of myocardial ischaemia-reperfusion injury. The principal aims to achieve this were:

(1) Investigate the long-term cardioprotective efficacy of Cyp-D inhibition in the established model of global genetic ablation of Cyp-D;

(2) Investigate the role of Cyp-D in the heart by establishing and investigating a model of cardiac-specific genetic ablation of Cyp-D.

5.3. Aim 1: Investigate long-term cardioprotection of Cyp-D ablation

5.3.1. Background

The Cyp-D genetic knockout mouse model is an important experimental tool for investigating the roles of Cyp-D and the mPTP in the pathophysiology of ischaemia-reperfusion. Cyp-D genetic ablation, by deletion of the *Ppif* gene, allows a more elegant elucidation of the roles of Cyp-D without the confounding non-selective effects of many of the small molecule inhibitors of Cyp-D described in the literature (detailed in chapter 1; see 1.4.1). This is particularly important since most of the available pharmacological

Cyp-D inhibitors, including CsA and Debio-025, also inhibit the other cyclophilin proteins making it difficult isolate the roles of Cyp-D (reviewed by Hausenloy et al., 2012).

Global genetic ablation of Cyp-D was simultaneously published by three independent research groups in 2005 (Basso et al., 2005; Baines et al., 2005; Nakagawa et al., 2005). This Cyp-D knockout system allowed characterisation of the baseline and stressed phenotypes of cells devoid of Cyp-D protein; characterisation of these animals is described in detail in chapter 1 (see 1.4.1, Table 1.2). Briefly, mitochondria isolated from Cyp-D knockout mice were more resistant to mPTP opening in response to simulated triggers of ischaemia-reperfusion including calcium and ROS. Importantly, Baines et al. (2005) and Nakagawa et al. (2005) also showed that global genetic ablation of Cyp-D significantly reduced myocardial infarct size *in vivo* in mice subjected to ischaemia-reperfusion. These studies confirmed the predicted role of Cyp-D in the susceptibility to ischaemia-reperfusion injury and provided a valuable model system in which to further examine the potential of Cyp-D as a therapeutic target in this setting.

However, these studies examined only the relatively short-term cardioprotective efficacy of Cyp-D genetic ablation, examining 24 hours reperfusion at most (Baines et al., 2005). Our group has shown that Cyp-D knockout mice are resistant to development of cardiac failure in response to myocardial ischaemia (by permanent coronary artery ligation) at 28 days (Lim et al., 2011). However, the long-term efficacy of Cyp-D inhibition by genetic ablation in the clinically relevant setting of myocardial ischemia-reperfusion injury has not been examined. The main objective of this chapter was to investigate the long-term effects of Cyp-D genetic ablation in the setting of myocardial ischaemia-reperfusion injury using the *in vivo* model developed in chapter 4.

Aim 1: This first aim of this chapter was to investigate the effect of global Cyp-D genetic ablation in mediating long-term cardioprotection against myocardial ischaemia-reperfusion. The central hypothesis in relation to this research objective was:

(1) Cyp-D global genetic ablation would significantly reduce myocardial infarct size following prolonged periods of reperfusion.

To investigate the long-term cardioprotective efficacy of Cyp-D genetic ablation it was necessary to first determine the expected effect size of myocardial infarct size reduction in order to determine the sample sizes required for subsequent long-term studies. This section describes the initial evaluation of the effect of Cyp-D global genetic ablation on infarct size following myocardial ischaemia-reperfusion injury.

5.3.2. Detailed methods

i Cyp-D global knockout mice

The Cyp-D global genetic ablation model used in this thesis was obtained from Prof J. Molkentin (Cincinnati Children's Hospital Medical Centre Laboratories, USA) from the colony created and published by his laboratory (Baines et al., 2005). Global somatic genetic ablation of Cyp-D in this colony was achieved by deletion of the first three coding exons of the endogenous *Ppif* gene according to standard transgenic methods, outlined in chapter 3 (see 3.1.2). A targeting vector was designed with homology to the non-coding regions of the *Ppif* locus surrounding the first three coding exons and containing the neomycin-resistance gene (*neo*), which upon insertion into SV129 derived embryonic stem cells resulted in generation of *Ppif* null mice (Figure 5.1). Cyp-D knockout mice were partially backcrossed onto a C57BL/6 background (approximate genetic background 75% C57BL/6 - 25% SV129).

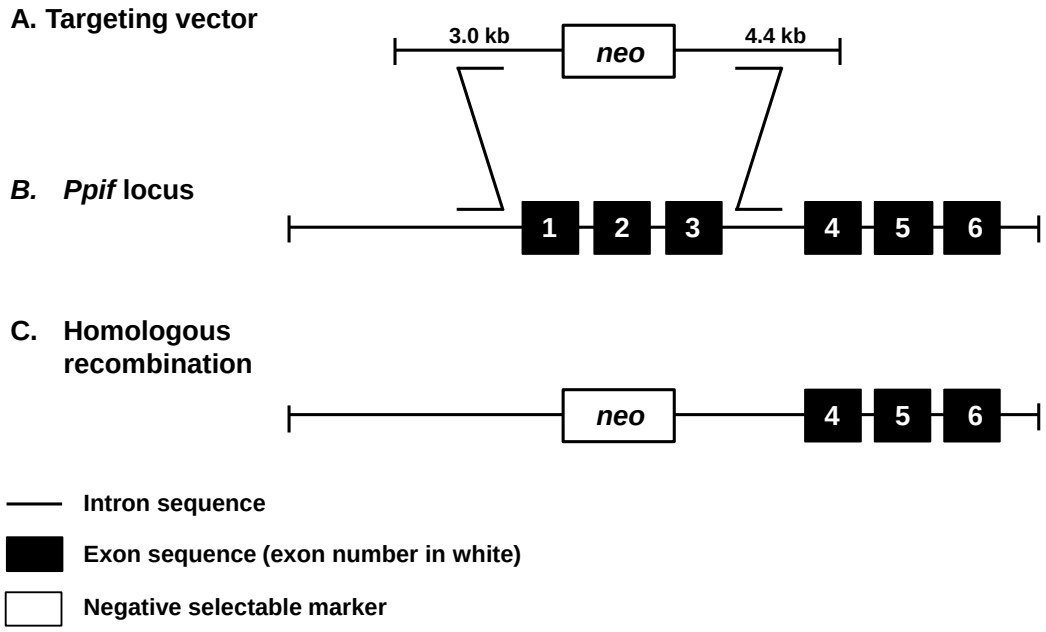

Figure 5.1: Generation of Cyp-D global knockout mice by Baines et al. (2005)
Global Cyp-D knockout was achieved by standard transgenic methods targeting the *Ppif* gene which encodes Cyp-D. Homologous recombination of the targeting vector and endogenous *Ppif* gene in embryonic derived stem cells resulted in deletion of the first three coding exons and insertion of the neomycin-resistance gene. *Ppif* KO cells were selected by neomycin resistance and used to create Cyp-D KO mice. Figure modified from Baines et al. (2005).

Mice provided by Prof J. Molkentin (Cincinnati Children's Hospital Medical Centre, USA).

Colony maintenance: The Cyp-D global transgenic colony was previously maintained as knockout breeding crosses and B6/SV129 mice used as approximate wildtype control animals (Figure 5.2 A). For the purposes of this thesis, a more appropriate breeding schedule was established to provide true littermate control animals. A series of genetic

backcrossing stages were also undertaken to minimise any potential effects of variations in background genetic strain in experiments using this transgenic colony. The breeding schedule undertaken in this thesis is summarised in Figure 5.2 and described below.

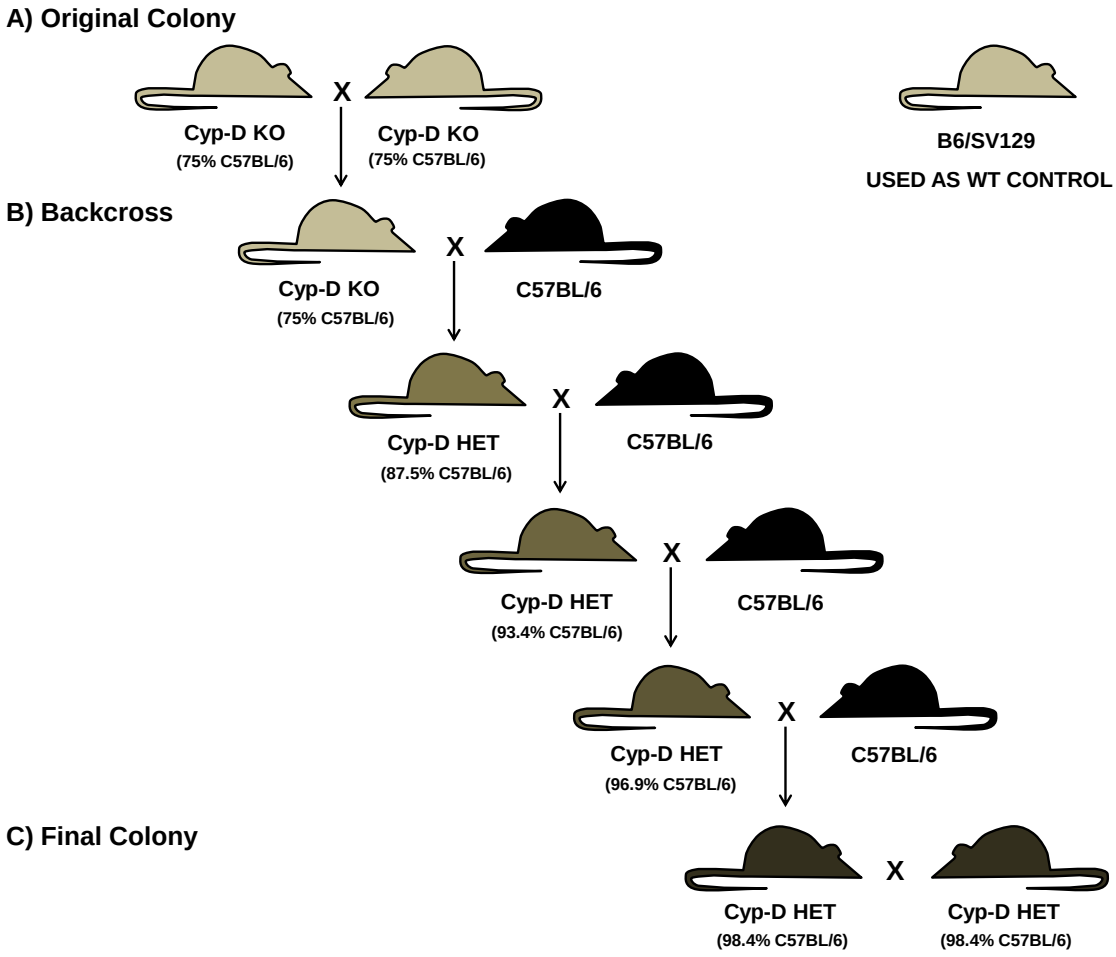

Figure 5.2: Cyp-D global knockout mouse colony backcrossing and maintenance
A) Original colony: Cyp-D KO mice were originally bred in-house with an approximate genetic background of 75% C57BL/6 and 25% SV129. Commercially available B6/SV129 mice were used as WT controls. B) Backcrossing stages were completed by initially crossing Cyp-D KO mice with C57BL/6 mice to produce Cyp-D HET mice. Cyp-D HET mice were crossed with C57BL/6 mice to produce Cyp-D HET (and WT) mice and Cyp-D HET progeny subsequently crossed with C57BL/6 mice. Backcrossing was completed for four generations to obtain Cyp-D HET mice with an approximate genetic background of 98.4% C57BL/6 and 1.6% SV129. C) Final colony was maintained as HET x HET crosses to produce Cyp-D WT, KO and HET progeny.

All breeding stages undertaken in the generation of this colony used a number of randomly selected animals from different parents in line with best practice breeding guidance (Wolfensohn and Lloyd, 2003). A number of animals from the original Cyp-D KO mouse colony maintained within our laboratory were bred with commercially obtained C57BL/6 mice (C57BL/6NCrl males and females; Charles River Laboratories, UK) to produce Cyp-D HET progeny. Cyp-D HET mice were subsequently bred with C57BL/6 animals to produce Cyp-D HET (and Cyp-D WT) progeny. This breeding

regime was undertaken for a total of four generations to produce a final colony with a genetic background of approximately 98.4% C57BL/6 and 1.6% SV129 (Figure 5.2 B). The colony was maintained as Cyp-D HET crosses to produce Cyp-D WT, HET and KO progeny for experimental use (Figure 5.2 C).

ii Genotyping for global genetic ablation of Cyp-D

All animals from this colony were genotyped prior to use; the genotyping method used here was based on that described in chapter 3 (see 3.1.2) with the following modifications. DNA samples were prepared from ear biopsies exactly as described previously and processed within 7 days of sampling. The PCR reaction mix was based on the standard PCR reaction optimised in this thesis and informed by Baines et al. (2005). The primers and cycling parameters for this reaction are described in Table 5.1. This protocol yielded DNA products of 600 base pairs (bp) (Neo-forward – Exon-4 reverse product) and 850 bp (Exon-3 forward – Exon-4 reverse product) corresponding to the mutant and wildtype DNA products. The genotype of each animal was decoded based on the presence or absence of these DNA bands: WT 850 bp only, KO 600 bp only and HET both 600 and 850 bp bands (Figure 5.3).

This PCR protocol was robust and reliably produced clear DNA bands for the determination of the genotypes of animals from the Cyp-D transgenic colony. This protocol was further confirmed by Western blot analysis of heart samples from Cyp-D WT and KO animals (example Western blot is shown subsequently in Figure 5.15).

A) Cyp-D PCR primer sequences

PRIMER	SEQUENCE	PROPERTIES	
		Length	T_m (ºC)
Primer 1 / Exon-4 reverse	5'-ATTGTGGTTGGTGAAGTCGCC-3'	21	57.3
Primer 2 / Exon-3 forward	5'-CTCTTCTGGGCAAGAATTGC-3'	20	59.8
Primer 3 / Neo forward	5'-GGCTGCTAAAGCGCATGCTCC-3'	21	63.7

B) Cyp-D PCR reaction mix

REAGENT	VOLUME/SAMPLE (µl)	FINAL CONCENTRATION
Qiagen 10X PCR Buffer	2.0	1X
10 mM dNTPs	0.4	200 µM
Primer 1 Exon-4R 100 µM	0.2	1 µM
Primer 2 Exon-3F 100 µM	0.2	1 µM
Primer 3 Neo-F 100µM	0.2	1 µM
Taq polymerase	0.2	-
Autoclaved distilled water	15.8	-
Crude DNA lysate †	1.0	-
TOTAL VOLUME/SAMPLE (µl)	**20.0**	

C) Cyp-D PCR thermocycling parameters

PCR STAGE	TEMPERATURE AND DURATION	PCR DESCRIPTION
1	95 ºC for 3 minutes	Hot start
2	95 ºC for 30 seconds	DNA separation
3	59 ºC for 30 seconds	Primer annealing
4	72 ºC for 1 minute	DNA synthesis
5	95 ºC for 30 seconds	DNA separation
6	57 ºC for 30 seconds	Primer annealing
7	72 ºC for 1 minute	DNA synthesis
8	Go to step 5 for 32 cycles	DNA synthesis
9	72 ºC for 10 minutes	Final extension
10	4 ºC for ever	Intermediate storage

Table 5.1: Cyp-D global transgenic colony genotyping protocol
A) Cyp-D primer sequences and properties. B) A single master mix was made based on Qiagen *Taq* kit (Qiagen, UK) and aliquots taken for each reaction. † 1 µl crude DNA lysate was added to each aliquot. C) PCR was performed using a thermal cycler (MJ Research, Canada).

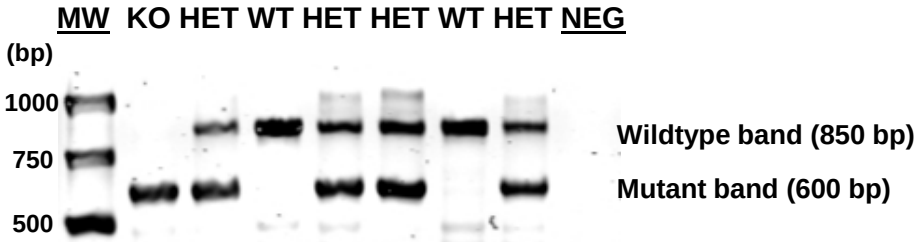

Figure 5.3: Cyp-D global transgenic colony representative genotyping result
The genotype of each animal was determined by the presence or absence of the expected PCR products: WT 850 bp band only, KO 600 bp band only and HET both bands (as annotated above the gel). A negative control (NEG) was run to ensure there was no external DNA contamination.

iii Ischaemia-reperfusion injury in vivo

Surgical protocol: The susceptibility of Cyp-D knockout and wildtype littermate controls was assessed using the *in vivo* recovery model of ischaemia-reperfusion injury developed previously in this thesis using the standard protocol of 30 minutes myocardial ischaemia and 72 hours reperfusion (see Figure 3.6). All surgeries were conducted on male mice aged 10-16 weeks from the Cyp-D global knockout transgenic colony or B6/SV129 mice from Harlan Laboratories, UK, as indicated in the results section below.

Endpoint 1 – IS/AAR%: The primary endpoint assessed in this study was myocardial infarct size by *ex vivo* histological staining using TTC and Evans blue staining, exactly as described previously, to calculate the infarct size as a percentage of AAR. The pre-defined surgical and AAR exclusion criteria were applied to this dataset (see 3.2.4).

All infarct size and AAR values are presented as mean ± SEM. Where two groups were compared, data were statistically analysed using an unpaired t-test. Where more than two groups were compared, data were statistically analysed by one-way ANOVA, followed by Bonferroni test comparing relevant columns of data. Where appropriate, Deming (Model II) regression analysis was performed to define the relationship between infarct size and AAR and reported as: $y=mx+c$ where m is the slope and c is the intercept when $x=0$. All statistical analysis was completed using GraphPad Prism® version 5.0 (GraphPad Software, USA). Statistical significance was reported where $P<0.05$ using standard significance coding.

Statistical power calculations were performed to retrospectively evaluate the power of statistical tests undertaken in this chapter to facilitate their interpretation. Where sufficient statistical power (80%) was not reached, the effect size and standard deviation were used to determine the sample size required to reach sufficient statistical power. For all tests, the minimal level of statistical power was judged to be 80%, in accordance with published guidelines (Cohen, 1988; Townend, 2002). All power calculations were performed using GraphPad StatMate version 2.0 (GraphPad Software, USA).

Endpoint 2 – Survival: Survival rates of Cyp-D mice were recorded and probable cause of death assessed by post-mortem investigation. Kaplan-Meier survival plots were plotted using GraphPad Prism® version 5.0 (GraphPad Software, USA). Significance was analysed by log-rank tests and significance was reported where $P<0.05$.

5.3.3. Results

This study first undertook a comprehensive backcrossing breeding schedule to allow generation of true wildtype littermate control mice and to theoretically reduce strain related variability in future experiments. All experiments using Cyp-D knockout and wildtype mice presented in this thesis were performed using true littermate control animals with a genetic background of approximately 98.4% C57BL/6 and 1.6% SV129. The first stage of this study to investigate the long-term cardioprotective efficacy of Cyp-D global genetic ablation aimed to characterise the backcrossed Cyp-D knockout colony produced here. These experiments are described below and the implications of these findings for future studies are discussed in detail subsequently.

i True littermate controls

Since previous studies of the Cyp-D global genetic knockout mice within our laboratory had utilised B6/SV129 mice as wildtype control animals, it was pertinent to examine myocardial infarct size in B6/SV129 mice and Cyp-D wildtype mice (backcrossed to 98.4% C57BL/6 and 1.6% SV129 genetic background) bred as a part of this thesis.

B6/SV129 and Cyp-D wildtype mice were subjected to the standard *in vivo* recovery ischaemia-reperfusion model developed in chapter 4 (30 minutes ischaemia and 72 hours reperfusion). There was no significant difference in myocardial infarct size between B6/SV129 and Cyp-D wildtype mice subjected to this standard protocol (Figure 4.9: IS/AAR% B6/SV129 30.3±3.8 versus Cyp-D WT 35.4±4.3; n≥6/group, $^{NS}P>0.05$). There was no significant difference in AAR (AAR/LV% B6/SV129 56.1±1.9 versus Cyp-D WT 55.6±2.8; n≥6/group, $^{NS}P>0.05$) or survival (% survival to 72 hours reperfusion: B6/SV129 85.7%, n=7 versus Cyp-D WT 90.0%, n=10) between these groups.

Although there was a trend towards an increased infarct size in Cyp-D wildtype mice in this study, substantially larger sample sizes would be required to detect such a small effect size. This was not examined further here since it does not represent a key study and would require a large number of animals. However, this experiment highlights the importance of using true littermate control animals in the study of myocardial infarction. Although this difference is unlikely to be biologically significant, the subsequent effect of this could artificially influence the outcome of studies not using correct littermate controls. All studies of transgenic animals in this thesis used true littermate animals.

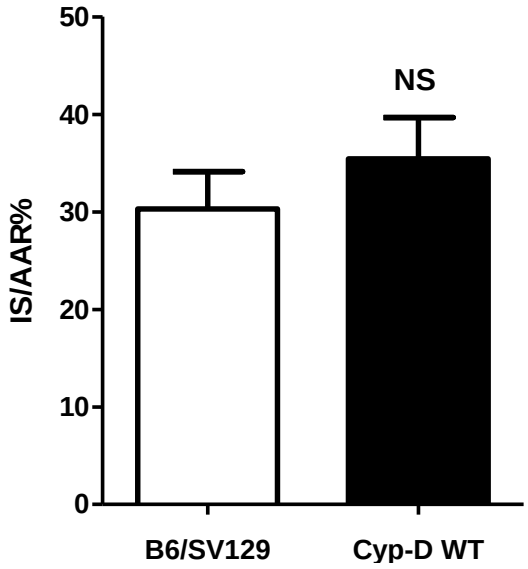

Figure 5.4: Infarct size in B6/SV129 and backcrossed Cyp-D WT animals
Infarct size following 30 minutes ischaemia and 72 hours reperfusion in B6/SV129 and backcrossed Cyp-D WT mice (98.4% C57BL/6 and 1.6% SV129); IS/AAR% was not significantly different between these mice: IS/AAR% B6/SV129 mice 30.3±3.8 (n=6) versus Cyp-D WT 35.4±4.3 (n=9). Statistical significance assessed by unpaired t-test, $^{NS}P>0.05$.

ii Effect size of Cyp-D global genetic ablation

To assess the effect size of cardioprotection by global Cyp-D genetic ablation, Cyp-D knockout and wildtype (true littermate) mice were subjected to the standard *in vivo* ischaemia-reperfusion protocol (30 minutes ischaemia and 72 hours reperfusion). Cyp-D knockout mice exhibited significantly smaller infarct sizes as compared to Cyp-D wildtype true littermate controls (Figure 5.5: IS/AAR% Cyp-D WT 35.4±4.3 versus Cyp-D KO 22.6±2.4; n=9/group, *P<0.05). This corresponds to a relative reduction in infarct size of approximately 36.2% (IS/AAR) and an absolute effect size of 12.8% (IS/AAR).

There was no significant difference in AAR between these groups (AAR/LV% Cyp-D WT 55.6±2.8 versus Cyp-D KO 62.2±3.0; n=9/group, $^{NS}P>0.05$), although the mean AAR was slightly larger in the Cyp-D KO group, this small difference is unlikely to affect the result especially since the infarct sizes presented here are controlled to AAR. This is discussed further below in relation to the need to measure AAR (see section iii).

There was no statistically significant difference in survival between Cyp-D knockout and wildtype littermate control mice subjected to this protocol (Figure 5.6: % survival to 72 hours reperfusion: Cyp-D WT 90.0%, n=10 versus Cyp-D KO 90.0%, n=10).

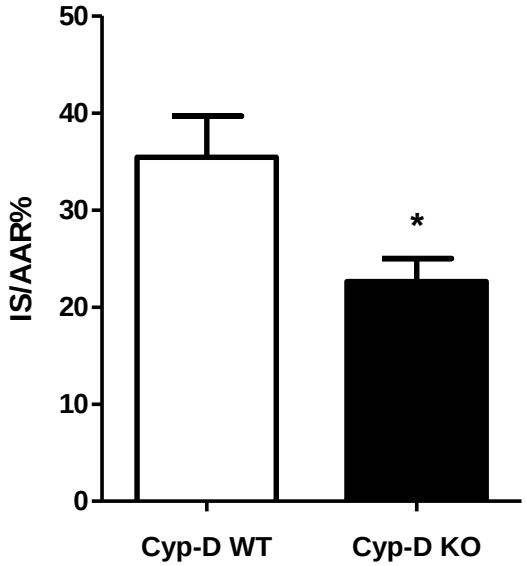

Figure 5.5: Infarct size in Cyp-D knockout mice following ischaemia-reperfusion
Infarct size following 30 minutes ischaemia and 72 hours reperfusion in Cyp-D KO and Cyp-D WT true littermate control animals. Cyp-D KO mice demonstrated significantly smaller infarct sizes compared to Cyp-D WT controls: IS/AAR% Cyp-D WT 35.4±4.3 (n=9) versus Cyp-D KO 22.6±2.4 (n=9). Statistical significance assessed by unpaired t-test, *P<0.05.

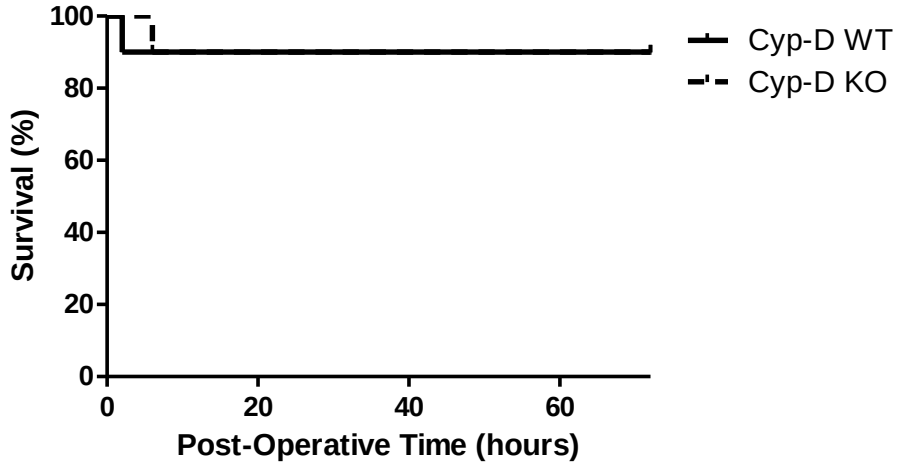

Figure 5.6: Survival of Cyp-D global knockout mice subjected to ischaemia-reperfusion
Survival of Cyp-D KO and WT littermates subjected to *in vivo* recovery ischaemia-reperfusion. There was no significant difference in survival to 72 hours between Cyp-D KO and WT control mice: survival to 72 hours was 90% for Cyp-D WT (n=10) and KO mice (n=10). No deaths were observed 6-72 hours post-surgery. Statistical significance assessed by log-rank test, ^{NS}P<0.05.

The high survival of animals subjected to this protocol reflects the low incidence of cardiac failure due to the short ischaemic duration examined in this model. This is important in order to evaluate the number of animals required to be operated on in subsequent studies of long-term cardioprotective efficacy in this thesis.

iii Long-term cardioprotective efficacy of global Cyp-D ablation

The overall objective of this chapter was to investigate the long-term cardioprotective efficacy of Cyp-D global genetic ablation in mice subjected to myocardial ischaemia-reperfusion. Since established cardiac MRI protocols to investigate long-term changes in infarct size have been validated to quantify infarct size only and not AAR (as described in chapter 1; see 1.5.2), it was important to evaluate whether the effect size of Cyp-D global genetic ablation on absolute infarct size observed in this study would allow detection of a statistically significant difference between these groups.

The data obtained in the previous study (presented in Figure 5.5) was re-expressed as absolute infarct size: infarct size as a percentage of total left ventricle area (IS/LV%). Comparison of IS/LV% was not sufficiently sensitive to detect a statistically significant difference between Cyp-D knockout and wildtype animals using this sample size (Figure 5.7: IS/LV% Cyp-D WT 19.3±2.0 versus Cyp-D KO 14.5±2.0; n=9/group, $^{NS}P>0.05$).

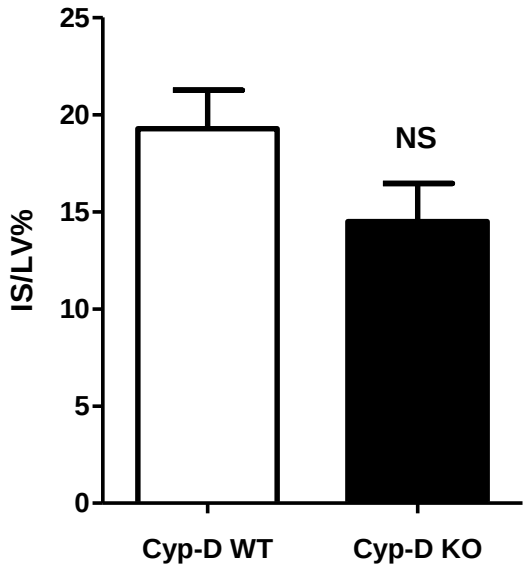

Figure 5.7: Absolute infarct size in Cyp-D global knockout mice
Evaluation of effect size of Cyp-D global genetic ablation by comparison of absolute infarct size (IS/LV%). The significant difference between Cyp-D WT and KO animals could no longer be seen when this data was not controlled to myocardial AAR: IS/LV% Cyp-D WT 19.3±2.0 (n=9) versus Cyp-D KO 14.5±2.0 (n=9). Statistical significance assessed by unpaired t-test, $^{NS}P>0.05$.

Given the smaller effect size of absolute infarct size (IS/LV%) reduction, it is expected that substantially larger sample sizes would be required to reach appropriate statistical power (80%). Indeed, evaluating the approximate standard deviation ($\sigma\approx5.9$; based on Cyp-D WT $\sigma=5.94$ and Cyp-D KO $\sigma=5.89$) and the expected effect size (≈4.78 IS/LV%) from this study, a prospective statistical power calculation shows that sample sizes of approximately 25 animals per group would be required to reach 80% statistical power.

Given the substantial samples sizes required for a study of absolute infarct size reduction in these animals, it was not feasible to subject these mice to long-term investigation of infarct size using cardiac MRI to assess infarct size alone. It is therefore not possible to evaluate the long-term cardioprotective efficacy of Cyp-D global genetic ablation. Further development of cardiac MRI for this purpose is addressed in chapter 8.

It is important to note that the low statistical power of examining absolute infarct size in this study could potentially be partially overcome by reducing variation in myocardial AAR between groups. Comparison of absolute infarct size (IS/LV%) is particularly susceptible to variations in AAR, since AAR is an important determinant of infarct size. This can be demonstrated by regression analysis of infarct size and AAR where increased AAR (AAR/LV%) is positively correlated with increased infarct size (IS/LV%) (Figure 5.8: Cyp-D WT r^2=0.75 and Cyp-D KO r^2=0.71). This analysis illustrates the importance of normalising absolute infarct size (IS/LV%) to AAR (AAR/LV%) to increase the sensitivity of the comparison of infarction and thus cardioprotective efficacy.

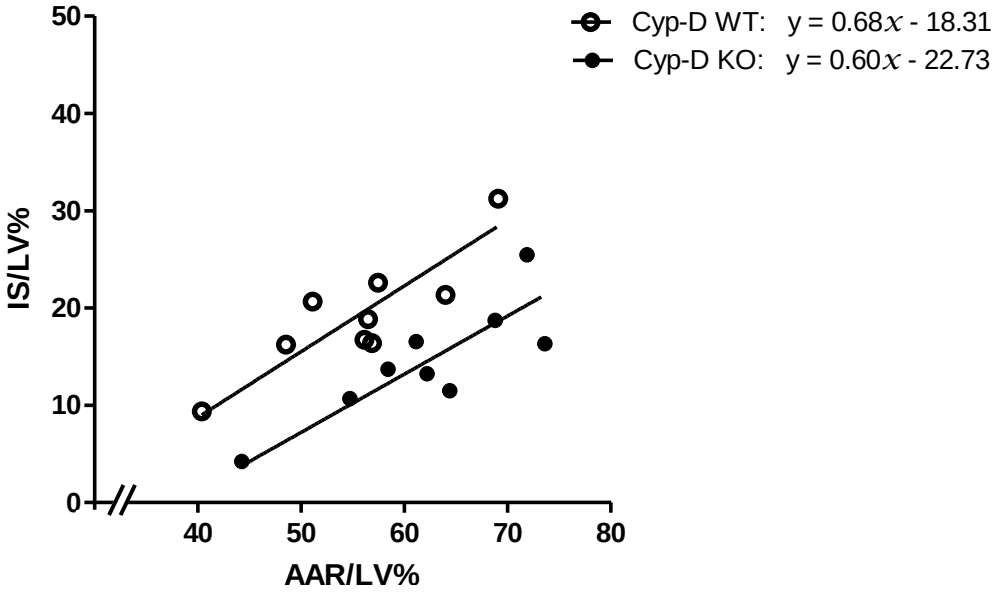

Figure 5.8: Regression analysis of infarct size and AAR in Cyp-D mice
Regression analysis of myocardial infarct size (Y) and AAR (X) in Cyp-D WT and KO mice. There was no significant difference in the slopes of these relationships: Cyp-D WT slope 0.68±0.1 versus Cyp-D KO slope 0.60±0.1; ^{NS}P>0.05. The elevations (intercepts) of these two relationships were significantly different: Cyp-D WT intercept -18.3 versus Cyp-D KO -22.7; ***P<0.001. Regression analysis and statistical significance assessed by Deming regression.

It is also interesting to note that regression analysis of infarct size and AAR of this dataset showed that there was no significant difference in the slope (indicative of the relationship between infarct size and AAR) between these groups, although the elevations (determined by the intercepts) were significantly different, which reflects the trend of difference in susceptibility to infarction expected in Cyp-D knockouts.

5.4. Aim 2: Further investigate the roles of Cyp-D in the heart

5.4.1. Background

The role of Cyp-D in regulating mPTP opening following myocardial ischaemia-reperfusion injury is widely accepted, as discussed above (see section 5.1). Published *in vivo* studies investigating the role of Cyp-D in cardioprotection against myocardial infarction have examined the whole-heart effects of Cyp-D genetic ablation or pharmacological inhibition. Results of these studies have been used to infer the role of Cyp-D in cardiomyocytes. This conclusion has been supported by *in vitro* studies of isolated cardiomyocytes in which Cyp-D genetic ablation and pharmacological inhibition also confer significant cardioprotective effects.

This section aims to further investigate the roles of Cyp-D in the pathophysiology of myocardial ischaemia-reperfusion injury *in vivo*, with regards to two specific aims:

(1) Cardiomyocyte-specific roles of Cyp-D: Investigate the contribution of Cyp-D in the cardiomyocytes specifically and the cardioprotective efficacy of cardiomyocyte-specific Cyp-D genetic ablation.

(2) Temporal roles of Cyp-D: Investigate the time-course of efficacy of Cyp-D genetic ablation in conferring cardioprotection against myocardial infarction; specifically, investigate the potential for a late-window of cardioprotection by Cyp-D genetic ablation following differing durations of reperfusion.

The development of cardiac-specific inducible transgenic systems provides an interesting potential opportunity to investigate these two important aims. Cardiac-specific and inducible genetic ablation of Cyp-D in a mouse model may permit investigation of these aims *in vivo* without the non-selective effects of pharmacological Cyp-D inhibitors.

The second part of this chapter investigates the potential application of an inducible cardiomyocyte–specific transgenic model of Cyp-D genetic ablation and its suitability for investigating the wider research aims outlined above.

Aim 2: The initial aim of this section was to establish and characterise an *in vivo* transgenic model of inducible cardiac-specific Cyp-D genetic ablation. The central hypothesis in relation to this research objective was:

(1) Generation of an α-MHC-MerCreMer – Cyp-D floxed transgenic mouse would allow cardiomyocyte-specific genetic ablation of Cyp-D upon treatment with tamoxifen.

5.4.2. Detailed methods

i Cyp-D cardiac-specific genetic ablation model

The first stage of this study was to establish a transgenic mouse colony of floxed Cyp-D and α-MHC-MerCreMer. The rationale of this inducible cardiac-specific system is described in detail in chapter 3 (see 3.1.2 ii). The Cyp-D gene is flanked by *loxP* sites (termed floxed Cyp-D) in all tissues and thus upon activation of MerCreMer activity in the cardiomyocytes, Cre-recombination of *loxP* sites excises the Cyp-D gene. Upon degradation of the existing Cyp-D protein, the cardiomyocytes of these animals theoretically become Cyp-D null; this genetic system is summarised in Figure 5.9.

The individual transgenic strains required for this model were imported into our laboratory and an extensive breeding schedule undertaken to obtain Cyp-D floxed – α-MHC MerCreMer mice; this breeding protocol is summarised in Figure 5.10.

Cyp-D floxed: The Cyp-D floxed mouse was originally created by Schinzel et al. (2005) by insertion of *loxP* sites using standard transgenic methods (see section 3.1.2 ii). A targeting vector containing *loxP* sites and the neomycin-resistance gene (*neo*) was inserted into 129/SvJ RW4 derived embryonic stem cells and transgenic stem cells used to create Cyp-D floxed mice (Cyp-D^{flox}) in a C57BL/6 strain. The *loxP* sites were placed to surround exons 3, 4 and 5 of the *Ppif* gene to allow excision of these exons upon Cre-driven recombination (Schinzel et al., 2005). These transgenic mice were then bred with C57BL/6 mice for two generations to give an approximate genetic background of 87.5% C57BL/6 and 12.5% 129/SvJ. The Cyp-D floxed mice were obtained from Jackson Laboratories, USA (strain *Ppif^{tm1Mmos}/J*; stock 005737) and imported into our facility.

The breeding schedule used to create the colony is summarised in Figure 5.10 A. Standard terminology is used for floxed genotypes throughout this thesis: wildtype (WT/WT), heterozygote floxed (WT/FL) and homozygous floxed (FL/FL) (Figure 5.10 A).

α-MHC-MerCreMer: The cardiac-specific MerCreMer (α-MHC-MerCreMer) transgenic construct used here was exactly as described previously (see 3.1.2 ii). The α-MHC-MerCreMer transgene was expressed in FVB/N embryos using standard methods. The resulting transgenic animals were bred with C57BL/6 mice for a total of 15 generations to a genetic background of B6/SV129 and subsequently onto a C57BL/6 genetic background. The α-MHC-MerCreMer transgenic mice used in this study are considered to be fully backcrossed on to a C57BL/6 genetic background. This cardiac-specific MerCreMer transgenic strain was provided as a kind gift from a collaborator (Dr R. Breckenridge, University College London, UK) which was originally from Jackson Laboratories, USA (strain B6.FVB[129]-Tg[Myh6-cre/Esr1*]1Jmk/J; stock 005657).

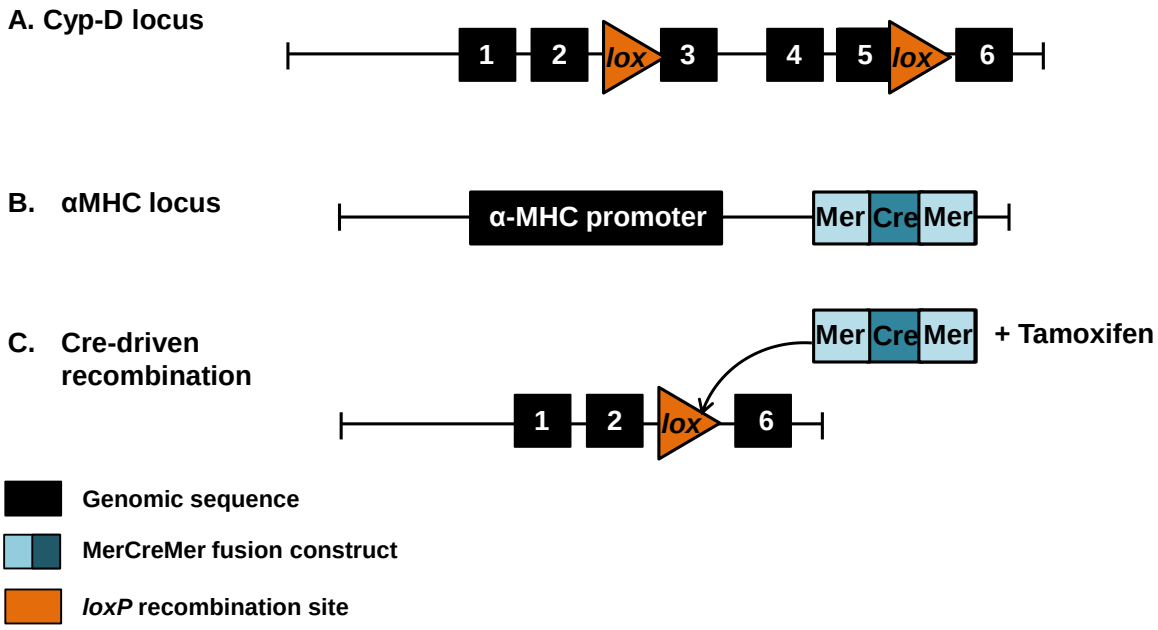

Figure 5.9: Generation of inducible cardiac-specific Cyp-D genetic ablation
Cardiac-specific genetic ablation of Cyp-D was achieved using a *loxP* and Cre-recombinase system. A) Cyp-D was flanked by *loxP* sites surrounding exons 3-5. B) MerCreMer double fusion construct was inserted under regulation of the α-MHC cardiac-specific promoter. C) Genetic recombination occurs upon activation of MerCreMer by tamoxifen to delete *Ppif* exons 3-5.

Standard terminology is used for genotypes of α-MHC-MerCreMer transgenic animals: wildtype (WT/WT) and MerCreMer heterozygote (WT/Cre). The established genotyping protocol for these animals did not permit the distinction between the heterozygous and homozygous introduction of MerCreMer and so the breeding schedule was designed to ensure that animals were either wildtype (WT/WT) or heterozygous (WT/Cre) (see Figure 5.10); this is described further below.

Colony maintenance: An intermediate cross between the Cyp-D FL/FL and MerCreMer heterozygous mice (MCM +/-) was undertaken to obtain animals transgenic for both Cyp-D floxing and MerCreMer (Figure 5.10 B). This breeding strategy was designed such that it never produced MerCreMer homozygous animals (Cre/Cre) given the difficulties associated with distinguishing between single or double insertion of the MerCreMer gene (i.e. WT/Cre and Cre/Cre) (as discussed by Davis et al., 2012). The final Cyp-D floxed – MerCreMer colony was maintained by crossing Cyp-D WT/FL mice with MerCreMer wildtype and heterozygous animals (Figure 5.10 C).

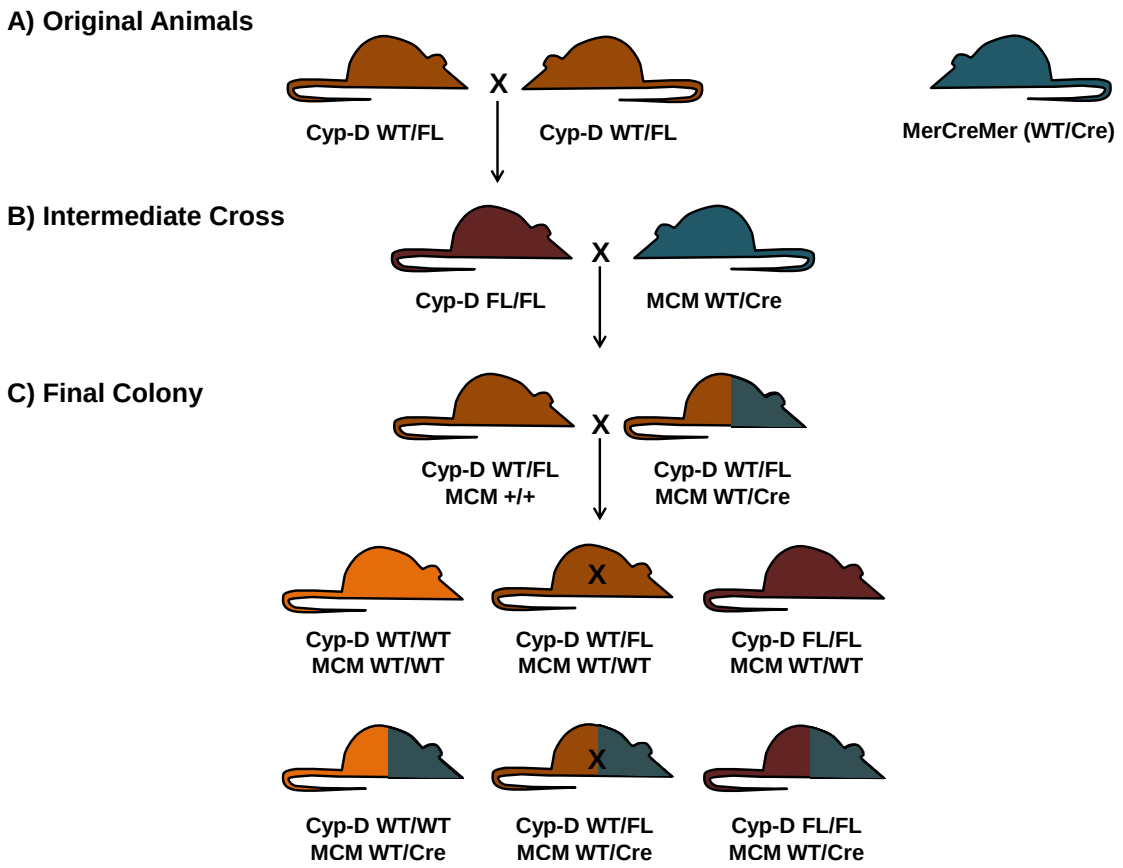

Figure 5.10: Cyp-D flox – α-MHC-MerCreMer transgenic colony and maintenance
A) Original colony: Cyp-D heterozygous floxed (WT/FL) and MerCreMer mice. Cyp-D heterozygous floxed mice were bred to produce Cyp-D FL/FL mice. B) Intermediate cross: Cyp-D FL/FL mice and MerCreMer heterozygous mice were bred to produce progeny containing the Cyp-D floxed gene and MerCreMer. C) Final colony: maintained as Cyp-D WT/FL Cre WT/WT with Cyp-D WT/FL Cre WT/CRE to produce the required transgenic animals.

ii Genotyping for floxed Cyp-D

All animals from this transgenic colony were genotyped for the presence of floxed Cyp-D using a standard PCR method based on that described earlier (see 3.1.2 iii). DNA samples were prepared from ear biopsies exactly as described previously and processed within a maximum of 7 days but ideally within 6 hours. The PCR reaction for floxed Cyp-D was based on the standard protocol optimised in this thesis. The PCR primers and cycling parameters used here were informed by the protocol provided by Jackson Laboratories, USA, who originally supplied these animals (Table 5.2). These PCR primers were designed to bind either side of the *loxP* insertion sites meaning that presence of *loxP* sites produces a larger PCR product (400 bp) compared to the wildtype (250 bp). The genotype of each animal was decoded based on these DNA bands: WT 250 bp only, homozygous (FL/FL) 400 bp only and heterozygous floxed (WT/FL) 400 and 250 bp bands (Figure 5.11). This protocol was robust and reliable.

A) Cyp-D floxed PCR primer sequences

PRIMER	SEQUENCE	PROPERTIES	
		Length	Tm (ºC)
Primer 1 / Cyp-D reverse	5'-TCTCACCAGTGCATAGGGCTCTG-3'	23	64.2
Primer 2 / Cyp-D forward	5'-GCTTTGTTATCCCAGCTGGCGC-3'	22	64.0

B) Cyp-D floxed PCR reaction mix

REAGENT	VOLUME/SAMPLE (µl)	FINAL CONCENTRATION
Qiagen 10X PCR Buffer	2.0	1X
10 mM dNTPs	0.4	200 µM
Primer 1 100 µM	0.2	1 µM
Primer 2 100 µM	0.2	1 µM
Taq polymerase	0.2	-
Autoclaved distilled water	16.0	-
Crude DNA lysate †	1.0	-
TOTAL VOLUME/SAMPLE (µl)	**20.0**	

C) Cyp-D floxed PCR thermocycling parameters

PCR STAGE	TEMPERATURE AND DURATION	PCR DESCRIPTION
1	94 ºC for 3 minutes	Hot start
2	94 ºC for 30 seconds	DNA separation
3	62 ºC for 30 seconds	Primer annealing
4	72 ºC for 1 minute	DNA synthesis
5	Go to step 2 for 35 cycles	DNA synthesis
6	72 ºC for 10 minutes	Final extension
7	4 ºC for ever	Intermediate storage

Table 5.2: Cyp-D floxed genotyping protocol
A) Cyp-D floxed primer sequences and properties. B) A single master mix was made based on Qiagen *Taq* kit (Qiagen, UK) and aliquots taken for each reaction. † 1 µl crude DNA lysate was added to each reaction. C) PCR was undertaken by a thermal cycler (MJ Research, Canada).

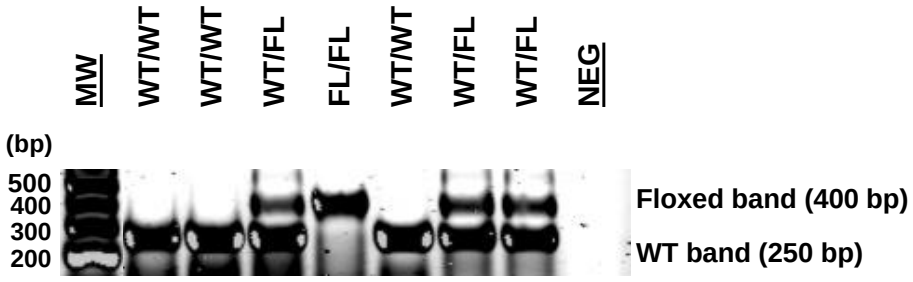

Figure 5.11: Cyp-D floxed representative genotyping result
The genotype of each animal was determined by the presence or absence of the expected PCR products: 250 bp wildtype band and 400 bp mutant band. Genotypes were determined by the presence or absence of these bands: WT 250 bp, homozygous floxed 400 bp and heterozygous floxed both bands. A negative control (NEG) was run to ensure there was no DNA contamination.

iii Genotyping for α-MHC-MerCreMer

These animals were also genotyped for the α-MHC-MerCreMer construct. The genotyping protocol was based on the standard protocol described in chapter 3 (see 3.1.2 iii). As detailed above, lysis of DNA samples for this PCR reaction was ideally undertaken within 6 hours of the biopsies being taken. Delayed sample lysis resulted in poor definition of the PCR DNA bands (particularly the internal control DNA band), which in some cases required re-sampling of ear biopsies. The PCR reaction for MerCreMer was based on the standard reaction optimised in this thesis and is detailed in Table 5.3. This PCR protocol yielded DNA products of 440 and 324 bp corresponding to the mutant (MerCreMer) and wildtype DNA products respectively. The internal control band was expected to be present in every reaction and the transgenic band only in samples heterozygous for Cre. The genotype of each animal was decoded based on the presence of the transgenic DNA band: WT 324 bp control band only and heterozygous MerCreMer (WT/Cre) both 324 bp control and 440 bp transgenic bands (Figure 5.12).

This PCR was generally robust, however, on some occasions the internal control bands were difficult to obtain and additional PCR attempts were required. The success of this PCR was improved by increasing the DNA concentration (final reaction detailed in Table 5.3) and ensuring that samples were lysed immediately upon biopsy (maximum 6 hour delay). For samples where the internal control product was not present, repeat reactions were run and fresh ear biopsies taken where clear PCR products could not be obtained.

A) MerCreMer PCR primer sequences

PRIMER	SEQUENCE	PROPERTIES	
		Length	Tm (ºC)
Primer 1 / Control forward	5'-CTAGGCCACAGAATTGAAAGATCT-3'	24	59.3
Primer 2 / Control reverse	5'-GTAGGTGGAAATTCTAGCATCATCC-3'	25	61.3
Primer 4 / TC forward	5'-ATACCGGAGATCATGCAAGC-3'	20	57.3
Primer 3 / TG reverse	5'-AGGTGGACCTGATCATGGAG-3'	20	59.4

B) MerCreMer PCR reaction mix

REAGENT	VOLUME/SAMPLE (µl)	FINAL CONCENTRATION
Qiagen 10X PCR Buffer	2.0	1X
$MgCl_2$ 25 mM	0.8	2.5 mM ‡
10 mM dNTPs	0.4	20 µM
Primer 1 100 µM	0.1	0.5 µM
Primer 2 100 µM	0.1	0.5 µM
Primer 3 100 µM	0.2	1 µM
Primer 4 100 µM	0.2	1 µM
Taq polymerase	0.12	-
Autoclaved distilled water	12.78	-
Crude DNA lysate †	3.3	-
TOTAL VOLUME/SAMPLE (µl)	**20.0**	

C) MerCreMer PCR thermocycling parameters

PCR STAGE	TEMPERATURE AND DURATION	PCR DESCRIPTION
1	94 ºC for 3 minutes	Hot start
2	94 ºC for 30 seconds	DNA separation
3	70 ºC for 45 seconds	Primer annealing
4	72 ºC for 45 seconds	DNA synthesis
5	Go to step 2 for 35 cycles	DNA synthesis
6	72 ºC for 2 minutes	Final extension
7	4 ºC for ever	Intermediate storage

Table 5.3: α-MHC MerCreMer genotyping protocol
A) MerCreMer genotyping primer sequences and properties. B) A single master mix was made (Qiagen, UK). † 3.3 µl crude DNA lysate was added to each master mix aliquot; ‡ $MgCl_2$ concentration was based on addition of $MgCl_2$ and existing $MgCl_2$ in standard Qiagen 10X buffer solution (15 mM $MgCl_2$). C) PCR was performed by a thermal cycler (MJ Research, Canada).

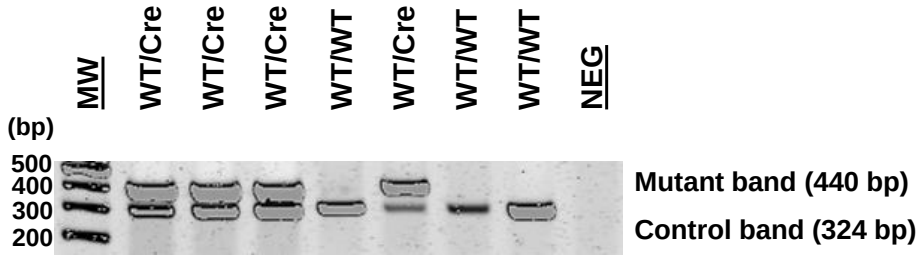

Figure 5.12: α-MHC-MerCreMer representative genotyping result
Two PCR bands were expected: 440 bp transgenic band and 324 bp internal control band. Genotypes of animals were determined by the presence or absence of the transgenic band: WT 324 internal control band only and heterozygous MerCreMer 440 and 324 bp.

iv Tamoxifen treatment of Cyp-D cardiac-specific mice

To achieve genetic ablation of Cyp-D in cardiomyocytes it was necessary to treat these animals with tamoxifen to allow entry of the MerCreMer protein into the nucleus where its Cre-recombinase activity drives homologous genetic recombination of the *loxP* sites flanking Cyp-D. An overview of the refinement of the tamoxifen dosing protocol is provided below and the final dosing regime is detailed subsequently.

Refinement of tamoxifen dosing regime: *Refinement of the tamoxifen protocol was undertaken in collaboration with Dr A. Hall within our laboratory, as detailed below.*

In accordance with a previous tamoxifen dosing regime used within our laboratory, tamoxifen (Sigma-Aldrich, UK) was dissolved in vehicle comprising ethanol-100% and corn oil (1 part ethanol to 9 parts corn oil) to give a final dosing concentration of 20 mg/kg (administration of 100 µl of 5 mg/ml tamoxifen per 25 g mouse). However, tamoxifen has a very low solubility even in this vehicle and so required sonication or agitation at 37ºC to achieve complete tamoxifen dissolution. The previous method within our laboratory had used sonication to achieve rapid and total tamoxifen dissolution. However, initial trials of this regime showed no significant difference in Cyp-D protein levels following 5 days tamoxifen treatment or 5 days treatment with 7 days washout.

Investigation of tamoxifen dosing protocol by Dr A. Hall: This dosing regime was concurrently applied to a different tamoxifen-inducible α-MHC-MerCreMer cardiac genetic ablation model within our laboratory and showed a very large degree of variation in final protein levels between experiments. This suggested that there may be a problem with the method used to prepare the tamoxifen solutions. It was observed that the sonication durations used in these studies may have varied between preparations and that sonication resulted in significant heating of the solution dependent upon the duration of sonication. This was investigated in this separate tamoxifen-inducible genetic model due to the low number of Cyp-D floxed – MerCreMer animals available.

Subsequent investigations used gentle agitation of the tamoxifen-vehicle mix at 37ºC for 4 hours to dissolve the tamoxifen. Administration of this tamoxifen solution (20 mg/kg) resulted in death of a number of animals following 3-5 days tamoxifen. This suggested that the method of preparing the tamoxifen solution here did not significantly affect the activity of tamoxifen, hence its increased toxicity. The tamoxifen dose was reduced to 18 mg/kg and showed improved survival of treated animals. Application of the refined tamoxifen protocol (18 mg/kg tamoxifen, solution prepared by warmed agitation) showed significant and consistent target gene ablation (reported by Dr A. Hall).

These preliminary studies demonstrated that the refined tamoxifen dosing protocol was effective at inducing MerCreMer recombination of *loxP* sites and this was employed in all subsequent experiments of the inducible genetic ablation system presented here.

Final tamoxifen dosing regime: The final tamoxifen dosing protocol used in this thesis was 18 mg/kg tamoxifen administered daily as an intraperitoneal bolus for 5 days. All mice used in this study weighed approximately 25 g and animals were administered approximately 100 µl of this 4.5 mg/ml tamoxifen solution, where the exact volume was calculated for each animal based on its weight to give a final dose of 18 mg/kg. The tamoxifen dosing solution was prepared to a concentration of 4.5 mg/ml by dissolution in ethanol-100% and corn oil vehicle (1 part ethanol to 9 parts corn oil) incubated at 37ºC with gentle agitation for 4 hours until total dissolution of tamoxifen. Tamoxifen solutions were freshly prepared for each study and stored for a maximum of 6 days at 4ºC.

Animals were dosed daily between 09:00 and 10:00 and monitored closely for the duration of the dosing protocol. Consistent timing of tamoxifen dosing was observed throughout to ensure that the effects of tamoxifen were closely matched between groups. Control animals were administered matched volumes of ethanol / corn oil vehicle. Animals were dosed for 5 consecutive days and hearts extracted at baseline (prior to dosing), following 5 days treatment (on day 6), following 5 days treatment and 7 days washout and following 5 days treatment and 14 days washout; this dosing protocol is summarised in Figure 4.15. The extraction protocol is described below (see section v).

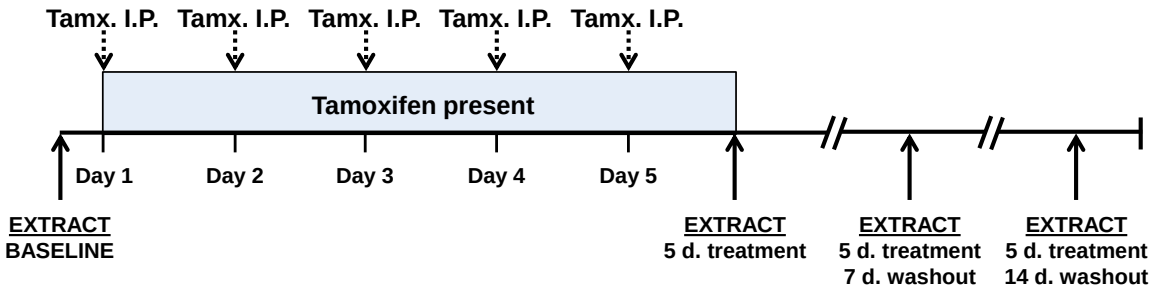

Figure 5.13: Tamoxifen dosing protocol for investigating inducible Cyp-D genetic ablation
Schematic of tamoxifen dosing protocol for investigating genetic ablation of Cyp-D in Cyp-D floxed α-MHC-MerCreMer model. Tamoxifen was administered at 18 mg/kg (100 µl of 4.5 mg/ml tamoxifen solution per 25 g mouse) as an I.P. bolus daily for 5 consecutive days (dashed arrows). Control animals were administered a matched volume of ethanol / corn oil vehicle. At the pre-defined time-point, the ventricles were removed and frozen for analysis of Cyp-D protein levels by Western blot. Mice were randomised to the 4 groups indicated (solid arrows).

v Assessment of Cyp-D protein levels by Western blot

To assess the efficacy of Cyp-D genetic ablation in the cardiomyocytes using this genetic model and tamoxifen dosing regime, a preliminary study to assess total heart levels of Cyp-D was undertaken using Western blot analysis. The Western blot protocol is described in chapter 3 (see 3.4.2) and the precise details provided below.

Preparation of heart samples: Hearts were extracted from anaesthetised mice and cannulated for manual perfusion exactly as described previously. The atria were removed and discarded and the left and right ventricular tissue immediately frozen in liquid nitrogen and stored at -80ºC until further processing. Tissues were homogenised using a glass pestle and mortar in standard homogenisation buffer (described in 3.4.1 i).

Immediately prior to use for Western blot analysis, the protein concentration of the ventricular tissue samples was assessed using a standard BCA protein assay exactly as described previously (see 3.4.1 iii). Tissue samples were diluted to a set protein concentration informed by the most dilute tissue sample by addition of homogenisation buffer detailed above. Tissue samples were stored on ice for the duration of processing (maximum 2 hours) to avoid multiple freeze-thaw cycles.

Western blotting protocol: Western blot analysis was performed by standard SDS-PAGE of protein samples performed exactly as described in chapter 3 (see 3.4.2).

Primary antibodies (detailed in Table 5.4 A) were diluted 1:1000 (final concentration of 1 µg/ml) in 5% milk / PBS + Tween solution and incubated with the membrane for 45-60 minutes at room temperature with agitation. Since the expected molecular weights of the two proteins of interest (Cyp-D and α-tubulin) are sufficiently different it was possible to probe membranes for these proteins simultaneously without the need for stripping antibodies. Following incubation of primary antibodies, excess unbound antibody was removed by washing the membrane six times for 10 minutes each in PBS + Tween.

An anti-mouse secondary antibody (detailed in Table 5.4 B) was diluted 1:2000 (final concentration of 0.5 µg/ml) in 5% milk PBS + Tween and incubated with the membrane for 1 hour at room temperature with agitation. This secondary antibody was conjugated to the HRP enzyme to allow subsequent visualisation of antibody binding using the standard chemiluminescence reaction described below. Following incubation of the secondary antibody, membranes underwent six 10 minute washes with PBS + Tween to remove unbound secondary antibody prior to chemiluminescence detection.

A) Primary antibodies:

ANTIBODY	ANTIBODY DETAILS
Cyp-D	Anti-cyclophilin-D mouse monoclonal antibody to Cyp-D (also termed Cyp-F) Purchased from Abcam Mitosciences® UK (catalogue number: ab110324) Stock 1 mg/ml; diluted 1:1000 to give working concentration 1 µg/ml Predicted molecular weight 22 kDa
α-tubulin	Anti-α-tubulin monoclonal antibody to α-tubulin Purchased from Abcam® UK (catalogue number: ab7291) Stock 1 mg/ml; diluted 1:1000 to give working concentration 1 µg/ml Predicted molecular weight 50 kDa

B) Secondary antibody:

ANTIBODY	ANTIBODY DETAILS
Anti-mouse	Horse anti-mouse IgG HRP-linked polyclonal antibody Purchased from Cell Signalling, USA (catalogue number: 7076S). Stock 1 mg/ml; diluted 1:2000 to give working concentration 0.5 µg/ml

Table 5.4: Antibodies for Western blot analysis of Cyp-D protein levels
A) Primary antibodies anti-Cyp-D and anti-α-tubulin. B) Secondary antibody was an anti-mouse IgG polyclonal antibody conjugated to HRP to allow subsequent detection by standard ECL. Antibodies were purchased from Abcam® (UK) or Cell Signalling Technology (USA) as detailed.

Protein bands were visualised using a standard HRP chemiluminescence reaction exactly as described previously (see 3.4.2 iv). Protein band intensity from these photographic films was quantified by densitometry performed using ImageJ software (version 1.45s, National Institutes of Health, USA) as described in chapter 3 (see 3.4.2 iv). Protein levels were quantified and normalised to the α-tubulin loading control for each sample and expressed in arbitrary units (A.U.). All values are presented as mean A.U. ± SEM. Data were analysed by one-way ANOVA followed by Bonferroni test using GraphPad Prism® version 5.0 (GraphPad Software, USA). Statistical significance was reported where $P<0.05$. Representative protein bands are shown alongside average densitometry quantifications presented in this chapter.

5.4.3. Results

The Cyp-D floxed – α-MHC-MerCreMer transgenic colony was established by series of genetic crosses of previously generated separate colonies. The breeding schedule undertaken to achieve this was complex and was further complicated by very poor breeding of these animals. There was no known reason for the poor pregnancy rate of these animals; however, this hindered experimental investigation of these animals.

i Investigation of tamoxifen dosing protocol

The first stage to investigate the use of this genetic ablation model for subsequent ischaemia-reperfusion experiments was to characterise an appropriate tamoxifen dosing regime and the resulting extent of reduction in Cyp-D protein levels in the heart.

Initial experiments used a tamoxifen dose of 20 mg/kg prepared by sonication; however, this showed no appreciable reduction in Cyp-D protein levels in whole heart homogenates; this data is not presented in this thesis since the dosing regime was subsequently suggested to be unreliable. Further experiments by Dr A. Hall within our laboratory using this dosing regime in a separate tamoxifen inducible α-MHC-MerCreMer genetic ablation model indicated that the sonication method for preparation of the tamoxifen solution was likely to be adversely affecting tamoxifen activity. The optimisation of a refined dosing protocol used for the experiments presented in this chapter is described above (see 5.4.2 v). Initial experiments using this potentially variable dose of tamoxifen were therefore discarded and all data presented in this thesis used the refined protocol described thereafter (18 mg/kg; prepared in 1 part ethanol-100% and 9 parts corn oil by agitation at 37ºC).

ii Investigation of Cyp-D genetic ablation – Cyp-D protein levels

Analysis of Cyp-D protein levels at baseline in Cyp-D floxed (FL/FL) – MerCreMer (WT/Cre) and Cyp-D (WT/WT) – MerCreMer (WT/Cre) showed a significance difference in Cyp-D protein levels between these genotypes (Figure 5.14). Although it should be noted that this analysis was based on a relatively small number of animals (n=2/group) and should be repeated for further investigation of this genetic ablation model.

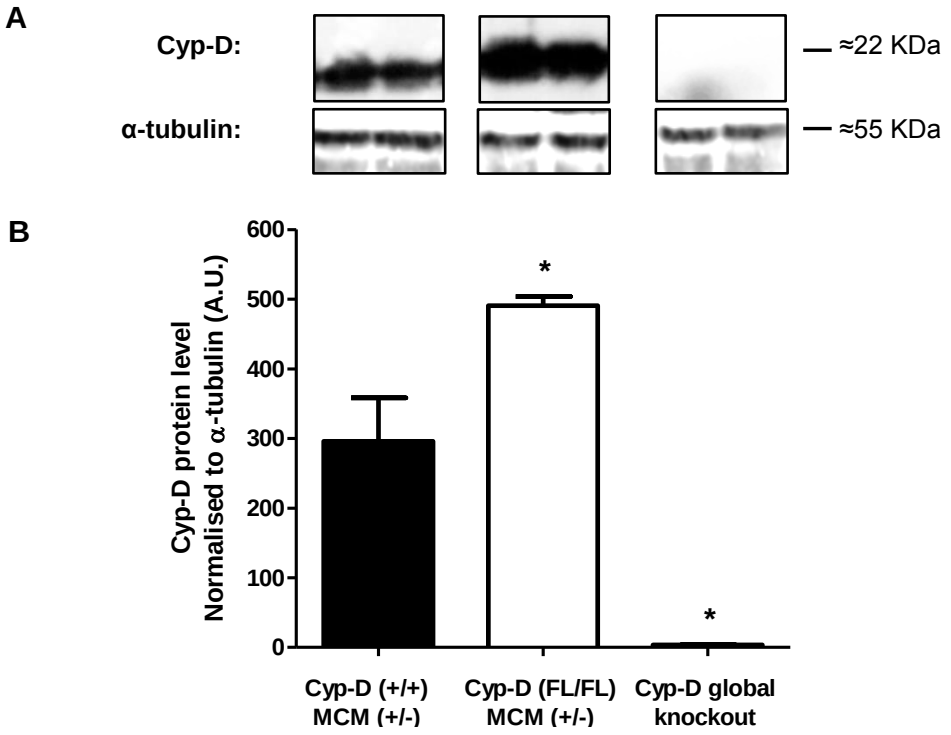

Figure 5.14: Cyp-D levels at baseline in wildtype and floxed animals
Western blot analysis to quantify Cyp-D protein levels in ventricular tissue at baseline. A) Representative protein bands from Western blot. B) Densitometry of Western blot to calculate Cyp-D protein levels normalised to α-tubulin protein levels. Statistical significance was assessed by one-way ANOVA comparing to Cyp-D (+/+) MerCreMer (+/-); Cyp-D levels were significantly increased in Cyp-D floxed mice compared to WT littermates (*P<0.05). Ventricular tissue samples from Cyp-D global KO mice were included as a negative control for Cyp-D protein levels. (n=2/group).

This suggests that insertion of the *loxP* sites flanking Cyp-D has affected Cyp-D protein expression. This presents an important consideration for future investigation of these animals since Cyp-D (+/+) MerCreMer treated animals would ordinarily be used as a tamoxifen treated control group to evaluate any effects of Cre-toxicity. However, given that Cyp-D baseline expression differed between these genotypes, this may affect susceptibility to myocardial infarction. This did not affect the interpretation of the data presented below in Figure 5.15 since all animals in this experiment were Cyp-D FL/FL.

Cyp-D protein levels were examined in Cyp-D floxed (FL/FL) – MerCreMer (WT/Cre) mice before tamoxifen treatment and at various time-points following 5 days tamoxifen treatment (see Figure 5.13 for protocol timings). There was no statistically significant difference in Cyp-D protein levels in ventricular tissue extracted from these animals (Figure 5.15; comparing white and blue bars, P>0.05, n=3/group), although there appeared to be a trend towards decreased Cyp-D protein levels following 7 and 14 days washout of tamoxifen treatment. This should now be investigated further.

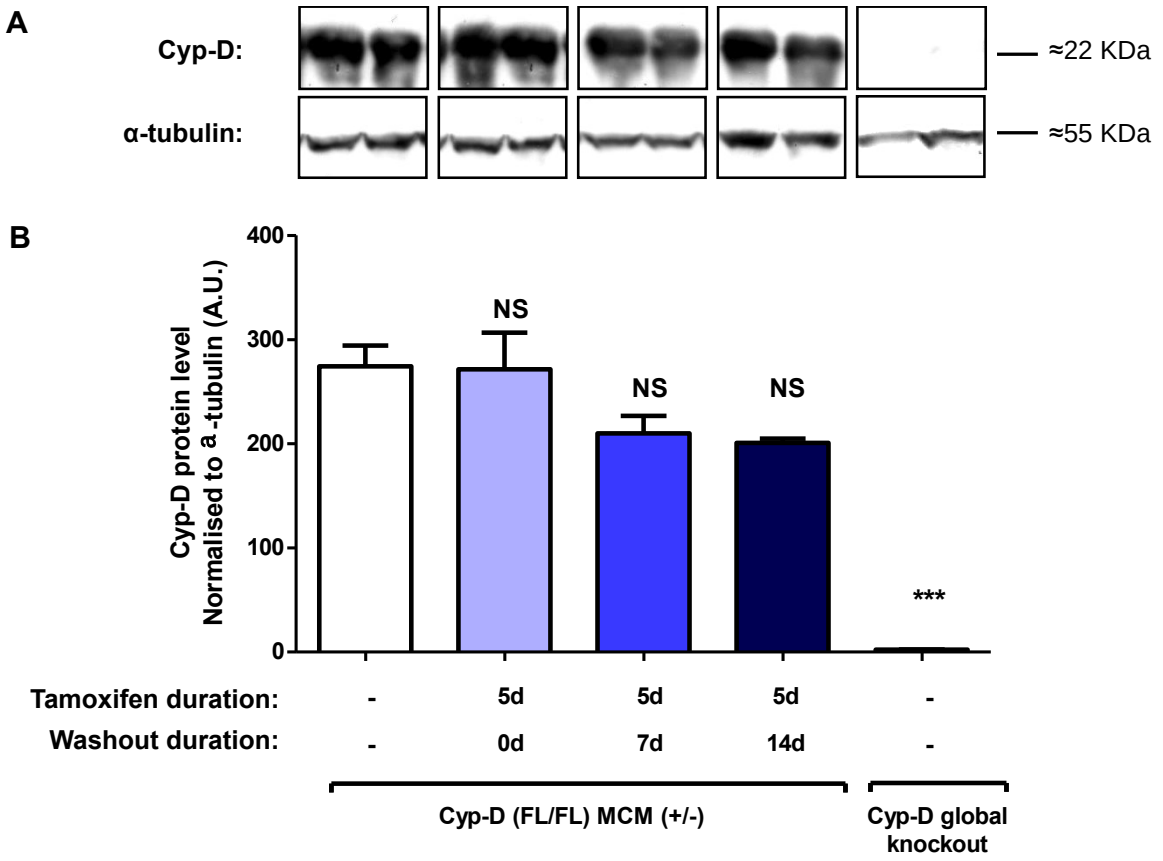

Figure 5.15: Cyp-D levels in tamoxifen treated animals
Western blot analysis of Cyp-D protein levels in ventricular tissue of Cyp-D floxed (FL/FL) MerCreMer (WT/Cre) animals at baseline and following 5 days tamoxifen treatment with varied washout periods. A) Representative protein bands from Western blot. B) Densitometry to calculate Cyp-D protein levels normalised to α-tubulin. Statistical significance assessed by one-way ANOVA comparing treated animals (blue bars; n=3/group) with baseline (white bar; n=3); no significant difference in Cyp-D protein levels ($P>0.05$). Ventricular tissue samples from Cyp-D KO mice were included as a negative control for Cyp-D protein (significantly different compared to other groups; ***$P<0.001$, n=2).

5.5. Discussion

The overall research objective of this chapter was to investigate the long-term efficacy of Cyp-D genetic ablation in protecting against myocardial ischaemia-reperfusion. The initial stage of this was to investigate the effect of global and cardiac-specific genetic ablation of Cyp-D on the susceptibility to myocardial infarction in the *in vivo* recovery model of ischaemia-reperfusion injury developed here. This chapter describes the experiments undertaken towards this aim and the obstacles to further investigation.

5.5.1. Aim 1: Investigate long-term cardioprotection by Cyp-D ablation

This first section of this chapter aimed to investigate the use of the well-established Cyp-D global genetic knockout model to examine the long-term efficacy of Cyp-D inhibition in the setting of myocardial ischaemia-reperfusion injury. This is an important outstanding research question since although several studies have shown that genetic ablation of Cyp-D reduces myocardial infarct size following ischaemia-reperfusion when assessed following short reperfusion durations (Baines et al., 2005; Nakagawa et al., 2005; Lim et al., 2007), it is not known whether this would confer long-term cardioprotective effects.

Given recent reports that Cyp-D knockout mice are more susceptible to cardiac failure upon physiological stress (Elrod et al., 2010), it is ever more pertinent to determine whether Cyp-D knockout mice remain cardioprotected at extended periods of myocardial reperfusion. This has been suggested by Gomez et al. (2007) who reported that administration of the Cyp-D inhibitor, Debio-025, improved cardiac function and survival 30 days following ischaemia-reperfusion (Gomez et al., 2007). However, this study did not examine infarct size at this extended time-point and furthermore cannot exclude the influence of non-selective effects of Debio-025 on the other cyclophilin proteins.

Although pharmacological inhibition of Cyp-D would be more clinically relevant, selective inhibitors of Cyp-D are not yet available (as reviewed in chapter 1; see 1.4.1) and therefore models of Cyp-D genetic ablation provide a more selective and elegant system in which to investigate the roles of Cyp-D. The Cyp-D global genetic knockout mouse colony is an important model for the proof-of-concept study proposed here.

Before embarking on this large-scale and costly long-term study of the cardioprotective efficacy of Cyp-D genetic ablation, a pilot study was undertaken to assess the expected effect size and variability of myocardial infarct size reduction in these animals.

Effect of using true littermate control animals: This study first sought to improve the breeding strategy of the existing Cyp-D global genetic knockout mouse colony within our laboratory to allow investigation of true littermate control mice. Myocardial infarct size in

commercially available B6/SV129 and Cyp-D wildtype mice was assessed to evaluate whether this subtle difference in genetic background influenced myocardial infarct size. This was important to allow interpretation of future experimental results obtained using this backcrossed colony in the context of previous studies of non-backcrossed animals.

It is important to note that infarct sizes resulting from this model are subject to inherent variation due to the *in vivo* nature of this myocardial insult and the relatively basic quantification method. This model is therefore not sufficiently sensitive to detect very small differences in infarct size, whereby very large and unfeasible sample sizes would be required to reach the required level of statistical power. As such, this study was not expected to discern a statistically significant difference between these groups but was instead intended to permit a qualitative comparison of the potential influence of subtle strain differences in the susceptibility to myocardial infarction. There was a slight but non-significant trend to increased infarct size in Cyp-D wildtype mice (98.4% C57BL/6 and 1.6% SV129 genetic background) compared to B6/SV129 mice (Figure 5.4).

Although this small difference in infarct size (approximately 5.1% IS/AAR) is unlikely to be biologically significant with regards to outcomes of myocardial ischaemia-reperfusion injury, this study highlights the importance of using appropriate littermate control animals. The small difference in infarct size between these genetic backgrounds could adversely affect the outcome of studies using inappropriate genetic controls. For example, this study suggests that comparison of infarct size between B6/SV129 and Cyp-D knockout mice would result in a smaller effect size and thus a possibly increased probability of concluding a false negative result (type II error).

Indeed, published studies have identified variations in cardiovascular traits between strains of inbred mice, including differences in LV function, heart rate and susceptibility to cardiac rupture in response to myocardial infarction (Hoit et al., 2002; Gao et al., 2005). Notably, Gorog et al. (2003) showed statistically significant differences in myocardial infarct size between sub-strains of C57BL/6 mice bred within their laboratory (Gorog et al., 2003). These studies confirm the assertion that all experiments using transgenic animals should ensure that correct true littermate control animals are investigated. All studies of transgenic mice in this thesis used true littermate controls in accordance with best practice (as evaluated and recommended by Davis et al., 2012).

Effect of global genetic ablation of Cyp-D: The effect of global knockout of Cyp-D on the susceptibility to myocardial infarct size was examined in animals subjected to the standard *in vivo* recovery model of ischaemia-reperfusion developed in this thesis. Cyp-D knockout mice exhibited significantly smaller infarct sizes compared to true wildtype littermate controls (Figure 5.5). This is in agreement with previous studies showing that

Cyp-D knockout mice are protected against ischaemia-reperfusion at shorter reperfusion durations (Nakagawa et al., 2005; Baines et al., 2005; Lim et al., 2007).

This study did not show any effect of Cyp-D genetic ablation on survival following ischaemia-reperfusion (Figure 4.). Given the profound reduction in myocardial infarct size in Cyp-D knockout mice it could perhaps be expected that this would correlate with improved survival. Indeed, a previous study by our laboratory showed that Cyp-D knockout mice exhibited improved survival following permanent coronary artery ligation (Lim et al., 2011). However, this model of cardiac failure examined a greater ischaemic insult and longer term prognosis (to 28 days) of these animals which showed a higher control mortality rate. Interestingly, Lim et al. (2011) showed that all deaths occurred 3-5 days following the onset of ischaemia. This may suggest that the ischaemia-reperfusion model here could cause increased mortality at further extended reperfusion periods; however, the pathophysiology of this model is different due to the effects of reperfusion. The ischaemia-reperfusion model presented here was not optimised to detect differences in mortality and further characterisation studies at extended reperfusion durations would be required to investigate this further.

This study provides the first demonstration, to our knowledge, that Cyp-D knockout mice remain cardioprotected in terms of reduced myocardial infarct size at an extended duration of reperfusion. This provides further support that Cyp-D inhibition is likely to confer long-term cardioprotective benefits and thus represents an important target.

It is expected that the cardioprotective effect exerted by genetic ablation of Cyp-D observed here is mediated by reduced mPTP opening. Although reduced mPTP opening in these animals has not been directly implicated here, this is strongly supported by previous studies investigating mPTP opening in these animals. Indeed, the initial generation of Cyp-D global knockout mice showed that mitochondria devoid of Cyp-D protein exhibited resistance to mPTP opening, mitochondrial swelling and loss of mitochondrial membrane potential in response to calcium and ROS triggers of mPTP opening (Nakagawa et al., 2005; Baines et al., 2005; Basso et al., 2005; Schinzel et al., 2005). Although only Baines et al. (2005) directly investigated this in cardiac mitochondria, it is widely accepted that the phenotypes observed in Cyp-D knockout mice are likely to result from reduced mPTP opening (reviewed by Bernardi, 2013; Elrod and Molkentin, 2013; Javadov and Kuznetsov, 2013).

However, Cyp-D genetic ablation may confer further biological effects due to reduced mPTP opening. The seminal study by Elrod et al. (2010) alluded to the potential physiological role of Cyp-D in calcium regulation, whereby reduced mPTP opening in mitochondria devoid of Cyp-D resulted in increased mitochondrial matrix calcium levels

and in turn altered metabolic flexibility. Specifically, increased mitochondrial calcium in these animals resulted in increased activation of mitochondrial dehydrogenase enzymes, increased glucose oxidation and decreased fatty acid metabolism (Elrod et al., 2010). This study demonstrates the wider role of Cyp-D and mPTP opening in cellular homeostasis and metabolism and is suggestive of some of the likely pathways indirectly influenced by Cyp-D. It is therefore important to consider these wider effects when interpreting the phenotypes of Cyp-D knockout mice.

In addition to the consequences of Cyp-D genetic ablation on metabolic flexibility, it is also important to consider the potential interference of these indirect effects for the interpretation of the phenotypes of Cyp-D knockout mice. Indeed, a recent study by Murphy's group (Menazza et al., 2013) showed that genetic ablation of Cyp-D caused altered expression of a number of mitochondrial proteins, including several important metabolic proteins involved in pyruvate and fatty acid oxidation (Menazza et al., 2013). This is particularly important given the essential roles of mitochondrial function and respiration in determining cell survival upon myocardial ischaemia-reperfusion (reviewed in chapter 1; see 1.2.3). However, it should be noted that this study did not detect any resulting difference in mitochondrial respiration in Cyp-D knockout hearts (Menazza et al., 2013). The importance of Cyp-D in metabolic regulation is also shown by the manifestation of adult-onset obesity in Cyp-D knockout mice (Luvisetto et al., 2008). It is therefore important to consider the effects of Cyp-D on metabolism when interpreting the susceptibility of these mice to myocardial infarction.

Further to this, a very recent study by Murphy's group (Nguyen et al., 2013) showed that the acetylation of a number of mitochondrial proteins was altered in Cyp-D knockout hearts. Although this study did not show direct regulation of acetylation and deacetylation by Cyp-D, it was proposed that increased mitochondrial calcium in the absence of transient mPTP opening in Cyp-D knockout mitochondria causes increases mitochondrial dehydrogenase enzyme activity, thereby increasing NADH / NAD^+ levels (by approximately 80%). This was predicted to reduce deacetylase enzyme activity. Interestingly, despite the previously asserted role of Sirt-3 as the major mitochondrial deacetylase protein, this study provided some evidence that the increased acetylation here was not the result of decreased Sirt-3 activity. Since this reduced deacetylase activity appeared to be linked to NADH / NAD^+ levels (Nguyen et al., 2013), this appears to implicate one or more Sirt proteins, since these are the only known KDAC proteins with NAD^+ sensitivity. This study therefore poses the intriguing possibility that the other mitochondrial Sirt proteins (Sirt-4 and -5) may be exerting modified deacetylase activity in the absence of Cyp-D, although this was not investigated by this study. However, since previous studies have suggested that Sirt-4 and -5 mediate only modest

deacetylase activity (Lombard et al., 2007), the involvement of these proteins in the altered acetylome of Cyp-D knockout mice remains speculative. It is possible that altered mitochondrial protein acetylation in Cyp-D knockout hearts may instead indicate increased activity of acetylation proteins, although this was not examined in this study. The role of acetyl-regulation of mitochondrial proteins is discussed in detail in chapter 6.

The role of Cyp-D in metabolic regulation is perhaps likely to become an increasing area of research interest given the recent implication of the ATP synthase enzyme (complex V) as the constituent protein of the mPTP (Bonora et al., 2013; Giorgio et al., 2013). The role of metabolic regulation in the pathophysiology of myocardial ischaemia-reperfusion injury is discussed in detail in relation to Sirt-3 in chapter 6.

Since the effects of Cyp-D on metabolic regulation are likely to become more profound following prolonged inhibition, temporal regulation of Cyp-D expression may provide a more elegant genetic model to investigate its role in cardioprotection and as a potential therapeutic target for long-term cardioprotection. Importantly, genetic ablation of Cyp-D following the onset of myocardial reperfusion would remove the potential confounding influences of these wider phenotypes exerted by Cyp-D knockout during ischaemia. Temporal regulation of Cyp-D genetic ablation is discussed subsequently (see 5.5.2).

Long-term cardioprotective efficacy of global Cyp-D ablation: The long-term efficacy of Cyp-D genetic ablation was not investigated here at further extended reperfusion durations due to the limitations of infarct size and AAR quantification using *ex vivo* histological endpoints; discussed in detail in chapter 4 (see 4.6.3; Reperfusion duration). Briefly, it is unclear whether histological staining provides accurate quantification of myocardial salvage at extended reperfusion durations due to the possible effects of inflammatory cell infiltration which may mask the true extent of infarction assessed by TTC staining and myocardial remodelling which may affect AAR measurement. The aim of this thesis was to investigate the long-term cardioprotective efficacy of modulating mitochondrial targets, however, this required development and validation of *in vivo* methods for quantifying infarct size and AAR *in vivo*; cardiac MRI methods for quantification of infarct size and AAR forms the focus of chapter 8.

With regards to the future investigation of the long-term cardioprotective efficacy of Cyp-D genetic ablation, the experiments presented here provide a valuable insight into the effect of Cyp-D knockout to inform the experimental design of future studies. Cyp-D knockout reduced absolute infarct size (IS/AAR%) by approximately 12.8% which corresponded to a relative reduction of approximately 36% (IS/AAR). The effect size and standard deviation of IS/AAR% and IS/LV% in this study can be used to inform the expected sample sizes required for future studies using cardiac MRI, discussed below.

To evaluate the possibility of using currently established cardiac MRI methods to assess myocardial infarct size over extended durations of reperfusion, this same dataset was re-expressed as infarct size as a percentage of left ventricle area (IS/LV%). As expected, not normalising infarct size to AAR reduced the statistical power of this comparison by increasing the relative error (standard deviation; σ) and reducing the absolute effect size. This reduction in statistical power meant that a significant difference could no longer be detected between these groups (Figure 5.7). Indeed, a prospective sample size calculation showed a predicted sample size of approximately 25 per group would be required to reach sufficient statistical power. This confirms that it would not be appropriate to investigate the long-term effect of Cyp-D genetic ablation on infarct size using current cardiac MRI protocols which have not been validated to quantify AAR.

It should however, be noted that the sensitivity of cardiac MRI quantification of infarct size using late-gadolinium enhancement imaging to detect cardioprotective efficacy has not been tested here. It is possible that this MRI method may have been sufficient to detect this cardioprotective effect given its increased sampling of the myocardium (due to it's three-dimensional nature). This was not tested in this thesis due to the practical and financial constrainsts of undertaking such a speculative study.

The long-term cardioprotective efficacy of Cyp-D genetic ablation was therefore not investigated further here. This study highlights the importance analysing myocardial AAR to assess cardioprotective efficacy and provides the impetus for investigation of cardiac MRI for determining AAR *in vivo* in the reperfused mouse heart. This is addressed in chapter 8 of this thesis.

5.5.2. Aim 2: Further investigate the roles of Cyp-D in the heart

The role of Cyp-D in regulating calcium sensitivity to mPTP opening upon myocardial reperfusion is widely accepted, however, the effect role of Cyp-D inhibition for long-term cardioprotection has not been confirmed *in vivo*, as discussed above. A further caveat to the use of the Cyp-D global genetic knockout mouse is the potential confounding effects of the timing of Cyp-D inhibition, whereby it is not possible to determine whether Cyp-D inhibition at the time of myocardial reperfusion or thereafter, as would occur in the clinical setting of acute myocardial infarction, would confer cardioprotection. Although pharmacological inhibition of Cyp-D would arguably represent the most immediately clinically translatable therapy, the lack of selective Cyp-D pharmacological inhibitors (see 1.4.1) complicates this. It is pertinent to determine whether specific inhibition of Cyp-D (i.e. by genetic ablation) at reperfusion reduces the susceptibility to infarction.

Development of inducible Cyp-D genetic ablation model: Development of inducible genetic ablation systems that allow regulation of the timing of genetic knockout of the target gene represent emerging and important models for proof-of-concept studies to dissect the role of proteins in pathophysiological processes. The second section of this chapter attempted to investigate the use of a floxed-MerCreMer system to knockout Cyp-D specifically in the cardiac muscle (i.e. only in cardiomyocytes) without the confounding non-selective effects of pharmacological Cyp-D inhibitors. The overall objective of this section was ultimately to investigate the role of Cyp-D specifically in the cardiomyocytes and importantly, investigate the time-course of Cyp-D involvement in the development of myocardial infarction; as discussed previously (see 5.4.1).

The Cyp-D floxed mouse line was developed by Schinzel et al. (2005) and crossed with the EIIa transgenic Cre mouse in which Cre-recombinase is expressed during early development (created by Lakso et al., 1996), to generate Cyp-D genetic knockout mice (Schinzel et al., 2005); described previously in chapter 1 (see 1.4.1). To examine the potential use of a Cyp-D floxed-MerCreMer cardiac-specific inducible genetic knockout model, the experiments presented in this chapter aimed to produce a more sophisticated transgenic colony to allow temporal and spatial regulation of Cyp-D genetic ablation. Intensive efforts were required to establish this final colony from the existing separate transgenic animals given the very poor breeding success encountered.

Efficacy of temporal genetic ablation of Cyp-D: Given the low number of animals produced by this Cyp-D floxed-MerCreMer colony, the tamoxifen dosing regime to drive MerCreMer-mediated recombination was optimised in a different transgenic system. Since this genetic system used the same MerCreMer strain, it was expected that the resulting Cre-recombinase activity of this tamoxifen regime would be consistent between these models. Optimisation of this tamoxifen dosing protocol considered the resulting animal mortality, off-target tamoxifen toxicity and genetic recombination efficacy

A refined tamoxifen dosing protocol was applied to Cyp-D floxed-α-MHC-MerCreMer (FL/FL; WT/Cre) mice. Investigation of ventricular Cyp-D protein levels showed no significant difference between any of the time-points tested up to 5 days tamoxifen treatment and 14 days protein washout (Figure 5.15). The greatest reduction in Cyp-D protein level compared to baseline was detected in tissues harvested 14 days following washout of tamoxifen treatment; however, this only corresponded to a 26.8% reduction in Cyp-D protein compared to baseline and was not statistically significant (Figure 5.15).

It is important to note that this experiment examined total ventricular tissue and since this model is expected to knockout the Cyp-D gene only in the cardiomyocytes, a residual level of Cyp-D protein was expected from other cell types within the heart

(namely fibroblasts). However, given that cardiomyocytes are highly mitochondria-enriched, it was expected that the majority of mitochondria (and thus Cyp-D protein) investigated by this protocol was from cardiomyocytes. It is therefore unlikely that the high level of Cyp-D protein remaining in these samples following this tamoxifen-treatment regime corresponded to non-muscle cells. This protocol was concluded to induce an unacceptably low knockout of Cyp-D protein to warrant investigation of the susceptibility to myocardial infarction in these animals. It is now important to investigate this further by examining Cyp-D protein levels in cardiomyocytes isolated from tamoxifen treated animals to confirm the level of Cyp-D protein remaining in the cardiomyocytes.

In addition, examination of Cyp-D mRNA levels in isolated cardiomyocytes would allow assessment of the efficacy of genetic ablation induced by this system. The tamoxifen dose used in this study (18 mg/kg) was slightly lower than that used in published studies (including Sohal et al., 2001 who originally published the protocol using 20 mg/kg tamoxifen) and thus may not induce sufficient activation of Cre-recombination. It may be interesting to examine the use of tamoxifen-containing chow since this has been suggested to result in increased MerCreMer activation and lower tamoxifen toxicity due to its more steady intake (Davis et al., 2012). However, since a concurrent study within our laboratory using this same MerCreMer strain and tamoxifen dosing regime provided genetic ablation of a different target gene, it is unlikely that this was a problem.

Although further investigation of Cyp-D mRNA and protein levels in cardiomyocytes is critical to evaluate the use of this genetic model for further studies, this was not undertaken here due to the poor availability of animals and low cardiomyocyte yield using the established primary isolation technique within our laboratory. This poor cardiomyocyte yield would have necessitated investigation of a large number of hearts; however, recent improvements to this protocol improve the feasibility of this study upon availability of animals. These experiments should be undertaken to continue the project.

Importantly, the time-course of the reduction in Cyp-D protein levels suggested by this study may potentially restrict the application of this model for the investigation of Cyp-D genetic ablation upon myocardial reperfusion. Since there was no appreciable reduction in Cyp-D levels following 5 days tamoxifen treatment (Figure 5.15), the effect of Cyp-D genetic ablation after myocardial ischaemia and during early reperfusion may not be possible. Future experiments should investigate a more detailed time-course of the reduction in Cyp-D levels within the first 7 days following tamoxifen treatment. Since the time-course of protein level reduction in this system depends on the time for genetic ablation and the rate of protein turnover, it would be important to examine mRNA and protein levels for further optimisation of this system. The turnover rate of Cyp-D is not

known and it may be that it is not sufficiently rapid to allow elegant knockout of Cyp-D in the early reperfusion period. Further studies should be undertaken to address this.

Limitations of Cre-loxP genetic ablation systems: It is also important to note that there was a significant difference in Cyp-D protein levels in Cyp-D floxed (FL/FL) mice compared to non-floxed wildtype controls (Figure 5.14). Although this was not investigated further in this study, this may present an important consideration for the future use of this genetic ablation system since these mice would ordinarily be used to control for any non-specific effects of tamoxifen (see 3.1.2 ii). This suggests that insertion of the *loxP* sites flanking the Cyp-D gene has changed Cyp-D gene expression, which is an unusual although important potential consequence of this system. Further examination of Cyp-D protein levels in the control mice outlined previously should be undertaken prior to use of these mice to investigate the susceptibility to infarction.

In addition to the potential effect of *loxP* site insertion, further confounding effects resulting from tamoxifen and / or Cre toxicity have been reported in previous studies utilising this method of genetic modification. These potential confounding effects have been discussed extensively in the literature (reviewed by Davis et al., 2012) and are summarised in chapter 3. These effects represent important considerations for the use of the tamoxifen-inducible genetic model presented here. Although this thesis describes only the early stages of development of this system, it is crucial to appreciate that this model will, in itself, impart some limitations and careful consideration of these limitations is required for subsequent interpretation of this model for studies of the role of Cyp-D.

The cardiac-specific inducible Cyp-D knockout model created here remains a potentially important tool for investigating the precise roles of Cyp-D in myocardial ischaemia-reperfusion injury with regards to tissue specificity and the timing of its involvement. The further experiments described above will be important for evaluating the future use of this model for dissecting the roles of Cyp-D in myocardial infarction.

5.5.3. Summary of potential limitations

The specific experimental limitations of this study have been discussed throughout this section. The main limitation with regards to the overall objective of this chapter to investigate the long-term cardioprotective efficacy of Cyp-D genetic ablation was the relatively small absolute effect size of Cyp-D global genetic ablation when assessing infarct size alone (IS/LV%), which precluded the further investigation of these mice using current MRI techniques. Given the financial costs of cardiac MRI, it was not feasible to undertake a pilot cardiac MRI study in these Cyp-D global knockout animals when this preliminary study suggests that substantial sample sizes would be required. This is

addressed in chapter 8 of this thesis which examines the importance of controlling infarct size measurements to AAR and investigates novel cardiac MRI methods to quantify AAR *in vivo* to enable this in future studies of cardioprotection.

5.5.4. Summary

The main research objective of this chapter was to investigate the long-term cardioprotective efficacy of Cyp-D genetic ablation in reducing myocardial infarct size.

(1) The Cyp-D global knockout mouse colony has been genetically backcrossed onto a C57BL/6 background to allow investigation of true littermate control animals. Although this study was not sufficiently statistically powered to detect such a small effect size, there was a slight trend towards increased myocardial infarct size in Cyp-D WT mice compared to the commercial B6/SV129 mice previously used as controls. This highlights the importance of using true littermate controls for the study of transgenic animals; this gold-standard practice was adhered to in all experiments.

(2) Global genetic ablation of Cyp-D significantly reduced myocardial infarct size in mice subjected to *in vivo* ischaemia-reperfusion injury investigated at 3 days reperfusion. Although Cyp-D genetic ablation did not affect survival of animals subjected to this model, the protocol used here did not elicit significant mortality of control (wildtype) mice and therefore was not sufficiently powered to detect differences in survival.

    This study provides the first demonstration of sustained cardioprotection in Cyp-D knockout mice following an extended reperfusion period and further supports the role of Cyp-D as a target for cardioprotection against ischaemia-reperfusion injury.

(3) To further investigate the specific role of Cyp-D in the development of myocardial infarction, a more elegant cardiac-specific transgenic model of Cyp-D genetic ablation was investigated. This thesis describes the establishment of a Cyp-D floxed – α-MHC MerCreMer colony from previous transgenic strains and the initial experiments to characterise its future use. Although the poor breeding success of this colony posed significant obstacles to this study, an initial tamoxifen dosing protocol showed only a modest and non-significant decrease in ventricular Cyp-D.

    Future experiments are required to further refine this tamoxifen inducible genetic ablation model to determine: (1) Cyp-D expression levels in isolated cardiomyocytes and (2) a more detailed time-course of the reduction in Cyp-D protein levels. These experiments were not completed here due to the restraints of poor breeding of this colony and the need to refine the cardiomyocyte isolation protocol.

CHAPTER 6: INVESTIGATION OF THE ROLE SIRTUIN-3 IN THE PATHOPHYSIOLOGY OF ISCHAEMIA-REPERFUSION

6.1. Introduction

The previous chapter of this thesis has highlighted the importance of mitochondria in the pathophysiological processes that occur upon myocardial ischaemia-reperfusion and the possibility for modulation of an important mitochondrial protein to elicit cardioprotective benefit. Sirt-3 has been identified as an important regulator of mitochondrial biology and may therefore be important in the pathophysiology of ischaemia-reperfusion injury. This chapter aimed to investigate the effects of modulating Sirt-3 activity to indirectly affect mitochondrial function and survival upon ischaemia-reperfusion. The overall objective of this chapter was to determine whether Sirt-3 is a feasible target for cardioprotection.

Sirt-3 is a key mitochondrial deacetylase protein which regulates the activity of a number of mitochondrial proteins involved in cell survival and energy production; as discussed in chapter 1 (see 1.4.2 ii). Amongst its numerous targets, Sirt-3 is known to deacetylate Cyp-D to reduce its PPIase activity, which is central to its regulation of mPTP opening. Indeed, genetic ablation of Sirt-3 results in hyper-acetylation of Cyp-D and increased PPIase activity, manifesting in increased mPTP opening in response to high calcium stresses (Hafner et al., 2010; Shulga et al., 2010). Although Sirt-3 appears to regulate the activity of a diverse array of mitochondrial proteins, its cumulative predicted actions in reducing mPTP opening, cellular acidosis and ROS levels and increasing oxidative phosphorylation, suggest that Sirt-3 activity may be beneficial for mitochondrial function and survival; as summarised in chapter 1 (see 1.4.2 iv, Figure 1.15).

Myocardial ischaemia-reperfusion is recognised to evoke substantial cellular metabolic stress and injury in which mPTP opening has been implicated as a major end-effector (see chapter 1; also reviewed by Yellon and Hausenloy, 2007). Given the importance of Sirt-3 deacetylation in reducing mPTP opening and potentially reducing extrinsic apoptotic cell death (summarised in Figure 1.15), it is expected that increased Sirt-3 activity may promote cell survival upon myocardial ischaemia-reperfusion. This chapter investigates modulation of Sirt-3 activity as a potential cardioprotective strategy.

This chapter aimed to investigate the effects of Sirt-3 genetic ablation and overexpression on the development of infarction upon ischaemia-reperfusion.

Investigation of the roles of Sirt-3 in myocardial ischaemia-reperfusion injury presented in this chapter was undertaken as a separate study to complement the in vitro investigation of Sirt-3 by Dr A. Hall and Dr S. Kumar; all in vivo data presented here was conducted independently and all references to the existing data are duly noted below.

6.2. Research objective and aims

The main objective of this chapter was to investigate modulation of Sirt-3 as a potential therapeutic target to protect against *in vivo* myocardial ischaemia-reperfusion injury. The principal research aims to achieve this objective were:

(1) Investigate the effect of Sirt-3 genetic ablation on the development of myocardial infarction in response to *in vivo* ischaemia-reperfusion;

(2) Investigate the effect of fasting-induced Sirt-3 overexpression on the development of myocardial infarction upon *in vivo* ischaemia-reperfusion.

6.3. Aim 1: Investigate Sirt-3 genetic ablation in myocardial infarction

6.3.1. Background and preliminary data

The overall aim of this chapter was to investigate the role of Sirt-3 in mediating the response to myocardial ischaemia-reperfusion injury *in vivo*. Sirt-3 is known to deacetylate a number of mitochondrial proteins including important proteins regulating mitochondrial function and cell survival (as described above and detailed in chapter 1; see 1.4.2). These roles of Sirt-3 led to the initial hypothesis investigated here.

Original hypothesis:

Ischaemia-reperfusion increases Sirt-3 mediated deacetylation of mitochondrial proteins to promote mitochondrial function and cell survival.

Initial preliminary studies within our laboratory aimed to investigate the potential roles of Sirt-3 in myocardial ischaemia-reperfusion injury using a number of well-established *in vitro* models using the HL-1 cardiac cell line. This cardiac cell line is a widely used and important *in vitro* model system, which has been reported to retain many cardiac phenotypes including cellular morphology, biochemistry and electrophysiology (developed by Claycomb et al., 1998). These studies of cell death, mPTP opening and

mitochondrial morphology provide an important initial stage of investigation to determine whether a protein of interest exerts significant effects in ischaemia-reperfusion injury.

These *in vitro* studies showed that Sirt-3 overexpression conferred a number of beneficial effects: reduced cell death in response to simulated ischaemia-reperfusion, delayed mPTP opening and increased mitochondrial fusion (Figure 6.1, blue bars; Experiments performed by Dr A. Hall and Dr S. Kumar). Importantly, overexpression of a mutated Sirt-3 protein with no deacetylase activity did not confer these beneficial effects to cell survival and indicators of mitochondrial health (Figure 6.1, black bars), therefore confirming the importance of Sirt-3 deacetylase activity in promoting these beneficial outcomes. The main results of these *in vitro* experiments are summarised in Figure 6.1 (experiments undertaken by Dr A. Hall and Dr S. Kumar) and discussed below in the context of the hypothesis investigated in the first part of this chapter.

Figure 6.1: Pilot *in vitro* studies investigating the role of Sirt-3
Preliminary studies to investigate the roles of Sirt-3 in ischaemia-reperfusion injury using well-established *in vitro* models. HL-1 cells were transfected with control empty plasmid (white bars), functional Sirt-3 (blue bars) and mutant Sirt-3 with no deacetylase activity (black bars).
A) Cell death: Susceptibility of HL-1 cells to cell death following simulated ischaemia-reperfusion (12 hours hypoxia and 1 hour re-oxygenation) was assessed as the percentage of transfected cells exhibiting propidium iodide (PI) staining (dead cells) using fluorescence microscopy. Cell death was significantly reduced by overexpression of Sirt-3. Statistical significance was assessed by one-way ANOVA, *P<0.05; n=4 group (30 random fields per sample).
B) Time to mPTP opening: Mitochondria were loaded with tetramethyl rhodaminemethyl ester (TMRM) dye which accumulates into the mitochondria where its fluorescence is quenched; confocal laser stimulation of TMRM generates ROS which induces mPTP opening allowing diffusion of TMRM into the cytosol where auto-quenching of its fluorescent signal is relieved. Time to mPTP opening was measured as the time to half maximum cytosolic TMRM signal. Time to mPTP opening was significantly delayed by Sirt-3 overexpression and there was mutant Sirt-3 had no effect. Statistical significance assessed by one-way ANOVA, n≥8/group.
C) Mitochondrial morphology: Representative images of mitochondrial morphology assessed by transfection of mitochondria with mitochondrial yellow fluorescent protein (mtYFP) to allow visualisation of mitochondria: i) Empty vector: baseline morphology; ii) Sirt-3 overexpression: predominantly fused mitochondria, iii) Mutant Sirt-3: largely normal morphology.
D) Quantification of mitochondrial morphology: Mitochondria were significantly more fused upon Sirt-3 overexpression. Statistical significance assessed by one-way ANOVA, *P<0.05; n≥6/group.

Experiments presented in this figure were performed by Dr A. Hall and Dr S. Kumar. Detailed methods for these experiments are outlined in a previous publication by our laboratory describing the application of these in vitro models (Ong et al., 2010). (Figure overleaf)

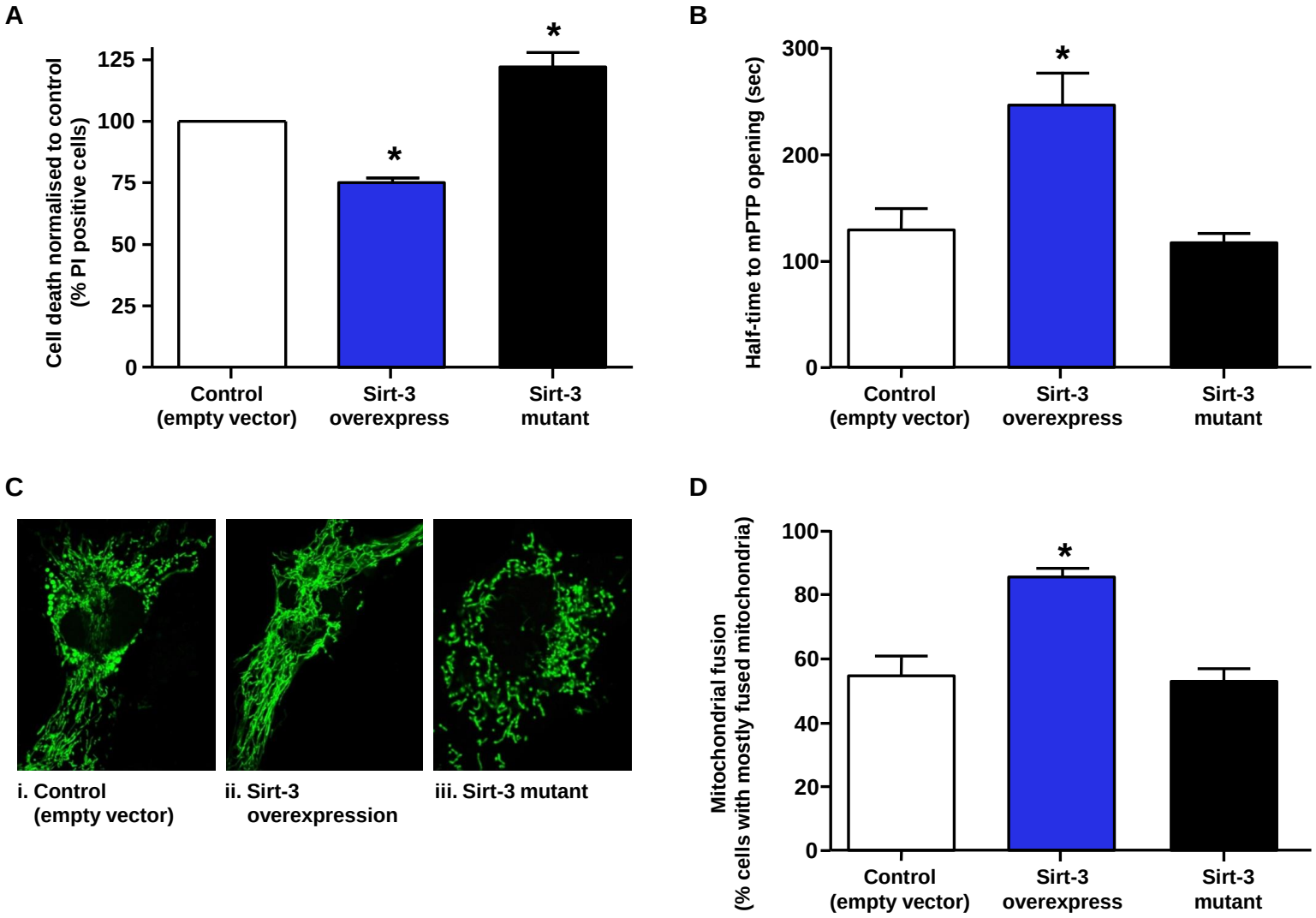

Figure 6.1: Sirt-3 *in vitro* pilot studies – constructed from data provided by Dr A. Hall and Dr S. Kumar – Full legend provided on the preceding page.

These studies appear to confirm the predicted role of Sirt-3 deacetylase activity in promoting mitochondrial and cellular survival upon stress stimuli. This suggests that increased Sirt-3 deacetylase activity may provide a viable therapeutic target for protecting against myocardial ischaemia-reperfusion.

This chapter aimed to investigate the effects of modulating Sirt-3 activity on the susceptibility to myocardial infarction *in vivo*. Since our laboratory did not have access to a Sirt-3 genetic overexpression model, an established Sirt-3 genetic ablation model (described in detail below) was used to investigate the roles of Sirt-3 in the development of myocardial infarction upon ischaemia-reperfusion. Silencing of Sirt-3 in an *in vitro* cell line model has been shown to result in increased cell death upon hypoxia (Pellegrini et al., 2012). Given the results of these *in vitro* studies, it was hypothesised that Sirt-3 genetic knockout mice would exhibit more rapid mPTP opening and increased cell death upon myocardial ischaemia-reperfusion.

Aim 1: The first aim of this chapter was to investigate the effect of global genetic ablation of Sirt-3 on the development of myocardial infarction following *in vivo* ischaemia-reperfusion injury. The central hypothesis in relation to this objective was:

(1) Sirt-3 genetic ablation would significantly increase myocardial infarct size upon *in vivo* ischaemia-reperfusion.

6.3.2. Detailed methods

i Sirt-3 global knockout mice

A Sirt-3 global genetic knockout mouse model was obtained from Dr D. Gius (Vanderbilt University Medical Centre, USA) from the colony originally created by Ahn et al. (2008). Genetic ablation of Sirt-3 was achieved by deletion of exons 2, 3 and 4 of the endogenous *Sirt-3* gene by insertion of *loxP* sites flanking these exons and crossing of Sirt-3 floxed mice with EIIa transgenic Cre-recombinase mice (developed by Lakso et al., 1996) to drive *loxP* site recombination to delete these exons (summarised in Figure 6.2). Mice were backcrossed onto a C57BL/6 background (Ahn et al., 2008).

Colony maintenance: Sirt-3 global knockout mice were obtained from Dr D. Gius (Vanderbilt University Medical Centre, USA) and a number of Sirt-3 knockout and heterozygous animals imported into our laboratory. A Sirt-3 transgenic colony was established from these original animals as outlined in Figure 5.2.

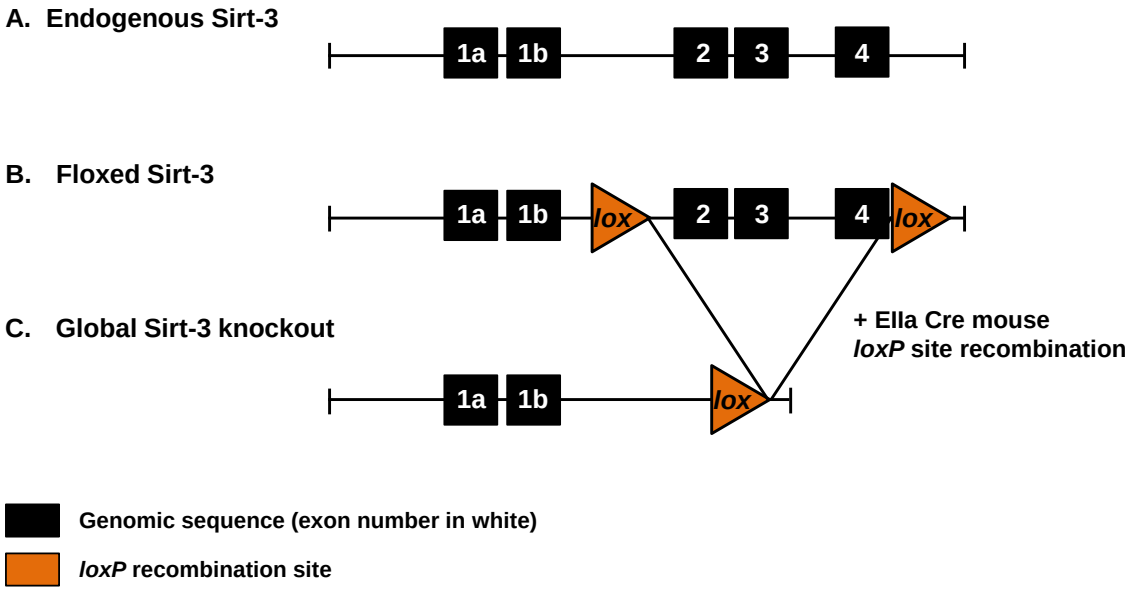

Figure 6.2: Generation of Sirt-3 global knockout mice by Ahn et al. (2008)
Global genetic knockout of Sirt-3 was achieved by insertion of *loxP* sites flanking exons 2-4 of the Sirt-3 gene using standard transgenic methods. Sirt-3 floxed mice were crossed with transgenic EIIa Cre-recombinase mice to cause Cre-driven recombination of Sirt-3 *loxP* sites to delete exons 2-4 of the Sirt-3 gene. Sirt-3 KO mice were bred with C57BL/6 mice to generate the colony and backcrossed onto a C57BL/6 genetic background. Figure modified from Ahn et al. (2008).

Mice were provided by Dr D. Gius (Vanderbilt University Medical Centre, USA).

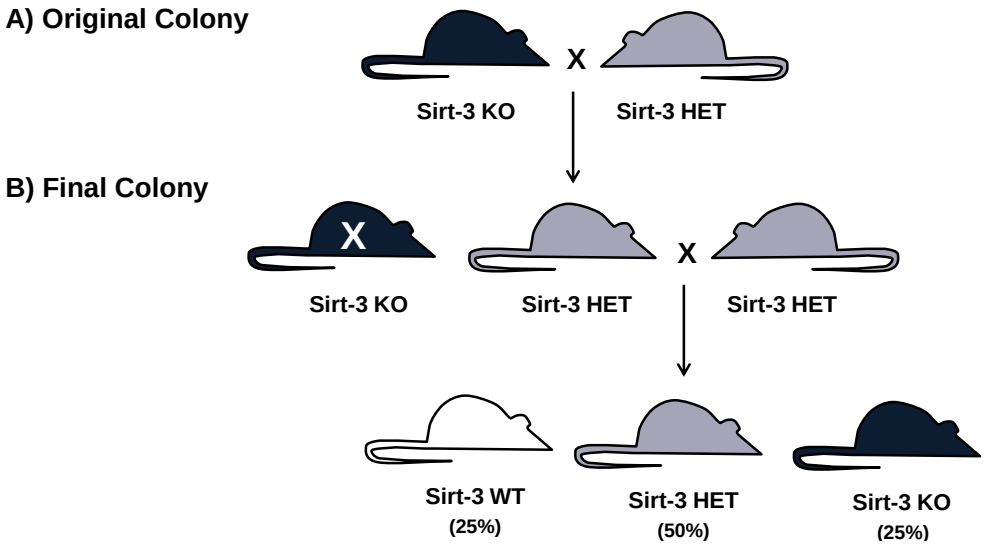

Figure 6.3: Sirt-3 colony establishment and maintenance
A) Original colony: Sirt-3 KO mice were crossed with Sirt-3 HET mice to create a stock of Sirt-3 HET animals. B) Final colony: maintained as Sirt-3 HET x HET crosses to produce progeny of Sirt-3 WT, KO and HET (in accordance with expected Mendelian ratios indicated in brackets).

ii Genotyping for Sirt-3 genetic ablation

The genotyping method used for these animals was based on the standard protocol described in chapter 3 (see 3.1.2 iii) with the following modifications. DNA samples were prepared from ear biopsies and processed within 6 hours, exactly as described previously. The PCR reaction mix was based on a standard reaction optimised in this thesis where the precise primers and sampling parameters are described in Table 6.1. The PCR primers and thermocycling conditions used in this reaction were informed by Dr D. Gius (personal communication) with further optimisation undertaken in this thesis.

The final PCR protocol developed here required the wildtype and mutant PCR product bands to be amplified in separate reactions to give optimal amplification of the required DNA bands. This protocol yielded DNA products with expected sizes of 499 bp (reaction A; KO) and 336 bp (reaction B; WT). The genotype of each animal was decoded based on the presence or absence of these DNA bands between the two separate reactions: KO 499 bp only, WT 336 bp only and HET both 499 and 336 bp bands (Figure 6.4).

When run separately these PCR reactions were robust and reliably produced clear DNA bands for genotyping. The success of these PCR reactions relied on immediate processing of ear biopsies, ideally within 2 hours of sampling (up to a maximum delay of 6 hours). Replacement ear samples were required where a clear PCR genotyping results could not be obtained after two attempts.

Given that PCR amplification of the wildtype and knockout DNA bands for these samples had to be separated to give optimal DNA amplification, it was vital that these reactions were as robust and reliable as possible. Particular care was taken to ensure successful and accurate addition of the crude DNA lysate samples to each sample to reduce the possibility of false negative results for the DNA bands. If there was any uncertainty regarding the presence or absence of a PCR band then the reactions for that animal were repeated to ensure accurate genotyping of all animals used in these studies. This genotyping protocol was confirmed by Western blot interrogation of Sirt-3 protein levels in samples from randomly selected Sirt-3 wildtype and knockout animals.

A) Sirt-3 PCR primer sequences

PRIMER	SEQUENCE	PROPERTIES	
		Length	Tm (ºC)
PCR REACTION A (KO):			
Primer 1: KO forward	5'-AACGATGAAATCTCCCGGTTTGGC-3'	24	62.7
Primer 2: KO reverse	5'-TCTTGCAGTTGCATCCGACTTGTG-3'	24	62.7
PCR REACTION B (WT):			
Primer 3: WT forward	5'-ATCTCGCAGATAGGCTATCAGC-3'	22	60.3
Primer 4: WT reverse	5'-AACCACGTAACCTTACCCAAGG-3'	22	60.3

B) Sirt-3 PCR reaction mix

REAGENT	VOLUME/SAMPLE (µl)	FINAL CONCENTRATION
Qiagen 10X PCR Buffer	2.0	1X
10 mM dNTPs	0.4	200 µM
Primer forward 100 µM	0.2	1 µM
Primer reverse 100 µM	0.2	1 µM
Taq polymerase	0.2	-
Autoclaved distilled water	15.5	-
Crude DNA lysate †	1.5	-
TOTAL VOLUME/SAMPLE (µl)	**20.0**	

C) Sirt-3 PCR thermocycling parameters

PCR STAGE	TEMPERATURE AND DURATION	PCR DESCRIPTION
1	95 ºC for 15 minutes	Hot start
2	94 ºC for 1 minute	DNA separation
3	60 ºC for 1minute	Primer annealing
4	68 ºC for 1 minute	DNA synthesis
5	Go to step 2 for 34 cycles	DNA separation
6	68 ºC for 7 minutes	Final extension
7	4 ºC for ever	Intermediate storage

Table 6.1: Sirt-3 global transgenic colony genotyping protocol
A) Sirt-3 primer sequences for reaction A (KO) and reaction B (WT). B) PCR was run as two separate reactions – reaction A for KO and reaction B for WT where a master mix for each reaction was made based on Qiagen *Taq* kit (Qiagen, UK) with addition of primers A or primers B. † 1.5 µl DNA lysate. C) PCR was undertaken by a thermal cycler (MJ Research, Canada).

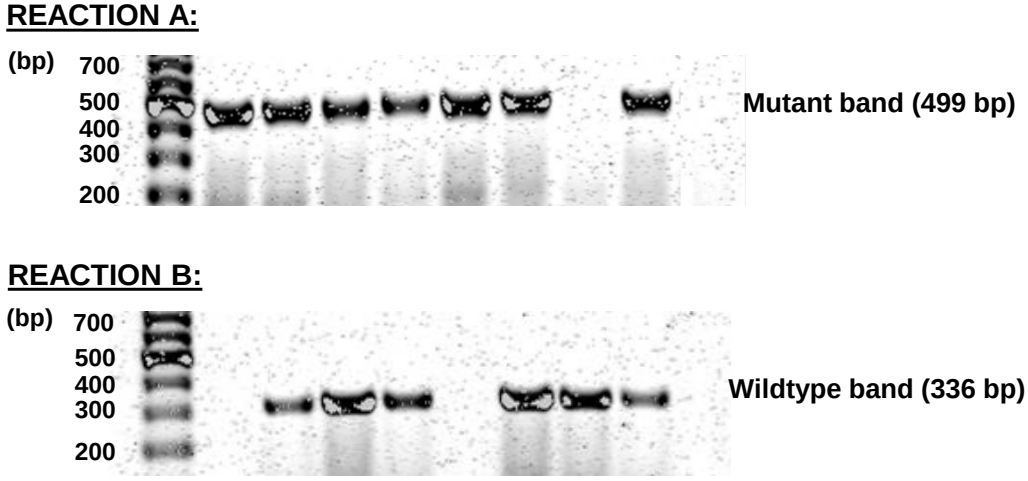

Figure 6.4: Sirt-3 transgenic colony representative genotyping result
The genotype of each animal was determined by the presence or absence of the expected PCR bands by comparison to the molecular weight ladder (lane 1) for reaction A KO 499 bp and reaction B WT 336 bp where HET animals were positive for both bands (as annotated). A negative control (NEG) was run to ensure there was no external DNA contamination.

iii Ischaemia-reperfusion injury in vivo

Surgical protocol: The susceptibility of Sirt-3 knockout and wildtype littermate controls was assessed using the *in vivo* recovery model of myocardial ischaemia-reperfusion injury developed previously in this thesis. Mice were subjected to either 30 or 45 minutes ischaemia followed by 24 hours reperfusion (Figure 4.10 B-C; overleaf). All surgeries were conducted on male mice aged 8-12 weeks from the Sirt-3 transgenic colony or C57BL/6 mice (Charles River Laboratories, UK) as indicated in the results section.

Endpoint 1 – IS/AAR%: The primary endpoint assessed in this study was infarct size by *ex vivo* histological staining using TTC and Evans blue staining exactly as described previously to calculate the infarct size as a percentage of AAR. The pre-defined surgical and myocardial AAR exclusion criteria were applied to this dataset (see 3.2.4).

All infarct size and AAR values are presented as mean ± SEM. All analysis was completed using GraphPad Prism® version 5.0 (GraphPad Software, USA) where the statistical tests and parameters were exactly as described in chapter 3 (see 3.2.4). Details of sample sizes and statistical tests are provided alongside results.

Endpoint 2 – Survival: Survival of Sirt-3 mice subjected to this protocol was analysed by Kaplan-Meier survival plots and long-rank tests using GraphPad Prism® version 5.0 (GraphPad Software, USA), exactly as described in chapter 3 (see 3.2.3). There was no statistical significance in survival between groups presented in this chapter.

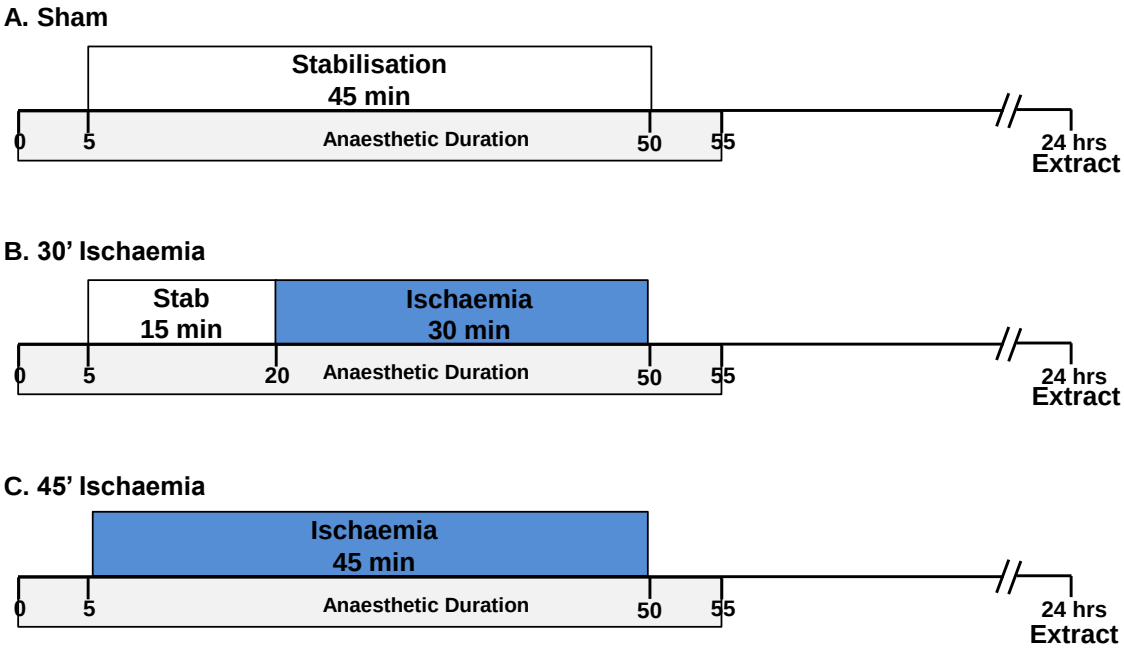

Figure 6.5: Sirt-3 ischaemia-reperfusion *in vivo* recovery protocol
Sirt-3 KO and WT littermate mice underwent the *in vivo* ischaemia-reperfusion protocol for either B) 30 minutes ischaemia or C) 45 minutes ischaemia. Sham operated animals underwent 45 minutes stabilisation (A). Hearts were extracted for staining for infarction at 24 hours reperfusion.

iv Assessment of Sirt-3 protein levels by Western blot

Sirt-3 protein levels were examined in C57BL/6 mice subjected to this surgical protocol to assess the effect of ischaemia and reperfusion on Sirt-3 protein levels. Western blot analysis was performed as previously (see 3.4.2) with the modifications below.

Preparation of heart samples: C57BL/6 mice underwent *in vivo* myocardial ischaemia-reperfusion surgery where hearts were extracted for analysis immediately following 30 minutes ischaemia or 30 minutes ischaemia and 16 hours reperfusion (Figure 6.6).

Processing of heart tissue was completed by Dr A. Hall within our laboratory:

Immediately following extraction, hearts were processed to isolate mitochondria for Western blot analysis. Hearts were extracted exactly as described previously and left and right ventricular tissue immediately homogenised using a glass pestle and mortar in standard homogenisation buffer. Mitochondrial proteins were isolated using a commercial kit (Qproteome mitochondria isolation kit, Qiagen, UK) according to the manufacturer's instructions (see 3.4.1 ii). Mitochondria were washed and re-suspended for Western blot analysis. The protein concentration of mitochondrial samples was assessed using a standard BCA protein assay. Samples were diluted to a set protein concentration by addition of the standard homogenisation buffer.

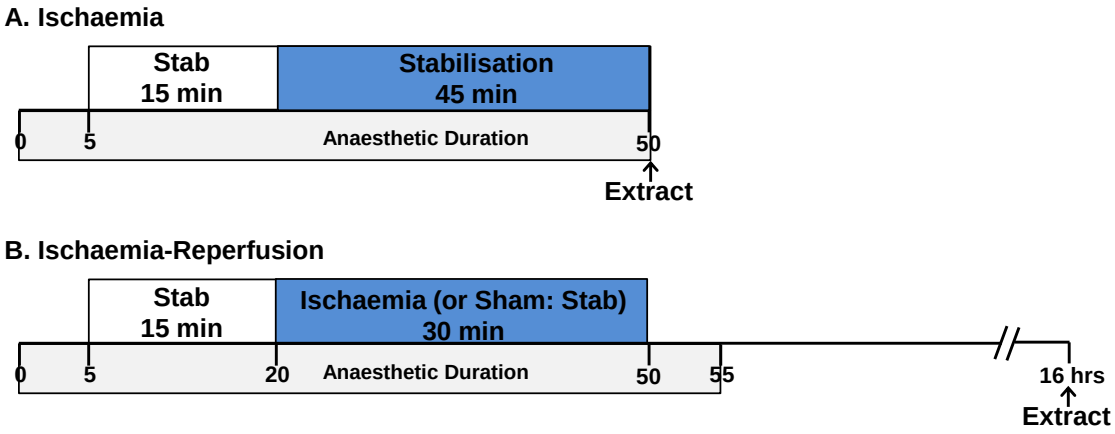

Figure 6.6: Surgical protocol to examine Sirt-3 expression levels
C57BL/6 mice underwent *in vivo* ischaemia with or without reperfusion. A) Sham: hearts were extracted following stabilisation or 16 hours recovery. B) Ischaemia / Reperfusion: hearts were extracted following 30 minutes ischaemia or 30 minutes ischaemia and 16 hours reperfusion.

Western blotting protocol: Western blot analysis was performed by SDS-PAGE of protein samples exactly as described in chapter 3 (see 3.4.2). Since Sirt-3 and VDAC (the intended control for protein loading) have very similar molecular weights (28 and 32 kDa respectively) and are detected using antibodies raised in the same species (rabbit; see Table 6.2) it was necessary to run two separate gels to assess the levels of these proteins. Previous attempts at stripping the membrane of bound antibody indicated that some primary antibody remained thereby precluding the use a single membrane for interrogation of both of these proteins. Particular care was taken to ensure protein loading was consistent between all samples. Normalisation of Sirt-3 protein levels to VDAC is discussed below in section 6.3.3.

Antibody interrogation of proteins: Primary antibodies (detailed in Table 6.2 A) were diluted 1:1000 (final concentration of 1 µg/ml) and incubated with the membrane for 45-60 minutes at room temperature with agitation. An anti-horse secondary antibody was used to detect primary antibody binding (detailed in Table 6.2 B).

A) Primary antibodies:

ANTIBODY	ANTIBODY DETAILS
Sirt-3	Anti-Sirt-3 rabbit monoclonal antibody to Sirt-3 Purchased from Cell Signalling, USA (catalogue number: 5490) Stock 1 mg/ml; diluted 1:1000 to give working concentration 1 µg/ml Predicted molecular weight 28 kDa
VDAC	Anti-VDAC rabbit monoclonal antibody to VDAC Purchased from Cell Signalling, USA (catalogue number: 4661) Stock 1 mg/ml; diluted 1:1000 to give working concentration 1 µg/ml Predicted molecular weight 32 kDa

B) Secondary antibody:

ANTIBODY	ANTIBODY DETAILS
Anti-rabbit	Horse anti-rabbit IgG HRP-linked polyclonal antibody Purchased from Cell Signalling, USA (catalogue number: 7074S). Stock 1 mg/ml; diluted 1:2000 to give working concentration 0.5 µg/ml

Table 6.2: Antibodies for Western blot analysis of Sirt-3 protein levels
A) Primary antibodies were anti-Sirt-3 and anti-VDAC. B) Secondary antibody was an anti-rabbit IgG polyclonal antibody conjugated to HRP to allow detection by a standard chemiluminescence reaction. All antibodies were purchased from Cell Signalling Technology (USA) as detailed here.

Chemiluminescence detection of antibody binding: Protein bands were visualised using a standard HRP chemiluminescence reaction as described previously (see 3.4.2). Protein levels were quantified and expressed as arbitrary units (A.U.) from densitometry analysis. Normalisation of Sirt-3 protein levels to VDAC as a control for protein loading was not undertaken here since VDAC expression appeared to vary between groups (see 6.3.3 for details). The potential effects of this are discussed in detail below. All values are presented as mean A.U. ± SEM. Data were analysed by one-way ANOVA and Bonferroni test using GraphPad Prism® version 5.0 (GraphPad Software, USA). Statistical significance was reported where $P<0.05$ using standard significance coding. Representative protein bands are shown alongside densitometry quantifications.

6.3.3. Results

To investigate the effect of global genetic ablation of Sirt-3 on myocardial infarct size following ischaemia-reperfusion injury, Sirt-3 knockout and wildtype (true littermate) mice were subjected to *in vivo* ischaemia and reperfusion. The standard 30 minute ischaemic protocol evoked an infarct size in Sirt-3 wildtype mice in accordance with that expected in previous studies of wildtype animals (Figure 5.5 A; WT). Importantly, there was no significant difference in infarct size between Sirt-3 knockout and wildtype animals (Figure 5.5 A: IS/AAR% Sirt-3 WT 36.3±2.0 versus Sirt-3 KO 33.3±4.1; n≥7/group, $^{NS}P>0.05$). There was no significant difference in AAR (AAR/LV% Sirt-3 WT 60.2±1.8 versus Sirt-3 KO 56.3±2.1; n≥7/group, $^{NS}P>0.05$) or survival (survival % to 24 hours reperfusion: Sirt-3 WT 87.5%, n=8 versus 88.9%, n=9) between these groups.

To investigate the potential role of Sirt-3 under more severe stress conditions, Sirt-3 mice were subjected to a longer ischaemic insult of 45 minutes; however, this also showed no significant difference in infarct size between Sirt-3 knockout and wildtype animals (Figure 5.5 B: IS/AAR% Sirt-3 WT 46.9±3.7 versus Sirt-3 KO 44.4±4.8; n=5/group, $^{NS}P>0.05$). There was no significant difference in AAR (AAR/LV%: Sirt-3 WT 63.5±7.3 versus Sirt-3 KO 63.5±3.4; n=5/group, $^{NS}P>0.05$) or survival (survival % to 24 hours reperfusion: Sirt-3 WT 71.4%, n=7 versus Sirt-3 KO 83.3%, n=6).

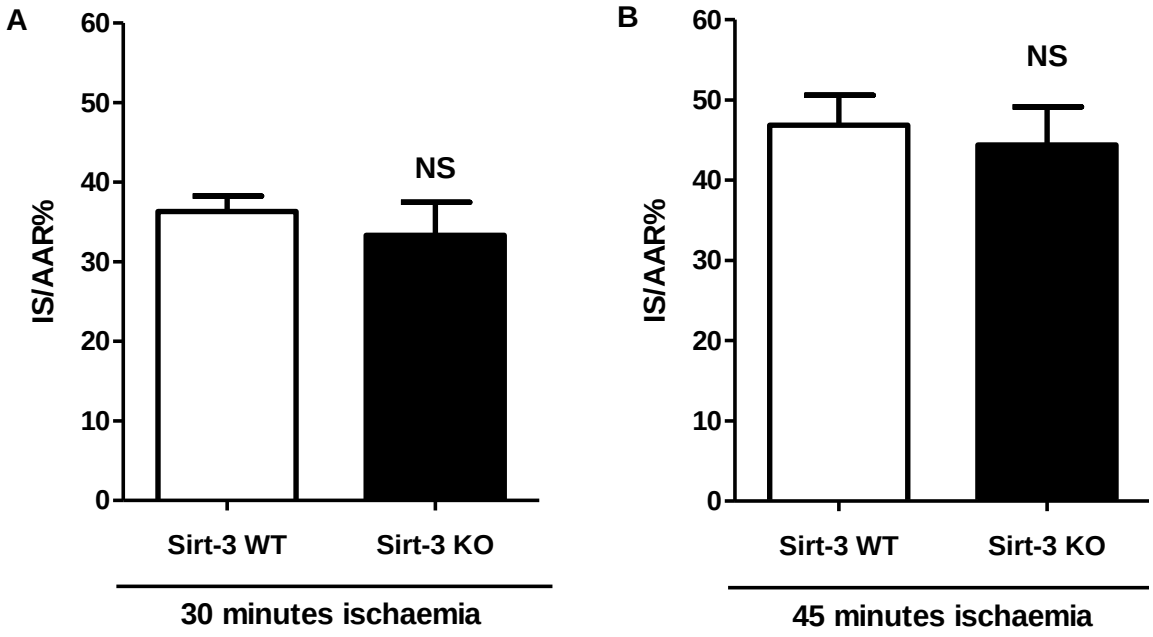

Figure 6.7: Infarct size in Sirt3 wildtype and knockout mice
Infarct size in Sirt-3 KO and WT littermate mice. A) 30 minutes ischaemia and 24 hours reperfusion: no significant difference in infarct size between Sirt-3 KO and WT mice: IS/AAR% Sirt-3 WT 36.3±2.0 (n=7) versus Sirt-3 KO 33.3±4.1 (n=8); $^{NS}P>0.05$. B) 45 minutes ischaemia and 24 hours reperfusion: no significant difference in infarct size between Sirt-3 KO and WT mice: IS/AAR% Sirt-3 WT 46.9±3.7 (n=5) versus Sirt-3 KO 44.4±4.8 (n=5), $^{NS}P>0.05$. Significance assessed by unpaired t-test.

Since genetic ablation of Sirt-3 did not appear to affect myocardial infarct size, these results suggest that Sirt-3 may not play an important role in the pathophysiology of myocardial ischaemia-reperfusion. This is unexpected given that Sirt-3 silenced cells were shown to exhibit increased cell death upon hypoxia in an *in vitro* model (Pellegrini et al., 2012; as discussed above); this is discussed in detail subsequently (see 6.5.1).

To investigate the effect of myocardial ischaemia and reperfusion on Sirt-3 expression levels, C57BL/6 were subjected to this surgical procedure and mitochondrial Sirt-3 protein levels examined immediately following ischaemia and after ischaemia and reperfusion. Analysis of Sirt-3 and VDAC protein levels in these samples showed increased levels of Sirt-3 protein in ischaemic samples compared to equivalent control operated animals. However, there was a large variation in VDAC protein levels between these samples, where it appeared that increased Sirt-3 levels appeared alongside decreased VDAC levels (Figure 5.14 A). Although there was no statistically significant difference in VDAC levels between these groups, absolute Sirt-3 levels were quantified without normalisation to VDAC to avoid any confounding effects of altered VDAC expression (quantification of absolute Sirt-3 protein levels is shown in Figure 5.14 B).

This analysis of mitochondrial Sirt-3 protein levels showed that myocardial ischaemia significantly increased Sirt-3 protein by approximately 3.0 fold compared to equivalent sham operated mice (Figure 5.14 B: white compared to white hashed bars, n=3/group, **P<0.01). Interestingly, animals subjected to the 16 hour sham procedure also showed a significant increase in mitochondrial Sirt-3 protein levels compared to 30 minute sham operated mice (Figure 5.14 B: white hashed compared to black hashed bars, n=3/group, *P<0.05). However, it should be noted that there was no significant difference in Sirt-3 protein levels following ischaemia-reperfusion compared to sham operated animals (Figure 5.14 B: black compared to black hashed bars, n=3/group, ^{NS}P>0.05).

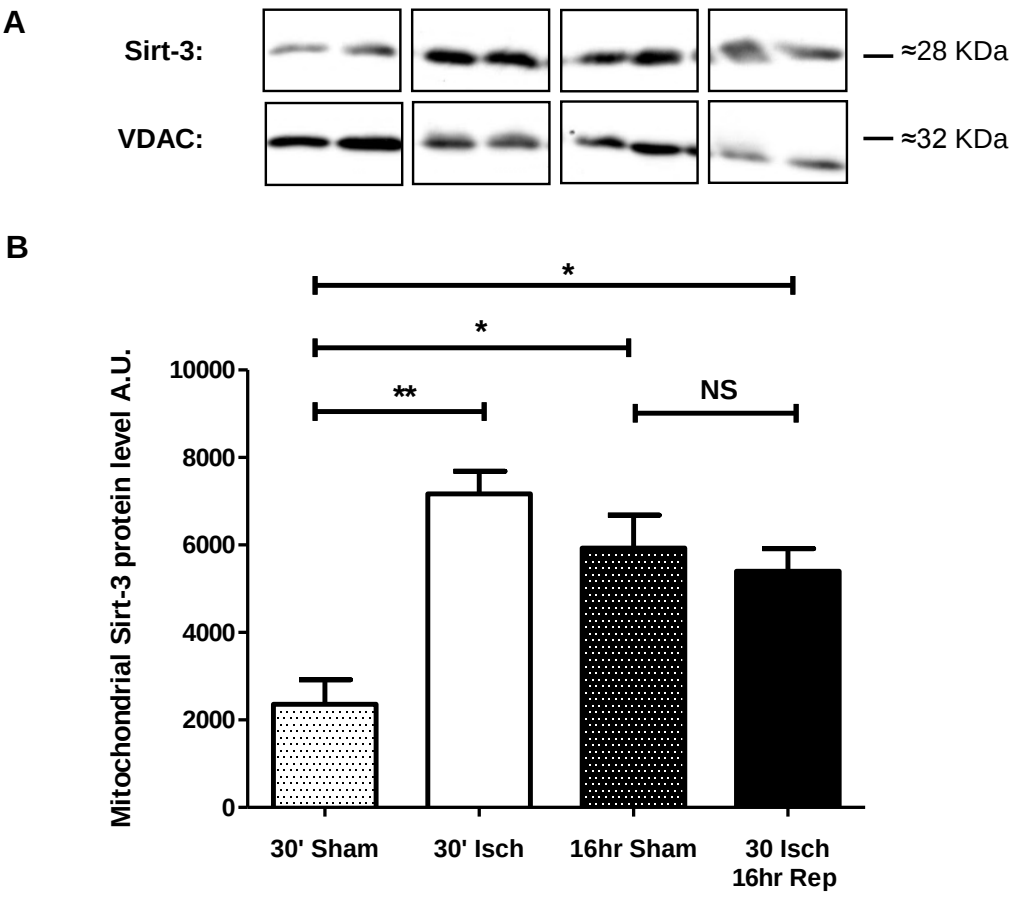

Figure 6.8: Sirt-3 protein levels following ischaemia and ischaemia-reperfusion
Western blot analysis to quantify Sirt-3 protein levels in mitochondria isolated from C57BL/6 mice immediately following ischaemia (white bar) and following ischaemia and reperfusion (black bar). Sirt-3 levels were also examined in equivalent sham operated animals (hashed bars); n=3/group. A) Representative protein bands from Western blot for Sirt-3 and VDAC. Since VDAC protein levels appeared to be variable between groups, this was not used as a loading control for normalisation of Sirt-3 levels. B) Densitometry of Western blot analysis to calculate Sirt-3 protein levels (absolute A.U. not normalised to VDAC). Statistical significance assessed by one-way ANOVA; mitochondrial Sirt-3 protein levels were significantly increased by ischaemia (comparison of white hashed and white bars; **P<0.01).There was no significant difference in mitochondrial Sirt-3 levels following ischaemia-reperfusion compared to sham (^{NS}P>0.05).

This study suggests that the surgical procedure used to induce myocardial ischaemia-reperfusion elicits a significant stress response. The potential implications of this are discussed in detail subsequently in this chapter (see 6.5.1).

6.4. Aim 2: Investigate Sirt-3 overexpression in myocardial infarction

6.4.1. Background

The demonstration that genetic ablation of Sirt-3 does not affect the susceptibility to myocardial infarction appears to suggest that Sirt-3 may not play a fundamental role in the pathophysiology of myocardial ischaemia-reperfusion injury. However, given the convincing *in vitro* data previously generated within our laboratory showing that Sirt-3 overexpression reduced cell death upon simulated ischaemia-reperfusion, delayed ROS-induced mPTP opening and promoted mitochondrial elongation (see pilot data by Dr A. Hall and Dr S. Kumar; Figure 6.1), the second part of this chapter sought to investigate the effects of Sirt-3 overexpression on the susceptibility to infarction *in vivo*.

Since our laboratory did not have access to a genetic model of Sirt-3 overexpression, a fasting protocol was utilised to increase Sirt-3 protein levels. Fasting has previously been shown to increase Sirt-3 expression in the liver and brown adipose tissue, where Hirschey et al. (2010) demonstrated maximal Sirt-3 protein levels were obtained following 18 hours fasting (Hirschey et al., 2010). A similar approach to induce Sirt-3 overexpression was undertaken by Lu et al. (2011), where fasting (24 hours but not 8 hours) was required to reveal a statistically significant difference in acetaminophen-induced liver injury between Sirt-3 knockout and wildtype mice, although this study did not report the extent of Sirt-3 overexpression induced by these fasting durations (Lu et al., 2011). The mechanism of increased Sirt-3 expression is expected to result from increased mitochondrial NAD^+ levels in response to fasting, since Sirt-3 activity is regulated by NAD^+ levels. Indeed, Yang et al. (2007a) showed that 48 hours fasting of rats resulted in an approximate 2.5-fold increase in NAD^+ levels (Yang et al., 2007a). These findings are in agreement with the well-defined role of the sirtuin proteins as a metabolic sensors (reviewed by Shinmura, 2013). The second part of this chapter aims to investigate the role of Sirt-3 in the pathophysiology of myocardial ischaemia-reperfusion injury using this model of increased Sirt-3 expression.

Aim 2: The second aim of this chapter was to investigate the effect of fasting-induced Sirt-3 overexpression on susceptibility to myocardial infarction. The central hypothesis in relation to this research objective was as described above, based on the *in vitro* data:

(1) Sirt-3 overexpression induced by fasting would significantly reduce myocardial infarct size upon *in vivo* ischaemia-reperfusion.

6.4.2. Detailed methods

The methods used in this section were largely based on those described in part 1 of this chapter (section 6.3.2) with additional experimental details provided here.

i Fasting protocol

Use of animals in this study was in accordance with the United Kingdom Animal (Scientific Procedures) Act of 1986. Fasting for a maximum of 16 hours is permitted without a specific Home Office protocol since it is not considered to be a procedure; the fasting protocol used here did not exceed 16 hours fasting. Fasting was initiated by removal of food from the housing cage, where animals were provided with water *ad libitum*. It was essential to ensure that all traces of food were removed from the floor of the cage. Animals were closely monitored during fasting to ensure maintained welfare.

ii Ischaemia-reperfusion injury in vivo

Following 16 hours fasting, animals were subjected to the *in vivo* ischaemia-reperfusion protocol developed in chapter 4 of this thesis, using a protocol of 30 minutes ischaemia and 24 hours reperfusion exactly as described above (see 6.3.2 iii, Figure 4.10 B). Particular care was taken to ensure that all animals were in good health prior to commencing surgery. The time-course of recovery and the observed activity of fasted animals (both Sirt-3 knockout and wildtype mice) following this surgical protocol was noticeably slower than expected from fed counterparts (although this was not formally assessed or quantified). There was no statistical difference in the survival of fasted versus fed wildtype mice. Animals were closely monitored by experienced technical staff to ensure that the severity limit of the procedural licence was not exceeded and that animals were in good health throughout this protocol.

Following 24 hours reperfusion, mice were anaesthetised and hearts extracted for *ex vivo* histological staining using TTC and Evans blue exactly as described above (see section 6.3.2 iii). The standard surgical and AAR exclusion criteria were applied.

This fasting study was undertaken in both Sirt-3 knockout and wildtype mice, since although it was only expected to increase Sirt-3 expression in the wildtype animals, it was important to include the Sirt-3 knockout control group to assess the involvement of Sirt-3 in any effect observed. For this same reason, additional surgeries of fed Sirt-3 knockout and wildtype mice were also performed during this study to permit inclusion of these groups in the final analysis of the effect of fasting on susceptibility to infarction.

6.4.3. Results

i Susceptibility to ischaemia-reperfusion injury

Although analysis of the time-course of Sirt-3 expression with incremental durations of fasting was not undertaken here, 16 hours fasting was shown to evoke Sirt-3 overexpression (Figure 6.9 A; corresponding to approximately a 1.5 fold increase in ventricular Sirt-3 protein level). This should be formally investigated in a larger sample.

To investigate the effect of fasting-induced Sirt-3 overexpression on the susceptibility to myocardial infarction, fasted Sirt-3 knockout and wildtype (true littermate) mice were subjected to 30 minutes ischaemia and 24 hours reperfusion. This study was undertaken with randomised additional surgeries for Sirt-3 knockout and wildtype fed mice to allow a comparison of the effect of fasting with fed control animals. Fasted wildtype animals exhibited significantly larger infarct sizes compared to fasted Sirt-3 knockout mice (Figure 6.9: IS/AAR% fasted Sirt-3 WT 52.8±4.7 versus fasted Sirt-3 KO 26.9±4.3; n=6/group, **P<0.01). There was no significant difference in AAR or survival. The lack of any effect of fasting on myocardial infarct size in Sirt-3 knockout mice confirms that the increased susceptibility to infarction in fasted wildtype mice results from Sirt-3 since there is no significant effect of fasting in Sirt-3 knockout mice.

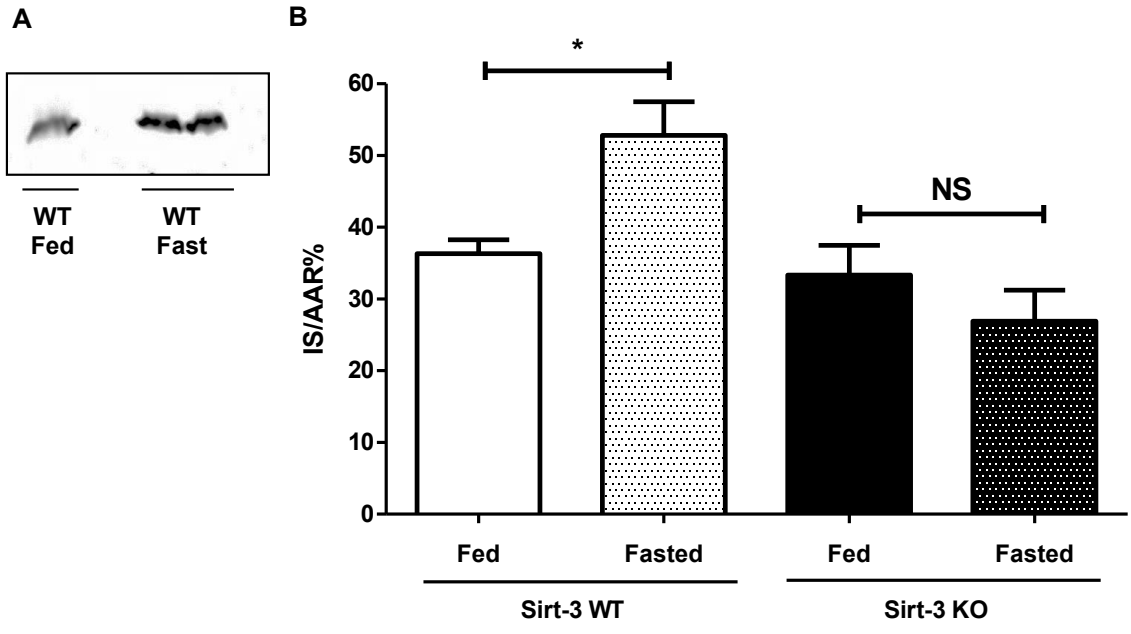

Figure 6.9: Infarct size in Sirt-3 fasted wildtype and knockout mice
A) Representative Western blot analysis of ventricular Sirt-3 protein levels in Sirt-3 WT fed and fasted mice. B) Infarct size in fasted Sirt-3 KO and WT littermate animals subjected to 30 minutes ischaemia and 24 hours reperfusion compared against fed controls. Infarct size in fasted Sirt-3 WT mice was significantly larger than in fasted Sirt-3 KO mice: IS/AAR% Sirt-3 WT fasted 52.8±4.7 (white hashed bar; n=6) versus Sirt-3 KO 26.9±4.3 (black hashed bar; n=6). Statistical significance was assessed by one-way ANOVA comparing relevant groups, *P<0.05.

6.5. Discussion

The overall research objective of this chapter was to investigate the potential modulation of Sirt-3 as a cardioprotective intervention to reduce myocardial infarction upon ischaemia-reperfusion. The initial *in vitro* studies within our laboratory indicated that Sirt-3 overexpression conferred a number of beneficial effects, notably increased cell survival upon simulated ischaemia-reperfusion injury. This chapter describes further investigation of the role of Sirt-3 in *in vivo* ischaemia-reperfusion injury.

6.5.1. Aim 1: Investigate the effect of Sirt-3 genetic ablation on susceptibility to myocardial infarction

Original research hypothesis and pilot data: Sirt-3 has been shown to mediate deacetylation of a number of key mitochondrial proteins, including proteins known to be important in controlling cell survival (summarised in chapter 1; see Table 1.3). Notably, Sirt-3 deacetylation of Cyp-D reduces its PPIase activity resulting in reduced mPTP opening (Shulga et al., 2010; Hafner et al., 2010). Further to this, Sirt-3 deacetylation increases the activity of the ROS scavenger enzyme, MnSOD (Jacobs et al., 2008; Chen et al., 2011), intracellular anhydrase (CA) (Pellegrini et al., 2012) and the Bax-binding protein, Ku70 (Sundaresan et al., 2008). It was, therefore, hypothesised that the cumulative actions of Sirt-3 on these important mitochondrial proteins would reduce mPTP opening directly by reducing Cyp-D activity and indirectly by reduced ROS levels. This would therefore be expected to reduce cell death upon myocardial ischaemia-reperfusion (summarised in chapter 1, Figure 1.15).

The *in vitro* pilot data from our laboratory showed that overexpression of Sirt-3 in the HL-1 cardiac cell line conferred several beneficial effects including reduced cell death following simulated ischaemia-reperfusion injury, delayed mPTP opening and increased mitochondrial fusion. Importantly, these beneficial effects were not observed following expression of mutated Sirt-3 lacking deacetylase activity, thereby confirming that Sirt-3 deacetylation mediates several beneficial effects which are expected to promote cell survival (summarised in Figure 6.1; experiments undertaken by Dr A. Hall and Dr S. Kumar). These studies provided initial evidence that Sirt-3 mediated deactylation may play an important role in the response to myocardial ischaemia-reperfusion injury and suggested that overexpression or increased activity of Sirt-3 may protect against the injurious effects of ischaemia-reperfusion *in vivo*.

Susceptibility of Sirt-3 knockout mice to myocardial infarction: The first section of this chapter investigated this original hypothesis using a model of global genetic ablation of Sirt-3. Given the apparent protective role of Sirt-3 overexpression *in vitro* in the HL-1 cardiac cell line, it was expected that genetic ablation of Sirt-3 would render the myocardium more susceptible to infarction from *in vivo* ischaemia-reperfusion. This was based on the assumed opposing effects of ablation and overexpression of this gene.

However, these experiments demonstrated that there was no difference in infarct size between Sirt-3 knockout and wildtype mice subjected to 30 minutes ischaemia (Figure 6.6 A). Since Sirt-3 activity is known to be upregulated by cellular stress, a more severe ischaemic insult (45 minutes myocardial ischaemia) was investigated, however, this also showed that Sirt-3 genetic knockout did not affect the susceptibility to infarction (Figure 6.6 B). This was unexpected based on the role of Sirt-3 overexpression previously demonstrated by our laboratory *in vitro* in the HL-1 cardiac cell line (Figure 6.1).

There are numerous potential explanations for this discrepancy between the *in vitro* and *in vivo* studies. The most obvious potential variable is the difference between the knockout and overexpression models investigated here. Genetic ablation of Sirt-3 may trigger some compensatory mechanism that is abrogating the effect of the knockout of Sirt-3. This was not expected given that the other sirtuin deacetylase proteins are not located in the mitochondria. It is possible however, that the other mitochondrial Sirt proteins, -4 and -5, exert deacetylase activities in the absence of Sirt-3. It should be noted however that these proteins have been shown to possess little deacetylase activity at baseline (Lombard et al., 2007). Further studies could investigate this by analysis of expression and activity of other Sirt proteins (potentially including normally cytosolic Sirt-1) in mitochondria isolated from Sirt-3 knockout hearts.

However, overexpression of Sirt-3 in the *in vitro* HL-1 cell model presented here may also introduce some artificial effects of Sirt-3 protein function. A potential pitfall of such transfection approaches is the potential for artificial localisation of the protein of interest. For example, overexpression of Sirt-3 may result in accumulation and activity of exogenous Sirt-3 protein in the cytosol. The precise localisation of Sirt-3 in the HL-1 cell system summarised here was not investigated in these experiments. In addition, further *in vitro* artefacts may derive from inherent differences in immortalised cells compared to *ex vivo* and *in vivo* cell preparations; this is discussed in more detail subsequently.

The potential influence of the difference between genetic overexpression and knockout was investigated further in part two of this chapter and is discussed in detail below. Additional potential reasons for the apparent discrepancy between these studies are discussed at the end of this chapter (see 6.5.3).

Increased Sirt-3 protein levels in response to stress: Since Sirt-3 is a stress protein known to be upregulated in response to stress stimuli, including calorie restriction and fasting (Sundaresan et al., 2008; Lu et al., 2011), mitochondrial Sirt-3 protein levels were examined in hearts extracted immediately following myocardial ischaemia and following ischaemia and reperfusion. This study did not examine total cell or cytosolic fractions and therefore provides an indication only of mitochondrial Sirt-3 protein levels.

It is important to note that there appeared to be a trend towards decreased VDAC protein levels in the mitochondrial samples with higher Sirt-3 protein levels. Although this procedure was not expected to affect VDAC levels, to avoid any confounding effects of this for the normalisation of Sirt-3 protein levels, analysis of Sirt-3 protein was computed as absolute band intensity and not normalised to VDAC levels. Since Sirt-3 protein levels have not been normalised to a loading control, the protein levels observed here are likely to be subject to slightly larger errors than would otherwise be expected. This Western blot analysis could be repeated using a different mitochondrial loading control, such as prohibitin, which has been suggested to be more stably expressed (Merkwirth and Langer, 2009; Verweij et al., 2013). However, this was not required since analysis of absolute Sirt-3 protein was sufficiently sensitive to detect significant changes.

This study showed that myocardial ischaemia significantly increased mitochondrial Sirt-3 protein levels by approximately 3.0-fold compared to sham operated animals (Figure 5.14 B). The short experimental protocol investigated here suggests that this increase in mitochondrial Sirt-3 protein results from either post-translational regulation (for example reduced Sirt-3 degradation) or intracellular targeting of the Sirt-3 protein and not *de novo* synthesis of Sirt-3. Sirt-3 is known to be targeted to the mitochondria by an N-terminal sequence which is subsequently cleaved within the mitochondrial matrix to form the functional Sirt-3 protein (Frye, 2000; Schwer et al., 2002). It is therefore possible that under baseline conditions there is a pool of inactive cytosolic Sirt-3 protein which is translocated to the mitochondria upon myocardial stress, as discussed further below.

To further investigate the effect of myocardial ischaemia and reperfusion on Sirt-3 protein levels it would be of interest to examine mitochondrial, nuclear and cytosolic cellular fractions to examine the subcellular localisation of Sirt-3. This would be particularly interesting given the potential nuclear role of Sirt-3 upon stress suggested by Sundaresan et al. (2008), where stress stimuli causeed nuclear-enrichment of Sirt-3 (Sundaresan et al., 2008). However, attempts at precise cellular fractionation within our laboratory showed notable contamination of these fractions and so this was not investigated further in this thesis. The mitochondrial fractions examined in this chapter were processed using a well-characterised commercial mitochondrial isolation kit proven

to provide an uncontaminated preparation. The precise mechanism of increased Sirt-3 protein levels following ischaemia therefore remains speculative and is an important direction for future experiments investigating the role of Sirt-3 in ischaemia-reperfusion.

Interestingly, the sham recovery procedure also evoked a significant increase in mitochondrial Sirt-3 protein levels (Figure 5.14 B), which was not further increased upon ischaemia-reperfusion. This suggests that the surgical protocol employed here evokes a significant stress response, as discussed briefly in chapter 4 (see 4.6.4). This increase in mitochondrial Sirt-3 protein levels may result from the potentially reduced calorie intake of these animals in the immediate post-operative period. Recovering mice (both sham and ischaemia-reperfusion operated) display reduced activity during recovery and appear to show reduced food and water intake during this period (however, it should be noted that activity levels and food intake have not been formally quantified). Once could speculate that the potentially reduced calorie intake or mild fasting of recovering animals may therefore evoke increased mitochondrial Sirt-3 protein levels; the effects of fasting on Sirt-3 protein expression are discussed in detail below. This also offers a possible reason for the absence of increased mitochondrial Sirt-3 protein levels in animals subjected to the 30 minute sham procedure. Given the extended time-course examined here (16 hours recovery), the increased mitochondrial Sirt-3 protein observed may result from *de novo* protein synthesis, although this has not been directly investigated here.

It is important to note that although the studies presented here have demonstrated increased Sirt-3 protein levels following ischaemia; increased Sirt-3 activity has not been investigated. Myocardial ischaemia is expected to increase NAD^+ levels (confirmed by Yang et al., 2007a) and is therefore expected to result in increased Sirt-3 activity. Sirt-3 deacetylase activity can be quantified using a radiolabelled acetyl-lysine assay or using more recently developed fluorescence labelling methods. A commercial assay kit from Cyclex (MBL International, USA) has been shown to provide a convenient and accurate method to quantify Sirt-3 deacetylase activity (as used by Shulga et al., 2010). This assay may serve as a useful tool for further investigation of the role of Sirt-3 in the experiments presented in this chapter, to confirm concomitant increased Sirt-3 activity.

6.5.2. Aim 2: Investigate fasting-induced Sirt-3 overexpression on the susceptibility to myocardial infarction

Given the role of Sirt-3 as a metabolic sensor, a fasting-induced model of Sirt-3 overexpression was examined in this thesis. This was particularly important given that under baseline (fed) conditions, Sirt-3 did not appear to be mediating a critical role in the pathophysiology of myocardial ischaemia-reperfusion and the development of infarction.

Hirschey et al. (2010) showed that fasting increases Sirt-3 protein levels which in turn reduces mitochondrial protein acetylation (confirming increased Sirt-3 activity) in liver and brown adipose tissue. A time-course study of these animals showed that Sirt-3 protein levels increased with the duration of fasting and maximal Sirt-3 levels were reached after 18 hours fasting (Hirschey et al., 2010). Importantly, Lu et al. (2011) demonstrated that following 24 hours (and not 8 hours) fasting there was a significant difference in the susceptibility of Sirt-3 fed and fasted mice to acetaminophen-induced liver toxicity (Lu et al., 2011). This illustrates that moderate durations of fasting (18-24 hours) can serve as an 'agonist' for identifying the pathophysiological roles of Sirt-3.

Fasting-induced increases in Sirt-3 expression were therefore investigated to provide a potentially more appropriate comparison with the previous *in vitro* studies that revealed an important role of Sirt-3 in cardiac cells. The second part of this chapter investigated the susceptibility to myocardial infarction of fed and fasted animals. This thesis used a 16 hour fasting protocol since this was permitted by the UK Home Office without requirement for a specific procedural licence. This 16 hour fasting protocol was expected to significantly increase Sirt-3 protein levels, based on the approximate time-course of Sirt-3 overexpression demonstrated by Hirschey et al. (2010).

Based on the pilot *in vitro* data (summarised in Figure 6.1), it was hypothesised that fasting-induced overexpression of Sirt-3 would protect against myocardial ischaemia-reperfusion, resulting in reduced myocardial infarct size in fasted wildtype mice. Interestingly, 3 days pre-operative fasting protects against renal and hepatic ischaemia-reperfusion, termed 'fasting induced preconditioning' (Mitchell et al., 2010). This group subsequently showed that 3 days fasting also reduced complex II driven mitochondrial respiration and mPTP opening (Mitchell et al., 2010; Verweij et al., 2013).

However, the 16 hour fasting protocol used here resulted in increased susceptibility to myocardial infarction in Sirt-3 wildtype animals (Figure 6.9). Since there was no equivalent increase in myocardial infarct size in fasted Sirt-3 knockout mice, it appears that this increased injury is mediated by the actions of Sirt-3. This fasting protocol was shown to increase myocardial Sirt-3 protein levels; however, the localisation and activity

of Sirt-3 should also be investigated in these animals, as discussed above. This detrimental effect of fasting in wildtype mice is apparently in conflict with the effect of fasting-mediated protection against renal and hepatic ischaemia-reperfusion (Mitchell et al., 2010; Verweij et al., 2013). This may result from the more severe fasting protocol used by these published studies (3 days fasting) or some organ-specific effects.

Indeed, the higher metabolic demand of the heart compared to the liver may account for some of this difference since fasting has been shown to cause downregulation of complexes I, IV and V and reduced oxidative phosphorylation (Verweij et al., 2013). It could be speculated that the heart may be less able to compensate for these changes induced by fasting. It would be pertinent to further investigate the metabolic changes in Sirt-3 wildtype and knockout hearts under fed and fasted conditions. Interestingly, Sirt-3 knockout (under fed conditions) significantly reduces ATP levels in mouse embryonic cells (Ahn et al., 2008) but not in the liver (Hirschey et al., 2010). Further studies should examine myocardial ATP levels in fed and fasted Sirt-3 wildtype and knockout mice.

The increased susceptibility to myocardial infarction in fasted Sirt-3 wildtype animals compared to Sirt-3 knockout mice (Figure 6.9) appears to conflict with the beneficial effect of Sirt-3 overexpression *in vitro* (summarised in Figure 6.1; experiments by Dr A. Hall and Dr S. Kumar) and appears to disprove our original hypothesis. However, a similar protective effect of Sirt-3 genetic ablation in fasted animals compared to wildtype fasted mice was observed in a model of liver toxicity discussed above (Hirschey et al., 2010). These studies appear to suggest that Sirt-3 may be associated with increased cell death under certain triggers of cell stress following fasting.

It is important to note that there are notable differences between the *in vitro* and *in vivo* model systems investigated here. A potential confounding factor influencing the interpretation of the *in vitro* data described here is the highly glycolytic metabolism of immortalised cell lines, including the HL-1 cell line, compared to the physiological metabolic state *in vivo*, where the heart is highly dependent on fatty acid oxidation (see chapter 1; 1.2.1). Indeed, the reduction in oxidative phosphorylation in HeLa cells has been shown to be manifested by a decrease in mitochondrial respiration (Rossignol et al., 2004), which could potentially influence the roles of metabolic sensor proteins, such as Sirt-3. The importance of the changed metabolic status of HeLa cells was shown by Shulga et al. (2010) where incubation of these cells in galactose-containing medium, which has been shown to stimulate a metabolic switch to oxidative phosphorylation, was required to detect a difference in Sirt-3 activity (Shulga et al., 2010). The altered changed metabolic state of HL-1 cells investigated in the *in vitro* experiments here may therefore influence the interpretation of the role of Sirt-3 from this study.

The relative merits and importance of these studies must now be evaluated to interpret the role of Sirt-3 in the pathophysiology of myocardial ischaemia-reperfusion injury.

6.5.3. Evaluation of the role of Sirt-3 as a potential cardioprotective target

It is important to note that this chapter of the thesis has not demonstrated a clear effect of Sirt-3 in ischaemia reperfusion injury in the normal physiological fed state. This poses the question as to whether Sirt-3 is an important mediator of ischaemia-reperfusion injury. The further studies discussed above would be necessary to address the revised working hypothesis of this research project; that Sirt-3 is detrimental in the setting of ischaemia-reperfusion injury. Investigation of the effect of Sirt-3 inhibition using a pharmacological inhibitor would provide an additional valuable insight into the potential for modulation of Sirt-3 activity as a therapeutic approach to reduce the susceptibility to myocardial infarction. Specifically, it would be important to investigate whether Sirt-3 inhibition at reperfusion could mediate a cardioprotective effect.

It remains interesting that there was no effect of Sirt-3 genetic ablation on the susceptibility to myocardial infarction in fed animals and this questions whether Sirt-3 represents a relevant target for cardioprotection against ischaemia-reperfusion. Given that it is evident that fasting-induced Sirt-3 overexpression elicits an increased infarct size, it would usually be suggested that inhibition of Sirt-3 as a therapeutic strategy may reduce infarct size. However, the data presented in the first part of this chapter suggests that this may not be the case. It is possible that this lack of reduction of infarct size in Sirt-3 knockout mice results from a compensatory mechanism in response to the absence of Sirt-3, especially since this is a global genetic knockout model. This could be addressed using inducible Sirt-3 knockout or a pharmacological inhibitor since this would more appropriately model the target of temporal Sirt-3inhibition. Unfortunately, inducible Sirt-3 knockout mice are not currently available. Although Galli et al. (2012) recently reported a pharmacological inhibitor with increased selectivity for Sirt-3 over Sirt-1 and -2, potential inhibition of other mitochondrial Sirt proteins (-4 and -5) has not be examined (Galli et al., 2012). A pharmacological approach may provide an important tool to investigate the role of Sirt-3 in myocardial ischaemia-reperfusion *in vivo*.

The precise role of Sirt-3 in the pathophysiology of myocardial ischaemia-reperfusion injury remains unclear; however, it appears that the metabolic status of the cells upon the onset of the ischaemia-reperfusion insult may influence the roles of this protein. Although Sirt-3 deacetylation has been linked with many beneficial effects for mitochondrial function and cell survival (as summarised in chapter 1; see Figure 1.15), there remains some controversy over the precise outcomes for cell death. The role of

Sirt-3 regulation of Bax-mediated cell death may be important in this setting, where Sirt-3 deacetylation of Cyp-D has been shown to result in hexokinase II (HKII) dissociation from the outer mitochondrial membrane (Shulga et al., 2010; Verma et al., 2013). Shulga et al. (2010) have provided some evidence that Cyp-D mediated dissociation of HKII is regulated by a conformational change in ANT, which has been shown to be influenced by the cellular metabolic status. It is therefore possible that the metabolic status of the cell upon the insult directs the balance of cell survival and death pathways (Shulga et al., 2010). Further investigation of prevalence of these cell survival and death signalling pathways in response to differential stress insults is required.

The effect of fasting on myocardial Sirt-3 expression levels and the resulting increased susceptibility to myocardial infarction is a particularly exciting finding. The biological basis of this is discussed above in relation to the pathophysiological roles of Sirt-3; however, this also represents a potentially important consideration clinically, where fasting prior to major surgeries is common practice. Experiments in this chapter suggest that fasting could actually increase injury resulting from myocardial ischaemia-reperfusion. This may be relevant for surgical procedures such as coronary artery bypass graft, where patients would be fasted prior to surgery and where the myocardium would be subjected to a degree of ischaemia-reperfusion. Although this has not been specifically investigated here, the initial data presented here would be useful to investigate in future studies. In particular, it would now be interesting to examine whether this increased susceptibility to myocardial infarction could be ameliorated by treatment with a pharmacological Sirt-3 inhibitor, such as that described by Galli et al. (2012). Finally, this study also highlights the importance of ensuring a constant supply of food for all experimental animals immediately prior to surgery.

6.5.4. Summary

The overall research objective of this chapter was to investigate the potential modulation of Sirt-3 as a cardioprotective intervention to reduce myocardial infarction upon ischaemia-reperfusion. The initial *in vitro* pilot studies undertaken within our laboratory using the cardiac HL-1 cell line showed that overexpression of Sirt-3 conferred several beneficial effects that may ultimately protect against ischaemia-reperfusion injury. This chapter aimed to further examine the potential therapeutic effects of modulation of Sirt-3 activity *in vivo*. The key findings of this chapter are summarised below:

(1) Genetic ablation of Sirt-3 did not affect the susceptibility of mice to myocardial infarction upon ischaemia-reperfusion. This was investigated following a standard *in vivo* ischaemic insult (30 minutes), widely used in this thesis, and also following an extended ischaemic insult (45 minutes). Since Sirt-3 genetic ablation did not affect infarct size, this study appears to suggest that Sirt-3 does not mediate a critical role in the pathophysiology of myocardial ischaemia-reperfusion injury.

(2) The *in vivo* recovery surgical protocol employed here evoked a significant increase in mitochondrial Sirt-3 protein levels. Since this increase was seen following only 30 minutes of myocardial ischaemia, it suggests that post-translational processing or cellular translocation provides a means by which mitochondrial Sirt-3 protein levels can be rapidly regulated in response to stress.

    The sham recovery surgical procedure with no myocardial ischaemia-reperfusion also significantly increased mitochondrial Sirt-3 protein levels, indicating that some element of this procedure elicits a significant stress response. This was not specifically investigated here; however, this provides an important consideration for the interpretation of future studies using this *in vivo* model.

(3) Fasting of wildtype mice increased Sirt-3 protein expression in the heart. Interestingly, wildtype fasted mice were more susceptible to myocardial infarction than fed animals, where this effect is confirmed to be the result of Sirt-3 activity since fasting did not affect infarct size in Sirt-3 knockout mice.

    This study suggests that under certain conditions, Sirt-3 may mediate a detrimental response to myocardial ischaemia-reperfusion, whereby Sirt-3 inhibition may provide a potential therapeutic target for cardioprotective benefit in this setting.

CHAPTER 7: INVESTIGATION OF THE ROLE OF DJ-1 IN THE PATHOPHYSIOLOGY OF ISCHAEMIA-REPERFUSION INJURY

7.1. Introduction

DJ-1 is another potentially important protein associated with the preservation of mitochondrial function. DJ-1 (also known as PARK7) is a highly conserved and widely expressed mitochondrial protein that has been implicated in numerous pathologies, notably in neurodegeneration where mutations in DJ-1 cause an early-onset heritable form of Parkinson's disease (Bonifati et al., 2003). Several studies have elucidated important roles for DJ-1 in the brain including sensing oxidative stress, scavenging ROS (Kinumi et al., 2004; Taira et al., 2004; Zhang et al., 2005) and preserving mitochondrial function (Canet-Aviles et al., 2004; Zhang et al., 2005; Krebiehl et al., 2010).

Given these crucial roles of DJ-1 in maintaining physiological mitochondrial function, modulation of DJ-1 represents a potential therapeutic target for pathological conditions involving mitochondrial dysfunction, including ischaemia-reperfusion injury (as detailed in chapter 1; see 1.4.3). Indeed, DJ-1 genetic ablation has been shown to render the brain more susceptible to ischaemia-reperfusion in an *in vivo* model of stroke (Aleyasin et al., 2007). Although DJ-1 protein is expressed in the heart (Bonifati et al., 2003), its roles in normal cardiomyocyte mitochondrial function and its potential importance in the pathophysiology of myocardial ischaemia-reperfusion are not well understood. The studies presented in this chapter aimed to examine the role of DJ-1 in myocardial infarction upon ischaemia-reperfusion to evaluate the potential future modulation of DJ-1 as a therapeutic target for cardioprotective in this setting.

Investigation of DJ-1 in myocardial ischaemia-reperfusion presented in this chapter was undertaken as a separate study to complement the in vitro investigation of DJ-1 by Ms U. Mukherjee within our laboratory; all in vivo data presented here was conducted independently and all references to existing data and technical assistance are duly acknowledged. The in vitro data presented in the introductory sections was prepared from the manuscript of this publication (Dongworth and Mukherjee et al.; in submission).

7.2. Research objective and aims

The main objective of this chapter was to investigate the role of mitochondrial DJ-1 in the heart, specifically its potential role in the pathophysiology of ischaemia-reperfusion. The principal research aims to achieve this objective were:

(1) Investigate the role of DJ-1 in normal cardiac physiology and function;

(2) Investigate the role of DJ-1 in the pathophysiology of myocardial ischaemia-reperfusion.

7.3. Aim 1: Investigate role of DJ-1 in cardiac physiology

7.3.1. Background and preliminary data

Previous studies investigating the role of DJ-1 have primarily examined its role in the brain; specifically in the development of Parkinson's disease upon mutation of the DJ-1 gene resulting in non-functional forms of the DJ-1 protein (Bonifati et al., 2003). As such, previous evaluations of the effects of global genetic ablation of DJ-1 have focused on the brain and the neurological symptoms displayed by these animals. DJ-1 knockout animals display no morphological differences in nervous system structure, including the brain itself (Yamaguchi and Shen, 2007). Furthermore, despite the reported roles of DJ-1 as an important sensor of oxidative stress and ROS scavenger, mitochondrial antioxidant protein levels are normal in young DJ-1 knockout mice (12-16 weeks); although it should be noted that mitochondrial MnSOD and glutathione peroxidase were upregulated in aged DJ-1 knockout animals (Andres-Mateos et al., 2007). Given the apparently normal neurological phenotype of DJ-1 knockout mice, it is pertinent to evaluate the role of DJ-1 in the heart, in which this protein is also highly expressed, to determine its roles in cardiac physiology and pathophysiology.

Initial studies undertaken within our laboratory investigated the role of DJ-1 in our well-established *in vitro* models of ischaemia-reperfusion injury using the HL-1 cardiac cell line. These studies demonstrated that at baseline, overexpression of DJ-1 increased the extent of mitochondrial fusion (Figure 6.1; experiment performed by Ms U. Mukherjee). Importantly, overexpression of mutant inactive forms of DJ-1 protein, DJ-1 L166P (which is unable to dimerise) and DJ-1 C106A (in which Cys106 is resistant to oxidation) did not confer this improved mitochondrial phenotype, thereby confirming that this beneficial phenotype is mediated by DJ-1 (Figure 6.1; experiment performed by Ms U. Mukherjee).

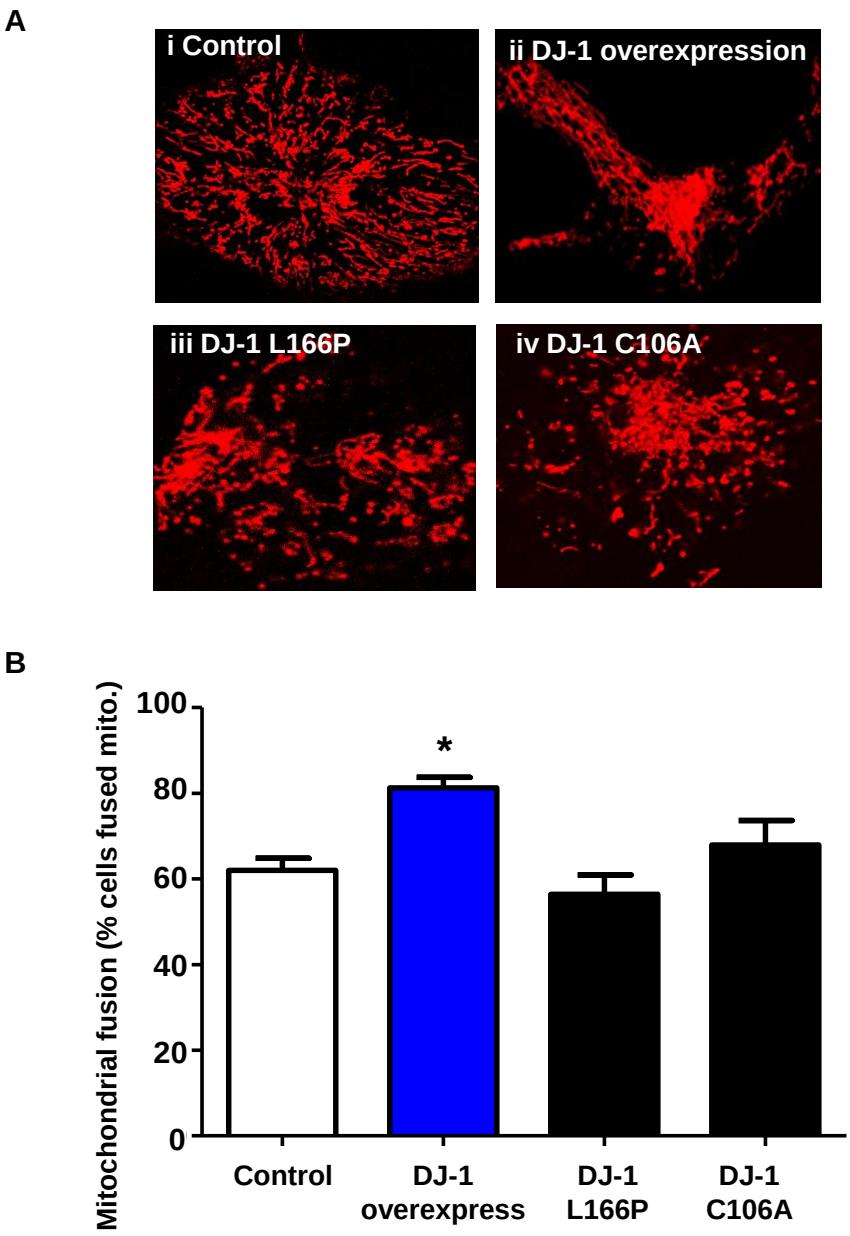

Figure 7.1: Initial *in vitro* investigation of the role of DJ-1
Initial *in vitro* studies performed by Ms U. Mukherjee to investigate the role of DJ-1 in the basal mitochondrial phenotype in the HL-1 cell model of mitochondrial morphology. HL-1 cells were transfected with the control empty plasmid (white bar), functional DJ-1 (blue bar) and mutant forms of DJ-1: L166P and C106A (black bars). A) Representative images of mitochondrial morphology assessed by transfection of mitochondria with mitochondrial red fluorescent protein (mtRFP): i) Empty vector: baseline morphology; ii) DJ-1 overexpression: predominantly fused mitochondria, iii) L166P mutant DJ-1: largely normal morphology and iv) C106A mutant DJ-1: largely normal morphology. D) Quantification of mitochondrial morphology. Statistical significance was assessed by one-way ANOVA, *P<0.05; n=6/group.

Experiments performed by Ms U. Mukherjee. Detailed methods are presented by a previous publication by our laboratory (Ong et al., 2010).

This study suggests that DJ-1 mediates an important regulatory role affecting mitochondrial morphology at baseline in this cardiac cell line; therefore suggesting that DJ-1 may confer a similar beneficial role *in* vivo. Unfortunately, attempts to develop an *in vitro* model of genetic knockdown of DJ-1 using lentiviral transfection of short-hairpin (sh) RNA did not sufficiently reduce DJ-1 protein levels to warrant further investigation for comparison with the *in vivo* knockout model; discussed subsequently (see 7.4).

The first section of this chapter aimed to investigate whether genetic ablation of DJ-1 resulted in any overt cardiac phenotype at baseline, whereby the *in vitro* data above led us to suggest that DJ-1 knockout mice would have some impairment of cardiac function.

Aim 1: This section aimed to investigate the effect of DJ-1 genetic ablation on cardiac physiology and function. It was hypothesised that DJ-1 knockout mice would display:

(1) Cardiac function: Unaffected baseline cardiac function but impaired stress response;

(2) Mitochondrial morphology: More fragmented mitochondria at baseline;

(3) Myocardial ATP levels: Lowered myocardial ATP levels at baseline.

7.3.2. Detailed methods

i DJ-1 global knockout mice

The DJ-1 global genetic knockout mouse model used here was obtained from Dr F Giorgini and Dr M Repici (University of Leicester, UK) from the initial colony created by Goldberg et al. (2005). Genetic ablation of DJ-1 was achieved by deletion of exon-2 of the endogenous *PARK7* gene using standard transgenic methods described in chapter 3 (see 3.1.2). The resulting DJ-1 knockout mice were backcrossed onto a C57BL/6 genetic background (Goldberg et al., 2005). DJ-1 knockout mice are also commercially available from Jackson Laboratories, USA (strain Cg-*Park7*$^{tm/Shn}$/J; stock 006577).

Colony maintenance: DJ-1 global knockout mice obtained from Dr F Giorgini and Dr M Repici (University of Leicester, UK) were used to establish a transgenic colony within our laboratory. Establishment and breeding of the DJ-1 knockout mouse colony was undertaken in collaboration with Ms U. Mukherjee and technical staff at University College London. DJ-1 knockout mice were crossed with commercially available C57BL/6 mice (Charles River Laboratories, UK) to generate a stock of DJ-1 heterozygous mice that were used to maintain the DJ-1 colony (Figure 5.2 B). The final colony was maintained as crosses of DJ-1 heterozygotes to produce DJ-1 WT, HET and KO mice.

All experiments were performed on DJ-1 knockout and wildtype true littermate controls. Due to time restraints and the poor breeding of these mice, experiments were conducted on mixed groups of male and female mice with equal numbers of males and females within and between all groups. It was not expected that there would be any confounding effects of sex on the data presented here since it was previously shown in this thesis that gender did not significantly affect the infarct sizes observed in this model (see chapter 4; see 4.5.3 iv). All mice used in these experiments were aged 12-16 weeks.

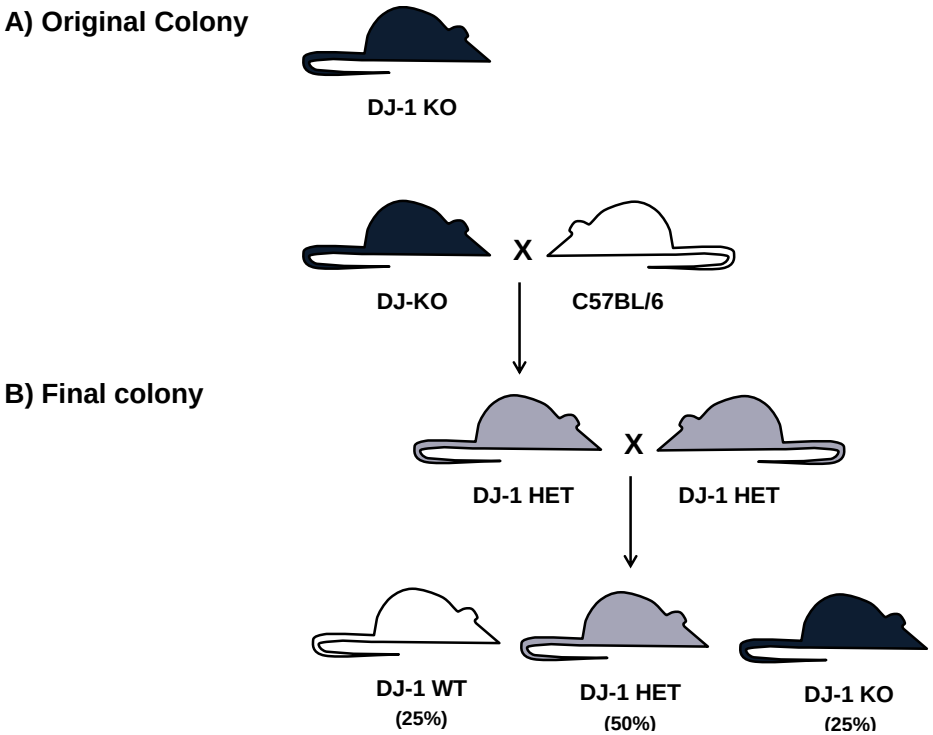

Figure 7.2: DJ-1 colony establishment and maintenance
Establishment and breeding of the DJ-1 KO mouse colony. A) Original colony: DJ-1 KO mice were crossed with commercially available C57BL/6 mice to create a stock of DJ-1 HETs. B) Final colony: was maintained as DJ-1 HET x HET crosses to produce progeny of DJ-1 WT, KO and HET (in accordance with expected Mendelian ratios indicated in brackets).

Establishment and initial breeding of this colony was undertaken in collaboration with Ms U. Mukherjee and technical staff at University College London, UK.

ii Genotyping for DJ-1 genetic ablation

The genotyping method used for these animals was based on that described in chapter 3 (see 3.1.2 iii). DNA samples were prepared from ear biopsies processed within 7 days exactly as described previously. The PCR reaction mix was based on the standard reaction optimised in this thesis. The PCR primers and thermocycling conditions used in this reaction were informed by Dr F Giorgini and Dr M Repici (personal communication) and are described in Table 7.1. This reaction yielded DNA products of 500 bp and 250 bp corresponding to knockout and wildtype bands respectively (Figure 7.3).

A) DJ-1 PCR primer sequences

PRIMER	SEQUENCE	PROPERTIES	
		Length	Tm (ºC)
Primer 1 / WT forward	5'-GATCCAGTGCTCTTAGCCACAGACTA-3'	26	64.8
Primer 2 / WT reverse	5'-GCATGACATCCACAGGAATCACT-3'	23	60.6
Primer 3 / KO reverse	5'-GGATCAATTCTCTAGAGCTCGCTGATCA-3'	28	65.1

B) DJ-1 PCR reaction mix

REAGENT	VOLUME/SAMPLE (µl)	FINAL CONCENTRATION
Qiagen 10X PCR Buffer	2.0	1X
10 mM dNTPs	0.8	400 µM
Primer 1 100 µM	1	5 µM
Primer 2 100 µM	1	5 µM
Primer 3 100µM	1	5 µM
Taq polymerase	0.3	-
Autoclaved distilled water	12.9	-
Crude DNA lysate †	1.0	-
TOTAL VOLUME/SAMPLE (µl)	**20.0**	

C) DJ-1 PCR thermocycling parameters

PCR STAGE	TEMPERATURE AND DURATION	PCR DESCRIPTION
1	94 ºC for 4 minutes	Hot start
2	94 ºC for 1 minute	DNA separation
3	65 ºC for 1minute	Primer annealing
4	72 ºC for 1 minute	DNA synthesis
5	Go to step 2 for 35 cycles	DNA synthesis
6	72 ºC for 7 minutes	Final extension
7	4 ºC for ever	Intermediate storage

Table 7.1: DJ-1 global knockout mouse genotyping protocol
A) DJ-1 primer sequences and properties. B) A single master mix was made based on the Qiagen *Taq* kit (Qiagen, UK) and aliquots taken for each reaction. † 1 µl crude DNA lysate was added. C) PCR was undertaken by a thermal cycler (MJ Research, Canada).

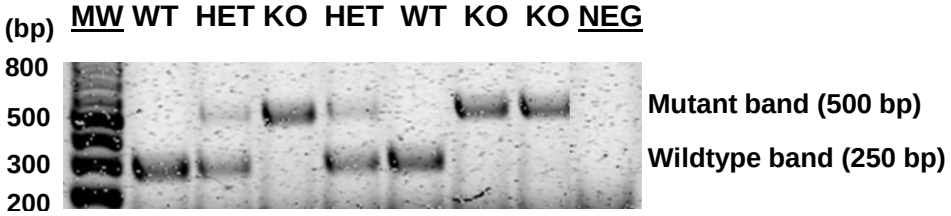

Figure 7.3: DJ-1 global transgenic colony representative genotyping result
The genotype of each animal was determined by the presence or absence of the expected PCR products by comparison to molecular weight ladder (lane 1): WT 250 bp band only, KO 500 bp band only and HET both bands (as annotated above the gel). A negative control (NEG) was run to ensure there was no external DNA contamination.

iii Cardiac phenotyping by echocardiography

Echocardiography evaluation of animals was undertaken in collaboration with Dr A. Dyson (Department of Medicine, University College London, UK).

Cardiac function of DJ-1 knockout and wildtype control mice was assessed using a standard small animal echocardiography setup as described in chapter 3 (see 3.7).

Echocardiography setup: The echocardiography setup was exactly as described previously in section 3.7. Echocardiography measurements were taken according to the parameters detailed previously and summarised in Table 7.2.

ENDPOINT	ECHOCARDIOGRAPHIC CALCULATION
Anatomical measurements	Left ventricle internal dimension and thickness of anterior and posterior walls; determined from parasternal short-axis view at papillary muscle.
Peak aortic blood flow velocity	Determined by pulsed-wave Doppler in the aortic arch where the direction of blow flow was confirmed by colour Doppler imaging. Peak velocity calculated as mean maximum of 6 velocity-time traces.
Heart rate (BPM)	Calculated as mean time between 6 Doppler velocity-time traces.
Stoke volume (µl)	Calculated as: (Velocity time integral * vessel cross section area). Vessel cross sectional area calculated as: (π x [0.5 x diameter]^2); where vessel diameter was assumed to be 1.34mm †
Cardiac output (ml/min)	Calculated as: (Heart rate * stroke volume)
Fractional shortening (%)	Calculated as: [(LV end diastolic diameter - LV end systolic diameter)/(LV end diastolic volume)]*100

Table 7.2: Echocardiographic measurements of cardiac structure and function
Summary of echocardiographic measurements of left ventricular ED and ES dimensions and measurements to assess principal features of cardiac function. † Based on previous studies.

Echocardiographic images and raw data analysis were performed by Dr A. Dyson.

Isoproterenol challenge: An isoproterenol cardiac stress protocol was investigated to induce inotropic and chronotropic stimulation of the heart to evaluate potential differences in cardiac function that may not be evident at baseline.

Optimisation of isoproterenol protocol – The isoproterenol dosing protocol used here was optimised to determine the time-course and magnitude of heart rate increase in response to different isoproterenol doses. C57BL/6 mice were anaesthetised with 1.8-2.0% isoflurane vaporised in oxygen (1.5 L/minute) and placed in the supine position. Heart rate was continually recorded using the standard ECG setup described previously (Powerlab coupled to Chart 7 software, AD Instruments, UK) with automated calculation of heart rate. Upon a steady state of anaesthesia using a consistent and minimal dose of isoflurane, isoproterenol was given as an intraperitoneal bolus and heart rate monitored.

This preliminary study showed that in the small sample size tested, 1 ng/g and 2 ng/g isoproterenol initiated only a moderate heart rate increase assessed at 4 minutes post-administration. An optimal dose of 4ng/g elicited a significant heart rate increase that reached its maximum within approximately 4 minutes of dosing and plateaued for approximately 20 minutes. An example of the heart rate increase evoked by this isoproterenol dose is shown in Figure 7.4. It should however, be noted that the starting heart rates in the pilot investigations of the effect of isoproterenol were slightly lower than expected using isoflurane anaesthesia. An increased dose of 8 ng/g isoproterenol caused immediate death of 2 animals and was therefore not investigated further.

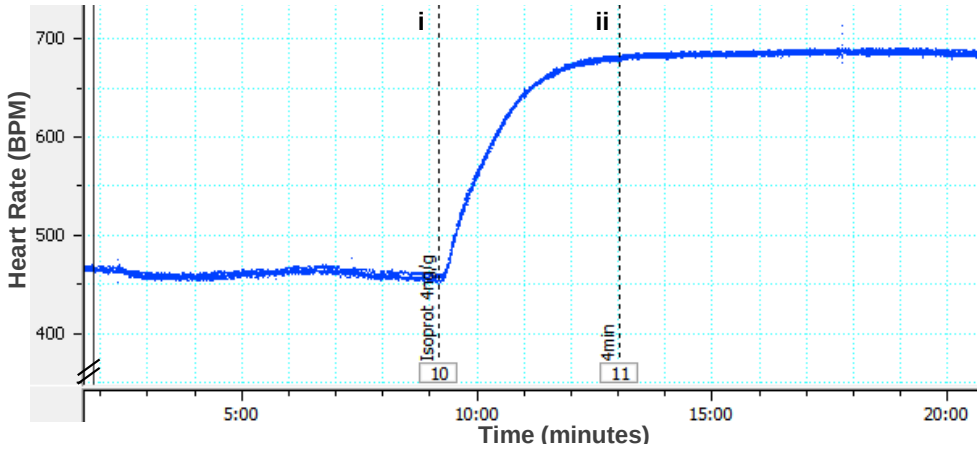

Figure 7.4: Representative heart rate increase in response to 4 ng/g isoproterenol
Example increase in heart rate following administration of 4 ng/g isoproterenol as a single intraperitoneal bolus at (i). Maximal increase in heart rate approximately 4 minutes post-administration. (ii) Plateau of increased heart rate continued for approximately 20 minutes (up to 8 minutes shown here). Heart rate increased from approximately 470 BPM to 600 BPM.

The final isoproterenol protocol using 4 ng/g was applied to all subsequent cardiac stress echocardiography measurements in this chapter. Isoproterenol (Sigma, UK) was dissolved in saline and 4 ng/g administered as a single intraperitoneal bolus (stock isoproterenol 1 µg/ml; administered 100 µl per 25 g mouse). Repeat echocardiographic measurements were started 4 minutes after administration of the isoproterenol bolus.

Statistical analysis: All values were calculated exactly as described in Table 7.2 and were reported as mean ± SEM. Data were analysed by one-way ANOVA and Bonferroni test using GraphPad Prism® version 5.0 (GraphPad Software, USA). Significance was reported where $P<0.05$ using standard coding.

iv Electron microscopy analysis of mitochondrial morphology

Preparation of heart samples: Hearts were prepared exactly as described in chapter 3 (see 3.6.1) using the non-recovery *in vivo* protocol. To assess baseline mitochondrial morphology, hearts were extracted from DJ-1 knockout and wildtype littermate control mice following 25 minutes *in vivo* stabilisation. Heart samples were processed for EM using a series of fixation and staining steps (described in chapter 3; see 3.6.2).
EM processing and imaging was undertaken by Mr M. Turmaine (Electron Microscopy Services Facility, University College London, UK).

Assessment of mitochondrial morphology: Mitochondrial morphology was evaluated by assessment of interfibrillar mitochondrial length compared to sarcomere length where normal mitochondrial length was considered to be approximately 1 sarcomere length. Mitochondria were defined as less than 1 sarcomere (fragmented), equal to 1 sarcomere (normal) or greater than 1 sarcomere (fused) as validated by Ong et al. (2010).
Analysis of images was performed by Dr S.B. Ong who was blinded to treatment groups.

The proportion of mitochondrial defined as normal, fragmented and fused was calculated for each heart (total of 500-600 mitochondria per heart) and expressed as mean percentage of mitochondria ± SEM. GraphPad Prism® version 5.0 (GraphPad Software, USA) was used to perform one-way ANOVA analysis and Bonferroni test comparing relevant groups. Statistical significance was reported where $P<0.05$.

v Myocardial ATP Assay

Baseline myocardial ATP levels were measured in left ventricle tissue samples from DJ-1 knockout and wildtype hearts using a standard commercial ATP assay kit.

Langendorff preparation of heart samples: Heart samples were prepared using Langendorff perfusion exactly as described previously (see 3.5.1); the total time from extraction to perfusion did not exceed 2 minutes 30 seconds for any heart preparation.

ATP luminescence assay: Myocardial ATP levels were measured using a commercial ATP assay kit (ATP Bioluminescent Assay Kit, Sigma, UK) in accordance with the manufacturer's instructions as detailed previously (see 3.5.2). Luminescence values were normalised to the average value recorded for wildtype control samples and expressed as a percentage of control ± SEM. All statistical analyses were completed using GraphPad Prism® version 5.0 (GraphPad Software, USA). Data were analysed by one-way ANOVA, followed by Bonferroni test comparing relevant groups. Statistical significance was reported where $P<0.05$.

7.3.3. Results

Following establishment of the DJ-1 colony within our laboratory, it was pertinent to investigate whether DJ-1 genetic ablation caused any overt cardiac phenotype.

i Cardiac phenotyping by echocardiography

Echocardiography of DJ-1 knockout and wildtype littermate control mice demonstrated no significant differences in anterior and posterior LV wall dimensions during systole or diastole. There were no significant differences in heart rate, fractional shortening cardiac output or stroke volume between DJ-1 knockout and wildtype littermates at baseline or following isoproterenol stress; representative M-mode echocardiography images are provided in Figure 7.5 and quantification of these endpoints summarised in Figure 7.6

Isoproterenol stress yielded a significant increase in heart rate in both DJ-1 knockout and wildtype mice (Figure 7.6 A: heart rate in BPM: DJ-1 WT baseline 498.5±19.9 and isoproterenol 620.2±10.2, n=6, $P<0.05$; DJ-1 KO baseline 505±25.9 and isoproterenol 628.8±17.0, n=5, $P<0.05$) and fractional shortening (Figure 7.6 B: fractional shortening % DJ-1 WT baseline 34.7±3.1 and isoproterenol 63.0±1.2, n=6, $P<0.05$; DJ-1 KO baseline 41.2±4.1 and isoproterenol 65.4±3.2, n=5, $P<0.05$). This demonstrated that this isoproterenol stress protocol evoked a sufficient cardiac stress response. There were no differences in stroke volume or cardiac output between DJ-1 knockout and wildtype mice at baseline or following isoproterenol challenge (Figure 7.6 C and D respectively).

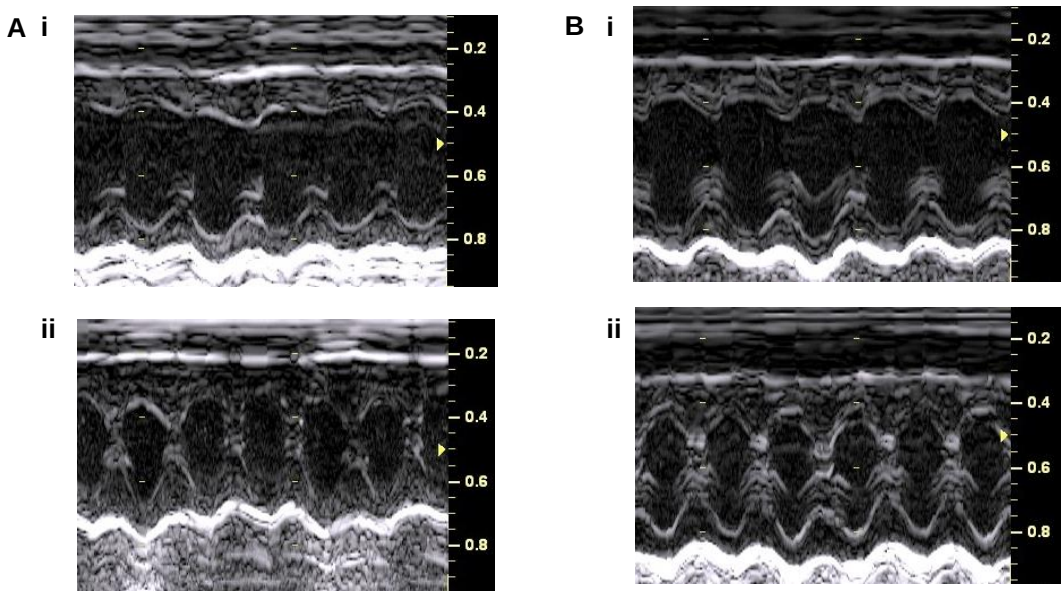

Figure 7.5: Representative echocardiographic phenotyping of DJ-1 knockout animals
Representative images from echocardiography of DJ-1 KO and WT littermate control mice at baseline and following isoproterenol treatment (4 ng/g, 4 minutes). A-B. Representative images of DJ-1 WT (A) and KO (B) at baseline (i) and following isoproterenol (ii).
Echocardiographic images and raw data analysis were performed by Dr A. Dyson.

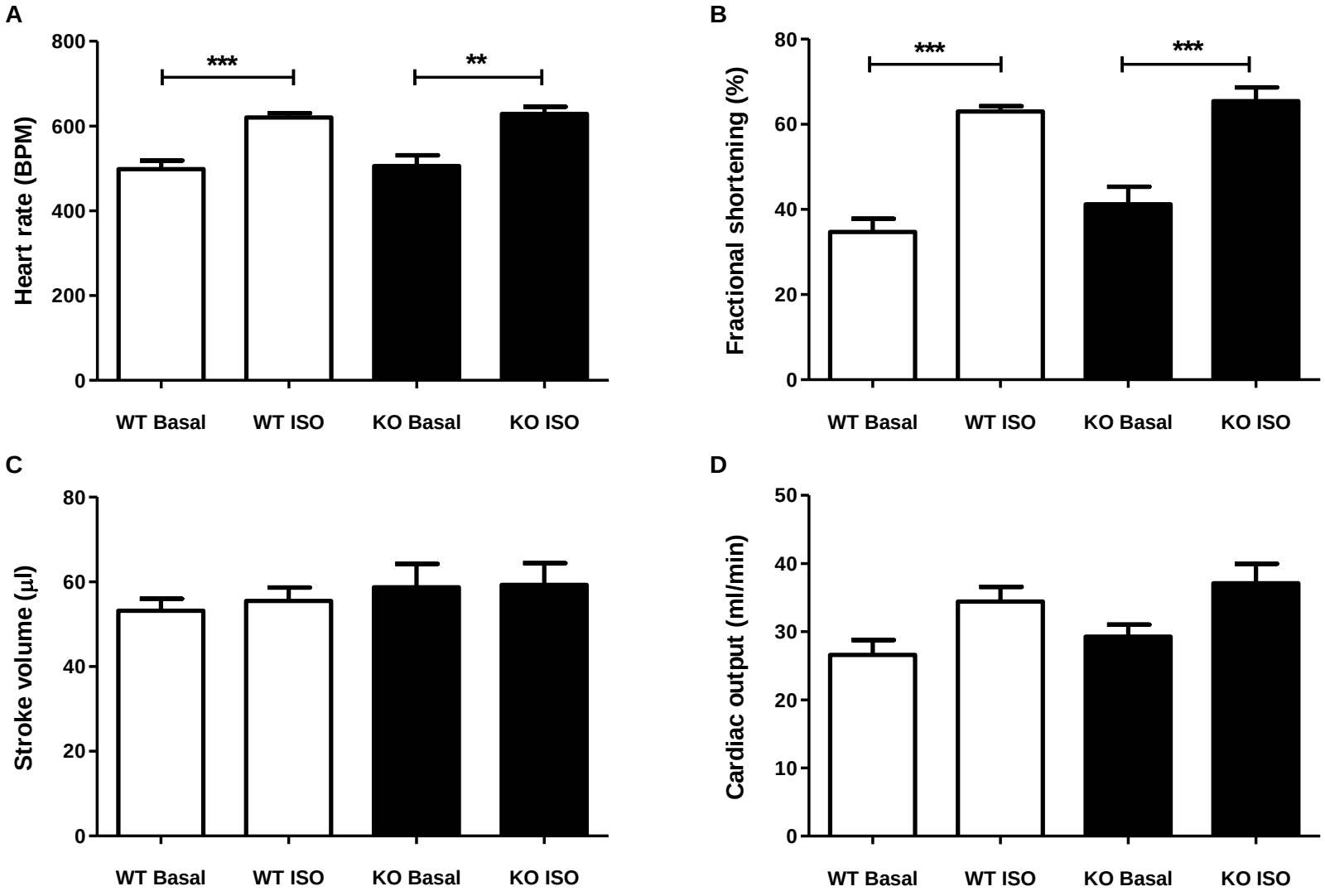

Figure 7.6: Echocardiographic phenotyping of DJ-1 knockout animals performed with Dr A. Dyson – Full legend is provided on the following page.

Figure 7.6: Echocardiographic phenotyping of DJ-1 knockout animals
A-D. Isoproterenol (4ng/g) treatment increased the heart rate and fractional shortening in DJ-1 knockout and wildtype mice (n≥5/group). Significance assessed by one-way ANOVA comparing WT Basal with WT ISO and KO Basal with KO ISO, P<0.05. (Figure on preceding page)
Echocardiographic images and raw data analysis were performed by Dr A. Dyson.

ii Mitochondrial morphology

Evaluation of the baseline mitochondrial morphology in DJ-1 knockout and wildtype littermate control hearts was performed using electron microscopy imaging of *ex vivo* prepared hearts. Classification of mitochondrial morphology in comparison to sarcomere length according to a protocol previously validated by our laboratory (Ong et al., 2010), demonstrated that there was a significant increase in the proportion of fragmented mitochondria in DJ-1 knockout hearts at baseline compared to wildtypes (Figure 7.7).

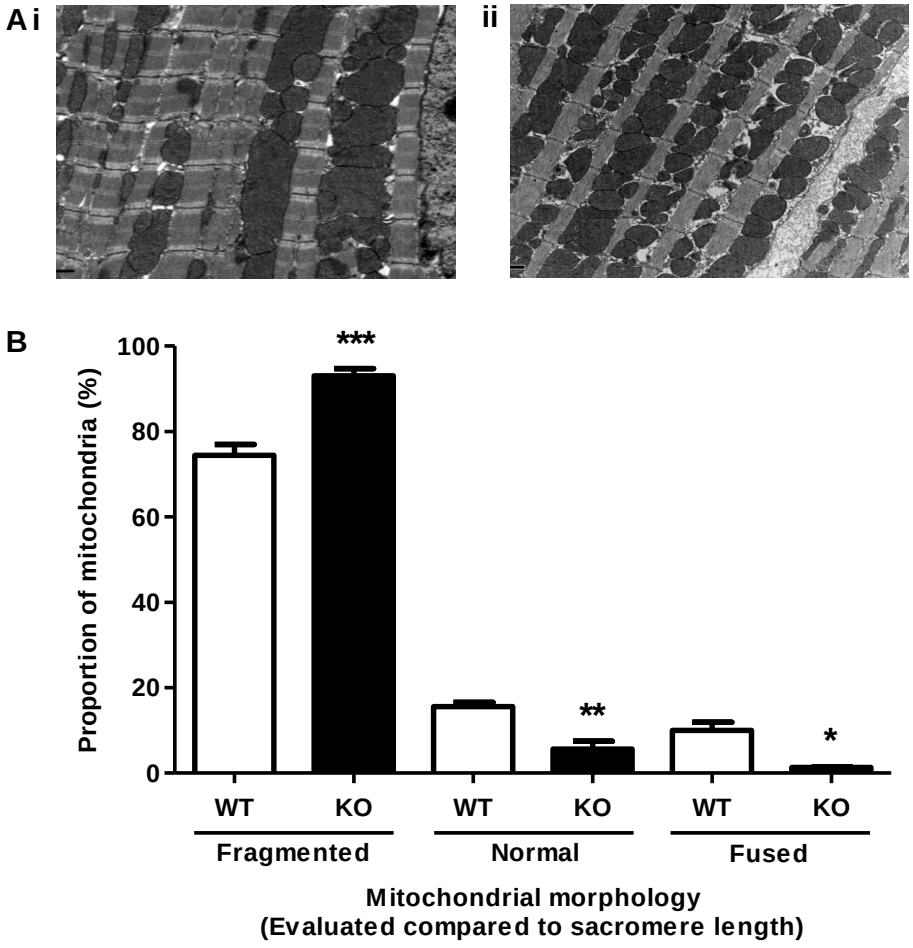

Figure 7.7: Baseline mitochondrial morphology in DJ-1 knockout hearts
Mitochondrial morphology at baseline in DJ-1 KO (n=5) and WT (n=3) hearts. A) Representative EM images showing mitochondrial morphology in i) DJ-1 WT and ii) DJ-1 KO heart samples. Mitochondrial morphology was evaluated against sarcomere length. There was a significant increase in the proportion of fragmented mitochondria in DJ-1 KO hearts compared to WT. Statistical significance assessed by one-way ANOVA comparing relevant groups; significance indicated for comparison of DJ-1 WT (white bar) and KO (black bar) for each classification.

iii Myocardial ATP levels

Assessment of myocardial ATP levels in Langendorff prepared hearts from DJ-1 knockout and wildtype littermate mice showed no significant difference between DJ-1 knockout and wildtype mice at baseline (Figure 4.19: n≥5/group, $^{NS}P>0.05$).

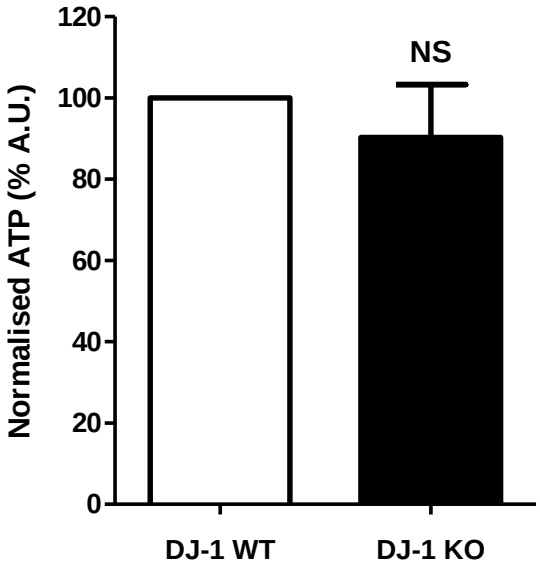

Figure 7.8: Myocardial ATP levels in DJ-1 knockout hearts
Hearts were extracted from DJ-1 KO (n=5/group) and WT littermate control (n=6/group) hearts and subjected to control or ischaemia on the Langendorff. ATP levels were measured using a luminescence kit and raw luminescence values normalised to DJ-1 WT control levels. There was no difference in ATP levels between DJ-1 KO and WT mice following control or ischaemic conditions. However, this ischaemic stimulus did not elicit a significant decrease in ATP levels. Statistical significance assessed by one-way ANOVA comparing all groups; n≥5/group, $^{NS}P>0.05$. (Extract from analysis presented in Figure 7.12 of all groups, hence the use of ANOVA test here)

These experiments appear to suggest that although DJ-1 affects cardiac mitochondrial morphology at baseline, it does not exert any substantial effect on myocardial phenotype with regards to mitochondrial function (inferred by ATP levels) or cardiac function.

7.4. Aim 2: Investigate role of DJ-1 in ischaemia-reperfusion injury

7.4.1. Background and preliminary data

The first section of this chapter demonstrated that although DJ-1 genetic ablation *in vivo* increased mitochondrial fragmentation, these animals did not display any overt cardiac phenotype at baseline. This next section aims to investigate the effect of DJ-1 knockout on the susceptibility of these animals to myocardial ischaemia-reperfusion.

As discussed above, DJ-1 has been implicated in the pathophysiology of neuronal ischaemia-reperfusion injury, where genetic ablation of DJ-1 rendered the brain more susceptible to infarction in an *in vivo* model of stroke (Aleyasin et al., 2007). This suggests that if DJ-1 plays a similar role in the heart, DJ-1 may represent a potential therapeutic target for protecting the heart against ischaemia-reperfusion injury.

Initial *in vitro* studies in our laboratory investigated the potential role of DJ-1 in cardiac ischaemia-reperfusion injury using a well-established model of HL-1 cardiac cell simulated ischaemia-reperfusion. This demonstrated a clear role of DJ-1 in the pathophysiology of cell survival, where overexpression of DJ-1 significantly increased cell survival (Figure 7.9 A; experiment performed by Ms U. Mukherjee). Interestingly, assessment of mitochondrial permeability transition *in vitro* in response to ROS-induced stress in HL-1 cells showed that overexpression of DJ-1 resulted in delayed mPTP opening (Figure 7.9 B; experiment performed by Ms U. Mukherjee). These *in vitro* studies provided an initial suggestion that DJ-1 mediates a similarly protective role against ischaemia-reperfusion in the heart as previously demonstrated in the brain.

To further investigate the cardioprotective role of DJ-1, additional studies were undertaken to examine the effect of DJ-1 knockout in native heart tissue.

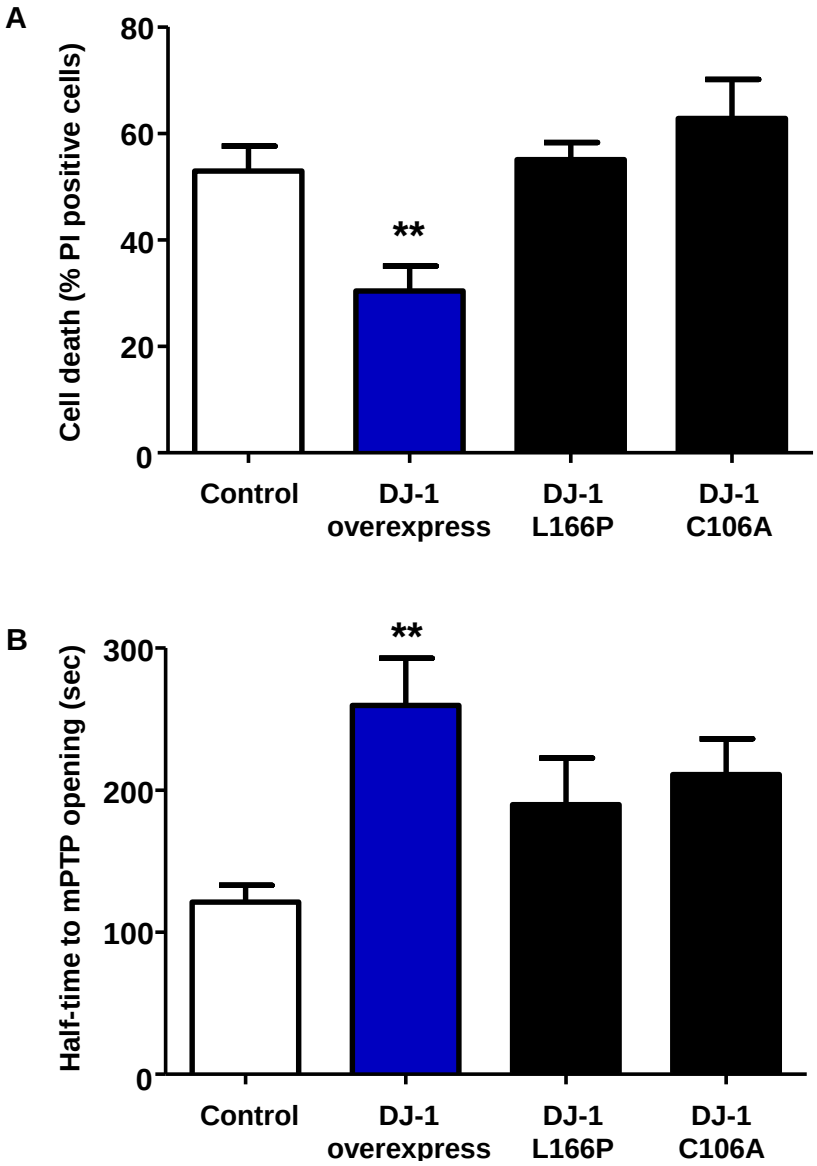

Figure 7.9: Initial *in vitro* investigation of the role of DJ-1 in ischaemia-reperfusion
Initial *in vitro* studies performed by Ms U. Mukherjee to investigate the role of DJ-1 in ischaemia-reperfusion in HL-1 cardiac cells. HL-1 cells were transfected with the control empty plasmid (white bars), functional DJ-1 (blue bars) and mutant DJ-1 (black bars): L116P and C106A.
A) Cell death: susceptibility of HL-1 cells to cell death following simulated ischaemia-reperfusion (12 hours hypoxia followed by 1 hour re-oxygenation) assessed as the percentage of transfected cells (taken a total cell number) exhibiting propidium iodide (PI) staining using fluorescence microscopy. Cell death is significantly reduced by overexpression of DJ-1. Statistical significance assessed by one-way ANOVA, **p<0.01; n=5/group (30 random fields per sample).
B) Time to mPTP opening: assessed using the TMRM laser-induced ROS model of mPTP opening; described briefly in chapter 6 (see 6.3.1). Time to mPTP opening was measured as the time to half maximum cytosolic TMRM fluorescence in seconds. mPTP opening was delayed by overexpression of DJ-1. Significance was assessed by one-way ANOVA, n=6/group.

Experiments presented in this figure were performed by Ms U. Mukherjee. Detailed methods are presented by a previous publication by our laboratory (Ong et al., 2010).

Aim 2: The second part of this chapter investigated the effect of global genetic ablation of DJ-1 on the susceptibility to myocardial infarction upon ischaemia-reperfusion. The central hypothesis in relation to this research objective was:

(1) DJ-1 genetic ablation would significantly increase the susceptibility to myocardial ischaemia-reperfusion injury.

It was hypothesised that upon myocardial ischaemia, DJ-1 knockout mice would display:

(1) Mitochondrial morphology: Increased mitochondrial fragmentation upon ischaemia;

(2) Myocardial ATP levels: Further lowered myocardial ATP levels upon ischaemia;

(3) Infarct size: Increased myocardial infarct size following ischaemia-reperfusion.

7.4.2. Detailed methods

The methods used in this section were largely based on those described in the preceding section (section 7.3.2) with additional experimental details provided here.

i Electron microscopy analysis of mitochondrial morphology

Preparation of heart samples: Hearts were prepared exactly as described above (see 7.3.2 iv). To assess mitochondrial morphology following myocardial ischaemia, animals were subjected to 20 minutes *in vivo* myocardial ischaemia by occlusion of the LAD; a summary of the non-recovery *in vivo* procedure used here is provided in chapter 3 (see 3.6.1; Figure 3.12). Hearts were extracted at the end of the defined ischaemia period with the occluding snare system still in place. Immediately following cannulation of the aorta, the snare system was released to allow complete perfusion and washout of the heart. Processing and EM analysis was exactly as described above (see 7.3.2 iv).

EM imaging was undertaken by Mr M. Turmaine (Electron Microscopy Services Facility, University College London, UK) and analysis of EM images was performed by Dr S.B. Ong (formerly of Hatter Cardiovascular Institute, University College London, UK).

ii Myocardial ATP Assay

Myocardial ATP levels were measured in left ventricle tissue samples isolated from DJ-1 knockout and wildtype hearts following a sublethal ischaemic insult.

Langendorff preparation of heart samples: Hearts were extracted from DJ-1 knockout and wildtype littermates and perfused on the Langendorff apparatus exactly as described above. Following 10 minutes stabilisation perfusion, myocardial ischaemia was simulated by closure of the flow regulator tap to stop perfusion for 20 minutes (see 3.5.1, Figure 3.16). Successful ischaemia was confirmed by lack of effluent from the heart and impaired contractile function. Processing of heart samples and the ATP assay were performed and analysed exactly as described above (see 7.3.2 v).

iii Myocardial ischaemia-reperfusion injury

Assessment of the susceptibility to myocardial infarction following ischaemia-reperfusion was performed in DJ-1 knockout and wildtype animals subjected to the *in vivo* recovery model of ischaemia-reperfusion injury developed in chapter 4 of this thesis.

Surgical protocol: The susceptibility of DJ-1 knockout and wildtype littermate control animals was assessed following 45 minutes ischaemia and 24 hours reperfusion (Figure 7.10 A). A standard IPC protocol of one cycle of 5 minutes ischaemia and 5 minutes reperfusion was also investigated (Figure 7.10 B). The increased ischaemic duration used in this study meant that the total anaesthetic duration of this surgical protocol was slightly extended in comparison to the standard protocol investigated previously (70 minutes duration compared to standard 55 minute duration).

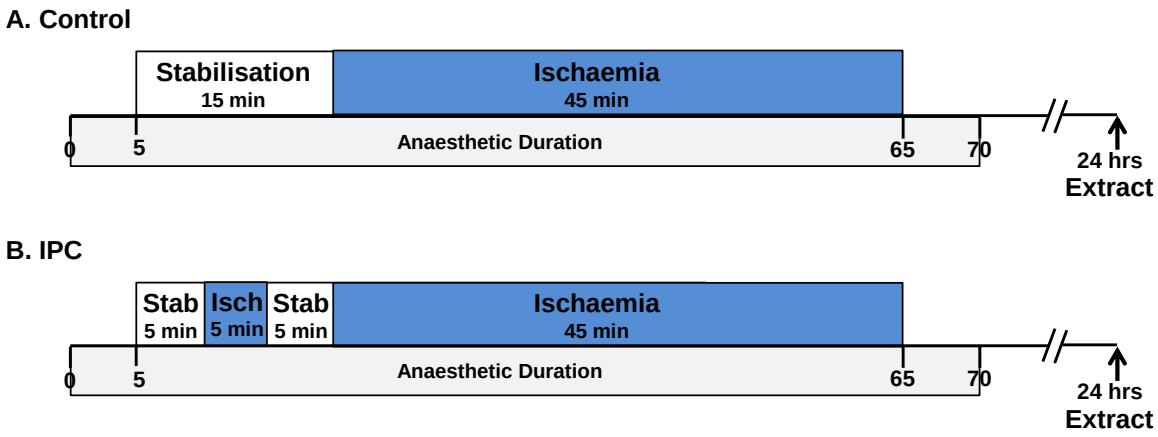

Figure 7.10: DJ-1 ischaemia-reperfusion *in vivo* recovery protocol
DJ-1 KO mice and true WT littermate controls were randomised to control or IPC protocols. A) Control: 15 minutes stabilisation, 45 minute ischaemia and 24 hours reperfusion. B) IPC: 5 minutes stabilisation, one cycle IPC consisting of 5 minutes ischaemia and 5 minutes reperfusion prior to the main ischaemic insult of 45 minutes followed by 24 hours reperfusion.

Endpoint 1 – IS/AAR%: The primary endpoint assessed in this study was infarct size by *ex vivo* histological staining using TTC and Evans blue staining, exactly as described previously, to calculate the infarct size as a percentage of AAR. The pre-defined surgical and myocardial AAR exclusion criteria were applied to this dataset (see 3.2.4).

All infarct size and AAR values are presented as mean ± SEM. All statistical analysis was completed using GraphPad Prism® version 5.0 (GraphPad Software, USA). Where two groups were compared, data were analysed using an unpaired t-test. Where more than two groups were compared, data were analysed by one-way ANOVA, followed by Bonferroni test comparing relevant columns of data. Statistical significance was reported where $P<0.05$ using standard significance coding.

Endpoint 2 – Survival: Survival rates of DJ-1 mice subjected to this surgical protocol were recorded and probable cause of death determined by post-mortem analysis. Kaplan-Meier survival plots were plotted using GraphPad Prism® version 5.0 (GraphPad Software, USA). Statistical significance was analysed by log-rank tests. There was no statistical significance in survival between groups presented in this chapter.

7.4.3. Results

Given the suggestion that DJ-1 overexpression *in vitro* in HL-1 cardiac cells protected against simulated ischaemia-reperfusion and delayed ROS-induced mPTP opening (summarised in Figure 7.9), the effect of DJ-1 genetic ablation was investigated *in vivo*.

i Mitochondrial morphology

Evaluation of the mitochondrial morphology in DJ-1 knockout and wildtype control mice following 20 minutes of *in vivo* ischaemia showed that there was no longer any significant difference in mitochondrial morphology between these animals (Figure 7.11).

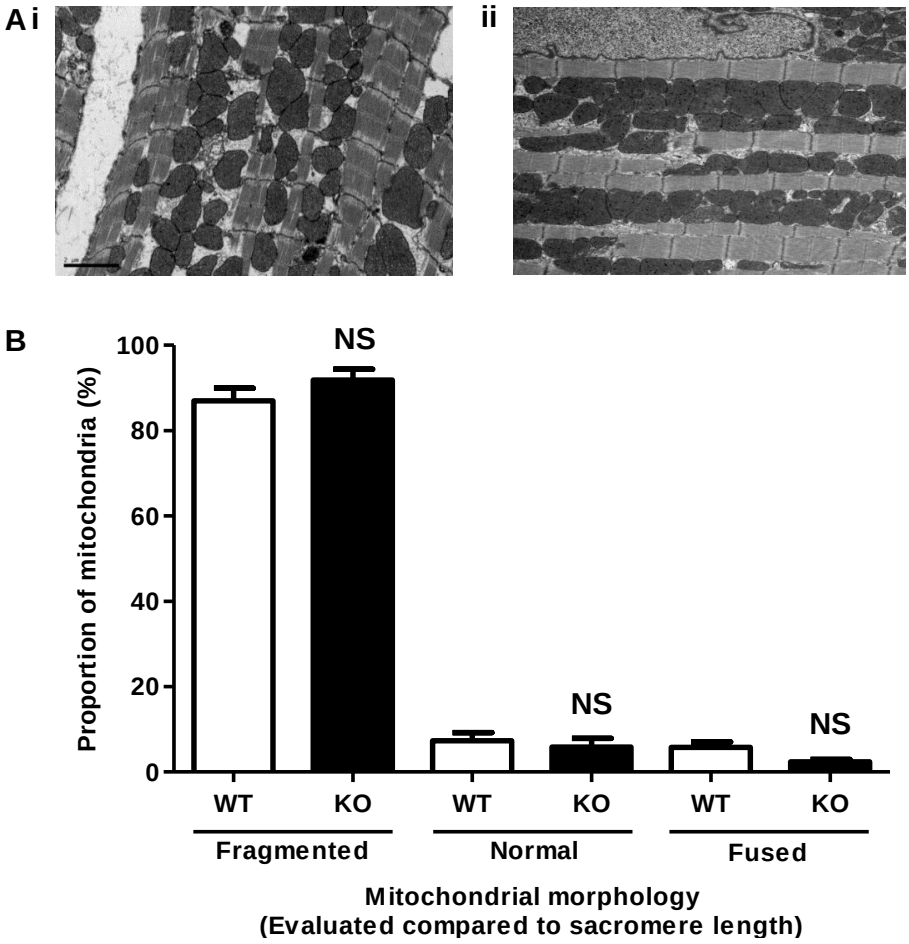

Figure 7.11: Mitochondrial morphology in DJ-1 knockout hearts following ischaemia
Assessment of mitochondrial morphology following 20 minutes *in vivo* myocardial ischaemia in heart samples from DJ-1 KO (n=5) and WT littermate controls (n=3). A) Representative EM images showing mitochondrial morphology in i) DJ-1 WT and ii) DJ-1 KO hearts following ischaemia. B) Mitochondrial morphology was determined by EM analysis for comparison of mitochondrial length against sarcomere length. There was no significant difference in mitochondrial morphology between DJ-1 KO and WT hearts following ischaemia; significance indicated for comparison of DJ-1 WT (white bar) and KO (black bar) for each classification.

ii Myocardial ATP levels

To assess the effect of ischaemia on myocardial ATP levels, Langendorff prepared hearts were subjected to 20 minutes global ischaemia and the resulting ATP levels assessed in left ventricle samples. However, this ischaemic protocol did not significantly reduce ATP levels in wildtype hearts (Figure 7.12: n≥5/group, $^{NS}P>0.05$) meaning that any comparison of DJ-1 knockout and wildtype hearts after ischaemia would be of limited value for assessing the effect of DJ-1 genetic ablation on myocardial ATP levels.

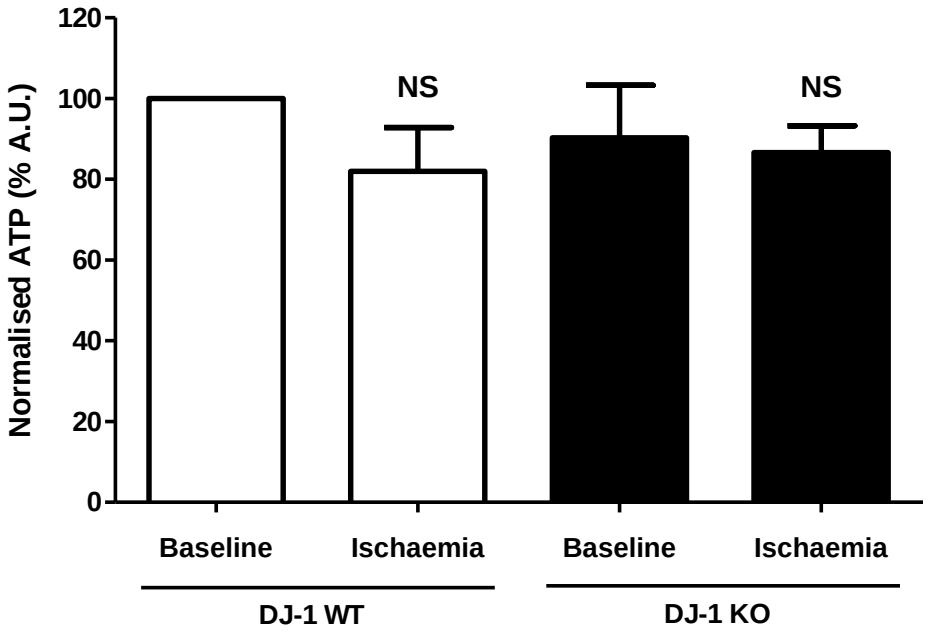

Figure 7.12: Myocardial ATP levels in DJ-1 knockout hearts
Hearts were extracted from DJ-1 KO (n=5/group) and wildtype littermates (n=6/group) and subjected to control or ischaemia on the Langendorff. ATP levels were measured using an ATP kit and raw luminescence values normalised to DJ-1 WT control levels. There was no difference in ATP levels between DJ-1 KO and WT mice following control or ischaemic conditions. However, this ischaemic stimulus did not elicit a significant decrease in ATP levels. Statistical significance assessed by one-way ANOVA comparing all groups; n≥5/group, $^{NS}P>0.05$.

The effect of myocardial ischaemia on ATP levels was not investigated further since an extended duration of ischaemia would be expected to induce a differential degree of cell death (based on the preliminary role of DJ-1 from the previous *in vitro* studies and subsequently confirmed below in section iii). Given the potential difference in cell death in DJ-1 wildtype and knockout hearts subjected to an extended ischaemic insult, it would not have been valid to evaluate mitochondrial function following a long ischaemic insult.

iii Susceptibility to ischaemia-reperfusion injury

The effect of DJ-1 knockout on the susceptibility to myocardial infarction upon ischaemia-reperfusion had not previously been investigated *in vivo*. DJ-1 wildtype and knockout mice were subjected to a modified protocol of 45 minutes ischaemia and 24 hours reperfusion. DJ-1 knockout mice exhibited significantly larger infarct sizes as compared to DJ-1 wildtype littermate controls (Figure 5.5: IS/AAR% DJ-1 WT 37.7±4.0 versus DJ-1 KO 50.9±3.5; n=8/group, *P<0.05). There was no significant difference in AAR (AAR/LV% DJ-1 WT 54.0±3.2 versus DJ-1 KO 48.2±1.9; n=8/group, ^{NS}P>0.05) or survival (% survival to 24 hours: DJ-1 WT 80%, n=10 versus DJ-1 WT 72.7%, n=11).

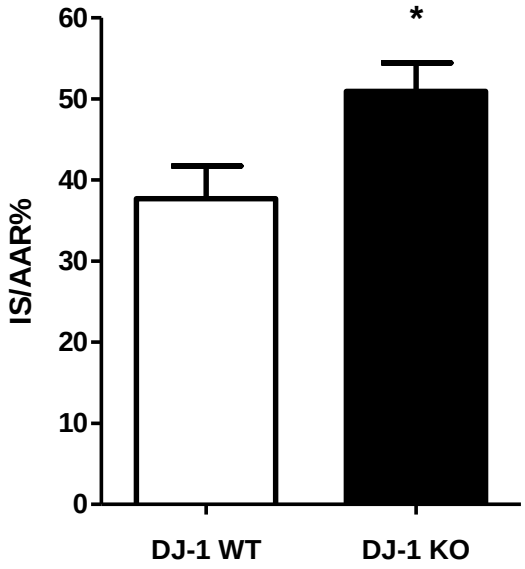

Figure 7.13: Infarct size in DJ-1 wildtype and knockout mice
Infarct size following 45 minutes ischaemia and 24 hours reperfusion in DJ-1 KO and WT littermate control animals. DJ-1 KO mice demonstrated significantly larger infarct sizes compared to DJ-1 WT controls: IS/AAR% DJ-1 WT 37.7±4.0 versus DJ-1 KO 50.9±3.5, n=8/group. Statistical significance assessed by unpaired t-test, *P<0.05.

Further to this, the susceptibility to cardioprotection by a standard IPC protocol was investigated in these animals. As expected, IPC significantly reduced myocardial infarct size in DJ-1 wildtype mice (Figure 4.12 A: IS/AAR% DJ-1 WT control 37.7±4.0 versus IPC 21.8±2.3, n=8/group, *P<0.05), thereby serving as a positive control for cardioprotection in this model. There was no significant difference in AAR (AAR/LV% DJ-1 WT control 54.0±3.2 versus DJ WT IPC 50.5±3.1, n=8/group, ^{NS}P>0.05) or survival (% survival to 24 hours: DJ-1 WT control 80%, n=10 versus DJ-1 WT IPC 80%, n=10).

Interestingly, IPC did not significantly reduce myocardial infarct size in DJ-1 knockout mice, where only a small trend towards decreased infarct size was observed in these animals (Figure 4.12 B: IS/AAR% DJ-1 KO control 50.9±3.5 versus IPC 39.4±4.1, n=8/group, ^{NS}P>0.05). There was no significant difference in AAR (AAR/LV% DJ-1 KO control 48.2±1.9 versus DJ KO IPC 54.3±3.8, n=8/group, ^{NS}P>0.05) or survival (% survival to 24 hours: DJ-1 KO control 72.7%, n=11 versus DJ-1 KO IPC 80%, n=10).

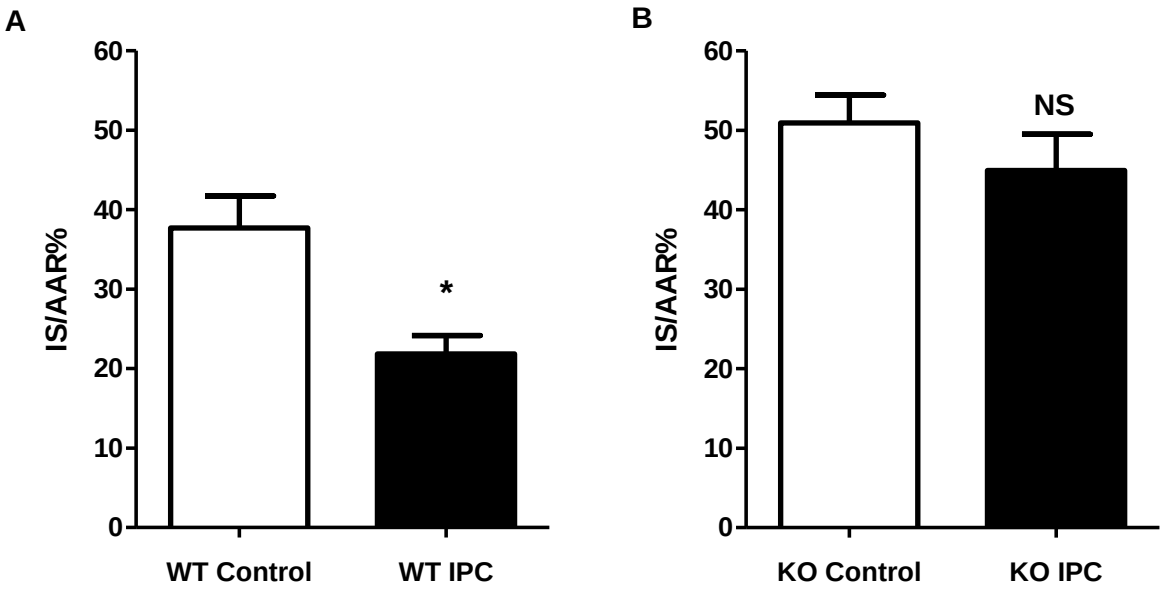

Figure 7.14: Susceptibility of DJ-1 knockout mice to cardioprotection by IPC
Cardioprotection by one cycle of IPC (5 minutes ischaemia and 5 minutes reperfusion) prior to the main ischaemic insult of 45 minutes and 24 hours reperfusion in DJ-1 KO and WT littermate controls. A) Significant reduction in infarct size by IPC in DJ-1 WT mice: IS/AAR% control 36.9±4.6 versus IPC 21.9±2.7, n=7/group, *P<0.05. B) No significant reduction in infarct size by IPC in DJ-1 KO mice: IS/AAR% control 51.3±4.0 versus 41.9±3.9, n=7 group, ^{NS}P>0.05. Statistical significance assessed by unpaired t-test.

This study suggests that DJ-1 may be involved in the cardioprotective pathway elicited by IPC. However, this apparent resistance to IPC was not investigated using additional cycles of preconditioning to assess whether this could be overcome with a higher IPC stimulus. The potential involvement of DJ-1 in IPC is discussed in detail below.

7.5. Discussion

The overall objective of this chapter was to investigate whether DJ-1 plays a role in the heart. Previous investigations have demonstrated a convincing role for DJ-1 in maintaining mitochondrial function in the brain at baseline in aged animals and in the pathophysiological response to neuronal ischaemia-reperfusion injury (Bonifati et al., 2003; Aleyasin et al., 2007). Indeed, DJ-1 knockout mice displayed increased cerebral infarct size in an *in vivo* stroke model (Aleyasin et al., 2007). Cumulatively these findings suggest the intriguing possibility that DJ-1 in the heart may be exhibiting a similar role in maintaining mitochondrial function and protecting against ischaemia-reperfusion injury.

The initial *in vitro* studies undertaken within our laboratory investigated the effect of overexpression of wildtype and mutant forms of DJ-1 in important models of mitochondrial and cell survival. These studies demonstrated a convincing role for DJ-1 in this cardiac cell line, where it was shown that overexpression of DJ-1 conferred beneficial outcomes of increased mitochondrial elongation and delayed mPTP opening. Our laboratory has previously shown that these mitochondrial phenotypes correlate with improved cell survival in response to simulated ischaemia-reperfusion injury in this cell line (Ong et al., 2010). Indeed, DJ-1 overexpression in this cell line reduced cell death upon simulated ischaemia-reperfusion (Dongworth and Mukherjee et al., in submission).

To extend the findings of this initial research and to confirm an *in vivo* role for DJ-1 in the pathophysiology of myocardial ischaemia-reperfusion, further studies were undertaken to investigate the effect of genetic ablation of DJ-1 on cardiac phenotype and susceptibility to infarction from ischaemia-reperfusion. Unfortunately it was not possible to directly compare the *in vitro* and *in vivo* systems since we did not have access to a DJ-1 overexpressing transgenic mouse line and attempts to create a DJ-1 knockdown *in vitro* system did not produce a sufficient reduction in DJ-1 protein levels (experiment conducted by Ms U. Mukherjee; data of DJ-1 knockdown not included here).

7.5.1. Role of mitochondrial DJ-1 in cardiac function

Cardiac phenotype: Given the known role of DJ-1 in maintaining mitochondrial function in the brain, it was hypothesised that this would result in impaired cardiac function at baseline and in response to isoproterenol stress in hearts devoid of DJ-1. However, this study showed that adult DJ-1 knockout mice display no overt cardiac phenotype at baseline or following isoproterenol stress (Figure 7.6), thereby suggesting that DJ-1 does not mediate a critical role in cardiac function under physiological conditions. Importantly since these DJ-1 knockout mice do not display any overt cardiac phenotype

such as LV hypertrophy, it was possible to examine the effect of DJ-1 knockout on susceptibility to ischaemia-reperfusion without any confounding myocardial pathology.

It is possible that the lack of any overt cardiac phenotype in DJ-1 knockout animals could be due to the relatively young age at which these animals were characterised (12-16 weeks old). Importantly, previous studies have shown that mitochondrial antioxidant protein expression is normal in young brain mitochondria from DJ-1 knockout animals and only exacerbated upon ageing (Andres-Mateos et al., 2007). It is possible that aged DJ-1 knockout animals may display an overt cardiac phenotype; however, investigation of aging was outside of the remit of this thesis. Additionally, it was advantageous to study the effect of DJ-1 without any confounding myocardial pathology, as discussed above, meaning that the effects demonstrated in the subsequent studies can be firmly concluded to result from the stress tested.

It would be interesting to examine the effect of DJ-1 genetic ablation on cardiac function following ischaemia-reperfusion. This could be undertaken in using cardiac MRI to assess cardiac function and infarct size at baseline and following ischaemia-reperfusion injury, which would provide a comprehensive investigation of the role of DJ-1 in the long-term pathophysiology of myocardial ischaemia-reperfusion; as discussed further below.

Mitochondrial morphology: Given that overexpression of DJ-1 resulted in increased mitochondrial elongation in the initial *in vitro* studies, it was expected that DJ-1 genetic ablation would cause increased mitochondrial fragmentation. Indeed, assessment of mitochondrial morphology at baseline showed an increased proportion of shorter mitochondria in DJ-1 knockout hearts compared to wildtypes at baseline (Figure 7.7). This is in agreement with several previous studies suggesting that DJ-1 knockout increases mitochondrial fragmentation in mouse embryonic fibroblasts and mitochondria isolated from brain and skeletal muscle (Irrcher et al., 2010; Krebiehl et al., 2010). However, there was no difference in mitochondrial morphology in DJ-1 knockout and wildtypes following a sublethal ischaemic insult (Figure 7.11; 20 minutes ischaemia).

This was unexpected, although it is possible that a greater ischaemic insult may have elicited a significant difference in mitochondrial morphology. However, for the reasons of differential cell death in DJ-1 knockout hearts discussed above, it was not feasible to investigate the effect of an extended lethal ischaemic insult. It should also be noted however, that the proportion of fragmented mitochondria at baseline in wildtype mice is higher than expected (Figure 7.7: DJ-1 wildtype mitochondria approximately 74% fragmented). There is no clear reason for this however, given that the extent of mitochondria fragmentation in DJ-1 knockout hearts at baseline was already 93%, it is likely that this would preclude observation of a further increase in fragmentation.

Additional investigation of the effect of DJ-1 in maintaining mitochondrial morphology at baseline and following sublethal myocardial ischaemia may benefit from a more sensitive method for measuring mitochondrial morphology. The development and validation of an improved assay of mitochondrial morphology represents a substantial undertaking and was outside of the defined remit of this thesis.

Myocardial ATP levels: Given that previous studies have shown that DJ-1 is important for maintaining mitochondrial function in the brain, it was hypothesised that DJ-1 adult hearts may have lower ATP levels at baseline and further upon myocardial ischaemia. Indeed, Giaime et al. (2012) showed reduced basal ATP levels in mouse embryonic fibroblast cells (Giaime et al., 2012). The effect of genetic ablation of DJ-1 on myocardial ATP levels was investigated in DJ-1 knockout and wildtype hearts at baseline and following a sublethal global ischaemic insult. This *ex vivo* approach allowed a large amount of tissue to be sampled from each heart and confirmed that all tissue sampled was ischaemic, which could not be ensured using an *in vivo* approach. There was no difference in myocardial ATP levels between DJ-1 knockout and wildtype littermates at baseline (Figure 4.19) suggesting that DJ-1 is not crucial for myocardial energy production, despite its effects on mitochondrial morphology.

Since the 20 minute sublethal ischaemic insult employed in this study did not elicit a statistically significant reduction in myocardial ATP (Figure 7.12), it was not possible to draw any firm conclusions regarding the role of DJ-1 in regulating ATP levels following ischaemia. This sublethal ischaemic duration was used to avoid any confounding effects of differential cell death following ischaemia-reperfusion injury that were expected to be present between DJ-1 knockout and wildtype animals, as described above. It was therefore not possible to increase the ischaemic duration since this may have resulted in increased cell death in the DJ-1 knockout animals and thus a reduction in myocardial ATP levels due increased cell death rather than providing a measure of mitochondrial function. Billia et al. (2013) showed that myocardial samples from DJ-1 knockout hearts subjected to transaortic constriction exhibited decreased ATP levels compared to equivalent treated wildtype hearts. However, the potential confounding effects of increased severity of cardiac failure in the knockout animals was not considered in this study (Billia et al., 2013). It is therefore difficult to conclude what role DJ-1 plays in mitochondrial ATP production following stress.

In summary, this suggests that although DJ-1 appears to be involved in maintaining cardiomyocyte mitochondrial dynamics, DJ-1 does not seem to be crucial for cardiac function. The second part of this chapter sought to investigate the role of DJ-1 following oxidative stress induced by myocardial ischaemia-reperfusion.

7.5.2. Role of DJ-1 in the pathophysiology of ischaemia-reperfusion injury

Previous studies of DJ-1 demonstrate that its genetic ablation renders the brain more susceptible to ischaemia-reperfusion injury (Andres-Mateos et al., 2007). This suggested the intriguing possibility that DJ-1 may also play a cardioprotective role in the heart, whereby genetic ablation of DJ-1 would be expected to increase infarct size upon myocardial ischaemia-reperfusion. Indeed, Billia et al. (2013) showed that DJ-1 knockouts were more susceptible to myocardial infarction induced by *in vivo* permanent coronary artery ligation. The second part of this chapter aimed to investigate the involvement of DJ-1 in the more clinically relevant setting of ischaemia-reperfusion.

Initial *in vitro* studies investigating the role of DJ-1 in HL-1 cardiac cells within our laboratory demonstrated that DJ-1 overexpression conferred several beneficial effects, notably reduced cell death in response to simulated ischaemia-reperfusion (Figure 6.1; Dongworth and Mukherjee et al., in submission). This is in agreement with previous studies of neuronal cell lines where DJ-1 overexpression protected against oxidative stress induced cell death (summarised in chapter 1; reviewed by Wilson, 2011). This is also supported by a recent study by Yu et al. (2013) in which DJ-1 overexpression in rat H9c2 myoblasts protected against simulated ischaemia-reperfusion.

The possible involvement of DJ-1 in the susceptibility to cell death following ischaemia-reperfusion was investigated further using the *in vivo* ischaemia-reperfusion model developed in chapter 4. A modified protocol of 45 minutes ischaemia and 24 hours reperfusion was applied to this study since a pilot study using 30 minutes ischaemia and 2 hours reperfusion did not detect a statistically significant difference in infarct size between DJ-1 knockout and wildtype animals. Following this extended ischaemic insult, these experimented indicated that DJ-1 knockout mice were more susceptible to myocardial infarction (Figure 5.5), exhibiting a 25.9% relative increase in infarct size (IS/AAR%). This is in agreement with the recent study by Billia et al. (2013) showing that genetic ablation of DJ-1 reduced myocardial infarct size resulting from permanent coronary artery ligation (often used as a model of cardiac failure) (Billia et al., 2013).

It should be noted however, that the control infarct size in the present model of 45 minutes ischaemia and 24 hours reperfusion is lower than that expected from previous control infarct data. The infarct size resulting from 45 minutes ischaemia and 24 hours reperfusion in DJ-1 wildtype mice was 37.7% (Figure 5.5) compared to 46.9% in Sirt-3 wildtype mice subjected to these same ischaemia and reperfusion durations (see chapter 6; Figure 6.7). These mice are of the same approximate genetic background (C57BL/6) and so the infarct sizes would be expected to be similar. By comparison with

infarct sizes from the *in vivo* ischaemia-reperfusion experiments presented in this thesis and others not presented here, the DJ-1 wildtype infarct size is lower than expected.

A potential explanation for this is the longer surgical protocol applied in this study, which was extended by an additional 15 minutes anaesthetic duration compared to all other surgeries in this thesis. The surgical protocols undertaken in the rest of this thesis were designed such that the surgical, and thus anaesthetic duration, could be matched by adjustment of the stabilisation period where ischaemic preconditioning is to be undertaken. However, since the protocol applied here used a longer ischaemic duration with application of IPC, an extended surgical time was required. It is possible therefore that the smaller infarct observed in this chapter resulted from some effect of anaesthetic conditioning. This may also be demonstrated by the slightly lower extent of cardioprotection elicited by IPC in these animals, where IPC reduced infarct size in DJ-1 wildtypes by approximately 42.2% (Figure 4.12 A). A detailed discussion of the potential pathways and the influence of anaesthetic conditioning evoked isoflurane anaesthesia in this model is provided in chapter 4 (see 4.6.1). However, a preliminary investigation of infarct size in these animals using the non-recovery *in vivo* protocol (with injectable anaesthesia) also showed that this standard IPC protocol did not elicit a significant cardioprotective effect in DJ-1 knockout mice, therefore confirming that the resistance to cardioprotection by IPC in these animals is a true effect of DJ-1 genetic ablation.

Overall this study suggests that endogenous DJ-1 may represent an important target for cardioprotection. This conclusion is supported by recent studies by Yu et al. (2013) and Billia et al. (2013) showing similar effects of DJ-1 *in vitro* overexpression and *in vivo* knockout. This thesis provides the first demonstration that DJ-1 genetic ablation increases the susceptibility to myocardial infarction upon *in vivo* ischaemia-reperfusion.

Susceptibility to cardioprotection by IPC: This study also showed that DJ-1 knockout mice were partially resistant to cardioprotection by a widely used standard IPC protocol (Figure 7.14). This suggests that DJ-1 may contribute to the signalling pathway underlying IPC. It is possible that a greater IPC stimulus (for example 3 cycles of 5 minutes ischaemia and 5 minutes reperfusion) could elicit a significant cardioprotective effect; however, this was not investigated further. A previous study by Lu et al. (2012) also suggested that DJ-1 may act as a mediator of hypoxic preconditioning in H9c2 rat myoblasts (Lu et al., 2012). Interestingly, it has been reported that neuronal DJ-1 can increase the activity of the pro-survival kinase, Akt (Kim et al., 2005a; Aleyasin et al., 2007; Lu et al., 2012). Whether DJ-1 is required for Akt activation in the setting of IPC is an intriguing question which remains to be explored and should now be investigated.

This study suggests that DJ-1 may modulate the response to myocardial ischaemia-reperfusion by its effects on the survival kinase (RISK) pathways known to be important in cell survival in this setting (for an overview of these pathways see 1.3.1). Overall, it appears that DJ-1 plays an important role in the pathophysiology of myocardial ischaemia-reperfusion injury, whereby genetic ablation of DJ-1 renders the heart more susceptible to myocardial infarction and less amenable to cardioprotection by IPC. This study concludes that DJ-1 may represent an important target for cardioprotection.

7.5.3. Summary of potential limitations

The results presented in this chapter confirm an important role for DJ-1 in ischaemia-reperfusion whereby genetic ablation of DJ-1 renders the heart more susceptible to infarction upon *in vivo* ischaemia-reperfusion. From this data, one could hypothesise that DJ-1 may represent an important therapeutic target for cardioprotection. However, the experiments described here have not explored the potential therapeutic application of DJ-1 to cardioprotection which would involve overexpression of DJ-1, which would be expected to reduce infarct size in this model. This is a key limitation of this study however; this could not be overcome here since we did not have access to DJ-1 overexpressing mice. Current pharmacological approaches to evoke increased DJ-1 expression have not been shown to be sufficiently selective to allow evaluation of the therapeutic benefit of DJ-1 overexpression (see 1.4.3).

In addition, all studies presented in this chapter were undertaken on young animals (12-16 weeks old). It is possible that the role of DJ-1 is exacerbated in aged animals, and as such, DJ-1 knockout mice may display an overt cardiac phenotype in aged animals. Given the demonstration of more overt neuronal phenotypes in aged DJ-1 animals (Andres-Mateos et al., 2007), it is possible that the increased susceptibility to myocardial infarction in DJ-1 knockout mice shown here may be exacerbated by aging. It may be particularly pertinent to investigate the cardioprotective efficacy of DJ-1 overexpression in aged animals to ensure that this therapeutic benefit translates to the aged heart. The importance of considering co-morbidities and ageing in pre-clinical studies was discussed in chapter 1 (see 1.5.1). This has not been investigated here but would be interesting to examine in further studies of the role of DJ-1 in myocardial ischaemia-reperfusion in order to examine the potential of this protein as a cardioprotective target.

7.5.4. Summary

The main research objective of this chapter was to investigate the role of DJ-1 in the heart and examine its potential as a therapeutic target to protect against ischaemia-reperfusion injury. This thesis, and the preliminary *in vitro* studies undertaken by our group, provides a solid proof-of-concept demonstration of the involvement of DJ-1 in the pathophysiology of myocardial ischaemia-reperfusion injury.

(1) Global genetic ablation of DJ-1 did not significantly affect cardiac phenotype in terms cardiac structure or function at baseline or following isoproterenol stress. Although DJ-1 cardiac mitochondria were shown to be significantly more fragmented at baseline conditions compared to wildtype control hearts, there was no significant difference in myocardial ATP levels in these hearts. These findings suggest that DJ-1 is dispensable for normal cardiac development and function.

(2) Investigation of the effects of ischaemia on mitochondrial morphology and myocardial ATP levels showed no significant difference between DJ-1 knockout and wildtype hearts. However, the relatively high extent of mitochondrial fragmentation at baseline is likely to have masked any further effect of ischaemia. Further examination of the effect of ischaemia on myocardial ATP levels in these animals was hindered by the absence of any significant effect of the 20 minute ischaemic insult, whereby the expected differential susceptibility to cell death precluded examination of a more severe ischaemic insult.

(3) DJ-1 knockout mice were more susceptible to infarction following myocardial ischaemia-reperfusion. Interestingly, DJ-1 knockout mice were partially resistant to cardioprotection by ischaemic preconditioning, suggesting that DJ-1 in the heart may be involved in the RISK pathway of cardioprotection.

The results presented here confirm that DJ-1 mediates an important role in the pathophysiology of myocardial ischaemia-reperfusion injury, whereby genetic ablation of DJ-1 renders the heart more susceptible to infarction *in vivo*. This chapter of the thesis suggests that DJ-1 overexpression may be an important cardioprotection strategy.

CHAPTER 8: INVESTIGATION OF *IN VIVO* IMAGING OF THE MYOCARDIUM USING CARDIAC MRI

8.1. Introduction

The overall research hypothesis of this thesis concerns the potential long-term efficacy of modulation of mitochondrial proteins to elicit cardioprotection. Previous chapters have highlighted and examined three important mitochondrial proteins that may represent therapeutic targets for cardioprotection. The *in vivo* model of myocardial ischaemia-reperfusion injury established in chapter 4 theoretically allows assessment of cardioprotective efficacy following extended reperfusion durations to evaluate the long-term efficacy of such interventions. However, this is complicated by the availability and validity of current methods for assessing cardioprotective efficacy, described previously.

Since myocardial infarct size is known to be a strong predictor of the prognosis of acute myocardial infarction patients, infarct size has become a widespread and important endpoint in pre-clinical and clinical cardioprotection studies. However, to determine the efficacy of cardioprotective therapies for reducing myocardial infarct size it is essential to consider the extent of 'myocardial salvage'. Typically myocardial salvage is defined as the proportion of myocardium at-risk (the AAR) that was salvaged by the intervention (calculated as: AAR minus infarct size divided by AAR). In practice, the majority of basic science studies evaluate the extent of injury normalised to the AAR (calculated as IS/AAR%, as presented in this thesis) since this also considers the extent of the AAR.

Variability in the AAR between animals in this model arises from subtle differences in coronary anatomy and the location of the occluding suture. This was discussed previously in relation to the establishment of the *in vivo* model developed in this thesis. Since the AAR is a critical determinant of infarct size, methods of controlling infarct size to AAR provide a more sensitive measure of cardioprotective efficacy than absolute infarct size. The importance of this was demonstrated in chapter 5 where assessment of absolute infarct size (IS/LV%) reduced the statistical power such that a statistical difference could not be detected (corresponding to a type II error) and required a sample size of 25 animals per group to obtain statistical power (see 5.3.3 iii, Figure 5.7).

Current methods for determining myocardial infarct size and AAR in experimental animal studies largely rely on *ex vivo* histological staining methods, for example using TTC and Evans blue as described in this thesis (see chapter 3; reviewed by Black and Rodger, 1996). Although these histological methods have been widely employed and validated

over many decades, there are some limitations to these approaches; most notably their terminal nature allowing only a single time-point to be assessed and the potential interference of long-term remodelling processes adversely affecting their validity; as discussed in detail in chapter 4 (see 4.6.3). Longitudinal animal studies and clinical studies investigating long-term cardioprotective efficacy require an *in vivo* method to determine AAR to allow assessment of myocardial salvage. This chapter investigates the use of cardiac MRI to assess myocardial salvage in the reperfused mouse heart.

Cardiac MRI has emerged as a possible non-invasive imaging modality for investigating cardioprotective efficacy in both *in vivo* experimental animal and clinical studies. An overview of the cardiac MRI methods investigated for *in vivo* quantification of infarct size and AAR is provided in chapter 1 of this thesis (see 1.5.2). This chapter evaluates the validity of cardiac MRI methods for quantifying AAR *in vivo* in reperfused hearts with the aim of providing a fully validated *in vivo* method of assessing myocardial salvage.

Investigation of the use of cardiac MRI for evaluation of myocardial salvage presented in this chapter was undertaken in collaboration with Prof M. Lythgoe at the Centre for Advanced Biomedical Imaging (CABI) at University College London, UK. MRI sequences were developed by Dr A. Campbell-Washburn and imaging undertaken in collaboration with Mr T Roberts; their contributions to this work are duly noted below.

8.2. Research objective and aims

The main objective of this chapter was to characterise and validate a method for the *in vivo* quantification of AAR in the mouse heart following *in vivo* ischaemia-reperfusion injury. The principal research aims to achieve this objective were:

(1) Develop and validate an *in vivo* cardiac MRI method for accurate assessment of myocardial AAR in mice subjected to ischaemia reperfusion injury;

(2) Investigate the validity of these *in vivo* cardiac MRI assessments of AAR in the presence of cardioprotective strategies.

8.3. Aim 1: Develop and validate an *in vivo* MRI method to assess myocardial area-at-risk

8.3.1. Background

A number of cardiac MRI methods have been investigated for the quantification of myocardial AAR in the reperfused heart, as outlined in chapter 1 (see 1.5.2, Table 1.5). These methods have had variable success at quantifying AAR, where T_2-weighted MRI approaches have been most widely investigated and applied in both experimental and clinical settings. This chapter investigates the use of a T_2-weighted cardiac MRI approach to *in vivo* AAR quantification. In addition, we also sought to investigate the use of a perfusion based cardiac MRI method to interrogate the reperfused mouse heart and potentially provide an additional method for quantifying AAR.

T2-weighted cardiac MRI methods: Numerous studies have suggested that T_2-weighted cardiac MRI provides an accurate method to quantify myocardial AAR following ischaemia-reperfusion. This method is based on the rationale that ischaemia-reperfusion causes oedema to develop within the AAR. The pathophysiological processes which cause myocardial oedema to develop in response to ischaemia-reperfusion are outlined in chapter 1 (see section 1.2). Since T_2-weighted MRI exploits the known linear correlation between tissue water content and T_2-relaxation time, this imaging modality allows delineation of areas of myocardial oedema which are hypothesised to equate to the AAR. Indeed, *in vivo* quantification of AAR by T_2-weighted cardiac MRI methods has been validated in a number of experimental animal species (Aletras et al., 2006; Bohl et al., 2010; Mewton et al., 2011; Beyers et al., 2012) and acute myocardial infarction patients (Berry et al., 2010; Fuernau et al., 2011). A detailed overview of the application and validation of T_2-weighted based cardiac MRI approaches for this purpose is provided in chapter (see 1.5.2 iii, Table 1.6).

Given the success of T_2-weighted cardiac MRI methods for quantifying AAR *in vivo*, this method is becoming more widely accepted and used in pre-clinical and clinical studies. However, applications of this technique to the reperfused mouse heart have been complicated by its small size and rapid heart rate, which impose signal-to-noise constraints. However, studies using this approach have provided promising results (Bohl et al., 2010; Beyers et al., 2012) and suggest that this could provide a feasible method for determining AAR and myocardial salvage *in vivo* in the mouse heart.

Perfusion cardiac MRI methods: Perfusion-based cardiac MRI methods have also been suggested as a potential approach to quantify myocardial AAR *in vivo*. These methods

are based on the premise that ischaemia-reperfusion causes some impairment to coronary perfusion even upon release of the coronary artery occlusion. The precise biological mechanism of this perfusion deficit has not been investigated to any significant extent; however, it is likely to represent decreased perfusion at the micro-circulatory level. Myocardial perfusion can be assessed *ex vivo* by perfusion of labelled microspheres of known diameters to allow identification of regions with poor perfusion. First-pass gadolinium (Gd) imaging has been the mostly widely investigated cardiac MRI method to quantify myocardial AAR (as detailed in chapter 1, see 1.5.2 iii) (reviewed by Arai, 2011a). Indeed, Gonzalez et al. (2008) used first-pass Gd MRI and histological analysis of microsphere perfusion to confirm the presence of subendocardial perfusion deficits in reperfused dog hearts following myocardial injury (Gonzalez et al., 2008). Despite the success of first-pass perfusion imaging in larger hearts, its application to the mouse heart is likely to be hindered by its smaller size and rapid heart rate, which limit the spatial and temporal resolution which are essential to this method.

Arterial spin labelling (ASL) is a newer MRI method of examining tissue perfusion which was first developed to examine cerebral blood flow but has since been applied to other organs, including the heart (reviewed by Petersen et al., 2006). The theoretical basis of this MRI method is described in detail in chapter 3 of this thesis (see 3.8.3). ASL MRI allows quantification of tissue perfusion and therefore allows comparison of relative perfusion rates within tissues. Indeed, ASL techniques have been shown to provide robust and reproducible quantification of myocardial blood *in vivo* in rodent hearts (Belle et al., 1998). Our collaborators at CABI have developed a multi-slice ASL MRI sequence for imaging the mouse heart (as described by Campbell-Washburn et al., 2012; 2013). This method has been shown to allow accurate interrogation of perfusion in the naïve mouse heart (Campbell-Washburn et al., 2012) and represents a valuable method to assess perfusion following ischaemia-reperfusion.

Since myocardial perfusion may provide a method of visualising the AAR in the reperfused heart following ischaemia-reperfusion injury, this thesis examines the application of this multi-slice ASL cardiac MRI method to detect areas of reduced perfusion in the mouse heart following *in vivo* ischaemia-reperfusion injury. Experiments here describe the first application of a multi-slice ASL MRI sequence to the reperfused mouse heart and its potential as a novel method for quantifying AAR *in vivo*.

Aim 1: The first aim of this chapter was to investigate the use of T_2-mapping and arterial spin labelling cardiac MRI protocols to assess AAR *in vivo.* The central hypotheses in relation to this research objective were:

(1) T_2-mapping cardiac MRI would allow accurate quantification of AAR *in vivo* in the reperfused mouse heart following ischaemia-reperfusion injury.

(2) ASL cardiac MRI would allow accurate quantification of area-at-risk *in vivo* in the reperfused mouse heart following ischaemia-reperfusion injury.

8.3.2. Detailed methods

All experiments presented in this chapter were undertaken using commercially available male B6/SV129 mice aged 10-14 weeks (Harlan Laboratories, UK). Mice were provided with a minimal acclimatisation period of one week prior to surgery and a further 2 days acclimatisation at the cardiac MRI facility prior to MRI investigation.

i Ischaemia-reperfusion injury in vivo

Surgical protocol: B6/SV129 mice underwent the standard protocol of *in vivo* ischaemia-reperfusion comprising 30 minutes ischaemia and approximately 72 hours reperfusion as described previously (see 3.2.1). Animals were monitored closely during the post-operative period and providing they displayed suitable surgical recovery they were transferred to the small animal cardiac MRI facility 16-24 hours following surgery.

ii Cardiac magnetic resonance imaging

Cardiac MRI was undertaken with Dr A. Campbell-Washburn and Mr T. Roberts, Prof M. Lythgoe (Centre for Advanced Biological Imaging, University College London, UK).

Following approximately 72 hours reperfusion, mice underwent cardiac MRI for the assessment of putative myocardial AAR and infarct size, as described in detail below.

Small animal cardiac MRI setup: A detailed description of the MRI instrumentation at CABI is provided by Price et al (2011), where the experimental setup used here was exactly as described in chapter 3 (see 3.8.1). The cardiac MRI protocol comprised: (1) ASL imaging and (2) T_2-mapping and (3) late-gadolinium enhancement imaging. An overview of the theoretical basis and methodological details of these of these methods is provided in chapter 3 (see section 3.8, Figure 3.20) and briefly described below.

Cine imaging – Cardiac function: Cinematic (cine) images of the heart were acquired to allow calculation of cardiac volumes and function. The precise MRI sequence parameters were exactly as described by Price et al. (2011) and detailed previously (see 3.8.2). Ten short-axis slices were imaged covering the whole heart from apex to base.

Quantification: Cardiac function was assessed from short-axis cine images. Segmentation of the myocardium was completed by semi-automated delineation of the epicardial and endocardial borders using Segment software version 8 (Segment, http://segment.heiberg.se/) with manual correction as required. The blood pool volume was plotted against time to determine the phases of cardiac cycle for quantification of cardiac function from images at end-diastole (ED) and end-systole (ES); see Table 8.1.

ENDPOINT	CALCULATION METHOD
Anatomical measurements	LV myocardial wall mass (LVM) [µg] = myocardial wall volume x 1.05 g/ml
Heart rate (BPM)	Calculated as: mean time between ECG trace R-waves
Stoke volume (SV) (µl)	Calculated as: (ED volume) – (ES volume)
Cardiac output (µl/min)	Calculated as: (Heart rate * stroke volume)
Ejection fraction (%)	Calculated as: (SV/EDV) x 100%

Table 8.1: Cine imaging cardiac MRI assessment of cardiac structure and function
Summary of cine imaging measurements of left ventricular end diastolic and systolic dimensions and measurements to assess principal features of cardiac function.
Cardiac MRI was performed by Dr A. Campbell-Washburn and Mr T. Roberts; analysis of MRI data was undertaken by Dr A. Campbell-Washburn.

Arterial spin labelling – Putative area-at-risk: ASL MRI evaluates tissue perfusion and was therefore considered as a potential method for evaluating perfusion defects and potentially quantifying myocardial AAR in this study. This thesis applied a multi-slice flow alternating inversion recovery (FAIR) ASL sequence developed by Campbell-Washburn et al. (2012; 2013). The theoretical basis of this technique is described in chapter 3 (see 3.8.3). Two acquisitions of three slices were used to image the whole heart (6 slices).

Quantification: Myocardial perfusion was assessed from the ASL perfusion maps of the 6 myocardial slices. Perfusion maps were produced for each slice by MATLAB compilation of the raw T_1-values and were displayed as heat-maps, in which normal perfusion appears in 'hot' colours (red – orange) and low perfusion appears in 'cold' colours (blue). Normal perfusion values were defined for each heart by selection of a region of interest in the second from most basal slice. Pixels with perfusion values less than 1 standard deviation below the 'normal' perfusion value for that heart were considered to have reduced perfusion. This threshold analysis of ASL maps was undertaken using a custom MATLAB script; as shown in Figure 8.1 (A – ASL).

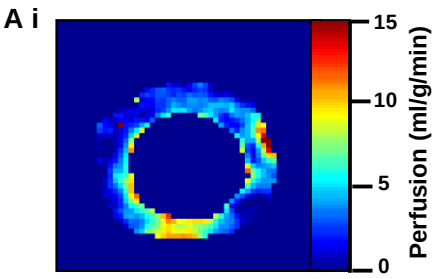

Figure 8.1: ASL-map threshold analysis of AAR A) Example images for a mid-slice of the myocardium interrogated by cardiac MRI ASL perfusion mapping (A) and histological staining (B). Regions of reduced perfusion were visible in ASL-maps and these appeared to be in the region of the AAR determined by histology. B) Threshold of AAR applied to cardiac MRI ASL-map (i) and histology (ii) – areas highlighted red were considered 'AAR' by these methods.

The area of reduced perfusion was calculated as a percentage of the total number of myocardial pixels (area of perfusion deficit / myocardial area %). Statistical analysis of the putative AAR defined by this method is described below (see section iv).

T_2-mapping – Putative area-at-risk: T_2-weighed MRI can be used to evaluate tissue water content as described above. Since myocardial ischaemia (and reperfusion) are known to cause tissue oedema within the AAR, T_2-weighted cardiac MRI has been investigated as a method to quantify AAR *in vivo* (reviewed by Garcia-Dorado et al., 2012). A T_2-mapping cardiac MRI protocol was applied to assess myocardial water content and investigate the potential use of this method to quantify AAR. A description of the theoretical basic of T_2-mapping is provided in chapter 3 (see 3.8.4).

Quantification: T_2-maps of the myocardium were produced by fitting exponential decay curves of T_2-relaxation time to T_2-signal intensity on a pixel-wise basis for each slice using MATLAB scripts (MATLAB Student Version R2008b, The MathWorks, USA). These T_2-maps were displayed as heat-maps, in which normal T_2-signal appears in 'colder' colours (green-yellow) and elevated T_2-signal appears in 'hot' colours (red). Normal T_2-signal values were defined by selection of a region of interest in the second from most basal slice. Pixels with T_2 values greater than 1 standard deviation above the 'normal' T_2-signal were considered to have elevated T_2-signal. This analysis method was in accordance with that used for a similar T_2-mapping interrogation of reperfused mouse hearts by Bohl et al. (2010). Threshold analysis was undertaken using a custom MATLAB script; an example of this approach is shown in Figure 8.2 (A – T_2-map).

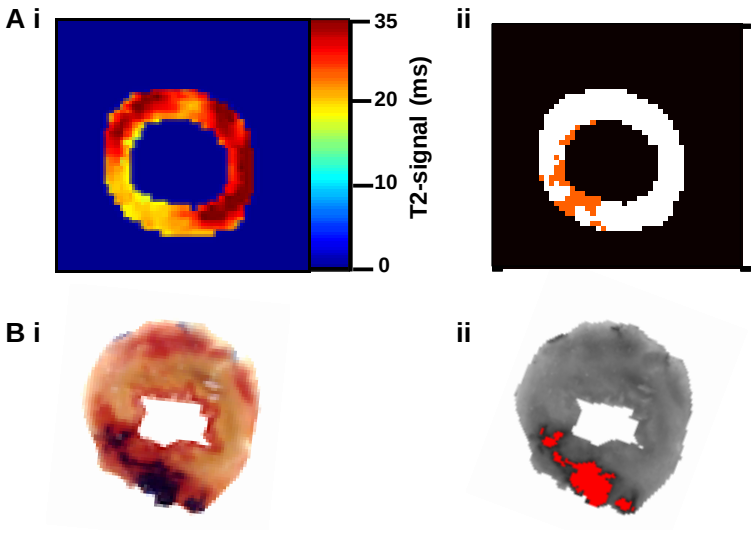

Figure 8.2: T_2-map threshold analysis of AAR
A) Example images for a mid-slice of the myocardium interrogated for AAR by cardiac MRI T_2-mapping (A) and histological staining (B). Regions of elevated T_2-signal were present in T_2-maps of the myocardium and these appeared to be in the region of the AAR determined by histology. B) Threshold of AAR applied to cardiac MRI T_2-map (i) and histology (ii) – areas highlighted red were considered 'AAR' by these methods.

The area of elevated T_2-signal was calculated as a percentage of the total number of myocardial pixels (area of elevated T_2 / myocardial area %). Statistical analysis of the putative AAR defined by this method is described below (see section iv).

Late-gadolinium enhancement – Infarct size: Late-gadolinium enhancement (LGE) cardiac MRI is a well-validated method of quantifying myocardial infarct size *in vivo*. A LGE cardiac MRI protocol was applied to allow quantification of myocardial infarct size and ultimately potentially myocardial salvage. A description of the theoretical basis of LGE imaging for infarct size quantification is provided in chapter 3 (see 3.8.5).

Quantification: The area of infarction was determined using an automated delineation method constrained by the myocardial borders using Segment software (version 8). Infarct size was calculated as the number of pixels with enhanced T_1 signal as a percentage of the total number of pixels. Analysis of infarct size is described below.

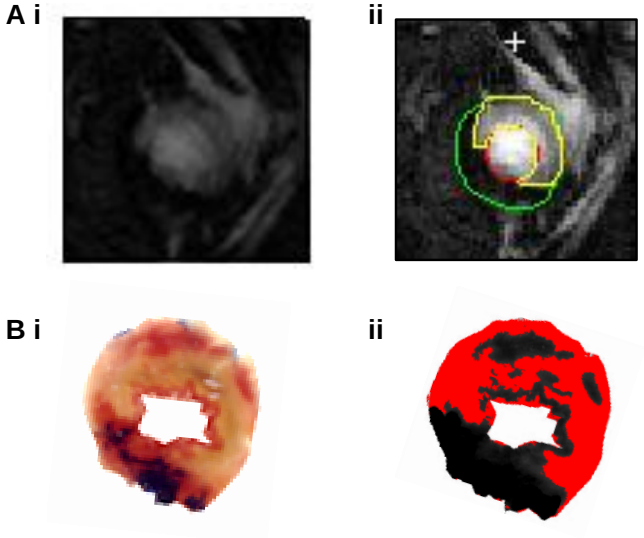

Figure 8.3: LGE threshold analysis of infarct size
A) Example images for a mid-slice of the myocardium interrogated for infarction by LGE imaging (A) and histological staining (B). The area of enhanced signal (bright area) corresponding to infarction was analysed to calculate infarct size. Analysis of area of infarct was completed using semi-automated Segment software: endocardial border red, epicardial border green, area of infarct encompassed in yellow. B) Threshold of LGE image (i) and histology (ii) – areas highlighted red were considered 'infarct' by these methods.

iii Histological staining for infarct size and area-at-risk

In order to validate cardiac MRI measurements of infarct size and AAR, animals evaluated by these MRI protocols were also subjected to classical *ex vivo* histological staining using perfusion of TTC and Evans blue, as described previously (chapter 3; see 3.2.4). Seven transverse slices of approximately 1 mm thickness were taken from the apex of the heart towards the base. Heart slices were processed and imaged exactly as described previously. Examples of histological staining of these hearts are presented in the preceding sections of this chapter describing threshold analysis of cardiac MRI images (see Figure 8.1 - Figure 8.3). It is important to note that it was not possible to completely align the histological and cardiac MRI myocardial slices due to the manual method of *ex vivo* slicing and possible effects of formalin storage of *ex vivo* heart slices; this is discussed in detail later in this chapter (see 8.5.1).

iv Statistical analysis of cardiac MRI and histological measurements

Percentage areas are reported as mean ± SEM for the endpoints determined by cardiac MRI and histological staining. All statistical analysis was completed using GraphPad Prism® version 5.0 (GraphPad Software, USA).

Validation of cardiac MRI quantification of myocardial infarct size and AAR was assessed by paired t-test comparisons of MRI and histology endpoints for each group. Statistical significance was reported where $P<0.05$ using standard significance coding.

Correlation analysis of this data for each group was not appropriate given the relatively small group sizes and close spread of data thereby invalidating any correlation statistics. Bland-Altman plots were constructed for each experimental group to assess the overall agreement in cardiac MRI and histological methods. Although Bland-Altman plots do not provide a formal structure for statistical testing, they provide a useful method of visualising the differences between these two methods. The endpoint for each method was plotted for each heart as the difference between histological and MRI quantification (Δ = cardiac MRI – histology endpoint) against the average quantification by these two methods. Bland-Altman plots were used to informally assess the size of bias (mean difference between methods) and the spread of variability. Details of statistical analyses and sample sizes are provided alongside the results presented in this chapter.

8.3.3. Results

This first part of this chapter examined the use of T_2-mapping and ASL cardiac MRI methods to quantify AAR in the reperfused mouse heart following 72 hours reperfusion.

An initial pilot study was undertaken to assess the feasibility of these cardiac MRI protocols to assess myocardial infarct size and AAR (n=4 animals; data not shown). This was the first application of LGE to reperfused mouse hearts by our research groups and demonstrated very good enhancement of areas of infarction which permitted accurate quantification of infarct size in line with those previously described by Price et al. (2011). In addition, this pilot study showed that the initial multi-slice T_2-mapping sequence investigated here allowed clear delineation of a region of the myocardium with increased T_2-signal indicating increased tissue water content (oedema). Interestingly, application of a preliminary single-slice ASL MRI sequence to a mid-ventricular slice of these hearts showed the presence of defined regions of reduced perfusion which appeared to be located in the approximate region of the AAR judged by histological staining. This suggested that ASL MRI of the full extent of the heart may provide a method of visualising, and potentially quantifying, myocardial AAR *in vivo*.

A multi-slice ASL cardiac MRI protocol was developed and applied in the subsequent studies in this thesis (Campbell-Washburn et al., 2012). The data from these pilot studies is not presented here since the small sample sizes investigated did not permit robust analysis of AAR quantification by these methods. All subsequent investigations of cardiac MRI methods to determine infarct size and AAR used multi-slice analysis of 6 or 7 myocardial slices, as described in section 8.3.2. The results of these studies of control operated animals are presented below for each cardiac MRI method.

i LGE – Myocardial infarct size

LGE cardiac MRI has been widely-validated and applied to quantify infarct size in small animals, including the reperfused mouse heart. This method was applied to all animals imaged in this chapter to allow final assessment of myocardial salvage.

This study showed that LGE imaging highlighted a clearly defined region of signal enhancement (bright appearance) within the LV which appeared to be spatially localised to the area of infarction determined by TTC staining (Figure 4.12). Although a slice-by-slice comparison of cardiac MRI and histology images was limited by subtle variations in the location and thickness of the histological slices, gross alignment of the slices for each heart provided a valid comparison of the identification of infarction.

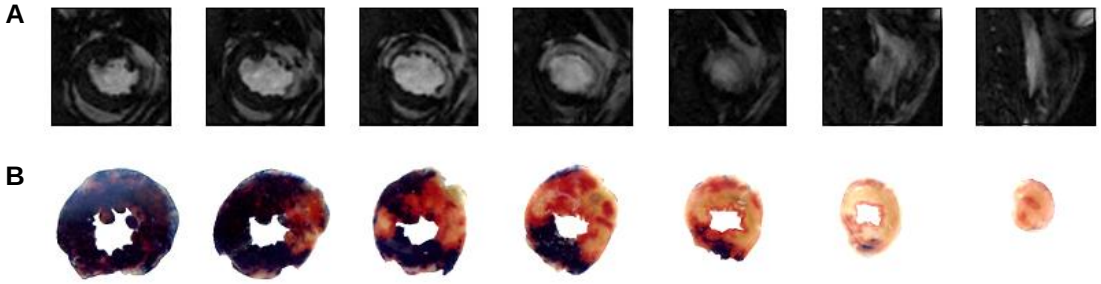

Figure 8.4: LGE imaging of myocardial infarction
Representative images for a control operated animal subjected to myocardial ischaemia-reperfusion. A) LGE images from base to apex. B) Histology images at approximate locations of MRI slices. Gross alignment of the 7 myocardial slices showed a good agreement of spatial localisation of infarction with 'gold-standard' histological staining for infarction using TTC.

Furthermore, quantification of myocardial infarct size as a percentage of the total ventricle area showed very good agreement between these two methods (Figure 4.12 A: IS/LV% histology TTC 30.9±0.6 versus MRI LGE 30.7±2.6; n=6/group, $^{NS}P>0.05$). Although some difficulties were encountered with delineation of the myocardial borders in LGE images of the most apical slices, this did not appear to affect the overall quantification of infarct size in these hearts. Bland-Altman analysis of this dataset showed a bias of -0.6±4.4 (standard deviation) (Figure 4.12 B) further indicating the robust nature of infarct size quantification by LGE cardiac MRI. Quantification of infarct size by this method is further investigated in the second part of this chapter.

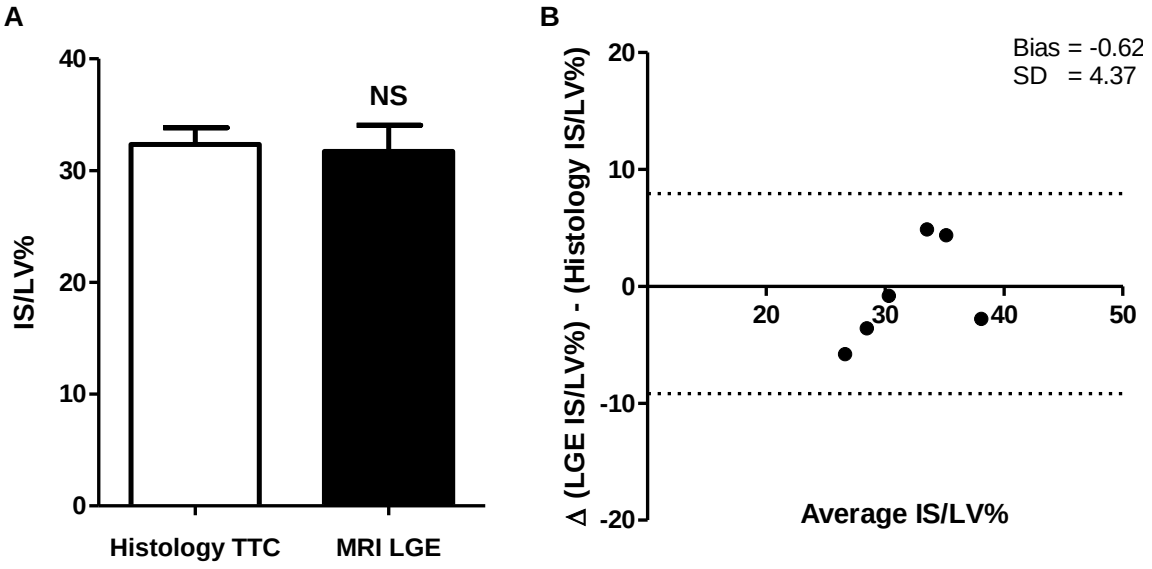

Figure 8.5: Infarct size assessment by LGE cardiac MRI
A) Quantification of infarct size as a percentage of LV area by histological TTC staining and cardiac MRI LGE imaging. There was no significant difference in infarct size quantification: IS/LV% histology TTC 30.9±0.6 versus MRI LGE 30.7±2.6. Statistical significance assessed by paired t-test, n=6, $^{NS}P>0.05$. B) Bland-Altman comparison of histological and LGE quantification of infarct size shows good agreement: bias -0.6 ± standard deviation 4.4.

ii Area-at-risk

The use of T_2-mapping and ASL cardiac MRI was assessed for *in vivo* quantification of AAR in this same cohort of animals. The results of these methods for AAR quantification for control operated animals are described in this section.

T_2-mapping MRI: A multi-slice T_2-mapping protocol was used to detect areas of increased tissue water content in reperfused mouse hearts. T_2-mapping highlighted clearly defined regions of enhanced of T_2-signal (seen as hot colours on T_2-maps) which appeared to be approximately localised to the AAR determined by 'gold-standard' histological staining (i.e. the area not stained by Evans blue) (Figure 8.6).

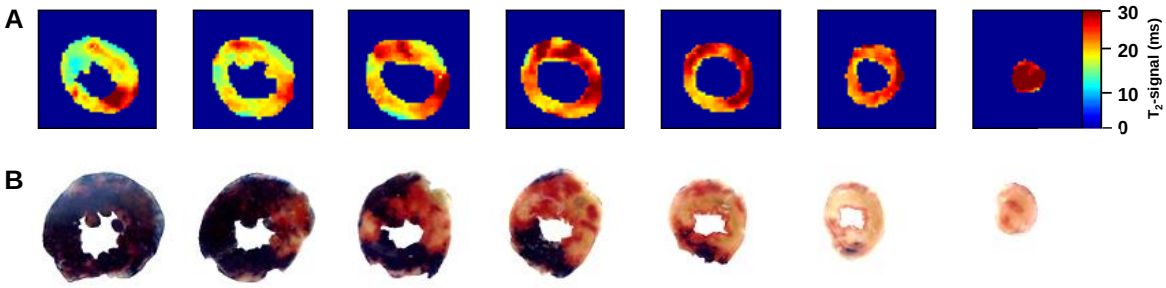

Figure 8.6: T_2-mapping imaging of myocardial oedema
Representative images for a control operated animal subjected to myocardial ischaemia-reperfusion. A) T_2-maps from base to apex: normal T_2-signal defined in septal region of slice 2. B) Histology images at approximate locations of MRI slices. Gross alignment of the 7 myocardial slices showed a good agreement of spatial localisation of oedema (putative measure of AAR) with histological staining for AAR by Evans blue (in which the AAR is the area not stained blue).

The area of oedema was defined as the area of myocardium exhibiting T_2 signal greater than 1 standard deviation above the 'normal' T_2 signal for that heart. This area of oedema (the putative AAR) was in very good agreement with that determined by histological staining in these control operated animals (Figure 8.7: AAR/LV% histology 64.3±2.5 versus MRI T_2-mapping 60.4±2.4; n=6/group, $^{NS}P>0.05$). Bland-Altman analysis of this dataset showed a bias of -3.9±11.4 (standard deviation) (Figure 8.7 B). This mean difference between histology and T_2-mapping quantification of AAR (-3.9% AAR/LV) is unlikely to be biologically significant for assessment of myocardial salvage.

Other threshold methods with subtle variations in the selection of the 'normal' T_2-value and threshold levels showed worse outcomes upon Bland-Altman analysis and were not investigated further. The threshold analysis method described here (see 8.3.2 ii) was used to quantify AAR by T_2-mapping MRI for all analyses presented in this thesis.

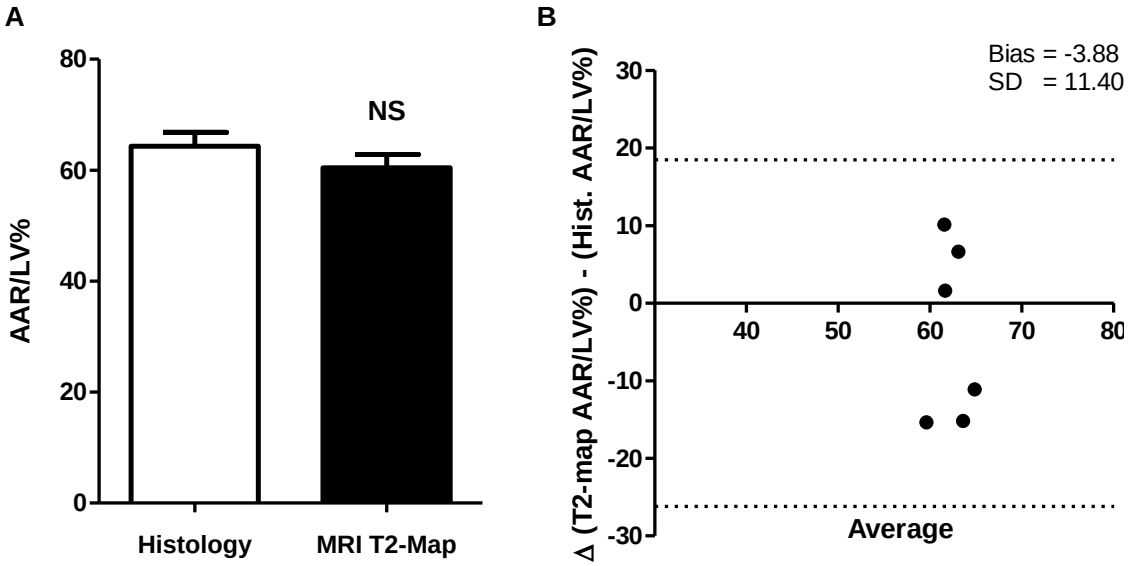

Figure 8.7: Putative AAR assessment by T_2-mapping cardiac MRI in control mice
A) Quantification of AAR as a percentage of LV area by histological staining and cardiac MRI T_2-mapping. There was no significant difference in AAR quantification by these methods, AAR/LV% histology 64.3±2.5 versus MRI T_2-mapping 60.4±2.4. Statistical significance assessed by paired t-test, n=6, $^{NS}P>0.05$. B) Bland-Altman comparison of histological and T_2-mapping AAR quantification shows acceptable agreement: bias -3.9 ± standard deviation 11.4.

ASL MRI: ASL cardiac MRI was used to assess myocardial perfusion in the same cohort of animals. This showed that distinct regions of the myocardium exhibited decreased perfusion and these appeared to correspond to the AAR judged by histological staining (Figure 8.9 A). The most apical slice commonly showed abnormal perfusion values which did not reflect biologically valid measurements and therefore this slice was excluded from quantification of the area of myocardial perfusion deficit.

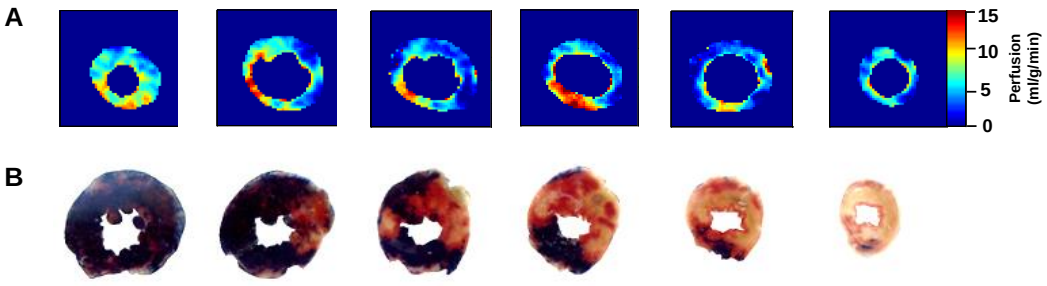

Figure 8.8: ASL imaging of myocardial perfusion
Representative images for a control operated animal subjected to myocardial ischaemia-reperfusion. A) ASP perfusion maps from base to apex: normal T_1 value defined in septal region of slice 2. B) Histology images at approximate locations of MRI slices. Gross alignment of the 6 myocardial slices shows a good agreement of spatial localisation of perfusion deficit (putative measure of AAR) with staining for AAR by Evans blue perfusion (AAR not stained in blue).

The area of reduced perfusion was defined as the area of myocardium exhibiting a T_1-perfusion value less than 1 standard deviation below the 'normal' T_1-perfusion value for that heart. The area of decreased perfusion (putative AAR) showed very good agreement with that determined by histological staining in control operated animals (Figure 8.9: AAR/LV% histology 64.3±3.9 versus MRI ASL 60.6±4.3; n=6/group, $^{NS}P>0.05$). Bland-Altman analysis of this dataset showed a bias of -3.7±11.9 (standard deviation) (Figure 8.9 B). This mean difference between histology and ASL quantification of AAR (-3.7% IS/LV) is unlikely to be biologically significant for the subsequent assessment of myocardial salvage.

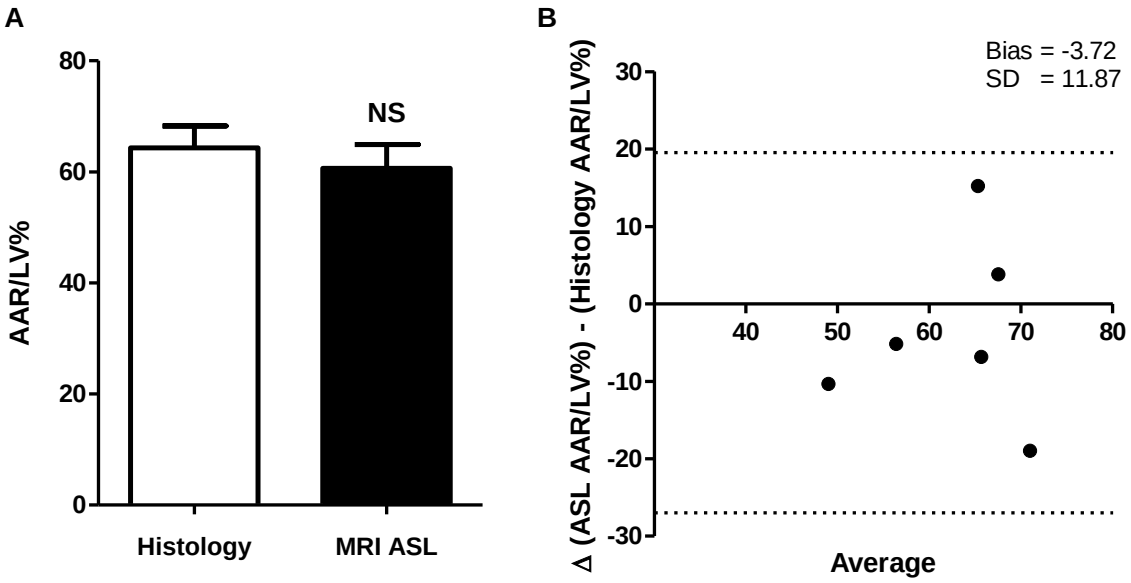

Figure 8.9: Area-at-risk assessment by ASL cardiac MRI and histology in control mice
A) Quantification of AAR as a percentage of left ventricle area by histological staining and cardiac MRI ASL perfusion imaging. There was no significant difference in infarct size quantification by these methods, AAR/LV% histology 64.3±3.9 versus MRI ASL 60.6±4.3. Statistical significance assessed by paired t-test, n=6, $^{NS}P>0.05$. B) Bland-Altman comparison of histological and ASL AAR quantification shows acceptable agreement: bias -3.7 ± standard deviation 11.9.

In summary, this study has shown that T_2-mapping and ASL cardiac MRI appear to provide valid and robust measures of myocardial AAR in the reperfused mouse heart. The bias calculated by Bland-Altman analysis was very similar between these methods (Bland-Altman bias: Figure 8.7 T_2-mapping bias -3.9±11.4; Figure 8.9 ASL -3.7±11.9; n=6). This suggests that either of these techniques could be used to assess myocardial salvage (reported here as IS/AAR%) in control operated animals. Indeed, comparison of IS/AAR% calculated by these cardiac MRI methods and 'gold-standard' histology shows that there is a striking agreement in mean IS/AAR% determined by these methods (Figure 8.10: paired t-tests comparing histology and cardiac MRI IS/AAR% confirmed there were no significant differences in quantification by histology and cardiac MRI).

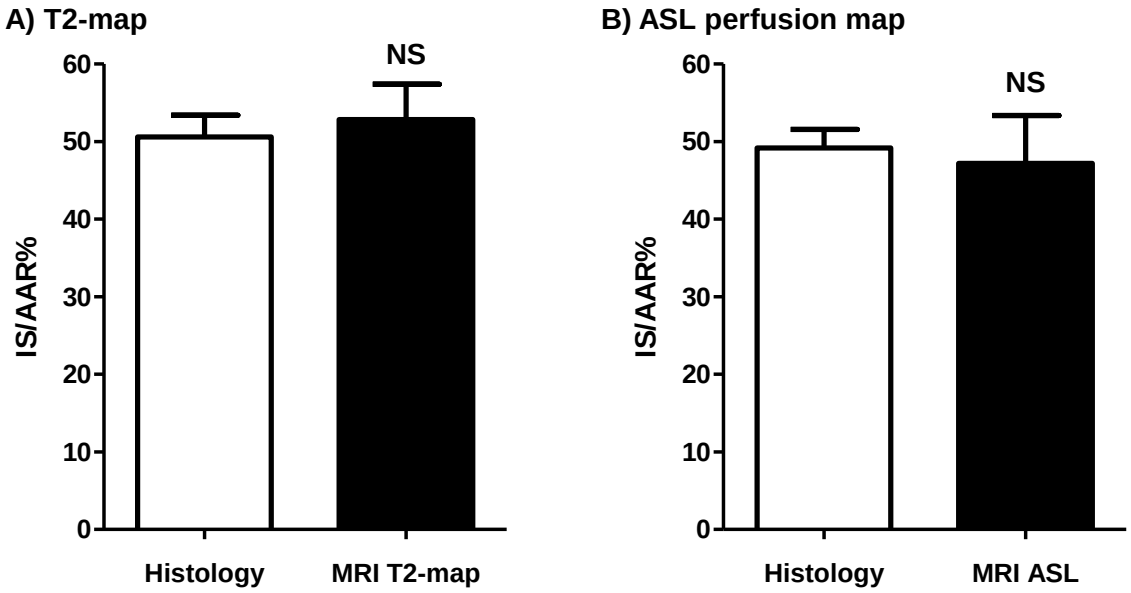

Figure 8.10: Quantification of infarct size controlled to AAR by cardiac MRI
Quantification of IS/AAR% in control animals. There was no significant difference in IS/AAR% calculation by cardiac MRI (black bars) and histological staining (white bars) for (A) T_2-mapping or (B) ASL cardiac MRI. Statistical significance assessed by paired t-test, n=6, $^{NS}P>0.05$.

The validity of these cardiac MRI methods for quantifying AAR *in vivo* is examined in the presence of cardioprotective interventions in the second part of this chapter below.

8.4. Aim 2: Validity of cardiac MRI assessments of area-at-risk in the presence of cardioprotective strategies

8.4.1. Background

To assess the validity of AAR quantification by these cardiac MRI methods it was crucial to determine whether cardioprotective interventions that reduce myocardial infarct size also affect the measure of AAR. This is a particularly pertinent research question concerning the use of T_2-weighted based cardiac MRI for this purpose since it has been previously suggested that certain cardioprotective interventions may reduce the extent of myocardial oedema. Notably, an early study of cardioprotection by IPC and ischaemic postconditioning (IPost) in dogs showed that both of these interventions significantly reduced the extent of myocardial oedema (Zhao et al., 2003). Furthermore, two recent landmark studies of clinical applications of T_2-weighted MRI showed that IPost (Thuny et al., 2012) and remote ischaemic postconditioning (RIPost) (Crimi et al., 2013) significantly reduced myocardial oedema. Although this is perhaps not surprising given that oedema is an outcome of injury, these studies suggest that T_2-weighted cardiac

MRI methods may not be appropriate for quantifying AAR in the presence of certain cardioprotective interventions. Since this study represents the first application of ASL cardiac MRI to quantify myocardial AAR, it is not known whether this technique will also be subject to these complications. The second part of this chapter investigates the effect of a cardioprotective interventions on AAR quantification by the T_2-mapping and ASL cardiac MRI methods described in part 1.

Aim 2: The second aim of this chapter was to investigate the validity of these cardiac MRI methods for assessing *in vivo* AAR in the presence of important cardioprotective interventions. The central hypotheses in relation to this research objective were:

(1) Cardioprotective interventions may reduce the extent of oedema meaning that these interventions T_2-mapping cardiac MRI may underestimate the AAR *in vivo*.

(2) Cardioprotective interventions are not expected to affect myocardial perfusion and thus ASL cardiac MRI should provide accurate quantification of AAR *in vivo* in the presence of cardioprotective interventions.

8.4.2. Detailed methods

The experiments presented in this section were undertaken using the exact experimental setup described previously (see 8.3.2) with the following additions.

i Ischaemia-reperfusion injury in vivo – Cardioprotective interventions

To investigate the effect of cardioprotective interventions on AAR quantification by these cardiac MRI methods, three interventions were examined: IPC, CsA and exenatide. The surgical procedure was exactly as described as above (see 8.3.2 i); 30 minutes ischaemia and 72 hours reperfusion with application of the interventions below.

Ischaemic preconditioning: A standard IPC protocol of 5 minutes ischaemia and 5 minutes reperfusion was applied immediately prior to the main 30 minute ischaemic insult exactly as described in chapter 4 (Figure 4.10). The IPC data presented in this section of thesis was conducted contiguously with the control data presented above (see 8.3.3) where these animals were randomised to receive either control or IPC treatment.

Cyclosporine-A: CsA treated animals received 10 mg/kg CsA as a single intravenous tail vein injection given 5 minutes prior to the onset of reperfusion, exactly as described in chapter 4 (Figure 4.11). Control animals received a matched volume of vehicle

(cremophor/ethanol-94%) 5 minutes prior to the onset of reperfusion. This study was completed as a separate experiment following completion of the IPC study.

Exenatide: Exenatide treated animals received 2.5 µg/kg given 5 minutes prior to the onset of reperfusion. Control animals received a matched volume of vehicle (saline) 5 minutes prior to the onset of reperfusion. Exenatide (trade name Byetta) was obtained from Eli Lilly and Company, UK as a pre-made solution of 0.25 mg/ml (pre-filled syringe). Exenatide was diluted in sterile saline to give an intermediate stock of 1.25 µg/ml (200-fold dilution). Dosing solutions were made fresh on each operating day to ensure that there was no loss of drug activity between experiments. This exenatide dosing stock was administered at 2 ml/kg both intravenously and subcutaneously; corresponding to 60 µl per 30 g mouse to give a final dosing concentration of 2.5 µg/kg I.V. and 2.5 µg/kg S.C.. Dosing was completed as described in chapter 3; animals were excluded where successful administration could not be confirmed.

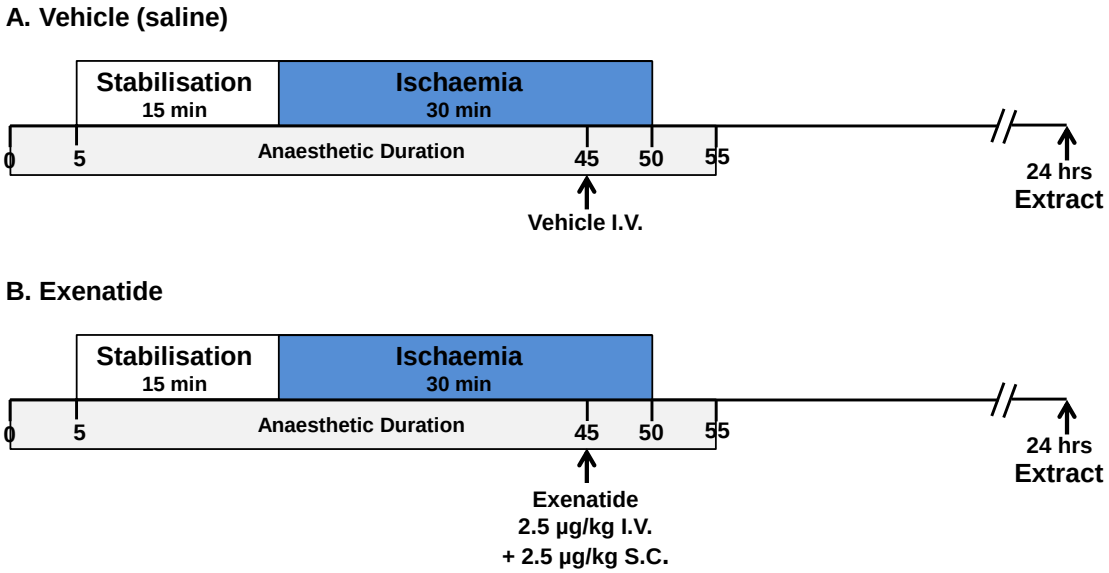

Figure 8.11: Exenatide dosing protocol
B6/SV129 mice were randomised to receive vehicle or exenatide administered 5 minutes prior to the onset of reperfusion. All dosing was as a single bolus administered I.V. immediately followed by a second bolus administered S.C.. A) Vehicle treated mice received a matched volume of saline. B) Exenatide treated received exenatide 2.5 µg/kg I.V. and S.C.. All mice were subjected to 15 minutes stabilisation, 30 minutes ischaemia and 72 hours reperfusion. Mice were subjected to histological staining for infarct size and AAR in a pilot study.

8.4.3. Results

i Pilot study – Cardioprotection by exenatide

Since both IPC and CsA cardioprotective interventions were previously investigated in this thesis, further pilot studies of these cardioprotective regimes were not required for this study (for details see chapter 4: IPC Figure 4.12 and CsA Figure 4.13). However, since exenatide had not been investigated in this model previously, an initial pilot study was required to evaluate the cardioprotective efficacy of this intervention. This pilot study showed that this exenatide dose (2.5 µg/kg I.V. and 2.5 µg/kg S.C. 5 minutes prior to the onset of reperfusion) did not elicit significant cardioprotection in this model (Figure 4.13: IS/AAR% vehicle control 42.5±4.4 versus exenatide 49.0±4.2; n=5/group, $^{NS}P>0.05$). There was no significant difference in AAR (AAR/LV% vehicle 65.4±4.2 versus exenatide 59.4±4.9; n=5/group, $^{NS}P>0.05$) or survival between these groups (survival to 24 hours reperfusion: vehicle 100% versus exenatide 100%, $^{NS}P>0.05$, excluding animals excluded due to unconfirmed dosing).

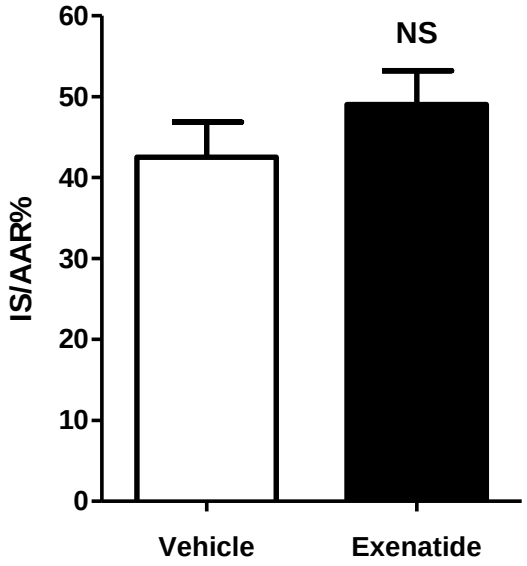

Figure 8.12: Pilot study of exenatide treatment
Pilot study investigating the effect of exenatide treatment on infarct size assessed by histological staining. B6/SV129 mice were randomised to receive either vehicle control or exenatide (2.5 µg/kg I.V. + 2.5 µg/kg S.C.). There was no significant difference in infarct size between these groups: IS/AAR% vehicle control 42.5±4.4 versus exenatide 49.0±4.2, n=5/group. Statistical significance assessed by unpaired t-test, $^{NS}P>0.05$.

Given the time and animals required to optimise this therapeutic strategy to evoke cardioprotection in this model, this therapeutic regime was not investigated further.

ii Cardioprotection by IPC and CsA

Histological analysis confirmed that IPC and CsA significantly reduced myocardial infarct size. Importantly, there was no significant difference in AAR between control and cardioprotected groups; thereby validating the comparison AAR quantification by cardiac MRI and histology in control and protected groups presented below.

A summary of the assessment of cardiac function in these animals is provided in Table 8.2. Although there were trends towards improved cardiac function in treated groups compared to the respective control group, there were no significant differences.

TREATMENT GROUP	Heart rate (BPM)	Stoke volume (µl)	Cardiac output (µl/min)	Ejection fraction (%)
Control	514.2 ±17.0	27.5 ±1.5	45.3 ±3.2	14.2 ±0.9
IPC	530.0 ±15.2	28.7 ±1.7	54.8 ±3.9	15.3 ±0.9
Vehicle	505.7 ±20.1	24.8 ±1.7	51.3 ±4.6	12.5 ±1.0
CsA	500.0 ±11.8	29.7 ±1.8	61.1 ±2.7	14.8 ±0.9

Table 8.2: Summary of MRI assessment of cardiac function
Endpoints of cardiac function for control and cardioprotected animals. Although there was a trend towards increased stroke volume, cardiac output and ejection fraction in cardioprotected animals compared to their respective controls (control versus IPC and vehicle versus CsA), there were no statistically significant differences. Significance assessed by unpaired t-test between control and treatment groups, $^{NS}P>0.05$.

iii Myocardial infarct size in cardioprotected hearts

To examine the validity of T_2-mapping and ASL cardiac MRI methods for quantifying myocardial AAR in the presence of cardioprotective interventions, the putative AAR determined by these cardiac MRI methods was compared with the histological AAR.

Quantification of absolute infarct size (IS/LV%) by LGE in these animals confirmed that there was no significant difference between 'gold-standard' histology and LGE methods for animals treated with IPC (Figure 8.13 A: histology IS/LV% 16.8±1.1 versus LGE MRI 18.0±1.6, n=10, P>0.05) or CsA (Figure 8.13 B: histology IS/LV% 21.9±1.5 versus LGE MRI 19.2±2.3, n=9, P>0.05). Bland-Altman analysis of LGE quantification of infarct size showed similar degrees of bias to that previously reported in control animals (Bland-Altman analysis bias ± standard deviation: IPC 1.2±3.9 versus CsA -2.7±9.4).

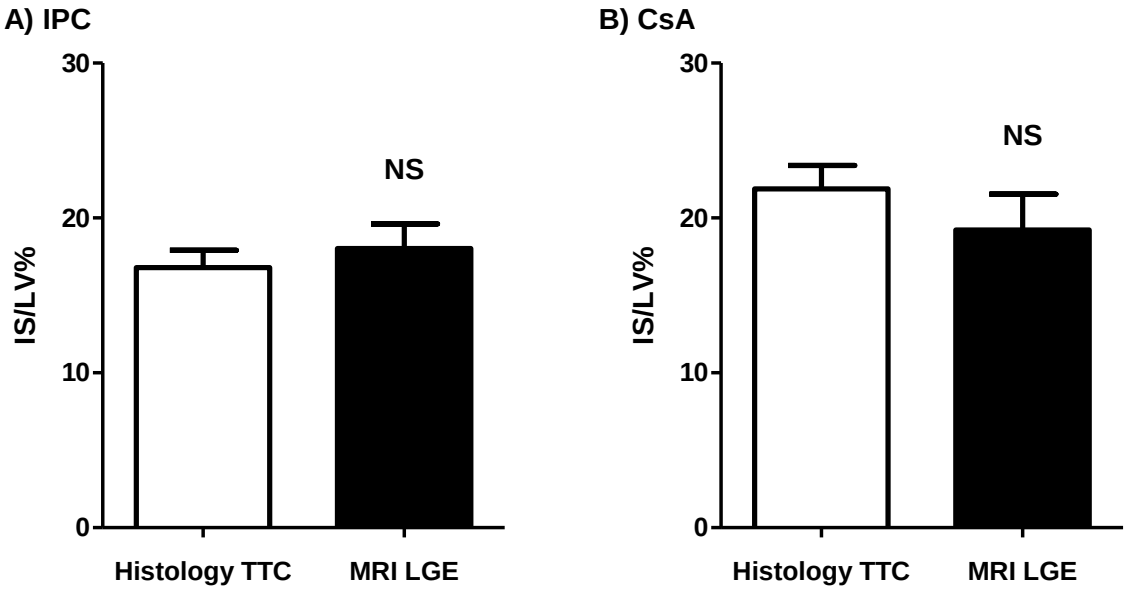

Figure 8.13: Infarct size assessment by LGE cardiac MRI
Quantification of infarct size as a percentage of LV area by histological TTC staining and cardiac MRI LGE imaging. A) IPC: IS/LV% histology TTC 16.8±1.1 versus MRI LGE 18.0±1.6, n=10, P>0.05. B) CsA: IS/LV% histology TTC 21.9±1.5 versus MRI LGE 19.2±2.3, n=9, P>0.05. Statistical significance assessed by paired t-test, ^{NS}P>0.05.

iv Area-at-risk in cardioprotected hearts

To evaluate the validity of T_2-mapping and ASL cardiac MRI quantification of myocardial AAR in the presence of cardioprotective interventions, IPC and CsA treated animals were imaged using these methods and the putative AAR calculated. It should be noted that the IPC control group data is described in the previous section and comparable results were obtained for control vehicle treated animals for the CsA study.

T_2-mapping MRI: This study showed that IPC significantly reduced the area of myocardial oedema meaning that T_2-mapping cardiac MRI significantly underestimated myocardial AAR (Figure 8.14 Ai: AAR/LV% histology 59.8±7.9 versus T_2-mapping cardiac MRI 46.0±13.2, n=10, *P<0.05). This was also evident in Bland-Altman analysis which showed a bias of -13.8 AAR/LV% (Figure 8.14 Aii). This degree of bias is likely to be biologically significant and therefore precludes the use of this T_2-mapping cardiac MRI method for AAR assessment in IPC treated animals in the model.

Interestingly, cardioprotection by CsA did not appear to affect the assessment of myocardial AAR using T_2-mapping cardiac MRI (Figure 8.14 Bi: AAR/LV% histology 58.0±4.2 versus T_2-mapping cardiac MRI 55.5±5.7, n=9, P>0.05). Bland-Altman analysis of AAR quantification by these methods in CsA treated animals showed reasonable agreement between the two methods with a mean bias of -2.50 AAR/LV% (Figure 8.14 Bii). This suggests that CsA does not significantly affect the area of oedema meaning that T_2-mapping cardiac MRI may be appropriate to assess AAR in these animals.

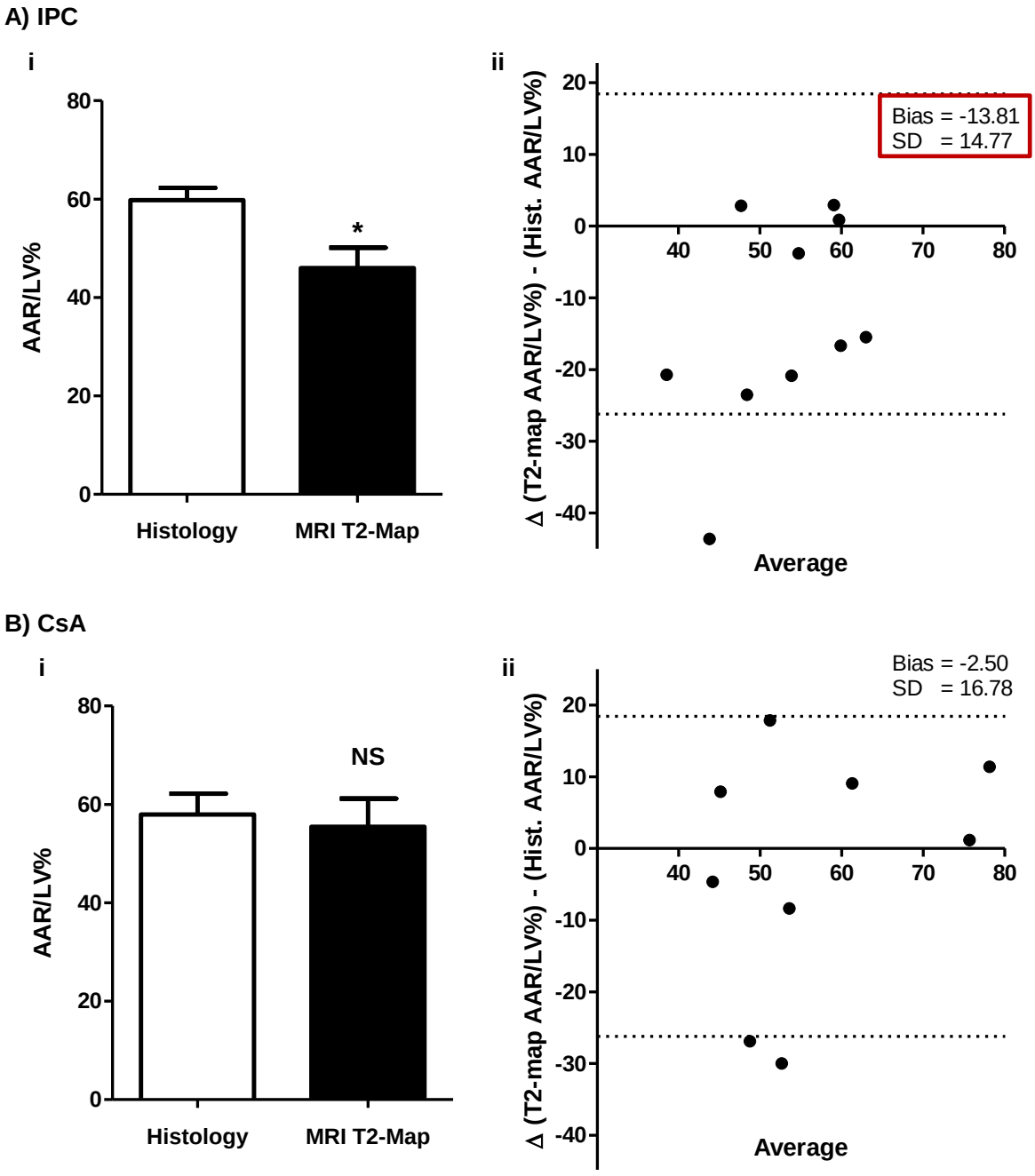

Figure 8.14: Area-at-risk assessment by T_2-mapping cardiac MRI in cardioprotected mice
Quantification of AAR as a percentage of LV area by histology (white bars) and cardiac MRI ASL (black bars) in cardioprotected mice. A) IPC: i) T_2-mapping cardiac MRI significantly underestimated myocardial AAR in IPC treated hearts; AAR/LV% histology 59.8±7.9 versus T_2-mapping MRI 46.0±13.2. Statistical significance assessed by paired t-test, n=10, *P<0.05. ii) Bland-Altman comparison of histological and T_2-mapping AAR quantification shows a large difference between AAR quantification by these two methods: bias -13.8±14.8 (SD). B) CsA: i) AAR/LV% histology 58.0±4.2 versus T_2-mapping MRI 55.5±5.7. Statistical significance assessed by paired t-test, n=8, ^{NS}P>0.05. B) Bland-Altman comparison of AAR quantification shows acceptable agreement: bias -2.50±16.8 (SD).

Comparison of mean T_2-values showed no difference between control and IPC hearts (Figure 8.15 A: mean T_2-value; normal T_2 control 17.0±0.6 versus IPC 19.8±1.4; elevated T_2 control 25.8±1.7 versus IPC 27.6±2.4; control n=6, IPC n=10) or vehicle and CsA hearts (Figure 8.15 B: mean T_2-value; normal T_2 vehicle 17.6±0.7 versus CsA 18.1±0.6; elevated T_2 vehicle 23.1±0.6 versus CsA 24.2±0.9; control n=7, IPC n=9).

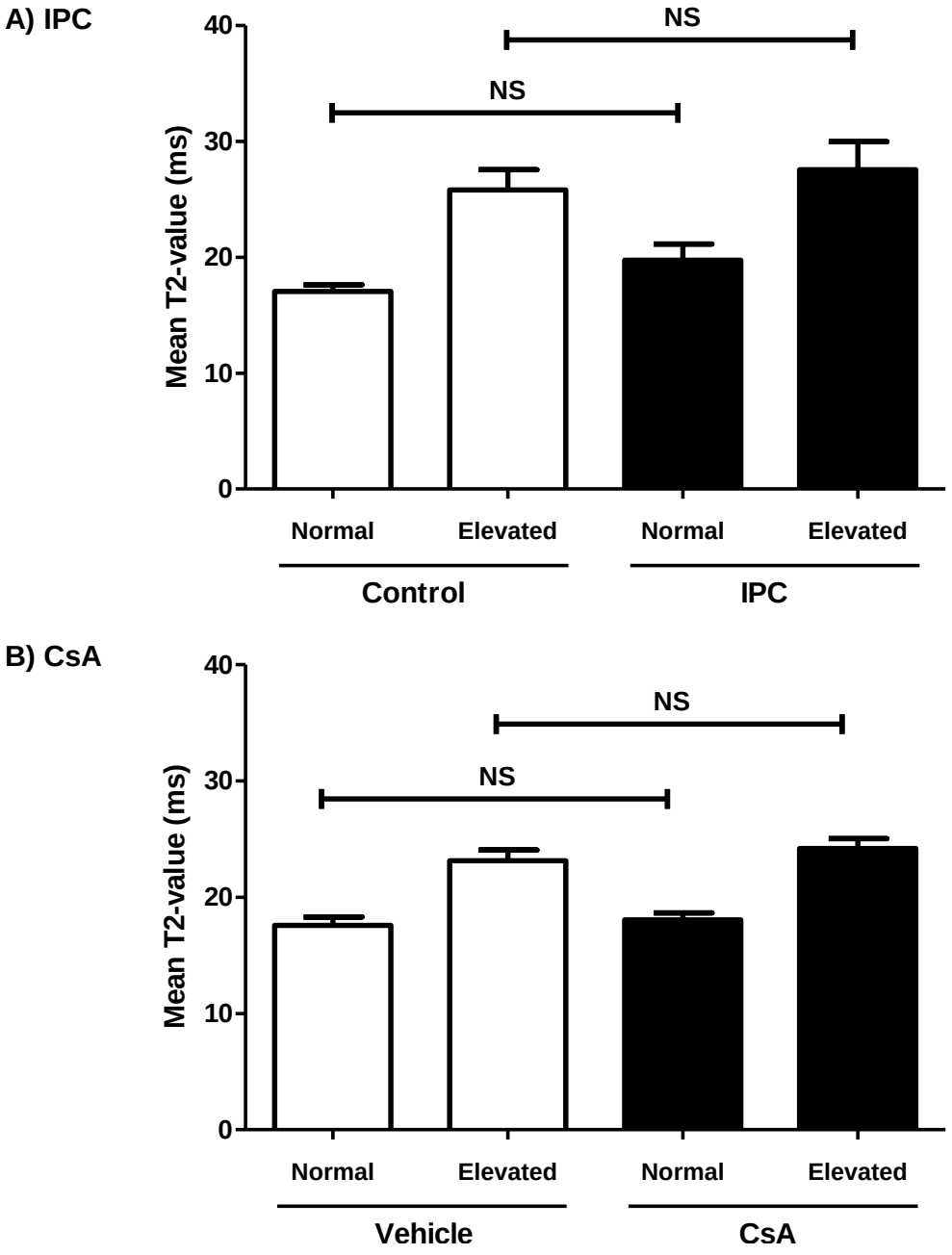

Figure 8.15: Absolute T_2-values for cardioprotected mice
Comparison of mean absolute T_2-values in areas deemed 'normal' and 'elevated' by threshold analysis. A) IPC: There was no difference in T_2-values between groups: normal T_2-value control 17.0±0.6 (n=6) versus IPC 19.8±1.4 (n=10) and elevated T_2 control 25.8±1.7 versus IPC 27.6±2.4. B) CsA: There was no difference in T_2-values between groups: normal T_2 control 17.6±0.7 (n=7) versus CsA 18.1±0.6 (n=9) and elevated T_2-value control 23.1±0.6 versus CsA 24.2±0.9. Statistical significance assessed by one-way ANOVA and Bonferroni test; $^{NS}P>0.05$.

This suggests that the absolute magnitude of myocardial oedema caused by ischaemia-reperfusion in these animals is not affected by the application of IPC or CsA and it is mainly the area of oedema that is changed in IPC treated mice (see Figure 8.14).

ASL MRI: ASL cardiac MRI was used to assess myocardial perfusion and quantify the putative AAR in the same cohort of animals. Importantly, this ASL method appeared to provide accurate quantification of AAR in IPC treated animals (Figure 8.16 Ai: AAR/LV% histology 58.0±3.0 versus T_2-mapping cardiac MRI 53.4±7.9, n=8, P>0.05). Bland-Altman analysis of this dataset showed a bias of -4.7 AAR/LV%, although it should be noted that the variation between these two methods is larger than is ideal. ASL cardiac MRI provided a good assessment of AAR in CsA treated animals (Figure 8.16 B: AAR/LV% histology 57.3±4.0 versus ASL cardiac MRI 63.0±4.3, n=9, P>0.05).

Comparison of the mean normal and decreased perfusion values from ASL-maps of these hearts showed no significant difference between control and IPC treated hearts (Figure 8.17 A: mean perfusion ± SEM; normal perfusion control 18.2±2.0 versus IPC 22.4±2.1; reduced perfusion control 5.6±0.6 versus IPC 6.4±0.5; control n=6, IPC n=7). Interestingly, the mean absolute perfusion value of 'normal' areas in the CsA treated group was significantly increased compared to vehicle controls (Figure 8.15 B: mean perfusion ± SEM; normal perfusion vehicle 16.9±0.5 versus CsA 29.5±3.6; reduced perfusion vehicle 4.8±0.7 versus CsA 9.1±1.2; vehicle n=6, CsA n=9). The increased magnitude of perfusion in CsA treated hearts does not appear to affect quantification of AAR from ASL-maps (Figure 8.16); discussed further later in this chapter (see 8.5.2).

In summary, IPC appears to reduce myocardial oedema thus invalidating the use of T_2-mapping cardiac MRI to asses AAR in these animals; interestingly, CsA did not appear to affect myocardial oedema. ASL cardiac MRI appeared to provide an appropriate measure of AAR in control, IPC and CsA treated animals.

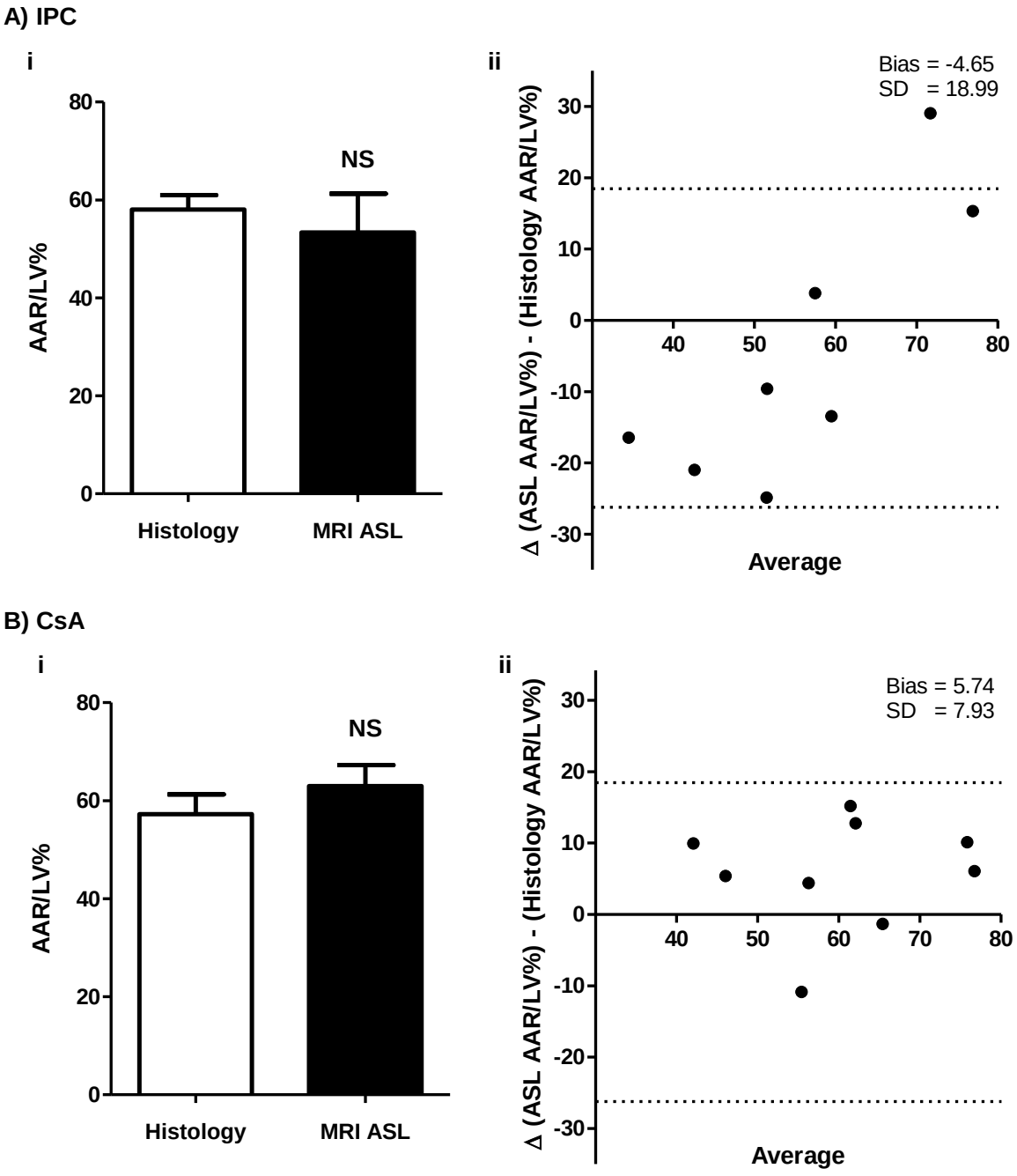

Figure 8.16: Area-at-risk assessment by ASL cardiac MRI in cardioprotected mice
Quantification of AAR as a percentage of LV area by histological staining (white bars) and cardiac MRI ASL (black bars) in cardioprotected mice. A) IPC: i) AAR/LV% histology 58.0±3.0 versus ASL MRI 53.4±7.9. Statistical significance assessed by paired t-test, n=8, $^{NS}P>0.05$. ii) Bland-Altman comparison of histological and ASL AAR quantification showed an acceptable average difference between AAR quantification by these two methods: bias -4.7±19.0 (SD). B) CsA: i) AAR/LV% histology 57.3±4.0 versus ASL MRI 63.0±4.3. Statistical significance assessed by paired t-test, n=9, $^{NS}P>0.05$. i) Bland-Altman comparison of histological and ASL AAR quantification showed an acceptable average difference between AAR quantification by these two methods: bias 5.7±7.9 (SD).

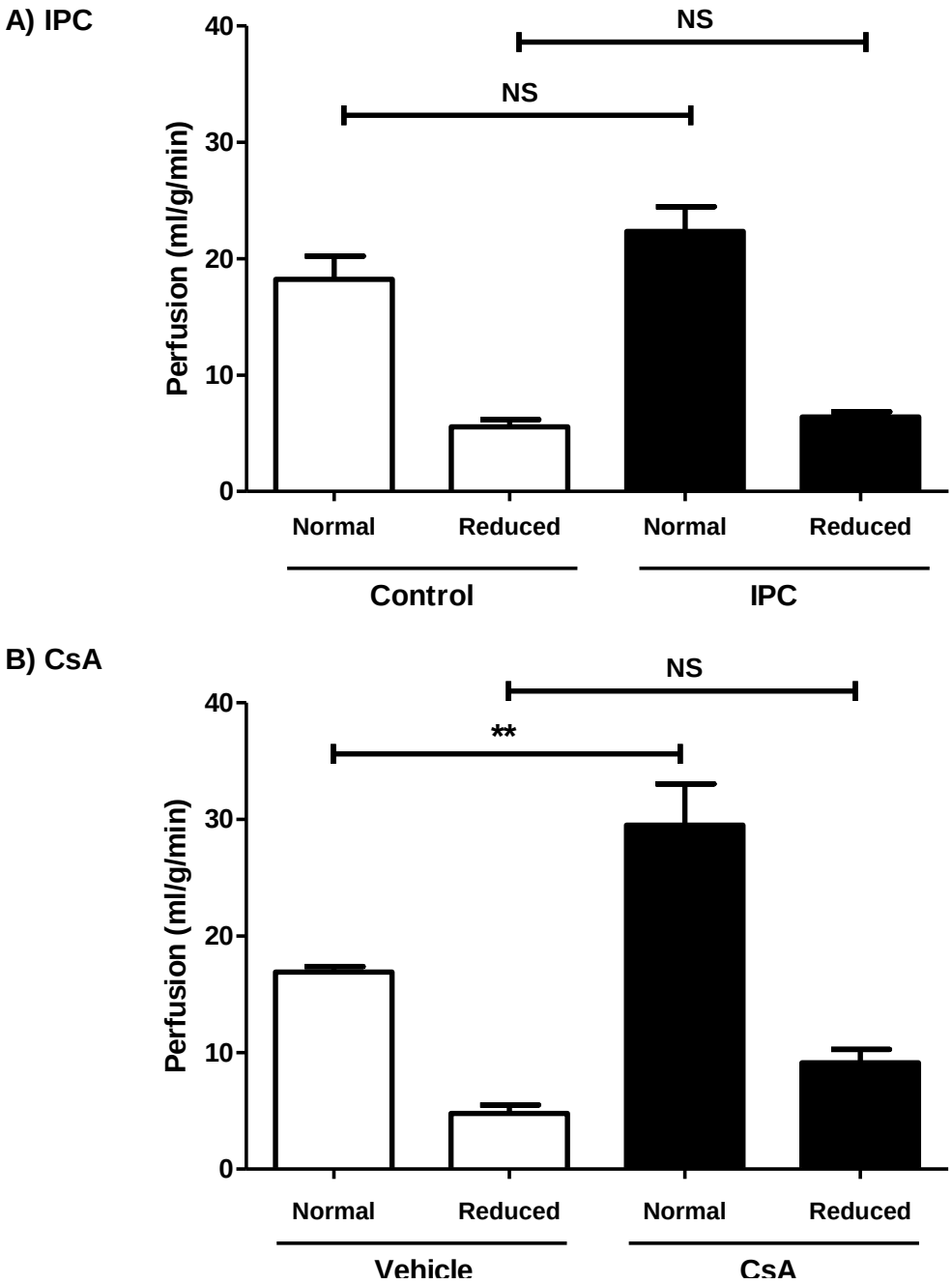

Figure 8.17: Absolute perfusion values for cardioprotected mice
Comparison of mean absolute perfusion values in areas of myocardium deemed 'normal' and 'AAR' by threshold analysis. A) IPC: There was no significant difference in perfusion between groups: normal perfusion control 18.2±2.0 (n=6) versus IPC 22.4±2.1 (n=7) and reduced perfusion control 5.6±0.6 versus IPC 6.4±0.5. Note: one IPC treated heart was excluded due to aberrant raw perfusion values. B) CsA: There was a significant increase in perfusion in 'normal' areas of CsA treated hearts (n=9) compared to vehicle controls (n=6): normal perfusion vehicle 16.9±0.5 versus CsA 29.5±3.6 and reduced perfusion vehicle 4.8±0.7 versus CsA 9.1±1.2. Note: one vehicle treated heart was excluded due to aberrant raw perfusion values. Significance assessed by one-way ANOVA and Bonferroni test comparing relevant groups.

Since this ASL method allows reasonably accurate AAR quantification, this method can be used to calculate IS/AAR%. This study demonstrated that there was no significant difference in IS/AAR% quantification by cardiac MRI (ASL and LGE) and histological staining for either IPC or CsA treated hearts. Crucially, this method allows detection of significant cardioprotection by these cardioprotective interventions compared to their respective controls (Figure 8.18; statistical significance assessed by unpaired t-tests).

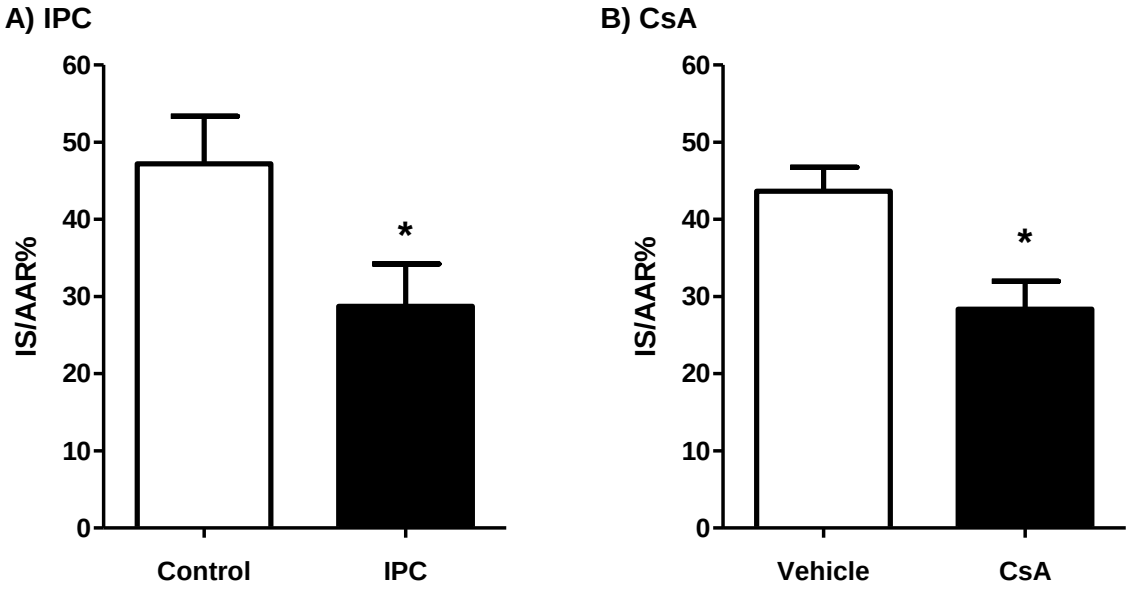

Figure 8.18: Quantification of infarct size controlled to AAR by cardiac MRI
Quantification of IS/AAR% by LGE and ASL cardiac MRI in animals subjected to IPC and CsA treatment (black bars) compared to respective control animals (white bars). A) IPC: IS/AAR% control 47.2±6.2 (n=6) versus IPC 28.7±5.5 (n=8), *P<0.05. B) CsA: IS/AAR% vehicle control 43.4±3.1 (n=6) versus CsA 28.4±3.7 (n=8). Statistical significance assessed by unpaired t-test.

8.5. Discussion

This chapter aimed to investigate and validate a cardiac MRI method of determining myocardial AAR *in vivo.* The need for this was highlighted in chapter 5 of this thesis where considering only absolute infarct size (IS/LV%) meant that very large sample sizes would be required to reach the appropriate statistical power to detect a significant difference in myocardial salvage between Cyp-D wildtype and knockout animals (see 5.3.3 iii, Figure 5.7). It had originally been intended that these mice would undergo long-term assessment of infarct size by serial cardiac MRI investigation; however, the lack of a fully validated method of determining AAR by cardiac MRI precluded this experiment.

The development of a robust and valid *in vivo* method for quantifying AAR would be widely applicable to many research projects within our laboratory and the wider field of ischaemia-reperfusion research. This chapter sought to investigate and validate a cardiac MRI method for quantifying AAR to complement LGE infarct size assessment.

8.5.1. Aim 1: Cardiac MRI for *in vivo* assessment of area-at-risk in control reperfused mouse hearts

Given the proposed use of T_2-weighted based cardiac MRI methods for quantifying AAR (reviewed by Garcia-Dorado et al., 2012), a T_2-mapping method was investigated in this chapter. In addition, an ASL perfusion based method was also applied to assess perfusion in the reperfused heart and potentially provide a measure of AAR. An initial pilot study developed and optimised multi-slice T_2-mapping and ASL cardiac MRI sequences to allow interrogation of the left ventricle (6-7 slices). This chapter describes the application of these sequences to mice following ischaemia-reperfusion where the validity of quantifications of putative AAR by these methods could be assessed by comparison with the AAR defined by 'gold-standard' histological staining methods.

T_2-mapping MRI: As expected from previous studies, T_2-mapping analysis of myocardial water content revealed spatially distinct regions of elevated T_2-signal which appeared to be located within the AAR judged by histological staining. Precise comparisons of the spatial distribution of the putative AAR determined by this method were hindered by the imprecise alignment of myocardial slices. This could be improved for future studies aimed at validating these cardiac MRI approaches, for example by using a slicing template for *ex vivo* preparation of hearts. However, since these methods provide a measure of the AAR over the whole heart (AAR/LV%), it is possible to compare the putative AAR calculated by cardiac MRI method to that obtained from 'gold-standard' histological staining. Evaluation of the putative AAR determined by T_2-mapping MRI showed that this was not significantly different to the quantification of AAR

by histology (Figure 8.7: bias -3.9±11.4 AAR/LV% ±SD). This indicates that on average across the control group examined here the T_2-mapping method slightly underestimated AAR by 3.9%. Although it should be noted that there is some spread in this dataset, it is unlikely that this bias in AAR calculation would be biologically significant.

This study therefore confirms that T_2-mapping cardiac MRI appears to be an appropriate method for quantifying myocardial AAR in control operated mice. This study is in accordance with previous studies in other experimental species and clinically (as summarised in chapter 1; see 1.5.2, Table 1.6). The validity of this cardiac MRI sequence for AAR quantification in cardioprotected animals is discussed below.

ASL MRI: This study also examined the use of an ASL approach to evaluate tissue perfusion in reperfused mouse hearts. Previous studies have shown that ischaemia-reperfusion causes impaired myocardial reperfusion and it has been hypothesised that the area of decreased perfusion may be confined to the AAR; thereby allowing potential quantification of AAR. Perfusion-based cardiac MRI has mainly examined the use of first-pass perfusion imaging where the perfusion of a contrast agent is used to identify areas of differential perfusion (an overview of these methods is provided in chapter 1; see 1.5.2 iii). The success of contrast perfusion methods in the mouse heart has been limited by the spatial and temporal resolution due to its small size and rapid heart rate.

The multi-slice ASL cardiac MRI sequence used here has been previously extensively developed by our collaborators at CABI. Application of this sequence to naïve mice showed good reproducibility of perfusion quantification between animals and scanning session to reveal normal perfusion values in the region of 10-15 ml/g/min with mean perfusion of 11.8±2.8 ml/g/min in standard CD1 mice (Campbell-Washburn et al., 2012). The studies undertaken in this thesis represents the first application of this multi-slice cardiac MRI sequence to the reperfused mouse heart.

ASL perfusion maps of the reperfused myocardium showed spatially distinct regions of reduced tissue perfusion which appeared to be spatially localised to the regions of AAR determined by histological staining. Given that the area of perfusion deficit was always larger than the area of infarction, it is unlikely that the measurement here reflects decreased perfusion within the infarcted area only. Quantification of the area of myocardium exhibiting decreased myocardial perfusion displayed good agreement with the AAR calculated by histological staining (Figure 8.9, bias -3.7±11.9 AAR/LV%±SD). This study provides the first suggestion that multi-slice ASL labelling may provide a means to determine myocardial AAR in reperfused hearts. The validity of this measurement is examined further below.

The biological basis of the perfusion deficit identified within the myocardial AAR has not been investigated here. The reduced perfusion within the AAR is not expected to correspond to unsuccessful reperfusion of the LAD coronary artery in this model but instead some impairment of microvascular perfusion within the capillary bed of these hearts. This is discussed below in relation to validity of ASL MRI for AAR quantification.

It should be noted that the extent of 'normal' tissue perfusion in these animals appeared to be higher than those previously published using this model (Figure 8.18 B: normal tissue perfusion in control mice 18.2±2.0 ml/g/min compared to the previous published study showing normal perfusion of 11.8±2.8 ml/g/min) (Campbell-Washburn et al., 2012). Previous investigations have shown that myocardial perfusion is very sensitive to isoflurane dosing, whereby increasing isoflurane concentration from 1.25% to 2.0% caused an approximate 2.5-fold increase in tissue perfusion (Kober et al., 2005; Campbell-Washburn et al., 2013). The slightly higher perfusion observed here could derive from a difference in isoflurane dosing of these animals. Although the experiments presented here used the minimal dose of isoflurane required to maintain steady anaesthesia, there may be subtle differences of anaesthetic sensitivity of the reperfused B6/SV129 mice compared to the CD-1 mice previously investigated. Tissue perfusion rates are discussed below in relation to the effect of cardioprotective interventions.

It should also be noted that the procedural survival of animals subjected to this cardiac MRI scanning protocol was lower than would ideally be expected. A number of animals did not survive to the end of the scanning protocol, likely due to complications arising from the prolonged duration of anaesthesia (which on occasion reached 3 hours). Animals which did not survive to the completion of the MRI protocol were excluded from the analyses of infarct size and area-at-risk quantification in this chapter. Further refinement of the MRI sequences in future may allow the overall scan time to be reduced. The resultant decrease in anaesthetic duration would likely improve procedural survival and would therefore be an important development for future applications of these methods for long-term studies of cardioprotective efficacy.

A further caveat to the interpretation of the quantification of AAR using both T_2-mapping and ASL methods presented here is the potential limitations of the thresholding technique used for analysis. The threshold method used here relied on the identification of a region-of-interest within the myocardium corresponding to the non-AAR to allow comparison of the rest of the tissue with this 'normal' region. This threshold approach was based on deviance in T_2-signal or perfusion value of 1 standard deviation from this mean normal value. There is significant future potential to improve this analysis method and this may improve the quantification of AAR using these methods in future studies.

8.5.2. Aim 2: Validity of cardiac MRI area-at-risk quantification in the presence of cardioprotective interventions

The second part of this chapter therefore sought to investigate the effect of cardioprotective interventions on the quantification of myocardial AAR by T_2-mapping and ASL cardiac MRI. This is particularly pertinent given the recent suggestions that certain cardioprotective interventions may reduce the extent of myocardial oedema (Thuny et al., 2012; Crimi et al., 2013). Since clinical assessments of the validity of cardiac MRI methods of determining AAR rely on imprecise comparisons with angiographic scores to infer the true AAR, the ability to directly compare AAR measurements across equivalent myocardial slices subjected to 'gold-standard' histological staining provides an important tool for accurate validation.

This thesis examined the effects cardioprotection by IPC and CsA on the validity of AAR assessment by these MRI methods. Histological analysis of these hearts showed that both of these cardioprotective interventions significantly reduced myocardial infarct size (IS/AAR%). Importantly, there was also no difference in AAR between groups thereby allowing comparison of the validity of AAR assessment by cardiac MRI.

T_2-mapping MRI: This study showed that IPC significantly reduced the area of myocardium exhibiting an elevated T_2-signal, therefore suggesting that IPC reduces the extent of myocardial oedema. Quantification of the putative AAR using this T_2-mapping protocol underestimated the AAR by approximately 13.8% in IPC treated animals (Figure 8.14; bias -13.8±14.8 AAR/LV% ±SD). This underestimation of AAR by T_2-mapping MRI is clearly shown by Bland-Altman analysis of AAR. Crucially, this corresponded to a statistically significant underestimation of AAR by T_2-mapping in this IPC treated group (Figure 8.14 A). This extent of bias in AAR quantification is likely to be biologically significant for any subsequent calculation of myocardial salvage and therefore suggests that T_2-mapping cardiac MRI is not appropriate for AAR quantification in the presence of cardioprotection by IPC in this model.

Interestingly, CsA did not appear to significantly affect the area of myocardium exhibiting an elevated T_2-signal and provided a reasonably accurate quantification of AAR in these animals (Figure 8.14 B; bias -2.5±16.8 AAR/LV% ±SD). The slight underestimation of AAR by ASL cardiac MRI (-2.5% AAR/LV) is unlikely to be biologically significant, although the variation in AAR assessment by this method was larger than is ideal. This may reflect the increased variation in the response to this intervention which is perhaps expected given the natural variation of any *in vivo* system and the potential variation in the success of intravenous drug dosing. This suggests that despite the cardioprotective effect of CsA in reducing infarct size, it does not appear to affect the development of

oedema. This could perhaps be taken as evidence that these interventions exert differential protective effects against ischaemia-reperfusion, this is discussed below.

The potential differential effects of IPC and CsA on the extent of myocardial oedema could provide support to the previous clinical studies which showed that the mechanical interventions, IPost and RIPost, but not the pharmacological intervention exenatide reduced myocardial oedema (Thuny et al., 2012; Lonborg et al., 2012a; 2012b; Crimi et al., 2013). However, these early studies do not provide sufficient evidence of a mechanistic difference between these mechanical and pharmacological interventions for which extensive further studies are now required. It is important to note however, that in the present study, there was a slight increase in the control infarct size caused by the vehicle meaning that despite significant cardioprotection by CsA, there was a difference in the infarct sizes between IPC and CsA treated animals. This may, therefore, account for some difference in the degree of myocardial oedema between these groups. It is therefore not possible to conclude from this study alone that IPC and CsA mediate differential effects on myocardial oedema.

These findings could suggest that myocardial oedema is related to the extent of myocardial infarction whereby it would be expected that myocardial oedema would increase with the duration of ischaemia. This may pose an additional confounding factor to the use of T_2-weighted based cardiac MRI methods for quantifying AAR clinically, where there is substantial variation in the ischaemic duration between patients. This has not yet been investigated directly, although Abel-Aty et al. (2009) showed that sublethal ischaemic durations caused myocardial oedema (Abdel-Aty et al., 2009). Since previous clinical studies have shown reasonably accurate assessment of AAR by T_2-weighted based MRI, it is likely that any potential effects of ischaemic duration do not preclude the use of this approach with large sample sizes. A measure of AAR that is not significantly affected by ischaemic duration may provide a more sensitive method of evaluating myocardial salvage and may therefore reduce the sample sizes required for clinical studies of cardioprotection; this is discussed further below.

The potential influence of reperfusion duration on the pathophysiology of myocardial oedema is also an important consideration for the further application of T_2-weighted based MRI approaches to quantifying AAR. Future studies could undertake an in-depth analysis of the time-course of manifestation of myocardial oedema over the initial period of reperfusion. Mather et al. (2011) showed significant resolution of myocardial oedema in acute myocardial infarction patients between days 2 and 7 of reperfusion (Mather et al., 2011). Oedema may become an interesting additional endpoint to assess the effects of potential therapeutic interventions in modulating the degree of myocardial injury. To

this end, it would be of value to assess the effect of interventions on the time-course of the development and resolution of oedema following ischaemia-reperfusion. However, since this study has shown that T_2-mapping MRI does not provide a reliable measure of AAR in the presence of IPC, this was not investigated further in this thesis.

ASL MRI: Given the promising nature of ASL perfusion mapping for quantification of AAR in control animals, the effect of cardioprotective interventions on the validity of this approach was also examined. This study showed that neither IPC nor CsA significantly affected the quantification of AAR by ASL cardiac MRI (Figure 8.16). It should be noted that there was a degree of bias associated with AAR quantification by this method (Figure 8.16: %AAR/LV bias in animals treated with IPC -4.7±19.0 and CsA 5.7±7.9). However, it was not expected that this would have a biologically significant effect for the quantification of myocardial salvage using this method of AAR calculation. Indeed, calculation of infarct size as a percentage of AAR (IS/AAR%) by LGE and ASL cardiac MRI showed that it was possible to detect significant cardioprotection by these interventions (Figure 8.18). This study therefore suggests that ASL cardiac MRI provides a valid method for quantifying myocardial AAR even in the presence of the cardioprotective interventions tested here.

It remains possible that other cardioprotective interventions may affect the validity of AAR quantification by ASL cardiac MRI. It could be expected that if an intervention were to modify myocardial perfusion that this may in turn affect the calculation of AAR by ASL MRI, since this method is based on detection of a perfusion deficit. Indeed, nitrate treatment has been shown to improve myocardial perfusion in reperfused canine hearts (Gonzalez et al., 2008). Interestingly, analysis of myocardial perfusion by ASL MRI showed that CsA treatment significantly increased the rate of 'normal' perfusion in the non-AAR (Figure 8.17: normal perfusion in vehicle 16.9±0.5 versus CsA 29.5±3.6 ml/g/min). Since an equivalent increase was not observed in IPC treated animals, it is unlikely that this corresponds to increased cardiac function in these animals. Although this remains an intriguing and unexplained effect of CsA, it did not influence the calculation of AAR by this method since the area of decreased perfusion was defined by a threshold approach based on this normal value (as described in section 8.3.2 ii). This study therefore suggests that ASL cardiac MRI may provide a valid method for AAR quantification even in the presence of cardioprotective interventions which increase myocardial perfusion. This should be investigated further in order to fully validate the use of this cardiac MRI method for assessing myocardial salvage.

It also remains to be seen whether the duration of myocardial ischaemia significantly affects the extent of perfusion deficit and AAR calculation by ASL MRI. However, the

immediate purpose of this study was to provide an *in vivo* method for AAR quantification for use in small animal studies, where the ischaemic duration is precisely controlled between animals. Investigation of the reliability of ASL AAR quantification at varied ischaemic durations would be required prior to clinical investigation of this method.

Overall, this study shows that ASL cardiac MRI may provide a more suitable method for quantifying myocardial AAR *in vivo* following ischaemia-reperfusion injury. Further studies are now required to complete the validation of this method for its wider use.

8.5.3. Summary

The main research objective of this chapter was to investigate and validate a cardiac MRI method to quantify myocardial AAR *in vivo* in the reperfused mouse heart. The ultimate aim of this study was to provide a fully validated method for calculating myocardial salvage in order to accurately assess the cardioprotective efficacy of novel therapeutic interventions. The main findings of this chapter are summarised below:

(1) T_2-mapping cardiac MRI detected clearly defined regions of elevated T_2-signal which appeared to be spatially localised within the known AAR. Although this T_2-mapping approach allowed accurate quantification of AAR in control operated animals, IPC significantly reduced the area of myocardial oedema and thus resulted in a significant underestimation of AAR by this method in IPC treated animals.

    Interestingly, CsA treatment did not appear to significantly affect the area of elevated T_2-signal meaning that this T_2-mapping approach still allowed accurate AAR quantification in CsA treated animals. Further studies are required to investigate the potential differential effects of cardioprotective interventions on myocardial oedema.

(2) ASL perfusion cardiac MRI showed clearly defined regions of decreased myocardial perfusion which appeared to be spatially localised within the known AAR. Quantification of the area of myocardium exhibiting decreased perfusion showed good agreement with the true AAR and therefore suggested that ASL cardiac MRI may provide a novel method to quantify AAR *in vivo* following ischaemia-reperfusion. Importantly, this study showed that cardioprotection by IPC and CsA did not significantly affect the validity of the quantification of AAR by ASL cardiac MRI.

Further investigations are now required to fully validate the use of ASL cardiac MRI to assess myocardial salvage. Since ASL cardiac MRI sequences are also available for use in clinical MRI, the work presented here may provide an important platform for the future direction of studies of cardioprotection in both the pre-clinical and clinical settings.

CHAPTER 9: OVERALL CONCLUSIONS

The overall aim of this thesis was to investigate the potential modulation of important mitochondrial proteins to confer long-term cardioprotection against myocardial ischaemia-reperfusion. This thesis has examined the potential cardioprotective efficacy of targeting cyclophilin-D, sirtuin-3 and DJ-1 to affect mitochondrial function and survival to ultimately affect cell survival. The cardioprotective efficacy of these potential targets has been discussed in detail in the previous chapters and since these represent distinct targets, the overall discussion of the findings of this thesis necessarily focuses on the main themes and future directions highlighted during the course of these studies.

Overall, it appears that modulation of each of these mitochondrial proteins may provide a therapeutic target for cardioprotection against myocardial ischaemia-reperfusion injury. This thesis highlights the importance of mitochondria for the maintenance of cellular function and survival in this pathological setting. Mitochondria are likely to represent important therapeutic targets for a number of pathologies involving cell death. The importance of mitochondrial function in the heart may be particularly acute given its high metabolic demand which means that mitochondrial dysfunction may manifest as a more severe phenotype. Further studies of the potential adverse side-effects of therapeutic targets aimed at mitochondrial proteins are required given the potential severity of metabolic dysfunction which could occur. This is particularly important for modulation of Cyp-D activity which has been shown to confer some adverse long-term effects (Oie et al., 2000; Elrod and Molkentin, 2013) and should be investigated further.

Although the use of genetic knockout models in this thesis has been fundamental to identifying the potential involvement of these mitochondrial proteins in the pathophysiology of ischaemia-reperfusion injury, their use may introduce further confounding effects. Global genetic ablation of proteins may result in compensatory mechanisms, which in turn may affect the phenotype of these animals at baseline and under pathological stress (reveiwed by Davis et al., 2012). This has been discussed in the relevant chapters of this thesis in relation to the proteins examined here and highlights the need for improved pharmacological inhibitors and activators of these proteins. Improvements to the chemical derivation of targeted drug therapies may facilitate the investigation of these mitochondrial targets in future. Mitochondrial-targeting of compounds presents an interesting and potentially improvement advance to this field. Although the development and characterisation of mitochondrial-targeted CsA is still in its infancy (Malouitre et al., 2010; Dube et al., 2012), this chemical approach

may provide further selectivity to existing pharmacological compounds and is likely to be an interesting direction of future research in the field of cardioprotection.

The importance of examining the long-term cardioprotective efficacy of potential therapeutic interventions has been discussed in detail in this thesis. The model of ischaemia-reperfusion injury developed here permits evaluation of myocardial infarct size, cardiac function and survival at prolonged durations of reperfusion. The assessment of cardioprotective efficacy however, requires assessment of both infarct size and the AAR to evaluate the extent of protection conferred by an intervention. Although the T_2-weighted cardiac MRI approaches currently in use in pre-clinical and clinical studies provide a reasonable measure of AAR under control conditions, there is mounting evidence that this may not be valid in all circumstances. The investigation of T_2-mapping cardiac MRI here showed that cardioprotection by a mechanical intervention, IPC, significantly reduced myocardial oedema and thus invalidated the quantification of AAR by this approach. In combination with the similar findings of two recent clinical studies (Thuny et al., 2012; Crimi et al., 2013), it appears that caution should be exercised with the use of T_2-weighted based cardiac MRI for quantifying myocardial AAR in the presence of cardioprotective interventions.

Investigation of a perfusion-based cardiac MRI method, ASL, to assess areas of the reperfused myocardium exhibiting decreased tissue perfusion, suggests that this may present a more appropriate and robust method for quantifying the AAR in this setting. Although further studies are required to fully validate this approach, the studies presented here support the use of ASL cardiac MRI as a novel method for determining AAR. Since ASL cardiac MRI sequences are already available clinically, it would be intriguing to now investigate the application of this method for clinical studies of cardioprotection. Further development of *in vivo* imaging methods has the potential to improve experimental pre-clinical and clinical studies of cardioprotection and thus potentially facilitate development and identification of novel cardioprotective therapies.

CHAPTER 10: REFERENCES

Abbott Animal Health. IsoFlo®; Isoflurane USP. 4. 2006. United Kingdom.

Abdel-Aty H, Cocker M, Meek C, Tyberg JV, Friedrich MG (Edema as a very early marker for acute myocardial ischemia: a cardiovascular magnetic resonance study. J Am Coll Cardiol 53:1194-1201.2009).

Ahn BH, Kim HS, Song S, Lee IH, Liu J, Vassilopoulos A, Deng CX, Finkel T (A role for the mitochondrial deacetylase Sirt3 in regulating energy homeostasis. Proc Natl Acad Sci U S A 105:14447-14452.2008).

Alberts B, Johnson A, Lewis J, Raff M, Roberts K, Walter P (2002) Molecular Biology of the Cell. USA: Garland Science.

Aletras AH, Tilak GS, Natanzon A, Hsu LY, Gonzalez FM, Hoyt RF, Jr., Arai AE (Retrospective determination of the area at risk for reperfused acute myocardial infarction with T2-weighted cardiac magnetic resonance imaging: histopathological and displacement encoding with stimulated echoes (DENSE) functional validations. Circulation 113:1865-1870.2006).

Aleyasin H, Rousseaux MW, Phillips M, Kim RH, Bland RJ, Callaghan S, Slack RS, During MJ, Mak TW, Park DS (The Parkinson's disease gene DJ-1 is also a key regulator of stroke-induced damage. Proc Natl Acad Sci U S A 104:18748-18753.2007).

Anderson EJ, Katunga LA, Willis MS (Mitochondria as a source and target of lipid peroxidation products in healthy and diseased heart. Clin Exp Pharmacol Physiol 39:179-193.2012).

Andres-Mateos E, Perier C, Zhang L, Blanchard-Fillion B, Greco TM, Thomas B, Ko HS, Sasaki M, Ischiropoulos H, Przedborski S, Dawson TM, Dawson VL (DJ-1 gene deletion reveals that DJ-1 is an atypical peroxiredoxin-like peroxidase. Proc Natl Acad Sci U S A 104:14807-14812.2007).

Appleton GO, Li Y, Taffet GE, Hartley CJ, Michael LH, Entman ML, Roberts R, Khoury DS (Determinants of cardiac electrophysiological properties in mice. J Interv Card Electrophysiol 11:5-14.2004).

Arai AE (Magnetic resonance imaging for area at risk, myocardial infarction, and myocardial salvage. J Cardiovasc Pharmacol Ther 16:313-320.2011a).

Arai AE (The cardiac magnetic resonance (CMR) approach to assessing myocardial viability. J Nucl Cardiol 18:1095-1102.2011b).

Argaud L, Gateau-Roesch O, Muntean D, Chalabreysse L, Loufouat J, Robert D, Ovize M (Specific inhibition of the mitochondrial permeability transition prevents lethal reperfusion injury. J Mol Cell Cardiol 38:367-374.2005).

Baines CP (The mitochondrial permeability transition pore and ischemia-reperfusion injury. Basic Res Cardiol 104:181-188.2009a).

Baines CP (The molecular composition of the mitochondrial permeability transition pore. J Mol Cell Cardiol 46:850-857.2009b).

Baines CP, Kaiser RA, Purcell NH, Blair NS, Osinska H, Hambleton MA, Brunskill EW, Sayen MR, Gottlieb RA, Dorn GW, Robbins J, Molkentin JD (Loss of cyclophilin D reveals a critical role for mitochondrial permeability transition in cell death. Nature 434:658-662.2005).

Balaban RS (The mitochondrial proteome: a dynamic functional program in tissues and disease states. Environ Mol Mutagen 51:352-359.2010).

Bao J, Sack MN (Protein deacetylation by sirtuins: delineating a post-translational regulatory program responsive to nutrient and redox stressors. Cell Mol Life Sci 67:3073-3087.2010).

Bao J, Scott I, Lu Z, Pang L, Dimond CC, Gius D, Sack MN (SIRT3 is regulated by nutrient excess and modulates hepatic susceptibility to lipotoxicity. Free Radic Biol Med 49:1230-1237.2010).

Barik S (Immunophilins: for the love of proteins. Cell Mol Life Sci 63:2889-2900.2006).

Basso E, Fante L, Fowlkes J, Petronilli V, Forte MA, Bernardi P (Properties of the permeability transition pore in mitochondria devoid of Cyclophilin D. J Biol Chem 280:18558-18561.2005).

Baxter GF, Goma FM, Yellon DM (Characterisation of the infarct-limiting effect of delayed preconditioning: timecourse and dose-dependency studies in rabbit myocardium. Basic Res Cardiol 92:159-167.1997).

Bell RM, Mocanu MM, Yellon DM (Retrograde heart perfusion: the Langendorff technique of isolated heart perfusion. J Mol Cell Cardiol 50:940-950.2011).

Belle V, Kahler E, Waller C, Rommel E, Voll S, Hiller KH, Bauer WR, Haase A (In vivo quantitative mapping of cardiac perfusion in rats using a noninvasive MR spin-labeling method. J Magn Reson Imaging 8:1240-1245.1998).

Berger F, Lau C, Dahlmann M, Ziegler M (Subcellular compartmentation and differential catalytic properties of the three human nicotinamide mononucleotide adenylyltransferase isoforms. J Biol Chem 280:36334-36341.2005).

Bergsma DJ, Eder C, Gross M, Kersten H, Sylvester D, Appelbaum E, Cusimano D, Livi GP, McLaughlin MM, Kasyan K, . (The cyclophilin multigene family of peptidyl-prolyl isomerases. Characterization of three separate human isoforms. J Biol Chem 266:23204-23214.1991).

Bernardi P (The mitochondrial permeability transition pore: a mystery solved? Front Physiol 4:95.2013).

Bernardi P, Scorrano L, Colonna R, Petronilli V, Di LF (Mitochondria and cell death. Mechanistic aspects and methodological issues. Eur J Biochem 264:687-701.1999).

Berry C, Kellman P, Mancini C, Chen MY, Bandettini WP, Lowrey T, Hsu LY, Aletras AH, Arai AE (Magnetic resonance imaging delineates the ischemic area at risk and myocardial salvage in patients with acute myocardial infarction. Circ Cardiovasc Imaging 3:527-535.2010).

Beyers RJ, Smith RS, Xu Y, Piras BA, Salerno M, Berr SS, Meyer CH, Kramer CM, French BA, Epstein FH (T(2) -weighted MRI of post-infarct myocardial edema in mice. Magn Reson Med 67:201-209.2012).

Billia F, Hauck L, Grothe D, Konecny F, Rao V, Kim RH, Mak TW (Parkinson-susceptibility gene DJ-1/PARK7 protects the murine heart from oxidative damage in vivo. Proc Natl Acad Sci U S A 110:6085-6090.2013).

Bitterman KJ, Anderson RM, Cohen HY, Latorre-Esteves M, Sinclair DA (Inhibition of silencing and accelerated aging by nicotinamide, a putative negative regulator of yeast sir2 and human SIRT1. J Biol Chem 277:45099-45107.2002).

Black SC, Rodger IW (Methods for studying experimental myocardial ischemic and reperfusion injury. J Pharmacol Toxicol Methods 35:179-190.1996).

Blackinton J, Ahmad R, Miller DW, van der Brug MP, Canet-Aviles RM, Hague SM, Kaleem M, Cookson MR (Effects of DJ-1 mutations and polymorphisms on protein stability and subcellular localization. Brain Res Mol Brain Res 134:76-83.2005).

Blackinton J, Kumaran R, van der Brug MP, Ahmad R, Olson L, Galter D, Lees A, Bandopadhyay R, Cookson MR (Post-transcriptional regulation of mRNA associated with DJ-1 in sporadic Parkinson disease. Neurosci Lett 452:8-11.2009a).

Blackinton J, Lakshminarasimhan M, Thomas KJ, Ahmad R, Greggio E, Raza AS, Cookson MR, Wilson MA (Formation of a stabilized cysteine sulfinic acid is critical for the mitochondrial function of the parkinsonism protein DJ-1. J Biol Chem 284:6476-6485.2009b).

Bohl S, Lygate CA, Schulz-Menger J, Neubauer S, Schneider JE. T2-mapping of ischaemia/reperfusion-injury in the in vivo mouse heart. Journal of Cardiovascular Magnetic Resonance 12[Supp 1]. 2010.

Bolli R, Becker L, Gross G, Mentzer R, Jr., Balshaw D, Lathrop DA (Myocardial protection at a crossroads: the need for translation into clinical therapy. Circ Res 95:125-134.2004).

Bolli R, Jeroudi MO, Patel BS, Aruoma OI, Halliwell B, Lai EK, McCay PB (Marked reduction of free radical generation and contractile dysfunction by antioxidant therapy begun at the time of reperfusion. Evidence that myocardial "stunning" is a manifestation of reperfusion injury. Circ Res 65:607-622.1989).

Bonifati V, Rizzu P, van Baren MJ, Schaap O, Breedveld GJ, Krieger E, Dekker MC, Squitieri F, Ibanez P, Joosse M, van Dongen JW, Vanacore N, van Swieten JC, Brice A, Meco G, van Duijn CM, Oostra BA, Heutink P (Mutations in the DJ-1 gene associated with autosomal recessive early-onset parkinsonism. Science 299:256-259.2003).

Bonora M, Bononi A, De ME, Giorgi C, Lebiedzinska M, Marchi S, Patergnani S, Rimessi A, Suski JM, Wojtala A, Wieckowski MR, Kroemer G, Galluzzi L, Pinton P (Role of the c subunit of the FO ATP synthase in mitochondrial permeability transition. Cell Cycle 12:674-683.2013).

Braunwald E, Kloner RA (Myocardial reperfusion: a double-edged sword? J Clin Invest 76:1713-1719.1985).

Bretaud S, Allen C, Ingham PW, Bandmann O (p53-dependent neuronal cell death in a DJ-1-deficient zebrafish model of Parkinson's disease. J Neurochem 100:1626-1635.2007).

Buckberg GD, Coghlan HC, Torrent-Guasp F (The structure and function of the helical heart and its buttress wrapping. V. Anatomic and physiologic considerations in the healthy and failing heart. Semin Thorac Cardiovasc Surg 13:358-385.2001).

Campbell-Washburn AE, Price AN, Wells JA, Thomas DL, Ordidge RJ, Lythgoe MF (Cardiac arterial spin labeling using segmented ECG-gated Look-Locker FAIR: variability and repeatability in preclinical studies. Magn Reson Med 69:238-247.2013).

Campbell-Washburn AE, Zhang H, Siow BM, Price AN, Lythgoe MF, Ordidge RJ, Thomas DL (Multislice cardiac arterial spin labeling using improved myocardial perfusion quantification with simultaneously measured blood pool input function. Magn Reson Med.2012).

Camper-Kirby D, Welch S, Walker A, Shiraishi I, Setchell KD, Schaefer E, Kajstura J, Anversa P, Sussman MA (Myocardial Akt activation and gender: increased nuclear activity in females versus males. Circ Res 88:1020-1027.2001).

Canet-Aviles RM, Wilson MA, Miller DW, Ahmad R, McLendon C, Bandyopadhyay S, Baptista MJ, Ringe D, Petsko GA, Cookson MR (The Parkinson's disease protein DJ-1 is neuroprotective due to cysteine-sulfinic acid-driven mitochondrial localization. Proc Natl Acad Sci U S A 101:9103-9108.2004).

Carmeliet E (Cardiac ionic currents and acute ischemia: from channels to arrhythmias. Physiol Rev 79:917-1017.1999).

Cell Signalling Technologies. Western blotting - Horseradish-peroxidase (HRP) linked secondary antibodies - Datasheet. 2012.

Chen J, Li L, Chin LS (Parkinson disease protein DJ-1 converts from a zymogen to a protease by carboxyl-terminal cleavage. Hum Mol Genet 19:2395-2408.2010).

Chen Y, Zhang J, Lin Y, Lei Q, Guan KL, Zhao S, Xiong Y (Tumour suppressor SIRT3 deacetylates and activates manganese superoxide dismutase to scavenge ROS. EMBO Rep 12:534-541.2011).

Chiong M, Wang ZV, Pedrozo Z, Cao DJ, Troncoso R, Ibacache M, Criollo A, Nemchenko A, Hill JA, Lavandero S (Cardiomyocyte death: mechanisms and translational implications. Cell Death Dis 2:e244.2011).

Choudhary C, Kumar C, Gnad F, Nielsen ML, Rehman M, Walther TC, Olsen JV, Mann M (Lysine acetylation targets protein complexes and co-regulates major cellular functions. Science 325:834-840.2009).

Cimen H, Han MJ, Yang Y, Tong Q, Koc H, Koc EC (Regulation of succinate dehydrogenase activity by SIRT3 in mammalian mitochondria. Biochemistry 49:304-311.2010).

Clarke SJ, McStay GP, Halestrap AP (Sanglifehrin A acts as a potent inhibitor of the mitochondrial permeability transition and reperfusion injury of the heart by binding to cyclophilin-D at a different site from cyclosporin A. J Biol Chem 277:34793-34799.2002).

Claycomb WC, Lanson NA, Jr., Stallworth BS, Egeland DB, Delcarpio JB, Bahinski A, Izzo NJ, Jr. (HL-1 cells: a cardiac muscle cell line that contracts and retains phenotypic characteristics of the adult cardiomyocyte. Proc Natl Acad Sci U S A 95:2979-2984.1998).

Cohen J (1988) Statistical Power Analysis for the Behavioral Sciences: L. Erlbaum Associates.

Connern CP, Halestrap AP (Recruitment of mitochondrial cyclophilin to the mitochondrial inner membrane under conditions of oxidative stress that enhance the

opening of a calcium-sensitive non-specific channel. Biochem J 302 (Pt 2):321-324.1994).

Cookson MR (DJ-1, PINK1, and their effects on mitochondrial pathways. Mov Disord 25 Suppl 1:S44-S48.2010).

Cooper HM, Huang JY, Verdin E, Spelbrink JN (A new splice variant of the mouse SIRT3 gene encodes the mitochondrial precursor protein. PLoS One 4:e4986.2009).

Costa AD, Garlid KD, West IC, Lincoln TM, Downey JM, Cohen MV, Critz SD (Protein kinase G transmits the cardioprotective signal from cytosol to mitochondria. Circ Res 97:329-336.2005).

Crimi G, Pica S, Raineri C, Bramucci E, De Ferrari GM, Klersy C, Ferlini M, Marinoni B, Repetto A, Romeo M, Rosti V, Massa M, Raisaro A, Leonardi S, Rubartelli P, Oltrona Visconti L, Ferrario M (Remote Ischemic Postconditioning of the Lower Limb During Primary PCI Safely Reduces Enzymatic Infarct Size in Anterior Myocardial Infarction: a Randomized Controlled Trial. JACC Cardiovasc Interv (In Press).2013).

Crompton M, Costi A (Kinetic evidence for a heart mitochondrial pore activated by Ca2+, inorganic phosphate and oxidative stress. A potential mechanism for mitochondrial dysfunction during cellular Ca2+ overload. Eur J Biochem 178:489-501.1988).

Crompton M, Costi A, Hayat L (Evidence for the presence of a reversible Ca2+-dependent pore activated by oxidative stress in heart mitochondria. Biochem J 245:915-918.1987).

Crompton M, Ellinger H, Costi A (Inhibition by cyclosporin A of a Ca2+-dependent pore in heart mitochondria activated by inorganic phosphate and oxidative stress. Biochem J 255:357-360.1988).

Cruz JI, Loste JM, Burzaco OH (Observations on the use of medetomidine/ketamine and its reversal with atipamezole for chemical restraint in the mouse. Lab Anim 32:18-22.1998).

Das AM (Regulation of mitochondrial ATP synthase activity in human myocardium. Clin Sci (Lond) 94:499-504.1998).

Davies MJ (The pathology of myocardial ischaemia. J Clin Pathol Suppl (R Coll Pathol) 11:45-52.1977).

Davis J, Maillet M, Miano JM, Molkentin JD (Lost in transgenesis: a user's guide for genetically manipulating the mouse in cardiac research. Circ Res 111:761-777.2012).

Dewald O, Ren G, Duerr GD, Zoerlein M, Klemm C, Gersch C, Tincey S, Michael LH, Entman ML, Frangogiannis NG (Of mice and dogs: species-specific differences in the inflammatory response following myocardial infarction. Am J Pathol 164:665-677.2004).

Di Lisa F, Bernardi P (A CaPful of mechanisms regulating the mitochondrial permeability transition. J Mol Cell Cardiol 46:775-780.2009).

Dirksen MT, Laarman GJ, Simoons ML, Duncker DJ (Reperfusion injury in humans: a review of clinical trials on reperfusion injury inhibitory strategies. Cardiovasc Res 74:343-355.2007).

Doetschman T, Azhar M (Cardiac-specific inducible and conditional gene targeting in mice. Circ Res 110:1498-1512.2012).

Dokmanovic M, Clarke C, Marks PA (Histone deacetylase inhibitors: overview and perspectives. Mol Cancer Res 5:981-989.2007).

Duan X, Kelsen SG, Merali S (Proteomic analysis of oxidative stress-responsive proteins in human pneumocytes: insight into the regulation of DJ-1 expression. J Proteome Res 7:4955-4961.2008).

Dube H, Selwood D, Malouitre S, Capano M, Simone MI, Crompton M (A mitochondrial-targeted cyclosporin A with high binding affinity for cyclophilin D yields improved cytoprotection of cardiomyocytes. Biochem J 441:901-907.2012).

Durgan DJ, Pulinilkunnil T, Villegas-Montoya C, Garvey ME, Frangogiannis NG, Michael LH, Chow CW, Dyck JR, Young ME (Short communication: ischemia/reperfusion tolerance is time-of-day-dependent: mediation by the cardiomyocyte circadian clock. Circ Res 106:546-550.2010).

Edwards NC, Routledge H, Steeds RP (T2-weighted magnetic resonance imaging to assess myocardial oedema in ischaemic heart disease. Heart 95:1357-1361.2009).

Elrod JW, Molkentin JD (Physiologic functions of cyclophilin D and the mitochondrial permeability transition pore. Circ J 77:1111-1122.2013).

Elrod JW, Wong R, Mishra S, Vagnozzi RJ, Sakthievel B, Goonasekera SA, Karch J, Gabel S, Farber J, Force T, Brown JH, Murphy E, Molkentin JD (Cyclophilin D controls mitochondrial pore-dependent Ca(2+) exchange, metabolic flexibility, and propensity for heart failure in mice. J Clin Invest 120:3680-3687.2010).

Fan J, Ren H, Fei E, Jia N, Ying Z, Jiang P, Wu M, Wang G (Sumoylation is critical for DJ-1 to repress p53 transcriptional activity. FEBS Lett 582:1151-1156.2008a).

Fan J, Ren H, Jia N, Fei E, Zhou T, Jiang P, Wu M, Wang G (DJ-1 decreases Bax expression through repressing p53 transcriptional activity. J Biol Chem 283:4022-4030.2008b).

Ferdinandy P, Schulz R, Baxter GF (Interaction of cardiovascular risk factors with myocardial ischemia/reperfusion injury, preconditioning, and postconditioning. Pharmacol Rev 59:418-458.2007).

Ferreira VM, Piechnik SK, Dall'Armellina E, Karamitsos TD, Francis JM, Choudhury RP, Friedrich MG, Robson MD, Neubauer S (Non-contrast T1-mapping detects acute myocardial edema with high diagnostic accuracy: a comparison to T2-weighted cardiovascular magnetic resonance. J Cardiovasc Magn Reson 14:42.2012).

Finley LW, Haas W, Desquiret-Dumas V, Wallace DC, Procaccio V, Gygi SP, Haigis MC (Succinate dehydrogenase is a direct target of sirtuin 3 deacetylase activity. PLoS One 6:e23295.2011).

Fischer G, Wittmann-Liebold B, Lang K, Kiefhaber T, Schmid FX (Cyclophilin and peptidyl-prolyl cis-trans isomerase are probably identical proteins. Nature 337:476-478.1989).

Fisher SG, Marber MS (An in vivo model of ischaemia-reperfusion injury and ischaemic preconditioning in the mouse heart. J Pharmacol Toxicol Methods 48:161-169.2002).

Forman MB, Puett DW, Virmani R (Endothelial and myocardial injury during ischemia and reperfusion: pathogenesis and therapeutic implications. J Am Coll Cardiol 13:450-459.1989).

Frantz S, Bauersachs J, Ertl G (Post-infarct remodelling: contribution of wound healing and inflammation. Cardiovasc Res 81:474-481.2009).

Freude B, Masters TN, Robicsek F, Fokin A, Kostin S, Zimmermann R, Ullmann C, Lorenz-Meyer S, Schaper J (Apoptosis is initiated by myocardial ischemia and executed during reperfusion. J Mol Cell Cardiol 32:197-208.2000).

Friedrich MG, Abdel-Aty H, Taylor A, Schulz-Menger J, Messroghli D, Dietz R (The salvaged area at risk in reperfused acute myocardial infarction as visualized by cardiovascular magnetic resonance. J Am Coll Cardiol 51:1581-1587.2008).

Fritz KS, Galligan JJ, Hirschey MD, Verdin E, Petersen DR (Mitochondrial acetylome analysis in a mouse model of alcohol-induced liver injury utilizing SIRT3 knockout mice. J Proteome Res 11:1633-1643.2012).

Fritz KS, Galligan JJ, Smathers RL, Roede JR, Shearn CT, Reigan P, Petersen DR (4-Hydroxynonenal inhibits SIRT3 via thiol-specific modification. Chem Res Toxicol 24:651-662.2011).

Frye RA (Characterization of five human cDNAs with homology to the yeast SIR2 gene: Sir2-like proteins (sirtuins) metabolize NAD and may have protein ADP-ribosyltransferase activity. Biochem Biophys Res Commun 260:273-279.1999).

Frye RA (Phylogenetic classification of prokaryotic and eukaryotic Sir2-like proteins. Biochem Biophys Res Commun 273:793-798.2000).

Fuernau G, Eitel I, Franke V, Hildebrandt L, Meissner J, de WS, Lurz P, Gutberlet M, Desch S, Schuler G, Thiele H (Myocardium at risk in ST-segment elevation myocardial infarction comparison of T2-weighted edema imaging with the MR-assessed endocardial surface area and validation against angiographic scoring. JACC Cardiovasc Imaging 4:967-976.2011).

Galli U, Mesenzani O, Coppo C, Sorba G, Canonico PL, Tron GC, Genazzani AA (Identification of a sirtuin 3 inhibitor that displays selectivity over sirtuin 1 and 2. Eur J Med Chem 55:58-66.2012).

Gao E, Lei YH, Shang X, Huang ZM, Zuo L, Boucher M, Fan Q, Chuprun JK, Ma XL, Koch WJ (A novel and efficient model of coronary artery ligation and myocardial infarction in the mouse. Circ Res 107:1445-1453.2010).

Gao XM, Xu Q, Kiriazis H, Dart AM, Du XJ (Mouse model of post-infarct ventricular rupture: time course, strain- and gender-dependency, tensile strength, and histopathology. Cardiovasc Res 65:469-477.2005).

Garcia-Dorado D, Andres-Villarreal M, Ruiz-Meana M, Inserte J, Barba I (Myocardial edema: a translational view. J Mol Cell Cardiol 52:931-939.2012).

Garcia-Dorado D, Oliveras J, Gili J, Sanz E, Perez-Villa F, Barrabes J, Carreras MJ, Solares J, Soler-Soler J (Analysis of myocardial oedema by magnetic resonance imaging early after coronary artery occlusion with or without reperfusion. Cardiovasc Res 27:1462-1469.1993).

Garcia-Dorado D, Piper HM (Postconditioning: reperfusion of "reperfusion injury" after hibernation. Cardiovasc Res 69:1-3.2006).

Garcia-Dorado D, Ruiz-Meana M, Piper HM (Lethal reperfusion injury in acute myocardial infarction: facts and unresolved issues. Cardiovasc Res 83:165-168.2009).

Geelen T, Paulis LE, Coolen BF, Nicolay K, Strijkers GJ (Contrast-enhanced MRI of murine myocardial infarction - part I. NMR Biomed 25:953-968.2012).

Giaime E, Yamaguchi H, Gautier CA, Kitada T, Shen J (Loss of DJ-1 does not affect mitochondrial respiration but increases ROS production and mitochondrial permeability transition pore opening. PLoS One 7:e40501.2012).

Giorgio V, Bisetto E, Soriano ME, Dabbeni-Sala F, Basso E, Petronilli V, Forte MA, Bernardi P, Lippe G (Cyclophilin D modulates mitochondrial F0F1-ATP synthase by interacting with the lateral stalk of the complex. J Biol Chem 284:33982-33988.2009).

Giorgio V, von SS, Antoniel M, Fabbro A, Fogolari F, Forte M, Glick GD, Petronilli V, Zoratti M, Szabo I, Lippe G, Bernardi P (Dimers of mitochondrial ATP synthase form the permeability transition pore. Proc Natl Acad Sci U S A 110:5887-5892.2013).

Goldberg MS, Pisani A, Haburcak M, Vortherms TA, Kitada T, Costa C, Tong Y, Martella G, Tscherter A, Martins A, Bernardi G, Roth BL, Pothos EN, Calabresi P, Shen J (Nigrostriatal dopaminergic deficits and hypokinesia caused by inactivation of the familial Parkinsonism-linked gene DJ-1. Neuron 45:489-496.2005).

Gomez L, Thibault H, Gharib A, Dumont JM, Vuagniaux G, Scalfaro P, Derumeaux G, Ovize M (Inhibition of mitochondrial permeability transition improves functional recovery and reduces mortality following acute myocardial infarction in mice. Am J Physiol Heart Circ Physiol 293:H1654-H1661.2007).

Gonzalez A, Ravassa S, Beaumont J, Lopez B, Diez J (New targets to treat the structural remodeling of the myocardium. J Am Coll Cardiol 58:1833-1843.2011).

Gonzalez FM, Shiva S, Vincent PS, Ringwood LA, Hsu LY, Hon YY, Aletras AH, Cannon RO, III, Gladwin MT, Arai AE (Nitrite anion provides potent cytoprotective and antiapoptotic effects as adjunctive therapy to reperfusion for acute myocardial infarction. Circulation 117:2986-2994.2008).

Gorog DA, Tanno M, Kabir AM, Kanaganayagam GS, Bassi R, Fisher SG, Marber MS (Varying susceptibility to myocardial infarction among C57BL/6 mice of different genetic background. J Mol Cell Cardiol 35:705-708.2003).

Griffiths EJ, Halestrap AP (Protection by Cyclosporin A of ischemia/reperfusion-induced damage in isolated rat hearts. J Mol Cell Cardiol 25:1461-1469.1993).

Griffiths EJ, Halestrap AP (Mitochondrial non-specific pores remain closed during cardiac ischaemia, but open upon reperfusion. Biochem J 307 (Pt 1):93-98.1995).

Gustafsson AB, Gottlieb RA (Heart mitochondria: gates of life and death. Cardiovasc Res 77:334-343.2008).

Hafner AV, Dai J, Gomes AP, Xiao CY, Palmeira CM, Rosenzweig A, Sinclair DA (Regulation of the mPTP by SIRT3-mediated deacetylation of CypD at lysine 166 suppresses age-related cardiac hypertrophy. Aging (Albany NY) 2:914-923.2010).

Halestrap AP, Clarke SJ, Khaliulin I (The role of mitochondria in protection of the heart by preconditioning. Biochim Biophys Acta 1767:1007-1031.2007).

Halestrap AP, Davidson AM (Inhibition of Ca2(+)-induced large-amplitude swelling of liver and heart mitochondria by cyclosporin is probably caused by the inhibitor binding to mitochondrial-matrix peptidyl-prolyl cis-trans isomerase and preventing it interacting with the adenine nucleotide translocase. Biochem J 268:153-160.1990).

Halestrap AP, Woodfield KY, Connern CP (Oxidative stress, thiol reagents, and membrane potential modulate the mitochondrial permeability transition by affecting nucleotide binding to the adenine nucleotide translocase. J Biol Chem 272:3346-3354.1997).

Hallows WC, Lee S, Denu JM (Sirtuins deacetylate and activate mammalian acetyl-CoA synthetases. Proc Natl Acad Sci U S A 103:10230-10235.2006).

Hansson MJ, Mattiasson G, Mansson R, Karlsson J, Keep MF, Waldmeier P, Ruegg UT, Dumont JM, Besseghir K, Elmer E (The nonimmunosuppressive cyclosporin analogs NIM811 and UNIL025 display nanomolar potencies on permeability transition in brain-derived mitochondria. J Bioenerg Biomembr 36:407-413.2004).

Hausenloy D, Wynne A, Duchen M, Yellon D (Transient mitochondrial permeability transition pore opening mediates preconditioning-induced protection. Circulation 109:1714-1717.2004a).

Hausenloy DJ, Baxter G, Bell R, Botker HE, Davidson SM, Downey J, Heusch G, Kitakaze M, Lecour S, Mentzer R, Mocanu MM, Ovize M, Schulz R, Shannon R, Walker M, Walkinshaw G, Yellon DM (Translating novel strategies for cardioprotection: the Hatter Workshop Recommendations. Basic Res Cardiol 105:677-686.2010).

Hausenloy DJ, Boston-Griffiths EA, Yellon DM (Cyclosporin A and cardioprotection: from investigative tool to therapeutic agent. Br J Pharmacol 165:1235-1245.2012).

Hausenloy DJ, Maddock HL, Baxter GF, Yellon DM (Inhibiting mitochondrial permeability transition pore opening: a new paradigm for myocardial preconditioning? Cardiovasc Res 55:534-543.2002).

Hausenloy DJ, Ong SB, Yellon DM (The mitochondrial permeability transition pore as a target for preconditioning and postconditioning. Basic Res Cardiol 104:189-202.2009).

Hausenloy DJ, Wynne AM, Yellon DM (Ischemic preconditioning targets the reperfusion phase. Basic Res Cardiol 102:445-452.2007).

Hausenloy DJ, Yellon DM (Preconditioning and postconditioning: united at reperfusion. Pharmacol Ther 116:173-191.2007).

Hausenloy DJ, Yellon DM (The second window of preconditioning (SWOP) where are we now? Cardiovasc Drugs Ther 24:235-254.2010).

Hausenloy DJ, Yellon DM (Myocardial ischemia-reperfusion injury: a neglected therapeutic target. J Clin Invest 123:92-100.2013).

Hausenloy DJ, Yellon DM, Mani-Babu S, Duchen MR (Preconditioning protects by inhibiting the mitochondrial permeability transition. Am J Physiol Heart Circ Physiol 287:H841-H849.2004b).

Hebert AS, Dittenhafer-Reed KE, Yu W, Bailey DJ, Selen ES, Boersma MD, Carson JJ, Tonelli M, Balloon AJ, Higbee AJ, Westphall MS, Pagliarini DJ, Prolla TA, Assadi-Porter F, Roy S, Denu JM, Coon JJ (Calorie restriction and SIRT3 trigger global reprogramming of the mitochondrial protein acetylome. Mol Cell 49:186-199.2013).

Herring N, Paterson DJ (ECG diagnosis of acute ischaemia and infarction: past, present and future. QJM 99:219-230.2006).

Heusch G (Cardioprotection: chances and challenges of its translation to the clinic. Lancet 381:166-175.2013).

Hirschey MD, Shimazu T, Goetzman E, Jing E, Schwer B, Lombard DB, Grueter CA, Harris C, Biddinger S, Ilkayeva OR, Stevens RD, Li Y, Saha AK, Ruderman NB, Bain JR, Newgard CB, Farese RV, Jr., Alt FW, Kahn CR, Verdin E (SIRT3 regulates mitochondrial fatty-acid oxidation by reversible enzyme deacetylation. Nature 464:121-125.2010).

Hoffman JW, Gilbert TB, Poston RS, Silldorff EP (Myocardial reperfusion injury: etiology, mechanisms, and therapies. J Extra Corpor Technol 36:391-411.2004).

Hoit BD, Khan ZU, Pawloski-Dahm CM, Walsh RA (In vivo determination of left ventricular wall stress-shortening relationship in normal mice. Am J Physiol 272:H1047-H1052.1997).

Hoit BD, Kiatchoosakun S, Restivo J, Kirkpatrick D, Olszens K, Shao H, Pao YH, Nadeau JH (Naturally occurring variation in cardiovascular traits among inbred mouse strains. Genomics 79:679-685.2002).

Honbou K, Suzuki NN, Horiuchi M, Niki T, Taira T, Ariga H, Inagaki F (The crystal structure of DJ-1, a protein related to male fertility and Parkinson's disease. J Biol Chem 278:31380-31384.2003).

Hu W, Chen Z, Ye Z, Xia D, Xia Z, Ma J, Zhu M, Chen G (Knockdown of Cyclophilin D Gene by RNAi Protects Rat from Ischemia/ Reperfusion-Induced Renal Injury. Kidney Blood Press Res 33:193-199.2010).

Huai Q, Sun Y, Wang H, Chin LS, Li L, Robinson H, Ke H (Crystal structure of DJ-1/RS and implication on familial Parkinson's disease. FEBS Lett 549:171-175.2003).

Humphreys RA, Kane KA, Parratt JR (The influence of maturation and gender on the anti-arrhythmic effect of ischaemic preconditioning in rats. Basic Res Cardiol 94:1-8.1999).

Iannitti T, Palmieri B (Clinical and experimental applications of sodium phenylbutyrate. Drugs R D 11:227-249.2011).

Ichas F, Jouaville LS, Mazat JP (Mitochondria are excitable organelles capable of generating and conveying electrical and calcium signals. Cell 89:1145-1153.1997).

Ingkanisorn WP, Rhoads KL, Aletras AH, Kellman P, Arai AE (Gadolinium delayed enhancement cardiovascular magnetic resonance correlates with clinical measures of myocardial infarction. J Am Coll Cardiol 43:2253-2259.2004).

Irrcher I, Aleyasin H, Seifert EL, Hewitt SJ, Chhabra S, Phillips M, Lutz AK, Rousseaux MW, Bevilacqua L, Jahani-Asl A, Callaghan S, MacLaurin JG, Winklhofer KF, Rizzu P, Rippstein P, Kim RH, Chen CX, Fon EA, Slack RS, Harper ME, McBride HM, Mak TW, Park DS (Loss of the Parkinson's disease-linked gene DJ-1 perturbs mitochondrial dynamics. Hum Mol Genet 19:3734-3746.2010).

Jacobs KM, Pennington JD, Bisht KS, Aykin-Burns N, Kim HS, Mishra M, Sun L, Nguyen P, Ahn BH, Leclerc J, Deng CX, Spitz DR, Gius D (SIRT3 interacts with the daf-16 homolog FOXO3a in the mitochondria, as well as increases FOXO3a dependent gene expression. Int J Biol Sci 4:291-299.2008).

Javadov S, Karmazyn M, Escobales N (Mitochondrial permeability transition pore opening as a promising therapeutic target in cardiac diseases. J Pharmacol Exp Ther 330:670-678.2009).

Javadov S, Kuznetsov A (Mitochondrial permeability transition and cell death: the role of cyclophilin d. Front Physiol 4:76.2013).

Jennings RB (Commentary on selected aspects of cardioprotection. J Cardiovasc Pharmacol Ther 16:340-348.2011).

Jennings RB, Reimer KA (Lethal myocardial ischemic injury. Am J Pathol 102:241-255.1981).

Jezek P, Hlavata L (Mitochondria in homeostasis of reactive oxygen species in cell, tissues, and organism. Int J Biochem Cell Biol 37:2478-2503.2005).

Johnson N, Khan A, Virji S, Ward JM, Crompton M (Import and processing of heart mitochondrial cyclophilin D. Eur J Biochem 263:353-359.1999).

Juhaszova M, Zorov DB, Kim SH, Pepe S, Fu Q, Fishbein KW, Ziman BD, Wang S, Ytrehus K, Antos CL, Olson EN, Sollott SJ (Glycogen synthase kinase-3beta mediates convergence of protection signaling to inhibit the mitochondrial permeability transition pore. J Clin Invest 113:1535-1549.2004).

Junn E, Taniguchi H, Jeong BS, Zhao X, Ichijo H, Mouradian MM (Interaction of DJ-1 with Daxx inhibits apoptosis signal-regulating kinase 1 activity and cell death. Proc Natl Acad Sci U S A 102:9691-9696.2005).

Kajitani K, Fujihashi M, Kobayashi Y, Shimizu S, Tsujimoto Y, Miki K (Crystal structure of human cyclophilin D in complex with its inhibitor, cyclosporin A at 0.96-A resolution. Proteins 70:1635-1639.2008).

Kato R, Foex P (Myocardial protection by anesthetic agents against ischemia-reperfusion injury: an update for anesthesiologists. Can J Anaesth 49:777-791.2002).

Katz AM (2001) Physiology of the Heart. USA: Lippincott Williams & Wilkins.

Kersten JR (Anesthetic preconditioning: an anesthesiologist's tale. 1997. Anesthesiology 114:162-166.2011).

Kim HS, Patel K, Muldoon-Jacobs K, Bisht KS, Aykin-Burns N, Pennington JD, van der Meer R, Nguyen P, Savage J, Owens KM, Vassilopoulos A, Ozden O, Park SH, Singh KK, Abdulkadir SA, Spitz DR, Deng CX, Gius D (SIRT3 is a mitochondria-localized tumor suppressor required for maintenance of mitochondrial integrity and metabolism during stress. Cancer Cell 17:41-52.2010).

Kim RH, Peters M, Jang Y, Shi W, Pintilie M, Fletcher GC, DeLuca C, Liepa J, Zhou L, Snow B, Binari RC, Manoukian AS, Bray MR, Liu FF, Tsao MS, Mak TW (DJ-1, a novel regulator of the tumor suppressor PTEN. Cancer Cell 7:263-273.2005a).

Kim RH, Smith PD, Aleyasin H, Hayley S, Mount MP, Pownall S, Wakeham A, You-Ten AJ, Kalia SK, Horne P, Westaway D, Lozano AM, Anisman H, Park DS, Mak TW (Hypersensitivity of DJ-1-deficient mice to 1-methyl-4-phenyl-1,2,3,6-tetrahydropyrindine (MPTP) and oxidative stress. Proc Natl Acad Sci U S A 102:5215-5220.2005b).

Kim RJ, Albert TS, Wible JH, Elliott MD, Allen JC, Lee JC, Parker M, Napoli A, Judd RM (Performance of delayed-enhancement magnetic resonance imaging with

gadoversetamide contrast for the detection and assessment of myocardial infarction: an international, multicenter, double-blinded, randomized trial. Circulation 117:629-637.2008).

Kim RJ, Fieno DS, Parrish TB, Harris K, Chen EL, Simonetti O, Bundy J, Finn JP, Klocke FJ, Judd RM (Relationship of MRI delayed contrast enhancement to irreversible injury, infarct age, and contractile function. Circulation 100:1992-2002.1999).

Kim RJ, Wu E, Rafael A, Chen EL, Parker MA, Simonetti O, Klocke FJ, Bonow RO, Judd RM (The use of contrast-enhanced magnetic resonance imaging to identify reversible myocardial dysfunction. N Engl J Med 343:1445-1453.2000).

Kim SC, Sprung R, Chen Y, Xu Y, Ball H, Pei J, Cheng T, Kho Y, Xiao H, Xiao L, Grishin NV, White M, Yang XJ, Zhao Y (Substrate and functional diversity of lysine acetylation revealed by a proteomics survey. Mol Cell 23:607-618.2006).

Kim YC, Kitaura H, Taira T, Iguchi-Ariga SM, Ariga H (Oxidation of DJ-1-dependent cell transformation through direct binding of DJ-1 to PTEN. Int J Oncol 35:1331-1341.2009).

Kinumi T, Kimata J, Taira T, Ariga H, Niki E (Cysteine-106 of DJ-1 is the most sensitive cysteine residue to hydrogen peroxide-mediated oxidation in vivo in human umbilical vein endothelial cells. Biochem Biophys Res Commun 317:722-728.2004).

Klocke R, Tian W, Kuhlmann MT, Nikol S (Surgical animal models of heart failure related to coronary heart disease. Cardiovasc Res 74:29-38.2007).

Kloner RA (Does reperfusion injury exist in humans? J Am Coll Cardiol 21:537-545.1993).

Kloner RA, Ganote CE, Jennings RB (The "no-reflow" phenomenon after temporary coronary occlusion in the dog. J Clin Invest 54:1496-1508.1974).

Kloner RA, Jennings RB (Consequences of brief ischemia: stunning, preconditioning, and their clinical implications: part 1. Circulation 104:2981-2989.2001).

Kloner RA, Rezkalla SH (Cardiac protection during acute myocardial infarction: where do we stand in 2004? J Am Coll Cardiol 44:276-286.2004).

Kober F, Iltis I, Cozzone PJ, Bernard M (Cine-MRI assessment of cardiac function in mice anesthetized with ketamine/xylazine and isoflurane. MAGMA 17:157-161.2004).

Kober F, Iltis I, Cozzone PJ, Bernard M (Myocardial blood flow mapping in mice using high-resolution spin labeling magnetic resonance imaging: influence of ketamine/xylazine and isoflurane anesthesia. Magn Reson Med 53:601-606.2005).

Kohr MJ, Sun J, Aponte A, Wang G, Gucek M, Murphy E, Steenbergen C (Simultaneous measurement of protein oxidation and S-nitrosylation during preconditioning and ischemia/reperfusion injury with resin-assisted capture. Circ Res 108:418-426.2011).

Kokoszka JE, Waymire KG, Levy SE, Sligh JE, Cai J, Jones DP, MacGregor GR, Wallace DC (The ADP/ATP translocator is not essential for the mitochondrial permeability transition pore. Nature 427:461-465.2004).

Korge P, Yang L, Yang JH, Wang Y, Qu Z, Weiss JN (Protective role of transient pore openings in calcium handling by cardiac mitochondria. J Biol Chem 286:34851-34857.2011).

Krauskopf A, Eriksson O, Craigen WJ, Forte MA, Bernardi P (Properties of the permeability transition in VDAC1(-/-) mitochondria. Biochim Biophys Acta 1757:590-595.2006).

Krebiehl G, Ruckerbauer S, Burbulla LF, Kieper N, Maurer B, Waak J, Wolburg H, Gizatullina Z, Gellerich FN, Woitalla D, Riess O, Kahle PJ, Proikas-Cezanne T, Kruger R (Reduced basal autophagy and impaired mitochondrial dynamics due to loss of Parkinson's disease-associated protein DJ-1. PLoS One 5:e9367.2010).

Krenz M, Cohen MV, Downey JM (The protective and anti-protective effects of ethanol in a myocardial infarct model. Ann N Y Acad Sci 957:103-114.2002).

Kristian T, Siesjo BK (Calcium in ischemic cell death. Stroke 29:705-718.1998).

Kumar D, Hacker TA, Buck J, Whitesell LF, Kaji EH, Douglas PS, Kamp TJ (Distinct mouse coronary anatomy and myocardial infarction consequent to ligation. Coron Artery Dis 16:41-44.2005).

Lakso M, Pichel JG, Gorman JR, Sauer B, Okamoto Y, Lee E, Alt FW, Westphal H (Efficient in vivo manipulation of mouse genomic sequences at the zygote stage. Proc Natl Acad Sci U S A 93:5860-5865.1996).

Lee SJ, Kim SJ, Kim IK, Ko J, Jeong CS, Kim GH, Park C, Kang SO, Suh PG, Lee HS, Cha SS (Crystal structures of human DJ-1 and Escherichia coli Hsp31, which share an evolutionarily conserved domain. J Biol Chem 278:44552-44559.2003).

Lev N, Barhum Y, Ben-Zur T, Melamed E, Steiner I, Offen D (Knocking out DJ-1 attenuates astrocytes neuroprotection against 6-hydroxydopamine toxicity. J Mol Neurosci 50:542-550.2013).

Lev N, Ickowicz D, Melamed E, Offen D (Oxidative insults induce DJ-1 upregulation and redistribution: implications for neuroprotection. Neurotoxicology 29:397-405.2008).

Levine B, Kroemer G (Autophagy in the pathogenesis of disease. Cell 132:27-42.2008).

Li Q, Guo Y, Xuan YT, Lowenstein CJ, Stevenson SC, Prabhu SD, Wu WJ, Zhu Y, Bolli R (Gene therapy with inducible nitric oxide synthase protects against myocardial infarction via a cyclooxygenase-2-dependent mechanism. Circ Res 92:741-748.2003).

Li S, Banck M, Mujtaba S, Zhou MM, Sugrue MM, Walsh MJ (p53-induced growth arrest is regulated by the mitochondrial SirT3 deacetylase. PLoS One 5:e10486.2010).

Liao XL, Hu XX, Chang FJ, Yuan HY, Ci HB, Wu JY, Xu Z, Wang ZP, Zhang X, Xia Z, Ou JS (A simple modification results in greater success in the model of coronary artery ligation and myocardial ischemia in mice. J Cardiovasc Pharmacol 61:430-436.2013).

Lim SY, Davidson SM, Hausenloy DJ, Yellon DM (Preconditioning and postconditioning: the essential role of the mitochondrial permeability transition pore. Cardiovasc Res 75:530-535.2007).

Lim SY, Hausenloy DJ, Arjun S, Price AN, Davidson SM, Lythgoe MF, Yellon DM (Mitochondrial cyclophilin-D as a potential therapeutic target for post-myocardial infarction heart failure. J Cell Mol Med 15:2443-2451.2011).

Lin DT, Lechleiter JD (Mitochondrial targeted cyclophilin D protects cells from cell death by peptidyl prolyl isomerization. J Biol Chem 277:31134-31141.2002).

Liu J, Farmer JD, Jr., Lane WS, Friedman J, Weissman I, Schreiber SL (Calcineurin is a common target of cyclophilin-cyclosporin A and FKBP-FK506 complexes. Cell 66:807-815.1991).

Lombard DB, Alt FW, Cheng HL, Bunkenborg J, Streeper RS, Mostoslavsky R, Kim J, Yancopoulos G, Valenzuela D, Murphy A, Yang Y, Chen Y, Hirschey MD, Bronson RT, Haigis M, Guarente LP, Farese RV, Jr., Weissman S, Verdin E, Schwer B (Mammalian Sir2 homolog SIRT3 regulates global mitochondrial lysine acetylation. Mol Cell Biol 27:8807-8814.2007).

Lonborg J, Kelbaek H, Vejlstrup N, Botker HE, Kim WY, Holmvang L, Jorgensen E, Helqvist S, Saunamaki K, Terkelsen CJ, Schoos MM, Kober L, Clemmensen P, Treiman M, Engstrom T (Exenatide reduces final infarct size in patients with ST-segment-elevation myocardial infarction and short-duration of ischemia. Circ Cardiovasc Interv 5:288-295.2012a).

Lonborg J, Vejlstrup N, Kelbaek H, Botker HE, Kim WY, Mathiasen AB, Jorgensen E, Helqvist S, Saunamaki K, Clemmensen P, Holmvang L, Thuesen L, Krusell LR, Jensen JS, Kober L, Treiman M, Holst JJ, Engstrom T (Exenatide reduces reperfusion injury in patients with ST-segment elevation myocardial infarction. Eur Heart J 33:1491-1499.2012b).

Long JS, Ryan KM (New frontiers in promoting tumour cell death: targeting apoptosis, necroptosis and autophagy. Oncogene 31:5045-5060.2012).

Lu HS, Chen HP, Wang S, Yu HH, Huang XS, Huang QR, He M (Hypoxic preconditioning up-regulates DJ-1 protein expression in rat heart-derived H9c2 cells through the activation of extracellular-regulated kinase 1/2 pathway. Mol Cell Biochem.2012).

Lu Z, Bourdi M, Li JH, Aponte AM, Chen Y, Lombard DB, Gucek M, Pohl LR, Sack MN (SIRT3-dependent deacetylation exacerbates acetaminophen hepatotoxicity. EMBO Rep 12:840-846.2011).

Lusis AJ (Atherosclerosis. Nature 407:233-241.2000).

Luvisetto S, Basso E, Petronilli V, Bernardi P, Forte M (Enhancement of anxiety, facilitation of avoidance behavior, and occurrence of adult-onset obesity in mice lacking mitochondrial cyclophilin D. Neuroscience 155:585-596.2008).

MacLellan WR, Schneider MD (Death by design. Programmed cell death in cardiovascular biology and disease. Circ Res 81:137-144.1997).

Mahrholdt H, Wagner A, Holly TA, Elliott MD, Bonow RO, Kim RJ, Judd RM (Reproducibility of chronic infarct size measurement by contrast-enhanced magnetic resonance imaging. Circulation 106:2322-2327.2002).

Malouitre S, Dube H, Selwood D, Crompton M (Mitochondrial targeting of cyclosporin A enables selective inhibition of cyclophilin-D and enhanced cytoprotection after glucose and oxygen deprivation. Biochem J 425:137-148.2010).

Manning AS, Hearse DJ (Reperfusion-induced arrhythmias: mechanisms and prevention. J Mol Cell Cardiol 16:497-518.1984).

Marber MS, Latchman DS, Walker JM, Yellon DM (Cardiac stress protein elevation 24 hours after brief ischemia or heat stress is associated with resistance to myocardial infarction. Circulation 88:1264-1272.1993).

Martinat C, Shendelman S, Jonason A, Leete T, Beal MF, Yang L, Floss T, Abeliovich A (Sensitivity to oxidative stress in DJ-1-deficient dopamine neurons: an ES- derived cell model of primary Parkinsonism. PLoS Biol 2:e327.2004).

Mather AN, Fairbairn TA, Artis NJ, Greenwood JP, Plein S (Timing of cardiovascular MR imaging after acute myocardial infarction: effect on estimates of infarct characteristics and prediction of late ventricular remodeling. Radiology 261:116-126.2011).

Mathers CD, Loncar D (Projections of global mortality and burden of disease from 2002 to 2030. PLoS Med 3:e442.2006).

Matsumoto H, Matsuda T, Miyamoto K, Shimada T, Mikuri M, Hiraoka Y (Peri-infarct zone on early contrast-enhanced CMR imaging in patients with acute myocardial infarction. JACC Cardiovasc Imaging 4:610-618.2011).

McCormack KJ, Chapleo CB (Opioid receptors and myocardial protection: do opioid agonists possess cardioprotective effects? Clin Drug Investig 15:445-454.1998).

McRobbie DW, Moore EA, Graves MJ, Prince MR (2006) MRI: From Picture to Proton. Cambridge: Cambridge University Press.

Menazza S, Wong R, Nguyen T, Wang G, Gucek M, Murphy E (CypD(-/-) hearts have altered levels of proteins involved in Krebs cycle, branch chain amino acid degradation and pyruvate metabolism. J Mol Cell Cardiol 56:81-90.2013).

Merkwirth C, Langer T (Prohibitin function within mitochondria: essential roles for cell proliferation and cristae morphogenesis. Biochim Biophys Acta 1793:27-32.2009).

Metzger D, Clifford J, Chiba H, Chambon P (Conditional site-specific recombination in mammalian cells using a ligand-dependent chimeric Cre recombinase. Proc Natl Acad Sci U S A 92:6991-6995.1995).

Mewton N, Rapacchi S, Augeul L, Ferrera R, Loufouat J, Boussel L, Micolich A, Rioufol G, Revel D, Ovize M, Croisille P (Determination of the myocardial area at risk with pre- versus post-reperfusion imaging techniques in the pig model. Basic Res Cardiol 106:1247-1257.2011).

Michael LH, Ballantyne CM, Zachariah JP, Gould KE, Pocius JS, Taffet GE, Hartley CJ, Pham TT, Daniel SL, Funk E, Entman ML (Myocardial infarction and remodeling in mice: effect of reperfusion. Am J Physiol 277:H660-H668.1999).

Michael LH, Entman ML, Hartley CJ, Youker KA, Zhu J, Hall SR, Hawkins HK, Berens K, Ballantyne CM (Myocardial ischemia and reperfusion: a murine model. Am J Physiol 269:H2147-H2154.1995).

Michishita E, Park JY, Burneskis JM, Barrett JC, Horikawa I (Evolutionarily conserved and nonconserved cellular localizations and functions of human SIRT proteins. Mol Biol Cell 16:4623-4635.2005).

Mitchell JR, Verweij M, Brand K, van d, V, Goemaere N, van den Engel S, Chu T, Forrer F, Muller C, de JM, van IW, Ijzermans JN, Hoeijmakers JH, de Bruin RW (Short-term dietary restriction and fasting precondition against ischemia reperfusion injury in mice. Aging Cell 9:40-53.2010).

Mitsumoto A, Nakagawa Y, Takeuchi A, Okawa K, Iwamatsu A, Takanezawa Y (Oxidized forms of peroxiredoxins and DJ-1 on two-dimensional gels increased in response to sublethal levels of paraquat. Free Radic Res 35:301-310.2001).

Miura T, Miki T (Limitation of myocardial infarct size in the clinical setting: current status and challenges in translating animal experiments into clinical therapy. Basic Res Cardiol 103:501-513.2008).

Miyazaki S, Yanagida T, Nunome K, Ishikawa S, Inden M, Kitamura Y, Nakagawa S, Taira T, Hirota K, Niwa M, Iguchi-Ariga SM, Ariga H (DJ-1-binding compounds prevent oxidative stress-induced cell death and movement defect in Parkinson's disease model rats. J Neurochem 105:2418-2434.2008).

Mo JS, Jung J, Yoon JH, Hong JA, Kim MY, Ann EJ, Seo MS, Choi YH, Park HS (DJ-1 modulates the p38 mitogen-activated protein kinase pathway through physical interaction with apoptosis signal-regulating kinase 1. J Cell Biochem 110:229-237.2010).

Mocanu MM, Yellon DM (PTEN, the Achilles' heel of myocardial ischaemia/reperfusion injury? Br J Pharmacol 150:833-838.2007).

Mortensen RM (Double knockouts. Production of mutant cell lines in cardiovascular research. Hypertension 22:646-651.1993).

Murphy E, Kohr M, Sun J, Nguyen T, Steenbergen C (S-nitrosylation: a radical way to protect the heart. J Mol Cell Cardiol 52:568-577.2012).

Murphy E, Steenbergen C (Gender-based differences in mechanisms of protection in myocardial ischemia-reperfusion injury. Cardiovasc Res 75:478-486.2007).

Murphy E, Steenbergen C (What makes the mitochondria a killer? Can we condition them to be less destructive? Biochim Biophys Acta 1813:1302-1308.2011).

Murry CE, Jennings RB, Reimer KA (Preconditioning with ischemia: a delay of lethal cell injury in ischemic myocardium. Circulation 74:1124-1136.1986).

Nakagawa T, Shimizu S, Watanabe T, Yamaguchi O, Otsu K, Yamagata H, Inohara H, Kubo T, Tsujimoto Y (Cyclophilin D-dependent mitochondrial permeability transition regulates some necrotic but not apoptotic cell death. Nature 434:652-658.2005).

Natanzon A, Aletras AH, Hsu LY, Arai AE (Determining canine myocardial area at risk with manganese-enhanced MR imaging. Radiology 236:859-866.2005).

Nazareth W, Yafei N, Crompton M (Inhibition of anoxia-induced injury in heart myocytes by cyclosporin A. J Mol Cell Cardiol 23:1351-1354.1991).

Nguyen TT, Stevens MV, Kohr M, Steenbergen C, Sack MN, Murphy E (Cysteine 203 of cyclophilin D is critical for cyclophilin D activation of the mitochondrial permeability transition pore. J Biol Chem 286:40184-40192.2011).

Nguyen TT, Wong RP, Menazza S, Sun J, Chen Y, Wang G, Gucek M, Steenbergen C, Sack MN, Murphy E (Cyclophilin D Modulates the Mitochondrial Acetylome. Circ Res.2013).

Nicolli A, Basso E, Petronilli V, Wenger RM, Bernardi P (Interactions of cyclophilin with the mitochondrial inner membrane and regulation of the permeability transition pore, and cyclosporin A-sensitive channel. J Biol Chem 271:2185-2192.1996).

Nogueiras R, Habegger KM, Chaudhary N, Finan B, Banks AS, Dietrich MO, Horvath TL, Sinclair DA, Pfluger PT, Tschop MH (Sirtuin 1 and sirtuin 3: physiological modulators of metabolism. Physiol Rev 92:1479-1514.2012).

Noll T, Koop A, Piper HM (Mitochondrial ATP-synthase activity in cardiomyocytes after aerobic-anaerobic metabolic transition. Am J Physiol 262:C1297-C1303.1992).

Nossuli TO, Lakshminarayanan V, Baumgarten G, Taffet GE, Ballantyne CM, Michael LH, Entman ML (A chronic mouse model of myocardial ischemia-reperfusion: essential in cytokine studies. Am J Physiol Heart Circ Physiol 278:H1049-H1055.2000).

O'Regan DP, Ahmed R, Neuwirth C, Tan Y, Durighel G, Hajnal JV, Nadra I, Corbett SJ, Cook SA (Cardiac MRI of myocardial salvage at the peri-infarct border zones after primary coronary intervention. Am J Physiol Heart Circ Physiol 297:H340-H346.2009).

Oerlemans MI, Koudstaal S, Chamuleau SA, de Kleijn DP, Doevendans PA, Sluijter JP (Targeting cell death in the reperfused heart: pharmacological approaches for cardioprotection. Int J Cardiol 165:410-422.2013).

Oie E, Bjornerheim R, Clausen OP, Attramadal H (Cyclosporin A inhibits cardiac hypertrophy and enhances cardiac dysfunction during postinfarction failure in rats. Am J Physiol Heart Circ Physiol 278:H2115-H2123.2000).

Olivetti G, Capasso JM, Sonnenblick EH, Anversa P (Side-to-side slippage of myocytes participates in ventricular wall remodeling acutely after myocardial infarction in rats. Circ Res 67:23-34.1990).

Olzmann JA, Brown K, Wilkinson KD, Rees HD, Huai Q, Ke H, Levey AI, Li L, Chin LS (Familial Parkinson's disease-associated L166P mutation disrupts DJ-1 protein folding and function. J Biol Chem 279:8506-8515.2004).

Ong SB, Subrayan S, Lim SY, Yellon DM, Davidson SM, Hausenloy DJ (Inhibiting mitochondrial fission protects the heart against ischemia/reperfusion injury. Circulation 121:2012-2022.2010).

Onyango P, Celic I, McCaffery JM, Boeke JD, Feinberg AP (SIRT3, a human SIR2 homologue, is an NAD-dependent deacetylase localized to mitochondria. Proc Natl Acad Sci U S A 99:13653-13658.2002).

Opie LH, Commerford PJ, Gersh BJ, Pfeffer MA (Controversies in ventricular remodelling. Lancet 367:356-367.2006).

Ordovas KG, Higgins CB (Delayed contrast enhancement on MR images of myocardium: past, present, future. Radiology 261:358-374.2011).

Ozden O, Park SH, Kim HS, Jiang H, Coleman MC, Spitz DR, Gius D (Acetylation of MnSOD directs enzymatic activity responding to cellular nutrient status or oxidative stress. Aging (Albany NY) 3:102-107.2011).

Patten RD, Aronovitz MJ, Deras-Mejia L, Pandian NG, Hanak GG, Smith JJ, Mendelsohn ME, Konstam MA (Ventricular remodeling in a mouse model of myocardial infarction. Am J Physiol 274:H1812-H1820.1998).

Peart JN, Gross ER, Gross GJ (Opioid-induced preconditioning: recent advances and future perspectives. Vascul Pharmacol 42:211-218.2005).

Pellegrini L, Pucci B, Villanova L, Marino ML, Marfe G, Sansone L, Vernucci E, Bellizzi D, Reali V, Fini M, Russo MA, Tafani M (SIRT3 protects from hypoxia and staurosporine-mediated cell death by maintaining mitochondrial membrane potential and intracellular pH. Cell Death Differ 19:1815-1825.2012).

Petersen ET, Zimine I, Ho YC, Golay X (Non-invasive measurement of perfusion: a critical review of arterial spin labelling techniques. Br J Radiol 79:688-701.2006).

Pfeffer MA, Braunwald E (Ventricular remodeling after myocardial infarction. Experimental observations and clinical implications. Circulation 81:1161-1172.1990).

Piot C, Croisille P, Staat P, Thibault H, Rioufol G, Mewton N, Elbelghiti R, Cung TT, Bonnefoy E, Angoulvant D, Macia C, Raczka F, Sportouch C, Gahide G, Finet G, Andre-Fouet X, Revel D, Kirkorian G, Monassier JP, Derumeaux G, Ovize M (Effect of cyclosporine on reperfusion injury in acute myocardial infarction. N Engl J Med 359:473-481.2008).

Piper HM, Garcia-Dorado D (Prime causes of rapid cardiomyocyte death during reperfusion. Ann Thorac Surg 68:1913-1919.1999).

Pons S, Fornes P, Hagege AA, Heudes D, Giudicelli JF, Richer C (Survival, haemodynamics and cardiac remodelling follow up in mice after myocardial infarction. Clin Exp Pharmacol Physiol 30:25-31.2003).

Price AN, Cheung KK, Lim SY, Yellon DM, Hausenloy DJ, Lythgoe MF (Rapid assessment of myocardial infarct size in rodents using multi-slice inversion recovery late gadolinium enhancement CMR at 9.4T. J Cardiovasc Magn Reson 13:44.2011).

Qiagen. Taq PCR Handbook. 3rd. 2010.

Rardin MJ, Newman JC, Held JM, Cusack MP, Sorensen DJ, Li B, Schilling B, Mooney SD, Kahn CR, Verdin E, Gibson BW (Label-free quantitative proteomics of the lysine acetylome in mitochondria identifies substrates of SIRT3 in metabolic pathways. Proc Natl Acad Sci U S A 110:6601-6606.2013).

Rasola A, Sciacovelli M, Chiara F, Pantic B, Brusilow WS, Bernardi P (Activation of mitochondrial ERK protects cancer cells from death through inhibition of the permeability transition. Proc Natl Acad Sci U S A 107:726-731.2010).

Reckitt Benckiser. Vetergesic - Product Data Sheet. 2011. United Kingdom.

Redel A, Jazbutyte V, Smul TM, Lange M, Eckle T, Eltzschig H, Roewer N, Kehl F (Impact of ischemia and reperfusion times on myocardial infarct size in mice in vivo. Exp Biol Med (Maywood) 233:84-93.2008).

Redel A, Stumpner J, Tischer-Zeitz T, Lange M, Smul TM, Lotz C, Roewer N, Kehl F (Comparison of isoflurane-, sevoflurane-, and desflurane-induced pre- and postconditioning against myocardial infarction in mice in vivo. Exp Biol Med (Maywood) 234:1186-1191.2009).

Reimer KA, Lowe JE, Rasmussen MM, Jennings RB (The wavefront phenomenon of ischemic cell death. 1. Myocardial infarct size vs duration of coronary occlusion in dogs. Circulation 56:786-794.1977).

Reimer KA, Vander Heide RS, Richard VJ (Reperfusion in acute myocardial infarction: effect of timing and modulating factors in experimental models. Am J Cardiol 72:13G-21G.1993).

Revollo JR, Grimm AA, Imai S (The NAD biosynthesis pathway mediated by nicotinamide phosphoribosyltransferase regulates Sir2 activity in mammalian cells. J Biol Chem 279:50754-50763.2004).

Rossignol R, Gilkerson R, Aggeler R, Yamagata K, Remington SJ, Capaldi RA (Energy substrate modulates mitochondrial structure and oxidative capacity in cancer cells. Cancer Res 64:985-993.2004).

Rottman JN, Ni G, Brown M (Echocardiographic evaluation of ventricular function in mice. Echocardiography 24:83-89.2007).

Sack MN (Emerging characterization of the role of SIRT3-mediated mitochondrial protein deacetylation in the heart. Am J Physiol Heart Circ Physiol 301:H2191-H2197.2011).

Sane DC, Mozingo WS, Becker RC (Cardiac rupture after myocardial infarction: new insights from murine models. Cardiol Rev 17:293-299.2009).

Sauve AA (Sirtuin chemical mechanisms. Biochim Biophys Acta 1804:1591-1603.2010).

Scher MB, Vaquero A, Reinberg D (SirT3 is a nuclear NAD+-dependent histone deacetylase that translocates to the mitochondria upon cellular stress. Genes Dev 21:920-928.2007).

Schinzel AC, Takeuchi O, Huang Z, Fisher JK, Zhou Z, Rubens J, Hetz C, Danial NN, Moskowitz MA, Korsmeyer SJ (Cyclophilin D is a component of mitochondrial permeability transition and mediates neuronal cell death after focal cerebral ischemia. Proc Natl Acad Sci U S A 102:12005-12010.2005).

Schlicker C, Gertz M, Papatheodorou P, Kachholz B, Becker CF, Steegborn C (Substrates and regulation mechanisms for the human mitochondrial sirtuins Sirt3 and Sirt5. J Mol Biol 382:790-801.2008).

Schneider A, Ad N, Izhar U, Khaliulin I, Borman JB, Schwalb H (Protection of myocardium by cyclosporin A and insulin: in vitro simulated ischemia study in human myocardium. Ann Thorac Surg 76:1240-1245.2003).

Schwartz LM, Verbinski SG, Vander Heide RS, Reimer KA (Epicardial temperature is a major predictor of myocardial infarct size in dogs. J Mol Cell Cardiol 29:1577-1583.1997).

Schwer B, North BJ, Frye RA, Ott M, Verdin E (The human silent information regulator (Sir)2 homologue hSIRT3 is a mitochondrial nicotinamide adenine dinucleotide-dependent deacetylase. J Cell Biol 158:647-657.2002).

Sclarovsky S (Physiological and pathological remodeling in acute inferior wall myocardial infarction. Isr Med Assoc J 15:143-146.2013).

Shanmuganathan S, Hausenloy DJ, Duchen MR, Yellon DM (Mitochondrial permeability transition pore as a target for cardioprotection in the human heart. Am J Physiol Heart Circ Physiol 289:H237-H242.2005).

Shao D, Oka S, Brady CD, Haendeler J, Eaton P, Sadoshima J (Redox modification of cell signaling in the cardiovascular system. J Mol Cell Cardiol 52:550-558.2012).

Shendelman S, Jonason A, Martinat C, Leete T, Abeliovich A (DJ-1 is a redox-dependent molecular chaperone that inhibits alpha-synuclein aggregate formation. PLoS Biol 2:e362.2004).

Shi T, Wang F, Stieren E, Tong Q (SIRT3, a mitochondrial sirtuin deacetylase, regulates mitochondrial function and thermogenesis in brown adipocytes. J Biol Chem 280:13560-13567.2005).

Shinmura K (Post-translational modification of mitochondrial proteins by caloric restriction: possible involvement in caloric restriction-induced cardioprotection. Trends Cardiovasc Med 23:18-25.2013).

Shinmura K, Tang XL, Wang Y, Xuan YT, Liu SQ, Takano H, Bhatnagar A, Bolli R (Cyclooxygenase-2 mediates the cardioprotective effects of the late phase of ischemic preconditioning in conscious rabbits. Proc Natl Acad Sci U S A 97:10197-10202.2000).

Shulga N, Wilson-Smith R, Pastorino JG (Sirtuin-3 deacetylation of cyclophilin D induces dissociation of hexokinase II from the mitochondria. J Cell Sci 123:894-902.2010).

Sigma-Aldrich. Adenosine 5'-triphosphate (ATP) Bioluminescent Assay Kit - Technical Bulletin. 2009. USA.

Smolina K, Wright FL, Rayner M, Goldacre MJ (Long-term survival and recurrence after acute myocardial infarction in England, 2004 to 2010. Circ Cardiovasc Qual Outcomes 5:532-540.2012).

Sobel BE, Bresnahan GF, Shell WE, Yoder RD (Estimation of infarct size in man and its relation to prognosis. Circulation 46:640-648.1972).

Sohal DS, Nghiem M, Crackower MA, Witt SA, Kimball TR, Tymitz KM, Penninger JM, Molkentin JD (Temporally regulated and tissue-specific gene manipulations in the adult and embryonic heart using a tamoxifen-inducible Cre protein. Circ Res 89:20-25.2001).

Song X, Li G, Vaage J, Valen G (Effects of sex, gonadectomy, and oestrogen substitution on ischaemic preconditioning and ischaemia-reperfusion injury in mice. Acta Physiol Scand 177:459-466.2003).

Steenbergen C, Perlman ME, London RE, Murphy E (Mechanism of preconditioning. Ionic alterations. Circ Res 72:112-125.1993).

Stowe DF, Kevin LG (Cardiac preconditioning by volatile anesthetic agents: a defining role for altered mitochondrial bioenergetics. Antioxid Redox Signal 6:439-448.2004).

Sundaresan NR, Samant SA, Pillai VB, Rajamohan SB, Gupta MP (SIRT3 is a stress-responsive deacetylase in cardiomyocytes that protects cells from stress-mediated cell death by deacetylation of Ku70. Mol Cell Biol 28:6384-6401.2008).

Szabo I, Zoratti M (The mitochondrial permeability transition pore may comprise VDAC molecules. I. Binary structure and voltage dependence of the pore. FEBS Lett 330:201-205.1993).

Taira T, Saito Y, Niki T, Iguchi-Ariga SM, Takahashi K, Ariga H (DJ-1 has a role in antioxidative stress to prevent cell death. EMBO Rep 5:213-218.2004).

Tao R, Coleman MC, Pennington JD, Ozden O, Park SH, Jiang H, Kim HS, Flynn CR, Hill S, Hayes MW, Olivier AK, Spitz DR, Gius D (Sirt3-mediated deacetylation of evolutionarily conserved lysine 122 regulates MnSOD activity in response to stress. Mol Cell 40:893-904.2010).

Tao X, Tong L (Crystal structure of human DJ-1, a protein associated with early onset Parkinson's disease. J Biol Chem 278:31372-31379.2003).

Tatou E, Mossiat C, Maupoil V, Gabrielle F, David M, Rochette L (Effects of cyclosporin and cremophor on working rat heart and incidence of myocardial lipid peroxidation. Pharmacology 52:1-7.1996).

Thermoscientific. Protein Assay Technical Handbook. 2. 2010. USA.

Thuny F, Lairez O, Roubille F, Mewton N, Rioufol G, Sportouch C, Sanchez I, Bergerot C, Thibault H, Cung TT, Finet G, Argaud L, Revel D, Derumeaux G, Bonnefoy-Cudraz E, Elbaz M, Piot C, Ovize M, Croisille P (Post-conditioning reduces infarct size and edema in patients with ST-segment elevation myocardial infarction. J Am Coll Cardiol 59:2175-2181.2012).

Thygesen K, Alpert JS, White HD, Jaffe AS, Apple FS, Galvani M, Katus HA, Newby LK, Ravkilde J, Chaitman B, Clemmensen PM, Dellborg M, Hod H, Porela P, Underwood R, Bax JJ, Beller GA, Bonow R, Van der Wall EE, Bassand JP, Wijns W, Ferguson TB, Steg PG, Uretsky BF, Williams DO, Armstrong PW, Antman EM, Fox KA, Hamm CW, Ohman EM, Simoons ML, Poole-Wilson PA, Gurfinkel EP, Lopez-Sendon JL, Pais P, Mendis S, Zhu JR, Wallentin LC, Fernandez-Aviles F, Fox KM, Parkhomenko AN, Priori SG, Tendera M, Voipio-Pulkki LM, Vahanian A, Camm AJ, De CR, Dean V, Dickstein K, Filippatos G, Funck-Brentano C, Hellemans I, Kristensen SD, McGregor K, Sechtem U, Silber S, Tendera M, Widimsky P, Zamorano JL, Morais J, Brener S, Harrington R, Morrow D, Lim M, Martinez-Rios MA, Steinhubl S, Levine GN, Gibler WB, Goff D, Tubaro M, Dudek D, Al-Attar N (Universal definition of myocardial infarction. Circulation 116:2634-2653.2007).

Tikhonova IM, Andreyev AY, Antonenko Y, Kaulen AD, Komrakov AY, Skulachev VP (Ion permeability induced in artificial membranes by the ATP/ADP antiporter. FEBS Lett 337:231-234.1994).

Townend J (2002) Practical Statistics for Environmental and Biological Sciences. Chichester: John Wiley and Sons Limited.

Tsang A, Hausenloy DJ, Mocanu MM, Carr RD, Yellon DM (Preconditioning the diabetic heart: the importance of Akt phosphorylation. Diabetes 54:2360-2364.2005).

Tsutsumi YM, Patel HH, Lai NC, Takahashi T, Head BP, Roth DM (Isoflurane produces sustained cardiac protection after ischemia-reperfusion injury in mice. Anesthesiology 104:495-502.2006).

Turcato S, Turnbull L, Wang GY, Honbo N, Simpson PC, Karliner JS, Baker AJ (Ischemic preconditioning depends on age and gender. Basic Res Cardiol 101:235-243.2006).

Ubachs JF, Engblom H, Erlinge D, Jovinge S, Hedstrom E, Carlsson M, Arheden H (Cardiovascular magnetic resonance of the myocardium at risk in acute reperfused myocardial infarction: comparison of T2-weighted imaging versus the circumferential endocardial extent of late gadolinium enhancement with transmural projection. J Cardiovasc Magn Reson 12:18.2010).

Ugander M, Bagi PS, Oki AJ, Chen B, Hsu LY, Aletras AH, Shah S, Greiser A, Kellman P, Arai AE (Myocardial edema as detected by pre-contrast T1 and T2 CMR delineates area at risk associated with acute myocardial infarction. JACC Cardiovasc Imaging 5:596-603.2012).

van den Borne SW, Diez J, Blankesteijn WM, Verjans J, Hofstra L, Narula J (Myocardial remodeling after infarction: the role of myofibroblasts. Nat Rev Cardiol 7:30-37.2010).

van den Doel MA, Gho BC, Duval SY, Schoemaker RG, Duncker DJ, Verdouw PD (Hypothermia extends the cardioprotection by ischaemic preconditioning to coronary artery occlusions of longer duration. Cardiovasc Res 37:76-81.1998).

van der Brug MP, Blackinton J, Chandran J, Hao LY, Lal A, Mazan-Mamczarz K, Martindale J, Xie C, Ahmad R, Thomas KJ, Beilina A, Gibbs JR, Ding J, Myers AJ, Zhan M, Cai H, Bonini NM, Gorospe M, Cookson MR (RNA binding activity of the recessive parkinsonism protein DJ-1 supports involvement in multiple cellular pathways. Proc Natl Acad Sci U S A 105:10244-10249.2008).

van Laake LW, Passier R, Monshouwer-Kloots J, Nederhoff MG, Ward-van OD, Field LJ, van Echteld CJ, Doevendans PA, Mummery CL (Monitoring of cell therapy and assessment of cardiac function using magnetic resonance imaging in a mouse model of myocardial infarction. Nat Protoc 2:2551-2567.2007).

Vandervelde S, van Amerongen MJ, Tio RA, Petersen AH, van Luyn MJ, Harmsen MC (Increased inflammatory response and neovascularization in reperfused vs. non-reperfused murine myocardial infarction. Cardiovasc Pathol 15:83-90.2006).

Verdouw PD, van den Doel MA, de ZS, Duncker DJ (Animal models in the study of myocardial ischaemia and ischaemic syndromes. Cardiovasc Res 39:121-135.1998).

Verma M, Shulga N, Pastorino JG (Sirtuin-3 modulates Bak- and Bax-dependent apoptosis. J Cell Sci 126:274-288.2013).

Vermeiren GL, Claeys MJ, Van BD, Grobben B, Slegers H, Bossaert L, Jorens PG (Reperfusion injury after focal myocardial ischaemia: polymorphonuclear leukocyte activation and its clinical implications. Resuscitation 45:35-61.2000).

Verweij M, Sluiter W, van den Engel S, Jansen E, Ijzermans JN, de Bruin RW (Altered mitochondrial functioning induced by preoperative fasting may underlie protection against renal ischemia/reperfusion injury. J Cell Biochem 114:230-237.2013).

Waak J, Weber SS, Gorner K, Schall C, Ichijo H, Stehle T, Kahle PJ (Oxidizable residues mediating protein stability and cytoprotective interaction of DJ-1 with apoptosis signal-regulating kinase 1. J Biol Chem 284:14245-14257.2009a).

Waak J, Weber SS, Waldenmaier A, Gorner K, Alunni-Fabbroni M, Schell H, Vogt-Weisenhorn D, Pham TT, Reumers V, Baekelandt V, Wurst W, Kahle PJ (Regulation of astrocyte inflammatory responses by the Parkinson's disease-associated gene DJ-1. FASEB J 23:2478-2489.2009b).

Wang M, Baker L, Tsai BM, Meldrum KK, Meldrum DR (Sex differences in the myocardial inflammatory response to ischemia-reperfusion injury. Am J Physiol Endocrinol Metab 288:E321-E326.2005).

Wehrens XH, Doevendans PA (Cardiac rupture complicating myocardial infarction. Int J Cardiol 95:285-292.2004).

Weinmann HJ, Brasch RC, Press WR, Wesbey GE (Characteristics of gadolinium-DTPA complex: a potential NMR contrast agent. AJR Am J Roentgenol 142:619-624.1984).

Weisman HF, Healy B (Myocardial infarct expansion, infarct extension, and reinfarction: pathophysiologic concepts. Prog Cardiovasc Dis 30:73-110.1987).

Wesbey GE, Higgins CB, McNamara MT, Engelstad BL, Lipton MJ, Sievers R, Ehman RL, Lovin J, Brasch RC (Effect of gadolinium-DTPA on the magnetic relaxation times of normal and infarcted myocardium. Radiology 153:165-169.1984).

Wiersema AM, Dirksen R, Oyen WJ, Van der Vliet JA (A method for long duration anaesthesia for a new hindlimb ischaemia-reperfusion model in mice. Lab Anim 31:151-156.1997).

Wilson MA (The role of cysteine oxidation in DJ-1 function and dysfunction. Antioxid Redox Signal 15:111-122.2011).

Wilson MA, Collins JL, Hod Y, Ringe D, Petsko GA (The 1.1-A resolution crystal structure of DJ-1, the protein mutated in autosomal recessive early onset Parkinson's disease. Proc Natl Acad Sci U S A 100:9256-9261.2003).

Wince WB, Kim RJ (Molecular imaging: T2-weighted CMR of the area at risk--a risky business? Nat Rev Cardiol 7:547-549.2010).

Wolfensohn S, Lloyd M (2003) Small laboratory animals. In: Handbook of Laboratory Animal Management and Welfare, pp 233-271 Oxford: Blackwell Publishing.

Woodfield KY, Price NT, Halestrap AP (cDNA cloning of rat mitochondrial cyclophilin. Biochim Biophys Acta 1351:27-30.1997).

Wu YT, Lee HC, Liao CC, Wei YH (Regulation of mitochondrial F(o)F(1)ATPase activity by Sirt3-catalyzed deacetylation and its deficiency in human cells harboring 4977bp deletion of mitochondrial DNA. Biochim Biophys Acta 1832:216-227.2013).

Xi J, Wang H, Mueller RA, Norfleet EA, Xu Z (Mechanism for resveratrol-induced cardioprotection against reperfusion injury involves glycogen synthase kinase 3beta and mitochondrial permeability transition pore. Eur J Pharmacol 604:111-116.2009).

Yamaguchi H, Shen J (Absence of dopaminergic neuronal degeneration and oxidative damage in aged DJ-1-deficient mice. Mol Neurodegener 2:10.2007).

Yanagida T, Kitamura Y, Yamane K, Takahashi K, Takata K, Yanagisawa D, Yasui H, Taniguchi T, Taira T, Honda T, Ariga H (Protection against oxidative stress-induced neurodegeneration by a modulator for DJ-1, the wild-type of familial Parkinson's disease-linked PARK7. J Pharmacol Sci 109:463-468.2009).

Yang H, Yang T, Baur JA, Perez E, Matsui T, Carmona JJ, Lamming DW, Souza-Pinto NC, Bohr VA, Rosenzweig A, de CR, Sauve AA, Sinclair DA (Nutrient-sensitive mitochondrial NAD+ levels dictate cell survival. Cell 130:1095-1107.2007a).

Yang Y, Fu W, Chen J, Olashaw N, Zhang X, Nicosia SV, Bhalla K, Bai W (SIRT1 sumoylation regulates its deacetylase activity and cellular response to genotoxic stress. Nat Cell Biol 9:1253-1262.2007b).

Yang YH, Chen YH, Zhang CY, Nimmakayalu MA, Ward DC, Weissman S (Cloning and characterization of two mouse genes with homology to the yeast Sir2 gene. Genomics 69:355-369.2000).

Yang Z, Berr SS, Gilson WD, Toufektsian MC, French BA (Simultaneous evaluation of infarct size and cardiac function in intact mice by contrast-enhanced cardiac magnetic resonance imaging reveals contractile dysfunction in noninfarcted regions early after myocardial infarction. Circulation 109:1161-1167.2004).

Yellon DM, Downey JM (Preconditioning the myocardium: from cellular physiology to clinical cardiology. Physiol Rev 83:1113-1151.2003).

Yellon DM, Hausenloy DJ (Myocardial reperfusion injury. N Engl J Med 357:1121-1135.2007).

Yu HH, Xu Q, Chen HP, Wang S, Huang XS, Huang QR, He M (Stable overexpression of DJ-1 protects H9c2 cells against oxidative stress under a hypoxia condition. Cell Biochem Funct.2013).

Yu W, Dittenhafer-Reed KE, Denu JM (SIRT3 protein deacetylates isocitrate dehydrogenase 2 (IDH2) and regulates mitochondrial redox status. J Biol Chem 287:14078-14086.2012).

Zhai X, Zhou X, Ashraf M (Late ischemic preconditioning is mediated in myocytes by enhanced endogenous antioxidant activity stimulated by oxygen-derived free radicals. Ann N Y Acad Sci 793:156-166.1996).

Zhang L, Shimoji M, Thomas B, Moore DJ, Yu SW, Marupudi NI, Torp R, Torgner IA, Ottersen OP, Dawson TM, Dawson VL (Mitochondrial localization of the Parkinson's disease related protein DJ-1: implications for pathogenesis. Hum Mol Genet 14:2063-2073.2005).

Zhao ZQ, Corvera JS, Halkos ME, Kerendi F, Wang NP, Guyton RA, Vinten-Johansen J (Inhibition of myocardial injury by ischemic postconditioning during reperfusion: comparison with ischemic preconditioning. Am J Physiol Heart Circ Physiol 285:H579-H588.2003).

Zhou W, Bercury K, Cummiskey J, Luong N, Lebin J, Freed CR (Phenylbutyrate up-regulates the DJ-1 protein and protects neurons in cell culture and in animal models of Parkinson disease. J Biol Chem 286:14941-14951.2011).

Zhou W, Zhu M, Wilson MA, Petsko GA, Fink AL (The oxidation state of DJ-1 regulates its chaperone activity toward alpha-synuclein. J Mol Biol 356:1036-1048.2006).

Zoratti M, Szabo I (The mitochondrial permeability transition. Biochim Biophys Acta 1241:139-176.1995).